Identification of selective chelators towards metals responsible for neurodegenerative diseases

Supervisore

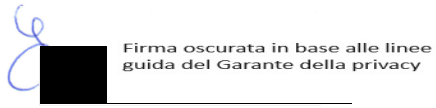

Dottoressa Emilia Furia

Dottoranda

Luana Malacaria

INDEX

ARTICLES PUBLISHED

1. Sequestering Ability of a Synthetic Chelating Agent towards Copper(II) and Iron(III): A Detailed Theoretical and Experimental Analysis
2. A review on coordination properties of Al(III) and Fe(III) towards natural antioxidant molecules: experimental and theoretical insights
3. Thermodynamic Study on the Dissociation and Complexation of Coumarinic Acid with Neodymium(III) and Dioxouranium(VI) in Aqueous Media
4. Experimental and theoretical study on the coordination properties of quercetin towards aluminum(III), iron(III) and copper(II) in aqueous solution
5. Modeling the Solubility of Phenolic Acids in Aqueous Media at 37 °C
6. Aluminum(III), iron(III) and copper(II) complexes of luteolin: Stability, antioxidant, and anti-inflammatory properties
7. Experimental insights on the coordination modes of coumarin-3-carboxilic acid towards Cr(III)-, Co(II)-, Ni(II)-, Cu(II)- and Zn(II): A detailed potentiometric and spectroscopic investigation in aqueous media
8. Experimental and theoretical study of the complexation of Fe^{3+} and Cu^{2+} by *L*-ascorbic acid in aqueous solution
9. Transition metal cations catalyze $^{16}O/^{18}O$ exchange of catechol motifs with $H_2{}^{18}O$
10. Insights into the complexation and oxidation of quercetin and luteolin in aqueous solutions in presence of selected metal cations
11. Wide pH range potentiometric and spectrophotometric investigation on the acidic constants of quercetin, luteolin and *l*-ascorbic acid in aqueous media

1. Introduction

The aim of this research project is to identify one or more ligands capable to capture selectively metal ions responsible of neurological diseases, belonging to the large group of dementias, such as Alzheimer's disease, thus facilitating their elimination from the body. The toxicity of heavy metals is one of the main threats to human health and, again, of the ecosystem in general. Heavy metals, in fact, are environmental pollutants and their toxicity is a problem of increasing importance for reasons ecological, evolutionary, nutritional, and environmental. Among these elements there are some able to exert a direct toxic effect, while others gradually accumulate in animals and plants, which are part of our food chain, then deposited in human tissues and organs. The function that metal ions play in biological systems depends on the nature of the metal. Some of them are fundamental for the correct action of enzymes that catalyze several metabolic functions, acting as cofactors and thus favoring the catalysis process of the enzymatic reactions. Low concentrations of specific metal ions can cause a malfunction in proteins, while if they or other metals are present in high concentrations, they can compete with other ions becoming harmful and dangerous. The dual property of metals, both to destroy and to sustain, has led to the development of many and complex cellular mechanisms, to regulate their location and intracellular availability.[1] The excessive exposure to these elements causes asthenia and excessive fatigue, damage to the brain, lungs, kidneys, liver, and abnormal changes in blood composition. Long-term exposure, generally, leads to progressive muscle and neurological degeneration, with the onset of symptoms and typical signs of other serious degenerative diseases, such as multiple sclerosis, Parkinson's disease, Alzheimer's disease, and muscular dystrophy. The binding molecules take on a biomedical interest in that they are potentially applicable in the processes of moving a metal from the body (*i.e.*, chelation therapy), in cases of pathologies due to bioaccumulation of heavy metals. Metals that are harmful to the body exert many of their adverse effects by forming complexes with DNA, with some enzymes and other molecules present in the body; these complexes exhibit properties that differ considerably from the original molecules. Therefore, an important aspect is the use of chelating agents capable of remove harmful metals from sites in which they are confined *in vivo*. The potential use of a chelating agent as a drug depends on its ability

to compete effectively with natural coordination sites to form a complex with the toxic metal ion. The essential requirement of a chelating agent is the formation with the metal ion of a more stable complex than that formed with its binding site *in vivo*. The ideal chelating agent must reduce the toxicity of the metal by promoting its mobilization from its compartment and its subsequent excretion. The ligand must be selective towards a particular metal ion, avoiding coordination with other metals, it should not interact with essential metals. Important parameters for the selection of the chelating agent are the stability of the complexes, the rate of formation of the complexes and the reaction stoichiometry. So that a ligand to be used as a drug, it is necessary to know its pharmacokinetics, and therefore the transformations of the drug by the body, and pharmacodynamics, *i.e.*, the actions of the drug on the different organs. The chelating agents examined are mainly natural molecules with different beneficial properties for humans.

The behavior of a metal under physiological conditions depends essentially on its speciation, *i.e.*, on the different forms in which it is found in each environment, characterized by conditions of temperature, pH and ionic strength. The thermodynamic study of chemical equilibria in solution allows to establish the stoichiometry of the different species present in the investigated systems and their corresponding concentrations. Furthermore, by evaluating the stability constants of the metal complexes formed in solution is possible to estimate the sequestering ability of ligands towards bioavailable metal ions. The thermodynamic approach provides, at first, the evaluation, under physiological conditions, of the acid-base properties of the ligand, to evaluate the competition between proton and metal cation for the ligand, and then the determination of the stability constants between a ligand and a specific metal ion. The potentiometry represents the most accurate and particularly economical method for the determination of equilibrium constants, allowing the evaluation of stoichiometric coefficients of the species and the corresponding stability constants. One of the fields of investigation of many chemists has been to analyze what happens in solution when two substances come into contact to reach a state of equilibrium. A great contribution to the development of equilibrium study is due to Professor Lars Gunnar Sillén, and one of the widely used theories is the Specific Interaction Theory (SIT[2,3]), based on the Sillén's studies, which can describe in detail what really happens

in solution. The amount of each species in equilibrium is expressed in terms of its activity, so it is necessary to evaluate its activity coefficients.[4] In this frame, the constant ionic medium method,[5] which involves the addition of a high and constant concentration of an inert salt in the test solutions, is used. This method gives us the opportunity to consider as constant all the activity coefficients and to work with concentrations. In the present work, the inert salts used were NaCl and $NaClO_4$ at a concentration of 0.16 M, and the measuring cell was maintained at 37 °C, to reproduce the physiological conditions of ionic strength and temperature. To identify the best model for an accurate explanation of the experimental data we have employed a graphic and a numerical procedures.[6]

References

1. R.A. Goyer, M.G. Cherian, *Toxicology of Metals. Biochemical Aspects, Handbook of Experimental Pharmacology*, (**1995)**.
2. L. Ciavatta, *The specific interaction theory in equilibrium analysis. Some empirical rules for estimate interaction coefficients of metal ion complexes, Ann. Chim.*, 80 (**1990)** 255.
3. L. Ciavatta, *The specific interaction theory in the evaluating ionic equilibria*, *Ann. Chim*., 70 (**1980)** 551.
4. K.S. Pitzer, *Activity Coefficients in Electrolyte Solutions*, (**1979)**, CRC Press, Boca Raton, Florida.
5. G. Biedermann, L.G. Sillén, *Arkiv för Kemi*, 40 (**1953)** 425.
6. L.G. Sillén, *Some Graphical Methods for Determining Equilibrium Constants. II. On "Curve-fitting" Methods for Two-variable Data*, *Acta Chem. Scand*., 10 **(1956)** 186–202.

2. Chelation Therapy

Neurodegeneration is the collective name for a vast group of pathological processes and conditions occurring in the brain, which usually leads to extensive neuronal death and consequent loss of function. Notably, the most important neurodegenerative diseases (ND), such as Alzheimer's disease (AD), Parkinson's disease (PD), Prion protein disease (PrD) and amyotrophic lateral sclerosis (ALS), are related to a progressive loss of specific neuronal cell populations and to an abnormal activity of protein components, which pathologically accumulate in the brain.[1,2] The observed protein misfolding is greatly affected by a variety of biophysical and chemical factors, including metal ions. In turn, the newly formed supramolecular structures may acquire the ability to bind bio-metals. Chelation therapy represents an attractive pharmacological option for the treatment of these diseases. Metal ions can generate, by redox cycling, a local excess of reactive oxygen species (ROS) which, for example, favors membrane depolarization resulting in a dangerous accumulation of calcium within the cell.[3] Oxidative stress is considered to be one of the main reasons related to a neuronal degeneration, most likely resulting from an enhanced level of some redox-active metal ions (*i.e.*, Cu and Fe) within the *substantia nigra*, a small area of dopaminergic cells located in the mid-brain. High levels of several metal ions, such as Mn, Cu, Fe, Zn, and Al, were, indeed, detected in the *substantia nigra* of PD patients.[4–6] The role of metal ions in neurodegeneration is still a highly controversial issue.[7,8] Metal dismetabolism (essentially due to genetic or environmental factors) and the consequent dramatic accumulation of a specific metal were clearly established as the primary cause of the disease for a few and very rare ND (*e.g.* Wilson disease's or neuroferritinopathy). The multifactorial character of the pathology and the overall modest increase in metals' concentration (though in the presence of evident metal dysmetabolism) makes it difficult to assign clear and conclusive roles to the various agents for most common ND (*e.g.* AD).

It is well known that the brain closely regulates metal ion homeostasis as an important part of its normal functioning. Zinc, for example, is a component of almost 300 enzymes either as a catalytic factor or as a co-factor.[9] Notably, during the normal neuronal activity, zinc is released into the synaptic cleft, where it can reach transient concentration as high as 300 μM;[10] afterwards, zinc must be efficiently removed to

avoid toxic effects. Disruption of this delicate equilibrium may have deleterious, often lethal, effects. Several recent studies highlighted that some metals are able to alter the biophysical properties of the Aβ peptide, thus accelerating Aβ aggregation, with the consequence of increasing neurotoxic effects on neuronal cells.[11–13] Accordingly, significant local increases in Cu (~400 μM) and Zn (~1 mM) concentration were found in senile plaques and in the neuropil.[14] The established metal imbalance (dishomeostasis), which occurs in several ND, has attracted the interest of several researchers, in particular, to the possible role that metal ions such as copper (Cu), iron (Fe), zinc (Zn), and the nonphysiological aluminum (Al) play in the etiology of some neurodegenerative conditions. Although these diseases generally present a complex and not yet fully understood pattern of pathological features, the disruption of this aberrant metal interaction through metal-targeted agents might represent a very challenging task for future pharmacological treatments.[15] As the demand of new and effective strategies for the treatment of ND increase, the use of chelating agents to scavenge free metals, present in the brain in large excess, may represent a very promising and well-grounded therapeutic option. In principle, treatment with chelating agents should aim at abstracting and removing metal ions such as Cu, Fe, Zn, and Al, which may be responsible for inducing direct neurotoxic effects. Indeed, this type of approach turned out to be successful for a few rare genetic diseases, where a dramatic brain metal accumulation takes place. The design of novel and effective nontoxic chelating molecules represents today a very challenging task, and several specific requirements must be met to obtain candidate drugs. An important requirement for an effective metal targeting agent in ND is its ability to cross the blood brain barrier (BBB). This excludes many common metal ligands because of a marked hydrophilic nature. Moreover, specific, and moderate, rather than indiscriminate and massive chelation of excess metals is highly preferred when dealing with the most frequent ND. Thus, ligands with intermediate affinity and appreciable metal selectivity should be designed, capable of disrupting a few relevant metal–peptide interactions[16] rather than inducing generalized, and thus highly toxic, metal depletion. Indeed, strong metal chelators are expected to compete successfully with metal-binding proteins, thereby altering physiological metal distribution and inhibiting essential metal-containing enzymes. These observations feature, for the major ND, a type of chelation therapy

that is radically different from the classical protocols, originally developed in the frame of clinical toxicology to contrast heavy metal poisoning. The goal may be achieved by abolishing abnormal metal/protein interactions, by contrasting localized metal excesses, or by normalizing intra/extra cellular metal ratios or, finally, by restoring the correct balance among the main bio-metals (*i.e.*, Cu, Fe and Zn). The last one could be reached by supplying a defective metal capable of counteracting the effects of the excess metal (for example, consider the well-known Cu/Zn antagonism) rather than by directly removing the excess metal itself. Specific attention must be paid to the nature of the ligand (hydrophobic/hydrophilic nature), to its toxicological profile, to the strength and selectivity of its metal binding, to its targeting to specific brain areas, and to the nature of the resulting metal complexes. Overall, these considerations justify novel and smart therapeutic approaches for the major ND, that are highly peculiar and might be better defined as metal-targeted strategies rather than metal chelation. Chelation therapy has been proposed as the appropriate treatment for reducing the abnormal accumulation of essential heavy metals, such as Fe, Cu and Zn, as well as of nonessential and poisonous ones, such as Pb, Hg, Cd and Al.[17,18]

Typically, chelators bind to metal ions enhancing their urinary and fecal excretion and causing a progressive decrease of their body concentrations. Chelation therapy became a common alternative treatment, despite its still controversial clinical results,[19,20] when ethylenediaminetetraacetic acid (EDTA) turned out to be effective in chelating and removing toxic metals from blood. Following the introduction of EDTA in clinical practice, other suggestions were based on a metal chelator that might benefit patients with atherosclerosis, as the hardened arteries could be "softened" due to removal of Ca from artery walls.[21] Regarding the effectiveness of chelation therapy, encouraging results from some laboratories are by no means unanimous, in fact contradictory evidence counterbalance these claims.[22,23] Thus, EDTA therapy in cardiology has been considered by the Food and Drug Administration (FDA) as a highly controversial and questionable issue. In contrast, the use of chelating agents to treat acute metal poisoning is now well established. Effective chelation treatments of metal poisoning require an accurate knowledge of the pharmacodynamic and pharmacokinetic of the administered chelator, that depends on the physical and chemical characteristics of metals and chelators (*i.e.*, ionic radius, solvation sphere size and deformability,

hardness/softness of electron donors and acceptors, chemical stability, administration route, bioavailability, metabolism, organ and intra/extra cellular specific compartmentalization, and, of course, natural excretion).[18] Hydrophilic chelators enhance renal excretion, but their extracellular localization confines the activity to extracellular metal pools only. On the other hand, lipophilic chelators might decrease intracellular stores, but may also redistribute toxic metals to more vulnerable organs, *e.g.*, the brain. The metal selectivity of chelators is particularly important, due to the risk of essential metal depletion. Moreover, in chronic metal induced disease, necessitating long-life chelation, toxicity and side effects of the chelator may drastically limit the time of treatment. Hence, development of new and not dangerous chelators, suitable to a long-term oral administration, remains an important research challenge. In addition, a significant teratogenic potential has been demonstrated for most chelators, due to induced trace element deficiencies.[24] Improved chelator design should aim to enhance selectivity, affinity, stability, renal clearance, and oral activity, while maintaining a low toxicity and a low cost. Finally, the adaptation of chelation therapy to neurodegenerative conditions is a very complex task. It may be preferred to denote these kinds of therapeutic approaches as metal targeted strategies for neurodegenerative diseases. The term chelator, originated from the Greek word "*chele*," which means "crab's claw"[25,26], defines the complexes formed by a ligand (a molecule with at least two donor groups or coordination number) with their substrates (ions), such that a "ring" system is established. The ring structure is well correlated with the formation of a more stable complex.[26] Denticity (from the word "*dens*," meaning tooth) is used to describe the number of available donor groups of a chelating agent to bind metal ions.[26] So, bidentate refers to two donor groups, tridentate to three, quinquedentate to five. Some chelators can form multidentate complexes, while others can only attain a monodentate or bidentate chelate rings. For multidentate ligands, the dissociation constant, K_d, that reflects the intrinsic strength of metal-ligand binding, can vary markedly for different species.[25] Some chelators can directly permeate cell membranes prior to or upon binding metal ions (*e.g.*, see Ref. 27). Other chelators become membrane permeable after esterification, or by acquiring a nonpolar state following metal complexation.[25] In addition, some chelators are ionophores since their chelating sites have limited flexibility and thus would prefer cations that fit easily into

their molecular structure.[26] Ionophores may selectively enhance the permeability of metal ions in lipid membranes of cells as in the case of calcium ionophore A23187 (calcimycin), which facilitates entry of calcium ions into cells.[28] Similarly, pyrithione is a zinc chelator that neutralizes zinc neurotoxicity.[27]

Hence chelators may act to either deprive biological systems of metal ions or may have the opposite effect of promoting metal uptake into cells.

References

1. A. Binolfi, R.M. Rasia, C.W. Bertoncini, M. Ceolin, M. Zweckstetter, C. Griesinger, T.M. Jovin, C.O. Ferna´ndez, *J. Am. Chem. Soc*., 128 (**2006**) 9893–9901.
2. P.M. Doraiswamy, A.E. Finefrock, *Lancet Neurol*., 3 (**2004**) 431–434.
3. M.P. Mattson, *Trends Neurosci*, 21 (**1998**) 53–57.
4. E.C. Hirsh, J.P. Brandel, P. Galle, F. Javoy-Agid, Y. Agid, *J. Neurochem*., 56 (**1991**) 446–451.
5. D.T. Dexter, A. Carayon, F. Javoy-Agid, Y. Agid, F.R. Wells, S.E. Daniel, A.J. Lees, P. Jenner, C.D. Marsden, *Brain*, 114 (**1991**) 1953–1975.
6. B.A. Fraucheux, M.E. Martin, C. Beaumont, J.J. Hauw, Y. Agid, E.C. Hirsch, *J. Neurochem*., 86 (**2003**) 1142–1148.
7. P. Zatta, *Singapore, London: World Scientific*; (**2003**) 1–511.
8. P. Zatta, A. Frank, *Brain Res. Rev*., 54 (**2007**) 19–33.
9. B.L. Vallee, K.H. Falchuk, *Physiol. Rev*., 73 (**1993**) 79–118.
10. S.Y. Assaf, S.H. Chung., *Nature*, 308 (**1984**) 734–736.
11. F. Ricchelli, D. Drago, B. Filippi, G. Tognon, P. Zatta, *Cell Mol. Life Sci*, 62 (**2005**) 1724–1733.
12. E. House, J. Collingwood, A. Khan, O. Korchazkina, G. Berthon, C. Exley, *J. Alzheimers Dis*., 6 (**2004**) 291–301.
13. C.J. Maynard, A.I. Bush, C.L. Masters, R. Cappai, Q.X. Li, *Int. J. Exp. Pathol*., 86 (**2005**) 147–159.
14. C.S. Atwood, G. Perry, H. Zeng, Y. Kato, W.D. Jones, K.Q. Ling, X. Huang, R.D. Moir, D. Wang, L.M. Sayre, M.A. Smith, S.G. Chen, A.I. Bush, *Biochemistry*, 43 (**2004**) 560–568.
15. G. Liu, M.R. Garrett, P. Men, X. Zhu, G. Perry, M.A. Smith, *Biochim. Biophys. Acta*, 1741 (**2005**) 246–252.
16. T. Storr, M. Merkel, G.X. Song-Zhao, L.E. Scott, D.E. Green, M.L. Bowen, K.H. Thompson, B.O. Patrick, H.J. Schugar, C. Orvig, *J. Am. Chem. Soc*., 129 (**2007**) 7453–7463.
17. K. Kalia, S.J. Flora, *J. Occup. Health*, 47 (**2005**) 1–21.
18. O. Andersen, *Mini Rev. Med. Chem*., 4 (**2004**) 11–21.

19. J.P. Carter, *J. Advancement Med*., 21 (**1989**) 213–226.
20. M.L. Knudtson, D.G. Wyse, P.D. Galbraith, R. Brant, K. Hildebrand, D. Paterson, D. Richardson, C. Burkart, E. Burgess, *JAMA*, 287 (**2002**) 481–486.
21. C.N. Clarke, N.E. Clarke, R.E. Mosher, *Am. J. Med. Sci*., 232 (**1956**) 654–656.
22. B. Guldager, E. Jelnes, S.J. Jorgensen, J.S. Nielsen, A. Klaerke, K. Mogensen, K.E. Larsen, E. Reimer, J. Holm, S. Ottesen, *J. Intern. Med*., 231 (**1992**) 261–267.
23. E. Ernst, *Am. Heart J*., 140 (**2002**) 139–141.
24. J.L. Domingo, Reprod. Toxicol., 9 (**1995**) 105–113.
25. D.P. Mellor, F.P. Dwyer, *Eds. Academic Press. New York*, (**1964**) 1–50.
26. P.M. May, R.A. Bulman, *Prog. Med. Chem*., 20 (**1983**) 225–336.
27. M.P. Cuajungco, G.J. Lees, *Brain Res*., 799 (**1998**) 97–107.
28. L. Blau, R.B. Stern, R. Bittman, *Biochim. Biophys. Acta*, 778 (**1984**) 219–223.

3. Ligands

Antioxidant molecules are capable of neutralizing free or incorrectly bound metals, thereby interfering with the 'down-stream' generation of ROS and other radicals. Therefore, antioxidants may be used mainly as a preventive approach.[1] Numerous molecules with antioxidant properties, such as estrogen, melatonin, vitamin C and E (*L*-ascorbate and α- topopherol, respectively), ginkgo bilboa extract, curcumin and flavonoids, have been shown to have neuroprotective effects against Aβ-induced toxicity in cell based experiments[2,3] and animal models.[4-7]

Natural polyphenols are largely distributed in the plant kingdom (*e.g*., fruit, vegetables, leaves and flowers). Polyphenols are π-conjugated compounds containing OH-phenolic groups (Fig. 1). There exist wide subclasses of natural and hemi-synthetic polyphenols, including the ''small'' phenolic acids (*i.e.*, molecular weight lower than 100), the intermediate-in-size flavonoids–lignans, coumarins, stilbenoids, isoflavonoids and flavonolignans (molecular weight ranging from 300 to 600) and the bigger oligomers and polymers (molecular weight ranging from 500 to 3000).

The flavonoid group is divided into numerous subgroups, including flavones, flavonols, anthocyanidins, chalcones, dihydroflavonols, flavanones and flavan-3-ols (Fig. 1). They are naturally synthesized by the secondary metabolism of plants. Chalcones (1,3-diaryl-2-propen-1-ones) are the precursors of the other flavonoids in plants. Most flavonoids appear in plants in their glycoside forms and a few of them in their aglycone form. Anthocyanidins, derivatives of the 2-phenylbenzopyrylium cation (Fig. 1), are responsible for red, blue and purple color (absorption of yellow wavelengths) of some flowers (*e.g*., orchids, roses), leaves (*e.g*., tobacco), fruit (*e.g*., berries, apples, plums, purple tomatoes) and vegetables (*e.g*., onions, aubergines).

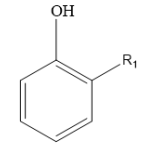

Phenol (R_1 = H)
Catechol (R_1 = OH)
Guaiacol (R_1 = OCH_3)

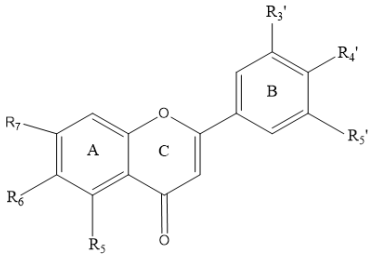

Flavone
1: 3',4'-diOH flavone ($R_{3'}$ = $R_{4'}$ = OH)
2: 3',4'-diOMe flavone ($R_{3'}$ = $R_{4'}$ = OCH_3)
3: Chrysin (R_5 = R_7 = OH)
4: Apigenin (R_5 = R_7 = $R_{4'}$ =OH)
5: Luteolin (R_5 = R_7 = $R_{3'}$ = $R_{4'}$ =OH)
6: 5,7-diOH- 3',4'-diOMe flavone (R_5 = R_7 = OH, ($R_{3'}$ = $R_{4'}$ = OCH_3)
7: 5,7-diOH- 3',4',5'-triOMe flavone (R_5 = R_7 = OH, ($R_{3'}$ = $R_{4'}$ = $R_{5'}$ = OCH_3)
8: Baicalein (R_5 = R_6 = R_7 = $R_{4'}$ =OH)

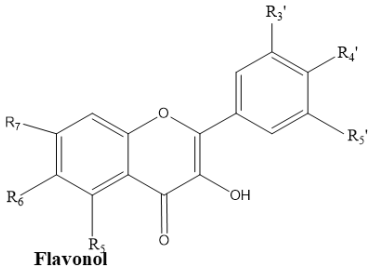

Flavonol
9: Galangin (R_3 = R_5 = R_7 = OH)
10: Kaempferol (R_3 = $R_{4'}$ = R_5 = R_7 = OH)
11: Quercetin ($R_{3'}$ = $R_{4'}$ = R_5 = R_7 = R_3 = OH)
12: Morin (R_3 = R_5 = R_7 = $R_{2'}$ = $R_{4'}$ =OH)
13: Myricetin (R_3 = R_5 = R_7 = $R_{3'}$ = $R_{4'}$ = $R_{5'}$ = OH)
14: Fisetin (R_3 = R_7 = $R_{3'}$ = $R_{4'}$ = OH)

Glycosylated flavonol
15: Rutin (R_5 = R_7 = $R_{3'}$ = $R_{4'}$ = $R_{5'}$ = OH and R_3 =rhamnosylglucoside)

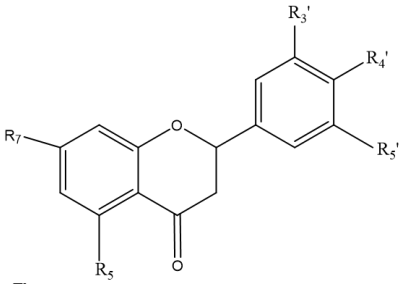

Flavanone
16: Eriodictyol ($R_{3'}$ = $R_{4'}$ = R_5 = R_7 = OH)
17: Hesperetin ($R_{3'}$ = R_5 = R_7 = OH and $R_{4'}$ = OCH_3)
18: Naringenin ($R_{4'}$ = R_5 = R_7 = OH)

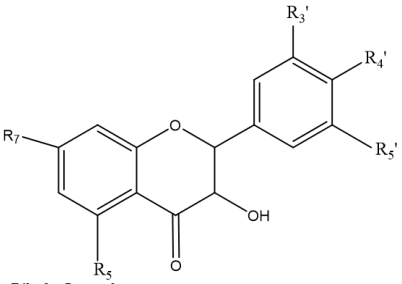

Dihydroflavonol
19: Aromadendrin ($R_{4'}$ = R_3 = R_5 = R_7 = OH)
20: Taxifolin (R_3 = R_5 = R_7 = $R_{3'}$ = $R_{4'}$ = OH)
21: Ampelopsin (R_3 = R_5 = R_7 = $R_{3'}$ = $R_{4'}$ = $R_{5'}$ = OH)

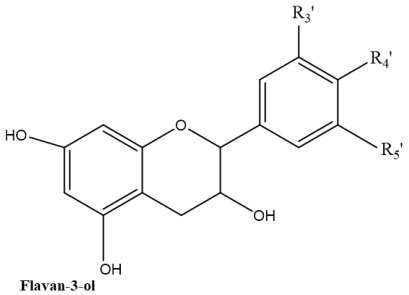

Flavan-3-ol
22: Catechin ($R_{4'}$ = OH)

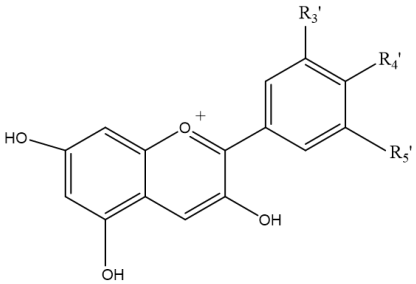

Anthocyanidin
23: Pelargonidinl ($R_{4'}$ = OH)
24: Cyanidin ($R_{3'}$ = $R_{4'}$ = OH)
25: Delphinidin ($R_{3'}$ = $R_{4'}$ = $R_{5'}$ = OH)

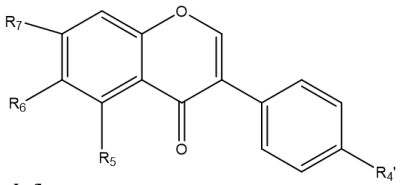

Isoflavone
26: Daidzein ($R_{4'}$ = R_7 = OH)
27: Genistein (R_5 = R_7 = $R_{4'}$ = OH)
28: Prunetin (R_5 = $R_{4'}$ = OH and R_7 = OCH_3)
29: Isoluteolin (R_5 = R_7 = $R_{3'}$ = $R_{4'}$ = OH)

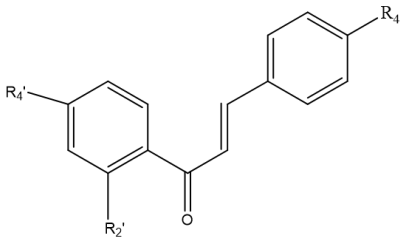

Chalcone
30: 4',4-diOH chalcone ($R_{4'}$ = R_4 = OH)
31: 2',4',4-diOH chalcone (R_4 = $R_{2'}$ = $R_{4'}$ = OH)
Or isoliquiritigenin

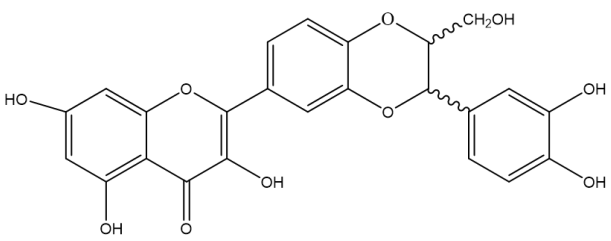

Dehydrosilybin
32: Dehydrosilybin

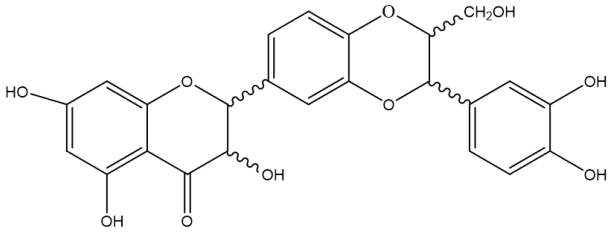

Silybin
33: Silybin

Fig. 1. Chemical structures of phenol, catechol, guaiacol and 33 different flavonoids and flavonolignans.

Chalcones provide yellow color (absorption of blue wavelengths). Some flavonols, flavones, flavan-3-ols and isoflavones are colorless, others provide yellow as well. They protect plants from UV-light, since most of them are known to absorb in this spectroscopic range. They are known to protect against DNA damage induced by UV-A and B light. Partially due to their optical properties, they may also significantly alter the interaction between plants and insects. The multitude of leaf, flower and fruit colors in nature is partly attributed to the variation of chemical structures of flavonoid pigments. The chemical structure of polyphenols is known to modulate UV/Vis absorption spectra, which depend on the number and the position of substitutions, mainly -OH, -OCH_3 and glycoside groups. The UV/Vis absorption and thus pigmentation may also be modulated by many other parameters, including pH, metal complexation, long-range intermolecular interactions (*e.g.*, via intra- and intermolecular π-stacking interactions between flavonoid moieties), which may induce co-pigmentation.[7] The UV/Vis spectra of polyphenols are generally attributed to electronic transitions between π-type molecular orbitals (MOs), that are extended over the molecular backbone. High molar absorption coefficients and thus large oscillator strengths are a product of (i) large LCAO (linear combination of atomic orbitals) coefficients, (ii) extended topology and (iii) similarity of topology in the contributing orbitals.[8] Flavonoids have several biological activities, including antimicrobial, anticarcinogenic, antimutagenic and antioxidative activities. It is well known that flavonoids are essential as they can reduce free radical formation, scavenge free radicals, and chelate metal ions such as iron and copper. Because of their unpaired electron, free radicals are highly reactive molecules. They can oxidize other molecules and convert them to radicals. Antioxidants are free radical scavengers which donate an electron or hydrogen atom to the free radical, thereby deactivating the radical. It is not clear whether the dominant mechanism of the antioxidant action of flavonoids occurs by electron donation or by hydrogen atom donation to radicals.

The antioxidant abilities of the flavonoids depend on their redox properties and chemical structures. The reduction potential of flavonoids is between 0.23-0.75 V, which depends on the electron-donating substituents in the B ring. Due to these low redox potentials, flavonoids can thermodynamically reduce highly oxidizing free radicals, such as peroxyl, superoxide, and hydroxyl radicals with redox potentials in

the range 1.0-2.13 V. A catechol group in the B ring, the 2,3-double bond in conjugation with 4-oxo in the C ring, and the additional presence of 3- and 5-hydroxyl groups in the flavonoids make them efficient antioxidants. The pyrogallol group in ring B also increases the antioxidant capacity. The proposed metal binding sites in flavonoids are the *ortho*-dihydroxyl groups in ring B, the 4-oxo and 5-hydroxyl groups, or the 4-oxo and 3-hydroxyl groups (Fig. 2).

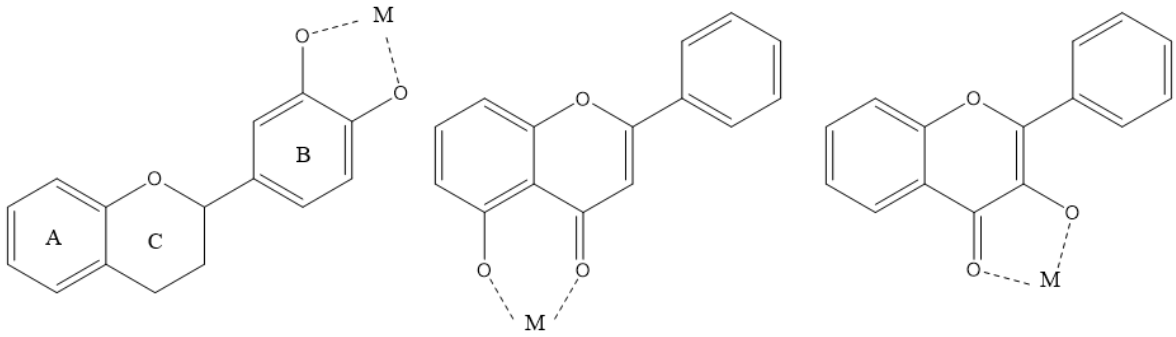

Fig. 2. Proposed Metal Binding Sites for Flavonoids.

Quercetin

Quercetin (3,5,7-trihydroxy-2-(3,4-dihydroxyphenyl)-4*H*-chromen-4-one, H_5Que) is a dietary flavonoid, which widely occurred in caper, black chokeberry, onion, tomato and lettuce. In plants, quercetin is usually bounded with sugars, ethers or phenolic acids. Different forms of quercetin derivatives seem to influence their rate of absorption in the small intestine and stomach. The content and form of its derivatives play a key role in their absorption. Quercetin has attracted increasing attention due to its antioxidant, anti-obesity,[9] anti-carcinogenic, antiviral,[10] antibacterial and anti-inflammatory effects. Moreover, quercetin has been reported to have a strong potential in the treatment of cancers. Quercetin has low water solubility and bioavailability, chemical instability, and short biological half-life, which may reduce its efficacy when used in the food and pharmaceutical fields. Quercetin is a lipophilic compound, and it is moderately soluble in ethanol (4.0 mg/mL, 37 °C) and highly soluble in dimethyl sulfoxide (150 mg/mL, 25 °C). However, its solubility in water is only approximately 0.01 mg/mL (at 25 °C). It is therefore difficult to directly incorporate high levels of quercetin into water-based food matrix. Quercetin has a typical flavonoid structure and

contains five hydroxyl groups. Fig. 3 displays the structural characteristics of flavonoids: 2 benzene rings (A and B) connected by an oxygen-containing pyrene ring (C). Quercetin is commonly found in its glycoside form, in which one or more hydroxyl group is replaced by different types of sugar groups. The main groups of quercetin derivatives are quercetin *O*-glycosides, and some other common derivatives are summarized in Fig. 3. The molecular structure and some physicochemical properties of quercetin and its derivatives are shown in Table 1.

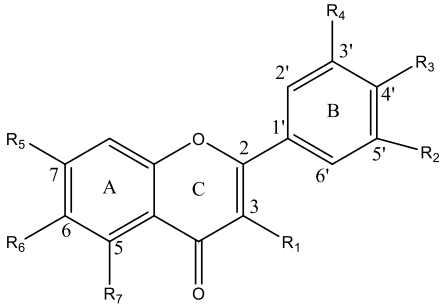

Systematic name	R_1	R_2	R_3	R_4	R_5	R_6	R_7
Quercetin	OH	OH	OH	H	OH	H	OH
Quercetin 3-*O*-rhamnoside (quercitrin)	O-Rha	OH	OH	H	OH	H	OH
Quercetin 3-*O*-rhamnozyl-(1-6)-glucoside (rutin)	O-RG	OH	OH	H	OH	H	OH
Quercetin 3-*O*-glucoside (isoquercitrin)	O-Glu	OH	OH	H	OH	H	OH
Quercetin 3-*O*-galactoside (Hyperoside)	O-Gal	OH	OH	H	OH	H	OH
Quercetin 7-*O*-glucoside	OH	OH	OH	H	OH	H	O-Glu
Quercetin	O-Rha	OH	OH	O-Glu	OH	H	OH
3-*O*-rhamnoside-7-*O*-glucoside	OH	OH	OH	H	OH	Glu	OH
Quercetin 3'-methyl ether (isorhamnetin)	OH	O-Met	OH	H	OH	H	OH
Quercetin 7-methyl ether (rhamnetin)	OH	OH	OH	H	OH	H	0-Met

Quercetin 4'-methyl ether (tamarixetin)	OH	OH	O-Met	H	OH	H	OH

Gal: galactose; Glu: glucose; Rha: rhamnose; RG: rhamnosyl glucose; Met: methyl

Fig. 3. Chemical structures of quercetin and its main derivatives.

Table 1. Summary of physicochemical properties of quercetin and its derivatives.

Chemical structure	*Molecular weight*	*Melting point (°C)*	*log P*	*Water solubility (mg/ml)*	*Physical state*	*UV.Vis max (nm)*	*Reported biological activities*
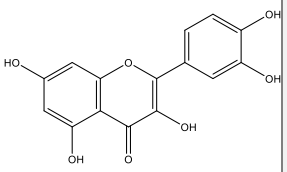 *Quercetin*	302.23	314-316	1.48	0.001	Yellow poweder	258, 360	Antioxidant, anti-inflammation, antiviral, anti-obesity, antidepressant as well as preventing cancer, diabetes, asthma, hypertension and cardiovascular diseases
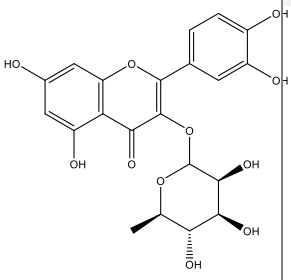 *Quercetin 3-O-rhamnoside*	448.38	174-179	0.90	0.024	Yellow powder	256, 346	Antioxidant, anti-inflammation, anticancer as well as inhibiting lipid peroxidation
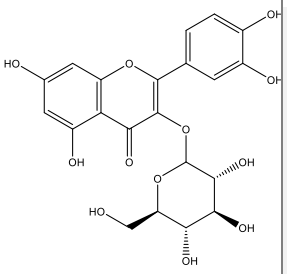 *Quercetin 3-O-glucoside*	464.38	188-189	0.83	0.095	Yellow powder	257, 362	Antioxidant, anti-inflammatory, antihypertensive, as well as cytoprotection; inhibiting melanogenesis and Ca^{2+} induced lipid peroxidation
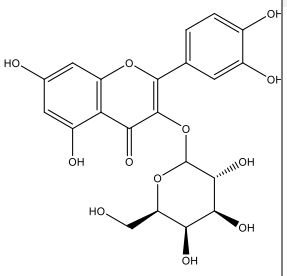 *Quercetin 3-O-galactoside*	464.38	227-230	0.43	NA	Yellow powder	256, 358	Antioxidant, antimicrobial, anti-inflammation, as well as preventing hypertension and cardiovascular diseases

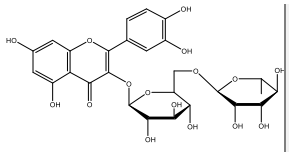 *Rutin*	610.52	190-192	-2.02	0.034	Faint yellow powder	256,351	Antioxidant, anticancer, anti-inflammation, cardioprotection as well as anticonvulsive
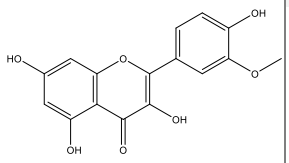 *Quercetin 3'-methyl ether*	316.26	305-307	2.79	0.037	Yellow crystal	255, 356	Antioxidant, anti-tumor as well as preventing endothelial dysfunction, hypertension and cardiovascular diseases

NA: not available

Quercetin and its derivatives usually exist in the form of yellow colored powder or crystals. Quercetin *O*-glycosides are the derivatives with at least one *O*-glycosidic bond. Many plants and vegetables contain quercetin *O*-glycosides, and the most common glycosylation site is located at the C3 carbon. The associated monosaccharides may include glucose, galactose, and xylose. Quercetin 3-*O*-glucoside has been found in beans,[12] salvia and buckwheat. Quercetin derivatives in the form of disaccharides are also widely occurred in plants and vegetables. Quercetin has been shown to be a strong antioxidant *in vitro* and is one of the most powerful scavengers of reactive oxygen species, such as $O_2^{\cdot -}$, $NO^{\cdot}$ and $ONOO^{-}$. Oxidative damage induced by $O_2^{\cdot -}$, $NO^{\cdot}$ and $ONOO^{-}$ can create deleterious effects on cells and tissues in human body and may cause many diseases, such as cardiovascular diseases, diabetes and cancers. Fortunately, peroxidation can be reduced by antioxidants, such as quercetin, which can interfere peroxidation by reacting with the radicals formed. Its antioxidative activity is ascribed to: (a) a catechol group in the B ring; (b) a 2,3-double bond in conjugation with a 4-oxo function in the C ring, and (c) -OH group at positions 3 and 5 in heterocyclic ring. Moreover, quercetin could significantly enhance the endogenous antioxidant capacity of scavenging ABTS (2,2'-azino-bis(3-ethylbenzothiazoline-6-sulfonic acid) radicals by 6.2 folds compared to that of Trolox, which can be ascribed to its contribution to the total antioxidant capacity of plasma. Some papers have dealt with complex formation of H_5Que with metals[13,14] and, generally, the chelation property of flavonoids towards metal ions have been attributed to the presence of the 3- or 5-hydroxypyran-4-one, rather than the 3',4'-dihydroxy group on B-ring (Fig. 3).[15,16] However, depending on pH and metal-to-ligand ratio, the potential different chelating sites of H_5Que have been observed to change their metal-chelating ability.[17,18]

Luteolin

Luteolin is a flavone present in many medical plants and in vegetables. However, concentrations are generally low compared to some of the flavonols like quercetin or kaempferol. Considerable concentrations are found in some spices like thyme, parsley, sage, in wild carrots, artichokes and in peanut hulls. Celery, spinach, some varieties of peppers and lettuce are our major nutritional luteolin sources.[19] While luteolin is only

a minor flavonoid component in food, high amounts can be isolated from peanut hulls and *Reseda luteola L*. that has been used as a dyeing plant due to its high luteolin content since ancient times.[20] While quercetin has been studied most intensively among the flavonoids during the last decades, recent research has provided a plethora of anti-oxidant, immunological, anti-carcinogenic, anti-bacterial, cardiovascular and other pharmacological mechanisms which suggest luteolin to be a valuable compound for many medical and food applications.[9,12] Some epidemiological investigations indeed indicate that luteolin intake may protect from cardiovascular diseases or some cancer species, but prospective clinical studies are widely lacking.

In a previous work, the redox potential of several radicals has been determined in aqueous solutions by a pulse radiolysis technique.[21] Main electron-donating system is the B-ring, if it is substituted with hydroxy groups. The A-ring is not a good electron donator and will scavenge alkyl peroxide radicals only when the B-ring is not substituted (Fig. 4).

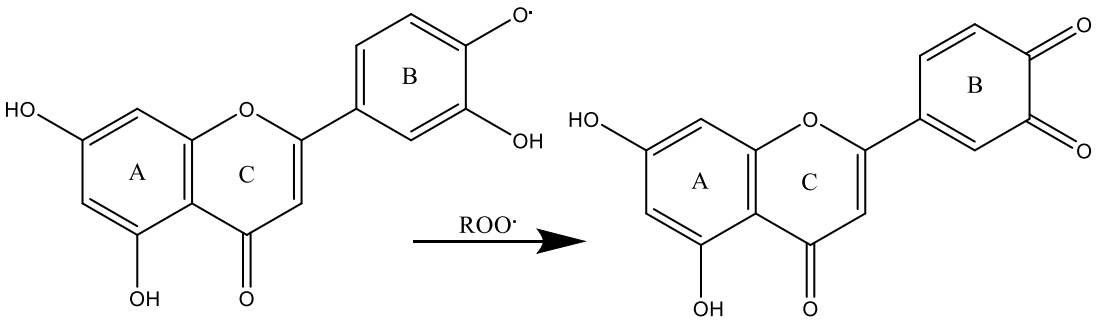

Fig. 4. Antioxidant mechanism of flavonoids.

Metal ions bound to biological structures may act as catalytic centers for multiple radical formation. Flavonoids with different -OH groups in the B ring, like quercetin and luteolin, can chelate with the metal ion and are very effective against the oxidative damage. Luteolin possesses two possible chelating sites: the 5-hydroxy-4-oxo and 3',4'-dihydroxyl (catechol) groups. As reported previously, the 5-hydroxy-4-oxo group is the preferred one.[22,23]

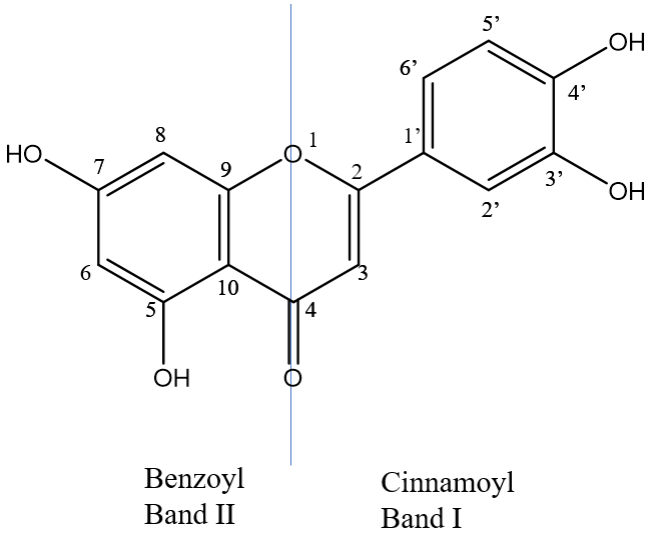

Fig. 5. Chemical structure of luteolin.

Coumarin

Coumarin derivatives are well known compounds found to be present in different food sources such as fruits, herbs, and vegetables.[24] They are of great interest owing to their important role in the fields of biology, medicine, industry, botany and chemistry.[25-29] Due to their versatility, the coumarin derivatives have been used in the pharmaceutical industry as antibiotics, antiviral, antimicrobial and anticoagulants agents and as pH indicators in biological systems and medical sciences.[30,31] Coumarin derivatives have also been used as sensitizers in phototherapy, as well as in the chemical industry as optical brightener and laser dyes.[32] The investigation of the binding properties of coumarin derivatives to different metal ions could help to understanding the factors controlling their biological activity. Natural as well as synthetic coumarins have recently drawn much attention due to their broad pharmacological activities.[33-35] The recognition of key structural features within coumarin family is crucial for the design and development of new analogues with improved activity and for the characterization of their mechanism of action and potential side effects. The different substituents in the coumarin nucleus strongly influence the biological activity of the resulting derivatives. Although some coumarins have been already characterized to evoke a particular biological activity, the challenge would be the design and synthesis of new derivatives with high specific activity for other pharmacological targets, to define their mechanism of action and achieve new therapeutic drugs. The ability of coumarins to bind metal ions represents an additional means of modulating their pharmacological

responses. Nowadays, a lot of studies report complexes of coumarin derivatives with metals, which possess biological activity. It has been found that the binding of a metal to the coumarin moiety retains or even enhances its biological activity.[36-38] The investigation of the binding properties of coumarin derivatives to different metal ions is essential for understanding the factors controlling their biological activity. Considerable efforts have now been given to the synthesis of coumarins with lanthanides. The coumarin-3-carboxylic acid (HCCA) contains abundance of coordination centers, and several ligand coordination modes are suggested in the metal complexes of HCCA, hence the determination of the metal coordination sphere is not a trivial task.

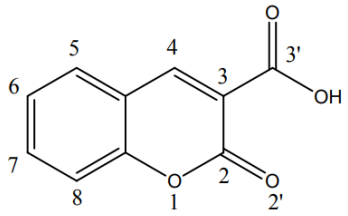

Fig. 6. Chemical structure of the ligand HCCA (coumarin-3-carboxylic acid).

The CCA^- anion is a polydentate system, it contains three potential donor atoms for coordination to metal ions one carbonylic oxygen (C=O), and two carboxylic oxygens (COO) and hence different monodentate and bidentate binding modes are possible.

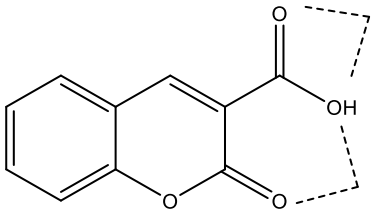

Fig. 7. Possible coordination sites of complexes between the coumaric acid species and a metal cation are shown.

L-Ascorbic acid

L-Ascorbic acid (H_2As), or 2,3-dehydro-L-gulonic acid γ-lactone **1** (scheme 1), also known as vitamin C, belongs to the most important substances involved in the metabolism of living organisms. This compound is widely occurring in both animal

and plant cells, where it performs various functions, in particular, participates in redox reactions, serves as a trap for toxic free radicals, and forms complexes with metals and proteins.[39] H_2As plays the role of cofactor of enzymatic hydroxylation by which proline residues in the collagen of the connective tissue are converted into 4-hydroxyproline residues, thus being involved in the process of formation of the main component of connective tissues of these higher animals. In addition, H_2As participates in the metabolism of phenylalanine and tyrosine, as well as in some other processes.[40] Various animals and plants can synthesize the necessary amounts of vitamin C proceeding from *D*-glucose. However, guinea pigs, primates, and humans do not possess this ability because of the absence of a necessary enzyme (*i.e.*, gulonolactone oxidaze) and, hence, must get H_2As by food.[40] The absence of sources of this vitamin leads to the development of *scorbutus*, a heavy form of avitaminosis. Microorganisms neither need H_2As nor synthesize it.[40] The antiscorbutic action of H_2As is specific: even stereomer **2** (see scheme 2) with respect to 5-C atom and stereomers **3** and **4** with respect to 4-C atom (*D*- and *L*-isoascorbic acids, respectively) exhibit either no such activity at all or produce a very low effect.[41] H_2As belongs to the class of weak acids: initially, it exhibits ionization of the hydroxy group at 3-C atom ($pK_{a1} = -3.86$). In weakly alkaline media, H_2As behaves as a monobasic acid and forms an ambidentate ascorbate anion **5** (Scheme 1). Under more basic conditions, H_2As is subject to ionization of the hydroxy group at 2-C atom ($pK_{a2} = -8.03$) with the formation of dianion **6**.[42] In the presence of very hard bases (*e.g.*, on boiling with KOH), H_2As forms a trianion **7** at the expense of proton detachment at position 4 (scheme 1). This is confirmed by the epimerization of H_2As and *D*- H_2As at high pH (scheme 2)[43] and by the formation of *L*-(4-^{3}H)H_2As upon tritium substitution for hydrogen at high pH in tritium-rich water (T_2O).[42]

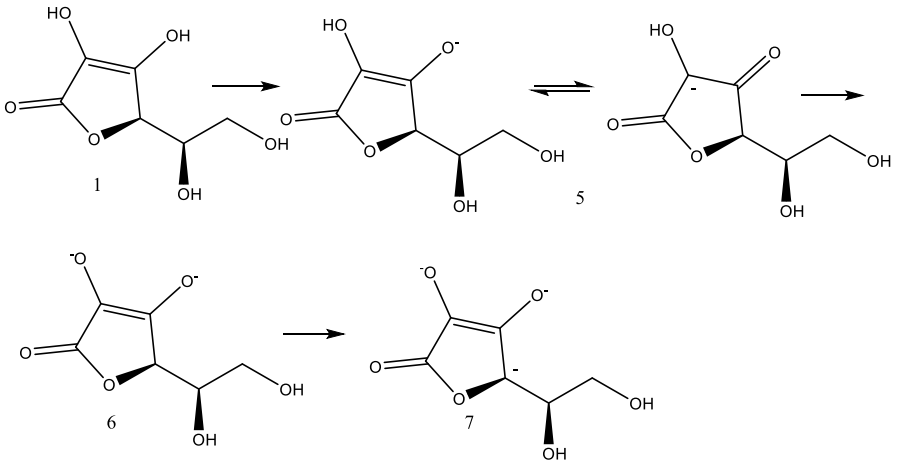

Scheme 1

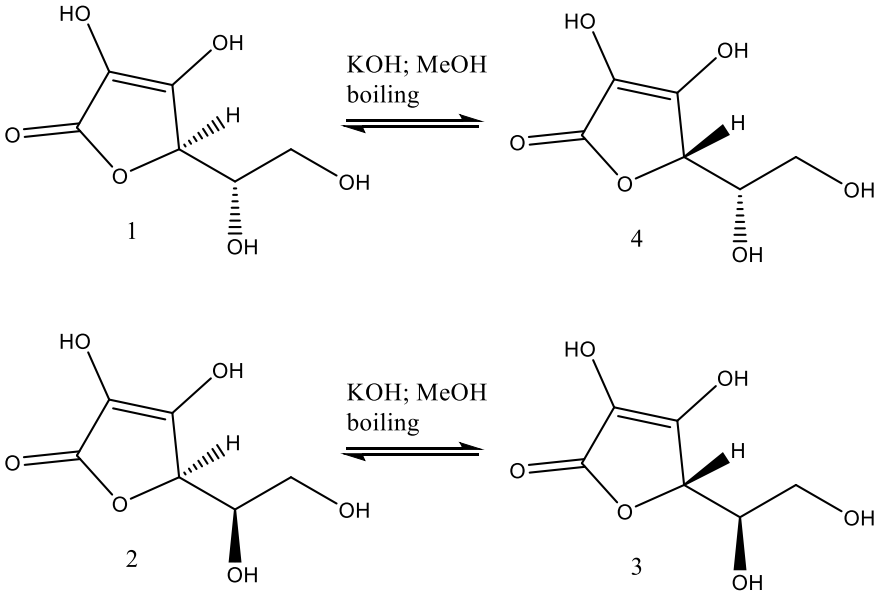

Scheme 2

The pK_a values of L-ascorbic acid were experimentally determined at 37 °C in aqueous solution. The pK_{a1} was determined potentiometrically and this allowed to obtain a very accurate value of the constant; pK_{a2} was determined spectrophotometrically by processing the experimental data with a calculation program, Hyperquad.

H_2As is stable when dry, but solutions readily oxidize, especially in presence of trace amounts of copper, iron and alkali. The first oxidation product of H_2As is the radical

monodehydroascorbate (MDHA), also known as semidehydroascorbate, or ascorbate free radical (Fig 8), (for a discussion of reaction mechanisms, see Refs 45, 46). MDHA, with a decay constant of $2.8x10^5 M^{-1} s^{-1}$ at pH 7,[47] is remarkably stable. *In vivo* MDHA is reduced back to H_2As by the activity of the NAD(P)-dependent enzyme, monodehydroascorbate reductase, or by electron transfer reactions. If allowed to persist though, two molecules of MDHA will also spontaneously disproportionate to H_2As and DHA. DHA itself is unstable and undergoes irreversible hydrolytic ring cleavage to 2,3-diketogulonic acid in aqueous solution.[49] The half-life for this breakdown was found to be 6 min at 37 °C,[50] although the rates of H_2As oxidation and DHA hydrolysis will be influenced by factors such as concentration, temperature, light and pH.

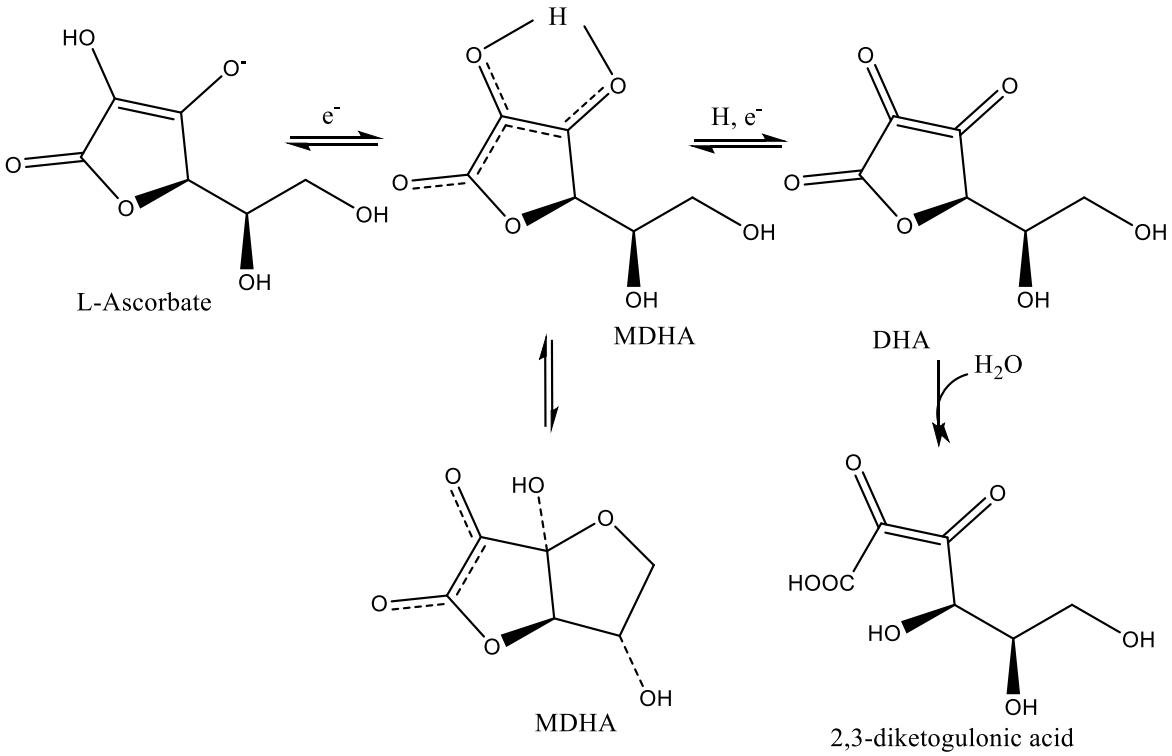

Fig. 8. Oxidation of *L*-ascorbate.

Physical properties of H_2As

Table 2. Physical properties of L-ascorbate (adapted from Ref 51)

Property	*Comments*
Appearance	White, odourless, crystalline solid with sharp acidic taste
formula/mol mass	$C_6H_8O_6$/176.13
m.p. (°C)	190–192
density, $g ml^{-1}$	1.65
pH	3 (5 $mg ml^{-1}$), 2 (50 $mg ml^{-1}$)
pK_1	4.17
pK_2	11.57
Redox potential	first stage: $E_1O + 0.166 V$ (pH 4)
Solubility ($g ml^{-1}$)	
water	0.33
95% ethanol	0.033
glycerol	0.01
fats and oils	insoluble
Spectral properties	
UV pH 2:	E_{max} (1%, 1 cm), 695 at 245 nm (undissociated)
pH 6.4:	E_{max} (1%, 1 cm), 940 at 265 nm (monodissociated form)

In both plant and animal systems H_2As interacts enzymatically and non-enzymatically with damaging oxygen radicals and their derivatives, so-called reactive oxygen species (ROS). These detoxification reactions can be an integral part of the housekeeping duties required of an aerobic existence in eukaryotic cells and the high intracellular concentrations of H_2As are an indication of the importance of these functions in eukaryotic organisms. In plants, the ability of H_2As to interact with physiologically generated ROS implicates H_2As in the modulation of processes such as lignification, cell division and the hypersensitive response. The biological importance of the antioxidant behavior of H_2As is that unlike other low-molecular-weight antioxidants (α-tocopherol, uric acid, carotenoids, flavonoids, *etc*.), H_2As can terminate radical chain reactions by disproportionation to non-toxic, non-radical products, *i.e.*, DHA and 2,3-diketogulonic acid (Fig 8). Further, since H_2As is only mildly electronegative, it can donate electrons to a wide range of substrates. Indeed, one of the most important features of the non-enzymatic antioxidant activity of H_2As, is its involvement in the regeneration of the lipophilic, membrane-associated α-tocopherol (vitamin E, α-

chromanoxy), radical. *L*-Ascorbic acid complexation with metal ions is of importance in explaining its biocoordination chemistry and the potential applications of formed complexes in many biological systems.[52,53] In spite of the presence of the dienol group in the molecule of the *L*-ascorbic acid, which allows possible complexation of the compound with metal ions, relatively little is known about the interactions of this water-soluble vitamin with metals.[54-56] Collecting more information on the elusive coordinating ability of vitamin C should be beneficial also for the exploitation of such ligand in chelating therapy.[57−64]

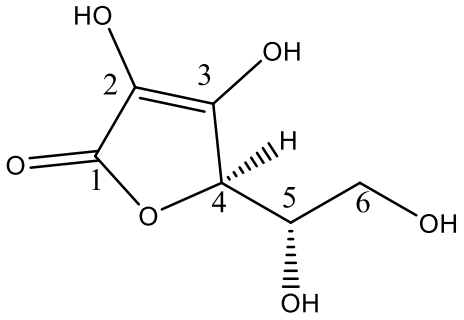

Fig. 9. Chemical Structure of *L*-Ascorbic Acid (H_2As)

References

1. C. Behl, B. Moosmann, *Free Radic. Biol. Med*., 33 (**2002**) 182–91.
2. P. Zatta, G. Tognon, P. Carampin, *J. Pineal. Res*., 35 (**2003**) 98–103.
3. S. Shishodia, G. Sethi, B.B. Aggarwal, *Ann. N. Y. Acad. Sci*., 1056 (**2005**) 206–17.
4. F. Yang, G.P. Lim, A.N. Begum, O.J. Ubeda, M.R. Simmons, S.S. Ambegaokar, P.P. Chen, R. R. Kayed, C.G. Glabe, S.A. Frautschy, G.M. Cole, *J. Biol. Chem*., 280 (**2005**) 5892–901.
5. F.V. Defeudis, *Pharmacol. Res*., 46 (**2002**) 565–8.
6. B.S. Oken, D.M. Storzbach, J.A. Kaye, *Arch. Neurol*., 55 (**1998**) 1409–15.
7. L.S. Schneider, S.T. DeKosky, M.R. Farlow, P.N. Tariot, R. Hoerr, M. Kieser, *Curr. Alzheimer Res.*, 2 (**2005**) 541–51.
8. K. Yoshida, M. Mori, T. Kondo, *Natural Product Report*, 26 (**2009**) 857–964.
9. S.F. Nabavi, G.L. Russo, M. Daglia, S.M. Nabavi, *Food Chemistry*, 179 (**2015**) 305-310.
10. S. Anandam, S. Selvamuthukumar, *Journal of Materials Science*, 49 (**2014**) 8140-8153.
11. K.A. Conklin, *Nutrition and cancer*, 37 (**2000**) 1-18.
12. Q. Chang, Y.S. Wong, *Journal of Agricultural and Food Chemistry*, 52 (**2004**) 6694-6699.
13. J.P. Cornard, J.C. Merlin, *J. Inorg. Biochem*., 92 (**2002**) 19.
14. J. Zhou, L.F. Wang, J.Y. Wang, N. Tang, *J. Inorg. Biochem*., 83 (**2001**) 41.
15. J.E. Brown, H. Khodr, R.C. Hider, C.A. Rice-Evans, *Biochem. J*., 330 (**1998**) 1173.
16. L. Mira, M.T. Fernandez, M. Santos, R. Rocha, M.H. Florencio, K.R. Jennings, *Free Radic. Res*., 36 (**2002**) 1119.
17. A. Torreggiani, M. Tamba, A. Trinchero, S. Bonora, *J. Mol. Struct*., 759 (**2005**) 744–747.
18. A. Torreggiani, A. Trinchero, M. Tamba, P. Taddei, *J. Raman Spectrosc*., 36 (**2005**) 380.
19. USDA databank for the flavonoid content of selected foods, 2nd release **2007**. Available at http://www.ars.usda.gov/nutrientdata; Accessed June 13, **2008**.

20. C.M. Schempp, A. Wähling, E. Lange, *European patent EP 1* 648 566 B1, (**2008**).
21. S.V. Jovanovic, S. Steenken, Y. Hara, M.G. Simic, *J. Chem. Soc*., [Perkin 2] (**1996**) 2497–504.
22. A. Primikyri, G. Mazzone, C. Lekka, A.G. Tzakos, N. Russo, I.P. Gerothanassis, *J. Phys. Chem. B*, 119 (**2015**) 83–95.
23. J. Ren, S. Meng, C.E. Lekka, E. Kaxiras, *J. Phys. Chem. B*, 112 **(2008)** 1845-1850.
24. H.E. Kleiner, S.V. Vulimiri, L. Miller, W.H. Johnson, C.P. Whitman, J. DiGiovanni, *Carcinogenesis*, 22 (**2001**) 73–82.
25. B. Thati, A. Noble, B.S. Creaven, M. Walsh, M. McCann, M. Devereux, K. Kavanagh, D.A. Egan, *European Journal of Pharmacology*, 602 (**2009**) 203–214.
26. P.B. Pansuriya, M.N. Patel, M.R. Chhasatia, P. Dhandhukia, V. Thakkar, *Journal of Coordination Chemistry*, 61 (**2008**) 3336–3349.
27. S. Lis, K. Staninski, T. Grzyb, *International Journal of Photoenergy*, 131702 (**2008**) 1–6.
28. P. Pansuriya, M. Patel, *Applied Organometallic Chemistry*, 21 (**2007**) 719–727.
29. I. Kempen, M. Hemmer, S. Counerotte, L. Pochet, P. de Tullio, J.M. Foidart, S. Blacher, A. Noël, F. Frankenne, B. Pirotte, *European Journal of Medicinal Chemistry*, 43 (**2008**) 2735–2750.
30. B.S. Creaven, D.A. Egan, K. Kavanagh, M. McCann, A. Noble, B. Thati, M. Walsh, *Inorganica Chimica Acta*, 359 **(2006)** 3976–3984.
31. I. Kostova1, G. Momekov, *Appl. Organometal. Chem*., 21 **(2007)** 226–233.
32. V. Sortur, J. Yenagi, J. Tonannavar, V.B. Jadhav, M.V. Kulkarni, *Spectrochimica Acta*, 64A (**2006**) 301–307.
33. I. Kostova, T. Stefanova, *J. Rare Earths*, 28 **(2010)** 40-46.
34. I. Kostova1, R.K. Agarwal, T Stefanova, *Int. J. Chem*., 1(2) **(2012)** 148-157.
35. M. Grazul, E. Budzisz, *Coordination Chemistry Reviews*, 253 **(2009)** 2588–2598.

36. B. Thati, A. Noble, B.S. Creaven, M. Walsh, M. McCann, M. Devereux, K. Kavanagh, D.A. Egan, *Eur. J. Pharmacol*., 602 (**2009**) 203.
37. B. Pansuriya, M.N. Patel, M.R. Chhasatia, P. Dhandhukia, V. Thakkar, *J. Coord. Chem*., 61 (**2008**) 3336.
38. G.B. Bagihalli, P.S. Badami, S.A. Patil, *J. Enzym Inhib. Med. Chem*., 24 (**2009**) 381.
39. M.L. Liao, P.A. Seib, *Food Technology*, 41(11) (**1987**) 104–107.
40. A. Lehninger, *Principles of Biochemistry*, Worth, New York (**1982**).
41. G.A. Melent'eva, L.A. Antonova, *Pharmaceutical Chemistry* [in Russian], Meditsina, Moscow (**1993**).
42. P.A. Seib, B.M. Tolbert, "*Ascorbic acid: Chemistry, Metabolism and Uses*," Advances in Chemistry Series, American Chemical Society, Washington, DC (**1982**).
43. G.S. Brenner, D.F. Hinkley, L.M. Perkins, S. Weber, *J. Org. Chem*., 29 (**1964**) 2389–2392.
44. S.J. Eitelman, R.H. Hall, A. Jordaan, *J. Chem. Soc*., *Chem. Commun*., (**1976**) 923–924.
45. E. Cadenas, *Oxidative Stress and Antioxidant Defences in Biology*, Ed by S. Ahmed, Chapman and Hall, New York, (**1995**) 1-61.
46. R.A. Larson, *Oxidative Stress and Antioxidant Defences in Biology*, Ed by S. Ahmed, Chapman and Hall, New York, (**1995**) 210-237.
47. C.H. Foyer, M. Lelandais, E.A. Edwards, P. Mullineaux, *Active Oxygen/Oxidative Stress and Plant Metabolism*, Ed by E. Pell and K. Steffen, American Society of Plant Physiologists, Rockville, (**1991**) 131-144.
48. P.W. Washko, R.W. Welch, K.R. Dhariwal, Y. Wang, M. Levine, *Anal. Biochem*., 204 (**1992**) 1-14.
49. J.C. Deutsch, *Anal. Biochem*., 260 (**1998**) 223-229.
50. J.K.C. Rose, *Biochim. Biophys. Acta*., 145 (**1987**) 685-692.
51. G.M. Jaffe, *in Encyclopedia of Chemical Technology*, 3rd ed, Ed by R.E. Kirk, D.F. Othmer, John Wiley & Sons, New York, 24 (**1984**) 8-40.
52. J.C. Deutsch, *J. Chromatog. A*, 881 (**200**0) 299−307.
53. B. Zü mreoğlu-Karan, *Chem. Rev*., 250 (**2006**) 2295−2307.

54. P.A. Seib, B.M. Tolbert, Ascorbic Acid: Chemistry, Metabolism and Uses, Washington D. C. (**1982**).
55. J. Maslowska, A. Owczarek, *Polish J. Chem*., 62 (**1988**) 75.
56. R.J. Kutsky, Hanbook of vitamins and hormons, Van Nostrand Reihold Company, New York (**1973**).
57. E. Kleszczewska, *J. Environ. Stud*., 8 (**1999**) 313−318.
58. J. Maslowska, A. Owczarek, *Polym. J. Chem*., 57 (**1983**) 719−726.
59. J. Maslowska, A. Owczarek, *Polym. J. Chem*., 62 (**1988**) 75−82.
60. A. De Robertis, A. Gianguzza, O. Giuffre, A. Pettignano, S.` Sammartano, *Appl. Organomet. Chem*., 20 (**2006**) 89−98.
61. V.M. Nurchi, M. Crespo-Alonso, L. Toso, J.I. Lachowicz, G. Crisponi, *Mini-Rev. Med. Chem*., 13 (**2013**) 1541−1549.
62. K.M. Buettner, J.M. Collins, A.M. Valentine, *Inorg. Chem*., 51 (**2012**) 11030−11039.
63. B. Zü mreoğlu-Karan, A.N. Ay, C. Ü naleroğlu, *Transition Met. Chem*., 30 (**2005**) 451−459.
64. C. Ü naleroğlu, B. Zümreoğlu-Karan, Y. Mert, *J. Mol. Struct*., 605 (**2002**) 227−233.

4. Elements in humans

The selection of the elements from the periodic table to be utilized by living organisms was, and still is, critically dependent upon the composition of the Earth's surface. "Life" on this planet began about 3.5 billion years ago from primitive cells.[1] Ostensibly, these cells evolved in oceans utilizing biochemicals synthesized on the surface of silicate particles on beaches. This evolution was based on the elements readily available in the ancient seas and seabeds. Understandably, the composition of the modern human body resembles the composition of these primitive synthetic arenas with the lighter elements of the periodic table being present but being challenged by an overlay of "modern" industrial elements mainly from lower in the table. As a result, the 'chemistry of life' is predominately the chemistry of the metals and non-metals of atomic number less than 35.[2,3] The heaviest essential metals to exist in primitive cells were selected from the first row of the transition series and existed in their lowest oxidation state because of the highly reducing atmosphere of water vapor, hydrogen sulfide, ammonia, and methane. Two billion years ago, the earliest cell contained the order of a hundred different protein molecules whereas today, a modern cell contains hundreds of thousands. Early cells required metal ions for structure, osmosis and as catalysts. For example, magnesium was present at high concentrations in early oceans and is likely to have been an effective catalyst in these early biological systems.[2] The amounts of essential elements in the body are normally controlled by physiological mechanisms, but for the non-essential, non-beneficial, elements there are generally no such controls and so the amounts in the body tend to reflect the natural abundance of the elements in food and water. For many such elements we may consider that there is a base load in the human body reflecting the natural intake of the elements in the diet.[1] Industrial, mining, or other human activities, have released metals into the environment. In order to fulfil all the necessary functions of life in an efficient way, humans need to sustain a healthy existence. Central to this is one's dependence upon the intake and uptake of several essential elements and on the absence, or below threshold, concentrations of several potentially toxic elements. Traditionally, for an element to be classed as "essential", it should pass certain criteria, *i.e.*, it must be present in all healthy tissues, and it must cause reproducible symptoms of ill health if excluded from the intake.[1,4] Approximately 32 elements in the periodic table are

believed to be essential or beneficial to life[4] (Figure 1). The remainder of the elements are adventitious, having been introduced by local dietary or environmental sources. Some of these elements are derived from pollutants present in water or food. Elements necessary for good health, food being by far the largest source, read H, C, N, O, S, Na, Mg, P, Cl, K and Ca as major elements and V, Cr, Mn, Fe, Co, Ni, Cu, Zn, Se, Mo, B, F, Si and I as minor species. Newer trace elements possibly having a health role include Sr, Ba, W, Cd, Sn, As and Br.[4] There is no perfect diet for the average human. The maintenance of good health depends on the supply of all 32 essential or beneficial elements in adequate, but not excessive, quantities and in a chemical form that is utilizable in the body.[4] The correct amount of trace metal to be taken up from the diet varies widely and is controlled by a large number of factors such as age, rate of tissue growth, general fitness, and activity parameters, for the individual concerned, and upon other foods co-consumed. In later life, the reduction in physical activity, in circulation and in appetite may lead to less trace elements being taken in adhering to carbohydrates and protein sources and so it is often advisable to increase the quantities of mineral-bearing foods as a person gets older.[5] The efficiency of intestinal uptake of several trace elements declines further in the elderly. For example, from diets containing ~10 mg of zinc per day, an elderly person may absorb as little as 1.5 mg/day[1,5] (Table 1).

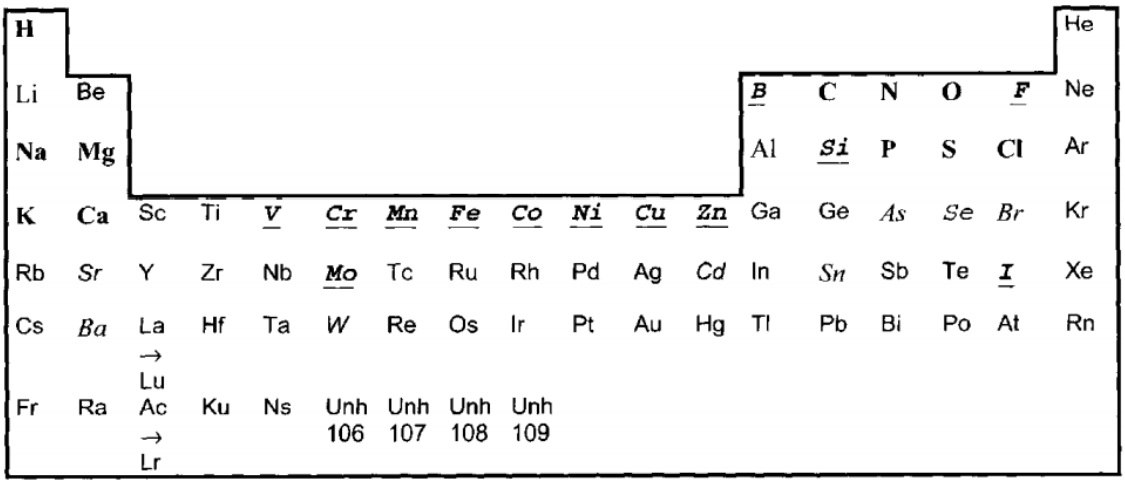

Fig. 1. The Periodic Table of the Elements indicating the bulk, essential and possibly essential elements.[4,3b]

Table 1. The masses of the essential and possibly essential elements occurring in 73 kg male and 60 kg female reference persons.[3b]

Element	Male		Female	
	grams	moles	grams	moles
Hydrogen	7300	7300	6000	6000
Carbon	16500	1375	13700	1140
Nitrogen	1880	134	1545	110
Oxygen	44900	2810	38900	2310
Phosphorus	730	23.5	600	19.3
Sulphur	146	4.6	120	3.8
Chlorine	104	2.9	85	2.4
Sodium	104	4.5	86	3.7
Potassium	144	3.7	103	2.6
Calcium	1180	29	860	22
Lithium	0.0007	0.0001	0.0006	0.00009
Boron	0.01	0.0009	0.009	0.00008
Fluorine	0.8	0.04	0.7	0.036
Magnesium	36	1.5	30	1.3
Silicon	1.5	0.05	1.3	0.046
Vanadium	0.02	0.0004	0.017	0.00034
Chromium	0.005	0.0001	0.0043	0.00008
Manganese	0.021	0.00038	0.017	0.00031
Iron	4.4	0.079	3.6	0.064
Cobalt	0.0007	0.00001	0.0006	0.00001
Nickel	0.01	0.0002	0.01	0.0002
Copper	0.12	0.0018	0.094	0.0015
Zinc	2.4	0.037	2.0	0.030
Arsenic	0.015	0.0002	0.012	0.00016
Selenium	0.02	0.0025	0.017	0.00022
Bromine	0.2	0.0026	0.17	0.0021
Molybdenum	0.005	0.00005	0.004	0.00004
Tin	0.03	0.00026	0.026	0.00022

Iodine	0.013	0.0001	0.011	0.00008
Barium	0.017	0.00012	0.015	0.00011

Shortages of essential trace elements can cause deficiency diseases, for example severe zinc deficiency in humans results in growth retardation, a delay in sexual development and skeletal malnutrition, acute dermatitis, and defects in the immune system. Mild zinc deficiency can result in impaired growth and poor resistance to infection. Many of these deficiency diseases have been well documented, for example, in areas where selenium is deficient, cardiomyopathy in children and women of childbearing age is endemic and a deficiency of chromium produces a glucose tolerance pattern like diabetes mellitus.[5] Toxic metals may reach our food from several sources, some of the most important being contaminated soil (often from sewage sludge and agricultural chemicals), unclean cooking water, storage containers and cooking utensils. Another problem is the distinction between metals required for health and toxic ones. This distinction is frequently one of amount rather than element. The mechanisms by which metals induce toxic effects are not well understood. The more toxic heavy metal ions (HMs), cadmium, lead and mercury are potent enzyme inhibitors because the ions are readily polarizable and bind to enzyme donor groups. Lipophilicity of the metal species usually dictates the extent of the toxicity and the body's ability to excrete the offending element.[6] Even excesses of essential elements can cause problems. Ingestion of large amounts of iron compounds (for example, supplements used to treat iron deficiency) can cause acute poisoning and chronic gastrointestinal disturbances and might even cause severe kidney and liver damage. Such chronic iron poisoning is often presented as siderosis or hemochromatosis. These conditions lead to the deposition of excess iron, in the form of ferritin and hemosiderin, in the liver, spleen and bone marrow, and they also lead to liver and kidney damage.

Anyway, some metal ions are necessary for the continuation of the vital functions of living organisms. For thousands of years, people have widely used metals for daily needs without considering their drawbacks and consequences. As a result, in addition to destroying the entire ecosystem, metal ions pollute the water resources and have seriously affected plant and animal life. Today, metal pollution is mostly caused by

mining, industrial sewage, urban wastes, acid rain, fossil fuel residues, fertilizers, and pesticides.[7] HMs are elements with a density above 5 g/mL.[8,9] They have been used in many different areas for thousands of years. The most common ones are Cr, Pb, Cd, Hg, Cu and Zn. In addition, as can be included in this group due to its similar physical and chemical properties to heavy metals.[10–12] Fe, Co and Mn are less common heavy metals. HMs can be examined under two groups as essential and non-essential HMs according to their toxicity, as said before. Essential HMs, including Zn, Cu, Fe and Co, are less effective or relatively harmless at low quantity. However, non-essential HMs, including Cd, Hg, As, and Cr are highly toxic even at low quantities.[13,14] On the other hand, HMs, including Zn, Cu and Fe, are obligatory for the biological activities of different proteins and enzymes as cofactors in distinct biological and physiological processes. For instance, Cu, Fe, Zn and Co demonstrate a vital role in the use of oxygen in the electron (e^-) transport chain, cell growth and differentiation, many enzymatic reactions, synthesis of biomolecules and the continuity of the immune system. The excess of HMs in the cytoplasm can disrupt the intracellular redox balance and cause changes in the cytoplasm's pH, alter protein conformation and inhibit enzyme's function. This situation can easily lead to cell dysfunction, necrosis, or apoptosis. In addition, HMs can interact with proteins thiol, carboxyl, and imidazole groups.[15,16] Iron is the best example of the metals that are taken or exposed to excessively in our daily life. An average person includes 4–5 g of elemental iron. Two-third of this amount exists in the hemoglobin as oxygen transporter protein and another one-third is stored in the iron-keeping proteins including hemosiderin or ferritin.[17] Fe exists in cytochromes, hemoglobin, myoglobin, and is essential for many enzymes, including peroxidases, catalase, succinate dehydrogenase, aconitase, aldehyde oxidase and oxygenase.[9,18] However, although the human body can tolerate relatively high iron levels, excess iron is quite toxic. Metal poisoning has become quite common in young children as a result of excessive iron intake due to iron-enriched food supplements. In addition, acute poisoning is less widespread in adults, but chronic Fe overload is usually encountered in β-thalassemia patients due to the mandatory and regular intake of whole blood transfusions.[17,19] The fatally accumulated iron level primarily affects the heart and liver. The regular evacuation of metal ions can be increased by the application of a convenient sequestering agent. Desferrioxamine B is one of the current

drugs of choice for Fe^{3+} removal. However, Desferrioxamine B can reduce the available iron level to about ten times of the normal level.[17,19,20] In humans, iron overloads can be decreased by the management of agents that can compete with the transferrin protein, which binds and transfers metal ions. Drugs that have a higher Fe^{3+} affinity than transferrin for effective chelation may damage natural iron stores under physiological conditions. Enterobactin as natural siderophore had high affinity toward Fe^{3+} ions.[21] Recent studies have proven that siderophores, which are small molecules produced by some microorganisms, make iron soluble and thus usable by plants. Siderophores from microbial origin are good iron chelating agents primarily due to powerful iron chelating components, such as hydroxamate, catecholate and α-hydroxocarboxylates. On the other hand, phytosiderophores such as mugineic acid and its derivatives are polydentate ligands with carboxylate and amine groups as metal chelators. Gramibactin has been reported to effectively form Fe^{3+} as an impressive example for a new group of diazeniumdiolate siderophores established on its ability to isolate iron. In the aforementioned study, it was reported that gramibactin forms quite stable complexes with Fe^{3+} ions in a broad pH range (Table 2).[22] Although there are many reasons for Fe pollution, it occurs especially with the corrosion of water pipes. The groundwater and soil are contaminated through industrial and agricultural human wastes including Fe. In addition, today, intense air pollution from the steel industry includes particulate iron and iron oxide together. Vomiting, nausea, diarrhea, abdominal pain, lethargy, and dehydration are the most common symptoms of iron toxicity.[23,24] Aluminum (Al) is the second plentiful metal in the earth's crust and constitutes about 8% of the total mineral quantity. It has an important place today because it is widely used in different industries. The acceptable daily intake limit of Al in humans is about 3 to 10 mg. Therefore, excessive, and irregular intake of Al causes dangerous effects for living creatures.[25] Al^{3+} toxicity is a major factor in living organisms. Due to its chemical properties, Al^{3+} leads to an imbalance of free radical metabolism, resulting in the oxidative injury of polysaccharides, proteins, nucleic acids, and membrane lipids, and disrupts the normal cell activities. Al toxicity is still not completely unraveled at the molecular level, but some potential mechanisms have been detailed. For example, it is known that Al exhibits an important pro-oxidant effect in living systems.[26] Al toxicity induces an excessive increase in ROS levels.

Especially, it promotes different neurodegenerative diseases including dementia and encephalopathy in humans. This toxicity also causes serious damage to biomolecules. The presence of Al in living systems creates different toxic effects. Another effect is the change in the natural structure and roles of proteins and enzymes in the glycolysis, cells, tissues, central nervous system (CNS), and other organs.[27] Al as a strong Lewis acid prefers oxygen donor ligands, including phosphates, nucleotides, carboxylates, and nucleic acids. It promotes hyperphosphorylation of normal proteins. In a recently proposed paradigm, it has been suggested that Al can interact directly with the backbone of proteins. It was suggested that Al coordinates directly to the carbonyl oxygen and protonated peptide nitrogen, occurring in stable structures with a 5-membered ring that forms strong covalent bonds, and can interact directly with the backbone of proteins.[28] It was reported that the patients affected by Al intoxication were treated successfully with the ethylenediaminetetraacetic acid (EDTA) as chelating agent over a short period (Table 2).[29] Copper (Cu) is compulsory for some metabolic enzymes, including cytochrome c oxidase, superoxide dismutase (SOD), tyrosinase, ceruloplasmin and dopamine-β-hydroxylase.[25] ROS can occur when liver cells are exposed to copper overload, and this is generally considered a critical event leading to cell death. Wilson's disease (WD) is a defect which blocks the body from getting rid of excessive Cu. In people with WD, copper accumulates in the brain, liver, and the other organs, especially the eyes. Whereas a small quantity of dietary Cu is sufficient to stay healthy, too much Cu quantity is toxic. In this case, excessive Cu^{2+} is effectively bounded either by ligands containing both hard and soft donors. The leading drug used for this purpose in the treatment of WD is penicillamine. This drug is a molecule including both types of donor atoms and selectively binds Cu^{2+} ions.[21] The ternary H-point standard addition method is simultaneously used to determine Cu^{2+} ions using murexide as chromogenic reagent. Murexide, a reddish-purple compound, has attracted much attention due to its application in chemical analysis and spectrophotometric fields (Table 2).[30] In addition, murexide as a metal ion indicator is used as a chromogenic reagent for the traditional spectrophotometric determination of some metals, especially copper. Furthermore, different complexation reactions were performed between murexide and Co^{2+}, Cu^{2+}, Ni^{2+}, Cd^{2+}, Zn^{2+}, and Pb^{2+} ions and recorded by a spectrophotometric technique (Table 2).[31] In the murexide method, a

simple and sensitive spectrophotometric method, spectrophotometric detection of Cu^{2+} with murexide, which is the ammonium salt of purpuric acid, had been developed. This method depends on the formation of a stable yellow greenish colored complex (at pH 5.0), which had a maximum absorption at 476 nm. Murexide is used in analytical chemistry for complexometric titrations, most often as a complexometric indicator for Ca^{2+} ions, but also for Co^{2+}, Cu^{2+}, Ni^{2+}, Cd^{2+}, Zn^{2+} and Pb^{2+} and rare earth metals.[32]

Table 2. Some metals and their chelating agents.

Metals	**Binding agent**	**References**
Pb^{2+}	Murexide	[31]
Cd^{2+}	Murexide	[31]
Hg^{2+}	Dimercaprol	[33]
	Murexide	[34]
Cu^{2+}	Penicillamine	[35]
	EDTA	[21]
Ni^{2+}	Murexide	[31]
Zn^{2+}	N,N,N',N'-tetrakis(2-pyridylmethyl)-ethylenediamine	[36]
	Desferrioxamine	[37]
	Enterobactin	[21]
Fe^{3+}	Deferoxamine	[38]
	Gramibactin	[22]
Al^{3+}	EDTA	[32]
Co^{2+}	Murexide	[32]
Mn^{2+}	Desferrioxamine	[32]
Ca^{2+}	Desferrioxamine	[29]

Zinc is the fourth most widespread metal in use after Fe, Al and Cu. It is stored and transferred in metallothionein and essential for the function of over three hundred enzymes and thousand transcription factors. Approximately 2–4 g Zn is distributed throughout the human body. An increase in the amount of Zn in the living environment can cause serious negative effects on living organisms. Zn homeostasis in the human body is controlled by the small intestines. Zn is stored in specific synaptic vesicles by

glutamatergic neurons in the brain and modulates neuronal excitement.[39] Since Zn has a flexible coordination geometry, they allow the conformation of the proteins they are in to change rapidly. Thus, biological reactions take place faster. The best example of Zn-containing enzymes is the carbonic anhydrase enzyme family, which can reversibly convert carbon dioxide (CO_2) and water to bicarbonate (HCO_3^-).[40–42] In addition, Zn is a cofactor of many metalloenzymes, including anhydrases, oxidases, dehydrogenases, and peroxidases. It plays a crucial role in the arrangement of nitrogen metabolism, cell proliferation, auxin synthesis and photosynthesis in plants.[39] This reagent readily permeates cell membranes and forms a stable 6-coordinate complex with Zn.[36] Furthermore, Zn is essential for folding of protein, configurational and conformational changes of proteins as well as DNA replication, growth hormones and fertility.[43] The most common intracellular Zn chelator is N,N,N',N'-tetrakis(2-pyridylmethyl)-ethylenediamine (Table 2). Cobalt, which is necessary for all animal metabolisms, is also an important element for the synthesis of cobalamin and vitamin B_{12}. Especially, bacteria in the ruminants' stomach convert Co salts into vitamin B_{12}.[44] Heavy metal pollution in water and soil has increased rapidly in recent years due to different reasons.[9] Similar to some earlier metals, a fully elucidated mechanism of Co toxicity has not been defined in general. In some studies, Co's high affinity for sulfhydryl (-SH) groups in biomolecules has been linked to oxidation and degradation of Krebs cycle intermediates, as well as damage to the transporting system resulting in enhanced intracellular Ca^{2+} ions.[45] Although As, Hg and Cd are not very active elements, they stimulate OS by inhibiting SOD, affecting antioxidants and binding to sulfhydryl group (-SH) of proteins. As they exist in trivalent form and, thus, induce OS by oxidation-reduction reactions. Because of their multivalent states, they also affect acid-base and methylation reactions. Hg toxicity has been shown to cause OS, enzyme inactivation, inflammation and autoimmunity. However, the specific molecular mechanisms of Hg toxicity have not yet been fully elucidated. On the other hand, Pb indirectly causes the OS by generating free radicals and ROS and decreases the antioxidant capacity of the cells. Prenatal exposure to As, Hg and Cd can result in brain dysfunction and neuronal diseases.[46] Although food is the main source of mercury poisoning, fish and dental amalgams are also considered as the most important sources of Hg exposure. People who consume a lot of fish meat from

polluted waters may be at increased risk of Hg exposure. Fetuses have a looser blood-brain barrier than adults. Therefore, mercury in the mother's bloodstream can reach the brain of the fetus. Therefore, pregnant women should avoid consuming fish caught from polluted waters.[47–49] Hg toxicity can cause many ailments, including hypertension, heart and kidney dysfunction.[50,51] Although Calcium is not a heavy metal, it is tightly bound by calbindins, which are a putative class of Ca^{2+}-binding proteins. Calbindins belong to the Ca^{2+} messenger system, which reply to the transitory in intracellular Ca^{2+} concentration (Table 2). A structural property of calbindins is their functional domain, which consists of two interacting binding sites. So, they have cooperative binding.[52] A similar situation to calbindins-Ca^{2+} co-binding is also observed between laurate and human serum albumin (HSA) that is commonly used as standard protein in biochemical assays.[53–56] It is known that HSA binds to a wide range of ligands, especially fatty acids. In addition, in another study, multiple binding equilibria were searched for HSA and laurate binding using by a dialysisexchange method.[52]

4.1 Metal Complexes

Other than the main group metal ions Na^+ and K^+, hydrated metal ions are rarely found in humans at physiological pH values because of hydrolysis; rather they are complexed to donor groups such as RS^-, NH_2, *etc*. The complex and its preferred ligand donor groups follow the order best described by the HSAB (hard and soft acids and bases) approach, chelation is widespread and polydentate ligands are extensively used.[57-59] Each complex has its own unique toxicology, and effectiveness; even slight differences in empirical formula, oxidation state, or chirality can change a beneficial species into a toxic agent.[1,4,60-63] For metal-ligand exchange reactions, which are rapid, there is thermodynamic control quantifiable using K values based upon equilibria and stoichiometry. For slower or catalyzed reactions kinetic constants, using k values, are useful in unravelling the competing species.[4,64]

4.2 Lability

A complex, which is formed with thermodynamically strong bonds, may exchange ligands quite readily when offered an equivalent replacement ligand. This is known as

bond lability. The opposite also occurs where a thermodynamically weak metal-ligand complex is reluctant to give up one of its ligands for a more strongly bonded replacement ligand.[65] The concept of lability depends upon the ability of the metal ion to be able to form the transition state intermediate involving the exchanging ligand and the target complex. Paradoxically, complexes having very large formation constants can readily exchange ligands in aqueous solution because they may be able to form an intermediate. In nature bonds are often made non-labile, *i.e.*, inert, by blocking the formation of a transition state intermediate species. Metal ions in biological systems are usually distributed between four different states *in vivo*. There are the (i) inert forms of the metal complex, which may either be laid down into a solid matrix, for example calcium in bones and teeth, or may be complexed into a non-reactive protein. There are three states of labile species: (ii) metal-proteins having reversibly bound metal ions known as high molecular mass species. These are in equilibrium with (iii) low molecular mass complexes. Thirdly, (iv) there must be some aquated metal ions, although this is highly unlikely with a pH = 7.4 because of hydrolysis.[66] The last three complexes have the metal ions in equilibrium so that excess metal can be circulated on labile proteins or even draw metal ions from it by ligand drugs or alternatively by depletion of lower molecular mass complexes. A rise in metal ion concentration present in the biological fluid will bring about an increase in all three types (ii)-(iv) of labile species - labile protein, low molecular mass and aquated metal ion concentrations - without necessarily increasing the amount of metal complexing to the inert protein. Building a metal into, or extracting a metal from, an inert protein usually involves a sophisticated biological process such as occurs in the liver or spleen.[1]

4.3 Metal ions in medicine, physiological role

The mechanisms by which organisms control metal ions and their role in cellular regulation has become an area of great scientific interest. Such metal ions include calcium, and the transition metals copper, zinc, manganese, and iron. These metals have been shown to be involved in cell-cell signaling, signal transduction, as well as, influencing transcription and translation via metal responsive regulators. There is an emerging view that cells are not buffer containers in which metals freely diffuse between thermodynamically controlled binding sites. Rather, a series of membrane

metal transporters, metal chaperones, and assembly complexes have recently been identified that regulate the uptake and delivery of metal ions to specific sites.[67] Metal ion dependent functions appears to be emerging as a new area of cell biology and is a potential site for therapeutic interventions. Normal metal metabolism maintains free metal ion concentrations at a very low level and delivers metals very selectively to their sites of action, while maintaining tight control over their reactivity. The macromolecular players and vesicular compartments involved in metal ion homeostasis and metal trafficking are only just being discovered. The brain is an example of a specialized organ that concentrates metal ions such as Fe, Zn, and Cu in concentrations in the order of 0.1–0.5 mM.[68] In healthy tissue, efficient homeostatic mechanisms and buffers are in place, compartmentalizing and regulating metal ion release.[69] Thus, despite reasonably high total concentrations, the concentration of free metal is very low. In the case of Zn^{2+}, for example, the balance between the cellular redox state, the concentration of other biological chelating agents, and the energy status of the cell, has been shown to determine Zn^{2+} distribution in the cell.[70] Physiological function relies, to a large extent, on the universal intracellular messenger calcium and cells have evolved a versatile calcium signaling toolkit.[71] The calcium concentration in cells is controlled by reversible binding to specific classes of proteins that act as Ca^{2+} sensors to decode its information before passing it on to targets. The decoding operation is based on specific conformational changes in the sensor proteins. Other proteins intrinsic to membranes simply control Ca^{2+} concentration without processing its message, by transporting it across membrane boundaries. They are in the plasma membrane and in the membranes of the endoplasmic reticulum (ER), the mitochondria, and most likely calcium containing organelles and the nuclear envelope, which play distinctive roles in the cellular homeostasis of Ca^{2+}.[72] This versatile system is exploited to control processes as diverse as fertilization, proliferation, development, learning and memory, contraction, and secretion. These normal processes must, however, be accomplished within the context of calcium being highly toxic since excess calcium can result in cell death through both necrosis and apoptosis. In neuronal systems, the ER localized to dendrites, axons, and their terminals, provides for local control of Ca^{2+} signals that effect changes in the structure and function of neuronal circuits.[73] Following activation of most excitatory synapses, calcium is released from

intracellular stores of central neurons. There is increasing evidence for the presence of local calcium signals caused by calcium-induced calcium release, coupling store signaling to activity-dependent synaptic plasticity. Calcium plays an important role in the regulation of neuronal gene expression; moreover, calcium influx has been shown to induce transcription of genes, which is regulated by the route of calcium entry into the cell.[74] Altered calcium homeostasis is also implicated in the normal aging process. In addition, zinc-mediated neuron signaling has been identified as a process analogous to other neurotransmitter mechanisms. Zinc is stored in presynaptic vesicles, released in brief pulses into the synaptic cleft, and acts on recognition sites in the postsynaptic membrane. Zinc-containing nerves are anatomically widely distributed in the brain, with the highest concentrations in the hippocampus. Metals ions are important cofactors for many transporters, transcription factors, and enzymes. For example, the metal-dependent matrix metalloproteinases (MMPs) are dependent on calcium and zinc, calpain cysteine proteases are calcium dependent, and the Cu/Zn-superoxide dismutases are copper and zinc dependent. MMPs are a family of calcium requiring and zinc containing proteinases that include gelatinases, collagenases, thermolysin, stromalysin, and membrane-bound proteases; they are involved in extracellular matrix degradation. MMPs are normally present in the brain in latent forms that require activation, which occurs at the cell surface by membrane-type metalloproteinases (MT-MMPs) and other proteases.[75] Their targets include other proteinases, proteinase inhibitors, clotting factors, chemotactic molecules, latent growth factors, growth factor-binding proteins, cell surface receptors, cell-cell adhesion molecules, and virtually all structural extracellular matrix proteins. More than 20 structurally homologous MMPs are known that differ in substrate specificity. Two calcium ions and a structural zinc site contribute to the stability of the enzyme structure, and an active site zinc is essential for catalytic activity.[76] Calpains are a family of non-lysosomal neutral cysteine proteases that form a growing family of structurally related intracellular multidomain cysteine proteinases containing a papain-related catalytic domain, whose activity depends on calcium. The calpains are believed to play important roles in cytoskeletal remodeling processes, cell differentiation, apoptosis, and signal transduction, but are also implicated in muscular dystrophy, cardiac and cerebral ischemia, platelet aggregation, restenosis, neurodegenerative diseases,

rheumatoid arthritis, and cataract formation. Current evidence points to a cooperative interaction of several sites, which, upon calcium binding, trigger the reformation of a papain similar catalytic domain. Copper, zinc superoxide dismutase (CuZnSOD), is an important antioxidant enzyme that requires two essential metals for catalytic function. It converts super oxide free radicals to the less active peroxide, which then can be further converted by other antioxidant enzymes into water. The balance of the Cu/Zn ratio is important in maintaining proper functioning of SOD and any imbalance can be damaging.

References

1. D.M. Taylor, D.R. Williams, Trace Element Medicine and Chelation Therapy, The Royal Society of Chemistry, Cambridge, (**1995**).
2. R. Osterberg, in An Introduction to Bioinorganic Chemistry (D. R. Williams, ed.), Thomas, Springfield, Illinois, (**1976**) 13-28.
3. (a) D.R. Williams, D.M. Taylor, in H.J. Smith and H. Williams' Introduction to the Principles of Drug Design and Action, 3rd. ed., Harwood Academic Publishers, (**1998**). (b) 4th ed., in press.
4. J.J.R. Frausto da Silva, R.J.P. Williams, The Biological Chemistry of the Elements, 2nd ed., Oxford University Press, (**2001**).
5. World Health Organisation, Trace Elements in Human Nutrition, WHO, Geneva, (**1996**).
6. G. Berthon (ed.), Handbook of Metal-Ligand Interactions in Biological Fluids, Vols. 1, 2, Bioinorganic Chemistry, Vols. 1, 2, Bioinorganic Medicine, Marcel Dekker, New York, (**1995**).
7. V.M. Nurchi, R. Cappai, G. Crisponi, G. Sanna, G. Alberti, R. Biesuz, S. Gama, , *Front. Chem.*, 8 (**2020**) 597400.
8. L. Jarup, Hazards of heavy metal contamination, *Br. Med. Bull*. 68 (**2003**) 167–182.
9. J.J. Kim, Y.S. Kim, V. Kumar, Heavy metal toxicity: An update of chelating therapeutic strategies, J. *Trace Elem. Med. Biol*., 54 (**2019**) 226–231.
10. M. Küçük, I. Gulcin, *Environ. Toxicol. Pharmacol*., 44 (**2016**) 134–139.
11. U.M. Kocyigit, P. Taslimi, I. Gulcin, *J. Biochem. Mol. Toxicol*., 32 (**2018**) e22172.
12. C. Caglayan, P. Taslimi, C. Türk, F.M. Kandemir, Y. Demir, I. Gulcin, *Comp. Biochem. Physiol*., 226 (**2018**) 108605.
13. R.A. Festa, D.J. Thiele, *Curr. Biol*., 21 (**2011**) R877–R883.
14. H. Haase, L. Rink, *Immun. Ageing*, 6 (**2011**) 9.
15. K. Jomova, M. Valko, *Toxicology.* 283 (**2011**) 65–87.
16. C. Caglayan, P. Taslimi, C. Turk, I. Gulcin, F.M. Kandemir, Y. Demir, S. Beydemir, *Environ. Sci. Pollut. Res*., 27 (**2020**) 10607–10616.

17. A. Vacca, C. Nativi, M. Cacciarini, R. Pergoli, S. Roelens, *J. Am. Chem. Soc*., 126 (**2004**) 16456–16465.
18. J.L. Beard, *J. Nutr*., 131 (**2001**) 568S–579S.
19. W.R. Harris, K.N. Raymond, F.L. Weitl, Ferric ion sequestering agents. 6. *J. Am. Chem. Soc*., 103 (**1981**) 2667–2675.
20. S. Roelens, A. Vacca, C. Venturi, *Chem. Eur. J*., 15 (**2009**) 2635–2644.
21. C. Bazzicalupi, A. Bianchi, C. Giorgia, M.P. Clares, E. Garcia-Espana, *Coord. Chem. Rev*., 256 (**2012**) 13–27.
22. S. Gama, R. Hermenau, M. Frontauria, D. Milea, S. Sammartano, C. Hertweck, W. Plass, *Chem. Eur. J*., 27 (**2021**) 2724–2733.
23. A.K. Baranwal, S.C. Singhi, *Ind. Pediatr*., 40 (**2003**) 534–540.
24. C. Hershko, Mechanism of iron toxicity, *Food Nutr. Bull*., 28 (**2007**) S500–S509.
25. V. Desai, S.G. Kaler, *Am. J. Clin. Nutr*., 88 (**2008**) 855S–858S.
26. E. Formoso, R. Grande-Aztatzi, X. Lopez, *J. Inorg. Biochem*., 92 (**2019**) 33–44.
27. C.I. David, H. Jayaraj, G. Prabakara, K. Velmurugan, D.P. Devi, R. Kayalvizhi, A. Abiram, V.R. Kannan, N. Nandhakumar, *Food Chem*., 371 (**2022**) 131130.
28. J.I. Mujika, G.D. Torre, E. Formoso, R. Grande-Aztatzi, S.J. Grabowski, C. Exley, X. Lopez, *J. Inorg. Biochem*., 181 (**2018**) 111–116.
29. A. Fulgenzi, R. De Giuseppe, F. Bamonti, D. Vietti, M.E. Ferrero, J. *Inorg. Biochem*., 152 (**2015**) 214–218.
30. M.S. Masoud, T.S. Kassem, M.A. Shaker, A.E. Ali, *J. Therm. Anal. Calorim*., 84 (**2006**) 549–555.
31. K. Grudpan, J. Jakmunee, Y. Vaneesorn, S. Watanesk, U.A. Maung, P. Sooksamiti, *Talanta*, 46 (**1998**) 1245–1257.
32. R.L. Martin, A.H. White, A.C. Willis, *J. Chem. Soc. Dalton Trans*., 14 (**1977**) 1336–1342.
33. A. Sigel, H. Sigel, (Eds.) Metal Ions in Biological Systems; Marcel Dekker: New York, NY, USA, (**2004**).
34. I. Ghasemi, M. Shamsipur, *J. Coord. Chem*., 36 (**1995**) 183–194.

35. G. Crisponi, V.M. Nurchi, D. Fanni, C. Gerosa, S. Nemolato, G. Faa, *Coord. Chem. Rev*., 254 (**2010**) 876–889.
36. R.J. Radford, S.J. Lippard, *Curr. Opin. Chem. Biol*., 17 (**2013**) 129–136.
37. J.L. Domingo, *J. Toxicol. Clin. Toxicol*., 27 (**1989**) 355–367.
38. G. Soybir, F. Köksoy, F. Ekiz, O. Yalçin, A. Oz¸seker, B. Cokne¸seli, *J. R. Coll. Surg. Edinb*., 43 (**1998**) 26–28.
39. R. Wirosoedarmo, F. Anugroho, S.D. Hanggara, K. Gustinasari, *Appl. Environ. Soil Sci*., 2018 (**2018**) 8259520.
40. F. Turkan, A. Cetin, P. Taslimi, M. Karaman, I. Gulcin, *Bioorg. Chem*., 86 (**2019**) 420–427.
41. B. Ozgeris, S. Goksu, L. Kose Polat, I. Gulcin, R.E. Salmas, S. Durdagi, F. Tumer, C.T. Supuran, *Bioorg. Med. Chem*., 24 (**2016**) 2318–2329.
42. I. Gulcin, M. Abbasova, P. Taslimi, Z. Huyut, L. Safarova, A. Sujayev, V. Farzaliyev, S. Beydemir, S.H. Alwasel, C.T. Supuran, *J. Enzyme Inhib. Med. Chem*., 32 (**2017**) 1174–1182.
43. C. Foresta, A. Garolla, I. Cosci, M. Menegazzo, M. Ferigo, V. Gandin, L. DeToni, *Hum. Reprod*., 29 (**2014**) 1134–1145.
44. T.J. Huat, J. Camats-Perna, E.A. Newcombe, N. Valmas, M. Kitazawa, R. Medeiros, *J. Mol. Biol*., 431 (**2019**) 1843–1868.
45. J.J. Devlin, A.C. Pomerleau, J. Brent, B.W. Morgan, S. Deitchman, M. Schwartz, *J. Med. Toxicol*., 9 (**2013**) 405–415.
46. S.J. Flora, V. Pachauri, *Int. J. Environ. Res. Public Health*, 7 (**2010**) 2745–2788.
47. C.L. Gilman, R. Soon, L. Sauvage, N.V. Ralston, M.J. Berry, *J. Trace Elem. Med. Biol*., 30 (**2015**) 17–24.
48. I. Kozikowska, L.J. Binkowski, K. Szczepanska, H. Slawska, K. Miszczuk, M. Sliwinska, T. Laciak, R. Stawarz, *Environ. Pollut*., 182 (**2013**) 256–262.
49. Z. Chen, R. Myers, T. Wei, E. Bind, P. Kassim, G. Wang, Y. Ji, X. Hong, D. Caruso, T. Bartell, et al., *J. Expo. Sci. Environ. Epidemiol*., 24 (**2014**) 537–544.
50. R.A. Bernhoft, *J. Environ. Public Health*, 2012 (**2012**) 460508.
51. M.J. Kosnett, *J. Med. Toxicol*., 9 (**2013**) 347–354.
52. A. Vacca, O. Francesconi, S. Roelens, *Chem. Rec*., 12 (**2012**) 544–566.

53. M. Nar, Y. Cetinkaya, I. Gulcin, A. Menzek, *J. Enzyme Inhib. Med. Chem*., 28 (**2013**) 402–406.
54. E. Koksal, I. Gulcin, *Protein Peptide Lett*., 15 (**2008**) 320–326.
55. F. Erdemir, D. Barut Celepci, A. Aktaş, P. Taslimi, Y. Gök, H. Karabıyık, I. Gulcin, *J. Mol. Struct*., 1155 (**2008**) 797–806.
56. M. Boztas, Y. Cetinkaya, M. Topal, I. Gulcin, A. Menzek, E. Sahin, M. Tanc, C.T. Supuran, *J. Med. Chem*., 58 (**2015**) 640–650.
57. R.G. Pearson, *Chem. Brit*., 3 (**1967**) 103.
58. R.G. Pearson, *J. Am. Chem. Soc*., 85 (**1963**) 3539.
59. J.A. Liyanage, Hard and Soft Acids and Bases, Monograph No. 16, Ceylon Institute of Chemistry, Sri Lanka, (**2002**).
60. A.M. Fiabane, D.R. Williams, The Principles of Bio-inorganic Chemistry, Monographs for Teachers Series No. 31, The Royal Society of Chemistry, Cambridge, (**1977**).
61. D.R. Williams (ed.), An Introduction to Bio-inorganic Chemistry, Thomas, Springfield, Illinois, (**1976**).
62. S.S. Brown, J. Savory (eds.), Chemical Toxicology and Clinical Chemistry of Metals, Academic Press, London, (**1983**) 412.
63. H.G. Seiler, H. Sigel, A. Sigel (eds.), Handbook on Toxicity of Inorganic Compounds, Marcel Dekker, New York, (**1988**) 1069.
64. K. Simkiss, K.M. Wilbur, Biomineralisation, Cell Biology and Mineral Deposition, Academic Press, San Diego, (**1989**).
65. F.A. Cotton, G. Wilkinson, Advanced Inorganic Chemistry, 5th ed., Wiley, New York, (**1988**) 1284.
66. J. Burgess, Metal Ions in Solution, Ellis Harwood, Chichester, (**1978**) 481.
67. C.E. Outten, T.V. O'Halloran, *Science*, 29 (**2001**) 2488–2492.
68. M.A. Lovell, J.D. Robertson, W.J. Teesdale, J.L. Campbell, W.R. Markesbery, *J. Neurol. Sci*., 158 (**1998**) 47-52.
69. A.I. Bush, Metals and neuroscience. *Curr. Opin. Chem. Biol*. 4 (**2000**) 184-191.
70. C. Jacob, W. Maret, B.L. Vallee, *Proc. Natl. Acad. Sci. USA*, 95 (**1998**) 3489-3494.

71. M.J. Berridge, P. Lipp, M.D. Bootman, *Nat. Rev. Mol. Cell. Biol*., 1 (**2000**) 11-21.
72. E. Carafoli, L. Santella, D. Branca, M. Brini, *Crit. Rev. Biochem. Mol. Biol*., 36 (**2001**) 107-260.
73. M.P. Mattson, F.M. LaFerla, S.L. Chan, M.A. Leissring, P.N. Shepel, J.D. Geiger, *Trends Neurosci*., 23 (**2000**) 222-229.
74. A.E. West, W.G. Chen, M.B. Dalva, R.E. Dolmetsch, J.M. Kornhauser, A.J. Shaywitz, M.A. Takasu, X. Tao, M.E. Greenberg, *Proc. Natl. Acad. Sci. USA*, 98 (**2001**) 11024-11031.
75. S.M. Bryce, G. Rosenberg, *J. Cereb. Blood Flow Metab*., 18 (**1998**) 1163–1172.
76. W. Bode, C. Fernandez-Catalan, H. Tschesche, F. Grams, H. Nagase, K. Maskos, *Cell. Mol. Life Sci*., 55 (**1999**) 639-652.

5 Methodology and data processing

5.1 Potentiometry

Potentiometry is the set of analytical methods that are based on the measurement of the potential difference of a galvanic cell in conditions of absence of current (static electrochemical method). The typical instrumentation used in potentiometry includes: a reference electrode, whose potential must be constant over time and independent of the composition of the solution containing the analyte in which it is immersed; a working electrode (or indicator electrode), whose response depends on the concentration of the analyte, so you can obtain information on its composition, especially on the constants of dissociation and formation of complexes; the potential of the working electrode depends on the concentration of a single ion. It is separated from the sample solution by a membrane, selectively permeable to the analyte under study. Finally, a device for measuring the potential which can be represented by a potentiometer or a modern electronic voltmeter. The electroneutrality of the cell is guaranteed by a salt bridge that carries the cations towards the cathodic part of the cell and the anions towards the anionic part of the cell.[1] Potentiometry is suitable in the case in which the measurement of the electromotive force of a cell is carried out in conditions of thermodynamic reversibility, or in equilibrium conditions with a substantial absence of current and in known solutions.

The above-mentioned potentiometric apparatus is shown in Fig. 1.

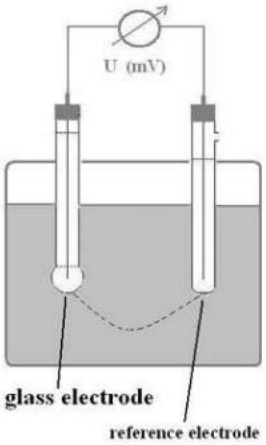

Fig. 1. Potentiometric cell.

Among the various reference electrodes, the best known are: the saturated calomel electrode (Hg / Hg_2Cl_2 in KCl) and the silver-silver chloride electrode (Ag / AgCl in KCl). Since it is of our interest to know the equilibria in solution for which the H^+ ion is responsible, in the following work, a glass membrane electrode is used as the indicator electrode, sensitive to the activity of H^+ ions. This is a particular membrane electrode which is the type of probe most used in chemical laboratories for measuring the pH of aqueous solutions through the pH-meter. The most common glass electrodes combine both the measuring electrode and a second internal electrode in a single body, which acts as a reference. A glass electrode of this kind is called combined. It owes its name to the fact that the part sensitive to pH is a thin glass membrane, sensitive to H^+ ions.

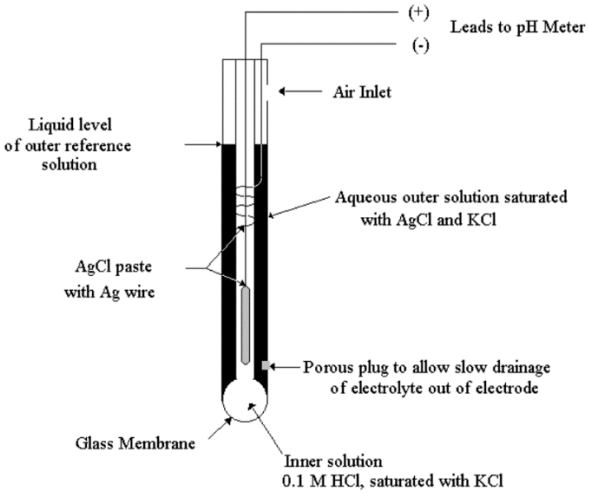

Fig. 2. Glass electrode

The electric potential that is created on the inner and outer sides of the membrane is a function of the pH of the solution in which the probe is immersed. The cell potential is calculated using the Nernst equation:

$$E_{\text{cell}} = E_{\text{reference}} - E_{\text{indicator}} + E_j \quad (1)$$

E_{cell} represents the electromotive force (f.e.m.) determined experimentally, $E_{\text{reference}}$ is the standard potential of the reference electrode, which is constant, E_j is the liquid junction potential of the cell that is established at the interface between two electrolytic solutions of different composition, specifically between the measurement solution and the ions of the ionic medium. Its value can be neglected under certain conditions of

ionic strength and hydrogen ionic concentration. $E_{\text{indicator}}$ is expressed according to the following equation:

$$E_{\text{indicator}} = \frac{RT}{nF} \ln \{X\}^n \quad (2)$$

Where R is the universal gas constant (8.314472 J / K mol), T the absolute temperature, F the faraday constant (96485.3415 C / mol), $\{X\}^n$ is the concentration of the analyte on which the value of the reference electrode potential depends and $\{H^+\}$ is the hydrogen ion activity. When the ionic strength is constant, the activities can be replaced by concentrations. When the ionic strength tends to zero, therefore at infinite dilution, the value of the activity coefficient is equal to one. If the concentrations of the species present in solution are at least 10 % lower than the concentration of the ionic medium, the activity coefficients are constant, even when the concentrations of the reagents vary. The relationship that links the potential of the indicator electrode to the value of the hydrogen ion concentration is as follows:

$$E_{\text{indicator}} = L - \frac{RT}{nF \cdot 0.4343} \text{pH} \quad (3)$$

Where 0.4343 is the conversion factor from the Neperian logarithms to the decimal logarithms, while L represents a constant value that considers various parameters relating to the reference electrode which will then be incorporated into the Reference. The work cell used is schematized as follows:

$$\text{Ag} \mid \text{AgCl (sat), NaCl (0,16M)} \parallel [H^+] = x \mid \text{(glass electrode)}$$

or more simply

$$\text{(RE} \mid \text{TS} \mid \text{GE).}$$

5.2 Constant ionic medium method

Given a generic reaction:

$$\alpha A + \beta B + \ldots \rightleftarrows \ldots + \sigma C + \delta D \quad (4)$$

the equilibrium constant can be written as:

$$K = \frac{\{D\}^{\delta}\{C\}^{\sigma}}{\{A\}^{\alpha}\{B\}^{\beta}} \quad (5)$$

in which the activities of the reaction products are reported in the numerator and those of the reactants in the denominator, all raised to their stoichiometric coefficients. Equation (5) expressed with the activities is strictly valid, at a constant temperature, regardless of the ideality or otherwise of the system. In very diluted solutions, where

the activity coefficients tend to one, the activities are identified with the concentrations and the laws of equilibrium are applied with the concentrations with good approximation. However, it should be noted that in electrolyte solutions, where the electrostatic interaction forces between charged particles are significant, even in dilute solutions there may be a significant deviation from ideality, such as not to allow the use of concentrations in the equilibrium laws. In the computation of equilibria, as in the evaluation of equilibrium constants from experimental data, it is advantageous to use concentrations instead of activity. For the definition of the activity coefficient ($y_i = a_i / c_i$, indicating the activity with a_i and the mole fraction or concentration with c_i) the equilibrium equation (5), it can also be written in the form:

$$K = \frac{[D]^{\delta}[C]^{\sigma}}{[A]^{\alpha}[B]^{\beta}} \frac{yd^{\delta}\, yc^{\sigma}}{ya^{\alpha}\, yb^{\beta}} \qquad (6)$$

The equilibrium constant is therefore divided into two terms, one containing the quotient of the concentrations, the other term containing the activity coefficients. Determination of *K* requires the evaluation of the activity coefficients or their removal. This is done in two ways:

1) the quotient of the concentrations is determined at different ionic strength and *K* is obtained by extrapolation to infinite dilution, where the activity coefficients tend to one;
2) activity coefficients are evaluated using theoretical relationships.

Both procedures give satisfactory results when the following conditions are met: in solution there is a single equilibrium, or several equilibria with very different constants.

Furthermore, it is essential that appreciable quantities of reaction products are formed, even in dilute solutions of reagents, where the quotient of the concentrations can be accurately evaluated, and the theoretical formulas of the activity coefficients are valid. Entirely different situations occur when several equilibria coexist in solution, or the species formed are so weak that high concentrations of reactants are required to achieve an appreciable concentration of reaction products. In recent times, it has been preferred to address these situations with the use of the constant ionic medium method. The solutions to be studied contain a high and constant concentration (generally 0.5, 1 or 3 M) of an inert electrolyte, such as $NaClO_4$, NaCl or KNO_3, whose ions do not participate in the equilibria investigated. In a constant ionic medium, the activity

coefficients of the reacting species remain constant if the concentration of these is small compared to that of the inert electrolyte.

The activity coefficients, if constant, can be incorporated into the equilibrium constant (6) and, consequently, the quotient of the concentrations becomes a constant. The law of mass action expressed by concentrations is, therefore, rigorously valid.

The constant expressed with the concentrations, also called stoichiometric, is a true constant if equilibria are discussed in solutions where the inert electrolyte always has the same high concentration, that is, in the same solvent. Stoichiometric constants are valid only in the ionic medium in which they are determined, therefore they have a limited field of applicability. If the standard state is chosen so that the activities of the reacting species tend to concentrations, when the composition of the solution tends to that of the ionic medium, the activity coefficients tend to one and therefore (6) can be written:

$$K = \frac{[D]^{\delta}[C]^{\sigma}}{[A]^{\alpha}[B]^{\beta}} \qquad (7)$$

(considering *p* and *T* constant and ionic medium constant).

Even if the equilibrium constants, determined in a constant ionic medium, are valid only in those conditions, their application is immediate.

Many fields of applied science, such as biochemistry and analytical chemistry, equilibria are often dealt with in solutions containing large amounts of electrolytes, such as ocean water or blood serum, where ionic forces are evaluated 0.7 M and 0.16 M in NaCl, respectively. The equilibrium constants determined at these ionic forces can be directly applied to the computation of equilibria affecting these systems of natural importance.

The great advantage that the constant ionic medium method offers is the description of complicated equilibria in terms of equilibrium constants and concentrations of the reacting species. The results directly give the concentration of free ions in solution and therefore usable in the law of mass action.[2] The constant ionic medium method is inappropriate in the study of unstable complex species since it would be necessary to use concentrated solutions of the reagents.

Activity of the species in solution

In extremely dilute solutions (the so-called infinite dilution) the particles of the solutes do not interact with each other, that is, they move freely throughout the volume of the solution and therefore they participate in the reactions in a measure directly proportional to their concentration. Instead in relatively concentrated solutions (more than 10^{-3} M) the "active" concentration of the solutes it is less than the nominal concentration, because the particles are "committed" to interacting with each other. Consequently, for each *i*-th solute is defined the activity (a_i) through the simplified report:

$$a_i = \gamma_i \times C_i$$

The activity coefficient (γ_i) is a pure number, less than or equal to 1, the value of which is the closer to 1 the more diluted the solution is. The activity coefficient, therefore, is that number which, multiplied by the concentration of a species in solution (C_i), provides its activity. In the case of electrolytic solutions, the forces exerted between the particles of the solutes are also of an electrostatic nature and the behavior of each ion depends significantly on the number (or rather on the concentration) and on the charge of all the other ions present in solution. In 1923 Peter Debye and Erich Hückel developed a theory to explain the behavior of electrolyte solutions. First, it is quite probable that in solution each ion is surrounded by ions of opposite charge, which envelop it in a sort of "ionic atmosphere", thus making it less active than would be expected if it interacted only with the solvent. The activity coefficient of each ion depends on the nature of the solvent, the temperature, the charge, and the concentration of all the other ions; more precisely, it depends on the ionic strength of the solution. The ionic strength (I) expresses the overall effect of all the ions present in solution:

$$I = \tfrac{1}{2} \Sigma_i C_i Z_i^2 = \tfrac{1}{2} (C_1 Z_1^2 + C_2 Z_2^2 + C_3 Z_3^2 + \ldots)$$

Where C_i is the concentration of each *i*-th ionic species (expressed in terms of molality, m, or in mol / 1000 g of solvent) and Z_i is the charge of each ion.

Stability Constants and their Determination

Complex formation takes place when water molecules around the metal ion are replaced by other ligands. Formation constants, also known as stability constants, are equilibrium constants used to describe the formation of a metal complex from a metal

ion and a ligand. Because some ligands are not soluble in water, mixed solvent systems are sometimes used when measuring the equilibrium constants. However, most complex formation reactions are studied in aqueous medium. To distinguish stepwise formation and overall formation constants, the symbol β is used for the latter. Values of K and β are related, and the β value can be expressed in terms of stepwise stability constants, as shown below:

$M + L \rightleftarrows ML$ $\quad K_1 = \frac{[ML]}{[M][L]}$ (8)

$ML + L \rightleftarrows ML_2$ $\quad K_2 = \frac{ML_2}{[ML][L]}$ (9)

$ML_2 + L \rightleftarrows ML_3$ $\quad K_3 = \frac{ML_3}{[ML_2][L]}$ (10)

$ML_3 + L \rightleftarrows ML_4$ $\quad K_4 = \frac{ML_4}{[ML_3][L]}$ (11)

$M + 4\,L \rightleftarrows ML_4$ $\quad \beta_4 = \frac{ML_4}{[M][L^4]}$ (12)

$\beta_n = K_1 \cdot K_2 \cdot K_3 \cdot \quad K_n$ (13)

$\beta_4 = K_1 \cdot K_2 \cdot K_3 \cdot K_4$ (14)

$\log\beta_4 = \log K_1 + \log K_2 + \log K_3 + \log K_4$ (15)

The equilibria (and associated formation constants) for protonation of the ligand (eqs 16-18), formation of ML_X complexes (eqs 19-21), formation of protonated complexes (eq. 22), formation of hydroxyl complexes (eq. 23), dissociation of water (eq. 24), and hydrolysis of metal ion (eq. 25), may be included in the model for complexation of M^{n+} (a metal) and H_xL^{n-}(a ligand):

$H^+ + L^{n-} \rightleftarrows HL^{(n-1)-}$ $\quad K_1^{HL} = \frac{[HL^{(n-1)-}]}{[H^+]\,[L^{n-}]}$ (16)

$H^+ + HL^{(n-1)-} \rightleftarrows H_2L^{(n-2)-}$ $\quad K_2^{H_2L} = \frac{[H_2L^{(n-2)-}]}{[H^+]\,[HL^{(n-1)-}]}$ (17)

$x\,H^+ + L^{n-} \rightleftarrows H_xL^{(n-x)-}$ $\quad \beta_x^{H_xL} = \frac{[H_xL^{(n-x)-}]}{[H^+]^x\,[L^{n-}]}$ (18)

$M^{m+} + L^{n-} \rightleftarrows ML^{(n-m)-}$ $\quad K_1 = \frac{[ML^{(n-m)-}]}{[M^{m+}][L^{n-}]}$ (19)

$ML^{(n-m)-} + L^{n-} \rightleftarrows ML_2^{(2n-m)-}$ $\quad K_2 = \frac{[ML_2^{(2n-m)-}]}{[ML^{(n-m)-}]\,[L^{n-}]}$ (20)

$M^{m+} + x\ L^{n-} \rightleftarrows ML_x^{(xn-m)-}$ $\beta_x = \frac{[ML_x^{(xn-m)-}]}{[M^{m+}]\,[L^{n-}]^x}$ (21)

$ML^{(m-n)-} + H^+ \rightleftarrows MHL^{(n-m+1)}$ $K^{MHL} = \frac{[MHL^{(n-m+1)}]}{[H^+]\,[ML^{(m-n)-}]}$ (22)

$ML^{(n-m)-} + OH^- \rightleftarrows M(OH)L^{(n-m+1)-}$ $K^{MOHL} = \frac{[M(OH)L^{(n-m+1)-}]}{[OH^-]\,[ML^{(n-m)-}]}$ (23)

$H_2O \rightleftarrows H^+ + OH^-$ $K_W = [H^+]\,[OH^-]$ (24)

$M(H_2O)^{m+} \rightleftarrows M(OH)^{(m-1)+} + H^+$ $K_M{}^{MOH} = \frac{[M(OH)^{(m-1)+}][H^+]}{[MH_2O^{m+}]}$ (25)

Potentiometric titration is one of the methods by which stability constants can be determined. In this type of titration, the negative log of hydrogen ion concentration is measured after additions of known volumes of acid or base titrant. These measurements are done on solutions containing ligand in the presence and absence of metal ions. The concentration of all species at each volume titrant is computed. The -log[H^+] (pH) calculated is compared with the experimental value. The stability constants are refined to minimize the difference between calculated and measured pH.

5.3 Data processing

The processing of the experimental results was conducted using a numerical calculation program, the SUPERQUAD.[3] As titrant aliquots are added to the reaction environment, the recorded potential values, the standard potential of the electrode, the initial volume of the titrant solution, the concentrations of the measurement and titrant solutions must be entered in the program. To determine the formation constants of the complex, it is necessary to enter the acid constants of the ligand and the formation constants of the hydrolysis products of metals as invariant parameters. The program relates the experimental data to those calculated according to the established speciation model. The program can provide the discrepancy between the experimental data and those calculated in order to verify the validity of the hypothesized speciation model.

The calculation of formation constants obtained by potentiometric titrations is a field of interest for many chemists.

For a long time, it was the MINIQUAD[4] program that was used, but with the onset of the complexity of the systems to be examined, it became necessary to perform improvements on the software in order to improve the ability to solve more complex

problems. MIQUV is born. This program has had limited use due to some formulas it uses for the calculation of derivatives. Another problem concerns the treatment of formation constants that take negative values during the processing procedure, so the model was rejected. The experience has given rise to the awareness that the refusal of the model at this point in processing is premature, so the MINIQUAD was used again, and later, to develop a new program that could fully assert itself, namely the SUPERQUAD. It can remedy the imperfections of the MINIQUAD. The problem of model selection arises in systems for which the equilibrium that is formed and the related species that take part in this equilibrium are difficult to interpret. Therefore, the HYPERQUAD[5] is developed, which is able to determine the equilibrium constants with the data obtained from the spectrophotometric methods in addition to the potentiometric data. It can perform a complete treatment of equilibrium solutions data. In the present work, the experimental data were processed using the SUPERQUAD as a calculation program. The HYPERQUAD was used as a calculation program for the determination of the acid constants of some binding molecules such as quercetin, luteolin and L-ascorbic acid; the HYPERQUAD it was useful for processing the spectrophotometric data at 37 °C in aqueous solution of the three binding molecules. This made it possible to determine the acid constants at basic pH which are difficult to determine through a potentiometric approach.

5.4 Superquad

The SUPERQUAD procedure is based on a series of assumptions:

1) For each chemical species in solution there is a formation constant expressed as the ratio between the concentrations of the products and the reactants. The constant can be expressed as a concentration ratio if the activities are constant. In fact, works in the presence of an inert ionic medium with a high concentration;
2) The electrodes used for potentiometric measurements must follow the law of Nernst (equation 26):

$$E = E^{\circ} + 59.16 \log [H^{+}] + E_j \quad (26)$$

3) Systematic errors must be minimized;

4) The independent variable (volume of titrant) is not subject to errors while the errors for the dependent variable (measured potential) assume a normal distribution. This allows you to use the least squares procedure;
5) There is a model of the equilibrium system, which adequately represents the experimental observations. The model is specified by a set of coefficients, one for each species formed. All least squares are processed in terms of the assumed model. Examining a sequence of models should produce a better model that is not significantly different from the real model. Choosing the best model is known as species selection.

The errors near the end point are greater than the errors in the middle points, so it is necessary to consider the points in a weighted way. The weight for each point of the titration is the inverse of the variance at that point (equation 27):

$$W_i = \frac{1}{\sigma^2} \tag{27}$$

while the error is defined as:

$$\sigma^2 = \sigma_E^2 + \left(\frac{\partial E}{\partial V}\right)^2 \cdot \sigma_v^2 \tag{28}$$

where σ^2, σ_E^2 and σ_v^2 are respectively: the variance calculated for the measurement, the variance of the potential read by the electrode and the variance of the volume of titrant read, while the derivative of the potential respect to the volume, represents the slope of the titration curve. The slope of the titration curve is greater at the end points and therefore their weight is less. The method of least squares allows to calculate a series of parameters that minimize the sum of the squared deviations between an observed quantity and a calculated one. Therefore, the process consists in determining the values of the constants that minimize the sum U of the squared weighted residuals (equation 29):

$$U = \sum_i w_i \left(E_{exp} - E_{calc}\right)^2 \tag{29}$$

For each i-th measure, E_{exp} is an experimental value, E_{calc} is a value calculated for each set of constants β obtained by assuming a given model and w_i are the weights assigned to each measure. For all the systems investigated in this work, has been assumed that $w_i = 1$. For the determination of the constants of formation of the complexes, the acid constants of the ligand are also defined. A preliminary model is provided below with

a given formation constant value from which E_{calc} is calculated. For each point, *i.e.*, added volume and read potential, an E_{calc} value is calculated according to the defined model and the function U is calculated. The program uses the Newton-Raphson method to find the minimum of the function; once this is done, the agreement between the experimental data and the corresponding calculated values is calculated. This agreement is expressed with the variance according to equation (30):

$$\sigma^2 = \frac{U_{min}}{(n-m)} \tag{30}$$

*n r*epresents the number of experimental data; *m* is the number of constants β. The standard deviations of the constants of formation of the complexes are obtained from the diagonal elements of the variance-covariance matrix, calculated according to equation (31):

$$M_v = \sigma^2 X^{-1} \tag{31}$$

where *X* represents the square matrix of order *m* of the normal equations.[6]

The program also evaluates χ^2, a parameter which for a random distribution of errors must be less than 12.6 to have a 95 % confidence level. If the standard deviation does not fall within the acceptable limit (0.2 mV), it means that the model described initially is not realistic, therefore it is necessary to hypothesize a new model with which to repeat the calculations. The program repeats the procedure a certain number of times, until it reaches a minimum, in which case it returns results for the training constants, the processing is, therefore, conducted in a cyclical manner.

5.5 Characterization methods

The characterization of the complexes was performed with UV-Visible spectrophotometry and with IR spectroscopy. UV-Vis is a molecular absorption spectroscopic technique commonly used in analytical chemistry. Spectroscopic techniques are based on the energy exchange that occurs between an incident electromagnetic radiation and the matter. UV-Visible spectroscopy deals the absorption phenomena of luminous radiations belonging to the visible (380-780 nm) and near ultraviolet (200-380 nm) spectral range. An electromagnetic radiation can be described as a particle, better known as photon, and like a wave consisting of an oscillating electric and magnetic field perpendicular to each other and to the direction of the radiation propagation. When an ultraviolet or visible photon is absorbed by a molecule, an increase of the absorbing species internal energy occurs, involving

vibrational, rotational, and electronic transitions from the ground state to those at higher energy, causing changes in the distribution of the molecule electron cloud. It can only happen if the incident photon energy and the ΔE between the fundamental state and the exited one are the same. The allowed transitions for this kind of spectroscopic technique are:

- $\sigma \rightarrow \sigma^*$
- $\pi \rightarrow \pi^*$
- $\pi \rightarrow \sigma^*$
- $n \rightarrow \pi^*$
- $n \rightarrow \sigma^*$

These ones are given by transition metals or molecules with double or triple bonds that are called chromophores. Measuring the absorbed radiation intensity, it is possible to draw the analyte information and carry out qualitative or quantitative analysis. The results of this measurement can be expressed graphically by means of a spectrum, which is a diagram of the intensity of the radiation absorbed as a function of wavelength. In a typical UV-Visible spectrum, the wavelength is reported on the abscissa and the absorbance (or, rarely, the transmittance) on the ordinate. If a material is not completely transparent, absorption occurs and therefore transitions between electronic energy levels. In this second case, the recorded spectrum will be characterized by a series of peaks of variable height for each transition, in relation to the intensity of the absorption itself. By exploiting this spectroscopic technique, it is possible to perform both quantitative and, albeit with greater difficulty, qualitative analyzes; moreover, it is possible to carry out kinetic studies (biochemical determinations of enzymes or more generic applications of chemical kinetics) and titrations. Among the most important applications are:

1) The study of solutions containing metals of the d block: these are often colored due to the electronic transitions that can occur between d orbitals of the metal concerned. In certain geometric coordinations, in fact, the initially degenerate d orbitals undergo an energetic separation comparable with a photon in the UV-Visible field. Knowledge of the energy gap between the orbitals may indicate the presence of certain ligands;

2) The study of organic compounds containing a high level of conjugation in π bonds: the energy required for electronic transitions between the different molecular orbitals falls within the visible spectrum. In general, the longer the conjugation system, the higher the absorbance and the lower the energy required and consequently the higher the photon wavelength.

For qualitative analysis purposes, this one is compared with other spectra proposed by literature or collected in special databases. The quantitative determination is carried out, instead, based on the *Lambert-Beer's law*, which correlates the intensity of the absorbed radiation to the analyte concentration and the thickness of the traversed medium. When a molecule is struck by an incident radiation, the attenuation of the incident ray, due to the absorption by an analyte solution, can be explained as *Transmittance* (T):

$$T = I_1/I_0 \quad (32)$$

where I_0 is the intensity of the incident radiation and I_1 is the intensity of the transmitted radiation by the solution. The absorbed radiation is more commonly measured as *Absorbance* (A) and it is related to the *Transmittance* (T) through the following relation:

$$A = \log 1/T = \log I_0/I_1 \quad (33)$$

By knowing A, it is possible to obtain the concentration of the absorbent species, thanks to *Lambert-Beer's law* which correlates these two ones.

$$A = \varepsilon\, b\, c \quad (34)$$

where:

ε = molar extinction coefficient (L mol^{-1} cm^{-1}), dependent on the wavelength of the absorbed radiation, on the solvent and chemical species that lead to the absorption;

b = thickness of the cell or optical path of the solution (cm), generally equal to 1 cm;

c = concentration of the absorbent species (mol L^{-1}).

The *Lambert-Beer's law* is, however, a limit law, as it applies to dilute solutions, *i.e.*, for concentrations ≤ 0.01 mol L^{-1}.

To verify the effective formation of the complexes, all solutions and solids gained at the end of each titration were analyzed by UV–Vis spectrophotometry. The blank for all solutions was carried out with a 0.16 M solution of the ionic medium

used in the experimental tests; the blank for solids of titration was carried out with ethanol.

Infrared spectroscopy or IR spectroscopy is an absorption spectroscopic technique normally used in the field of analytical chemistry, material chemistry and physical chemistry for the study of chemical bonds. When an infrared photon is absorbed by a molecule, it passes from its fundamental vibrational state to an excited vibrational state. In a typical infrared spectrum on the abscissa, we find a scale of frequencies expressed in wave number, or quantity of waves per centimeter, and in the ordinate the percentage of transmittance. If a material is transparent to infrared radiation, its spectrum will appear as a line parallel to the abscissa axis. If a material is not completely transparent there will be absorptions and, therefore, transitions between vibrational energy levels. In this second case the recorded spectrum will be characterized by a series of peaks of variable height for each transition.

Another characterization technique used is Nuclear Magnetic Resonance (NMR). NMR spectroscopy is an analytical chemistry technique used in quality control and research for determining the content and purity of a sample as well as its molecular structure. For example, NMR can quantitatively analyze mixtures containing known compounds. For unknown compounds, NMR can either be used to match against spectral libraries or to infer the basic structure directly. Once the basic structure is known, NMR can be used to determine molecular conformation in solution as well as studying physical properties at the molecular level such as conformational exchange, phase changes, solubility, and diffusion. To achieve the desired results, a variety of NMR techniques are available. The principle behind NMR is that many nuclei have spin and all nuclei are electrically charged. If an external magnetic field is applied, an energy transfer is possible between the base energy to a higher energy level (generally a single energy gap). The energy transfer takes place at a wavelength that corresponds to radio frequencies and when the spin returns to its base level, energy is emitted at the same frequency. The signal that matches this transfer is measured in many ways and processed to yield an NMR spectrum for the nucleus concerned.

The recently developed affinity NMR technique, which detects complexation of a small molecule with a “receptor”, promises to be a valuable tool to perform rapid screening of compounds for biological activity.[7,8] The basis of this technique is that the translational diffusion coefficient of a small ligand changes substantially upon binding to the target macromolecule receptor. Affinity NMR uses diffusion editing to “filter out” signals from nonbinding components, and thus, the bound ligands will be selected from the mixture. The criterion for affinity NMR is that there are considerable differences in observed translational diffusion coefficients between binding and nonbinding ligands in order for them to be distinguished. However, this condition is not always satisfied. The free and bound ligands are in fast exchange on the diffusion time scale; thus, the observed diffusion coefficients are the weighted average of the free and bound species. Ligands in the free form should diffuse at a much faster rate than those in the bound state, so that even a small amount of the ligand in the free state causes the apparent diffusion rate of binding ligand to increase considerably. This factor can greatly narrow the gap of diffusion coefficients between binding and nonbinding ligands, leaving little room to differentiate “active” compounds from the mixture. Under such circumstances, it is difficult to draw the line between binding and nonbinding ligands by diffusion experiments alone. In the various systems investigated, this technique was useful to identify the possible coordination sites in the complexes formed in aqueous solution.

UPLC refers to high Ultra Performance Liquid Chromatography. It improves in three areas: chromatographic resolution, speed and sensitivity analysis. UPLC comes from High Performance Liquid Chromatography (HPLC), is an advance technique of liquid chromatography where it takes advantage of innovation in various technologies such as instrumentation and particle size to achieve dramatic increases in resolution, speed and sensitivity of the liquid chromatography. It operates at higher pressure than that used in HPLC and uses fine particles (less than 2.5μm) and mobile phases at high linear velocities. UPLC technology is now applied throughout the world produce quality data with reproducible and robust methods as compared to the conventional HPLC. Therefore, by using smaller particles, speed and peak capacity (number of peaks resolved per unit time in

gradient separations) can be extended to new limits, termed UPLC. The technology takes full advantage of chromatographic principles to run separations using columns packed with smaller particles and/or higher flow rates for increased speed, this gives superior resolution and sensitivity. UPLC can be hyphenated with other techniques such as Mass spectrometer (MS), Ion chromatograph (IC), Nuclear magnetic resonance spectrometer (NMR) and Infrared spectrometer (IR) *etc*. This technique provides unique end-to-end solutions for all industries and has found application in various fields such as pharmaceutical, food, environmental, forensic, toxicology and pesticide.

The speciation profiles represent the starting point necessary to understanding the structure of metal-ligand complexes, which can be obtained from an experimental as well as from a theoretical point of view. In fact, in some works, the coordination sites of ligands to the different metal ions were determined with the aid of ^{1}H NMR and ^{13}C NMR spectroscopy as well as by a computational approach.

Furthermore, the use of a graphical method of normalized curves was very advantageous in the processing of experimental data. In particular, the average number of protons per ligand and the average number of protons per metal have been plotted as a function of pH. The graphic treatment allowed us to provide an explanation of the three stoichiometric coefficients obtained from the numerical processing of the experimental data.

6. Experimental details

The preparation of the reagents must be carried out with the utmost care to obtain solutions of known composition and in a state of high purity. All the solutions were prepared with double distilled water; in the preparation of the solutions, it is essential to minimize both the effects due to protolytic impurities, which can significantly interfere with acid-base reactions, and those related to oxidizing and reducing agents, whose effect can be deleterious if electrode reactions are studied. Below are the materials and measuring instruments, Gran's method, used for determining the standard potential of the reference electrode, and the details for the preparation of some solutions.

Sodium perchlorate was prepared according to Biedermann[9] starting from $HClO_4$ to 70 % and Na_2CO_3 solid (Carlo Erba RPE). The solution obtained was neutralized to pH 8 and left to digest for more than fifteen days, to favor the precipitation in the form of mixed oxides of any metallic impurities contained therein. The solution was then filtered, acidified to pH 3 and boiled to remove CO_2. The stock solution was analyzed by drying a known quantity at a temperature of 120 °C and weighing the residue as anhydrous $NaClO_4$. Acidity was determined by potentiometric titration with a glass electrode by adding known volumes of standardized $HClO_4$ solutions. The initial acidity value was extrapolated with Gran's method[10].

The stock solutions of *perchloric acid* were prepared by dilution with double distilled water from $HClO_4$ (Merck p.a.) and standardized by volumetric procedure using $KHCO_3$ as primary standard and with the use of the red methyl indicator to identify the final point of the titration. Analyzes coincided within ±0.1 %.

The stock solutions of *sodium hydroxide* were prepared by dilution with bidistilled water from a 50 % solution, previously filtered with a G3 *gooch* under nitrogen, and volumetrically standardized with $HClO_4$, with an accuracy of 0.1 %.

Stock solutions of *HCl*, *NaOH* and $AlCl_3(H_2O)_6$ were prepared on a volumetric basis in NaCl (dried at 220 °C for 2 h) media of total ionic strengths of 0.10, 0.60, 1.60, 3.00 and 5.00 $mol \cdot dm^{-3}$ (*i.e.*, 0.10, 0.61, 1.66, 3.20 and 5.61 $mol \cdot kg^{-1}$ NaCl, respectively) with doubly distilled deionized water. The solutions could therefore be mixed in different quantities without substantially compromizing the total ionic strength. A stock solution of ~0.500 $mol \cdot dm^{-3}$ HCl was standardized with tris(hydroxymethyl)- aminomethane (Trizma) with methyl red and used to prepare 20 $mmol \cdot dm^{-3}$ HCl titrants at each ionic strength. Stock solutions of ~20 $mmol \cdot dm^{-3}$ NaOH were made from a 50 % NaOH stock solution that was filtered under $N_2(g)$ and diluted in $N_2(g)$-degassed solutions of NaCl. These solutions were stored in sealed polyethylene titrant bottles and protected from atmospheric H_2O and CO_2 by an air inlet packed with drierite and ascarite. Volumetric Gran titrations of standardized solutions of HCl in the corresponding NaCl media were carried out to determine the NaOH concentration. Repeated NaOH determinations over the course of this study provided assurance that little or no contamination took place from atmospheric CO_2.

The *copper(II) perchlorate* stock solutions were prepared by dissolving CuO in a slight excess of standardized $HClO_4$. The oxide, very pure, was obtained by heating, at 500 °C, $Cu(NO_3)_2 \cdot 4H_2O$ prepared from electrolytic copper 99.99 % and HNO_3. The thermal decomposition of the nitrate was carried out by melting the salt under vigorous stirring and subsequent roasting in an electric stove for 10 hours. The decomposition product thus obtained appeared as an impalpable powder, more reactive and soluble in $HClO_4$ than the granular oxide available on the market. The latter has traces of metallic copper which, reacting with hot $HClO_4$, could induce chlorides in the solution. The Cu(II) concentration in the stock solutions was determined by electrogravimetry and iodometry.[11] The results agreed to 0.1 %. The hydrogen ion concentration was derived by $[ClO_4^-] = [H^+] + 2[Cu(II)]$.

The *uranyl perchlorate* stock solution was prepared from $UO_2(NO_3)_2(H_2O)_6$ (Carlo Erba). This compound was purified by successive extractions, then burned at a temperature of 900 °C to obtain U_3O_8. The oxide was dissolved in bidistilled HNO_3; nitric acid was removed with perchloric acid vapors in a closed glass system under an inert atmosphere by bubbling of N_2. The crystals of $UO_2(ClO_4)_2(H_2O)_6$, cold separated, were dissolved in double distilled water and analyzed for possible presence of Fe(III), Cl^-, NO_3^-, SO_4^{2-} and heavy metals. No significant amount of these impurities was found in the stock solution. The concentration of U(VI) was determined gravimetrically as uranium (VI)-oxinate according to Classen and Visser.[12] The results agreed within 0.1 %. The hydrogen ion concentration was determined by a potentiometric titration using Gran's method[10] to process the data.

The stock solution of *neodymium(III) perchlorate* was prepared by adding a slight excess of Nd_2O_3 (Fluka 99.9 %) to a hot 4 mol / kg solution of $HClO_4$. The solution was left to rest for a week to favor the precipitation, as hydroxides, of the heavy metals. The solution was filtered and acidified to pH 3. The concentration of Nd(III) in the stock solution was determined by chelometric titration with EDTA, using orange-xylenol as an indicator of the end point. The results agreed within 0.1 %. The hydrogen ion concentration was determined with a glass electrode by acid-base coulometric titration, and the end point was calculated with the Gran's

method[10]. The concentration of the perchlorate ion was obtained from the sum $[H^+]$ + 3[Nd(III)].

The stock solution of *aluminum(III) perchlorate* is prepared by oxidation, at room temperature, of an aluminum wire, whose weight is known exactly, using $Hg_2(ClO_4)_2$ in slight excess, according to the following reaction:

$$2Al_{(S)} + 3Hg_2(ClO_4)_2 \rightarrow 2Al(ClO_4)_3 + 6Hg_{(l)}$$

to obtain solutions of $Hg_2(ClO_4)_2$, pure mercury oxide, HgO, is dissolved in a standardized quantity of $HClO_4$, adding a slight excess (about 1 %). The solution is subsequently equilibrated with metallic mercury to transform Hg^{2+} in Hg_2^{2+}. Mercury (II) oxide is prepared by thermal decomposition of $Hg(NO_3)_2$ at 500 °C in a muffle, which is synthesized by dissolution of bidistilled mercury in concentrated nitric acid. The starting solution of $Hg_2(ClO_4)_2$ contains a known quantity of ClO_4^- ions and is about 0.01 M in $HClO_4$. At this acidity (pH = 2) and at room temperature, the oxidation of aluminum by the ClO_4^- ions is negligible and the chloride ions do not form appreciably. The collateral reaction is probably delayed by the mercury film that forms on the aluminum wire immediately after it is brought into contact with the solution. An important experimental detail is the introduction of aluminum in portions, to avoid an increase in temperature caused by the strong heating due to the oxidation reaction. After the complete dissolution of the aluminum, the excess of Hg_2^{2+} ions are removed by electrolysis with the aid of a cathode, consisting of a platinum mesh electrode, and a spiral platinum anode. There are no Hg_2^{2+}, Cl^- ions in the clear solution. The aluminum(III) concentration of the stock solution was controlled by gravimetric dosing by precipitation with ortho-hydroxyquinoline, as recommended by Berg,[13] and an agreement was found within 0.1 % with the value calculated on the basis of the quantity of metallic aluminum initially introduced.

Stock solution of *nickel(II) perchlorate* was prepared from the pure metal (Aldrich). A known quantity of metal was dissolved in an excess of HI (Merck) at 57 % to which a known quantity of standardized $HClO_4$ was subsequently added such as to guarantee an excess of 10 %. Most of the HI was transformed into molecular iodine by adding HIO_3 (Baker) and the released iodine was removed by boiling. The last traces of iodine have been eliminated by oxidation, causing

oxygen to bubble into the solution. At the end of the purification processes a qualitative assay was performed to verify the absence of chlorides in the stock solution.

With the procedures described below it was possible to accurately calculate the concentrations of nickel(II) and perchlorate ions.

The Ni(II) concentration was checked electrogravimetrically: approximately 15 cm^3 of concentrated ammonia was added to an aliquot of stock solution to be analyzed, diluting with bidistilled water up to a volume of 100 cm^3. The solution was electrolyzed, using a platinum mesh electrode as cathode, with a current intensity of 0.5 A for 12 hours. At the end of the electrodeposition, the nickel deposit was washed with double distilled water, dried with ethyl alcohol, and conditioned in an oven at 102 °C until the weight was constant. From the deposit weight it was possible to calculate the Ni(II) concentration. The perchlorate content of the stock solution was determined gravimetrically: a solution of $KHCO_3$ was added drop by drop to a known quantity of nickel stock solution until complete precipitation of $Ni(OH)_2$. To keep the pH of the filtrate around 5, a known quantity of perchloric acid was added. The solution was allowed to evaporate slowly and the precipitate, $KClO_4$, was dried in an oven at 120 °C until the weight was constant. The result obtained was corrected for the quantity of $HClO_4$ used. The agreement between the experimental result and the calculated (= mol_{HClO4} + $mol_{Ni(II)}$) was about 0.2 %.

The *NaCl* stock solution was prepared by weighing a known quantity of the salt subsequently dissolved in bidistilled water. The solution did not require standardization because NaCl is a primary substance.

Iron(III) perchlorate was prepared and standardized as reported by Ciavatta *et al.*[14]

A stock aqueous solution of *aluminum chloride* (~1.0 $molL^{-1}$) was prepared by dissolving a known amount of crystalline $AlCl_3 \cdot 6H_2O$ 99 % (Aldrich, Gillingham, UK) in distilled deionized water. Working solutions of $AlCl_3$ were prepared by dilution of the stock solution with deionized distilled water. The stock solution containing ~0.4 $molL^{-1}$ $AlCl_3$ and acidified with ~0.4 $molL^{-1}$ HCl, was prepared by dissolution of $AlCl_3 \cdot 6H_2O$ indistilled deionized water containing a pre-dispensed amount of 1.0 $molL^{-1}$ HCl (Fisher Scientific, Loughborough, UK) in a

volumetric flask of the required volume. The hydrogen ion concentration in metal stock solution was determined by potentiometry, using a glass electrode according to Gran's method.[10]

Fe(III) chloride stock solutions were prepared and standardized according to Khoe *et al.*.[15] The hydrogen ion concentration in metal stock solution was determined by potentiometry, using a glass electrode according to Gran's method.[10]

Hexaaquochromium(III) perchlorate was prepared by reducing reagent grade chromium trioxide with a slight excess of reagent grade formic acid in the presence of excess perchloric acid. The chromium(III) perchlorate was recrystallized twice from dilute perchloric acid and then was dissolved in perchloric acid solution. The acidity of the solution was determined by a method suggested by the work of Blaedel and Panos[16] on the determination of the acidity of aluminum(III) solutions; this method has been summarized elsewhere.[17] The chromium concentration was determined spectrophotometrically after oxidation to chromium- (VI) by peroxide in alkaline solution.

There is an important reference where is possible to see the preparation of the solutions metal-perchlorate.[18]

6.1 Materials and measuring instruments

For the potentiometric titrations, two different instrumental apparatuses were used: a combined glass electrode with internal Ag / AgCl reference (saturated), and an alkaline glass indicator electrode with an external Ag / AgCl (saturated) reference electrode. The first is the 411/CGG/12 model, while the second is the 6.01333.100 Metrohm model and has allowed us to have data with an accuracy of 10^{-4} V thanks to the external device for measuring the potential which is an analyzer of ion Orion model EA 940, while the first system has an accuracy of 10^{-3} V and the external device is a DIGITAL pH-METER MODEL 334-B from AMEL. Cells similar to that described by Forsling were used.[19] The Ag / AgCl reference electrodes were prepared according to Brown.[20] To prepare the solutions, the reagents and stock solutions were weighed on a Mettler Toledo AL204 analytical balance, the accuracy of which is 0.0001 g. Double-distilled water was used as the solvent. The

solids used, such as the salts for the preparation of the stock solutions, are of high purity. All measurements were carried out in a bath heated by a Julabo at a temperature of 37 °C, and this was constantly monitored with a special thermometer.

6.2 Gran's method and determination of standard potentials

Gran's idea, which dates back to the early 1950s, was to derive, based on Nernst's law, a function of the electrochemical potentials measured during titration that varied linearly with respect to the volume of added titrant.[21] The method is based on the linearization of the sigmoidal titration curve in the interval around the equivalent volume V_e. The use of linear diagrams offers several advantages:

- It is possible to record only a few points and not the entire titration curve;
- The equivalent point is obtained by extrapolation from a straight line; this linearization allows the identification of the equivalent point even when the titration curves do not allow it.

Starting from the Nernst equation, this is rewritten in exponential form, in order to isolate the concentration of the unknown species:

$$E = \frac{RT}{nF\ 0.4343} \log C_x \rightarrow C_x = 10^{(\frac{nF\ 0.4343}{RT}E)} \quad (35)$$

If C_x corresponds to the concentration of titrant, indicated with C_t, it can be written that:

$$C_t = \frac{N_t V_t - N_t V_e}{V_{tot}} \quad (36)$$

where N_t and V_t are the normality and the volume of titrant added respectively, V_e is the equivalent volume and V_{tot} is the total volume. Substituting equation (36) into (35) we get:

$$C_t = 10^{(\frac{nF\ 0.4343}{RT}E)} \rightarrow 10^{(\frac{nF\ 0.4343}{RT}E)} V_{tot} = N_t V_t - N_t V_e \quad (37)$$

An equation of the type $y = \alpha x + b$ is obtained, where, in the case under consideration, $y = 10^{(\frac{nF\ 0.4343}{RT}E)} V_{tot}$,

the angular slope $\alpha = N_t$, the independent variable is $x = V_t$, intercepts $b = N_t V_e$. For values of $y = 0$, we have that $V_t = V_e$. Remember that, working at a temperature of 37 ° C, the factor $\frac{nF\ 0.4343}{RT} = 0.06154\ V$. For the determination of the standard potential of the measuring electrode, a 0.16 M solution in NaCl was prepared and titrated with a known solution of HCl, recording the potential values. In this way the Gran function is shown in the graph and with the QB45 program the data to determine the standard potential have been processed. In the case of the combined electrode, the value is:

$$E° = 426.1 \pm 0.5 \text{ mV},$$

while in the case of the working electrode with external reference it is:

$$E° = 357.1 \pm 0.5 \text{ mV}.$$

References

1. D.A. Skoog, J.J. Leary, *Chimica analitica strumentale, EdiSES*, (**2000).**
2. S. Hietanen, L.G. Sillén, *Acta Chem. Scand.*, (**1959)**.
3. P. Gans, A. Sabatini, A. Vacca, *J. Chem. Soc. Dalton Trans.*, (**1985).**
4. A. Sabatini, A. Vacca, P. Gans, *Talanta*, (**1974)**.
5. P. Gans, A. Sabatini, A. Vacca, *Talanta*, (**1996)**.
6. L.G. Sillén, *Acta Chem. Scand*., (**1954)**.
7. M. Lin, M.J. Shapiro, J.R. Wareing, *J. Am. Chem. Soc*., 119 (**1997)** 5249.
8. M. Lin, M. J. Shapiro, J.R. Wareing, *J. Org. Chem*., 62 (**1997)** 8930.
9. S. Abbasi, B. Bhat, R. Singh, *Indian. J. Chem.*, 14B (**1976)** 718.
10. S. Abbasi, *J. Indian. Chem. Soc.*, 61 (**1984**) 125.
11. M. Bartusek, J. Zelinka, *Collec. Czech. Chem. Commun.*, 32 (**1967**) 992.
12. M. Maeda, Y. Murata, K. Ito, *J. Chem. Soc. Dalton Trans.*, (**1987**) 1853.
13. L. Ciavatta, *Ann. Chim.*, 80 (**1990**) 225.
14. L. Ciavatta, G. Nunziata, L.G. Sillén, *Acta Chem. Scand*., 23 (**1969**) 1637–1652.
15. G.H. Khoe, P.L. Brown, R.N. Sylva, R.G. Robins, *J. Chem. Soc. Dalton Trans.*, 9 (**1986**) 1901-1906.
16. W.J. Blaedel, J.J. Panos, *Anal. Chem*., 22 **(1950)** 910.
17. E.L. King, J.A. Neptune, *J. Am, Chem. Soc*., 77 **(1955)** 3180.
18. G. Biedermann, D. Ferri, *Chem Scripta*, 2 (**1972**) 57–61
19. W. Forsling, S. Hietanen, L.G. Sillén, *Acta Chem. Scand*., (**1952)**.
20. A.S. Brown, *J. Am. Chem. Soc*., (**1934)**.
21. G. Gran, *Acta Chem. Scand.*, (**1950)**.

7. Conclusive remarks

The entire research work concerned the study of the formation of complexes between antioxidant molecules and metal ions. In a thermodynamic approach of the chemical equilibrium in aqueous solution, there are several steps that must be followed with a very precise order. Having to work in aqueous solution and since these are binding molecules that are almost always organic acids, clearly the first thing to do is to evaluate how soluble these molecules are. Subsequently, the acid-base properties of the binding molecules are evaluated as what is studied is a competition between the metal and the proton on the binder; the metal must be competitive with the proton regardless of the dissociation of the acid. Once the solubility and acid-base properties of the ligand have been evaluated, we proceed with the study of the metal-ligand complexation equilibria. The calculation of the equilibrium constants requires the control of the ionic strength because the law of mass action is valid with the activities, and considering that the knowledge of the activity coefficients is not always simple, it is preferred to keep them constant, working in ionic medium conditions constant; the activity coefficients once constant, even if not known, can be incorporated in the constant *K*, determining a stoichiometric constant conditioned by the experimental conditions. Therefore, a constant is obtained which depends on the experimental conditions and in the specific case referred to quite natural conditions. The work is, in fact, carried out under physiological conditions at a temperature of 37 °C and controlling the ionic strength at a value of 0.16 M in NaCl or $NaClO_4$. The choice to work in physiological conditions is due to the fact that we already have an idea of what really happens in natural systems. The analysis of the chemical equilibrium allows to determine both the composition of the species that are formed between a generic metal and a binder, and the relative formation constants. This knowledge is necessary for an accurate and serious speciation that qualitatively and quantitatively describes a system in terms of complex formats. The potentiometric method is used in the whole work; this method represents one of the most accurate methods for the determination of equilibrium constants and like all instrumental methods it has advantages and limitations; the limitation is that it does not allow to determine the metal-ligand coordination sites. What we can evaluate, are the stoichiometric coefficients of the species that are present in solution, but we do not have the possibility of knowing with

certainty which complex corresponds to the three stoichiometric coefficients. A structure of the complexes formed in aqueous solution is hypothesized, based on the speciation profile obtained and considering the chemistry of the metal and of the binder. Among the advantages, we remember that it is an economic method, the experimental apparatus is simple, the measurements are reproducible and the speed depends on the tendency of the system being studied to go to equilibrium. The processing of the experimental data takes place with a calculation program, the SUPERQUAD, where the primary data of the titrations are entered, such as: the concentrations of the reagents, the volumes of titrant, the potentials recorded. SUPERQUAD is a program based on the least squares method; looks for the minimum of a function that is constructed by considering a particular model. Thus, it is possible to identify the best model that explains the experimental data.

The entire work carried out for the various metal-bonding systems investigated, allowed us to evaluate which species are formed in physiological conditions of temperature and ionic medium, and this undoubtedly represents a good starting point for carrying out subsequent experimental tests. Starting from the data obtained for the various systems investigated through this experimental approach, computational calculations can then be carried out to identify the most stable structure of the complexes, carry out tests on the antioxidant properties of the complexes, select the ligand that best sequestrates a metal ion under the physiological conditions. Important is also the use of instruments to characterize the complexes in solution for examples: RP-UHPLC-PDA-ESI-IT-MS (Reversed phase liquid chromatography) to identify and quantify the amount of the products, UV-vis spectrophotometric measurements, ESI-IT-MS (electrospray ionization ion trap mass spectrometry) to verify the species present in the systems and NMR (Nuclear Magnetic Resonance) to evaluate the possible coordination site on the structure of the ligand.

Abbreviations

Neurodegenerative diseases (ND)

Alzheimer's disease (AD)

Parkinson's disease (PD)

Prion protein disease (PrD)

Amyotrophic lateral sclerosis (ALS)

Reactive oxygen species (ROS)

Blood brain barrier (BBB)

Ethylenediaminetetraacetic acid (EDTA)

Food and Drug Administration (FDA)

Linear combination of atomic orbitals (LCAO)

Quercetin (H_5Que)

Coumarin-3-carboxylic acid (HCCA)

L-ascorbic acid (H_2As)

Monodehydroascorbate (MDHA)

Heavy metal ions (HMs)

Central nervous system (CNS)

Superoxide dismutase (SOD)

Wilson's disease (WD)

Human serum albumin (HSA)

Hard and soft acids and bases (HSAB)

Endoplasmic reticulum (ER)

Matrix metalloproteinases (MMPs)

Membrane-type metalloproteinases (MT-MMPs)

Transmittance (T)

Absorbance (A)

Infrared spectroscopy (IR)

Nuclear Magnetic Resonance (NMR)

Ultra performance liquid chromatography (UPLC)

High performance liquid chromatography (HPLC)

Mass spectrometer (MS)

Ion chromatograph (IC)

Reversed phase liquid chromatography (RP-UHPLC-PDA-ESI-IT-MS)

Electrospray ionization ion trap mass spectrometry (ESI-IT-MS)

INDEX

ACES Asian Chemical Editorial Society

DOI: 10.1002/asia.202000717

CHEMISTRY AN ASIAN JOURNAL Full Paper

Sequestering Ability of a Synthetic Chelating Agent towards Copper(II) and Iron(III): A Detailed Theoretical and Experimental Analysis

Alessandra G. Ritacca, Luana Malacaria, Vincenzo Algieri, Antonio De Nino, Nino Russo, Emilia Furia,* Loredana Maiuolo,* and Emilia Sicilia*[a]

Abstract: In the continuous effort to identify selective chelators towards bioavailable and toxic metal ions, the potential selectivity of a novel N,O chelating ligand, recently synthesized and claimed to be able to bind to Cu(II) ions forming stable complexes while leaving unaltered the level of essential metal ions, was scrutinized using a combined theoretical and experimental approach. A multistep synthetic procedure was used to synthesize the ligand, whose chelating properties along with the stability of the complexes formed binding Cu(II) and, for comparison, Fe(III) ions were evaluated using potentiometric measurements and UV-Vis spectroscopy. DFT analysis allowed to disclose the structural characteristics of the formed complexes. In the plethora of all the possible structures, a selection of the most reliable ones was achieved by means of a stringent comparison between experimental and simulated UV-Vis spectra. The outcomes of the present investigation demonstrate that the Cu(II) sequestering ability of the ligand is smaller than that towards Fe(III). The strategy used here should allow to check the propensity of ligands in selectively binding metal ions.

1. Introduction

Chelation therapy is a promising methodology for the treatment of pathological diseases arising from oxidative stress caused by excess or dysregulation of transition metals. Alzheimer's disease (AD), in particular, is a chronic neurodegenerative disorder that occurs mostly in people over the age of 65.[1] AD is the main source of dementia and one of the most difficult healthcare challenges of the last century.[2] The etiology of AD is still poorly understood and multifaceted. Indeed, it is currently conceived that a combination of factors, *i.e.*, genetics, environment, and lifestyle, may be responsible for the progression of AD, but the specific mechanism of its onset is still unclear and no cure exists for this disease. The most accredited hypothesis of amyloid cascade, which suggests that the aggregation of amyloid proteins is a stimulus for AD pathogenesis has dominated research in the field and drug development for the last 25 years.[3] However, as none of the drugs purposely developed has demonstrated significant efficacy, suggestions that additional factors, such as oxidative stress and disorders of metal ion metabolism, might be mutually operating in neurodegeneration have been reexamined.[4]

Metal ions are essential for life as they play a crucial role in many biochemical paths. Nevertheless, environmental exposure, genetic dysfunction, inadequate dietary consumption and drug interaction can induce an alteration of their physiological concentration leading to deleterious effects and neurotoxicity. Specifically, redox-active metal ions as Cu(II) and Fe(III) exert their toxic action through the formation of reactive oxygen species (ROS), which may result in tissue or organ damage.[5] In this framework, chelation therapy plays a central role in the clinical treatment of metal intoxications.[6] The poisoning action of toxic metal ions represents one of important health and social problem in the industrialized countries. The research on chelating agents to be used in clinical practice is mainly based on biology drivers and no attention is payed to the chemical knowledge of the mechanism involved in the complex formation. Drugs based on a chelating agent able to sequestering a specific metal are not necessarily the best, but only the most common drugs.[7–10] Specificity and stability of the metal-chelator complexes are extremely important in the choice of the most adequate chelating agent. Indeed, complexes stability is the first requirement to transform toxic metal ions in chelated species to be excreted. Chelators can be classified according to the number of coordinating groups on the molecule able to bind toxic metal ions. The chelating agents actually in use belong to few chemical categories (*i.e.*, poliaminocarboxylic acids; ligands containing mercapto groups; ligands with oxygen coordinating groups and dithiocarbamates). In our continuous effort to identify selective chelators towards bioavailable and toxic metal ions,[11–14] in the present work the attention was focused on the recently proposed N,O synthetic chelator **1** reported in Scheme 1.[15]

The authors showed that the novel proposed chelator **1** exhibits specific Cu(II) selectivity at physiological pH alleviating metal overload induced oxidative stress and assessed the stability of the formed copper complexes over time. As we considered to be of interest to verify such results using a

[a] *A. G. Ritacca, L. Malacaria, Dr. V. Algieri, Prof. A. De Nino, Prof. N. Russo, Dr. E. Furia, Dr. L. Maiuolo, Prof. Dr. E. Sicilia*
Department of Chemistry and Chemical Technologies
Università della Calabria
Ponte P. Bucci Cubo 14c, 87036 Arcavacata di Rende (CS) (Italy)
E-mail: emilia.sicilia@unical.it
emilia.furia@unical.it
loredana.maiuolo@unical.it

Supporting information for this article is available on the WWW under https://doi.org/10.1002/asia.202000717

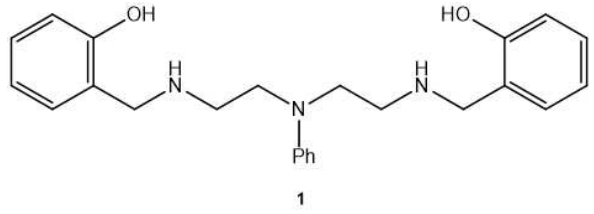

Scheme 1. Structure of the synthetic chelating agent **1**.

different combination of theory and experiments, herein we present a thorough study based on experimental methods (potentiometric and UV-Vis spectroscopy) combined with quantum-mechanical DFT calculations. The objective to determine stoichiometric composition and related stability constants in aqueous medium, i.e., at 37 °C and in 0.16 M NaCl to reproduce biological conditions, of the complexes formed with Cu(II) and, for comparison, Fe(III) ions was pursued. Thermodynamic and structural information on these systems in a wider pH range and in aqueous solution was obtained aiming at applying in the future such approach to novel proposed ligands.

2. Results and Discussion

2.1. Ligand synthesis

In the effort to explore the chelating behavior of the mixed *N*- and *O*-donor atom containing ligand **1**, a multistep synthetic procedure was developed as shown in Scheme 2. The synthesis started from the commercial material *N*-phenyldiethanolamine **2** that was symmetrically activated to oxygen moieties with tosyl groups. The reaction between **2** and *p*-toluenesulphonyl chloride **3** was performed in dry pyridine.[16]

In the next step, the bis-tosylate substrate **4**, purified by recrystallization and isolated in 80% yield, was allowed to react with potassium phthalimide **5** to produce the derivate **6**, as a consequence of the replacement of tosylates by phthalimide groups through SN2 reaction. The compound **6** was used as crude to furnish the deprotected diamine compound **7** in excellent yield (96%) through modified procedures of literature.[17] Subsequently, compound **7** was reacted with salicylaldehyde **8**, isolating the resulting bis-imine derivative **9**, which furnished ligand **1** *via* reduction reaction in excellent yield (92%).[15]

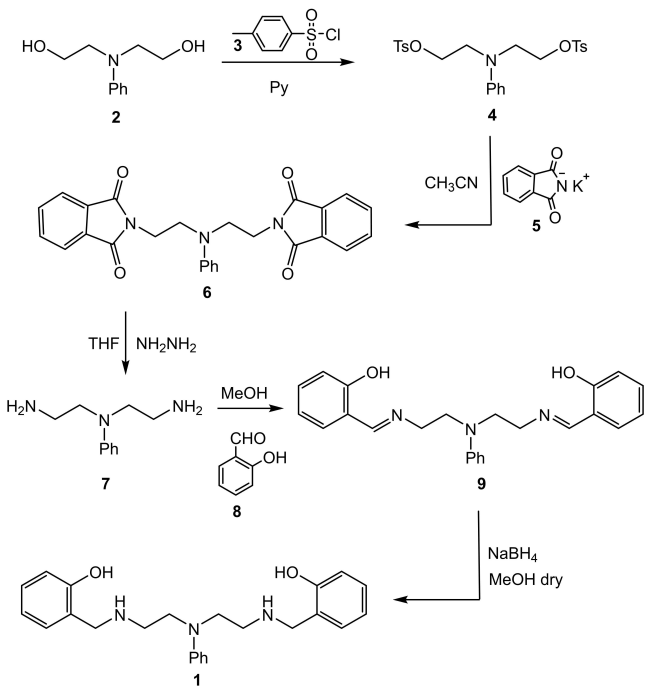

Scheme 2. Multistep procedure for the synthesis of the **1** ligand.

2.2. Chelating properties of the ligand and stability of formed complexes

The complex formation equilibria of Cu(II) and Fe(III) with **1**, which for the sake of simplification will be named H_2L from now on, were studied at 37 °C and in 0.16 M NaCl by measuring with a glass electrode the competition of the ligand for metal cations and H^+. After addition of reagents, the pH of the test solutions was stepwise increased by adding NaOH standard solutions. By using the experimental approach described previously[13], at first, we have determined the acidic constants of the ligand considering, together with the two phenolic moieties, also the protonation of the two secondary amino groups, that should occur in acidic environment (Eqs. 1–4):

$$H_4L^{2+} \rightleftharpoons H_3L^{+} + H^{+} \qquad pK_{a1} = 7.92 \pm 0.01 \tag{1}$$

$$H_3L^{+} \rightleftharpoons H_2L + H^{+} \qquad pK_{a2} = 8.42 \pm 0.06 \tag{2}$$

$$H_2L \rightleftharpoons HL^{-} + H^{+} \qquad pK_{a3} = 8.58 \pm 0.06 \tag{3}$$

$$HL^{-} \rightleftharpoons L^{2-} + H^{+} \qquad pK_{a4} = 8.9 \pm 0.1 \tag{4}$$

The uncertainties represent 3σ. The distribution of ligand at different pH is reported in Figure 1.

As can be seen, at physiological pH the ligand H_2L coexists with the bi- and the mono-protonated species H_4L^{2+} and H_3L^{+}, respectively. Metals (C_M) and ligand (C_L) concentrations were ranged from (0.25–5.0)×10^{-3} M and the ligand-to-metal ratio was varied between 1 and 6. The hydrogen ion concentration was ranged from 0.01 M (pH 2.0) for Fe(III) and from 3.15 10^{-3} M (pH 2.5) for Cu(II), to pH 7.5. The general equilibrium can be written as follows:

$$pM^{n+} + q(OH)^{-} + rH_2L \rightleftharpoons M_p(OH)_q(H_2L)_r^{(np-q)} \ \beta_{pqr} \tag{5}$$

Eq. 5 takes into account the possible formation of simple ($q = 0$), mixed ($q \neq 0$), mononuclear ($p = 1$) and polynuclear ($p > 1$) species. Equilibrium constants of the predominant hydrolysis products under our experimental conditions of Cu(II) and Fe(III)

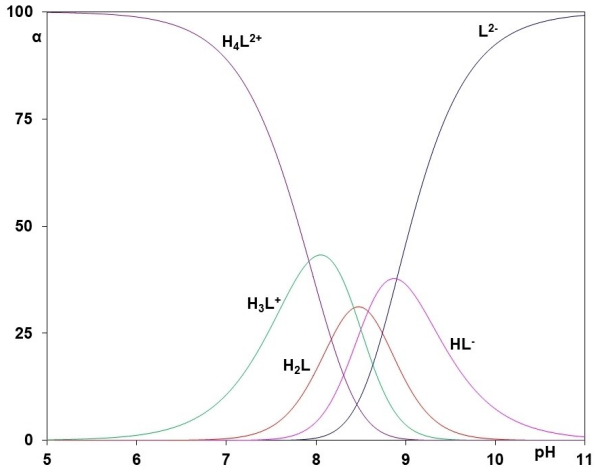

Figure 1. Distribution of H_2L in aqueous solution in a wide pH range.

cations (*i.e.*, $Cu(OH)^+$ and $Cu_2(OH)_2^{2+}$, and $Fe(OH)^{2+}$ and $Fe(OH)_2^+$ species, respectively) were taken from the literature.[18] The acidic constants of ligand (Eqs. 1–4) and the hydrolysis constants of metal cations were kept fixed in the evaluation of β_{pqr}. The stability constants of a chosen ternary species (p,q,r) were allowed to vary systematically to seek the best data fitting. Results obtained from numerical treatment of potentiometric data are reported in Table 1.[19]

Speciation profiles show that a complexation occurs at 1:1, 1:2 and 1:3 ligand-to-cation ratio for Cu(II) and at 1:1 and 1:2 for Fe(III). Results reported by Rakshit *et al.* proposed a single species at ligand to metal ratio 1:2 for Cu(II) with a log $\beta \geq 12$, and a single species at ligand to metal ration 1:1 for Fe(III) with a log $\beta = 3.39$.[15] As can be seen in Table 1, our results underline a different behavior for the two examined cations: the synthesized chelator, H_2L, is able to form several species distributed in the overall investigated pH range. The distribution diagrams (Figure 2a–b), in which the metal cation percentage in the complexes *versus* pH is reported, highlight these differences.

Figure 2a shows that the formation of the complexes between Cu(II) and H_2L is relevant from pH 3.5 and at a physiological pH the predominant species are the two simple complexes $Cu(H_2L)_2^{2+}$ and $Cu(H_2L)_3^{2+}$. Completely different is the behavior of Fe(III). As can be seen in Figure 2b the complexation takes place starting from a pH value of 2 and the only complex at physiological pH is $Fe(OH)_2(H_2L)_2^+$. By a comparison of the stability constant values for the two systems (Table 1), the sequestering ability of H_2L towards Cu(II) is smaller than that towards Fe(III) according to the strong acidity of the latter. The speciation models were verified by UV-Vis spectroscopy and by DFT theoretical investigations to define the possible structures of the complexes formed in aqueous solutions. A comparison of free ligand and coordinated species UV-Vis spectra is reported in Figure 3.

According to literature data[15], the spectrum of free H_2L shows three absorptions in the UV region, two intense bands at 272 and 241 nm and a shoulder at 308 nm. After addition of the metal cations, Cu(II) and Fe(III), the formation of two different phases, *i.e.*, solution and solid, was detected. After proper dilution, UV-Vis spectra of these solutions were registered. Concerning Cu(II), solid dissolved in ethanol shows a red-shift respect to free ligand at 281 and 248 nm, while the solution shows a slight shift of the 272 nm band at 276 nm. As regards Fe(III), solid dissolved in ethanol and solution opportunely

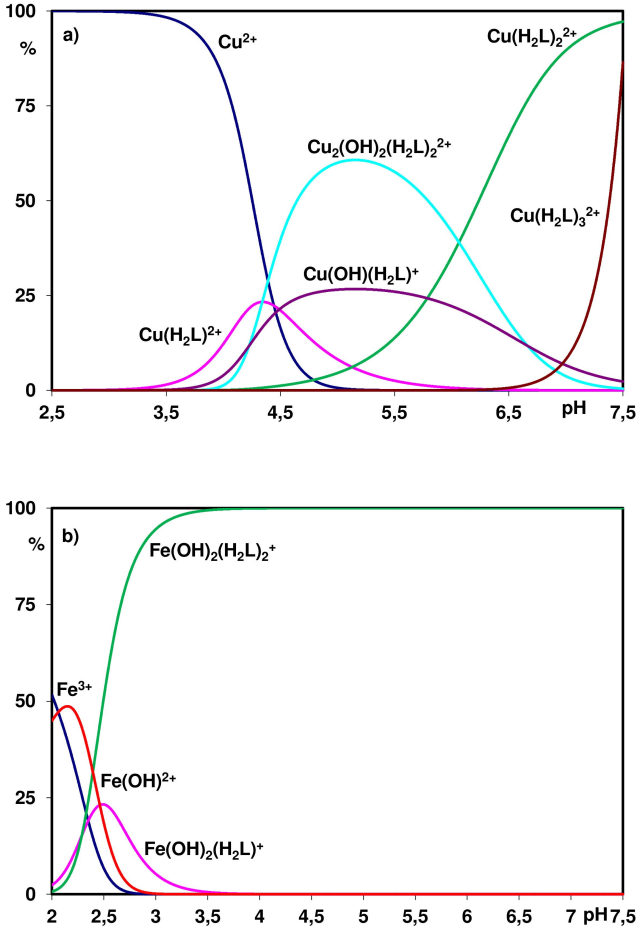

Figure 2. Distribution diagrams in the presence of H_2L of: a) Cu(II) ($C_M = 0.5$ mM and $C_L = 2.5$ mM) and b) Fe(III) ($C_M = 0.5$ mM and $C_L = 2.5$ mM).

Table 1. Formation constants of H_2L ligand complexes in NaCl 0.16 M and at 37 °C with Cu(II) and Fe(III) according to Eq. 5 compared with the corresponding calculated values.

Cations	Complexes	log $\beta_{pqr} \pm 3\sigma$	Calc. log β
Cu(II)	$Cu(H_2L)^{2+}$	10.13 ± 0.02	10.0
	$Cu(H_2L)_2^{2+}$	18.92 ± 0.02	12.4
	$Cu(H_2L)_3^{2+}$	24.63 ± 0.02	19.7
	$Cu(OH)(H_2L)^+$	19.0 ± 0.1	18.9
	$Cu_2(OH)_2(H_2L)_2^{2+}$	41.85 ± 0.06	77.7
Fe(III)	$Fe(OH)_2(H_2L)^+$	36.25 ± 0.06	72.5
	$Fe(OH)_2(H_2L)_2^+$	50.66 ± 0.03	84.6

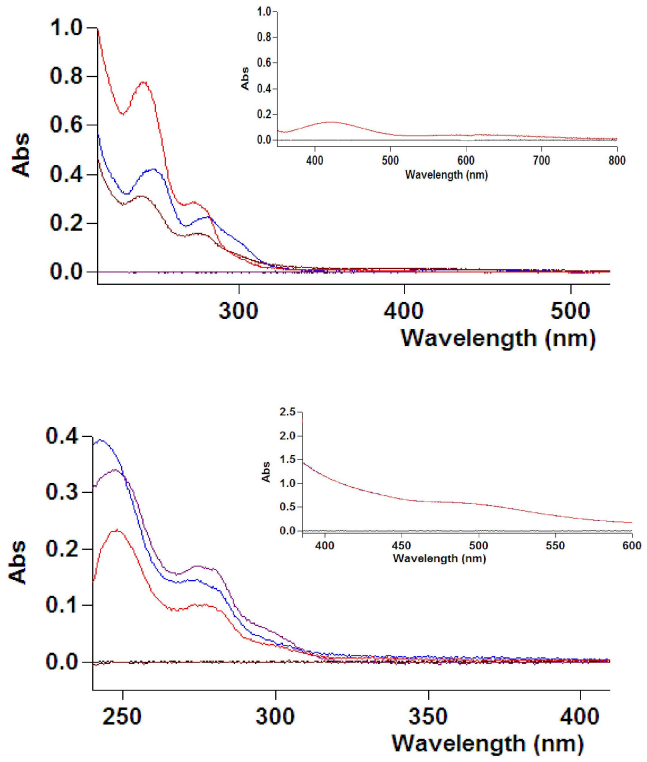

Figure 3. UV-Vis spectra of the free ligand and of the a) Cu(II) and b) Fe(III) complexes. In a) red line is free chelator, blue line is solid Cu(II)-H_2L and brown line is solution Cu(II)-H_2L In b) blue line is free chelator, red line is solid Fe(III)–H_2L and violet is solution Fe(III)–H_2L. Insets refer to the Vis region of the spectra (380–800 nm), in which the d–d bands are present.

diluted exhibits a bathochromic shift of both absorptions to 277 and 248 nm, and to 274 and 248 nm, respectively. the spectra of the coordination compounds in the visible region are reported in the insets of Figure 3. As it can be seen, after the addition of the metal cations absorptions appear in the visible region. In particular, for Cu(II)-H_2L system two different bands are detected at 621 and at 418 nm, while for Fe(III)–H_2L system just one at 480 nm. Spectroscopic results confirm the formation of complexes between metal cations and H_2L.

2.3. Computational analysis

2.3.1. Geometrical structure and stability of formed complexes

Starting from the information coming from experiments, structures and coordination modes of the formed complexes by binding of the **1** ligand, were investigated using DFT quantum mechanical calculations. In the reference paper[15] among all the structures of lowest energy calculated using molecular mechanics, that with a 1:2 metal to ligand ratio having a pseudo-square-planar geometry, where two N- and phenolate O-donor atoms each are coordinated to the central metal ion was selected as the most probable. Such structure, indeed, resulted to be in agreement with all the experimental findings.

Several possible alternative structures were taken into consideration. Concerning the ways of coordination of the ligand **1**, even if the available coordination sites are five, very likely due to geometric and steric constraints, all the optimizations carried out to go beyond tri-coordination failed. The possibility that the ligand is fully or partially deprotonated was examined. In addition, also the coordination of the ligand in a form that, for the sake of simplicity, we call zwitterionic was explored as during the optimization a spontaneous proton migration from the OH group to the NH occurred. All the starting geometries were assumed to be octahedral for the iron cation, whereas for copper several initial arrangements were considered. Water molecules were allowed to saturate the remaining coordination sites. Pseudo tetrahedral, square planar, square pyramidal or trigonal bipyramidal arrangements were obtained by spontaneous release of the ligands and reorganization of the initially assumed octahedral geometry. All the geometric arrangements reported here, have to be considered "distorted" with respect to the corresponding regular ones. For all the optimized structures the corresponding UV-Vis spectra were calculated for comparison with the experimental counterparts aiming at selecting the geometrical arrangements that better reproduce the experimentally detected transitions.

For all the complexation equilibria free energies were calculated for the substitution and release of water molecules in the reference hexaaquo complexes. The most stable structure chosen as a reference for Cu(II) is square planar around the metal cation with four water molecules in the first shell and two water molecules in the second coordination shell.[20,21] The reference structure for Fe(III) is octahedral.

For both Cu(II) and Fe(III) only complexes with stoichiometric ratios reproducing the indications coming from potentiometric measurements were examined and, for each proposed stoichiometric ratio, all the compatible arrangements were explored.

As shown by the distribution diagrams in Figure 2 panel b), for the Fe(III) ion only two complexes, $Fe(OH)_2(H_2L)^+$ and $Fe(OH)_2(H_2L)_2^+$, can be formed starting from pH = 2, being the latter the only complex existing at physiological pH. The Cu(II) ion appears to be able to form complexes with various metal-to-ligand ratios even if at physiological pH only one of them, $Cu(H_2L)_2^{2+}$, has a preponderant concentration,

The fully optimized geometrical structures of Cu(II) and Fe(III) complexes, in different stoichiometric ratios, selected on basis of the best fitting of the experimental UV-Vis spectra are reported in Figures 4 and 5, respectively, together with the corresponding calculated formation Gibbs free energies. In the same figures also key geometrical parameters for each of these complexes are provided.

For each of the suggested stoichiometric ratios, except the 1:2 ratio for Cu(II), only one plausible geometry, amongst all the possible alternatives, was intercepted reproducing the experimentally detected UV-Vis transitions.

For the copper complexes, the located structure with stoichiometric 1:1 metal-to-ligand ratio has a square-planar geometry with the ligand that is coordinated to the metal in a bidentate fashion together with two water molecules. Coordi-

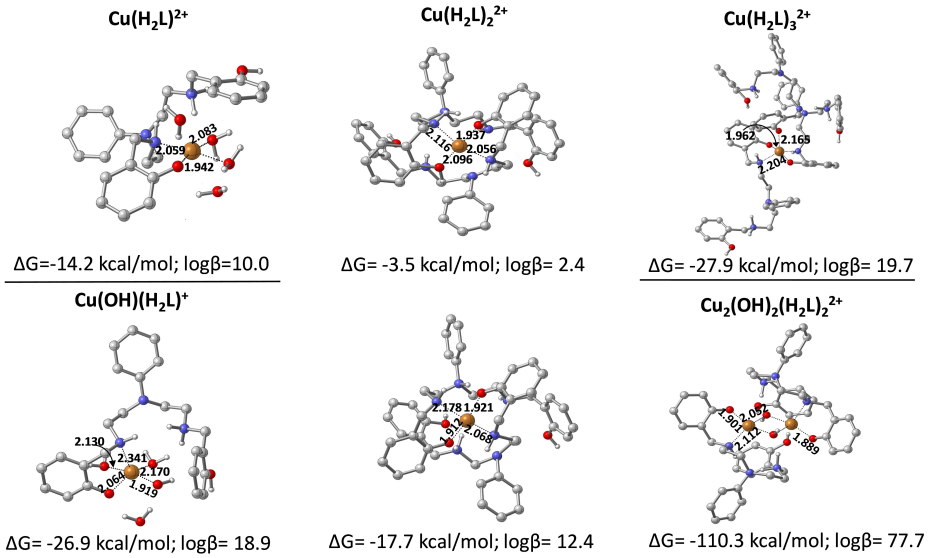

Figure 4. Fully optimized geometrical structures of Cu(II)-H_2L complexes with different stoichiometric ratios together with calculated reaction energies (kcal mol^{-1}) and log β values.

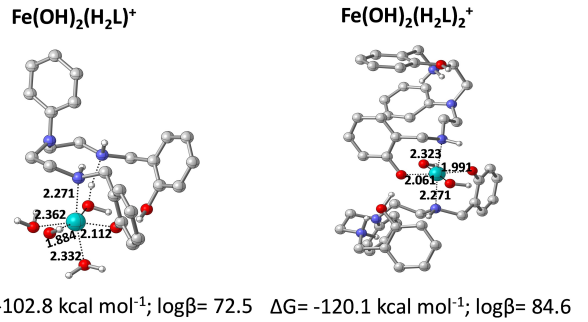

Figure 5. Fully optimized geometrical structures of Fe(III)–H_2L complexes in two stoichiometric ratios together with calculated reaction energies (kcal mol^{-1}) and log β values.

nation occurs through phenolate oxygen and secondary nitrogen of the ligand in a zwitterionic form. Formation energy of the complex is calculated to be −14.2 kcal mol^{-1} and log β = 10, in good agreement with the experimental value.

Two possible structures for the metal-to-ligand 1:2 ratio were intercepted. In the less stable complex, two *N,O* chelating zwitterionic ligands coordinate the copper center. The complexation energy is −3.5 kcal mol^{-1} and log β = 2.4. The second more stable complex differs with respect to the first one as in one of the coordinated ligands the proton from the OH group is transferred to the nitrogen of the tertiary amine. The complexation energy is −17.7 kcal mol^{-1} and logβ = 12.4. The better agreement in the latter case with the experimental value allows the selection of the most probable structure.

The complex for the copper:ligand 1:1 ratio, with charge +1 due to the coordination of a hydroxide ligand, adopts a square planar arrangement. The zwitterionic ligand is coordinated to the metal through the oxygen atom of the phenolate, whereas the three remaining positions are occupied by two water molecules and the hydroxide ligand. As it appears from the reported structure in Figure 4, the secondary nitrogen from the phenolate side establishes an additional interaction with the metal center at a Cu–N distance of 2.34 Å. Therefore, the geometry can be classified as square pyramidal. The complex is stabilized by 26.9 kcal mol^{-1} for a corresponding logβ = 18.9, in good agreement with experiments.

In the located structure, possessing a square pyramidal geometry, of the Cu(II) complex with a metal to ligand 1:3 ratio, two zwitterionic ligands coordinate the metal in a *N,O* bidentate fashion in the same equatorial plane. The third zwitterionic ligand coordinates only through the oxygen of the phenolate in axial position. The calculated energy of formation of the complex is −27.9 kcal mol^{-1} for a logβ value of 19.7. This value, even if lower than that experimentally measured, is in line with the expected trend. The last proposed arrangement for the 2:2 ratio between the metal and the ligand is a binuclear complex with two OH^- groups acting as bridging ligands. Each zwitterionic ligand chelates a metal center from opposite sides adopting a tetrahedral geometry. Complexation stabilizes the formed system by 110.3 kcal mol^{-1} with logβ = 77.7 on the basis of calculations. Such value is overestimated with respect to experiment, but, once again, in line with the proposed trend.

The fully optimized structures of the only two Fe(III) complexes selected on the basis of the same criterion used for Cu(II) complexes are depicted in Figure 5 together with the calculated values of the complexation energies.

The Fe(III) complex with a metal to ligand 1:1 ratio and charge +1 due to the coordination of two hydroxide ligands assumes a very distorted octahedral arrangement. The ligand, once again in its zwitterionic form, is coordinated to the metal center in a *N,O* chelating fashion. It is noteworthy, in this case, that the protonated secondary nitrogen partially transfers a proton to one of the OH^- groups. Therefore, the octahedron remaining positions are occupied by three water molecules and one hydroxido group.

The complex results to be stabilized by 102.8 kcal mol^{-1} for a logβ = 72.5. In this case the complexation energy is overestimated, but compatible with the values for the Cu(II) formed complexes.

The second iron complex, that is the only one existing at physiological pH, has a 1:2 metal-to-ligand ratio and charge +1 as, once again, two hydroxide ligands are bound to the metal. The two zwitterionic ligands are both *N,O* chelating in axial and equatorial positions, whereas both OH^- ligands occupy the equatorial positions of a distorted octahedral geometry. The complexation energy is −120.1 kcal mol^{-1} and logβ = 84.6. The calculated values of the complexation energies for both the iron complexes are overestimated with respect to the experimental counterparts. However, the trend is correct and the large values of the free energy confirm the ability of the ligand to form very stable complexes with the iron cation supporting the suggestion that the investigated ligand Fe(III) coordination is favored with respect to that of Cu(II).

2.3.2. Calculated UV-Vis spectra

Analysis of the absorption properties of optimized complexes started with the calculation of the absorption spectra of the free ligand **1** in its different forms, that is neutral, neutral zwitterionic, mono-deprotonated and doubly deprotonated. Transition wavelengths, oscillatory strengths and orbital contributions for each form of the free ligand are reported in Table S1 of the Supporting Information (SI). In the UV–Vis spectrum of the ligand, two absorption peaks were observed at 272 and 241 nm and a shoulder at 308 nm. Calculated wavelengths for all the different forms of the ligand reproduce very well the experimental values. However, a shoulder at 315 nm appearing only in the absorption spectrum of the neutral zwitterionic form should allow to identify such form as that present is solution and experimentally detected. Reported structure of the Molecular Orbitals (MOs) involved in transitions (Figure S1) show that peaks are assigned to $\pi\rightarrow\pi^*$ transitions of the aromatic rings. Complexation of the H_2L ligand with Cu(II) and Fe(III) causes some shifts in these transitions and, in addition, two new peaks appear for the Cu(II)-H_2L system at 621 and at 418 nm, and only one for the Fe(III)–H_2L system at 480 nm. Calculated wavelengths are rather far, as it often occurs with TDDFT spectra, from both shifted wavelengths and new detected ones upon coordination. Nevertheless, both the presence of peaks outside the regions of the spectrum individuated by the experimental detection and, on the other hand, the absence of peaks in the proper regions, allowed to exclude many of the possible alternative structures intercepted by computations. Comparison between experimental and computed absorption wavelengths is reported in Table 2 and 3 for Cu(II) and Fe(III) complexes, respectively. Absorption wavelengths of the complexes that on the basis of the experimental findings should be present at physiological pH have been marked in red.

Transition wavelengths, oscillatory strengths and orbital contributions are summarized in Table S2 of the SI. Plots of the molecular orbitals, involved in electronic transitions of the complexes, $Cu(H_2L)_2^{2+}$ and $Fe(OH)_2(H_2L)_2^{+}$ that for copper and iron, respectively represent the most abundant species at physiological conditions, are shown in Figure S2.

Table 2. Experimental and TDDFT calculated absorption wavelengths (cm^{-1}) for Cu(II) complexes. Calculated wavelengths for the complex present at physiological pH are marked in red.

Exp.	$Cu(H_2L)^{2+}$	$Cu(H_2L)_2^{2+}$ log β= 2.4	$Cu(H_2L)_2^{2+}$ log β = 12.4	$Cu(H_2L)_3^{2+}$	$Cu(OH)(H_2L)^{+}$	$Cu_2(OH)_2(H_2L)_2^{2+}$
272.0	271.8	293.9	276.0	317.7	293.9	319.5
276.0	325.6	325.5	304.1	346.7	346.4	335.6
418.0	458.2	447.8	407.6	428.4	455.0	471.6
621.0	634.2	676.4	600.8	601.4	689.3	640.8

Table 3. Experimental and TDDFT calculated absorption wavelengths (cm^{-1}) for Fe(III) complexes. Calculated wavelengths for the complex present at physiological pH are marked in red.

Exp.	$Fe(OH)_2(H_2L)^{+}$	$Fe(OH)_2(H_2L)_2^{+}$
248.0	303.2	306.2
274.0	363.9	357.8
480.0	486.7	428.3

As can be deduced from the spectra and the structure of the involved MOs, the nature of the involved transitions confirms what was previously reported.[15,22] The electronic transitions at 407 and 428 nm for Cu and Fe complexes, respectively, can be attributed to ligand to metal charge transfer (LMCT), that is from the phenolate to the metal center. The electronic transition with significantly lower intensity that in the Cu complex appears at 600 nm is a d–d transition.

Coordination of the ligand by the phenolate is confirmed in line with what previously suggested. However, the present investigation demonstrates that the ligand does not coordinate in deprotonated form because the phenolate moiety is formed by transfer of the proton from the OH group to the NH one.

3. Conclusion

In the present paper a combined theoretical and experimental approach was used to scrutinize the ability of a newly synthesized *N,O* chelating ligand **1** to selectively form stable complexes with copper and, therefore, leave unaltered the concentration of essential metal ions. Developing a multistep synthesis procedure, the ligand was prepared and examined for its complexation capability of both Cu(II) and Fe(III) by potentiometric measurements and UV-Vis spectroscopy. DFT quantum mechanical calculations were performed to identify the most reliable geometrical structures of the detected complexes at different metal-to-ligand ratios suggested by experiments. The comparison between experimental and simulated UV-Vis spectra allowed to discard many possible alternatives. Although the available coordination sites are five, very likely due to geometric and steric constraints, all the optimizations carried out to go beyond tri-coordination failed. The preferred form for the ligand to bind to the metal is what we named zwitterionic, obtained by migration of a proton from one of the phenol OH to one of the secondary nitrogen.

Experiments supported by calculations show that the affinity of the ligand for Fe(III) is higher than for Cu(II). The combined experimental and theoretical strategy used here will be applied in the future for testing the propensity of new ligands to selectively bind to toxic metal cations.

Experimental Section

Synthesis of ligand 1

All reagents were purchased from Sigma-Aldrich or Alpha Aesar and used without purification. Solvents are purified and dried through classical procedures. Reactions were monitored by TLC using silica plates 60-F264 commercially available from Merck. ^{1}H and ^{13}C APT NMR spectra were recorded at 300 and 75 MHz, respectively, in $CDCl_3$, CD_3OD and DMSO-d_6 using tetramethylsilane (TMS) as the internal standard (Bruker (Billerica,MA,USA) ACP300 MHz). Chemical shifts are given in parts per million and coupling constants in Hertz. Spectra ^{1}H and ^{13}C APT NMR of compounds **1**, **4**, **6**, **7** and **9** are reported in Supporting Information (SI).

Synthesis of N-*Ph*-O,O′-*Ts-diethanolamine (4).*

To a solution of *N*-phenyldiethanolamine **2** (5.0 g, 27.5 mmol) in 25 ml of dry pyridine, *para*-toluensulfonyl chloride **3** (6.4 ml, 66.6 mmol) was slowly added at 0 °C. The mixture was allowed to react at room temperature for 3 h. At the end of reaction, the pale yellow solution was put into a beaker containing ice water and stirred fast. The precipitated solid was filtered under vacuum and recrystallized from ethanol/toluene, isolating 10.77 g of **4** as a colourless crystalline solid in 80% yield.

^{1}H NMR ($CDCl_3$): δ (ppm) 2.42 (s, 6H, CH_3), 3.54 (t, J = 6.03 Hz, 4H, CH_2), 4.08 (t, J = 6.03 Hz, 4H, CH_2), 6.41 (d, J = 8.19 Hz, 2H, Ar), 6.70 (t, J = 7.27 Hz, 1H, Ar), 7.12 (t, J = 7.93 Hz, 2H, Ar), 7.27 (d, J = 7.93 Hz, 4H, Ar), 7.70 (d, J = 8.19 Hz, 4H, Ar). ^{13}C APT NMR ($CDCl_3$): δ (ppm) 21.66, 50.18, 66.62, 112.04, 117.60, 127.85, 129.49, 129.91, 132.62, 145.01, 145.76.

Synthesis of N-*Ph*-N,N-*bis-ethylene-phthalymide (6).*

Phthalimide potassium **5** (7.5 g, 40.4 mmol) was added to a solution of compound **4** (5.0 g, 10.2 mmol) solved in 150 ml of acetonitrile and the mixture was heated at reflux for 5 h. When the reaction was over, the solvent was removed under reduced pressure and water (80 ml) was added. The aqueous mixture was extracted with dichloromethane (3 × 25 ml) and the organic phase was dried with anhydrous sodium sulphate, filtered and evaporated under vacuum, obtaining 5.84 g of yellow solid **6** that were used in the subsequent reaction without any purification.

^{1}H NMR (DMSO-d_6): δ (ppm) 3.51–3.60 (m, 4H, CH_2), 3.67–3.79 (m, 4H, CH_2), 6.51 (t, J = 7.07 Hz, 1H, Ar), 6.82 (d, J = 8.10 Hz, 2H, Ar), 7.08 (t, J = 8.10 Hz, 2H, Ar), 7.76–7.89 (m, 8H, Ar). ^{13}C APT NMR (DMSO-d_6): δ (ppm) 39.88, 52.84, 116.88, 121.39, 128.11, 134.22, 136.69, 139.48, 152.14, 173.00.

Synthesis N-*Ph*-N,N-*bis-ethylamine (7)*

The compound **6** (2.0 g, 4.55 mmol) was solved in 40 ml of THF and aqueous hydrazine (11.35 ml, 363 mmol) was gently added. The mixture was stirred for 2 h at room temperature. Then, the solvent was removed by rotary evaporation and the residue was washed with hexane, isolating 2.86 g of an orange oil (**7**, 96% yield).

^{1}H NMR ($CDCl_3$): δ (ppm) 2.19 (s_b, 4H, NH_2), 2.91 (t, J = 6.60 Hz, 4H, CH_2), 3.41 (t, J = 6.60 Hz, 4H, CH_2), 6.61–6.77 (m, 3H, Ar), 7.15–7.25 (m, 2H, Ar). ^{13}C APT NMR ($CDCl_3$): δ (ppm) 39.50, 54,46, 112.53, 116,54, 129,21, 148,13.

Synthesis of N-*Ph*-N,N-*bis-ethylene-(*o–*hydroxyphenyl-methane-yl)- imine (9)*

To a solution of **7** (1.0 g, 5.58 mmol) in degased sodium acetate buffer, (0.1 M, pH 4.5), salicylaldehyde (1.89 ml, 25.5 mmol) in dry MeOH (40 ml) was added dropwise under nitrogen and the reaction was heated at 100 °C for 20 h. During the reaction, a brown gummy precipitate was observed. Then, the mixture was extracted in dichloromethane, dried with anhydrous sodium sulphate, filtered and evaporated under vacuum. The crude was purified by flash chromatography (exane/ethyl acetate, 6 : 4 v:v). A solid yellow was isolated in 90% yield (**9**, 1.96 g).

^{1}H NMR ($CDCl_3$): δ (ppm) 3.65–3.73 (m, 4H, CH_2), 3.73–3.81 (m, 4H, CH_2), 6.70–6.79 (m, 3H, Ar), 6.80–6.89 (m, 2H, Ar), 6.92–6.99 (m, 2H, Ar), 7.11–7.18 (m, 2H, Ar), 7.22–7.34 (m, 4H, Ar), 8.20 (s, 2H, N=CH), 13.32 (s_b, 2H, OH). ^{13}C APT NMR ($CDCl_3$, 75 MHz): δ (ppm) 52.76, 57.16, 114.40, 116.83, 117.02, 118.66, 118.74, 129.58, 131.37, 132.36, 146.92, 161.07, 166.48.

Synthesis of N-*Ph*-N,N-*bis-ethylene-(*o–*hydroxyphenyl-methylene)-amine (1)*

To a degased solution of **9** (0.50 g, 1.30 mmol) in dry methanol, sodium borohydride (0.39 g, 1.04 mmol) was added at 0° C under nitrogen and the mixture was stirred for 1 h. The mixture was treated with diluted hydrochloric acid and extracted with ethyl acetate. The organic phase was dried with anhydrous sodium sulphate, filtered and evaporated under vacuum. The crude was purified by recrystallization with ethyl acetate/methanol, isolating a pale orange solid in 92% yield (**1**, 0.47 g).

^{1}H NMR (CD_3OD): δ (ppm) 2.92 (s_b, 4H, CH_2), 3.56 (m, 4H, CH_2), 3.87 (m, 4H, CH_2), 6.68–6.88 (m, 7H, Ar), 7.02–7.25 (m, 6H, Ar). ^{13}C APT NMR (CD_3OD): δ (ppm) 38.40, 46.71, 50.79, 114.66, 118.61, 119.09, 120.28, 124.52, 129.96, 130.32, 140.71, 149.08, 157.95.

Potentiometric and spectrophotometric details

The sodium hydroxide titrant solutions, the hydrochloric acid, the sodium chloride and the metal cations chloride stock solutions were prepared and standardized as previously described.[14] All solutions were prepared with bidistilled water. The titrations were carried out with the same apparatus described previously.[11] The glass electrodes were manufactured by Metrohm; they acquired a constant potential within 30 minutes after the addition of the reagents. To avoid carbonate interference, a slow stream of nitrogen gas was passed through three bottles (a–c) containing: (a) 1 M NaOH, (b) 1 M H_2SO_4 and (c) 0.16 M NaCl, and then into the test solutions, stirred during titrations, through the gas inlet tube. The cell assembly was placed in a thermostat kept at (37.0 ± 0.1) °C. The spectrophotometric measurements were carried out with a Varian Cary 50 Scan UV Visible Spectrophotometer. Absorbance values between (240 and 800) nm were measured each 1 nm. The temperature of the cell holder was kept at (37.0 ± 0.3) °C by a Grant circulating water bath. Matched quartz cells of thickness 1 cm were employed. The absorbance, A_λ, was recorded to 0.001 units.

Computational details

The geometries of the copper(II) and iron(III) complexes were optimized at the DFT level of theory using the hybrid Becke three parameter exchange functional[23] and the Lee-Yang-Parr correlation functional[24] B3LYP. In order to properly take into account non-bonding interactions, that play a very important role in the present case, Grimme dispersion correction[25] have been included using atom pair-wise additive scheme, DFT-D3 method. Recontracted LANL2DZ effective core potential[26] and corresponding valence basis set was used to describe Cu and Fe atoms, whereas the. 6-31G* basis set was adopted to describe all the other atoms. Calculations were carried out by means of the Gaussian09 software package.[27] All the structures were fully relaxed without imposing any constrain and were confirmed to be minima by harmonic vibrational frequencies. For all the complexation equilibria free energies were calculated for the substitution and release of water molecules in the reference hexaaquo complexes, that is square planar around the metal cation with four water molecules in the first shell and two water molecules in the second coordination shell for Cu(II)[20,21]] and octahedral for Fe(III).

The overall process in solution corresponds to:

$$[M(H_2O)_6]^z + \{nL\}^c \rightarrow [ML]^{c+z} + (6-n-t)H_2O \quad (6)$$

where $L = L^{2-}$, HL^-, H_2L and OH^-; c is the total formal charge of the n ligands; z the charge of the hexaaquo complex; and t = 0,1, 2, 3 takes into account the possibility that the ligands are mono, bi or tridentate. Therefore, the formation energies of these complexes were calculated as:

$$\Delta G = \Delta G([ML]^{c+z}) + (6-n-t)\Delta G(H_2O) - \Delta G([M(H2O)_6]^z - \Delta G(nL)^c \quad (7)$$

the stability constant (log β) value is related to free energy change for the complexation reaction by the following equation:

$$log\beta = -\Delta G/2.303RT \quad (8)$$

To simulate the aqueous environment, the implicit SMD solvation model, with a dielectric constant of 78.35, was employed. Enthalpies and Gibbs free energies were obtained using standard statistical procedures at 298 K and 1 atm from total energies, including zero-point, thermal and solvent corrections. As the free energy corrections in the Gaussian's default standard state corresponds to an ideal gas at a standard pressure of 1 atm, the computed free energies have been converted[28] to yield Gibbs energies with a solution phase standard state of 1 mol L^{-1} for all the species except water solvent. For water molecules a standard state of 55.5 M was used. Cu(II) and Fe(III) hexaaquo complexes were used for establishing the most stable spin state of the investigated complexes, which resulted to be doublet and sextet, respectively. Spin multiplicity was also tested and confirmed for some of the metal:ligand complexes. Several computational protocols were tested for the calculation of the UV-Vis absorption spectra in water using the time-dependent extension of DFT, TDDFT. Calculations using more extended basis sets together with a series of xc functionals and solvent models were tested. The best performing adopted protocol was CAM–B3LYP xc functional[29] in conjunction with the recontracted LANL2DZ pseudo potential for metals and 6–31G* basis set for the rest of the atoms and SMD to simulate implicit solvent.

Acknowledgements

University of Calabria and Calabria Region (PAC CALABRIA 2014–2020 – Asse Prioritario 12, Azione B) 10.5.12 CUP: H28D19000040006) are acknowledged for financial support.

Conflict of Interest

The authors declare no conflict of interest.

Keywords: *N,O* chelating ligand · Cu(II) and Fe(III) complexes · DFT · neurodegenerative diseases · stability constants

[1] G. Livingston, A. Sommerlad, V. Orgeta, S. G. Costafreda, J. Huntley, D. Ames, C. Ballard, S. Banerjee, A. Burns, J. Cohen-Mansfield, C. Cooper, N. Fox, L. N. Gitlin, R. Howard, H. C. Kales, E. B. Larson, K. Ritchie, K. Rockwood, E. L. Sampson, Q. Samus, L. S. Schneider, G. Selbæk, L. Teri, N. Mukadam, *The Lancet* **2017**, *390*, 2673–2734.
[2] P. Scheltens, K. Blennow, M. M. Breteler, B. de Strooper, G. B. Frisoni, S. Salloway, W. M. Van der Flier, *The Lancet* **2016**, *388*, 505–517.
[3] J. Hardy, D. Allsop, *Trends Pharmacol. Sci.* **1991**, 12, 383–388.
[4] K. Herrup, *Nat. Neurosci.* **2015**, *18*, 794–799.
[5] T. B. Chaston, D. R. Richardson, *JBIC J. Biol. Inorg. Chem.* **2003**, *8*, 427–438.
[6] V. M. Nurchi, M. Crespo-Alonso, L. Toso, J. I. Lachowicz, G. Crisponi, *Mini-Rev. Med. Chem.* **2013**, 13, 1541–1549.
[7] O. Bortolini, I. Mulani, A. De Nino, et al., *Tetrahedron* **2011**, *67*, 5635–5641.
[8] O. Bortolini, G. Fantin, M. Fogagnolo, S. Rossetti, L. Maiuolo, G. Di Pompo, S. Avnet, D. Granchi, *Eur. J. Med. Chem.* **2012**, *52*, 221–229.
[9] P. Merino, L. Maiuolo, I. Delso, V. Algieri, A. De Nino, T. Tejero, *RSC Adv.* **2017**, *7*, 10947–10967.
[10] O. Bortolini, I. Mulani, A. De Nino, L. Maiuolo, A. Melicchio, B. Russo, D. Granchi, *Curr. Org. Synth.* **2014**, *11*, 461–465.
[11] E. Furia, *J. Solution Chem.* **2017**, 46, 1596–1604.
[12] D. Aiello, E. Furia, C. Siciliano, D. Bongiorno, A. Napoli, *J. Mol. Liq.* **2018**, *269*, 387–397.
[13] E. Furia, A. Beneduci, N. Russo, T. Marino New, *J. Chem.* **2018**, *42*, 11006–11012.
[14] A. Beneduci, G. A. Corrente, T. Marino, et al., *J. Mol. Liq.* **2019**, *296*, 111805–111814.
[15] A. Rakshit, K. Khatua, V. Shanbhag, P. Comba, A. Datta, *Chem. Sci.* **2018**, *9*, 7916–7930.
[16] I. D. Kostas, *J. Organomet. Chem.* **2001**, *626*, 221–226.
[17] R. Nguyen, N. Jouault, S. Zanirati, et al., *Soft Matter* **2014**, *10*, 3926–3937.
[18] C. F. Baes, R. E. Mesmer, The Hydrolysis of Cations; A Wiley-Interscience Publication: New York, **1976**.
[19] P. Gans, A. Sabatini, A. Vacca, *J. Chem. Soc. Dalton Trans.* **1985**,, 1195–1200.
[20] R. Rios-Font, M. Sodupe, L. Rodríguez-Santiago, P. R. Taylor, *J. Phys. Chem. A* **2010**, *114*, 10857–10863.
[21] A. Bérces, T. Nukada, P. Margl, T. Ziegler, *J. Phys. Chem. A* **1999**, *103*, 9693–9701.
[22] S. Y. Ebrahimipour, I. Sheikhshoaie, J. Castro, et al., *Inorg. Chim. Acta* **2015**, *430*, 245–252.
[23] A. D. Becke, *J. Chem. Phys.* **1993**, *98*, 5648–5652.
[24] C. Lee, W. Yang, R. G. Parr, *Phys. Rev. B* **1988**, *37*, 785–789.
[25] S. Grimme, J. Antony, S. Ehrlich, H. Krieg, *J. Chem. Phys.* **2010**, *132*, 154104.
[26] S. Chiodo, N. Russo, E. Sicilia, *J. Chem. Phys.* **2006**, *125*, 104107.
[27] M. J. Frisch, G. W. Trucks, H. B. Schlegel, G. E. Scuseria, M. A. Robb, J. R. Cheeseman, G. Scalmani, V. Barone, G. A. Petersson, H. Nakatsuji, X. Li, M. Caricato, A. Marenich, J. Bloino, B. G. Janesko, R. Gomperts, B. Mennucci, H. P. Hratchian, J. V. Ortiz, A. F. Izmaylov, J. L. Sonnenberg, D. Williams-Young, F. Ding, F. Lipparini, F. Egidi, J. Goings, B. Peng, A. Petrone, T. Henderson, D. Ranasinghe, V. G. Zakrzewski, J. Gao, N. Rega, G. Zheng, W. Liang, M. Hada, M. Ehara, K. Toyota, R. Fukuda, J. Hasegawa, M. Ishida, T. Nakajima, Y. Honda, O. Kitao, H. Nakai, T. Vreven,

K. Throssell, J. A. Montgomery Jr., J. E. Peralta, F. Ogliaro, M. Bearpark, J. J. Heyd, E. Brothers, K. N. Kudin, V. N. Staroverov, T. Keith, R. Kobayashi, J. Normand, K. Raghavachari, A. Rendell, J. C. Burant, S. S. Iyengar, J. Tomasi, M. Cossi, J. M. Millam, M. Klene, C. Adamo, R. Cammi, J. W. Ochterski, R. L. Martin, K. Morokuma, O. Farkas, J. B. Foresman, D. J. Fox, Gaussian 09, Revision D. 01, Gaussian. *Inc.: Wallingford, CT* **2009**.

[28] A. V. Marenich, C. J. Cramer, D. G. Truhlar, *J. Phys. Chem. B* **2009**, *113*, 6378–6396.

[29] C. A. Guido, S. Knecht, J. Kongsted, B. Mennucci, *J. Chem. Theory Comput.* **2013**, *9*, 2209–2220.

Manuscript received: June 25, 2020
Accepted manuscript online: August 11, 2020
Version of record online: September 9, 2020

CHEMISTRY
AN ASIAN JOURNAL

Supporting Information

Sequestering Ability of a Synthetic Chelating Agent towards Copper(II) and Iron(III): A Detailed Theoretical and Experimental Analysis

Alessandra G. Ritacca, Luana Malacaria, Vincenzo Algieri, Antonio De Nino, Nino Russo, Emilia Furia,* Loredana Maiuolo,* and Emilia Sicilia*

Table S1

Compound	λ	*f*	Transitions	λ_{exp}
H_2L	238.6	0.3891	H->L+5 (92%)	241.0
	275.3	0.0399	H->L+3 (75%)	272.0
H_2L zwitt	239.7	0.2049	H-1->L+3 (79%)	
	270.4	0.091	H->L+3 (69%)	
	315.2	0.0026	H->L (100%)	
HL^-	239.5	0.3525	H-1->L+4 (92%)	
	271.3	0.0564	H->L+3 (54%)	
L^{2-}	240.5	0.3183	H-2->L+3 (90%)	
	272.4	0.0925	H-1->L+1 (40%) H->L+1 (31%)	

Figure S1

H_2L	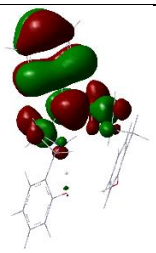 H	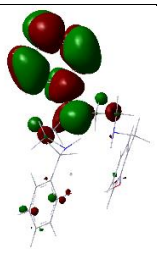 L+5	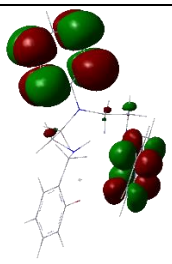 L+3	
H_2L zwitt	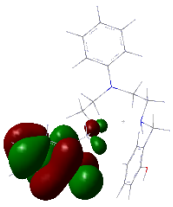 H	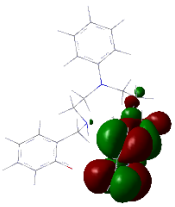 L	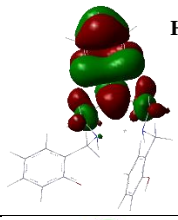 H-1	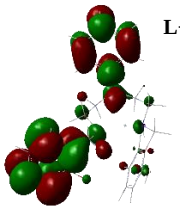 L+3
HL^-	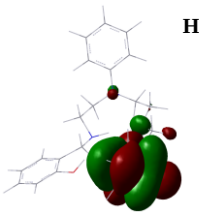 H	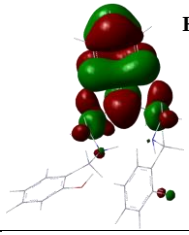 H-1	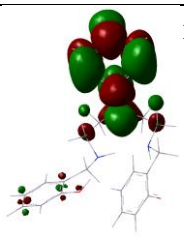 L+4	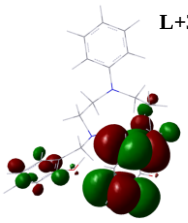 L+3
L^{2-}	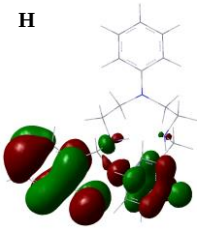 H	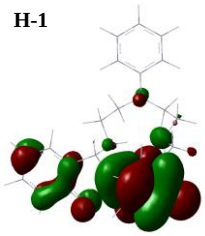 H-1	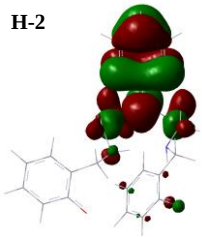 H-2	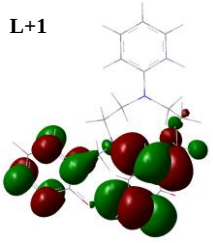 L+1 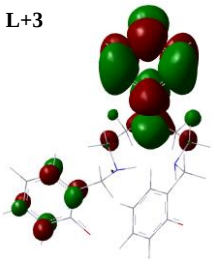 L+3

Table S2

Compound	λ	*f*	Transitions	λ_{exp}
$Cu(H_2L)^{2+}$	271.8	0.0604	H-8(B)->L(B) (44%)	272.0
	325.6	0.0951	H-6(B)->L(B) (77%)	
	458.2	0.0263	H-1(B)->L(B) (63%)	276.0
	634.2	0.0001	H-19(B)->L(B) (63%)	418.0
				621.0
log β = 2.4 $Cu(H_2L)_2^{2+}$	293.9	0.0133	H-7(B)->L(B) (45%) H-2(B)->L(B) (19%)	
	325.5	0.1214	H-15(B)->L(B) (29%) H-6(B)->L(B) (42%)	
	447.8	0.0101	H(B)->L(B) (47%)	
	676.4	0.0061	H (B)->L(B) (4%) H-39(B)->L(B) (13%) H-36(B)->L(B) (14%)	
log β = 12.4 $Cu(H_2L)_2^{2+}$	276.0	0.0493	H-15(B)->L (B) (48%) H-6(B)->L (B) (25%)	
	304.1	0.119	H-12(B)->L (B) (14%) H-11(B)->L(B) (20%) H-3(B)->L(B) (14%)	
	407.6	0.0429	H(B)->L (B) (59%)	
	600.8	0.0024	H-30(B)->L (B) (13%) H-27(B)->L(B) (13%) H-16(B)->L(B) (10%)	
	671.1	0.0007	H-18(B)->L (B) (11%) H-1(B)->L (B) (17%)	
$Cu(H_2L)_3^{2+}$	317.7	0.0683	H-11(B)->L (B) (17%) H-9(B)->L (B) (32%)	
	346.7	0.023	H-2(A)->L+18(A) (8%) H-1(B)->L+19(B) (6%)	
	428.4	0.1026	H-1(B)->L (B) (51%) H(B)->L (B) (26%)	
	601.4	0.0015	H-61(B)->L (B) (20%) H-59(B)->L(B) (19%)	
	705.4	0.0031	H-31(B)->L (B) (17%) H-30(B)->L (B) (19%)	
$Cu(OH)(H_2L)^{+}$	293.9	0.0748	H-11(B)->L (B) (22%) H-9(B)->L (B) (30%)	
	346.4	0.034	H-8(B)->L (B) (22%) H-3(B)->L (B) (24%)	
	455.0	0.03	H(B)->L (B) (69%)	
	689.3	0.0017	H-29(B)->L (B) (12%)	

			H-27(B)->L (B) (29%)	
$Cu_2(OH)_2(H_2L)_2^{2+}$	319.5	0.0723	H-14(B)->L+1(B) (44%) H-14(B)->L (B) (4%)	
	335.6	0.1251	H-15(B)->L(B) (26%) H-15(B)->L+1(B) (4%)	
	471.6	0.0684	H(B)->L (B) (55%) H(B)->L+1(B) (4%)	
	640.8	0.0006	H-49(B)->L+1(B) (18%) H-49(B)->L(B) (2%)	
$Fe(OH)_2(H_2L)^+$	303.2	0.0080	H-1(B)->L+2(B) (30%)	248.0
	363.9	0.0111	H-9(B)->L (B) (50%) H-8(B)->L (B) (26%)	274.0
	486.7	0.0077	H (B)->L(B) (82%)	
				480.0
$Fe(OH)_2(H_2L)_2^+$	319.3	0.0212	H-1(B)->L+3(B) (48%)	
	357.8	0.0135	H-6(B)->L+1(B) (13%)	
	428.3	0.0086	H-1(B)->L (B) (80%)	

Figure S2

	H	L	H-15	H-6
$Cu(H_2L)_2^{2+}$	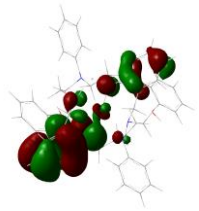	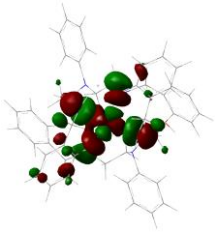	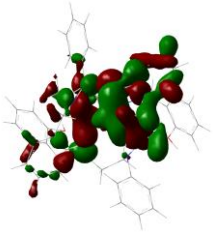	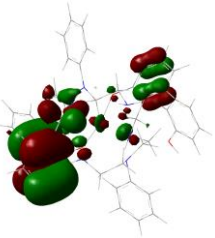
	H-12	**H-11**	**H-3**	**H-30**
	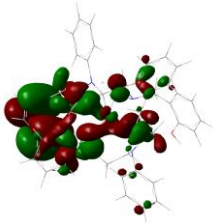		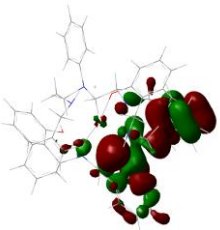	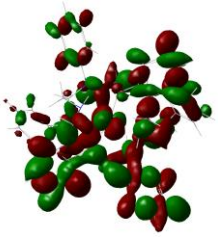
	H-27	**H-16**	**H-18**	**H-1**
	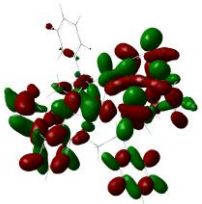	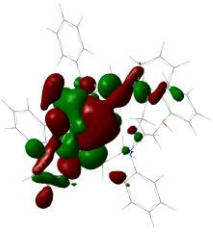	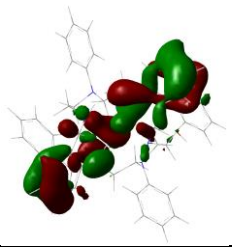	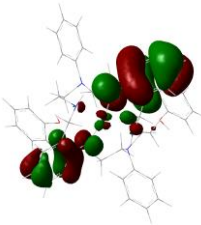

	H-1	L	L+3	H-6
$Fe(OH)_2(H_2L)_2^{+}$	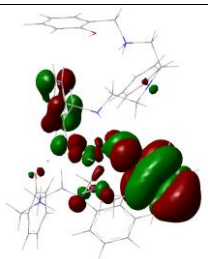	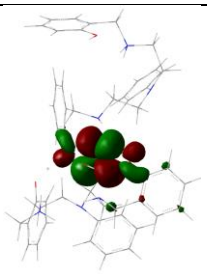	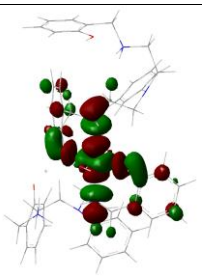	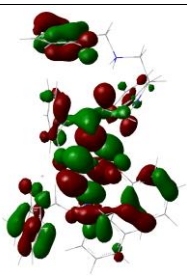
	L+1			
	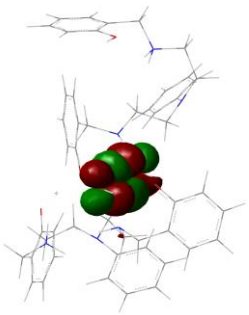			

N-Ph-N,N-bis-ethylene-(o-hydroxyphenyl-methylene)-amine (**1**)

^{1}H NMR

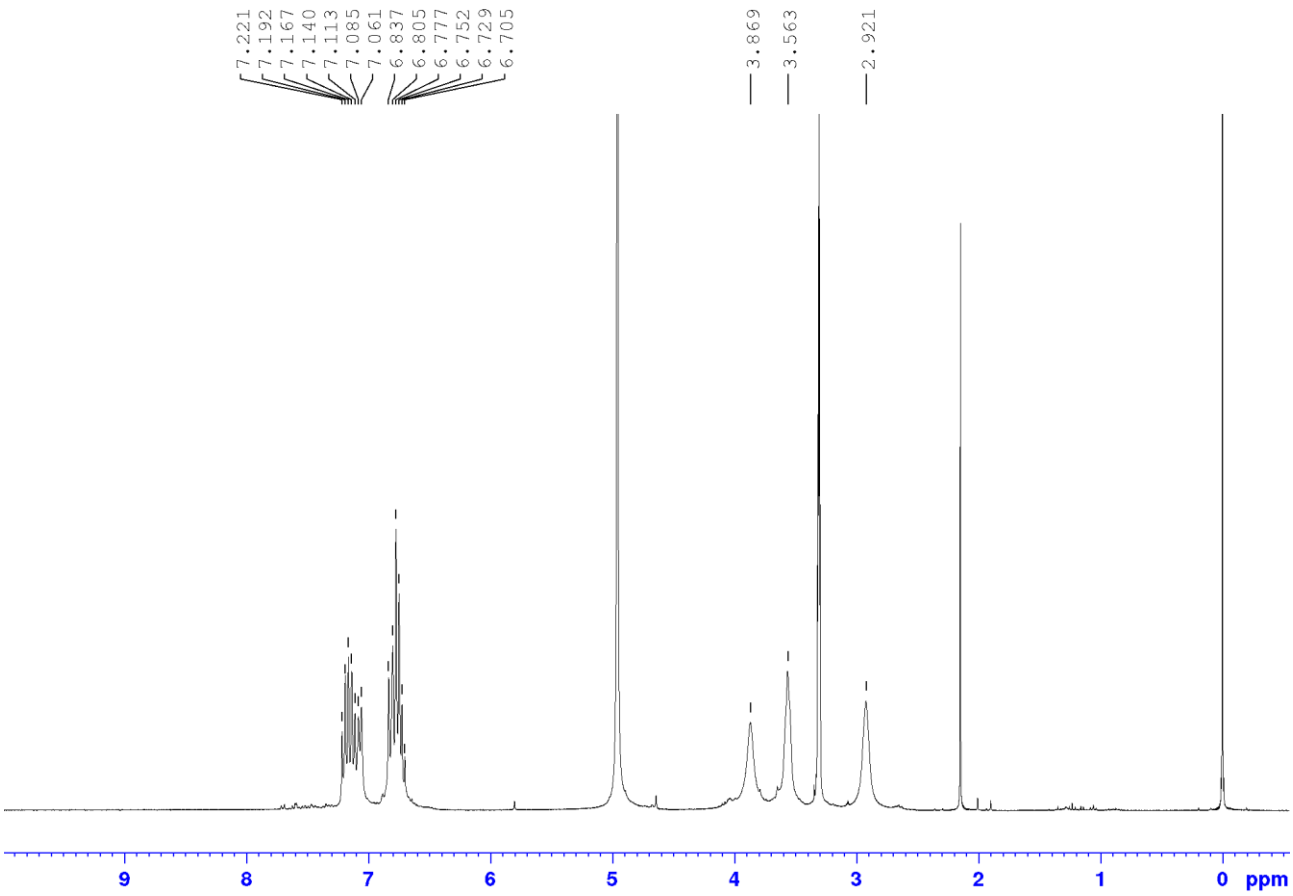

^{13}C APT NMR

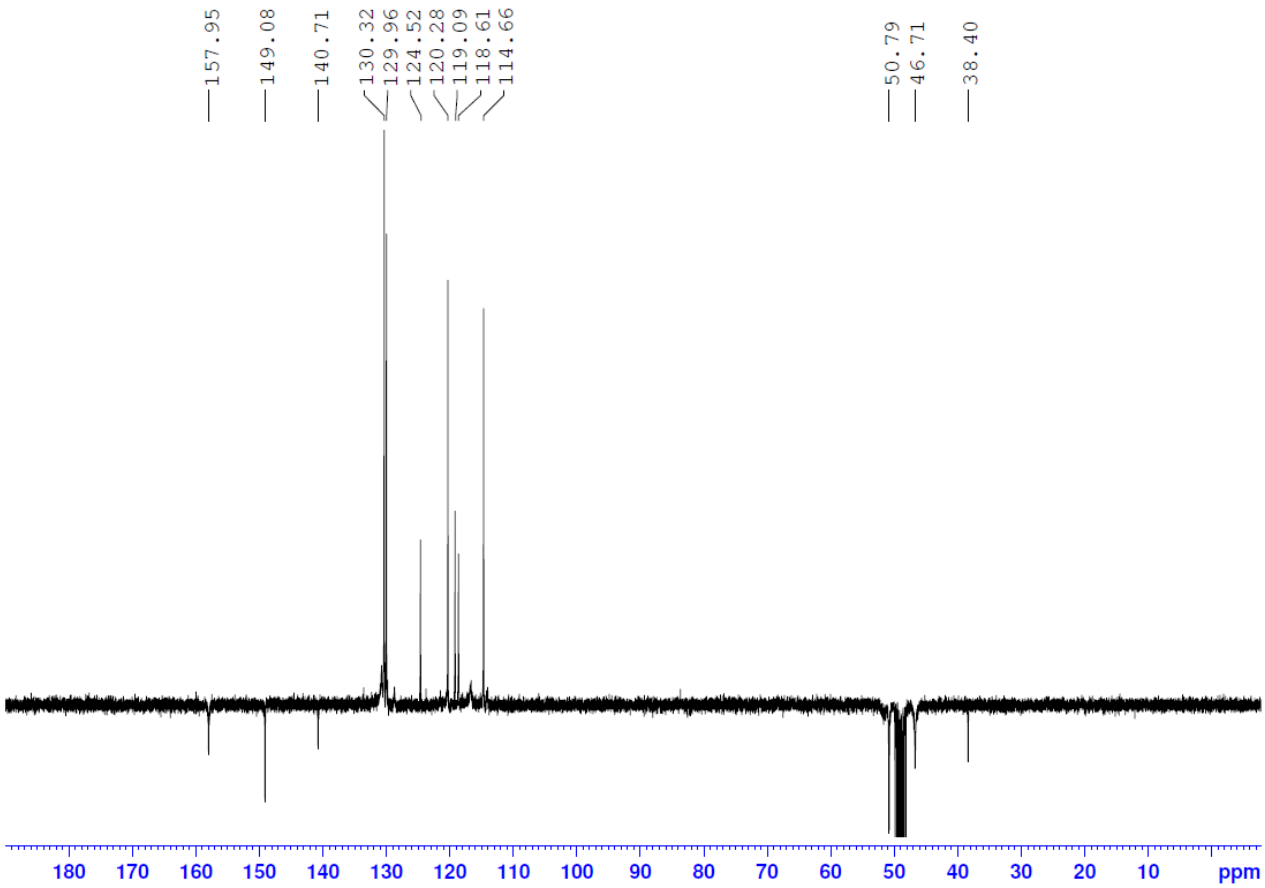
157.95
149.08
140.71
130.32
129.96
124.52
120.28
119.09
118.61
114.66
50.79
46.71
38.40
180
170
160
150
140
130
120
110
100
90
80
70
60
50
40
30
20
10
ppm

N-Ph-O,O'-Ts-diethanolamine **(4)**

^{1}H NMR

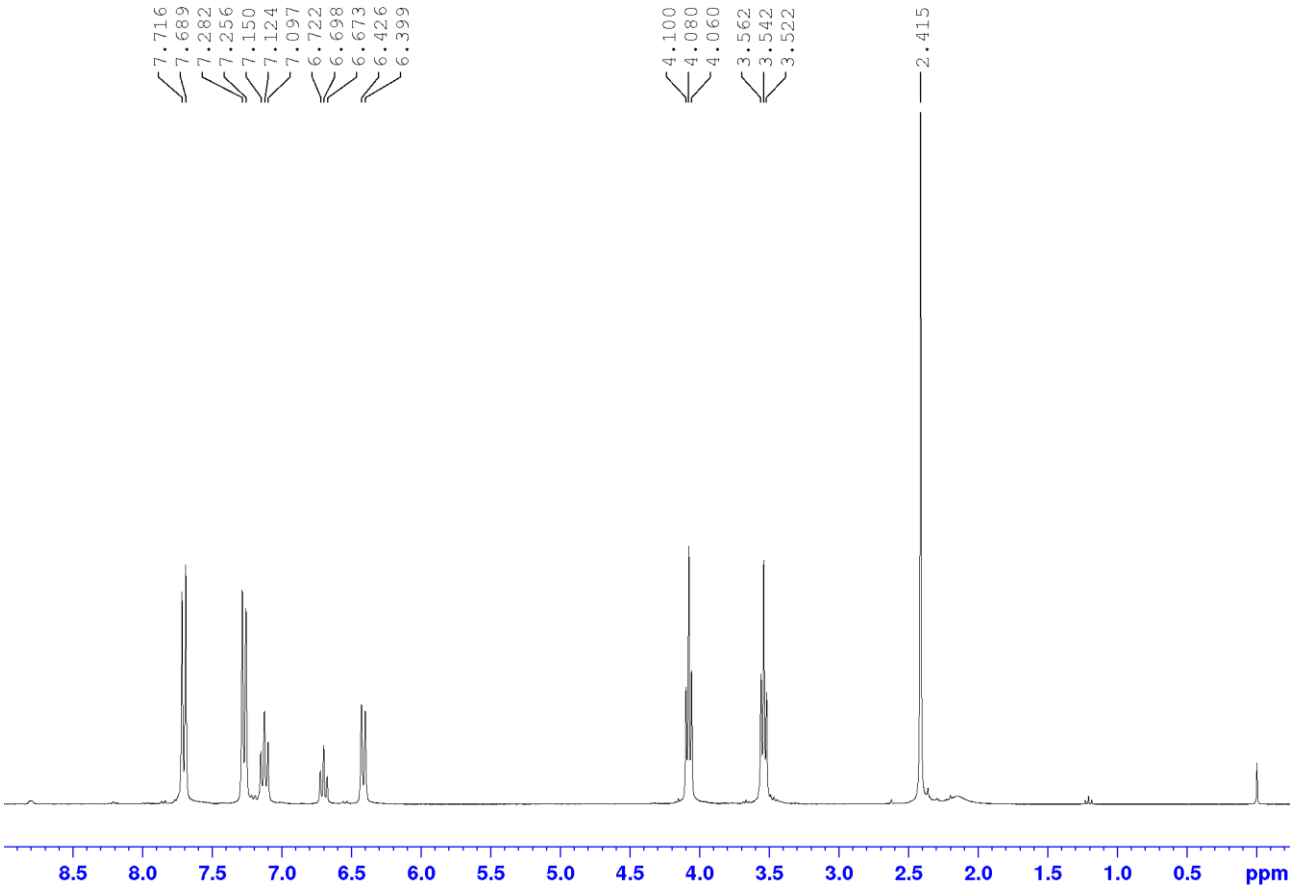

^{13}C APT NMR

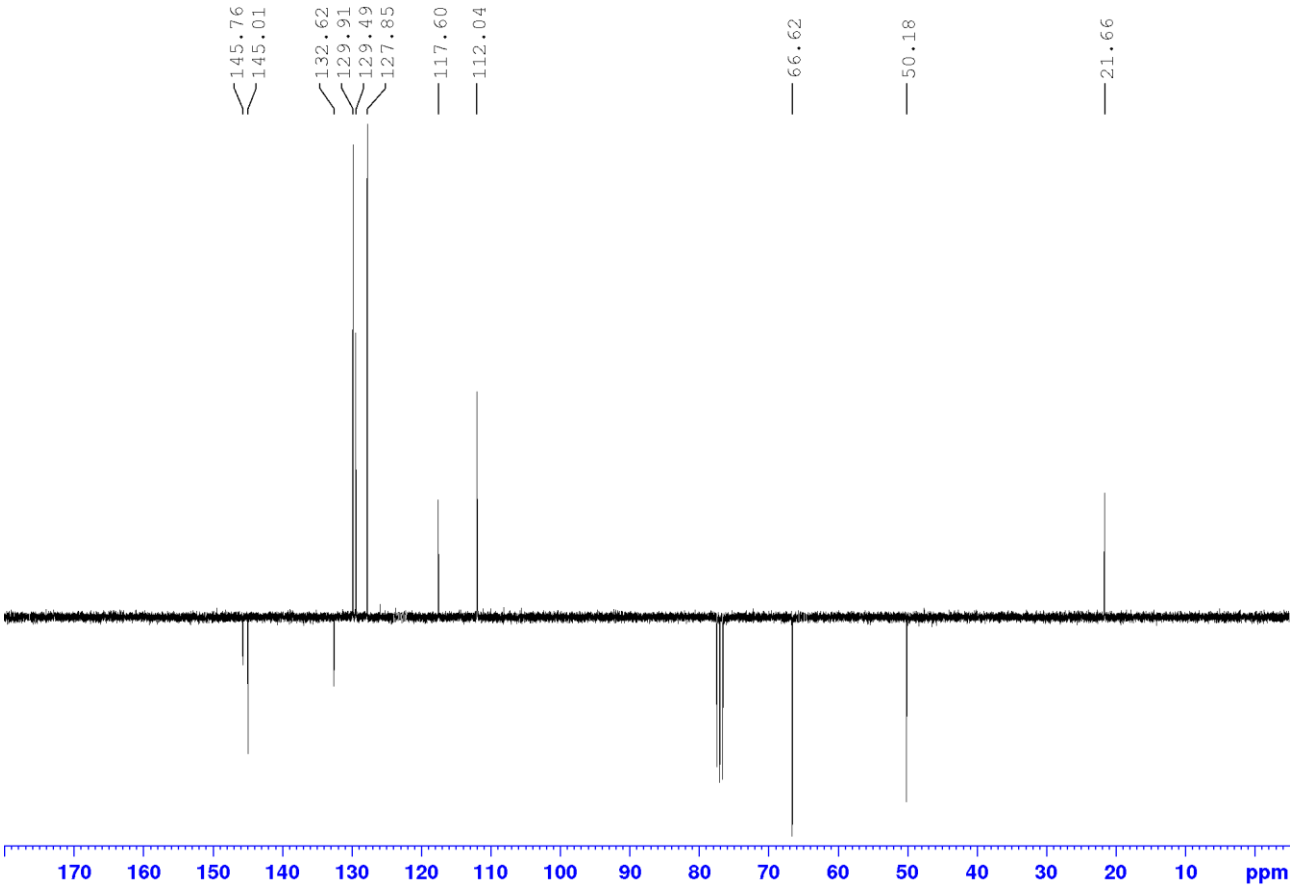
145.76
145.01
132.62
129.91
129.49
127.85
117.60
112.04
66.62
50.18
21.66
170
160
150
140
130
120
110
100
90
80
70
60
50
40
30
20
10
ppm

N-Ph-N,N-bis-ethylene-phthalymide (**6**)

^{1}H NMR

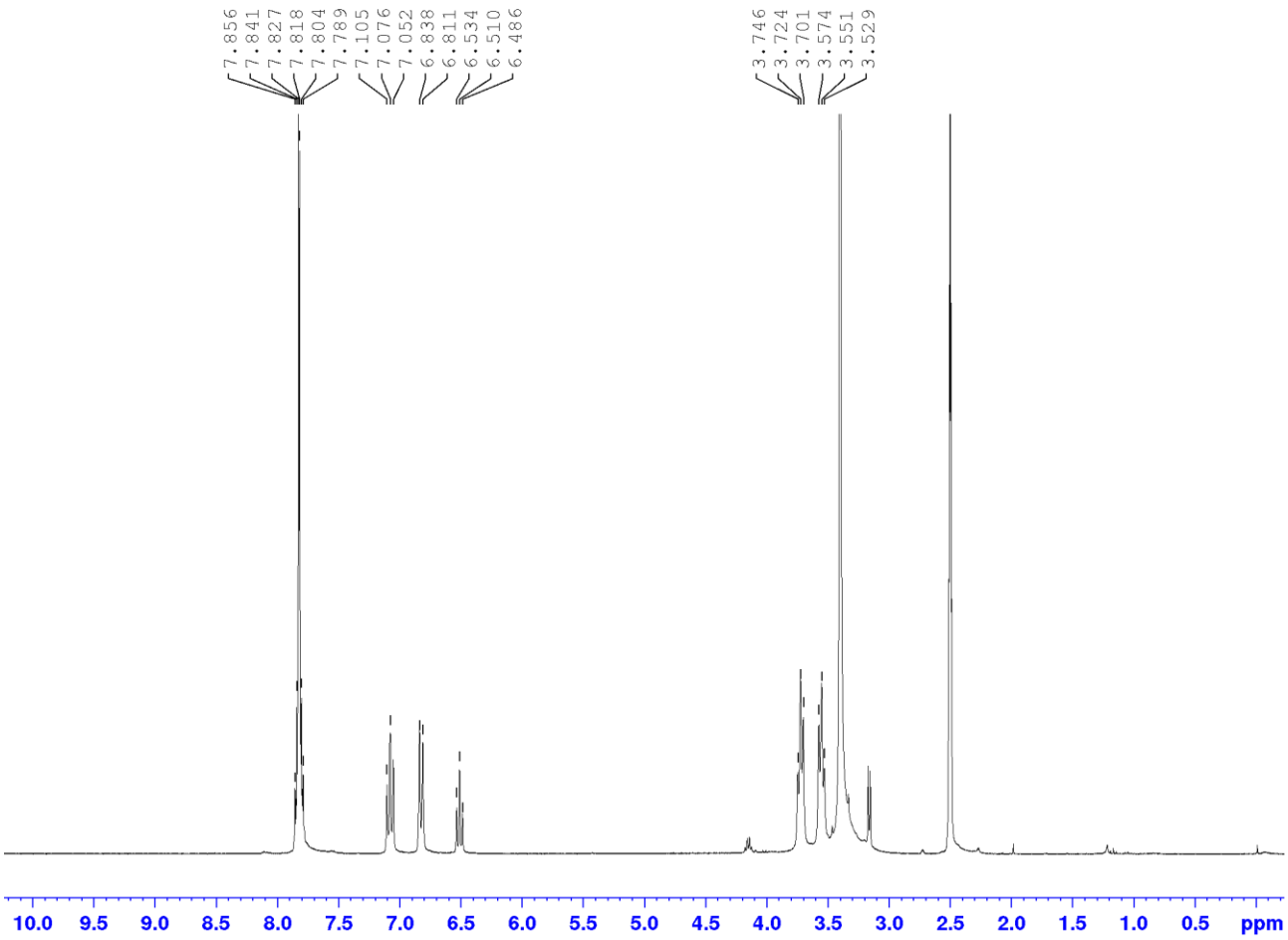

^{13}C APT NMR

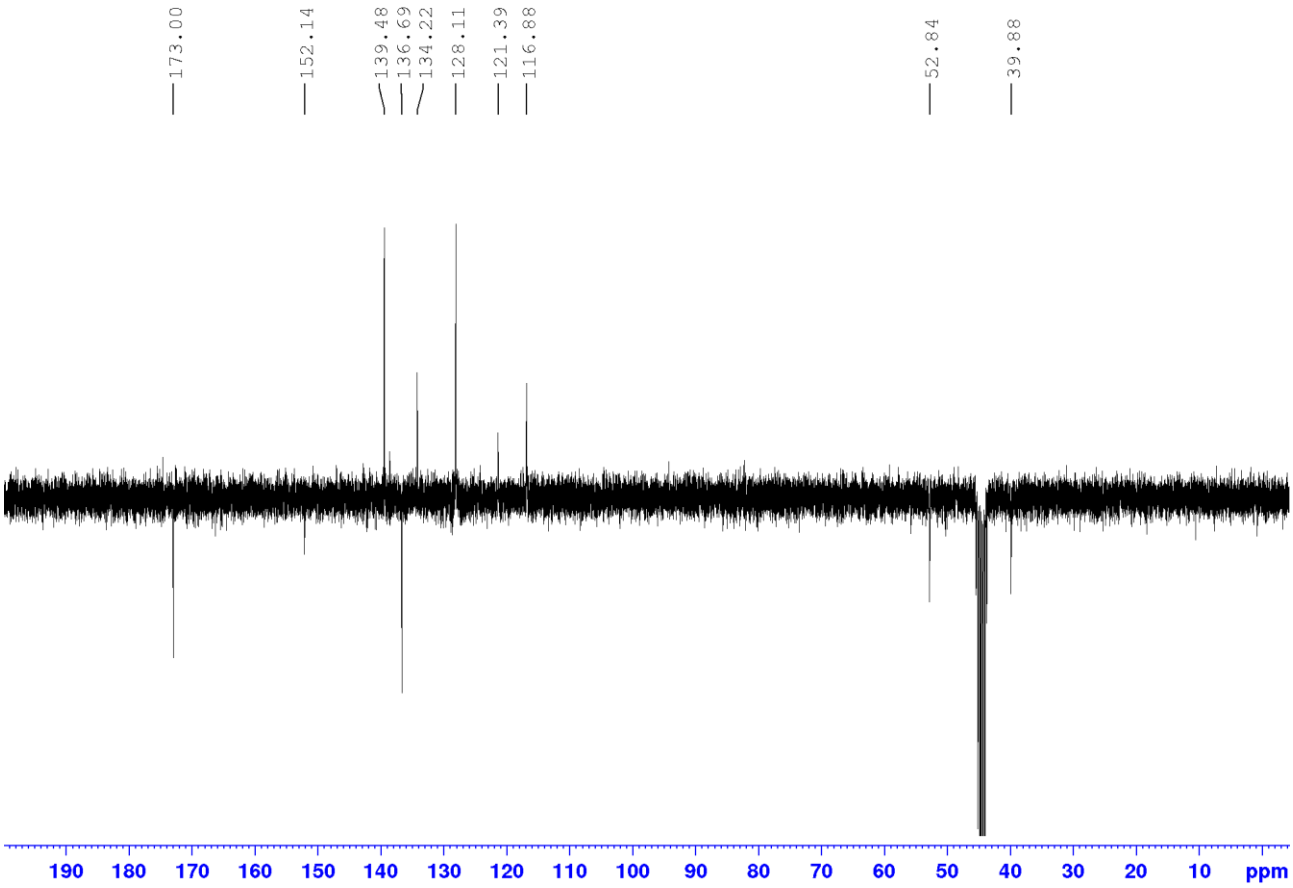
173.00
152.14
139.48
136.69
134.22
128.11
121.39
116.88
52.84
39.88
190 180 170 160 150 140 130 120 110 100 90 80 70 60 50 40 30 20 10 ppm

N-Ph-N,N-bis-ethylamine (**7**)

^{1}H NMR

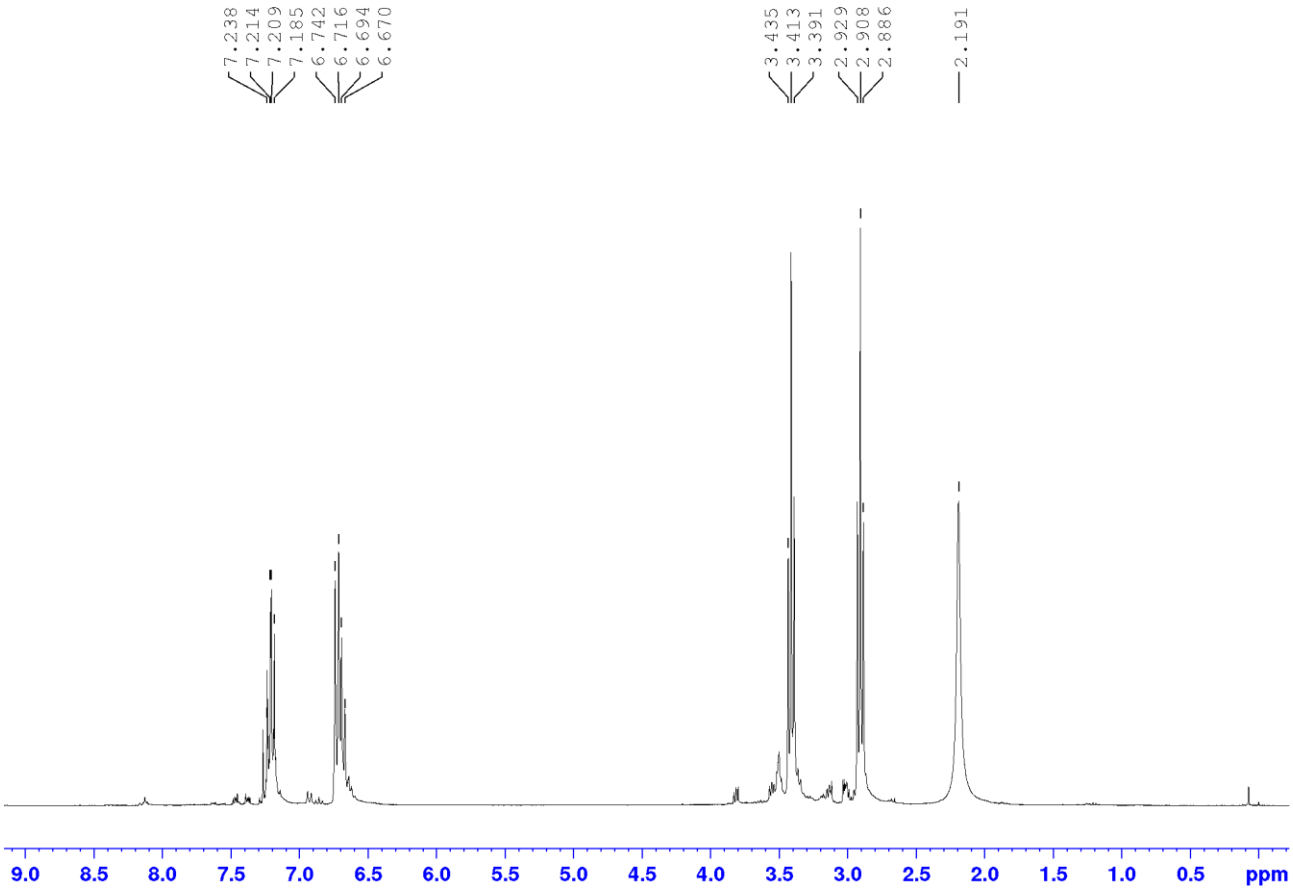

^{13}C APT NMR

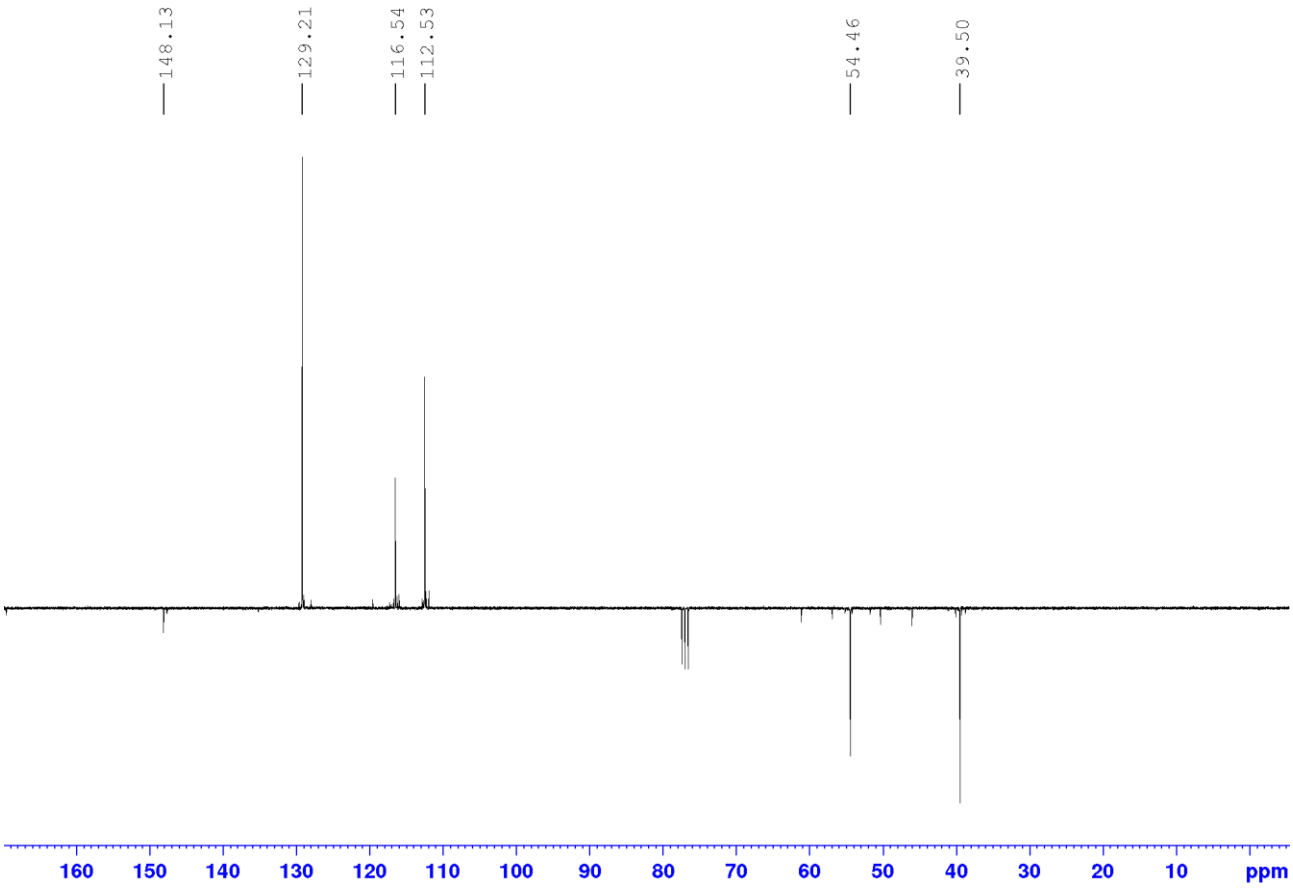
148.13
129.21
116.54
112.53
54.46
39.50
160
150
140
130
120
110
100
90
80
70
60
50
40
30
20
10
ppm

N-Ph-N,N-bis-ethylene-(o-hydroxyphenyl-methane-yl)-imine (**9**)

^{1}H NMR

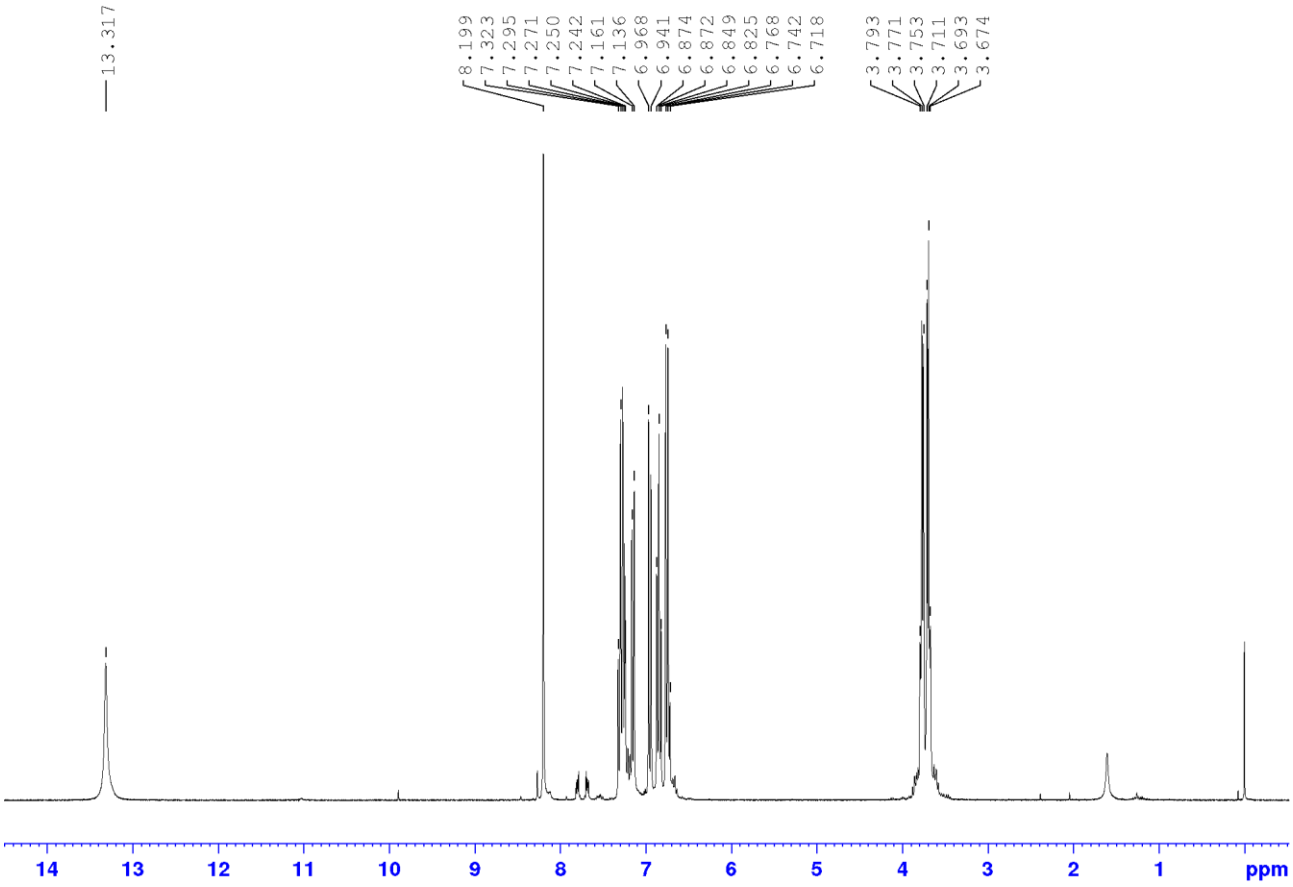

^{13}C APT NMR

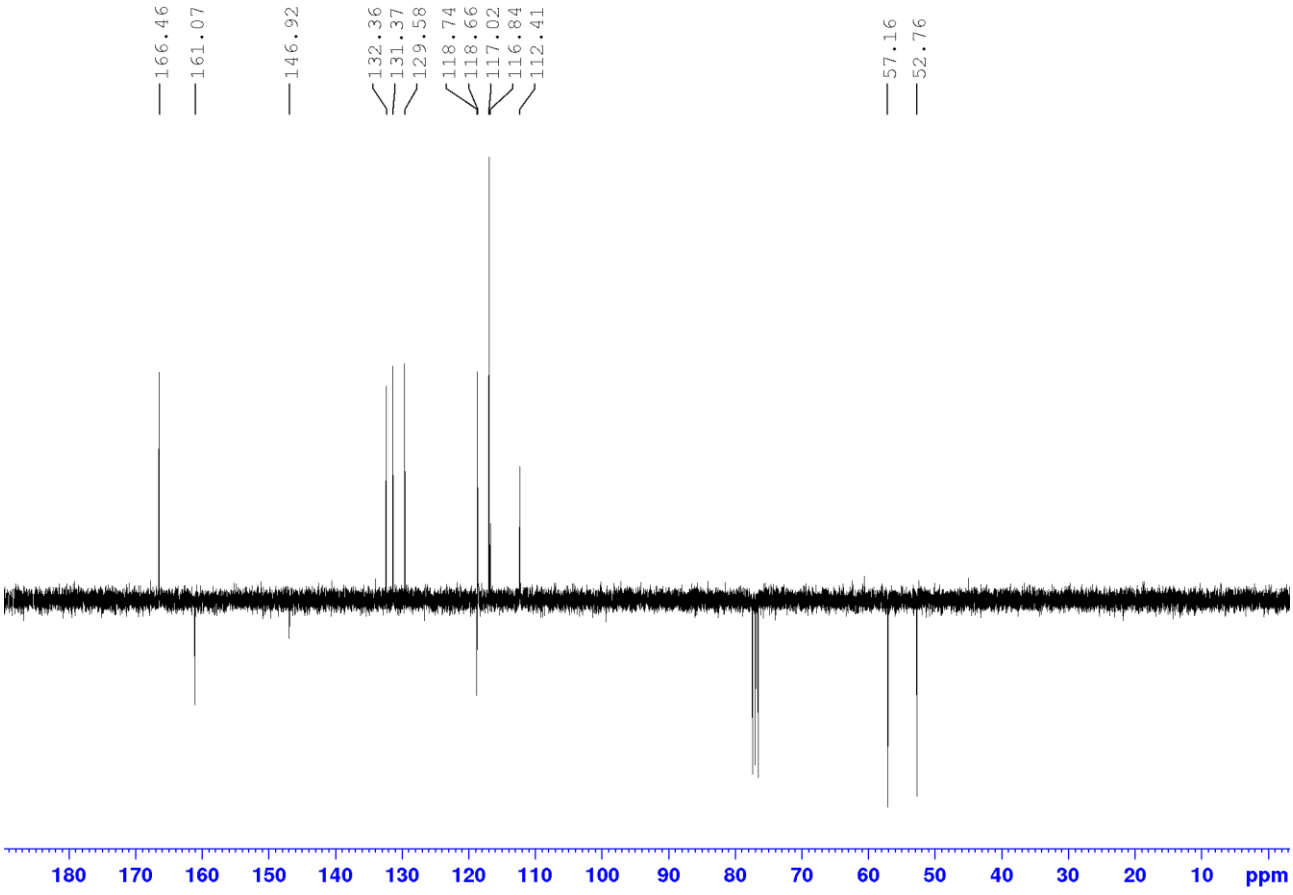
166.46
161.07
146.92
132.36
131.37
129.58
118.74
118.66
117.02
116.84
112.41
57.16
52.76
180
170
160
150
140
130
120
110
100
90
80
70
60
50
40
30
20
10
ppm

molecules

MDPI

Review

A Review on Coordination Properties of Al(III) and Fe(III) toward Natural Antioxidant Molecules: Experimental and Theoretical Insights

Luana Malacaria †, Giuseppina Anna Corrente †, Amerigo Beneduci, Emilia Furia, Tiziana Marino and Gloria Mazzone *

Department of Chemistry and Chemical Technologies, University of Calabria, Via P. Bucci, I-87036 Rende, CS, Italy; luana.malacaria@unical.it (L.M.); giuseppina.corrente@unical.it (G.A.C.); amerigo.beneduci@unical.it (A.B.); emilia.furia@unical.it (E.F.); tiziana.marino65@unical.it (T.M.)

* Correspondence: gloria.mazzone@unical.it

† These authors contributed equally to this work.

Abstract: This review focuses on the ability of some natural antioxidant molecules (i.e., hydroxycinnamic acids, coumarin-3-carboxylic acid, quercetin, luteolin and curcumin) to form Al(III)- and Fe(III)-complexes with the aim of evaluating the coordination properties from a combined experimental and theoretical point of view. Despite the contributions of previous studies on the chemical properties and biological activity of these metal complexes involving such natural antioxidants, further detailed relationships between the structure and properties are still required. In this context, the investigation on the coordination properties of Al(III) and Fe(III) toward these natural antioxidant molecules might deserve high interest to design water soluble molecule-based metal carriers that can improve the metal's intake and/or its removal in living organisms.

Keywords: natural antioxidants; Al(III) complexes; Fe(III) complexes; chelating ability; spectroscopic characterization; DFT

Citation: Malacaria, L.; Corrente, G.A.; Beneduci, A.; Furia, E.; Marino, T.; Mazzone, G. A Review on Coordination Properties of Al(III) and Fe(III) toward Natural Antioxidant Molecules: Experimental and Theoretical Insights. *Molecules* **2021**, *26*, 2603. https://doi.org/10.3390/molecules26092603

Academic Editors: Enrico Bodo and Franck Rabilloud

Received: 21 March 2021
Accepted: 27 April 2021
Published: 29 April 2021

1. Introduction

1.1. Role of Al(III) and Fe(III) Ions

Diseases related to the accumulation of metals, which play several critical roles in the human body, are attracting increasing attention in the scientific community [1]. Under normal conditions, some metals are considered micronutrients, being cofactors of numerous enzymes involved in many biological processes. However, they become toxic if present in relatively high amounts above a certain threshold, especially the first-row transition metal ions (e.g., Fe, Cu, and Zn), which seems to be related to severe degenerative diseases such as Alzheimer's disease [2].

Human exposure to metals has increased over time due to their increased use, particularly with industrialization [3,4]. Toxicity due to metal exposure can also arise from their accidental ingestion through food and beverages (drinking water) [5]. Indeed, metals can be present naturally in many foods, but their uptake can be increased due to food contamination arising from some methods used in the production stages. Prevention and treatment of diseases caused by metals often occurs with the use of coordination compounds [6]. Many organic molecules, in fact, behave as ligands and can form stable complexes with metal ions, used as therapeutic agents for the treatment of metal accumulation. In particular, some transition metal complexes have shown high therapeutic potential in the treatment of different disorders, being used as antitumor, anti-inflammatory, and antidiabetic agents as well as in the treatment of diseases of the nervous system [1,3,6].

In this context, the research into suitable chelating agents against toxic metal ions overload in human tissues and the understanding of their behavior become crucial for

the improvement of chelation therapy [1]. This is a promising strategy for reducing the redox stress lethal for neurons aimed at removing toxic metal ions from the human body or reducing their toxicity by transforming them into less toxic compounds or by dislocating them from the site where they exert a harmful action [6].

This review focuses on the coordination properties of aluminum(III) and iron(III) metal ions, potentially implicated in degenerative processes, since they can be targeted by metal chelators to regenerate the normal trafficking of metal [3].

The source of aluminum in humans is essentially oral intake from food, drinking water, and Al-containing drugs [1,7]. Since the 1970s, this metal has been recognized as the cause of different diseases and as a neurotoxic agent associated with encephalopathies due to its accumulation in brain tissues [8]. Currently, however, aluminum's role in Alzheimer neuropathology is still not clear, although several experimental and clinical evidences have pointed out its implication as a primary etiological factor of Alzheimer's disease [8–10].

Aluminum, with a crystal radius of 0.675 Å (coordination number VI) [11], is a typical hard metal ion. In biological systems, the majority of binding sites for it are negatively charged oxygen donors as carboxylates, phenolates, catecholates, and phosphates. The hydrolytic chemistry of aluminum affects its solubility and its bioavailability in biological environments. At pH $\leq$ 5, the main species is the $[Al(H_2O)_6]^{3+}$ ion; the mononuclear species $Al(OH)^{2+}$ and $Al(OH)_2{}^{+}$ are formed by the deprotonation of coordinated water molecules with increasing pH values. Polynuclear species $Al_2(OH)_2{}^{4+}$ and $Al_3(OH)_4{}^{5+}$ are also formed, but their concentration is strictly related to that of the total aluminum. At neutral pH, a precipitate of $Al(OH)_3$ is formed, while at higher pH, the species $Al(OH)_4{}^{-}$ becomes soluble. The speciation equilibria of the soluble and insoluble forms of the hydroxo complexes and of the complexes with other competing ligands must be considered to better understand and describe the solution chemistry of aluminum in biological systems.

Due to the similar ionic radius of Al(III) and Fe(III) (0.675 Å for Al(III), 0.690 and 0.785 Å for low and high spin Fe(III), respectively) [11], Al(III) can compete with Fe(III) for binding to the biological transporter systems as transferrin. Indeed, high-spin Fe(III) is classified as a hard Lewis acid and, in analogy with Al(III), forms very stable bonds with hard ligands. Iron overload is the most common metal toxicity disease worldwide. Under normal conditions, body iron levels are governed by homeostatic controls of iron uptake, distribution, and storage. Several factors may affect iron absorption: the amount of iron present in the diet, its chemical species, the ligands coordinating iron in the intestine and the presence of other potential iron chelators. Pathological conditions may result from gastrointestinal iron absorption and/or multiple red blood cell transfusions [6].

In this review, experimental and computational results on the ability of some natural antioxidant molecules (NAMs) (i.e., hydroxycinnamic acids, coumarin-3-carboxylic acid, quercetin, luteolin, and curcumin, Scheme 1) to form Al(III)- and Fe(III)-complexes are reported and discussed. Since the coordination chemistry background is necessary to drive the selection of drug candidates suitable to discriminate between different metal ions, the coordination properties of Al(III) and Fe(III) in aqueous solution toward the selected NAMs shown in Scheme 1 were investigated. Understanding the interactions of these metals with this class of ligands is helpful to design water soluble molecule-based metal carriers aimed to improve the metal's intake and/or its removal in living organisms.

1.2. Choice of the Ligands

On the basis of the structure–activity relationship, several NAMs are well known to be effective metal chelators due to the presence of carbonyl groups as well as of phenolic hydroxyls, and carboxylic groups that, regardless of their pK_a values, can be deprotonated upon metal interaction. Thus, their ability to bind transition metal ions make these classes of molecules particularly interesting to counteract the metal-related damage. Among the numerous NAMs able to exert such activity, we focused on those derivatives whose chelating ability was investigated in aqueous solution, an environment that better mimics the physiological one.

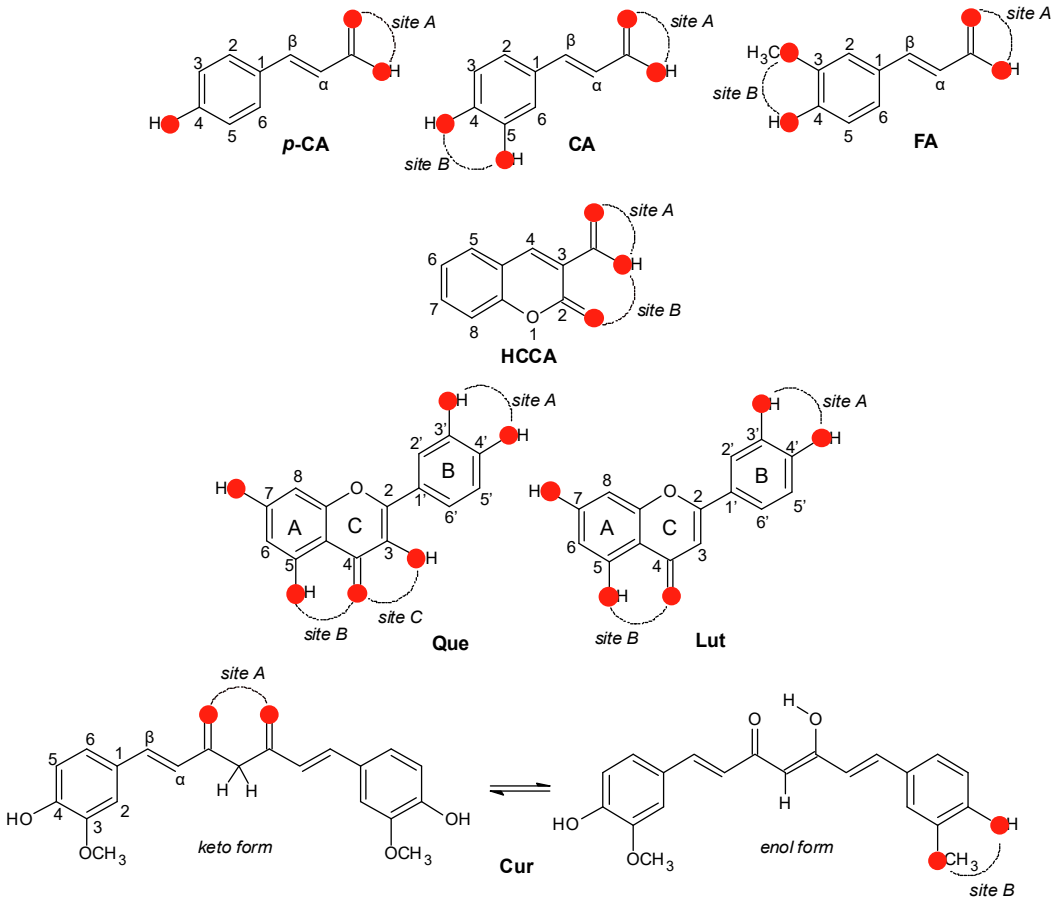

Scheme 1. NAMs considered here for coordination of Al(III) and Fe(III) ions: *p*-coumaric (*p*-CA), caffeic (CA), ferulic (FA), and coumarin-3-carboxylic (HCCA) acids, quercetin (Que), luteolin (Lut), and curcumin (Cur). All the potential binding sites are highlighted with red circles and dashed arcs.

1.2.1. Hydroxycinnamic Acid Derivatives

Hydroxycinnamic acids (Scheme 1) and their derivatives are derived from cinnamic acid, an unsaturated carboxylic acid. They display interesting health benefits such as antioxidant, anti-collagenase, anti-inflammatory, antimicrobial, and anti-tyrosinase activities as well as ultraviolet (UV) protective effects [12]. The pharmacological potential exhibited by these phenolic acids and derivatives has been attributed to the presence of multiple hydroxyl groups in their chemical structure, which make them active as free radical scavengers. The presence of a double bond in the side chain leads to the possible existence of two isomeric forms: *cis* (*Z*) and *trans* (*E*). The diversity and their resultant nutraceutical properties are derived from the nature of the bonds and that of the molecules involved [13]. They are found both covalently linked to the plant cell wall polysaccharides and in their free soluble forms in the cytoplasm and are synthesized from either L-phenylalanine or L-tyrosine as part of the lignin precursor pathway.

In the present work, we focused on the sequestering ability of *p*-coumaric, caffeic, and ferulic acids (*p*-CA, CA, and FA, respectively, Scheme 1).

In *p*-CA, position 4 of the phenyl ring of the skeleton of cinnamic acid bears a hydroxyl group. It is the major precursor in the synthesis of other phenolic acids such as caffeic, chlorogenic, rosmarinic, and ferulic acids. It is widely present in fruits, vegetables, cereals, and mushrooms. Studies on *p*-CA and its conjugated forms have even revealed, besides the properties listed above, antiplatelet aggregation activity.

CA is a cinnamic acid where the phenyl ring is substituted by hydroxyl groups at positions 3 and 4. It is one of the most common phenolic acids found in fruits, vegetables,

mushrooms, and herbs. It is biosynthesized by the hydroxylation of *p*-coumaric acid and has several medicinal properties, among which antidiabetic activity.

FA, known also as 4-hydroxy-3-methoxycinnamic acid, is widely distributed in beverages (coffee, beer), fruits (cabbage, potatoes, carrots), vegetables (broccoli, spinach, tomato), cereals (wheat, corn, maize), flowers, and nuts. It is a caffeic acid derivative formed by the action of the enzyme caffeate *O*-methyltransferase.

1.2.2. Coumarin Derivatives

Coumarins, a family of 1,2-benzopyrones widely diffused in plants, and their derivatives have stimulated interesting research in biology and medicine due to their antioxidant, antibiotic, anticoagulant, anticancer, and anti-inflammatory properties. Coumarins can exist in a variety of forms due to the various substitutions possible in their basic structure, which modulate their biological activity. Therefore, their physicochemical properties and therapeutic applications may depend upon the substitution pattern. In addition, coumarin derivatives can yield a wide variety of metal complexes, and their complexation with d-block metal cations has been recognized as a promising route toward the development of new therapeutic agents and can be used, in principle, in specific chelation therapies [14]. Belonging to this category, the coumarin-3-carboxylic acid (HCCA) here considered, has an oxygen atom in the third position of the basic coumarin skeleton (see Scheme 1), creating a single charged ligand that can chelate, through two O donors, metal ions. HCCA behaves as a scavenger of the hydroxyl radical generated chemically or by gamma radiation, as a selective inhibitor of monoamine oxidase or as an antibacterial agent.

1.2.3. Flavonoids

Flavonoids are secondary plant metabolites of the polyphenol family and form one of the most numerous and widespread families of natural substances accumulated in significant amounts in fruits and vegetables [15,16]. The increasing interest in flavonoids is due to their wide biological and pharmacological effects such as anti-cancer, anti-ulcer, anti-allergic, antioxidant, antiviral, and anti-inflammatory properties [17,18]. The antiradical activity of flavonoids depends on their structure, the position of OH groups, and interaction with biological membranes.

Flavonoids are classified into six main subgroups according to their structure: flavan-3-ols, anthocyanins, flavonols, flavones, flavanones, and isoflavones. Many health benefits are connected with the high consumption of flavonoid-rich foods including reduced risk for heart diseases, cancer, neurodegenerative psychic diseases, and many other chronic diseases. It is assumed that oxidative stress plays an important role in the genesis of these diseases, and therefore flavones may possess therapeutic effects through antioxidant mechanisms. In addition to their antioxidant properties, flavonoids exhibit other multiple biological effects (i.e., antibacterial, antiviral, anti-inflammatory, anticarcinogenic, anti-ischemic, hypolipidemic, antimutagenic, and many others [19]. The present article reviews the coordination properties of two specific flavonoids, namely quercetin and luteolin.

Quercetin (Que) is the most commonly studied flavonol, since it can chelate the metals as a bidentate O,O-coordinating ligand. Furthermore, it is the most important and naturally occurring cancer-preventing agent [20]. The cancer preventive and therapeutic effects of quercetin have been demonstrated through in vitro as well as in vivo experimental findings [21,22]. As depicted in Scheme 1, Que consists of three phenolic rings (A, B, and C rings); it has three available sites for metal chelation including ortho-dihydroxyl (catechol) group of the B ring (site A), 5-hydroxy-4-keto group (site B), and 3-hydroxy-4-keto group (site C), since both hydroxyl and keto groups of Que have the ability to form metal complexes [23–35]. Interestingly, it was observed that some biological properties of quercetin such as antioxidant, antibacterial, and antitumor activities, change with metal chelation.

Luteolin (Lut) is a common flavone with several biological effects [36,37] that is often found in leaves, rinds, barks, and flowering plants. It possesses two metal ion chelating

sites: the 3′,4′-dihydroxy group in ring B and the 5-hydroxy and 4-carbonyl group in ring C (see Scheme 1).

Because of poor water solubility and the bioavailability of flavonoids, their use in the food industry or pharmacy is limited. However, the formation of metal complexes may increase solubility, hydrophilicity, and bioavailability of flavonoids and therefore enlarge the area of new applications.

1.2.4. Curcumin

Curcumin (1,7-bis-(4-hydroxy-3-methoxyphenyl)-1,6-heptadiene-3,5-dione, Cur) is a component of the Indian spice turmeric, manufactured from the rhizome of the perennial herb *Curcuma longa* that is widely cultivated in tropical countries in South and South East Asia, especially in China and India [38]. Curcumin is a typical example of polyphenol-rich natural remedies, and has been used for centuries in Indian traditional medicine (Ayurveda) and traditional Chinese medicine. The medicinal activity of curcumin has been known since ancient times. It has also been used as a photodynamic agent for the destruction of bacteria and tumor cells. Multiple therapeutic activities have been attributed to curcumin mostly because of its anti-inflammatory and antioxidant effects. As such, curcumin was predominantly used to treat inflammatory conditions including bronchitis, colds, parasitic worms, leprosy, arthritis, and inflammations of bladder, liver, kidney, and skin, and to improve symptoms such as fever and diarrhea. In addition, curcumin is thought to have beneficial effects in diseases of the neurological system including Alzheimer's disease [39]. As can be evinced from Scheme 1, Cur has three chemical moieties in its structure: two aromatic ring systems containing methoxy and phenolic groups connected by a seven carbon linker consisting of an α,β-unsaturated β-diketone moiety. A keto-enol tautomeric equilibrium (as shown also in Scheme 1) characterizes the diketo moiety, which can therefore exist in different types of tautomers, depending on the environment. In the crystal state, it exists in a *cis*-enol configuration, where it is stabilized by resonance assisted hydrogen bonding and the structure consists of three substituted planar groups interconnected through two double bonds. In most of the non-polar and moderately polar solvents, the enol form is generally more stabilized than the keto form by 5 to 8 kcal mol^{-1}, depending on the nature of the solvent. Due to extended conjugation, the π electron cloud is distributed along the whole molecule. In solution, it exists as *cis-trans* isomers; the *trans*-form, in which the two phenolic-methoxy groups are on the opposite sides of the curcumin backbone, is slightly more stabilized than the *cis*-form, where the phenolic methoxy groups are on the same side up the backbone [40]. The bis-keto form predominates in acidic and neutral aqueous solutions. At pH 3–7, curcumin is an extraordinarily potent H-atom donor. In the keto form, the heptadienone linkage between the two methoxyphenol rings contains a highly activated carbon atom, whose C–H bonds are very weak due to delocalization of the unpaired electron on the adjacent oxygen. In contrast, above pH 8, the enolate form of the heptadienone chain predominates, and curcumin behaves mainly as an electron donor, a more typical mechanism for phenolic antioxidant scavenging activity [41,42].

The ability of curcumin in free radical reactions may be due to the presence of two phenolic groups, the enol form of the diketone moiety, and the extended conjugated structure. Barik et al. showed that the antioxidant activity of curcumin in the β-keto-enol form is higher than those in the β-diketone form [43]. There are three factors that influence its antioxidant activity: (i) the redox state of the biological environment, (ii) the presence of metal ions, and (iii) of substituents on the side chain [44]. The strong chelating ability of diketones has been widely investigated toward some metal ions, depending on the molar ratio between metal ions and curcumin, the solvent, the metal salt, and the pH media. Over the past few decades, several studies have been published dealing with metal curcumin complexes and their applications [40,45].

2. Measurement of the Stability of Metal–Ligand Complexes in Aqueous Solution

The stability of metal–ligand complexes can be primarily described with three different amounts: cumulative, stepwise, and conditional stability constants. Cumulative, also called overall stability constants, are commonly indicated as β, which characterizes each complex formed in solution. If M is the metal ion, H the proton, and L the ligand, and $M_mH_hL_l$ is the complex formed according to the general equilibrium in Equation (1),

$$m\,M + h\,H + l\,L \leftrightarrows M_mH_hL_l \quad (1)$$

β is defined as:

$$\beta = [M_mH_hL_l]/[M]^m[H]^h[L]^l \quad (2)$$

where square brackets denote the concentrations at equilibrium. The use of concentration amounts as a replacement for the activities is usually allowed by maintaining a constant ionic strength during the experimental measurements. The overall constants are usually given as log β, and their knowledge is required for performing metal–ligand speciation calculations. In order to obtain accurate results, many experimental details have to be considered so the experimental determination of β values is complicated. β values are affected by the acid–base properties of the metal ion and ligand, by the total metal (C_M) and ligand (C_L) concentrations and by the pH. For this reason, the overall constants do not allow us to state the effective complex stability. Moreover, log β values cannot be used to compare the stability of complexes formed by different metal ions and ligands.

Stepwise stability constants are generally indicated as K and are commonly employed when the complexes existing in solution contain one metal ion and one or more ligands (ML_l, with $l \geq 1$). Stepwise and overall constants are related to each other: for the complexes ML and ML_2, log β_{ML} = log K_{ML} and log β_{ML2} = log K_{ML} + log K_{ML2}, respectively.

Conditional stability constants may be cumulative or stepwise and are commonly indicated with the apostrophe (i.e., β′ or K'). These constants can be used to compare the stability of complexes formed by different metal ions and ligands. However, the comparison is possible only when the complexes have the same stoichiometry.

The acidity constants of each ligand, the stability constants of the metal ion hydrolysis products, and the ionic product of water have to be considered to complete the speciation picture and allow speciation calculations.

For some metal–ligand complexes, more than one speciation profile has been reported in the literature, and different log β values have also been proposed. However, speciation data obtained at ionic strength as close as possible to 0.15 M and at 37 °C, which would better resemble physiological conditions, are uncommon. The information arising from these studies can be useful to identify potential complexes that can be formed in vivo; furthermore, the overall charge of the complexes is crucial in determining their partitioning in a biological environment: generally, a charged complex is hydrophilic, preferring to be solubilized in aqueous solutions (i.e., in the blood), and is unable to pass cellular barriers. In contrast, a neutral species should behave in the opposite way. Therefore, the structure of any complex, deductible from its stoichiometry, has a central role in determining its properties and toxicity.

Taking into account the importance of the metal cations and the ligands as the object of this review, results obtained from measurements carried out under physiological conditions of ionic strength and temperature (i.e., close to 0.15 M and at 37 °C) as well as the most studied temperature of 25 °C have been considered.

Table 1 reports the selected speciation information, determined by potentiometry and UV–Vis spectroscopy regarding Al(III) and Fe(III) with some NAMs, according to the general equilibrium reported in Equation (3):

$$pM^{3+} + q(OH)^- + rL^- \rightleftarrows M_p(OH)_q(L)r^{(3p-q-r)} \qquad \beta_{pqr} \quad (3)$$

Table 1. Formation of complexes of some natural antioxidants with Al(III) and Fe(III), according to Equation (3). Standard deviations are reported as 3σ.

Al(III)				
Ligand	**(pqr)**	**log β**	**Temperature**	**Reference**
CA	(111) (121) (131) (142)	13.40 ± 0.03 22.26 ± 0.06 30.87 ± 0.09 42.53 ± 0.09	37 °C	[13]
FA	(121) (131) (142)	21.3 ± 0.3 30.31 ± 0.02 42.24 ± 0.02	37 °C	[13]
p-CA	(131)	30.21 ± 0.09	37 °C	[13]
HCCA	(121) (131)	25.9 ± 0.2 36.5 ± 0.3	37 °C	[14]
Que	(121) (111) (101)	29.25 ± 0.06 16.1 ± 0.1 23.0 ± 0.5	37 °C 37 °C 25 °C	[34] [26] [27]
Cur	(111)	16.4 ± 0.1	37 °C	[45]
Fe(III)				
HCCA	(122)	28.35 ± 0.06	37 °C	[14]
Que	(121) (112) (122)	37.24 ± 0.06 43.9 ± 0.1 53.1 ± 0.1	37 °C	[26]
	(101) (102)	5.5 9.56	25 °C	[46]
Lut	(101)	8.4	25 °C	[47]
Cur	(131)	41.4 ± 0.3	37 °C	[45]

This equation takes into account the possible formation of simple ($q = 0$), mixed ($q \neq 0$), mononuclear ($p = 1$), and polynuclear ($p > 1$) species.

The speciation profiles represent the starting point necessary for understanding the structure of metal–ligand complexes, which can be obtained from an experimental as well as theoretical approach using different characterization techniques and computational methods that will be discussed in the following sections.

3. Binding Sites and Complexes Formation

The ability of chelating agents to block metal-related damage has been widely explored over the past ten years and even earlier by applying quantum mechanics-based approaches [13,14,18,31,34,45–53]. In particular, DFT and its time dependent (TD) extension have been used to identify binding sites and complex stoichiometry, structurally characterizing the ligand–metal complexes, and comparing the outcomes with the available experimental data.

All the ligands considered in this review present more than one possible mono coordinating or chelating site, as highlighted in Scheme 1 by red circles and dashed arcs. Furthermore, to identify the most probable complexes in an aqueous environment, neutral and anionic species were taken into consideration as plausible ligands depending on the experiments or simulation conditions for complex formation [47,50,51]. From a modeling point of view, despite the wide literature on the complex formation of different antioxidants with several metal ions [18,52,53], only a few of these take into consideration the aqueous physiological environment and thus consider the metal ion surrounded by solvent molecules [13,14,31,34,45,47,51]. Some of these computational studies are supported by experiments on the complexes' stability [13,14,31,34,45], while others have taken into account

only the general physiological conditions considering neutral or deprotonated antioxidant species as a function of their pK_as [47,50,51].

In the search for the most probable binding site, key outcomes can come from spectroscopic characterization that is often used to detect the most probable complexes. Figure 1 shows the comparison of the absorption shift in the UV–Vis region of the most sensible band upon complex formation as revealed by experimental evidence and simulated by TDDFT calculations, coming from those works that better fit the aim of the present review (i.e., to describe the coordination properties of Al(III) and Fe(III) toward NAMs in aqueous environment) [13,14,31,34,45].

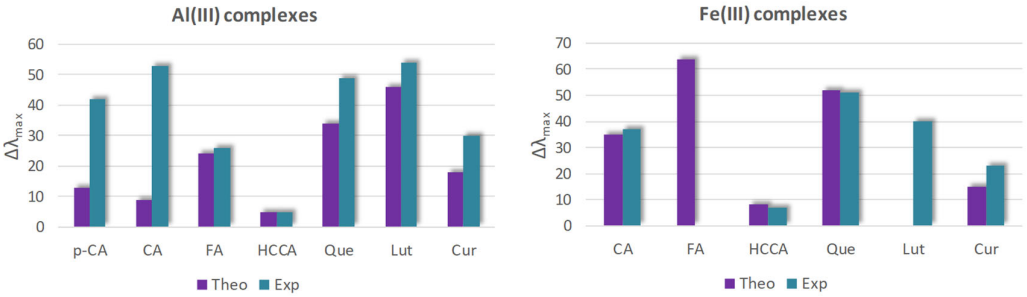

Figure 1. Bathochromic shift of the first absorption band upon complexation with Al(III) and Fe(III) metal ions of the different NAMs. Data were taken from references collected in Table 2, with the exception of: Fe(III)-CA spectrum recorded in aqueous solution at pH = 9 [54] and here calculated; Fe(III)-FA spectrum here calculated; Lut-Al(III) in MeOH-water (1/2 *v*/*v*) [55]; Lut-Fe(III) in EtOH [56].

Table 2. Free energy formation (ΔG_f) of the complexes formed between the selected natural antioxidants and Al(III) or Fe(III), calculated according to Equation (5).

		Al(III)		
Ligand (L)	**Complex**	**ΔG_f**	**Level of Theory**	**Reference**
CA	$[Al(H_2O)_3(OH)(L_A)]^+$	−119.4	M052X/6-31+G(d) − SMD, water	[13]
FA	$[Al(H_2O)(OH)_3(L_A)]^-$	−158.4	M052X/6-31+G(d) − SMD, water	[13]
p-CA	$[Al(H_2O)(OH)_3(L_A)]^-$	−159.5	M052X/6-31+G(d) − SMD, water	[13]
HCCA	$[Al(H_2O)_2(OH)_2(L_B)]$ $[Al(H_2O)_2(OH)_2(L_A)]$ $[Al(H_2O)(OH)_3(L_B)]^-$ $[Al(OH)_3(\eta^1\text{-}L_A)]^-$	−145.3 −139.5 −157.7 −159.0	M052X/6-31+G(d) − SMD, water	[14]
Que	$[Al(H_2O)_2(OH)_2(L_B)]$ $[Al(H_2O)_2(OH)_2(L_C)]$	−123.7 −119.0	M052X/6-31+G(d) − SMD, ethanol	[31]
	$[Al(H_2O)_3(OH)(L_B)]^+$ $[Al(H_2O)_3(OH)(L_C)]^+$ $[Al(H_2O)_4(L_A)]^+$	−71.2 −68.6 −55.9	M052X/6-31+G(d) − SMD, water	[34]
Lut	$[Al(H_2O)_4(L_A)]^{2+}$ $[Al(H_2O)_4(L_B)]^{2+}$ $[Al(H_2O)_2(L_B)_2]^+$ $[Al(H_2O)_2(L_A)_2]^+$	−1.5 2.5 −6.8 −1.1	B3LYP/6-31G ** − CPCM, water	[51] [a]
Cur	$[Al(H_2O)_3(OH)(L_A)]^+$ $[Al(H_2O)_3(OH)(L_B)]^+$	−135.1 −124.9	M052X/6-31+G(d) − SMD, water	[45]
		Fe(III)		
CA	$[Fe(H_2O)_4(L_A)]^{2+}$ $[Fe(H_2O)_4(L_A)_2]^+$	5.8 16.0	M052X/6-31+G(d) − SMD, water	This work
FA	$[Fe(H_2O)_4(L_A)]^{2+}$ $[Fe(H_2O)_4(L_A)_2]^+$	–49.7 –85.4	M05/6-311++G(d,p) − SMD, water	[50]
HCCA	$[Fe(OH)_2(\eta^1\text{-}L)_2]^-$ $[Fe(OH)_2(\eta^2\text{-}L)_2]^-$	−27.1 −19.2	M052X/6-31+G(d) − SMD, water	[14]
Que	$[Fe(H_2O)_2(OH)_2(L_A)]^-$ $[Fe(H_2O)(OH)(L_A)_2]^-$ $[Fe(OH)_2(L_A)_2]^-$	−99.4 −113.7 −125.8	M052X/6-31+G(d) − SMD, water	[34]
Cur	$[Fe(H_2O)(OH)_3(L_A)]^-$ $[Fe(H_2O)(OH)_3(L_B)]^-$	−57.1 −55.5	M052X/6-31+G(d) − SMD, water	[45]

[a] Optimization in vacuum, single point in solvent; ΔG_f for the reaction $nAl(H_2O)_6^{3+} + mL \rightarrow Al_nX^yL^k{}_m + (l - (3n - k))H_2O + (3n - k)H_3O^+$, where l is the number of water molecules detached from $Al(H_2O)_6^{3+}$ upon ligand complexation by using the experimental value of $-\Delta G_{vap}(H_2O)$ as $\Delta G_{solv}(H_2O)$ in the calculation of the Gibbs free energy for the formation of one mole of the considered complexes.

With the final aim of comparing the ability of the different ligands to bind Al(III) and Fe(III) metal ions in aqueous solution, metal binding affinity was here estimated (when possible on the basis of data available in the literature) by calculating the reaction free energies of the complexation reaction for the substitution of water molecules in the hexaaquo complex and considering the overall process in solution (Equation (4)):

$$\{nL\}^c + [M(H_2O)_6]^z \rightarrow [ML_n]^{z+c} + (6\text{-}n\text{-}t)H_2O \quad (4)$$

where c is the total formal charge of the n ligands; L = ligand (neutral or deprotonated) OH^-; z is the charge of the hexaaquo complex; and t = 0, 1 takes into account the possibility that the ligands are mono or bidentate. Therefore, the formation energies of these complexes were calculated as:

$$\Delta G_f = \Delta G([ML_n]^{z+c}) + (6 - nt)\Delta G(H_2O) - (\sum_i^n (L))^c - \Delta G([M(H_2O)_6]^z) \quad (5)$$

Most of the literature works considered here refer to measurements in aqueous solutions with pH values within the range 3.5–5, thus the accessible species and the corresponding most probable structures are of different types, depending on both the metal and ligand (Table 1) [13,14,31,34,45].

Data collected in Table 2 from the most recent studies on the selected NAMs, support the ability of Al(III) and Fe(III) metal ions to bind oxygen sites, essentially arranging in octahedral complexes (see Scheme 2). However, when metal ions and ligands exist in 1:2 stoichiometric ratios, $[M(OH)_2(L)_2]^-$, or the ligand is monocoordinated, $[M(OH)_3L]^-$, the tetrahedral structure is plausible [14].

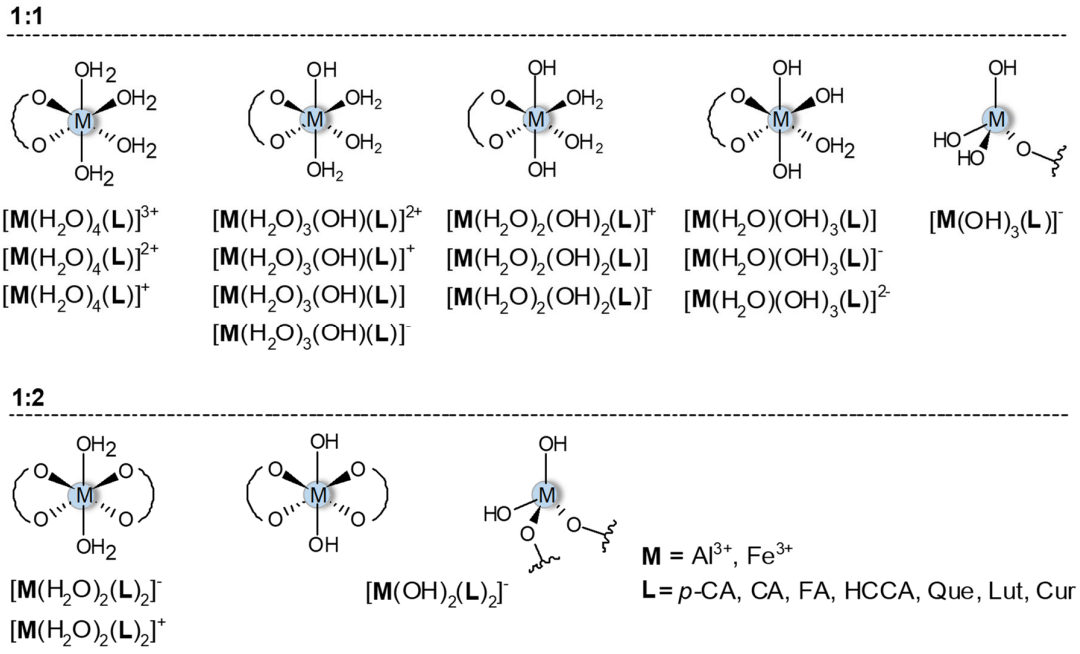

Scheme 2. Metal–ligand complexes in aqueous solution for 1:1 and 1:2 stoichiometric ratios.

4. Complex Characterization by Spectroscopic and Spectrometric Techniques

The structural characterization of Al(III) and Fe(III) complexes with the NAMs reported in Scheme 1, is of primary importance for understanding their potential applicability. The NAM derivatives generally form complexes with a 1:1 and 1:2 metal to ligand ratio. However, the different number of binding sites offered by each of them (Scheme 1), which is very intriguing, makes a straightforward identification of the structure of the complexes more difficult. To this aim, several spectroscopic and spectrometric techniques have

been used for metal-NAM complex characterization, which allows for attribution and discrimination among the different chelation sites.

Among the spectroscopic techniques, the most useful and widespread are ultraviolet-visible (UV–Vis), Fourier transform infrared (FTIR), nuclear magnetic resonance (NMR), and fluorescence spectroscopy. Mass spectrometry (MS) is also used in several instances because it provides crucial insights into the stoichiometry of the complexes. The UV–Vis characterization gives information on the d–d* transitions of the metal and on the possible geometry of the coordination complex. FTIR provides information on the functional groups of the ligand that may be involved in the complexation. The complexation is usually accompanied by a loss of some OH protons or it may cause significant proton and carbon resonance variation of the ligand close to the metal binding sites. In this context, ^{1}H and ^{13}C-NMR are powerful tools for elucidating the interaction between metal cations and ligands. The fluorescence emission spectra provide useful insights to identify the coordination site from the enhancement or quenching of the fluorescence as well as from the shift of the excitation and emission wavelength. Table 3 reports the results concerning the metal-to-ligand stoichiometric ratio, the solvent used for the synthesis and characterization of the complex, and the main spectroscopic and spectrometric methods used for their characterization.

Table 3. Methods used to characterize the complexes between the selected natural antioxidants and Al(III) or Fe(III) in the reported metal to ligand (M:L) stoichiometric ratios.

			Al(III)	
Ligand	**M:L**	**Solvent**	**Characterization Methods**	**Reference**
CA	1:1 1:2	water	UV–Vis, ^{1}H-NMR	[13]
FA	1:1 1:2	water	UV–Vis, ^{1}H-NMR	[13]
p-CA	1:1	water	UV–Vis, ^{1}H-NMR	[13]
HCCA	1:1	water	UV–Vis, ^{1}H, ^{13}C-NMR	[14]
Que	1:2	methanol	FTIR, ^{1}H, ^{13}C MAS NMR	[57]
	1:1	water	UV–Vis, ^{1}H, ^{13}C-NMR	[34]
Lut	1:1 2:1	methanol:water (9:1)	UV–Vis, FT-IR, RAMAN	[58]
	1:2	ethanol	UV–Vis, FTIR, fluorescence, ESI-MS	[59]
Cur	1:1 2:1 3:1	methanol	^{1}H, ^{13}C, ^{27}Al-NMR, MALDI-TOF	[60]
	1:1 1:2	water	UV-Vis, ESI MS/MS, LD-MS, MS/MS	[45]
			Fe(III)	
HCCA	1:2	water	UV–Vis, ^{1}H, ^{13}C-NMR	[14]
Que	1:2	methanol	UV–Vis, FTIR, ESI MS, ^{1}H-NMR	[29]
	1:2	water	UV–Vis, ^{1}H, ^{13}C-NMR	[34]
Lut	1:1	ethanol	UV–Vis, FT-IR, ESI MS	[56]
	1:2 1:2 [a]	water	ESI MS, ESI-TOF MS	[37]
Cur	1:2	water	UV–Vis, ESI MS/MS, LD-MS, MS/MS	[45]
	1:2	methanol	FTIR	[61]
	1:2	water:methanol (1:1)	UV–Vis, FTIR, RAMAN, ESR, ^{1}H-NMR, X-ray	[62]
	1:2	methanol	UV–Vis, FTIR	[63]

a. Fe(II)-Lut [37].

In the following section, the importance of the aforementioned characterization techniques in discriminating the coordination site/sites will be highlighted, discussing the interaction of Al(III) and Fe(III) cations with hydroxycinnamic acids, coumarinic acid, quercetin, luteolin, and curcumin.

5. Discussion

The combination of different approaches permitted to unravel the different affinity of the two metal cations for a specific binding site of the selected NAMs. Indeed, while speciation studies allowed to predict which metal and ligand species exist in solution at a given pH, metal, and ligand total concentrations, spectroscopic, spectrometric, and computational studies provide pivotal information for identifying the preferred binding site of a metal for a specific ligand and thus the most probable complexes. All the experimental methods addressed here to describe the interactions of Al(III) and Fe(III) with the selected NAMs and information stemming from them are summarized in Table 4.

5.1. Hydroxycinnamic Acid Derivatives

Al(III) ions can form 1:1 and 1:2 stoichiometric ratio species with CA and FA, and only a 1:1 stoichiometric ratio species with *p*-CA (Table 3). As can be seen in Table 1, the sequestering ability of CA toward the aluminum cation is higher than that of FA and *p*-CA as it forms complexes with four different stoichiometry. This result can be explained considering the higher solubility of CA than the other two hydroxycinnamic acids, which allows for working with a higher ligand to metal ratio, thus facilitating the water substitution in the aluminum coordination sphere [13].

Metal coordination by the selected hydroxycinnamic acids can occur on the carboxylic site (site A) or on the catechol-like site (site B) in the case of CA and FA (see Scheme 1), as reported by different authors in the search for the most probable one in metal coordination [13,49,52,53]. One of the first studies in an aqueous solution (pH = 5) reported site B of CA as the preferred one for Al(III) coordination, on the basis of a comparison between recorded and simulated UV–Vis absorption spectra of selected metal–ligand complexes, identifying the three complexes of the type $[M(H_2O)_4(L)]$, $[M(H_2O)_3(OH)(L)]^-$ and $[M(H_2O)_4(L)]^+$ (see Scheme 2) as the most plausible under such physicochemical conditions [46]. However, more recently, Beneduci et al. observed the formation of Al(III)–CA complexes by combining potentiometric measurements, UV–Vis and ^{1}H-NMR spectra with computational studies. The monoanionic species were considered as the only possible CA, FA, and *p*-CA active species at pH within the range 3.5–5, thus taking into account the coordination of Al(III) only on site B of CA completely protonated, which resulted in being much more instable than the coordination on the carboxylate site, site A [13]. A similar behavior was found for FA and *p*-CA, for which the most probable complex resulted for a stoichiometric ratio (131), $[Al(OH)_3(H_2O)(L_A)]^-$. The formation of these complexes was clearly indicated by the huge bathochromic shift observed (up to 60 nm) in all the UV–Vis spectra with respect to those of the free ligands. According to the thermodynamic results, ligand complexation is strongly influenced by pH. In particular, it occurs just at pH 3.5 for caffeic acid, while a pH higher than 4 is needed for the other two ligands. UV–Vis spectroscopy alone cannot provide straightforward evidence on the complexation site involved. In this case, very clear insights on the structures of the complexes were obtained by ^{1}H-NMR. These α, β unsaturated acids are very interesting because the doublet at about 7.6 ppm related to the proton in β can be used as an automatic alert system for the detection of changes in the electronic configuration on the carboxylic site. Thus, when the Al(III) cation interacts with this functional group, a pH-dependent shielding effect is induced, which determines a significant shift (up to 0.06 ppm) of the doublet to the lower field (Figure 2). The reason for this sensitivity is due to the positive charge delocalization on the β-carbon atom, following deprotonation caused by a pH increase or by the Al(III) complexation on the carboxylic group.

Table 4. Details of the identification and characterization methods.

Experimental Methods	Methodology	Principle	Analysis Results	Reliability and Quality of the Results on the Complex Formation
Potentiometry	✔ Measurements in aqueous solution	The complexation equilibria are studied by measuring, with a glass electrode, the competition of the ligand for H^+ and metal cations.	The experimental data, obtained at different metal and ligand total concentrations, and processed by numerical procedures, were rationalized according to a general equilibrium, to obtain the complexes existing in solution at a given pH.	Speciation studies allow to predict the most probable stoichiometric coefficients of the complexes and the corresponding stability constants.
UV-Vis	✔ Spectroscopic technique ✔ No sample preparation ✔ Measure in solution	Absorption of ultraviolet and visible photons by a molecule causes a change from its fundamental electronic state to an excited electronic state.	In a typical UV–visible spectrum the wavelength is reported in the abscissa ($190 < \lambda < 780$ nm) and the absorbance (or the transmittance) in the ordinate. The recorded spectrum will be characterized by a series of bands of variable intensity.	Complexation leads to specific band shifts in the spectrum of the ligand that, in several cases, can be directly related to the involvement of a specific complexation site of the ligand. In addition, metal-to-ligand charge transfer transitions and d-d transition bands may occur
^{1}H, ^{13}C, ^{27}Al-NMR	✔ Spectroscopic technique ✔ Measure in solids and in solution	Absorption of a radio frequency radiation is measured after immersing a molecule in a strong static magnetic field, which causes nuclear spin transitions.	An NMR spectrum shows the frequency absorbed and then emitted by the atoms of the nucleus under examination, which depends on the chemical environment around it (chemical shift).	Upon complexation huge shielding or deshielding effects may be induced on the magnetic nuclei of the ligand, generally placed close to the binding site. However, significant chemical shift displacement can occur far from the binding site when resonance structures are involved in the ligand. Quantitative information on the structural properties of the complexes may also be obtained from the spectra of magnetic metals such as ^{27}Al.
FTIR	✔ Spectroscopic technique ✔ Measure in solution and in solid	Absorption of an infrared photon by a molecule, causes its transition from its fundamental vibrational state to an excited vibrational state.	In a typical IR spectrum, the percentage of transmittance is plotted against the wave number ($4000\ cm^{-1} < \lambda < 400\ cm^{-1}$). Each peak in the spectrum can be assigned to a specific functional group.	Formation of a complex usually leads to the appearance of specific peaks related to the metal-heteroatom bond (e.g., Al-O). Moreover, metal binding affects the bond vibrational energies of the functional groups of the ligand involved in the complexation, leading to related peak shifts.
Mass spectrometry	✔ Spectrometric techniques ✔ Measure in solution and in solid ✔ Destructive technique	This technique allows separating a mixture of ions according to their mass/charge ratio. Molecules are ionized and fragmented into lighter ions according to typical patterns depending on their chemical structure.	The diagram showing the abundance of each ion as a function of the mass/charge ratio (m/z) is the so-called mass spectrum, typical of each compound as it is directly related to its chemical structure and to the ionization conditions it has been subjected.	Upon complexation, specific m/z fragments containing the metal can be detected, indicative of the specific binding site involved. The stoichiometry of the complex (M:L ratio) can be easily determined.

Table 4. *Cont.*

Experimental Methods	Methodology	Principle	Analysis Results	Reliability and Quality of the Results on the Complex Formation
Fluorescence	✔ Spectroscopic technique ✔ Measure in solution ✔ Non-destructive technique	An incident photon excites the fluorophore from the ground state to a higher energy state (electronically and vibrationally) with the same spin. In a few nanoseconds, the excited electron returns to the ground electronic state passing through one or more excited states at intermediate energy. All decays except one are usually non-radiative, while the last one emits light with a longer wavelength than the incident radiation, that is the fluorescence.	In a typical fluorescence spectrum, the fluorescence intensity is plotted vs. the wavelength of emission.	Complex formation between a metal and a fluorophore may lead to a significant fluorescence enhancement due to restricted intramolecular rotations of the ligand, as well as a huge shift of the emission maximum.
RAMAN	✔ Spectroscopic technique ✔ Measure in solution, solid and gas phase ✔ Non-destructive technique	This technique is based on the diffusion (scattering) of a monochromatic electromagnetic radiation by the analyzed sample. The diffused radiation contains the components with different energy (Rayleigh, Stokes and anti-Stokes) associated to molecular vibrations of different functional groups.	In a Raman spectrum the intensity of the signals proportional to the number of Stokes photons, are plotted against the Raman shift (in $cm^{-1)}$, corresponding to the energy difference associated to transitions between fundamental vibrational levels.	Upon complexation specific band shifts (i.e., inplane skeletal vibrations as well as stretching vibrations) occurs in the RAMAN spectra indicating which part of the ligand takes part in the metal binding.
ESR	✔ Spectroscopic technique ✔ Measure in solution	It detects the induced transition by a microwave radiation between the energy levels of electron spins under a static magnetic field. It allows the study of organic and inorganic free radicals, odd electrons molecules, molecules in the triplet state, transition metal complexes, etc.	The EPR spectrum is the first derivative of the absorption spectrum obtained in the microwave range	ESR measurements of the magnetic moment, is indicative of low or high spin configuration around the metal, thus providing information on the coordination geometry
X-ray Diffraction	✔ Spectroscopic technique ✔ Measure on powder ✔ Non-destructive technique	It allows the structural characterization of crystalline materials. It is based on the constructive interference of an x-ray monochromatic beam which is scattered at specific angles from each set of lattice planes in a sample.	The x-ray pattern is the fingerprint of the periodic atomic arrangement in the material	X-ray diffraction provides insight on the coordination geometry around the metal ion as well as on the degree of crystallinity of the complexes.

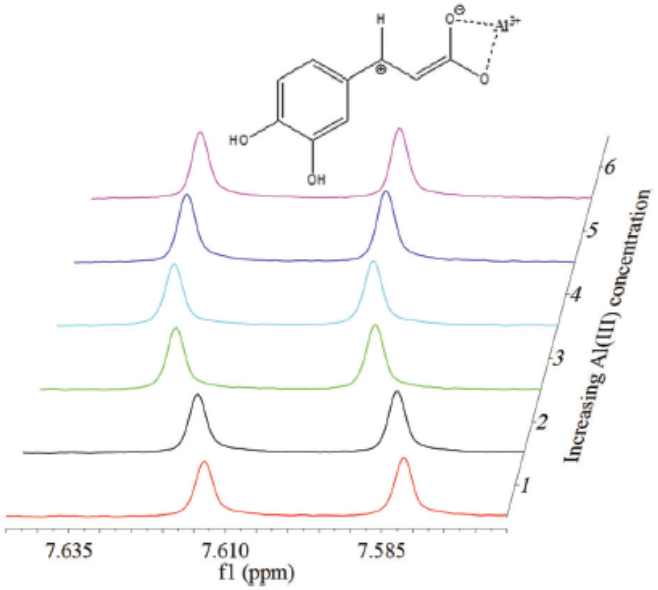

Figure 2. ^{1}H-NMR doublet of the b proton of caffeic acid at pH = 3.5 and the deshielding effect caused by the formation of the complex with Al(III). Reproduced from [14] with permission from the Centre National de la Recherche Scientifique (CNRS) and the Royal Society of Chemistry.

Regarding the Fe(III) complexation, no experimental structural characterization is available for CA and *p*-CA while the carboxylate anion was found as the most abundant species for FA in the complexes formed under a physiological environment in a computational work by Truong et al. They explored several complexes and concluded that the most stable ones involved the coordination of Fe(III) on site A of FA and are of the type $[M(H_2O)_4(L)]^{2+}$ and $[M(H_2O)_2(L)_2]^{+}$ for 1:1 and 1:2 metal to ligand stoichiometric ratios, respectively [50]. On these complexes, we performed TDDFT calculations to get an indication of the changes in the absorption spectrum of the ligand after the complexation. Bathochromic shifts of 64 and 47 nm were found for the 1:1 and 1:2 complexes, respectively, the former are included in Figure 1. Though additional studies should be undertaken to unequivocally identify the preferred metal-to-ligand stoichiometric ratios, the most plausible complex is likely to involve the coordination of FA to Fe(III) through the carboxylate site (site A).

Interestingly, the same authors found a very similar behavior for Fe(II) metal ions, though the energies involved were of different magnitude. Data available in the literature for the Fe(II)–CA complex [47] were thus used here as a guide to calculate the ΔG_f and to simulate the absorption spectrum of a plausible Fe(III)–CA complex with the metal binding through site A. Thus, both 1:1 and 1:2 complexes with CA in its monoanionic form were considered. The simulated electronic spectra showed a red shift of 35 and 27 nm for the two complexes, respectively, and the former perfectly fits the experimental observation [54], as evident from Figure 1. Similar to the outcomes of Truong et al. [50] about FA, the obtained ΔG_f suggests a higher affinity of CA for ferrous ions rather than for the ferric one [47].

5.2. Coumarin Derivatives

For the aluminum–coumarin-3-carboxylic acid system, the complexes are in stoichiometric ratio 1:1 and also include hydroxyl group in the coordination sphere of the metal cation (i.e., $[Al(OH)_2(L)]$ and $[Al(OH)_3(L)]^{-}$). The stability of these species is relatively high, particularly when compared to the constant's value for the Fe(III)–HCCA complex (see Tables 1 and 2). The sequestering ability of HCCA toward the Al(III) cation was higher than that toward Fe(III) [14]. HCCA can form only one type of Fe(III) complex in aqueous solution (122), which contains two hydroxyl ligands together with the two

anionic antioxidant molecules. In this case, two coordination modes were found as the ligand binds the metal center in η^1 or η^2 fashion. The former result was the most stable $[Fe(OH)_2(\eta^1\text{-}L)_2]^-$, in accordance with the experimental evidence (see log β in Table 1), and thus the complex arranges in a tetrahedral structure (Figure 3).

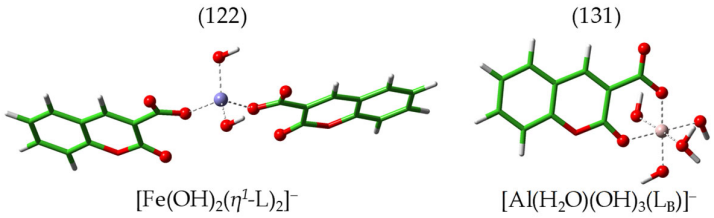

Figure 3. Optimized structures of the tetrahedral 1:2 Fe:HCCA and octahedral 1:1 Al:HCCA complexes.

Despite a similar hard Lewis acid nature of the ions, the coordination of HCCA to the Al(III) metal ion leads to more stable complexes as evidenced by the calculated metal binding affinity (Table 2), in which the ligand chelates the metal surrounded by two or three OH^- ligands, $[Al(H_2O)_2(OH)_2(L)]$, and $[Al(H_2O)(OH)_3(L)]^-$, respectively. Such structures have the metal coordination on site B, involving both the carboxylate and lactone moieties and forming a six-membered cycle. Even in the case of Al(III) complexes, the formation of a tetrahedral structure is possible, $[Al(OH)_3(L)]^-$; the ligand coordinates the metal, surrounded by three OH^-, in η^1 fashion. Based on the determined binding constants and the computed binding energies, the (131) stoichiometry is the most probable one at the working pH of 3.5. Furthermore, the coexistence of both tetrahedral and octahedral complexes with such a stoichiometric ratio, $[Al(H_2O)(OH)_3(L_B)]^-$ and $[Al(OH)_3(\eta^1\text{-}L)]^-$, is supported by NMR measurements and by the very similar values of the calculated formation energies (Table 2). Indeed, both ^{1}H- and ^{13}C-NMR highlight that the overall effect caused by the complexation is a down-field shift of all signals with respect to the free ligand. It is important to note that the proton adjacent to the carboxylic acid (H in C4), is the least shifted in the ^{1}H-NMR spectrum of the complex, whereas the hypothetic complexation on that moiety would have led to the opposite result. In addition, the ^{13}C-NMR highlighted that the carbon atom in C2 was the most shifted, pointing out a strong interaction of the Al(III) cation with the oxygen atom of the aromatic ring. These evidences indicate that the coordination occurs through site B, which involves a relatively low electronic rearrangement of the ligand upon complex formation. Actually, the optical absorption spectrum of the free ligand was not significantly affected by the metal binding, with only a slight red shift for the Al(III)–HCCA system (see Figure 1). The excellent agreement between experiments and simulations supported the implication of site B in HCCA coordination. Overall, the HCCA prefers to bind both the metals through site B in η^1 and η^2 for Fe(III) and Al(III) ions, respectively, with a major affinity for Al(III) ion [14].

5.3. Flavonoids

Data on the complexation behavior of Que and Lut by Al(III) and Fe(III) ions come from several studies [26,33,64,65], some of which combine experimental and computational approaches [31,34]; others have reported the calculated structures of the complexes optimized under physiological conditions [51] while others have focused on their spectroscopic characterization [26,55,56].

Among the ligands described in this review, Que has the highest number of complexation sites, the 3′,4′-dihydroxyl groups (site A), the 5-hydroxychromone (site B), and the 3-hydroxychromone (site C), leading to an intricate and intriguing complexation behavior.

The structural characterization of the Al(III)–Que complexes in aqueous and in mixed hydro-alcoholic solutions is not very easy due to the poor solubility of quercetin and the formation of low-soluble complexes [57,66]. Useful insights on its complexation behavior come from several studies in methanol and ethanol. Ahmedova et al. reported on the

synthesis of the Al(III)–Que complex in methanol and its characterization by elemental analyses, IR, and ^{1}H-^{13}C MAS NMR [57]. This study suggested the formation of a complex with a metal-to-ligand ratio of 1:2. The involvement of the carbonyl group in the complexation was demonstrated by a significant shift at lower energy (>50 cm^{-1}) of its stretching vibration in the IR spectrum of the complex as well as by the disappearance of the broad resonance signal assigned to the intramolecular C5-OH/O = C4 hydrogen bond in the ^{1}H MAS NMR. Further ^{13}C MAS NMR data showed that the complex formation occurs by chelation involving the oxygen atom in position 5, which is downfield shifted according to the analysis of the electron distribution.

The complexation behavior of quercetin for iron(III) as well as the antioxidant and anti-diabetic activity of the Fe(III)–Que complexes were also studied in methanol [24,29]. Interestingly, Raza et al. reported on a 1:2 stoichiometric metal-to-ligand ratio, where iron chelates quercetin through site C [29]. This was confirmed by (i) a strong red shift (>65 nm) of the longer wavelength band in the electronic absorption spectrum, associated with the cinnamoyl system, (ii) the presence in the IR spectra of the Fe–O stretching vibration and a significant shift of the C = O stretching vibration, (iii) the ESI-MS experiments, which showed a peak at m/z 658.54 assigned to the $[Fe(L)_2]^+$ species, and (iv) the disappearance of the hydroxyl proton (3-OH) signal in the ^{1}H-NMR of the complex.

Quercetin can preferentially bind Al(III) by its chelating sites B and C, as has been previously highlighted by Furia et al., who characterized a neutral 1:1 Al(III):Que complex formed in ethanol/water mixture [31]. The computational study showed that this complex, with the formula $[Al(H_2O)_2(OH)_2(Que)]$, had the lowest energy when 5-hydroxychromone was involved in the complexation, though the complex involving the coordination of the 3-hydroxychromone site was only slightly less stable. UV–Vis spectroscopy investigation showed a huge bathochromic shift of the quercetin absorption spectrum, especially of band I (429 nm vs. 368 nm), which was attributed to the conjugation of B and C rings. Strong experimental support on the involvement of the B ring in the coordination can be obtained from the comparison between the FTIR spectra of the complex and of the free ligand. The analysis of the characteristic bands of quercetin highlights a significant reduction of the stretching vibration of the carbonyl group (ν(C = O) 1639 cm^{-1} vs. 1666 cm^{-1}) and of the C–C stretching vibration of the B ring (ν(C–C) 1598 cm^{-1} vs. 1611 cm^{-1}) in the spectrum of the complex, which also showed the characteristic Al–O stretching vibration band of the complex at 636 cm^{-1}. However, the experimental data did not allow for a clear discern between the chelating sites B and C, indicating that both complexes could be populated, as suggested by the computational results showing the kinetically possible interconversion between the two isomers in solution [31].

More recently, a comprehensive experimental and computational study on the Al(III)–Que and Fe(III)–Que complexes was conducted, for the first time, entirely in aqueous solution [34]. The speciation studies showed the formation of several complexes in the 2–5 pH range, with the precipitation of neutral solid species at higher pHs. The sequestering ability of Que toward Fe(III) was higher than that toward Al(III). Speciation profiles from potentiometric titrations showed that complexation occurs at a 1:1 ligand-to-Al(III) ratio and at 1:1 and 2:1 ligand-to-Fe(III) ratios. The stability of all these complexes was high, particularly when the hydroxyl group was involved in the coordination [34]. Computational data showed that this stability comes from the bidentate nature of the ligand. For Al(III), the most stable complex was formed when the site B was involved, irrespective of the charge of the systems. However, the speciation study showed the formation of a complex with the ligand doubly deprotonated, of the type $[Al(Que)]^+$, which must necessarily involve site A in the coordination with both the hydroxyl groups deprotonated. This complex is only slightly higher in energy than the $[Al(OH)(Que)]^+$, where the Al ion bound to site B, suggesting that the complex involving the catechol moiety would be kinetically favored.

For Fe(III), instead, among the mononuclear bidentate complexes that could be formed, the most stable was the one involving the catechol site A, with stoichiometry

$[Fe(OH)_2(Que)]^-$. The neutral species formed during the titrations were characterized by ^1H and ^{13}C-NMR spectroscopy after their dissolution in DMSO. Unexpectedly, the proton spectra of the above samples showed all the OH proton signals, but with large shift ($\Delta\delta$, ppm) and intensity changes compared to the free quercetin. This suggests that the dissolved solids were a mixture of different complexes that come into a rapid equilibrium in solution in the NMR time scale. It was shown that the magnitude of the chemical shift change and its sign (downfield or up-field shift) reflects a complicated electrostatic charge distribution over the entire quercetin molecule (maps of molecular electrostatic potential, MEP), which cannot be accounted for by the presence of only one complex in solution (Figure 4). Therefore, the qualitative comparison between the NMR maps of the relative chemical shift changes and the MEPs supports the hypothesis that the spectrum of the M(III)–Que mixture is a weighted average of those of the individual complexes and free quercetin. The simulated NMR spectra of the neutral complexes are consistent with the presence of a mixture of more than one complex, thus highlighting the tendency of Que to bind these metals at different coordination sites.

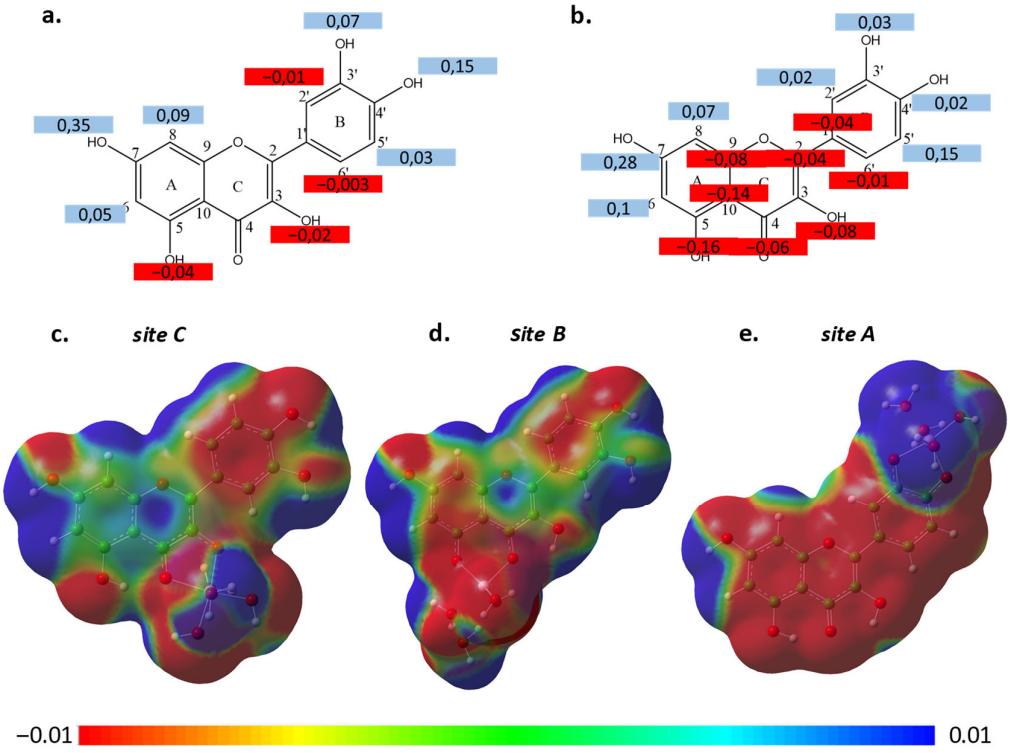

Figure 4. Chemical shift changes maps. (**a**) ^1H-NMR, (**b**)^{13}C-NMR. Maps of the molecular electrostatic potential (MEP) of (**c**) site C, (**d**) site B [$Al(OH)_2(Que)$] complexes, and (**e**) site A [Al(OH)(Que)] complex. Reproduced from [34], Copyright Elsevier 2021.

To our knowledge, no experimental data on the Al(III)–Lut complexes formed in aqueous solution have ever been reported. Nonetheless, a comprehensive TDDFT investigation by Amat et al. was performed on the spectroscopic properties of Al(III)–Lut complexes, where the Gibbs free energy of complex formation in water were computed considering the hexaaquo complex $Al(H_2O)_6^{3+}$ as the starting reagent in the complexation reaction [51]. According to the absorption spectra obtained in methanol [55], the authors suggested the formation of three different complexes with increasing $[Al^{3+}]/[Lut]$ ratio: the 1:2 metal to ligand complex $[Al(H_2O)_2(L_B)_2]^+$ and the subsequent formation of the $[Al(H_2O)_4L_B]^{2+}$ complex with a 1:1 Al:Lut stoichiometry, both with Lut chelating through site B, and the formation of two binuclear complexes with a 2:1 Al:Lut stoichiometric ratio in equilibrium between them, both involving the bidentate sites (4–5 and 3′–4′).

Looking at the ΔG_f values reported in Table 2, we note a scarce ability of Lut to bind Al(III), especially when compared with the Que complexes obtained in the same stoichiometric ratio (101), though they are calculated in a different way (see footnote of Table 2) [34,51]. In contrast, by comparing the species with the same stoichiometry (i.e., 101) between Fe(III)–Que [53] and Fe(III)–Lut [56] (see Table 1), it was possible to observe that Lut formed a slightly more stable complex than Que. This behavior could be related to the structure of the species, with a formation of five-membered and six-membered cycles, respectively. Spectroscopic and spectrometric investigations through UV–Vis, IR, ESI-MS, ESI-TOF MS, and spectrofluorometric determination were employed to study the interaction of Lut and Fe(II), Fe(III), and Al(III) [58,59]. As already noted, Lut can chelate metals by two sites: the 3′,4′-dihydroxyl group in the B ring (site A) and the 5′-hydroxy and 4-carbonyl group in the C ring (site B). Yang at al. were able to discriminate between these sites, defining the stoichiometry of the Fe(III)–Lut complexes and the chelating sites involved, by UV–Vis, IR, and ESI-MS characterization. Lut has two absorption bands in the UV–Vis region, the first one, a $\pi-\pi^*$ transition, assigned to the B ring system (cinnamoyl system) and the other, at low wavelength, representing the A ring system (benzoyl system). The UV–Vis spectra of luteolin and different Fe(III)–Lut complexes at different molar ratio (L:M = 1:1, 1:2, 1:3) acquired in ethanol solution [56] showed that the overall effect of iron addition is a bathochromic shift of these bands, with that related to the cinnamoyl system highly marked (~40 nm), and the appearance of a new band clearly indicating the complex formation. The molar ratio plot (absorbance vs. Fe(III)–Lut mole ratio) indicates the formation of a 1:1 Fe(III)–Lut complex. Significant information was obtained in this study by comparing the IR spectra of the free ligand and that of the Fe(III)–Lut complex, where many characteristic signals of the Lut cinnamoyl moiety were shifted. Among these, the most important are those assigned to the C=C stretching vibration of the benzene ring, due to an enhancement of the conjugation after coordination (38 cm^{-1}), and of the C–O vibration relative to the phenolic hydroxyl groups (~13 cm^{-1}), indicating their involvement in the coordination. Moreover, of noteworthy importance was the peak at 639 cm^{-1} assigned to the stretching of the O–Fe(III) bond. The ESI-MS experiments gave direct information on the 1:1 Fe(III):Lut stoichiometry of the complex since, irrespective of the molar ratio investigated (L:M = 1:1, 1:2, 1:3), the same three major peaks were always found at m/z 402.7, 431.6, and 448.8 corresponding, respectively, to the following ions: $[(Lu\text{-}2H)^{2-} + Fe^{3+} + NO^{3-} + H^+]$, $[(Lu\text{-}2H)^{2-} + Fe^{3+} + 2\ CH_3CH_2OH]$, and $[(Lu\text{-}2H)^{2-} + Fe^{3+} + NO^{3-} + CH_3CH_2OH + H^+]$. Thus, the above data overall indicate the formation of the 1:1 M:L complex with coordination on site A.

Very recently, a thorough study on the interaction and coordination modes between Lut and iron by using electrospray ionization time-of-flight mass spectrometry (ESI-TOF MS) was reported [37]. The reaction between Lut and iron was performed in hot water to simulate the intake of this flavonoids in the human body, which is generally found in edible plants and is taken after boiling. The supernatant obtained after the reaction was measured by direct injection in the ESI-TOF MS. The results highlight the presence of a complex (m/z 626), which was assumed to be the Fe(III)–Lut 1:2 complex [37]. Moreover, analogously to other flavonoids, luteolin can reduce Fe(III) to Fe(II) under acidic conditions, leading to the formation of Fe(II)–Lut complexes [67,68]. Specifically, the presence of a 1:2 Fe(II):Lut complex was confirmed by the ESI experiment. As further evidence, the presence of Fe(II) in the Fe(III)–Lut complex solution was detected by using the indicator 1,10-phenanthroline, which forms an intense red colored complex with the Fe(II) ion.

Different photoluminescent flavonoids such as morin, luteolin, and quercetin can be used as fluorogenic ligands for metal cation detection through a chelation mechanism [69–72]. The fluorometric method can be used for the study of the chelation mechanism, since it can reduce the interference from the matrix compared with other spectroscopic methods. Sun et al. reported on the use of Lut in the spectrofluorometric determination of aluminum, based on the complex formation. Indeed, the free ligand in ethanol solution shows only a weak fluorescence due to the quenching mechanism associated with the proton transfer

from the hydroxyl to the carbonyl group of the C (pyrone) ring. The formation of the Al(III)–Lut complex upon addition of Al(III) to the solution leads to a significant increase in the fluorescence emission due to the lack of the above quenching mechanism and the increase in the rigidity of the molecules that minimizes the non-radiative dissipation processes. Moreover, the emission maximum shifted considerably (>100 nm) as Al^{3+} concentration increased (from 10^{-4} to up 10^{-3} M). UV–Vis and IR spectroscopy also gave clear indication of complexation by significant signal shifts in the complex with respect to the free ligand. ESI-MS measurements provided evidence of a singly-charged complex at a m/z 579 ([Al(III) + (luteolin−2H) + (luteolin−H) + H]$^+$) ratio corresponding to a 1:2 Al:Lut molar ratio. The authors proposed a dimeric structure in which one luteolin is coordinated through site A and the other through site B.

5.4. Curcumin

The speciation profiles obtained by potentiometric titrations in aqueous solution up to pH 4.5 showed that curcumin forms complexes with a 1:1 molar ratio, with a positive charge in the case of Al(III) and a negative one for Fe(III). At higher pH values, the formation of neutral insoluble species with a 1:2 stoichiometry occurs. The binding modes of curcumin with metal cations were evaluated combining UV–Vis and MS characterizations with computational studies [45,60]. Beneduci et al. found a different propensity of the two metal ions in the complexation with curcumin. Indeed, while Al(III) preferred the diketo moiety (by about 10 kcal mol^{-1}), Fe(III) formed two almost equally stable complexes for the coordination to the keto-enolic and guaiacol sites. The UV–Vis spectrum of free curcumin showed two absorption bands, one in the UV region ascribed to the phenolic moiety and the other in the visible region (λ_{max} = 434 nm), with a shoulder at lower wavelengths. More specifically, this band reflects the equilibrium between the keto and enol forms of the curcumin and is strongly dependent on the pH value and on the type of solvent (polarity and protic/aprotic) [62,73,74]. The absorption spectra of the investigated Al–Cur complexes showed significant spectral changes with the shoulder of the Vis-band that seemed to disappear. In order to better clarify this point, the experimental Vis band of the free ligand and of the complexes were fitted with multiple Gaussian functions (Figure 5a). Indeed, this structured absorption in the free curcumin can be well deconvoluted by two bands, centered at 358 nm (assigned to the keto form) and at 434 nm (assigned to the enol form) ($R^2 > 0.999$, $\chi^2 < 1.3 \times 10^{-4}$). The band deconvolution of the spectra of the complexes highlights that the enol band remained almost peaked at 434 nm, while a red shift of 30 nm was calculated for the diketo band ($R^2 > 0.998$, $\chi^2 < 3 \times 10^{-4}$). This analysis revealed that the most important spectral changes could be detected in the keto-enol absorption band, thus indicating the involvement of the keto-enol site in the complexation. To support these hypotheses, a full characterization of the complexes was carried out by mass spectrometry (ESI MS/MS, LD-MS, and MS/MS). The mass spectrum, obtained by direct infusion into an electrospray mass spectrometer, clearly indicates the formation in solution of a 1:1 Al:Cur complex (signal at m/z 429), which also coordinates a water molecule and a hydroxyl moiety, as indicated by the fragmentations. The high resolution (HR) laser desorption (LD) MS and MS/MS experiments provide insight on the neutral complex obtained during titrations. Direct and consecutive fragmentations of the complex did not show specific peaks associated with the keto-enol moiety, suggesting that the coordination of the aluminum occurs via the enol oxygen with the assistance of the oxygen lone pairs of the ketonic group (Figure 5f).

The above reported spectroscopic and spectrometric characterization was also extended to investigate the ability of Fe(III) to coordinate curcumin and to study the relative coordination site. The UV–Vis spectra of the Fe(III)–Cur complexes showed significant changes in the keto-enol absorption band, which appeared much more structured than in the spectrum of free curcumin, with the appearance of a new band at around 500 nm, usually associated with a metal-to-ligand-charge transfer transition (MLCT) [62]. Gaussian deconvolution analysis showed a red shift (15 nm) of the diketo band and a relative

intensity increase of this band at the expense of the enolic one with respect to the free curcumin. The increased intensity of the band assigned to the keto tautomer indicates that iron, unlike aluminum, stabilizes the keto form of curcumin. The ESI MS/MS of the neutral Fe(III)–curcumin complex (m/z 790) showed a very rich profile and many fragments could be identified to give useful insights such as those at m/z 423, probably due to the loss of a curcumin ligand, which also involves the reduction of Fe(III) to Fe(II); at m/z 177, arising from the formation of the feruloyl moiety; and at m/z 572, which is very interesting because it supports the hypothesis that the site of complexation is on the guaiacol moiety. From the LD/MS and MS/MS study, the most abundant signal resulted from the overlap of the complexes with a stoichiometry of 1:2 (M:L) containing the species $[Fe(II)(Cur)_2]^+$ (m/z 790.17) and $[Fe(III)(Cur)_2]^+$ (m/z 791.18), indicating that two molecules of curcumin chelate iron via the hydroxyl oxygen with the assistance of the oxygen lone pairs of the methoxyl groups. In addition, the formation of a fragment at m/z 599.1, due to the cleavage of the bond among the diketone functionalities, and loss of the neutral 1-aryl-3-hydroxy-1,3-butadiene moiety, confirms the results obtained by ESI MS/MS that iron coordination occurs on the guaiacol moiety (Figure 5f).

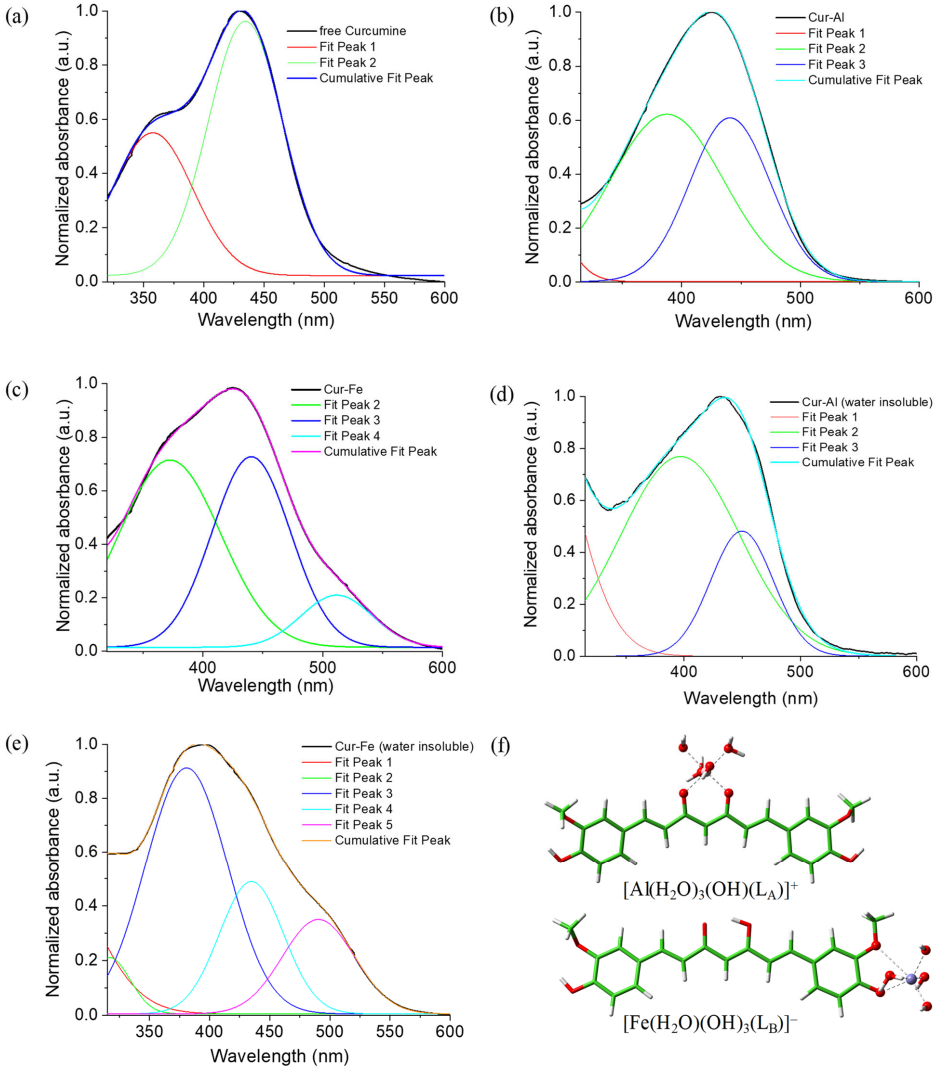

Figure 5. Deconvolution analysis of UV–Vis Spectra: (**a**) free Cur; (**b**) Al(III)–Cur aqueous solution; (**c**) Fe(III)–Cur aqueous solution; (**d**) Al(III)–Cur solid; (**e**) Fe(III)–Cur; and (**f**) optimized structures of the most probable Al– and Fe–Cur complexes. Adapted from [45], Copyright Elsevier 2019.

Other studies on the complexation between curcumin and iron (Fe(II) and Fe(III)) in methanol or methanol/water mixtures have been reported in the last few decades, showing the formation of complexes with a 1:2 M:L molar ratio where the ligand behaves as a bidentate by chelating the metal ion with the keto-enol moiety [61–63,75,76]. Generally, this coordination mode is accompanied by a hypsochromic shift in the UV–Vis spectrum of the complex with respect to the free curcumin [63] as well as by a significant shift (~40 cm^{-1}) in the IR spectrum of the complex of the following vibrations: ν(CO)keto, δ(CO)enol, and ν(C=C) aromatic [62].

6. Conclusions

In this review, experimental and computational results on the ability of some natural antioxidant molecules, NAMs, to form Al(III)– and Fe(III)–complexes are collected. The chelating ability of selected NAMs (i.e., hydroxycinnamic acids (*p*-coumaric, caffeic and ferulic acids), coumarin-3-carboxylic acid, quercetin, luteolin and curcumin), well known to be effective metal chelators, was investigated in aqueous solution, an environment that better mimics the physiological one. Data collected here evidence that:

- hydroxycinnamic acids (*p*CA, CA, and FA) are able to form more stable complexes with Al(III) than with Fe(III) coordinating the metal ion through the carboxylate site in all cases.
- coumarin-3-carboxylic acid, similarly, prefers to bind Al(III) rather than Fe(III), forming 1:1 and 1:2 M:L stoichiometric ratio complexes, respectively. Consequently, octahedral complexes with Al(III), involving both carboxylate and lactone moieties, and tetrahedral complex with Fe(III) in a η^1 ligand's coordination were analyzed.
- flavonoids (Que and Lut) formed 1:1 and 1:2 M:L complexes with both metal ions, though they showed a more intricate behavior, as more than one coordination mode was found plausible with both metal ions, making the identification of the preferred coordination site and thus the most probable complex in a water environment, especially in the case of Que, difficult.
- Curcumin discriminates well between the two metal ions since it prefers to coordinate Al(III) through the diketo site while the Fe(III) results most probably bound to the guaiacol site.

The excursus of data available for the selected NAMs toward bioavailable Al(III) and Fe(III) metal ions confirms the ability of phenolic compounds to trap metals preventing their accumulation and their harmful action to human health.

Author Contributions: Conceptualization, validation, writing—review and editing, supervision, A.B., E.F., T.M. and G.M.; Methodology, software, visualization, data curation, formal analysis, investigation, G.A.C., L.M., and G.M.; Writing—original draft preparation, G.A.C., E.F., and G.M.; Project administration, T.M. All authors have read and agreed to the published version of the manuscript.

Funding: This research received no external funding.

Acknowledgments: The authors thank the Dipartimento di Chimica e Tecnologie Chimiche, Università della Calabria and Ministero degli Affari Esteri e della Cooperazione Internazionale, MAECI-CUP H28D20000370001 for their financial support.

Conflicts of Interest: The authors declare no conflict of interest.

References

1. Crisponi, G.; Nurchi, V.M.; Bertolasi, V.; Remelli, M.; Faa, G. Chelating agents for human diseases related to aluminium overload. *Coord. Chem. Rev.* **2012**, *256*, 89–104. [CrossRef]
2. Liu, Y.; Guo, M. Studies on Transition Metal-Quercetin Complexes Using Electrospray Ionization Tandem Mass Spectrometry. *Molecules* **2015**, *20*, 8583–8594. [CrossRef] [PubMed]
3. Nurchi, V.M.; Crespo-Alonso, M.; Toso, L.; Lachowicz, J.I.; Crisponi, G. Chelation Therapy for Metal Intoxication: Comments from a Thermodynamic Viewpoint. *Mini-Rev. Med. Chem.* **2013**, *13*, 1541–1549. [CrossRef] [PubMed]

4. Arias Arias, F.E.; Beneduci, A.; Chidichimo, F.; Furia, E.; Straface, S. Study of the adsorption of mercury (II) on lignocellulosic materials under static and dynamic conditions. *Chemosphere* **2017**, *180*, 11–23. [CrossRef] [PubMed]
5. Hofer, T.; Jørgensen, T.O.; Olsen, R.L. Comparison of food antioxidants and iron chelators in two cellular free radical assays: Strong protection by Luteolin. *J. Agric. Food Chem.* **2014**, *62*, 8402–8410. [CrossRef]
6. Crisponi, G.; Dean, A.; Di Marco, V.; Lachowicz, J.I.; Nurchi, V.M.; Remelli, M.; Tapparo, A. Different approaches to the study of chelating agents for iron and aluminium overload pathologies. *Anal. Bioanal. Chem.* **2013**, *405*, 585–601. [CrossRef]
7. Drüeke, T.B. Intestinal absorption of aluminium in renal failure. *Nephrol. Dial. Transplant.* **2002**, *17*, 13–16. [CrossRef]
8. Exley, C. Aluminum Should Now Be Considered a Primary Etiological Factor in Alzheimer's Disease. *J. Alzheimer's Dis. Reports* **2017**, *1*, 23–25. [CrossRef]
9. Munoz, D.G. Is exposure to aluminum a risk factor for the development of Alzheimer disease?—No. *Arch. Neurol.* **1998**, *55*, 737–739. [CrossRef]
10. Lidsky, T.I. Is the Aluminum Hypothesis Dead? *J. Occup. Env. Med.* **2014**, *56*, S73–S79. [CrossRef]
11. Shannon, R.D. Revised effective ionic radii and systematic studies of interatomic distances in halides and chalcogenides. *Acta Cryst.* **1976**, *32*, 751–767. [CrossRef]
12. León-Carmona, J.R.; Alvarez-Idaboy, J.R.; Galano, A. On the peroxyl scavenging activity of hydroxycinnamic acid derivatives: Mechanisms, kinetics, and importance of the acid-base equilibrium. *Phys. Chem. Chem. Phys.* **2012**, *14*, 12534–12543. [CrossRef] [PubMed]
13. Beneduci, A.; Furia, E.; Russo, N.; Marino, T. Complexation behaviour of caffeic, ferulic and p-coumaric acids towards aluminium cations: A combined experimental and theoretical approach. *New J. Chem.* **2017**, *41*, 5182–5190. [CrossRef]
14. Furia, E.; Beneduci, A.; Russo, N.; Marino, T. Structural characterization of aluminium(III) and iron(III) complexes of coumarinic acid in aqueous solutions from combined experimental and theoretical investigations. *New J. Chem.* **2018**, *42*, 11006–11012. [CrossRef]
15. Jabeen, E.; Janjua, N.K.; Ahmed, S.; Murtaza, I.; Ali, T.; Hameed, S. Radical scavenging propensity of Cu^{2+}, Fe^{3+} complexes of flavonoids and in-vivo radical scavenging by Fe^{3+}-primuletin. *Spectrochim. Acta Part A Mol. Biomol. Spectrosc.* **2017**, *171*, 432–438. [CrossRef]
16. Cherrak, S.A.; Mokhtari-Soulimane, N.; Berroukeche, F.; Bensenane, B.; Cherbonnel, A.; Merzouk, H.; Elhabiri, M. In Vitro Antioxidant versus Metal Ion Chelating Properties of Flavonoids: A Structure-Activity Investigation. *PLoS ONE* **2016**, *11*, e0165575. [CrossRef]
17. Selvaraj, S.; Krishnaswamy, S.; Devashya, V.; Sethuraman, S.; Krishnan, U.M. Flavonoid-Metal Ion Complexes: A Novel Class of Therapeutic Agents. *Med. Res. Rev.* **2014**, *34*, 677–702. [CrossRef]
18. Kasprzak, M.M.; Erxleben, A.; Ochocki, J. Properties and applications of flavonoid metal complexes. *RSC Adv.* **2015**, *5*, 45853–45877. [CrossRef]
19. Kostyuk, V.A.; Potapovich, A.I.; Kostyuk, T.V.; Cherian, M.G. Metal complexes of dietary flavonoids: Evaluation of radical scavenger properties and protective activity against oxidative stress in vivo. *Cell. Mol. Biol.* **2007**, *53*, 62–69. [CrossRef]
20. Corradini, E.; Foglia, P.; Giansanti, P.; Gubbiotti, R.; Samperi, R.; Laganà, A. Flavonoids: Chemical properties and analytical methodologies of identification and quantitation in foods and plants. *Nat. Prod. Res.* **2011**, *25*, 469–495. [CrossRef]
21. Ravishankar, D.; Rajora, A.K.; Greco, F.; Osborn, H.M.I. Flavonoids as prospective compounds for anti-cancer therapy. *Int. J. Biochem. Cell Biol.* **2013**, *45*, 2821–2831. [CrossRef]
22. Spoerlein, C.; Mahal, K.; Schmidt, H.; Schobert, R. Effects of chrysin, apigenin, genistein and their homoleptic copper(II) complexes on the growth and metastatic potential of cancer cells. *J. Inorg. Biochem.* **2013**, *127*, 107–115. [CrossRef] [PubMed]
23. Chebotarev, A.N.; Snigur, D.V. Study of the acid-base properties of quercetin in aqueous solutions by color measurements. *J. Anal. Chem.* **2015**, *70*, 55–59. [CrossRef]
24. Jabeen, E.; Janjua, N.K.; Ahmed, S.; Murtaza, I.; Ali, T.; Masood, N.; Rizvi, A.S.; Murtaza, G. DFT predictions, synthesis, stoichiometric structures and anti-diabetic activity of Cu (II) and Fe (III) complexes of quercetin, morin, and primuletin. *J. Mol. Struct.* **2017**, *1150*, 459–468. [CrossRef]
25. Escudero, L.B.; Fusari, C.M.; Altamirano, J.C.; Camargo, A.B.; Wuilloud, R.G. Stability of Iron-Quercetin Complexes in Synthetic Wine under In Vitro Digestion Conditions. *J. Food Sci.* **2014**, *79*, C1933–C1938. [CrossRef]
26. Pękal, A.; Pyrzynska, K. Evaluation of Aluminium Complexation Reaction for Flavonoid Content Assay. *Food Anal. Methods* **2014**, *7*, 1776–1782. [CrossRef]
27. Zhang, C.; Korshin, G.V.; Kuznetsov, A.M.; Yan, M. Experimental and quantum-chemical study of differential absorbance spectra of environmentally relevant species: A study of quercetin deprotonation and its interactions with copper (II) ions. *Sci. Total Environ.* **2019**, *679*, 229–236. [CrossRef] [PubMed]
28. Ravichandran, R.; Rajendran, M.; Devapiriam, D. Antioxidant study of quercetin and their metal complex and determination of stability constant by spectrophotometry method. *Food Chem.* **2014**, *146*, 472–478. [CrossRef] [PubMed]
29. Raza, A.; Xu, X.; Xia, L.; Xia, C.; Tang, J.; Ouyang, Z. Quercetin-Iron Complex: Synthesis, Characterization, Antioxidant, DNA Binding, DNA Cleavage, and Antibacterial Activity Studies. *J. Fluoresc.* **2016**, *26*, 2023–2031. [CrossRef]
30. Normaya, E.; Fazli, M.; Norazmi Ahmad, M.; Ku Bulat, K.H. COSMO-RS and DFT studies on development and optimization of quercetin as a chemosensor for Fe 3+ recognition in aqueous medium. *J. Mol. Struct.* **2019**, *1184*, 538–545. [CrossRef]

31. Furia, E.; Marino, T.; Russo, N. Insights into the coordination mode of quercetin with the Al(III) ion from a combined experimental and theoretical study. *Dalt. Trans.* **2014**, *43*, 7269–7274. [CrossRef]
32. Samsonowicz, M.; Regulska, E. Spectroscopic study of molecular structure, antioxidant activity and biological effects of metal hydroxyflavonol complexes. *Spectrochim. Acta Part A Mol. Biomol. Spectrosc.* **2017**, *173*, 757–771. [CrossRef] [PubMed]
33. De Castilho, T.S.; Matias, T.B.; Nicolini, K.P.; Nicolini, J. Study of interaction between metal ions and quercetin. *Food Sci. Hum. Wellness* **2018**, *7*, 215–219. [CrossRef]
34. Corrente, G.A.; Malacaria, L.; Beneduci, A.; Furia, E.; Marino, T.; Mazzone, G. Experimental and theoretical study on the coordination properties of quercetin towards aluminum(III), iron(III) and copper(II) in aqueous solution. *J. Mol. Liq.* **2021**, *325*, 115171. [CrossRef]
35. Çıkla Yılmaz, D.; Pekin, M. Potentiometric and Chromatographic Study of Cu(II) and Al(III) Complexes of Quercetin. *Marmara Pharm. J.* **2017**, *21*, 330–337. [CrossRef]
36. Wang, Q.; Zhao, L.; Zhao, H.; Liu, X.; Gao, L.; Cheng, N.; Cao, W. Complexation of luteolin with lead (II): Spectroscopy characterization and theoretical researches. *J. Inorg. Biochem.* **2019**, *193*, 25–30. [CrossRef] [PubMed]
37. Zheng, K.; Xiong, Y.; Li, Z.; Peng, L.; Guo, Q.; Li, X.; Deng, X. ESI-TOF MS analysis and DNA cleavage activity of complexes formed by luteolin and five metal ions in hot water. *Inorg. Nano-Metal Chem.* **2020**, *50*, 1181–1188. [CrossRef]
38. Cione, E.; La Torre, C.; Cannataro, R.; Caroleo, M.C.; Plastina, P.; Gallelli, L. Quercetin, Epigallocatechin Gallate, Curcumin, and Resveratrol: From Dietary Sources to Human MicroRNA Modulation. *Molecules* **2019**, *25*, 63. [CrossRef]
39. Kim, J.; Lee, H.J.; Lee, K.W. Naturally occurring phytochemicals for the prevention of Alzheimer's disease. *J. Neurochem.* **2010**, *112*, 1415–1430. [CrossRef]
40. Banerjee, S.; Chakravarty, A.R. Metal Complexes of Curcumin for Cellular Imaging, Targeting, and Photoinduced Anticancer Activity. *Acc. Chem. Res.* **2015**, *48*, 2075–2083. [CrossRef]
41. Sen, S.; Sharma, H.; Singh, N. Curcumin enhances Vinorelbine mediated apoptosis in NSCLC cells by the mitochondrial pathway. *Biochem. Biophys. Res. Commun.* **2005**, *331*, 1245–1252. [CrossRef]
42. Khopde, S.M.; Priyadarsini, K.I.; Venkatesan, P.; Rao, M.N.A. Free radical scavenging ability and antioxidant efficiency of curcumin and its substituted analogue. *Biophys. Chem.* **1999**, *80*, 85–91. [CrossRef]
43. Barik, A.; Mishra, B.; Shen, L.; Mohan, H.; Kadam, R.M.; Dutta, S.; Zhang, H.Y.; Priyadarsini, K.I. Evaluation of a new copper(II)-curcumin complex as superoxide dismutase mimic and its free radical reactions. *Free Radic. Biol. Med.* **2005**, *39*, 811–822. [CrossRef]
44. Dutta, S.; Murugkar, A.; Gandhe, N.; Padhye, S. Enhanced antioxidant activities of metal conjugates of Curcumin derivatives. *Met. Based. Drugs* **2001**, *8*, 183–188. [CrossRef] [PubMed]
45. Beneduci, A.; Corrente, G.A.; Marino, T.; Aiello, D.; Bartella, L.; Di Donna, L.; Napoli, A.; Russo, N.; Romeo, I.; Furia, E. Insight on the chelation of aluminum(III) and iron(III) by curcumin in aqueous solution. *J. Mol. Liq.* **2019**, *296*, 111805. [CrossRef]
46. Cornard, J.P.; Lapouge, C. Absorption spectra of caffeic acid, caffeate and their 1:1 complex with AI(III): Density functional theory and time-dependent density functional theory investigations. *J. Phys. Chem. A* **2006**, *110*, 7159–7166. [CrossRef] [PubMed]
47. Mazzone, G. On the Inhibition of Hydroxyl Radical Formation by Hydroxycinnamic Acids: The Case of Caffeic Acid as a Promising Chelating Ligand of a Ferrous Ion. *J. Phys. Chem. A* **2019**, *123*, 9560–9566. [CrossRef]
48. Leopoldini, M.; Russo, N.; Chiodo, S.; Toscano, M. Iron Chelation by the Powerful Antioxidant Flavonoid Quercetin. *J. Agric. Food Chem.* **2006**, *54*, 6343–6351. [CrossRef] [PubMed]
49. Villuendas-Rey, Y.; Alvarez-Idaboy, J.R.; Galano, A. Assessing the Protective Activity of a Recently Discovered Phenolic Compound against Oxidative Stress Using Computational Chemistry. *J. Chem. Inf. Model.* **2015**, *55*, 2552–2561. [CrossRef]
50. Truong, D.H.; Nhung, N.T.A.; Dao, D.Q. Iron ions chelation-based antioxidant potential vs. pro-oxidant risk of ferulic acid: A DFT study in aqueous phase. *Comput. Theor. Chem.* **2020**, *1185*, 112905. [CrossRef]
51. Amat, A.; Clementi, C.; Miliani, C.; Romani, A.; Sgamellotti, A.; Fantacci, S. Complexation of apigenin and luteolin in weld lake: A DFT/TDDFT investigation. *Phys. Chem. Chem. Phys.* **2010**, *12*, 6672–6684. [CrossRef] [PubMed]
52. Primikyri, A.; Mazzone, G.; Lekka, C.; Tzakos, A.G.; Russo, N.; Gerothanassis, I.P. Understanding zinc(II) chelation with quercetin and luteolin: A combined NMR and theoretical study. *J. Phys. Chem. B* **2015**, *119*, 83–95. [CrossRef]
53. Dimitrić Marković, J.M.; Marković, Z.S.; Brdarić, T.P.; Pavelkić, V.M.; Jadranin, M.B. Iron complexes of dietary flavonoids: Combined spectroscopic and mechanistic study of their free radical scavenging activity. *Food Chem.* **2011**, *129*, 1567–1577. [CrossRef]
54. Singh, K.; Kumar, A. Kinetics of complex formation of Fe(III) with caffeic acid: Experimental and theoretical study. *Spectrochim. Acta Part A Mol. Biomol. Spectrosc.* **2019**, *211*, 148–153. [CrossRef]
55. Favaro, G.; Clementi, C.; Romani, A.; Vickackaite, V. Acidichromism and ionochromism of luteolin and apigenin, the main components of the naturally occurring yellow weld: A spectrophotometric and fluorimetric study. *J. Fluoresc.* **2007**, *17*, 707–714. [CrossRef] [PubMed]
56. Yang, A.H.; Shi, X.Y.; Li, X.; Li, F.F.; Zhang, Q.Q.; Jiang, S.X.; Cui, J.Z.; Gao, H.L. Spectroscopic and electrochemical studies on the evaluation of the radical scavenging activities of luteolin by chelating iron. *RSC Adv.* **2014**, *4*, 25227–25233. [CrossRef]
57. Ahmedova, A.; Paradowska, K.; Wawer, I. 1H, 13C MAS NMR and DFT GIAO study of quercetin and its complex with Al(III) in solid state. *J. Inorg. Biochem.* **2012**, *110*, 27–35. [CrossRef]

58. Rygula, A.; Wrobel, T.P.; Szklarzewicz, J.; Baranska, M. Raman and UV-vis spectroscopy studies on luteolin-Al(III) complexes. *Vib. Spectrosc.* **2013**, *64*, 21–26. [CrossRef]
59. Sun, J.; Wu, Y.; Xiao, D.; Lin, X.; Li, H. Spectrofluorimetric determination of aluminum ions via complexation with luteolin in absolute ethanol. *Luminescence* **2014**, *29*, 456–461. [CrossRef]
60. Jiang, T.; Wang, L.; Zhang, S.; Sun, P.C.; Ding, C.F.; Chu, Y.Q.; Zhou, P. Interaction of curcumin with Al(III) and its complex structures based on experiments and theoretical calculations. *J. Mol. Struct.* **2011**, *1004*, 163–173. [CrossRef]
61. Bicer, N.; Yildiz, E.; Yegani, A.A.; Aksu, F. Synthesis of curcumin complexes with iron(III) and manganese(II), and effects of curcumin-iron(III) on Alzheimer's disease. *New J. Chem.* **2018**, *42*, 8098–8104. [CrossRef]
62. Refat, M.S. Synthesis and characterization of ligational behavior of curcumin drug towards some transition metal ions: Chelation effect on their thermal stability and biological activity. *Spectrochim. Acta Part A Mol. Biomol. Spectrosc.* **2013**, *105*, 326–337. [CrossRef]
63. Bagchi, A.; Mukherjee, P.; Bhowmick, S.; Raha, A. Synthesis, characterization and antibacterial activity of a novel curcumin metal complex. *Int. J. Drug Dev. Res.* **2015**, *7*, 11–14.
64. Kejík, Z.; Kaplánek, R.; Masařík, M.; Babula, P.; Matkowski, A.; Filipenský, P.; Veselá, K.; Gburek, J.; Sýkora, D.; Martásek, P.; et al. Iron Complexes of Flavonoids-Antioxidant Capacity and Beyond. *Int. J. Mol. Sci.* **2021**, *22*, 646. [CrossRef] [PubMed]
65. De Souza, R.F.V.; De Giovani, W.F. Antioxidant properties of complexes of flavonoids with metal ions. *Redox Rep.* **2004**, *9*, 97–104. [CrossRef] [PubMed]
66. De Souza, R.F.V.; De Giovani, W.F. Synthesis, spectral and electrochemical properties of Al(III) and Zn(II) complexes with flavonoids. *Spectrochim. Acta Part A Mol. Biomol. Spectrosc.* **2005**, *61*, 1985–1990. [CrossRef] [PubMed]
67. Macáková, K.; Mladěnka, P.; Filipský, T.; Říha, M.; Jahodář, L.; Trejtnar, F.; Bovicelli, P.; Proietti Silvestri, I.; Hrdina, R.; Saso, L. Iron reduction potentiates hydroxyl radical formation only in flavonols. *Food Chem.* **2012**, *135*, 2584–2592. [CrossRef]
68. Mira, L.; Fernandez, M.T.; Santos, M.; Rocha, R.; Florêncio, M.H.; Jennings, K.R. Interactions of Flavonoids with Iron and Copper Ions: A Mechanism for their Antioxidant Activity. *Free Radic. Res.* **2002**, *36*, 1199–1208. [CrossRef]
69. Lopes, G.K.B.; Schulman, H.M.; Hermes-Lima, M. Polyphenol tannic acid inhibits hydroxyl radical formation from Fenton reaction by complexing ferrous ions. *Biochim. Biophys. Acta Gen. Subj.* **1999**, *1472*, 142–152. [CrossRef]
70. Pękal, A.; Biesaga, M.; Pyrzynska, K. Interaction of quercetin with copper ions: Complexation, oxidation and reactivity towards radicals. *BioMetals* **2011**, *24*, 41–49. [CrossRef]
71. MacCarrone, G.; Caruso, R.; Contino, A.; Giuffrida, A.; Messina, M.; Cucinotta, V. The contribution of electrospray mass spectrometry to the study of metal complexes: The case of copper(II)-dipeptide systems. *Eur. J. Inorg. Chem.* **2009**, *2009*, 2612–2620. [CrossRef]
72. Jovanovic, S.V.; Steenken, S.; Tosic, M.; Marjanovic, B.; Simic, M.G. Flavonoids as antioxidants. *J. Am. Chem. Soc.* **1994**, *116*, 4846–4851. [CrossRef]
73. Bernabé-Pineda, M.; Ramírez-Silva, M.T.; Romero-Romo, M.; González-Vergara, E.; Rojas-Hernández, A. Determination of acidity constants of curcumin in aqueous solution and apparent rate constant of its decomposition. *Spectrochim. Acta Part A Mol. Biomol. Spectrosc.* **2004**, *60*, 1091–1097. [CrossRef]
74. Priyadarsini, K.I. Photophysics, photochemistry and photobiology of curcumin: Studies from organic solutions, bio-mimetics and living cells. *J. Photochem. Photobiol. C Photochem. Rev.* **2009**, *10*, 81–95. [CrossRef]
75. Shakeri, A.; Panahi, Y.; Johnston, T.P.; Sahebkar, A. Biological properties of metal complexes of curcumin. *BioFactors* **2019**, *45*, 304–317. [CrossRef]
76. Saithongdee, A.; Praphairaksit, N.; Imyim, A. Electrospun curcumin-loaded zein membrane for iron(III) ions sensing. *Sensors Actuators B Chem.* **2014**, *202*, 935–940. [CrossRef]

applied sciences

MDPI

Article

Thermodynamic Study on the Dissociation and Complexation of Coumarinic Acid with Neodymium(III) and Dioxouranium(VI) in Aqueous Media

Luana Malacaria, Giuseppina Anna Corrente and Emilia Furia *

Department of Chemistry and Chemical Technologies, University of Calabria, 87036 Rende (CS), Italy; luana.malacaria@unical.it (L.M.); giuseppina.corrente@unical.it (G.A.C.)
* Correspondence: emilia.furia@unical.it; Tel.: +39-0984-492831

Abstract: In the frame of a systematic study on the sequestering ability of natural antioxidants towards metal cations, the complexation of coumarin-3-carboxilic acid (HCCA) with neodymium(III) and dioxouranium(VI) (uranyl, UO_2^{2+}), and overall stability constants of the resulting complexes, were evaluated from the pH-potentiometric titration data at 37 °C and in an aqueous solution (i.e., 0.16 mol/L $NaClO_4$). The graphic representation of the complex's concentration curves is given by the distribution diagrams, which provide a depiction of all the species present in the solution in the selected pH ranges. The protonation constant of HCCA was also determined to evaluate the competition of the ligand for the metal cations and H^+. The ligand-to-metal concentration ratio was varied between 1 and 10, and the hydrogen ion concentration was decreased stepwise until the incipient precipitation of a basic salt of the metal, which occurred at different values depending on the specific metal cation and the ligand to metal ratio. Speciation profiles obtained by potentiometric titrations and supported by UV-Vis data show that a complexation occurs at a ligand-to-Nd(III) and to $-UO_2^{2+}$ ratio of 1:1 and 2:1, with different degrees of deprotonation: $Nd(OH)(CCA)^+$, $UO_2(OH)(CCA)$, $UO_2(OH)_2(CCA)^-$, and $Nd(OH)(CCA)_2$, $UO_2(CCA)_2$ and $(UO_2)_2(OH)_2(CCA)_2$.

Keywords: coumarin-3-carboxilic acid; Nd(III) complexes; UO_2^{2+} complexes; sequestering ability; stability constants

Citation: Malacaria, L.; Corrente, G.A.; Furia, E. Thermodynamic Study on the Dissociation and Complexation of Coumarinic Acid with Neodymium(III) and Dioxouranium(VI) in Aqueous Media. *Appl. Sci.* **2021**, *11*, 4475. https://doi.org/10.3390/app11104475

Academic Editors: Giuseppe Cassone, Claudia Foti, Ottavia Giuffré and Franz Saija

Received: 21 April 2021
Accepted: 11 May 2021
Published: 14 May 2021

1. Introduction

The poisoning action of toxic metal ions represents one of the most important problems for health. In this context, metal chelation therapy was proposed more than 50 years ago for the treatment of pathologies produced in the body by an overload of a metal ion, and it is the most efficient therapeutic approach [1,2]. The choice of the most adequate chelating agent is related to the specificity and stability of the metal–chelator complexes. Metal chelation therapy involves the use of a chelating agent, which consists of an organic molecule that possesses a chelator located at one terminus of the agent and an active functionality located at the other end of the molecule to connect with the vector molecule [3]. Among chelators, the most used are macrocyclic ligands, which are to be preferred with respect to their acyclic counterparts from a thermodynamic and kinetic point of view. Their drawback is related to their slow binding kinetics, which necessitates high temperatures. Coumarin and its derivatives can form complexes with different metal ions, and therefore, in principle, can be used in specific chelation therapies. This class of ligands can form complexes with several toxic metal ions, and has attracted the interest of researchers, also in consideration of their antibiotic, anticoagulant, anticancer and anti-inflammatory properties [4]. Complexes of this class of ligands with several transitions, lanthanide and actinide metal ions have been studied previously to gain insight into their coordination chemistry and their biological activity [5–15]. Some reviews summarize the advances in various medicinal applications of metal complexes of coumarins [15–18]. It was reported that the biological activity of some

coumarin derivatives significantly improves by binding to metal ions; this behavior could be attributed to an increase in the lipophilicity of the systems. However, the relationship between the structure and properties of complexes is still unknown. Nevertheless, to achieve insight into the factors controlling the metal complex biological activity, it is first necessary to know the binding properties of coumarins to the metal ions. In 2001, attempts to determine the structure of a copper(II) complex of coumarin-3-carboxylic acid (HCCA), analyzing spectroscopic data, suggested a binuclear structure [4]. Synthesis was carried out using copper(II) chloride as the salt yielding a very insoluble product. Overall complexes of Ni(II), Co(II), Zn(II) and Mn(II) with HCCA were studied at experimental and theoretical levels. The complexes were characterized by elemental analyses, FT-IR, ^{1}H-NMR, ^{13}C-NMR and UV-Vis spectroscopy, and by magnetic susceptibility measurements [19]. Recently, we have reported on the complexation of HCCA with Al(III) and Fe(III), in aqueous solutions at 37 °C and in 0.16 M NaCl, to evaluate the selectivity of this ligand towards bioavailable metal cations [20].

HCCA exhibits two different coordination sites (Figure 1): it can play as monodentate or bidentate ligand via carboxylic moiety involving one or both oxygen atoms, respectively, as well as bidentate ligand through the lactone and the carboxylic oxygen to realize a high stabilized 6-membered metallocycle. Simultaneous bidentate and monodentate coordination mode by the free carbonyl oxygen was shown in the presence of lanthanides [12].

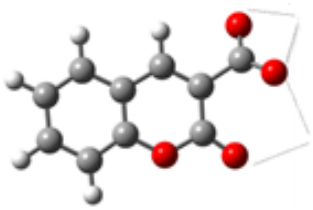

Figure 1. Coordination sites of HCCA.

In view of its potential application as a chelating agent, herein we present a study on the complexation ability of coumarin-3-carboxylic acid towards neodymium(III) and dioxouranium(VI) (uranyl, UO_2^{2+}) under the physiological conditions of temperature and ionic strength (i.e., 37 °C and 0.16 mol/L $NaClO_4$), evaluating the stability constants of the complexes and the corresponding structures by potentiometric measurements and UV-Vis spectrophotometry. This work is the first one entirely in an aqueous medium; although the ligand's antioxidant activity involves water as a natural solvent in the biological media, most of the studies reported in the literature refers to measurements carried out in mixed solvents, due to the low solubility in water of HCCA.

2. Materials and Methods

2.1. Chemicals

Sodium hydroxide titrant solutions, perchloric acid and sodium perchlorate stock solutions were prepared and standardized as previously described [21]. Neodymium and uranyl perchlorate stock solutions were prepared and standardized as reported previously [22]. HCCA (≥99%, Sigma–Aldrich, Munich, Germany), kept in a desiccator over silica gel, was used without further purification. The ionic strength of all the solutions was adjusted to 0.16 mol/L at 37 °C by adding the appropriate amount of $NaClO_4$ as the background electrolyte. All solutions were freshly prepared with double-distilled water.

2.2. Potentiometry and Spectrophotometry

The potentiometric apparatus used to carry out the titrations was described previously [21]. The glass electrodes were manufactured by Metrohm (Swiss) and acquired, after the addition of the reagents, a constant potential within 45–60 min that remained unchanged within ±0.01 mV. To avoid carbonate interference, a slow stream of nitrogen

gas was passed into the test solutions, kept under magnetic stirring during titrations. The cell assembly was placed in a thermostat kept at (37.0 ± 0.1) °C.

The complexation equilibria were studied, at 37 °C and in 0.16 mol/L $NaClO_4$, by measuring, with a glass electrode (GE), the competition of HCCA for H^+ and metal cations. Measurements were performed as potentiometric titrations with cell (G)

$$\text{RE} \mid \text{Test Solution} \mid \text{GE} \qquad \text{(G)}$$

in which RE is the reference electrode (Ag | AgCl | 0.01 mol/L NaCl | 0.15 mol/L $NaClO_4$ | 0.16 mol/L $NaClO_4$) and the Test Solution contained C_M mol/L $M(ClO_4)_n$ (i.e., $Nd(ClO_4)_3$ and $UO_2(ClO_4)_2$), C_L mol/L HCCA, C_A mol/L $HClO_4$, C_B mol/L NaOH, and (0.16 − nC_M − C_A − C_B) mol/L $NaClO_4$. The EMF of cell (G) can be written, in mV, at the temperature of 37 °C, as Equation (1):

$$E = E^\circ + 61.54 \log[H^+] + E_j \qquad (1)$$

where E° was constant for each series of measurements and E_j is the liquid junction potential, which is a function of $[H^+]$ only [23]. E_j value under our experimental conditions (i.e., 37 °C and 0.16 mol/L $NaClO_4$) was determined by acid-base titration with cell (G) when metal ions and HCCA were absent. The data for $[H^+] \leq 0.100$ mol/L could be well approximated by the linear slope E_j $([H^+])_I = -j_I$ $[H^+]$. The value of j (mV/M) is 337 ± 1.

Each titration was divided into two parts. In the first part, E° was determined in the absence of HCCA and metal cations; in the $[H^+]$ range 10^{-4}–10^{-2} mol/L values constant to within 0.1 mV were calculated according to the Gran's method [24,25]. In the second part, after the addition of the reagents, the acidity was stepwise decreased by adding known volumes of NaOH standard solution. The concentration of HCCA (C_L) was varied within 1 and $5{\cdot}10^{-3}$ mol/L, while the concentration of metal ions (C_M) ranged within 0.5 and $5{\cdot}10^{-3}$ mol/L, and the ligand to metal concentration ratio was varied within 1 and 10. The hydrogen ion concentration was varied from $1{\cdot}10^{-2}$ mol/L (pH 2.0) to incipient precipitation of a neutral salt, which takes place in the range $[H^+] = (3.2–0.032){\cdot}10^{-5}$ mol/L (pH 4.5–6.5) depending on the specific metal ion and on the ligand-to-metal ratio. The primary C_M, C_L, C_A, C_B and $[H^+]$ data form the basis of the treatment to obtain the stability constants.

The spectrophotometric measurements were carried out with a Varian Cary 50 Scan UV Visible Spectrophotometer. Absorbance values between 210 and 450 nm were measured each 1 nm. The temperature of the cell holder was kept at (37.0 ± 0.3) °C by a Grant circulating water bath. Matched quartz cells of thickness 1 cm were employed. The absorbance, A_λ, was recorded to 0.001 units. The acquisition of data was controlled with the aid of a computer connected to the instrument.

2.3. Synthesis of the Complexes

An amount of 0.560 g of $Nd(ClO_4)_3$ (0.119 mmol) and 0.435 g of $UO_2(ClO_4)_2$ (0.2196 mmol) stock solutions were added to 10.0 mg (0.0521 mmol) and 5.0 mg of coumarin-3-carboxylic acid, respectively, and then dissolved in water (i.e., 100 mL) under constant stirring and at 37 °C over a period of 24 h.

Taking into account the distribution diagrams of the metal ions in the presence of HCCA, the pH of these solutions was controlled (i.e., pH = 6 and pH = 4 for neodymium and uranyl, respectively). The complexation resulted in pallid yellow aqueous solutions and two solids, white for neodymium and orange for uranyl, the latter removed by filtration. Aqueous solutions, as well as solids, dissolved in DMSO, and opportunely diluted with water, were analyzed by UV–Visible spectroscopy.

3. Results

The experimental data (C_M, C_L, C_A, C_B, $[H^+]$), processed by graphical, as well as numerical procedures, were explained according to the general equilibrium reported in the Equation (2):

$$p\,M^{n+} + q\,OH^- + r\,CCA^- \rightleftarrows M_p(OH)_q(CCA)_r^{(np-q-r)} \qquad \log \beta_{pqr} \tag{2}$$

The graphical methods consist essentially in the comparison of experimental plots with model functions [26]. To explain the experimental data, the simple hypothesis was made that the main reaction products are binary ($q = 0$) complexes, mononuclear in metal ion ($p = 1$), formed according to equilibrium (3):

$$M^{n+} + r\,CCA^- \rightleftarrows M(CCA)_r^{(n-r)} \qquad \log \beta_{10r} \tag{3}$$

The validity of this assumption was tested by constructing the graphs Z as a function of log ($[HCCA]/[H_3O^+]$) from the primary data. Z represents the average number of ligand for metal ion, as reported in Equation (4):

$$Z = (C_A - [HCCA] - [CCA^-])/C_B \tag{4}$$

Thus, when complexes of general formula $M(CCA)_r^{(n-r)}$ predominate, the points Z versus log ($[HCCA]/[H_3O^+]$), at different C_L and C_M, should fall on a unique curve. The experimental functions Z for Nd^{3+}-HCCA and UO_2^{2+}-HCCA are reported in Figure 2a,b, respectively.

Table 1. Formation of complexes of coumarin-3-carboxylic acid with Nd^{3+} and UO_2^{2+} according to Equation (2). Values of log β in $NaClO_4$ 0.16 mol/L at 37 °C were obtained by numerical procedure. Standard deviations are reported as 3σ.

Metal Ions	Species	log β ± 3σ
Nd^{3+}	$Nd(OH)(CCA)^+$	9.2 ± 0.1
	$Nd(OH)(CCA)_2$	11.9 ± 0.3
UO_2^{2+}	$UO_2(CCA)_2$	8.2 ± 0.1
	$UO_2(OH)(CCA)$	13.0 ± 0.3
	$UO_2(OH)_2(CCA)^-$	21.6 ± 0.1
	$(UO_2)_2(OH)_2(CCA)_2$	28.9 ± 0.3

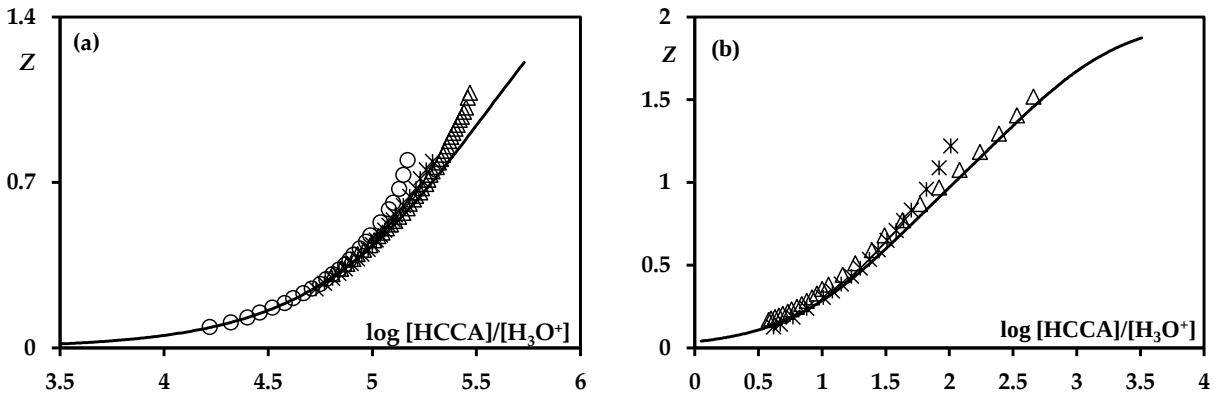

Figure 2. Z as a function of log($[HCCA]/[H_3O^+]$) for (**a**) Nd^{3+}-HCCA and (**b**) UO_2^{2+}-HCCA systems. Triangles (0.5, 5); diamond (5, 5); circles (1, 2). The curve was calculated with the constants obtained by numerical treatment and reported in Table 1.

As Figure 2 shows, most of the experimental points fall on a unique curve, which tends to 2, though a careful inspection of the graphs shows that small, but systematic, deviations from the model including only simple complexes were observed. These deviations

were evidence that some additional species are present. The probable composition of the complexes, responsible for these deviations, was obtained by numerical treatment by the least-square program SUPERQUAD [27], to seek the minimum of the function:

$$U = \sum (E_i^{obs} - E_i^{cal})^2 \quad (2)$$

where $E^{obs} = E + j\,[H_3O^+] = E^\circ + 0.06154 \log [H_3O^+]$ and E^{cal} is a value calculated for a given set of parameters.

The most probable p, q and r values and the corresponding constants log β_{pqr} (Equation (2)) were achieved by varying systematically the stability constants of a chosen ternary species (p,q,r) to obtain the best data fitting. In the numerical treatments, the acidic constant of coumarin-3-carboxylic acid, according to equilibrium (5) and reported with the relative standard deviation (3σ), was kept invariant.

$$HCCA \leftrightarrows CCA^- + H^+ \qquad \log K_a = -3.08 \pm 0.01 \quad (5)$$

This constant, unknown from the literature, was determined by potentiometric measurements under the same experimental conditions used for the evaluation of the stability constants between ligand and metal ions (i.e., at 37 °C and in 0.16 mol/L $NaClO_4$).

Considering the low solubility of HCCA in an aqueous solution [20], all the experiments were carried out by adding an exactly weighed quantity of solid ligand in the titration's apparatus. When equilibria (2) and (5) take place, HCCA dissolved into the aqueous medium. In the numerical treatment, the constants of the predominant hydrolysis products of Nd^{3+} and UO_2^{2+}, taken from the literature [28], (i.e., $Nd(OH)^{2+}$ and $Nd_2(OH)_2^{4+}$, $(UO_2)_2(OH)_2^{2+}$, $(UO_2)_3(OH)_5^+$, $UO_2(OH)^+$ and $(UO_2)_3(OH)_4^{2+}$, respectively), were kept invariant and were used to construct the distribution diagrams reported in Figure 3a,b. In the construction of these diagrams, the same pH range investigated for the study of the complexes was considered. As can be seen in Figure 3a, the only hydrolytical species of neodymium is $Nd(OH)^{2+}$, which nevertheless does not reach percentages greater than 10%. In regard to uranyl ion (Figure 3b), the complexes $(UO_2)_2(OH)_2^{2+}$ and $(UO_2)_3(OH)_5^+$ are the predominant hydrolytical species, while $(UO_2)_3(OH)_4^{2+}$ and $(UO_2)(OH)^+$ are minor species, with percentages that do not exceed 10% and 1%, respectively.

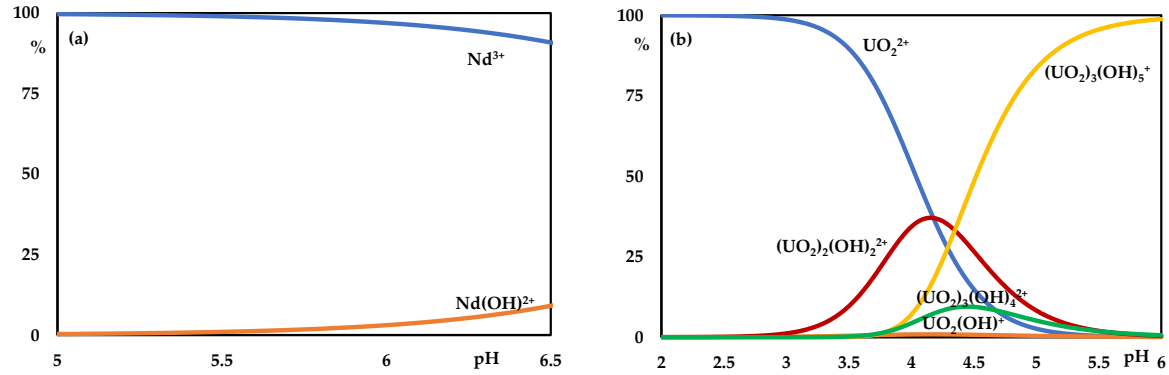

Figure 3. Distribution diagrams of hydrolytical species of (**a**) Nd^{3+} (C_M = 1.0 mM) and (**b**) UO_2^{2+} (C_M = 2.5 mM).

The results obtained for the neodymium- and uranyl-HCCA systems are reported in Table 1. For the neodymium-HCCA system, experimental data were explained with the formation of one complex, and the best minimum was obtained with the $Nd(OH)CCA^+$ species. A substantial decrease in the square error sum U (66.85%) was obtained considering also the presence of $Nd(OH)(CCA)_2$. No other complexes improved the fit.

Moreover, the uranyl-HCCA system data were explained with one complex: the best model comprised $UO_2(CCA)_2$. Different models that consider the presence of two species were also tested; among these, the best fit was obtained with the presence of $UO_2(CCA)_2$ and $UO_2(OH)(CCA)$, which corresponds to a decreasing of U (57%). A lower

error square sum (71%) was still obtained on adding the species $UO_2(OH)_2(CCA)^-$. Finally, the inclusion of the polynuclear complexes $(UO_2)_2(OH)_2(CCA)_2$, though present in small amounts, lowers the minimum of the square error sum by more than 40%. No other species, introduced to improve the fit, was retained. Speciation profiles show that in an aqueous solution a complexation occurs at 1:1 and 2:1 ligand-to-cations ratio with different degrees of deprotonation for both cations. A direct comparison between species with the same stoichiometry shows that the complex of uranyl is more stable than that of neodymium (i.e., 13.0 vs. 9.2).

4. Discussion

In this work, we have investigated the acid−base equilibrium of coumarinic acid and the chelating properties of its deprotonated form towards neodymium and uranyl at 37 °C and in 0.16 mol/L $NaClO_4$. Coumarinic acid anion forms 1:1 and 2:1 complexes with both metal ions. The uranyl ion is also capable to form a polynuclear complex with stoichiometry 2:2. Furthermore, from the data reported in Table 1, it may be noted that the complex $UO_2(OH)(CCA)$ is stronger than the corresponding neodymium species, $Nd(OH)(CCA)^+$.

The stability constants reported in Table 1 were used to represent the distribution diagrams (Figure 4a,b), in which the percentage of metal cations into the complexes as a function of pH is depicted.

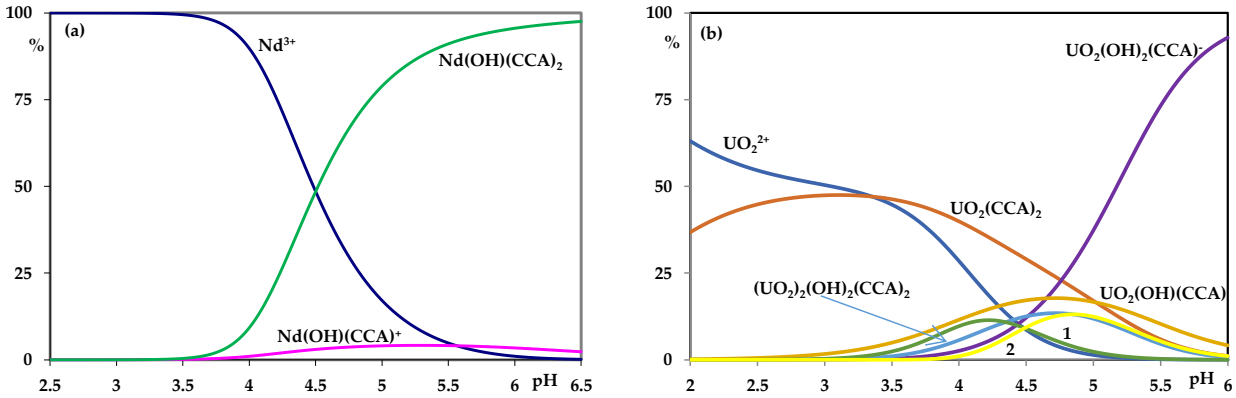

Figure 4. Distribution diagrams in the presence of HCCA of (**a**) Nd^{3+} (C_M = 1.0 mM and C_L = 2.0 mM) and (**b**) UO_2^{2+} (C_M = 2.5 mM and C_L = 2.5 mM). One (green line) and 2 (yellow line) in (**b**) are the hydrolytical species $(UO_2)_2(OH)_2^{2+}$ and $(UO_2)_3(OH)_5^+$, respectively.

As can be seen in Figure 4a, the complexation between HCCA and Nd(III) starts at a pH higher than 3.5 with the neutral species $Nd(OH)(CCA)_2$, which is predominant in the whole pH range. The complex $Nd(OH)(CCA)^+$, instead, is a minor species with a percentage that does not reach values higher than 5%. The neodymium hydrolytical species $Nd(OH)^{2+}$ does not exist in the pH range investigated, supporting that the complexes between the ligand and metal ion could also involve the hydroxyl group.

Regarding the system UO_2^{2+}-HCCA (Figure 4b), all of the complexes reach significant percentages. The complexation starts from pH 2 with the formation of the neutral species $UO_2(CCA)_2$, which is predominant until pH 5. The anionic complex $UO_2(OH)_2(CCA)^-$ is the main from pH 5, while the other two minor species, $(UO_2)_2(OH)_2(CCA)_2$ and $UO_2(OH)(CCA)$, start to have significant percentages at the same pH value (i.e., 4) and coexist in the whole investigated pH range. As can be seen in Figure 4b, the percentage of the predominant uranyl hydrolytical complexes, $(UO_2)_2(OH)_2^{2+}$ and $(UO_2)_3(OH)_5^+$, decreases drastically in the presence of coumarin-3-carboxylic acid, confirming that the complexes between UO_2^{2+} and HCCA could be mixed species involving hydroxyl ion too.

To verify the effective formation of the complexes, a comparison of the UV-Vis spectra for free ligand and coordinated species is reported in Figure 5.

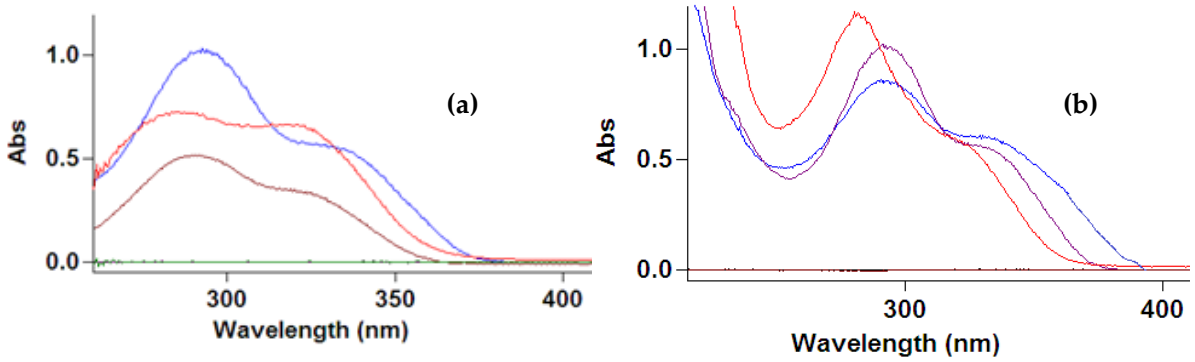

Figure 5. UV-Vis spectra of (**a**) Nd^{3+}-HCCA: free ligand (blue line), solution (brown line) and solid (red line); (**b**) UO_2^{2+}-HCCA: free ligand (violet line), solution (red line) and solid (blue line).

According to the literature [19], the UV-Vis spectrum of free coumarin-3-carboxylic acid shows two characteristic absorption bands, at 333 nm (low intensity) and 292.5 nm. The addition of the metal cations, Nd^{3+} or UO_2^{2+}, in the aqueous suspension containing HCCA, brought solid ligand into the aqueous phase as soluble complexes. Figure 5 shows the absorption spectra of the Nd^{3+}-HCCA (brown line in Figure 5a) and UO_2^{2+}-HCCA (red line in Figure 5b) complexes. Due to the low electronic rearrangement, which is induced on the ligand upon complex formation, the free ligand absorption spectrum was not significantly affected by the complexation.

Indeed, the band at 333 nm undergoes, in both spectra, a slight blue shift (i.e., at 320 nm). The most interesting spectral change can be detected for the band at 292.5 nm, which undergoes a significant hypsochromic shift, especially for the uranyl system (i.e., at 280 nm). As a further product of both syntheses, a solid was obtained, which was dissolved in a 1:1 ethanol:water mixture and analyzed, after the appropriate dilution with water, spectrophotometrically (red line in Figure 5a and blue line in Figure 5b). The UV-Vis spectra of these complexes show analogous spectral features to those analyzed before, suggesting that these insoluble species are formed by the soluble complexes, possibly upon the additional inclusion of a ligand or a hydroxide in the metal coordination sphere, in order to obtain a neutral species of the type $M_p(OH)_q(CCA)_r$.

All the complexes' spectra contain a broad band in the UV region (i.e., at λ = 320 nm), with tailing into the visible region. These bands were assigned to a ligand to metal change transfer transition.

The molar absorption coefficients of the complexes are reported in Figure 6: for the two complexes of neodymium, i.e., $Nd(OH)(CCA)^+$ and $Nd(OH)(CCA)_2$, ε values of 5870 and 4360 $M^{-1}cm^{-1}$, respectively, were recorded at λ_{max} of 290 nm. Higher ε values are obtained for the uranyl-HCCA system, which are $4 \cdot \times 10^5$ for the neutral species and 7×10^5 for the charged one.

Our results can only be partially compared with those proposed by Georgieva et al. [15] and by Martin et al. [29]; in these works, the complex of formula $Nd(CCA)_2(NO_3)(H_2O)$ was synthesized and characterized by spectroscopic and computational methods. According to our hypothesis, the spectroscopic results suggest that CCA^- is bidentate bound to the metal ion through the carboxylic and the carbonylic moiety. The model calculations of both bidentate modes of CCA^- to Nd(III) showed that the bidentate binding form through the carboxylic and the carbonylic oxygen atoms is energetically preferred as compared to that through both the carboxylic atoms.

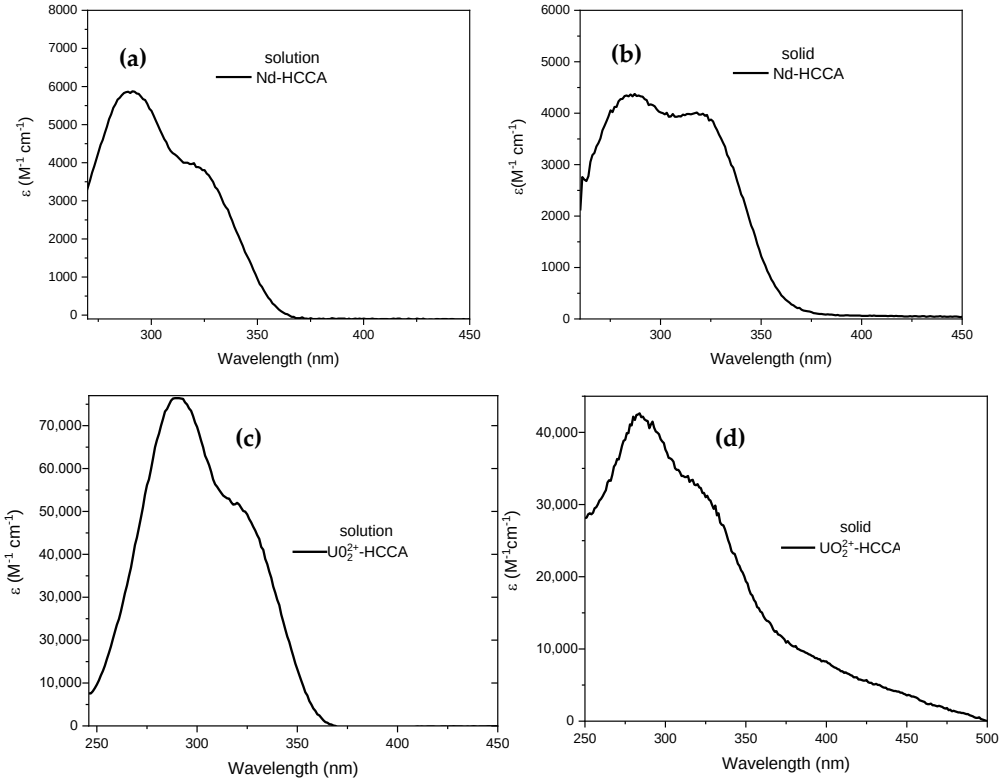

Figure 6. Absorption spectra of (**a**,**b**) neodymium-HCCA and (**c**,**d**) uranyl-HCCA. complexes, obtained by analyzing solution and solid, respectively.

Author Contributions: Conceptualization: E.F. Investigation: L.M., G.A.C. Resources: E.F. Writing—Original Draft: E.F., L.M. All authors have read and agreed to the published version of the manuscript.

Funding: This research received no external funding.

Institutional Review Board Statement: Not applicable.

Informed Consent Statement: Not applicable.

Data Availability Statement: Data sharing not applicable.

Acknowledgments: We thank the University of Calabria.

Conflicts of Interest: The authors declare no conflict of interest.

References

1. Malacaria, L.; Corrente, G.A.; Beneduci, A.; Furia, E.; Marino, T.; Mazzone, G. A review on coordination properties of Al(III) and Fe(III) towards natural antioxidant molecules: Experimental and theoretical insights. *Molecules* **2021**, *26*, 2603. [CrossRef] [PubMed]
2. Ritacca, A.G.; Malacaria, L.; Algieri, V.; De Nino, A.; Russo, N.; Furia, E.; Maiuolo, L.; Sicilia, E. Sequestering ability of a synthetic chelating agent towards copper(II) and iron(III): A detailed theoretical and experimental analysis. *Chem. Asian J.* **2020**, *15*, 3266–3274. [CrossRef] [PubMed]
3. Zhu, L.; Liu, B.; Yang, X.; Zhuo, L.; ·Mu, W.; Chen, Y.; ·Yang, Y.; ·Wei, H.; Li, X. Complexation of 1,3 Diamino 2 hydroxypropane N,N,N′,N′ tetraacetic Acid (DHPTA) with Heavy Lanthanides (Tb^{3+}, Ho^{3+}, Lu^{3+}) in Aqueous Solution. *J. Sol. Chem.* **2020**, *49*, 166–178. [CrossRef]
4. Karaliota, A.; Kretsi, O.; Tzougraki, C. Synthesis and characterization of a binuclear coumarin-3-carboxylate copper (II) complex. *J. Inorg. Biochem.* **2001**, *84*, 33–37. [CrossRef]
5. Creaven, B.S.; Devereux, M.; Karcz, D.; Kellett, A.; McCann, M.; Noble, A.; Walsh, M. Copper (II) complexes of coumarin-derived Schiff bases and their anti-Candida activity. *J. Inorg. Biochem.* **2009**, *103*, 1196–1203. [CrossRef]

6. Creaven, B.S.; Egan, D.A.; Karcz, D.; Kavanagh, K.; McCann, M.; Mahon, M.; Noble, A.; Thati, B.; Walsh, M. Synthesis, characterisation and antimicrobial activity of copper(II) and manganese(II) complexes of coumarin-6,7-dioxyacetic acid (cdoaH_2) and 4-methylcoumarin-6,7-dioxyacetic acid (4-MecdoaH_2): X-ray crystal structures of [Cu(cdoa)(phen)$_2$]·8.8H_2O and [Cu(4-Mecdoa)(phen)$_2$]·13H_2O (phen = 1,10-phenanthroline). *J. Inorg. Biochem.* **2007**, *101*, 1108–1119.
7. Creaven, B.S.; Egan, D.A.; Kavanagh, K.; McCann, M.; Mahon, M.; Noble, A.; Thati, B.; Walsh, M. Synthesis and antimicrobial activity of copper(II) and silver(I) complexes of hydroxynitrocoumarins: X-ray crystal structures of [Cu(hnc)$_2$(H_2O)$_2$]·2H_2O and [Ag(hnc)] (hncH = 4-hydroxy-3-nitro-2*H*-chromen-2-one). *Polyhedron* **2005**, *24*, 949–957. [CrossRef]
8. Creaven, B.S.; Egan, D.A.; Kavanagh, K.; McCann, M.; Noble, A.; Thati, B.; Walsh, M. Synthesis, characterization and antimicrobial activity of a series of substituted coumarin-3-carboxylatosilver (I) complexes. *Inorg. Chim. Acta* **2006**, *359*, 3976–3984. [CrossRef]
9. Thati, B.; Noble, A.; Rowan, R.; Creaven, B.S.; Walsh, M.; McCann, M.; Egan, D.; Kavanagh, K. Mechanism of action of coumarin and silver (I)–coumarin complexes against the pathogenic yeast Candida albicans. *Toxicol. Vitr.* **2007**, *21*, 801–808. [CrossRef]
10. Grazul, M.; Budzisz, E. Biological activity of metal ions complexes of chromones, coumarins and flavones. *Coord. Chem. Rev.* **2009**, *253*, 2588–2598. [CrossRef]
11. Kulkarni, A.; Patil, S.A.; Badami, P.S. Synthesis, characterization, DNA cleavage and in vitro antimicrobial studies of La (III), Th (IV) and VO (IV) complexes with Schiff bases of coumarin derivatives. *Eur. J. Med. Chem.* **2009**, *44*, 2904–2912. [CrossRef]
12. Roh, S.-G.; Baek, N.S.; Hong, K.-S.; Kim, H.K. Synthesis and Photophysical Properties of Luminescent Lanthanide Complexes Based on Coumarin-3-carboxylic Acid for Advanced Photonic Applications. *Bull. Korean Chem. Soc.* **2004**, *25*, 343–344.
13. Georgieva, I.; Trendafilova, N.; Aquino, A.J.A.; Lischka, H. Theoretical study of metal− ligand interaction in Sm(III), Eu(III), and Tb(III) complexes of coumarin-3-carboxylic acid in the gas phase and solution. *Inorg. Chem.* **2007**, *46*, 10926–10936. [CrossRef] [PubMed]
14. Mihaylov, T.; Trendafilova, N.; Kostova, I.; Georgieva, I.; Bauer, G. DFT modeling and spectroscopic study of metal–ligand bonding in La (III) complex of coumarin-3-carboxylic acid. *Chem. Phys.* **2006**, *327*, 209–219. [CrossRef]
15. Georgieva, I.; Trendafilova, N.; Kiefer, W.; Rastogi, V.K.; Kostova, I. Vibrational and theoretical study of coumarin-3-carboxylic acid binding mode in Ce (III) and Nd (III) complexes. *Vibr. Spectr.* **2007**, *44*, 78–88. [CrossRef]
16. Kostova, I.; Manolov, I.; Nicolova, I.; Konstantinov, S.; Karaivanova, M. New lanthanide complexes of 4-methyl-7-hydroxycoumarin and their pharmacological activity. *Eur. J. Med. Chem.* **2001**, *36*, 339–347. [CrossRef]
17. Kostova, I.; Manolov, I.; Konstantinov, S.; Karaivanova, M. Synthesis, physicochemical characterisation and cytotoxic screening of new complexes of cerium, lanthanum and neodymium with Warfarin and Coumachlor sodium salts. *Eur. J. Med. Chem.* **1999**, *34*, 63–68. [CrossRef]
18. Kostova, I.; Momekov, G.; Zaharieva, M.; Karaivanova, M. Cytotoxic activity of new lanthanum (III) complexes of bis-coumarins. *Eur. J. Med. Chem.* **2005**, *40*, 542–551. [CrossRef]
19. Creaven, B.S.; Devereux, M.; Georgieva, I.; Karcz, D.; McCann, M.; Trendafilova, N.; Walsh, M. Molecular structure and spectroscopic studies on novel complexes of coumarin-3-carboxylic acid with Ni(II), Co(II), Zn(II) and Mn(II) ions based on density functional theory. *Spectrochim. Acta Part A* **2011**, *84*, 275–285. [CrossRef]
20. Furia, E.; Beneduci, A.; Russo, N.; Marino, T. Structural characterization of aluminium(III) and iron(III) complexes of coumarinic acid in aqueous solutions from combined experimental and theoretical investigations. *New J. Chem.* **2018**, *42*, 11006–11012. [CrossRef]
21. Furia, E.; Sindona, G. Complexation of L-Cystine with Metal Cations. *J. Chem. Eng. Data* **2010**, *55*, 2985–2989. [CrossRef]
22. Furia, E.; Porto, R. 2-Hydroxybenzamide as a Ligand. Complex Formation with Dioxouranium(VI), Aluminum(III), Neodymium(III), and Nickel(II) Ions. *J. Chem. Eng. Data* **2008**, *53*, 2739–2745. [CrossRef]
23. Biedermann, G.; Sillén, L.G. Studies on the hydrolysis of metal ions. IV. Liquid junction potentials and constancy of activity factors in $NaClO_4$–$HClO_4$ ionic medium. *Arkiv Kemi.* **1953**, *5*, 425–440.
24. Gran, G. Determination of the equivalent point in potentiometric titrations. *Acta Chem. Scand.* **1950**, *4*, 559–577. [CrossRef]
25. Gran, G. Determination of the equivalence point in potentiometric titrations. Part II. *Analyst* **1952**, *77*, 661–670. [CrossRef]
26. Sillén, L.G. Some Graphical Methods for Determining Equilibrium Constants. II. On "Curve-fitting" Methods for Two-variable Data. *Acta Chem. Scand.* **1956**, *10*, 186–202. [CrossRef]
27. Gans, P.; Sabatini, A.; Vacca, A. Superquad: An improved general program for computation of formation constants from potentiometric data. *J. Chem. Soc. Dalton Trans.* **1985**, *6*, 1195–1200. [CrossRef]
28. Baes, C.F.; Mesmer, R.E. *The Hydrolysis of Cations*; Wiley Interscience: New York, NY, USA, 1976.
29. Martin, J.; Mladěnka, P.; Saso, L.; Kostova, I. Lanthanide(III) complexes are more active inhibitors of the Fenton reaction than pure ligands. *Redox Rep.* **2016**, *21*, 84–89. [CrossRef]

Journal of Molecular Liquids 325 (2021) 115171

Contents lists available at ScienceDirect

Journal of Molecular Liquids

journal homepage: www.elsevier.com/locate/molliq

Experimental and theoretical study on the coordination properties of quercetin towards aluminum(III), iron(III) and copper(II) in aqueous solution

Giuseppina A. Corrente, Luana Malacaria, Amerigo Beneduci, Emilia Furia *, Tiziana Marino, Gloria Mazzone

Dipartimento di Chimica e Tecnologie Chimiche, Via P. Bucci, Cubo 12/D, Università della Calabria, I-87036 Arcavacata di Rende (CS), Italy

ARTICLE INFO

Article history:
Received 23 October 2020
Received in revised form 10 December 2020
Accepted 20 December 2020
Available online 24 December 2020

Keywords:
Aluminum quercetin complexes
Iron quercetin complexes
Copper quercetin complexes
Stability constants
DFT
NMR

ABSTRACT

In this work we have studied the complexation of quercetin (3,3′,4′,5,7-pentahydroxyflavone, H_5Que) with aluminum(III), iron(III) and copper(II) at 37 °C and in aqueous solution (0.16 M NaCl). To evaluate the competition of the ligand for the metal cations and H^+, the protonation constant of quercetin was also determined under the same experimental conditions. Speciation profiles obtained by potentiometric titrations and supported by UV–Vis data show that in aqueous solution a complexation occurs at 1:1 ligand-to-cations ratio for Al(III) and Cu(II), and at 1:1 and 1:2 ligand-to-Fe(III) ratio. The coordination sites of quercetin to the different metal ions were determined with the aid of ^{1}H NMR and ^{13}C NMR spectroscopy as well as by a computational approach. Synergies between experiment and computation show that aluminum and iron ions show no clear preference towards any of the complexation sites of quercetin, while for copper the **4,5** site (*i.e.*, the 4-carbonyl-5-hydroxyl site of the A and C rings of the ligand) could be excluded.

1. Introduction

Heavy metals are environmental pollutants, and their toxicity is a problem of growing importance from ecological, evolutionary, nutritional and environmental point of view. On the other hand, metal cations play important roles in biological systems including action as cofactors for enzymes that catalyze different metabolic functions [1]. Metal ions can be absorbed by ingestion, inhalation and for contact through the skin. When absorbed metal ions and their compounds pass in the bloodstream, mainly by blood plasma proteins [2,3]. Redox-active metal ions such as Cu(II) and Fe(III) exert their toxic action through the formation of reactive oxygen species (ROS), which may result in tissue or organ damage [4]. Additionally, Cu(II) is involved in the metabolism of dioxygen and plays a fundamental role in the respiratory chain. Moreover, iron overload is a common consequence of the chronic transfusion therapies [5] and aluminum excess may be observed in uremic patients. The overload of Fe(III) and Al(III) in the central nervous system has been suggested to be involved in neurodegenerative disorders [6]. Al(III) is third most abundant element in the Earth's crust and can enter in the biotic cycle in many different ways [7]. It is well known that aluminum does not serve any essential function in human biochemistry and a small increase seems sufficient to produce neurotoxicity [8,9]. For this reason, the presence of Al(III) in the human brain has been associated to the Alzheimer's and other neurodegenerative diseases [10].

Current treatment options for metal cation overload are designed to remove tissue deposits, which cause the toxic effects. Metal chelation therapy was proposed more than 50 years ago for the treatment of pathologies produced in the body by an overload of a metal and it is the most efficient therapeutic approach. Metal chelation therapy involves the use of a chelating agent, *i.e.*, a molecule which forms stable coordination complexes with the target metal ion. The behavior of a specific metal under physiological conditions depends essentially on its speciation profile. The formation of complexes between bioavailable metal cations and natural ligands can play an important role in chelation therapy for pathologies deriving from the accumulation of heavy metals. In this context, stability and specificity of metal-chelator complexes are extremely important in the choice of the most adequate chelating agent. The knowledge of metal-ligand speciation can allow modeling the chelating agent activity *in vitro* or *in vivo*, *i.e.*, to perform calculations describing the distribution of the metal ion of interest at any conditions. Phenolic and/or aromatic molecules such as flavonoids have been shown to be excellent chelating compounds for bioavailable metal ions. Quercetin (3,3′,4′,5,7-pentahydroxyflavone, H_5Que, Scheme 1) is one of the most common flavonols present in nature, and is one of the most biologically active and common dietary flavonoid present in vegetables and fruits. It may chelate metal cations, preventing the generation of damaging oxidizing radicals whose formation is mediated by metals and thus protecting the biological targets against oxidative stress [11–13]. As can

* Corresponding author.
E-mail address: emilia.furia@unical.it (E. Furia).

https://doi.org/10.1016/j.molliq.2020.115171
0167-7322/

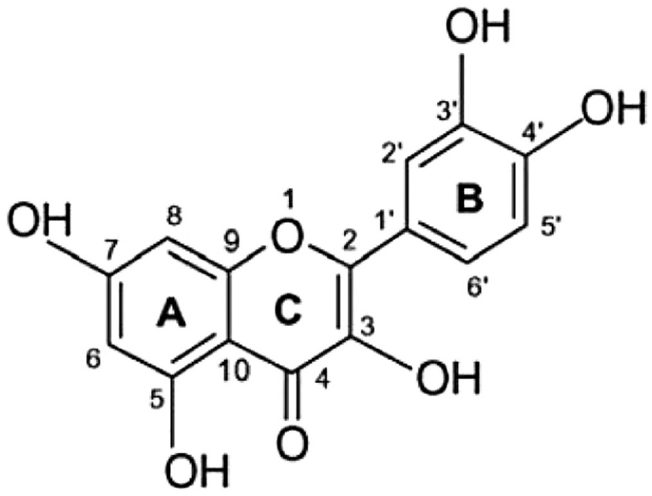

Scheme 1. Chemical structure of quercetin, H_5Que.

be seen in the Scheme 1, in the quercetin structure three chelation sites are possible: the 3-hydroxy-carbonyl, the 5-hydroxy-carbonyl and the 3′,4′-dihydroxyl functions.

The possible correlation between these different coordination sites and the nature of the metal cation is worth of being investigated. In this framework, the aim of this work was to determine the stoichiometric composition and the corresponding stability constants of complexes between quercetin and Al(III), Fe(III) and Cu(II) ions at 37 °C and in 0.16 M NaCl. Following our previous studies, here we present an experimental investigation (potentiometric, UV–Vis, ^{1}H and ^{13}C NMR spectroscopy) combined with a computational approach (Density Functional Theory, DFT) to obtain structural properties of these systems in aqueous solution [11,14–16]. Speciation calculations allow to predict which complexes exist in solution at a given pH and metal and ligand total concentrations. The information regarding the most abundant complex existing at physiological conditions can be useful for two reasons: the identity of the existing complexes, and in particular of the most abundant one, and their charge, crucial in determining their redistribution once the target metal ion has been complexed by the chelating agent. For example, a charged complex is expected to be hydrophilic, thus being unable to pass cellular barriers and preferring to be solubilized in aqueous solutions (*e.g.*, in the blood), whereas neutral species should behave in an opposite way. Previous experimental and theoretical investigations have considered the complexation of quercetin with Al(III), Fe(III) and Cu(II) in solution and at different stoichiometric ratios [17–24]. Despite the presence of these works, the structure and the complex formation features are somehow contradictory. Whereas, the structure of the complexes, which might be deduced from the stoichiometry, has a main role in determining their properties and toxicity.

2. Experimental section

2.1. Materials

Sodium chloride, hydrochloric acid and sodium hydroxide titrant solutions were prepared and standardized as previously described [16]. Aluminum(III), iron(III) and copper(II) chloride stock solutions were prepared and standardized as reported previously [16,25]. Quercetin (Sigma, ≥95%) was kept in a desiccator over silica gel and was used without further purification. All solutions were freshly prepared with bidistilled water.

2.2. Potentiometric and spectrophotometric measurements

The potentiometric apparatus and the titrations carried out were described in a previous work [16]. To avoid carbonate interference, a slow stream of nitrogen gas was passed through the gas inlet tube into the test solutions, stirred during titrations. During the EMF measurements, the cell assembly was placed in a thermostat kept at (37.0 ± 0.1) °C.

Spectrophotometric measurements were carried out with a Varian Cary 50 Scan UV Visible Spectrophotometer by measuring the absorbance values, A_λ, (to 0.001 units) between 200 and 700 nm each 1 nm. Matched quartz cells of thickness 1 cm were employed. The temperature of the cell holder was maintained at (37.0 ± 0.3) °C by a Grant circulating water bath. The acquisition of data and the formulations of the parameters were managed with the aid of a computer connected to the instrument.

2.3. NMR method

^{1}H and ^{13}C NMR spectra were acquired on a Bruker Avance 500 spectrometer. The pulse sequence zgpg30 was used for the ^{13}C spectra acquisition, with a 30° pulse of 9 ms and 2 s inter-pulse delay. Proton decoupling was performed by applying the Composite Pulse Decoupling Program CPDPRG. All spectra were stored in 64 k digital data points with a spectral width of 30,000 and a number of scans equal to 20,480. The temperature of the samples inside the probe was maintained at 37 ± 1 °C by a Bruker VT2000 variable temperature control unit.

2.4. Computational details

All the calculations performed with the Gaussian 09 computational package [26] were carried out in the framework of density functional theory employing the M052X [27] exchange-correlation functional coupled with the 6–31+G(d) basis set for C, O, Al and H atoms except for Cu and Fe atoms, for which the relativistic compact Stuttgart/Dresden effective core potential was used in conjunction with its split valence basis set. The structures were fully optimized in aqueous solution taking into account the impact of the solvent used in the speciation experiments by means of the SMD version of the polarizable continuum model (PCM) [28]. For this purpose, the dielectric constant of water (ε=78.0) has been considered. Harmonic vibrational frequencies have been performed on each optimized structure at the same level of theory of the optimizations and the thermochemical analysis has been used to correct the electronic energies in order to obtain the Gibbs free energies.

According to previous results on the iron(III)-coumarin system [15], the most stable spin multiplicity was obtained with a value of 6, which arises from a high-spin configuration of the Fe(III) center. In particular, from the unrestricted Kohn–Sham (UKS) calculations no spin contamination was found, being the $\langle S^2 \rangle$ value equal to 8.75. In the case of copper ion the spin multiplicity with the value of 2 was considered.

With the aim to obtain the vertical excitation energies, the TD-DFT approach has been also used in agreement to that previously and successfully used on similar chemical systems [11,14–16,29,30].

For each metal ion the complexes having neutral charge and characterized by the **3–4**, **4–5** and **3′-4′** coordination sites have been subjected to the geometry optimization at the B3LYP/6–311+G(d,p) in DMSO (ε=46.826) and then the gauge-independent atomic orbital (GIAO) method [31,32] has been used to estimate the absolute chemical shielding as implemented in the Gaussian 09. Chemical shifts have been then obtained from absolute shieldings by subtraction of a calculated reference. In this regard the absolute chemical shielding of TMS have been computed at the same level of theory.

Natural Bond Orbitals (NBO) analysis was performed using the Gaussian 09.

Furthermore to estimate the binding energies (BE) related to two different coordination sites (4–5 or 3′-4′), the complexes of Al(III), Fe

(III) and Cu(II) ions have been separated into two fragments according to a cleaved metal–ligand bond as shown by the following expression:

$$BE = -(\Delta H_{complex} - \sum \Delta H_{monomer})$$

The BE is calculated as the difference between the enthalpy of the whole complex and the enthalpy of the individual subsystem. Such obtained binding energies represent the energy involved in the formation of the metal ion-ligand complex.

Metal binding affinity of quercetin to Al(III), Fe(III) and Cu(II) has been evaluated, as previously reported [29,33], by calculating the reaction free energies in the general complexation reaction for the substitution of water molecules in the hexaaquo complex.

3. Results and discussion

3.1. Chelating properties of quercetin and stability of formed complexes

The complex formation equilibria between H_5Que and Al(III), Fe(III) and Cu(II) cations were studied at 37 °C and in 0.16 M NaCl. Quercetin is essentially insoluble in water, for this reason all the experiments were carried out by adding an accurately weighed quantity of solid quercetin in the titration's apparatus. After addition of the other reagents, the pH of test solutions was stepwise increased from 2 to 7.5 by adding NaOH standard solutions. When the generic equilibrium reported in Eq. (1) takes place, quercetin dissolved into the aqueous medium to form complexes.

$$pM^{n+} + rH_5Que \rightleftarrows M_p(H)_{-q}(H_5Que)_r^{(np-q)} + qH^+ \quad \log \beta_{p,q,r} \tag{1}$$

The equilibrium reported in Eq. (1) takes into account all the possible complexes formed in solution (*i.e.*, simple $q=r$, mixed $q \neq r$, mononuclear p and $r = 1$, and polynuclear p and $r > 1$ species), and all the potential chelation sites of quercetin which correspond to a different number of protons involved in the coordination. However, β values do not allow to assess the effective complex stability, which is also affected by the acid-base properties of the metal cations and of the ligand. For this reason, to evaluate the competition of the ligand for metal cations and H^+, preliminarily it was necessary to determine under the same experimental conditions the first acidic constant of quercetin (Eq. (2)):

$$H_5Que \rightleftarrows H_4Que^- + H^+ \quad pK_{a1} = 8.79 \pm 0.09 \tag{2}$$

The uncertainty on the values represents 3σ. Assignment of this value is still under question [34], though, most of the literature converges on the deprotonation of the 7-OH group [35,36]. Support to the last assignment comes from the computational evaluation of the stability of the conjugate bases of the various acidic hydroxyl groups of quercetin (*i.e.*, 7OH > 3′OH > 4′OH > 5OH > 3OH), that shows that deprotonation of the 7-OH position is favored.

In line with literature [34,37], we have experienced that quercetin undergoes degradation in alkaline medium, which is more rapid than potentiometric measurement time. Therefore, no additional efforts were made to determine the acidity of the other hydroxyl groups. The acidic constant of quercetin as well as the constants of principal cationic hydrolysis products, taken from literature [16,38] (*i.e.*, $Al(OH)^{2+}$ and $Al(OH)_2^+$, $Fe(OH)^{2+}$ and $Fe(OH)_2^+$, $Cu(OH)^+$ and $Cu_2(OH)_2^{2+}$), were kept invariant in the numerical treatment to determine stability constants $\beta_{p,q,r}$. The potentiometric measurements were performed as titrations with cell (G):

Reference Electrode/Test Solution/Glass Electrode → (G)

the general composition of Test Solution was CM mol·dm−3 MCln, CL mol·dm−3 H5Que, CA mol·dm−3 HCl, CB mol·dm−3 NaOH, and (0.16-nCM-CA-CB) mol·dm−3 NaCl. Metal and ligand concentrations were ranged from (0.25·10−3) to (1.05·10−3) mol·dm−3 and the ligand to metal ratio was varied between 1 and 4. The pH was ranged from 2.5 for Al(III) and Cu(II) and from 2 for Fe(III) to the precipitation of a neutral species, involving ligand and metal ion, which takes place at different pH depending on the specific ligand to metal ratio investigated and evidently on the nature of metal. The most probable p, q, and r values and the corresponding constants $\log \beta_{p,q,r}$ were computed by a numerical approach [39], and results obtained are reported in the Table 1.

Speciation profiles show that in aqueous solution a complexation occurs at 1:1 ligand-to-cations ratio for Al(III) and Cu(II), and at 1:1 and 1:2 ligand-to-Fe(III) ratio. Any comparison with previous literature data was not possible, as this work is the first one entirely in aqueous medium. The distribution diagrams in Fig. 1 a-c show the percentage of metal cations into the complexes with respect to pH.

As can be seen in Fig. 1a, the complexation between quercetin and Al(III) starts at pH higher than 3.5 and the complex $Al(H)_{-2}(H_5Que)^+$ reaches percentage lower than 50%, confirming that the sequestering ability of quercetin towards Al(III) is not efficient. Regarding the system Fe(III)-Que (Fig. 1b) all the complexes reach a percentage higher than 30%. The complexation starts from pH 2 with the formation of the species $Fe(H)_{-5}(H_5Que)_2^{2-}$ which is predominant until pH 4. The other two complexes, $Fe(H)_{-4}(H_5Que)^-$ and $Fe(H)_{-6}(H_5Que)_2^{3-}$, start to form at the same pH value (*i.e.*, 2.5) and coexist in the whole investigated pH range. Interestingly, the distribution of the hydrolytical complexes, $Fe(OH)^{2+}$ and $Fe(OH)_2^+$, shows that percentages decrease drastically in the presence of quercetin. This led us to hypothesize that the complexes between iron and quercetin could be mixed species involving hydroxyl ion. Finally, the speciation diagram of the system Cu(II)-Que (Fig. 1c) shows that the neutral complex $Cu(H)_{-2}(H_5Que)$ starts to form at pH 5.5 and is the predominant species from pH 6.5, with percentage higher than 70%. The other two species, $Cu(H)_{-1}(H_5Que)^+$ and $Cu(H)_{-3}(H_5Que)^-$, exist in two different pH ranges, in particular from pH 4 to pH 7.5, with a maximum value at pH 6.5, and from pH 6.5, respectively. The anionic complex, $Cu(H)_{-3}(H_5Que)^-$, is a minor species as it reaches a percentage lower than 15%.

In order to verify the effective formation of the complexes, all solutions and solids gained at the end of each titration were analyzed by UV–Vis spectrophotometry. A comparison of the UV–Vis spectra of free ligand (H_5Que) and of the coordinated species is reported in Fig. 2a-c. According to literature, the UV–Vis spectrum of free quercetin shows two characteristic absorption bands of flavonoid compounds [40,41]: band I at 377 nm is due to the conjugation between B and C ring (cinnamoyl system), and band II at 258 nm deriving from the A-C ring (benzoyl system), which are highlighted in Fig. 2b. Moreover, there are two other less intense absorption bands at 303 and 280 nm. The UV–Vis spectra recorded on the solutions containing metal cations show a significant shift of the characteristic bands of quercetin, confirming the occurred complexation.

3.2. Computational analysis

Although the quercetin has been the subject of several theoretical works, in order to obtain the ligand key properties at the same level of

Table 1
Formation of complexes of quercetin with Al(III), Fe(III) and Cu(II), according to Eq. (1). Values of $\log \beta_{p,q,r}$ in NaCl 0.16 M at 37 °C were obtained by numerical procedure (standard deviations are reported as 3 σ).

	Species	$\log \beta_{p,q,r} \pm 3\sigma$
Al(III)	$Al(H)_{-2}(H_5Que)^+$	−6.0 ± 0.1
	$Fe(H)_{-4}(H_5Que)^-$	−6.98 ± 0.06
Fe(III)	$Fe(H)_{-5}(H_5Que)_2^{2-}$	−4.6 ± 0.1
	$Fe(H)_{-6}(H_5Que)_2^{3-}$	−8.7 ± 0.1
	$Cu(H)_{-1}(H_5Que)^+$	−3.12 ± 0.03
Cu(II)	$Cu(H)_{-2}(H_5Que)$	−9.91 ± 0.03
	$Cu(H)_{-3}(H_5Que)^-$	−18.00 ± 0.09

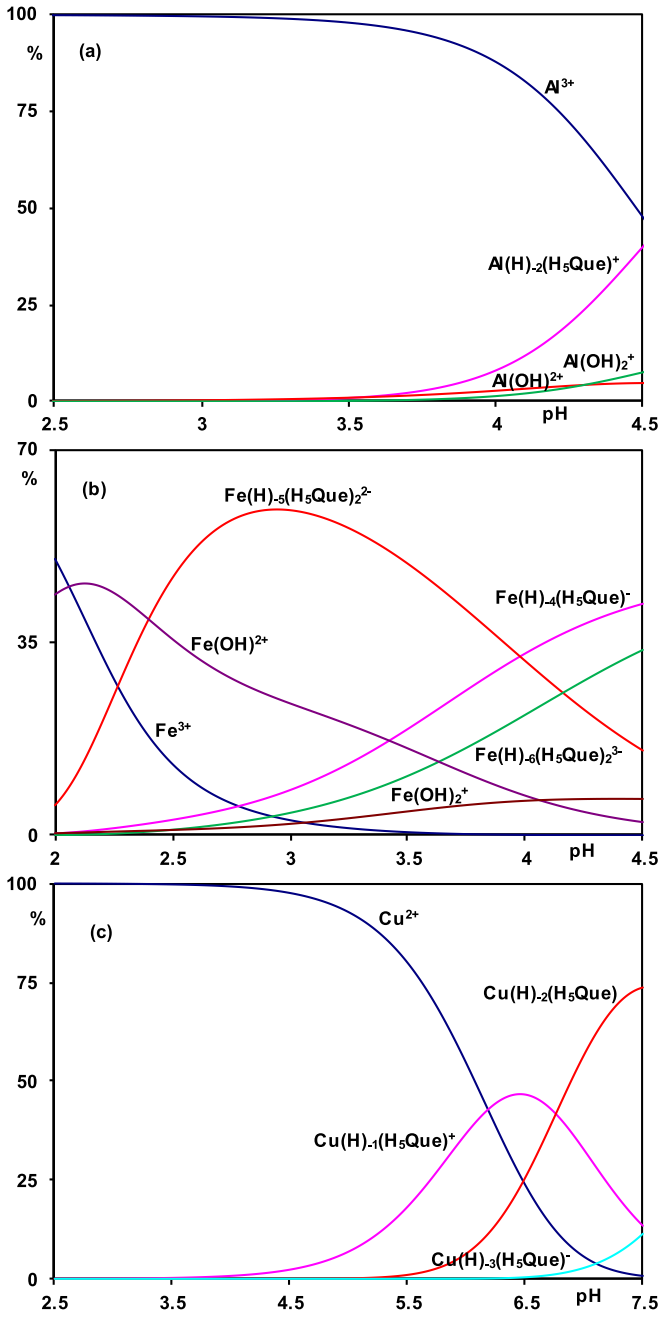

Fig. 1. Distribution diagrams in the presence of H_5Que of: (a) Al(III) (C_M=0.25 mM and C_L=1.0 mM); (b) Fe(III) (C_M=0.5 mM and C_L=0.7 mM) and (c) Cu(II) (C_M=0.25 mM and C_L=1.0 mM).

theory used for the complexes, the first step of our investigation was the optimization of quercetine (Que) alone considering the two different conformations accounting for the position of the 3′OH site from the same side of 3OH (*s-cis*) or from the other side (*s-trans*). Thus, the two considered values of the Φ angle (C3-C2-C1'-C2', see Scheme 1), for the rotation around the 2–1′ bond, account for the two conformations of the catechol ring, as well as for the system planarity. The resulting conformers are isoenergetic, *i.e.*, energy range of 0.2 kcal/mol, but the related electrostatic potential map (reported in Fig. 3) clearly exhibits the influence of the Φ angle on the charge distribution in the region including the OH moiety of the ring C (in C3 position) and C2'H of the ring B. Furthermore, the planarity of the ligand is associated with the highest conjugation and it is also relevant for the effect of metal chelation on the antioxidant properties of quercetin [18].

Quercetin is a multidentate ligand and metal coordination can take place *via* the 3-hydroxyl and 4-carbonyl group of the C ring (denoted as **3–4** site), the 4-carbonyl-5-hydroxyl site of the A and C rings (**4–5** site) or *via* the catechol moiety of the B ring (**3′-4′** site) (see Scheme 1). The preferred binding site can depend on the metal ion and on the pH value, as also evidenced by the speciation described therein. Moreover, the polarity of the solvent plays an important role in metal ion/ligand interaction. Overall, these features can result also on different metal/ligand stoichiometry as it emerged in the case of iron (see Table 1). Following the experimental indications arising from the speciation profiles of Fig. 1, to gain structural features and binding modes of Al(III), Fe(III) and Cu(II) ions complexes with quercetin, at the pH range of 2.5–4.5 for Al(III) and Fe(III) and of 2.5–7.5 for Cu(II), different structures have been investigated. Despite the numerous experimental and theoretical works devoted to modeling the geometric parameters of flavonoid complexes [17,20,21,41–48], the concern for this topic is still persistent and current due to the limited X-ray data availability that encourages to deeply explore their behavior in different environments and pH conditions.

The search for the most plausible metal/quercetin complexes was driven by the metal to ligand stoichiometric ratio and the total charge suggested by the potentiometric analysis (see Table 1), by considering the loss of protons from both quercetin and water molecules coordinated to the metal. In particular, given the pH range at which the experiments were conducted (see Fig. 1), the quercetin can be anionic (see Eq. (2)) only once it is coordinated to the metal center, thus different deprotonation sites were considered in the complex's formation depending on the site involved in the coordination to the metal centre. Only in some cases, in order to hypothesize the formation with specific stoichiometric ratio and charge, the possibility that the 4′-anionic quercetin could be involved in the complex formation was taken into consideration (see Supplementary Material). The starting structures of the complexes were obtained by chelation of the metal ion close to the 3–4, 4–5, and 3′-4′ sites of quercetin, considering both its isomeric forms abovecited, and saturing the coordination sphere of each metal with water molecules (or OH^- depending on the complex total charge). In principle, also the site 7-OH of the quecetin was considered but, since it mainly generates monocoordinated species, it resulted to be less favored for all the metal complexation. So, all the species characterized by the presence of metal ion monocoordinated to the ligand were discarded, independently on the charge and the considered coordination site, and they are reported in the Supplementary Material. While the outcomes for the most stable complexes of the three metal ions with quercetin, as preferred isomer in each complex, were collected in Fig. 4 and Table 3.

3.2.1. Al(III)-Quercetin

For aluminum, different combinations of deprotonated quercetin forms associated with total charge +1 of the complexes ($Al(H)_{-2}(H_5Que)^+$) in the 1:1 metal/ligand ratio were taken into account that lead to $Al(OH)H_4Que^+$ or $Al(H_3Que)^+$ species. The most plausible complexes are depicted in Fig. 4a together with the relative free energy values calculated with respect to the most stable complex, while all the other optimized structures are shown in Fig. S1 of the Supplementary Material.

When the quercetin acts as monodentate ligand, the generated complexes (Fig. S1) are higher in energy regardless the considered species, $Al(OH)H_4Que^+$ or $Al(H_3Que)^+$. Anyway, the latter complex is the least favored one as it can be arisen from the relative energy values in Fig. S1. In the three monodentate structures intercepted, the metal ion assumes a trigonal bipyramid geometry.

The bidentate nature of the ligand results in very stable complexes with Al(III) ion (see Table S1). Regardless the Φ value and charge of the systems, the preferred chelation occurs through the A/C rings with the **4–5** site rather than the **3–4**. In particular, for $Al(OH)H_4Que^+$ the six-membered chelate ring of the **4–5** site is favored on that five-membered generated by the **3–4** site metal coordination by about

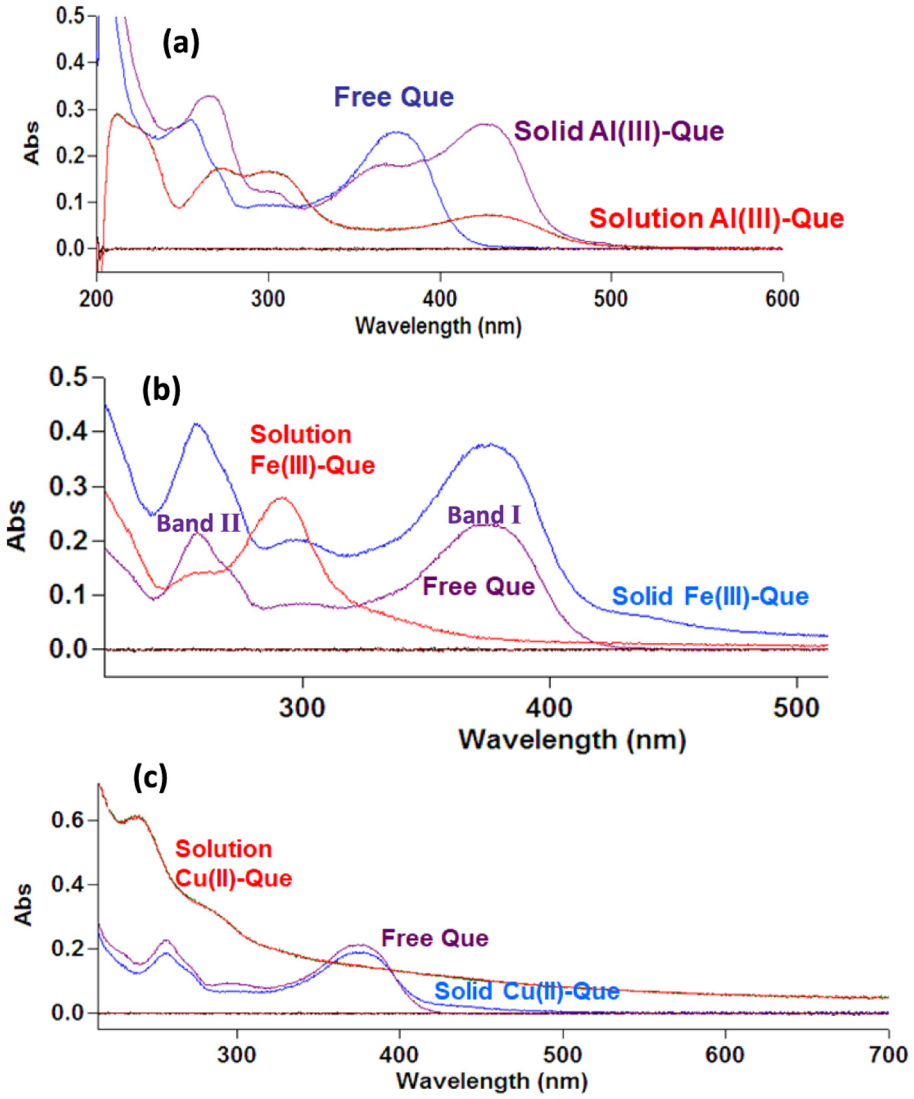

Fig. 2. UV–Vis spectra of the free ligand and of the complexes. (a) Al(III)-Que; (b) Fe(III)-Que and (c) Cu(II)-Que.

3.5 kcal/mol (see Fig. S1 and Table S1). Analogous outcomes were found in previous works [11,15,16,22]. In all the bidentate complexes of the Al(*OH*)H_4Que^+ species the aluminum retains the octahedral geometry (Fig. 4a and S1). When the catechol moiety is implicated in the metal ion coordination, the complexes **3′$_H$-4′** and **3′-4′$_H$** of Fig. S1 can be formed and they lie 10.7 and 9.1 kcal/mol, respectively, higher in energy than the **4–5** complex in Fig. 4a, evidencing site **3′-4′** as the less preferred site for Al(III) bearing an OH^- ligand in acqueous solution. On the contrary, based on the speciation diagram of Fig. 1a, the Al$(H_3Que)^+$ can be formed only if the site **3′-4′** is involved in the coordination, while for obtaining the other coordination sites, the most acid site should be considered deprotonated (see Fig. S1b) and they were excluded because of the experimental pH condition. The resulted most probable species, having the catechol group completely deprotonated (see Fig. 4a), results to be just over 4 kcal/mol higher in energy than the lowest energy structure, that is the **4–5** of Al(*OH*)H_4Que^+.

This behavior well accounts for the hard acid nature of the Al(III) that prefers binding to the hard bases to give complexes having a rather ionic nature as confirmed by the NBO charges analysis (Table 2) deriving from −0.930 |e| for O3′ and −0.922 |e| for O4′ more negative by 0.191 |e| and 0.199 |e| with respect to the neutral quercetin. This difference reflects the clear electrostatic nature of the interaction that, as a consequence, gives rise to a higher binding energy (Table 2). In the **4–5** complex of Al(*OH*)H_4Que^+, the natural charges of the oxygen atoms involved in the coordination resulted to be −0.886 |e| and −0.790 |e|, respectively, more negative by 0.162 |e| and 0.046 |e| than in the ligand alone. The different topology of the complex along with a local different nature charge surrounding the metal ion causes a minor binding energy (Table 2).

Furthermore in **3′-4′** complex of Al$(H_3Que)^+$, the torsional angle Φ deviates from the planarity more than the **4–5** complex of Al(*OH*)H_4Que^+ (46.1 *vs* −152.9 degrees). This finding is in agreement with the non-planar ligand usually found in the Al coordination to the catechol moiety [11,21,22,49]. On the contrary, when Al binds to the 3–4 site it was possible to observe a more complete planarity of the ligand with the five membered chelate ring generated by the metal ion coordination (see Fig. S1), as already found in other works [11,49].

The calculated formation free energies reported in Table S1, suggest the **3′-4′** coordination of the Al$(H_3Que)^+$ species as possible kinetically favored candidate (−55.9 kcal/mol) whereas the **5–4** of the Al(*OH*)H_4Que^+ one as thermodymically favored (−71.2 kcal/mol) confirming what previously declared for alluminium complexes [11,49].

3.2.2. Fe(III)-Quercetin

According to the speciation diagrams (Fig. 1b), in the case of Fe(III) geometry optimization of both 1:1 and 1:2 metal to ligand

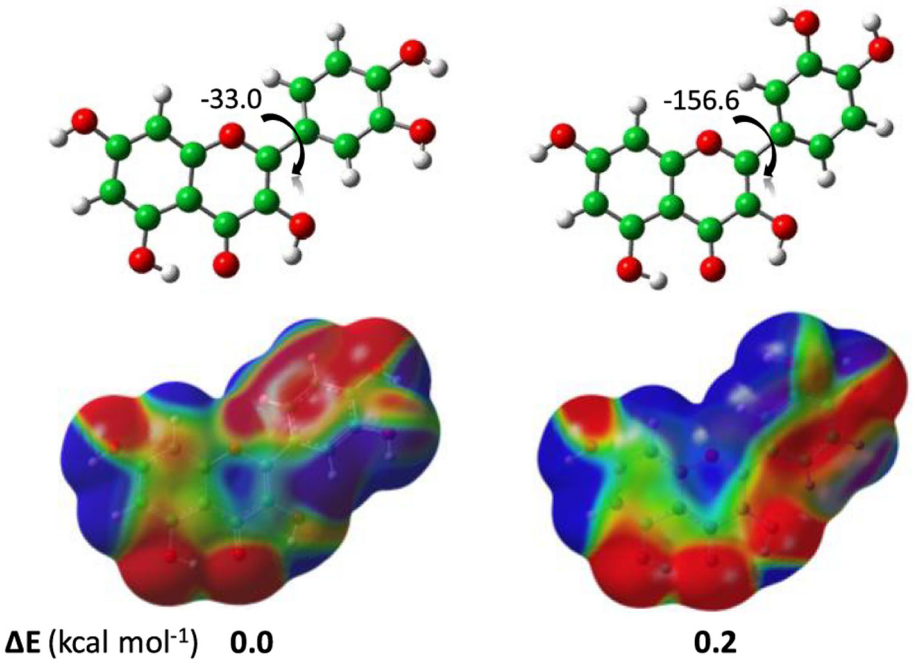

Fig. 3. Optimized structures of quercetin in both *s-cis* and *s-trans* isomeric forms.

stoichiometric ratio were performed. In Fig. 4b are depicted the complexes of the $Fe(OH)_2(H_3Que)^-$ representative of the most probable structures in which catechol moiety (**3′-4′**) is implicated in the complexation. Two iron-containing complexes (very close in energy) are displayed accounting for both geometric isomers of quercetin. The other considered species are reported in Fig. S2. In all the intercepted complexes, the deviation from the planarity of ring B is less pronounced with respect to that observed in the case of aluminum complexes in the same conditions (see Fig. 4a and S1). As above anticipated in the experimental section, differently from the aluminum ion, the species in ratio 1:1 for iron complexes exhibit a negative charge that necessarely have to provide the presence of two hydroxyl groups (see dark red line in Fig. 1b) and the doubly charged ligand, that can be realized only in **3′-4′** site coordination. Also in the case of Fe(III) complexes in $Fe(OH)_2(H_3Que)^-$ stochiometric ratio and charge, the possibility that the other binding sites could be involved in the Fe(III) complexation requires Que. to have a deprotonate hydoxyl group not involved in the metal coordination, possibility that was discarded based on pH condition. The NBO charge values reported in Table 2 evidence the different behavior of the Fe(III) ion related to the aluminum one since the positive charge on the metal ion decreased by 0.370 |e|. Catechol group of quercetin is an affective metal chelator; its deprotonated form behaves as hard Lewis base and exhibits a particular affinity for hard Lewis acids like Fe(III) and the delocalized electron density of the catechol donor groups stabilize the ferric state. Taking into account all these relevant factors and contrary to what happened in aluminum, the **3′-4′** binding site is that involved in the most favored complex. This well matches with the available data that propose the iron strongest affinity for the ortho-dihydroxyl group of quercetin [45] in acidic solution, though several experimental and theoretical studies on the coordination properties of flavonoids present in literature provided often contradictory results concerning the binding site and metal/ligand stoichiometric ratio [18,19,21,42–44,49].

Irrespective of the applied combination of charge and coordination site, the d^5 high-spin Fe(III) in the complexes, where the quercetin acts as bidentate ligand, appears hexacoordinate (see Fig. 4b and S2) with the **4–5** and **3–4** complexes less stable by about 5 kcal/mol than the **3′-4′** one. In the only complex with the monocoordinated iron to quercetin (**3′** of Fig. S2), characterized by a coordination number (CN) equal to 5, a trigonal bipyramidal geometry can be observed. However, the formation of this complex in solution can be confidently excluded as it lies at about 13.0 kcal/mol above the **3′-4′** one.

3.2.3. Cu(II)-Quercetin

In the same pH range explored for Al(III) and Fe(III) complexes, the $Cu(H_4Que)^+$ species results the only species present in solution (see Fig. 1c). Thus, the monodeprotonated ligand on its possible OH groups (3-OH, 5-OH, 3′-OH and 4′-OH) has been considered in the complexes formation with metal ion. Based on the energetic unfavorability of monodentate quercetin complex, the bidentate nature of the ligand was mainly examined. The investigated complexes well account for the different orientation of catechol moiety and the planarity deviation along with the mono- and bi-coordination of the ligand (see Fig. 4c and S3). In the case of copper-containing complexes, all the considered structures are enclosed in a range of about 6 kcal/mol pointing out a substantial different behavior with respect to both Al(III) and Fe(III) metal ions. In particular, in Fig. 4c the structures related to the possible $Cu(H_4Que)^+$ species within the range of 5 kcal/mol and representative of the most stable conformation for the three considered coordination sites have been collected. The lowest minimum exhibits the metal ion coordinated to the **4–5** site followed by those with the metal cation linked to the **3–4** (2.0 kcal/mol) and **3′-4′$_H$** (4.7 kcal/mol) sites. In the **4–5** and **3′-4′$_H$** complexes, the ion is pentacoordinated outlining a square planar pyramid. In fact a water molecule initially placed as sixth ligand, after minimization is retained in the outer coordination shell of the copper ion by H-bond with the oxygen atoms (see Fig. 4c). This behavior can be ascribed to the axial distortion very common in the d^9 configuration of copper ion [41,50]. In the six membered chelate ring **4–5** complex, the orientation of the catechol ring is in *trans* owing to the torsional angle Φ equal to 157.3°. The **3–4** complex lying at only 2.0 kcal/mol above the **4–5** one, shows a dihedral angle value (Φ=19.5°) pointing out a catechol ring that does not deviate so much from the planarity. The copper ion on the contrary, appears tetracoordinated having pushed out of the inner coordination sphere

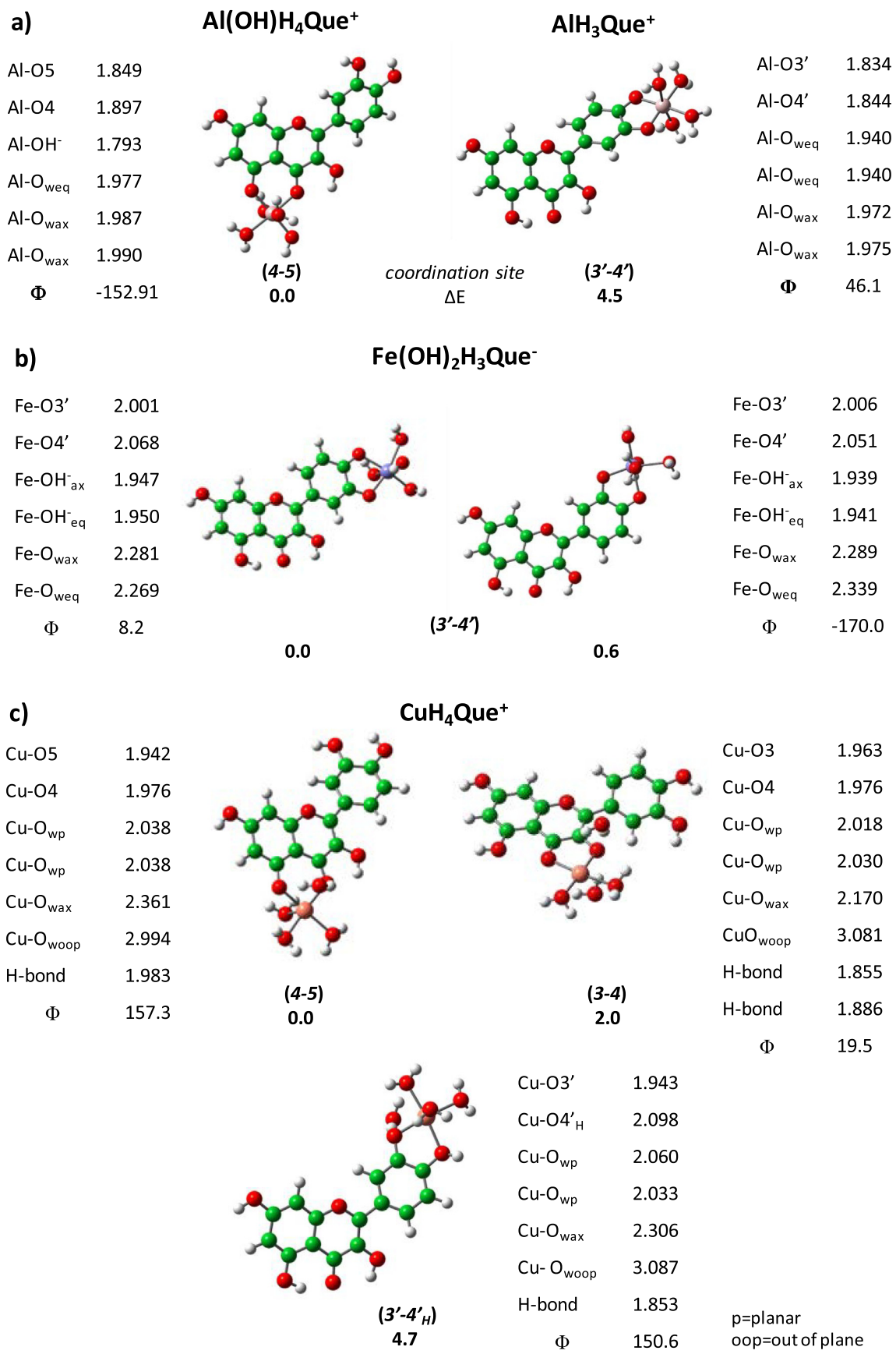

Fig. 4. Optimized Structures for the most plausible complexes of H_5Que with a) Al(III), b) Fe(III) and c) Cu(II). In parenthesis is specified the coordination site. Gibbs free energy differences with respect to the most stable complexes are reported in kcal/mol.

Table 2
BE differences (kcal/mol) between the most stable complexes and the others for each metal and natural charges for metal and oxygen atoms within each complexes.

Species	Coord. site[a]	ΔBE	O5 (O3′ or O3)	O4 (O4′)	M^{n+}	O_{Weq}	O_{Wax}	$O_{ox(eq)}$ (O_W)	$O_{ox\ (ax)}$(O_W)
Al									
$Al(OH)H_4Que^+$	**4–5**	13.7	−0.886	−0.790	1.922	−0.949	−0.947	−1.245	−0.946
AlH_3Que^+	**3′-4′**	0.0	−0.930	−0.922	1.919	−0.954	−0.951	−0.957	−0.955
Fe									
$Fe(OH)_2H_3Que^-$	**3′-4′** *s-cis*		−0.873	−0.842	1.549	−0.924	−0.925	−1.140	−1.130
Cu									
CuH_4Que^+	**4–5**	28.2	−0.844	−0.751	1.327	–	−0.962	−0.940	−0.940
CuH_4Que^+	**3′-4′$_H$**	53.4	−0.887	−0.377	1.377	−1.021	−0.963	−0.942	−0.949
CuH_4Que^+	**3–4** *s-cis*	0.0	−0.911	−0.735	1.410	−0.949	–	−0.949	–

[a] H atoms are always removed from the OH binding sites unless denoted with a subscript H.

two water molecules, so a square planar geometry has been obtained. The two water molecules are now located out of plane at 1.855 Å and 1.886 Å from the O3 deprotonated atom. The analogue having the dihedral angle equal to −160.5° (species **3–4** *s-trans* of Fig. S3) is almost isoenergetic owing to only 0.2 kcal/mol less stable.

Analyzing the natural charges of the atoms involved in the coordination for the **3–4** complex (Table 2), it is possible to note that the electrostatic component of the interaction is more evident with respect to that observed for the **4–5** for both donor atom and metal ion. In particular, the atom O5 (−0.844 |e|) is less negative than O3 (−0.911 |e|) and the copper ion retains more positive charge since 1.411 |e| and 1.327 |e| in **3–4** and **4–5**, respectively. This behavior is reflected on the higher binding energy by 28.2 kcal/mol than **4–5** (see Table 2) and deviates from that of the other two metal ions examined because it advises that the **3–4**, very close in energy to **4–5**, can coexist with it in aqueous environment. Furthermore its free formation energy (22.7 kcal/mol) smaller than that of **4–5** (24.3 kcal/mol) corroborates the consequence of the chelate effect, which is due to the bidentate ligand that prefers the formation of a six-membered ring (**4–5**) on the five-membered one (**3–4**), which is therefore the kinetically favored complex. However unlike the aluminum and iron ions, the monocoordination to the deprotonated 3′-OH produced a complex at 4.7 kcal/mol above the lowest energy minimum since the stabilizing effects from the H-bonds network including that with the neighbohring oxygen atom (O3) (see **3′-mono** of Fig. S3). This behavior is also enabled by the *cis* orientation of catechol moiety (Φ=33.6°).

3.2.4. UV–Vis simulated spectra in acqueous solution

To confirm the formation in aqueous solution of the most probable complexes above-described UV–Vis spectra were simulated. Table 3 collects the outcomes of TDDFT for neutral quercetin and for the most palusible complexes obatined with Al(III), Fe (III) and Cu(II) ions.

The computed excitation energies (Table 3) give for the quercetin two main bands: an intense absorption ($f = 0.674$) at 324 nm which is mainly due to a H→L transition (92%) and a band at 222 nm that, keeping in mind the overestimation of excitation energies provided by TDDFT method [51], well reproduce the experimental ones (377 nm and 258 nm, respectively). Analog behavior was encountered in previous works [11,19,29]. The frontier orbitals energy levels and the related electronic distribution isodensity plots are reported in Fig. S4. The displayed frontier orbitals clearly show the interested regions in the UV absorption, *i.e.*, the cinnamoyl moiety for HOMO-LUMO transition in the 320–385 nm range and the benzoyl one in the 240–280 nm.

Table 3
Computed wavelength (nm) for quercetin and the selected Al(III)-, Fe(III)- and Cu(II)-Que complexes. The experimental values are also reported.

Species	Coordination site	Calc.[a]		Exp.	
		I	II	I	II
Quercetin	–	222	324	258	377
$Al(OH)H_4Que^+$	**4–5**	238(0.51)[b]	358(0.63)	267	426
$Al(H_3Que)^+$	**3′-4′**	228(0.64)	328(0.68)		
$Fe(OH)_2H_3Que^-$	**3′-4′**	243(0.18)	376(0.81)	269	427
$Cu(H_4Que)^+$	**4–5**	243(0.45)	358(0.57)	264	431
$Cu(H_4Que)^+$	**3′-4′$_H$**	237(0.29)	349(0.95)		
$Cu(H_4Que)^+$	**3–4** ***s-cis***	228(0.54)	357(0.65)		

[a] Only electronic transitions having an oscillator strength higher than 0.1 were included.
[b] Oscillator strength in parenthesis.

The Al(III) complexation retains two main absorption bands attributed to H→L energy gaps with the first absorption band having π → π* character. The computed excitation energies for the two considered complexes propose a better reproduction of the experimental absorption for the $Al(OH)H_4Que^+$ (**4–5** of Fig. 4a) because for $Al(H_3Que)^+$ (**3′-4′** of Fig. 4a) the absorption band does not show the usual bathochromic shift in quercetin, before observed. The electronic density on the LUMO of the **4–5** complex is predominantly localized on both A and C rings (see Fig. S4). The UV–Vis results support the $Al(OH)H_4Que^+$ (**4–5**) as the most probable Al(III)-Que complex in the examined aqueous conditions. Although the ion is more likely to interact with the cathecol region in $Al(H_3Que)^+$ (see ΔBE in Table 2), the result is in agreement with other works [11,17], proposing $Al(OH)H_4Que^+$ (**4–5**) to be the kinetically favored complex.

When quercetin is coordinated to Fe(III) *via* catechol region, complex (**3′-4′**), the band belonging to the cynnamoyl moiety (323 nm, see Table 3), suffers a bathochromic shift (Δλ~50 nm). This behavior is in agreement with the experimental counterpart of this work and the previous one [43].

Looking at the main electronic transitions of the considered copper-containing complexes reported in Table 3, it is important to note that all of them exhibit a bathochromic shift of the band related to the cinnamoyl moiety by 35 nm, 26 nm and 34 nm and by 21 nm, 15 nm and 6 nm for the band belonging to the benzoyl moiety for **4–5**, **3′-4′** and **3–4** *s-cis*, respectively, caused by the deprotonation of quercetin and the formation of the complexes. This finding confirms that whatever the A-C rings (**5–4** site) or only the C ring (**3–4** site) is implicated in the coordination, the cinnamoyl band does not show significant difference to allow to discriminate the preferred complex, matter that, indeed, should be assigned to the benzoyl band that presents a more consistent difference (21 nm *versus* 6 nm). A further important consequence is that the different coordination geometry of the copper ion in **4–5** and **3–4** *s-cis* does not play a crucial role. The **3′-4′** complex, in turn, shows a small shift for both bands with respect to the alone quercetin proposing that the coordination on the catechol moiety (B ring) produces electronic effects on the A-C rings.

3.3. NMR spectroscopy characterization

To gain insights into the coordination behavior of quercetin towards the three different metal cations, Al(III), Fe(III) and Cu(II), ^{1}H NMR and

^{13}C NMR spectra were recorded on the DMSO-d_6 solutions prepared by dissolving the insoluble products formed during the potentiometric titration experiments and were compared to that of the free ligand (Fig. 5). The ^{1}H NMR spectrum of quercetin exhibits a sharp and extremely deshielded resonance at 12.45 ppm, which is usually attributed to the 5OH proton that participates in a strong intramolecular hydrogen bond with the 4O carbonyl oxygen atom [52,53]. Also, the C3, C3′, C4′ and C7 OH groups appear as extremely sharp singlets in the region 9.2–10.7 ppm (Fig. 5 and Table 4).

As shown before, complex formation leads to the substitution of one or two acidic protons of quercetin by the metal cation. While in aqueous solution, an equilibrium between the free quercetin and the metal-quercetin complex is expected [54,55], in non protic solvents, such as DMSO, complexation should lead to the disappearance of those proton signals involved in the complexation reaction [56,57]. This should be expected also for the DMSO solution obtained by dissolving the water insoluble complexes formed during the titration experiment. Instead, the ^{1}H NMR spectra acquired on these samples contains all the signals relative to the five OH groups of quercetin (Fig. 5). This evidence could suggest that the insoluble products collected during titration could be undissolved/unreacted quercetin. However, the UV–Vis spectra (Fig. 2) clearly show the formation of the complexes. In addition, we observe significant shift of the above proton signals and of significant changes in their relative signal intensity with respect to the free ligand (Fig. 5 and Table S2). The presence of all the acidic proton signals of quercetin makes difficult any univocal identification of the complexation site involved, and leads to the necessary assumption that the dissolved solid is a mixture of different species which come into a rapid equilibrium in solution within the NMR time scale. This equilibrium being facilitated by the presence of water in the solid which is due to the drying at air. Under this hypothesis, the NMR spectrum should reflect a weighted average over the spectra of each species in solution.

Table 4
OH*i*/OH3 intensity ratio in free quercetin and in the Cu(II)–Que complex.

	I_{OH5}/I_{OH3}	I_{OH7}/I_{OH3}	$I_{OH4'}/I_{OH3}$	$I_{OH3'}/I_{OH3}$
Que	2.2	1.4	0.92	1.6
Cu(II)–Que	1.0	0.56	0.63	1.2

Based on the above assumption, the possible neutral species in the Al(III)-Que system are those where the quercetin is deprotonated once, $Al(OH)_2H_4Que$, at the 7OH/5OH/3OH, or twice, $Al(OH)H_3Que$, at the 3′,4′-OH dihydroxyl site.

The schematic map in Fig. 6a shows the chemical shift changes associated to each proton in the molecular structure of Que., where the shielding and deshielding effect, deriving from the complexation, is indicated by the red and blue color code, respectively. It is rather impressive to see that a large deshielding effect occurs on the 3′,4′-OH dihydroxyl site (up to 0.17 as ppm change) and on the extreme opposite side of the molecule on the A ring (at the 7OH, H6 and H8 positions), with the largest shift for the OH-7 ($\Delta\delta \sim 0.35$ ppm). While, a moderate to low shielding effect is found for the 5OH, 3OH and the other protons in the B ring (Fig. 5, Fig. 6a and Table S2).

A similar map can be built from the ^{13}C NMR chemical shift changes of the Al(III)-Que complexes with respect to that of pure Que. (Fig. 6b) which highlights also a strong shielding effect on the C5-C10-C9 segment adjacent to the **4**–**5** coordination site. Therefore, ^{1}H and ^{13}C NMR data show significant changes in the chemical shifts of specific regions of the quercetin molecule upon complexation, including that bearing the hydroxyl site in position 7. Thus, although the bidentate complexes are much more stable, the monodentate complexes involving this site cannot be totally excluded.

The above maps reflect, to some extent, the change in the distribution of the electronic charge density of quercetin which is due to the

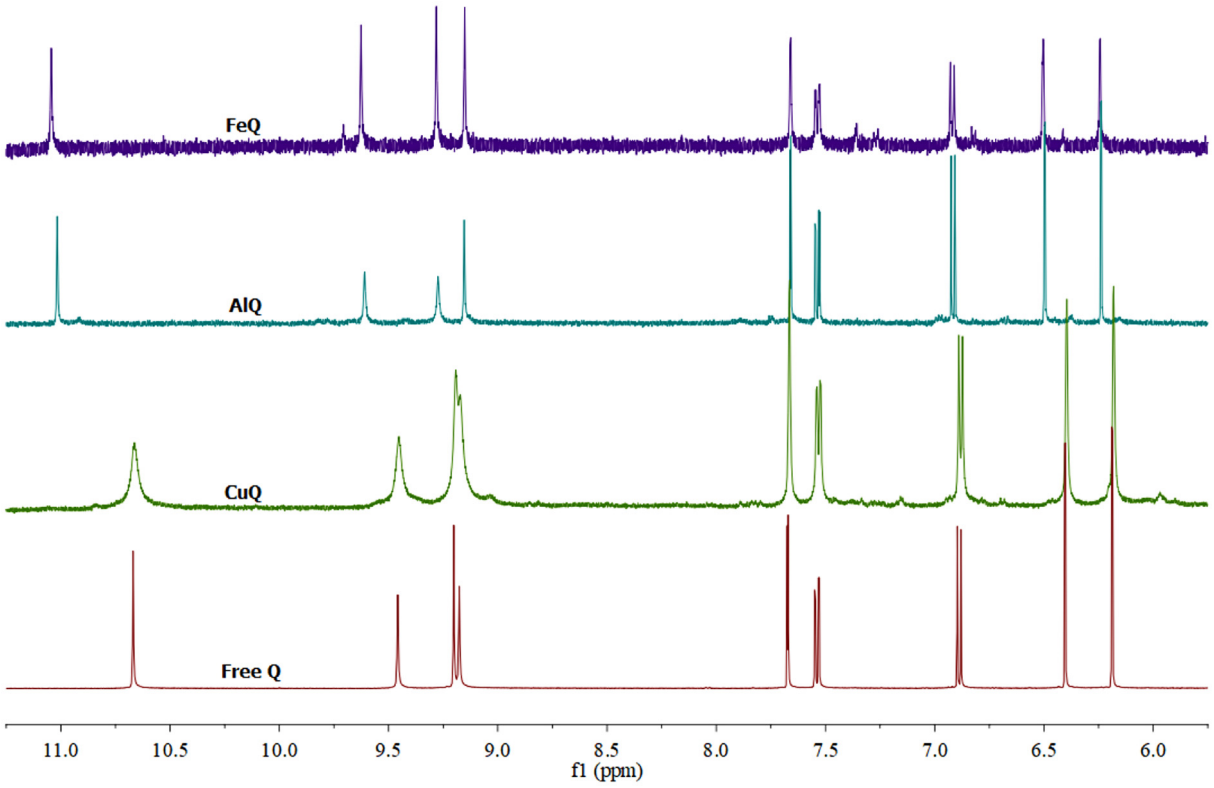

Fig. 5. ^{1}H NMR spectra of pure quercetin and of the complexes in DMSO.

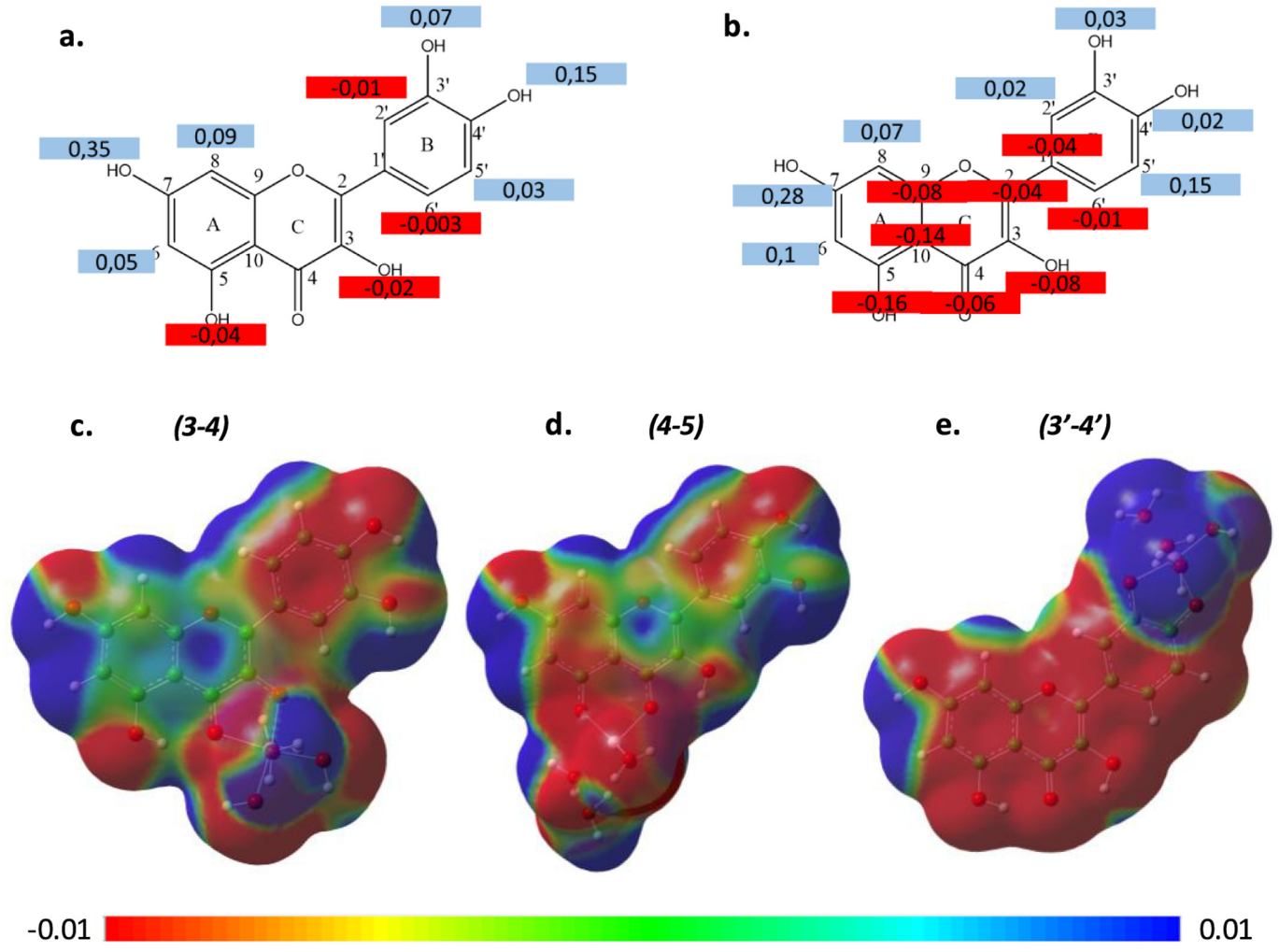

Fig. 6. Chemical shift changes maps a) ^{1}H NMR, b)^{13}C NMR. Maps of the molecular electrostatic potential (MEP)of c) 3–4, d) 4–5 Al(OH)$_2$H$_4$Que complexes and e) 3′,4′-OH Al(*OH*)H$_3$Que complex.

complexation with the Al(III) cation, because a shielding/deshielding effect on an atom should correspond to an increase/decrease of the electronic charge density in the molecule close to that atom. MEPs were computed considering all the possible Que. chelating sites for metal cation and are reported in Fig. 6 (panel c, d, e). If compared with the MEP of the neutral quercetin (Fig. 3), when the cation binds at the **3–4** site, an increase of the negative charge density essentially occurs on ring B, while a relatively high positive charge density is generated on rings A and C (Fig. 6c). Though, this charge distribution in **3–4** complex may explain the observed high field shifts of the NMR signals and the low-field shift in the C6-C7-C8 segment, it however, does not explain the strong deshielding effect observed on the 3′,4′ dihydroxyl site. This may be induced only when the metal coordination occurs on the catechol site (Fig. 6e). Therefore, the qualitative comparison between the NMR maps and the MEPs supports the hypothesis that the spectrum of the Al(III)-Que mixture is a weighted average of those of the individual complexes and free quercetin.

The simulated NMR spectra (Table S3) of the three plausible Al(III)-Que neutral complexes, whose MEPs are included in Fig. 6, confirm the coexistence of different complexes as well. Indeed, the computed ^{1}H chemical shifts endorse the observed (Fig. 6a,b) deshielding of 7OH and the shielding of H6 and H8 in those complexes whose aluminum coordination leads to the formation of the five-membered rings (for coordination at **3–4** and **3′-4′** sites). In particular, the large deshielding of 7OH as well as the shielding of H2' and H6' can be found only if the complexation occurs on site **3′-4′**. From the other hand, the low-field shift of 3′OH and 4′OH is observed when the **5–4** site is that involved in the metal coordination. Considering also the ^{13}C spectra, the shielding of the C5-C9-C10 segment occurs only if Que. coordinates Al(III) through the **3–4** site, while the downfield shift of most of carbon atoms of ring B is found for **4–5** coordination of the metal. Thus, based on this comparison, it cannot be excluded the presence in the examined solid of none of the three plausible Al(III)-Que complexes.

Based on the recorded ^{1}H NMR spectrum, similar hypotheses on coordination and nature of the complexes can be done on the Fe(III)-Que system, showing the same behavior as that of the Al(III)-Que one in terms of NMR chemical shifts (Table S4). Also the simulation of the ^{1}H NMR spectrum (Table S5) of the three possible metal coordination (**3–4**, **4–5** and **3′-4′**), suggests the coexistence of different species also in the case of Fe(III) complexation. However, differently from Al (III)-Que complexes, the presence of the **4–5** coordination mode can be excluded as none of the shifts experimentally found is observed in the simulated spectrum of such a complex. Indeed, the electrostatic potential map for coordination to **4–5** site (Fig. S5), evidences a negative charge density on ring A which does not explain the deshielding effect on protons of such ring that is experimentally observed. Most of those shifts are instead found for the complexation of Fe(III) through **3–4** site, while the shielding of H2' can be ascribed only to the **3′-4′** Fe(III)-Que complex. In addition, they are the most stable neutral complexes of Fe(III)-Que in DMSO and their relative stability differs of less than

1 kcal/mol, so they are formed with equal probability and can be considered as the most plausible species in the characterized solid.

In contrast to the above findings, the ^{1}H NMR signals of the Cu(II)–Que complex are all upfield shifted as compared to the free quercetin (Table S4), though the absolute chemical shift changes are relatively smaller than those observed on the other complexes (Table S2 and S4). The electrostatic density maps of Que. coordinated to the Cu(II) ion at the **3′-4′** site (Fig. S6) show a general increase of the negative charge density on the whole molecule, thus supporting the shielding effect observed in the proton spectrum of the complex.

A similar shielding effect was observed previously on Cu(II)–Que complex with a ligand to metal ratio of 1:2 where, chelation occurs in the **3′-4′** dihydroxyl and **3–4** positions and was attributed to the increase of the conjugation caused by the metal coordination, which increases the planarity of the flavonoid molecule [57]. In addition, a strong support towards the coordination on the 3-hydroxochrome position comes from the systematic decrease of the OH*i*/OH3 intensity ratio in the complex with respect to that of free quercetin (Table 4). Therefore, the evidence points towards the formation of the solid species Cu(*OH*)H$_4$Que with coordination in 3OH/4O, which is in rapid equilibrium with free quercetin in solution. However, the coordination in **3′-4′** cannot be excluded based on the MEPs reported in Fig. S6 showing that when the Cu cation is coordinated to this site a significant charge density is induced on the whole Que. molecule. Therefore, the generalized upfield shift of the NMR peaks (Fig. 5 and Table S4), similar to that found when the Cu cation binds both the **3–4** and **3′-4′** sites [57], agrees well with the presence of both complexes in our solid.

The simulated ^{1}H NMR spectra for Cu(II) coordination to the three possible sites of Que., evidence an upfield shift for most of the protons essentially in all the three cases, with the exception of 3OH and H6' protons in **4–5** metal coordination and 5OH proton in **3′-4′** Cu(II)-Que complex that, in principle, could exclude the presence of such complexes in the experimentally characterized solid. However, while for Cu(II) coordination at site **3–4** the signals of all the protons result upfield shifted or not shifted, the shielding of 3OH can be found only admitting the presence of **3′-4′** coordination of Que. to ferric ion. In addition, from the computational outcomes in DMSO, the **3′-4′** Cu(II)-Que complex emerges as the most stable species in such environment. Therefore, only considering the presence of both **3–4** and **3′-4′** complexes the observed shielding of the protons chemical shift with respect to free quercetin can be rationalized.

4. Conclusions

The coordination properties of quercetin towards Al(III), Fe(III) and Cu(II) in aqueous solution at 37 °C and in 0.16 M NaCl have been discussed. Speciation profiles from potentiometric titrations show that a complexation occurs at 1:1 ligand-to-cations ratio for Al(III) and Cu(II), and at 1:1 and 1:2 ligand-to-Fe(III) ratio. To achieve insights on the binding modes of the metal ions complexes, UV and ^{1}H and ^{13}C NMR spectra and DFT calculations have been performed. In all the complexes examined by the computational approach, the water solvent was represented using a combined model: esplicit water molecules to achieve a starting coordination number of six for alluminium, iron and copper and then the solvent in the region around the complex was implicitily described. Simulations of the UV–Vis spectra conducted at the time-dependent density functional theory level yielded results consistent with the experiemental ones and the features in the absorbance were primarily associated to the electron transitions from the highest occupied molecular orbital to the lowest unoccupied molecular orbital in the complexes.

The NMR analysis of the solid samples, obtained during the titration experiments, is consistent with the presence of a mixture of more than one complex thus, highlighting the tendency of quercetin to bind the three cations at different coordination sites, agreeing with the comparatively similar stability of the various possible complexes. Specifically, aluminum and iron show no clear preference towards any of the three complexation sites while, for copper the **4–5** site could be excluded based on experimental findings, computational results and literature data.

The use of quercetin in chelation therapy could be advantageous for the following reasons: its high ability in sequestering different metal ions deriving from its three coordination sites with different characteristics and the high stability of the complexes formed; its lipophilicity that could likely allow it to pass the cell membranes.

Conceptualization: Emilia Furia, Amerigo Beneduci, Tiziana Marino Investigation: Giuseppina Anna Corrente, Luana Malacaria, Gloria Mazzone Resources: Tiziana Marino, Amerigo Beneduci, Emilia Furia Writing - Original Draft: Emilia Furia, Giuseppina Anna Corrente, Gloria Mazzone Writing - Review & Editing: Emilia Furia, Amerigo Beneduci, Tiziana Marino.

Declaration of Competing Interest

The authors declare that they have no known competing financial interests or personal relationships that could have appeared to influence the work reported in this paper.

Acknowledgements

The authors thank Dipartimento di Chimica e Tecnologie Chimiche, Università della Calabria for the financial support. The authors also thank the Ministero degli Affari Esteri e della Cooperazione Internazionale (MAECI - CUP H28D20000370001).

Appendix A. Supplementary data

Supplementary data to this article can be found online at https://doi.org/10.1016/j.molliq.2020.115171.

References

[1] R.A. Goyer, M.G. Cherian (Eds.), Toxicology of Metals: Biochemical Aspects, Springer-Verlag, Berlin Heidelberg, 1995.
[2] H. Seiler, A. Sigel, H. Sigel, Handbook on Metals in Clinical and Analytical Chemistry, CRC Press, 1994.
[3] V.M. Nurchi, M. Crespo-Alonso, L. Toso, J.I. Lachowicz, G. Crisponi, Chelation therapy for metal intoxication: comments from a thermodynamic viewpoint, Mini-Rev. Med. Chem. 9 (2013) 1541–1549.
[4] T.B. Chaston, D.R. Richardson, Interactions of the pyridine-2-carboxaldehyde isonicotinoyl hydrazone class of chelators with iron and DNA: implications for toxicity in the treatment of iron overload disease, J. Biol. Inorg. Chem. 8 (2003) 427–438.
[5] G. Capolongo, M. Zacchia, A. Beneduci, S. Costantini, P. Cinque, A. Spasiano, G. De Luca, M.E. Di Pietro, P. Ricchi, F. Trepiccione, G. Capasso, A. Filosa, Urinary metabolic profile of patients with transfusion-dependent β-thalassemia major undergoing deferasirox therapy, Kidney Blood Press. Res. 45 (2020) 455–466.
[6] A. Dean, M.G. Ferlin, P. Brun, I. Castagliuolo, R.A. Yokel, D. Badocco, P. Pastore, A. Venzo, G.G. Bombi, V.B. Di Marco, 1,6-Dimethyl-4-hydroxy-3-pyridinecarboxylic acid and 4-hydroxy-2-methyl-3-pyridinecarboxylic acid as new possible chelating agents for iron and aluminium, Dalton Trans. 10 (2009) 1815–1824.
[7] C. Exley, Human exposure to aluminium, Environ Sci Process Impacts 15 (2013) 1807–1816.
[8] C. Exley, Aluminum should now be considered a primary etiological factor in Alzheimer's disease, J. Alzheimer's Dis. Rep. 1 (2017) 23–25.
[9] R.A. Yokel, The pharmacokinetics and toxicology of aluminum in the brain, Curr. Inorg. Chem. 2 (2012) 54–63.
[10] C. Exley, A molecular mechanism of aluminium-induced Alzheimer's disease? J. Inorg. Biochem. 76 (1999) 133–140.
[11] E. Furia, T. Marino, N. Russo, Insights into the coordination mode of quercetin with the Al(III) ion from a combined experimental and theoretical study, Dalton Trans. 43 (2014) 7269–7274.
[12] J.B. Harborne, C.A. Williams, Advances in flavonoid research since 1992, Phytochemistry 55 (2000) 481–504.
[13] Z. Jurasekova, C. Domingo, J.V. Garcia-Ramos, S. Sanchez-Cortes, Effect of pH on the chemical modification of quercetin and structurally related flavonoids characterized by optical (UV-visible and Raman) spectroscopy, Phys. Chem. Chem. Phys. 16 (2014) 12802–12811.
[14] A. Beneduci, E. Furia, N. Russo, T. Marino, Complexation behaviour of caffeic, ferulic and *p*-coumaric acids towards aluminium cations: a combined experimental and theoretical approach, New J. Chem. 41 (2017) 5182–5190.

[15] E. Furia, A. Beneduci, N. Russo, T. Marino, Structural characterization of aluminium (III) and iron(III) complexes of coumarinic acid in aqueous solutions from combined experimental and theoretical investigations, New J. Chem. 42 (2018) 11006–11012.
[16] A. Beneduci, G.A. Corrente, T. Marino, D. Aiello, L. Bartella, L. Di Donna, A. Napoli, N. Russo, I. Romeo, E. Furia, Insight on the chelation of aluminum(III) and iron(III) by curcumin in aqueous solution, J. Mol. Liq. 296 (2019) 111805–111814.
[17] A. Torreggiani, M. Tamba, A. Trinchero, S. Bonora, Copper(II)–Quercetin complexes in aqueous solutions: spectroscopic and kinetic properties, J. Mol. Struct. 744–747 (2005) 759–766.
[18] M. Leopoldini, N. Russo, S. Chiodo, M. Toscano, Iron chelation by the powerful antioxidant flavonoid quercetin, J. Agric. Food Chem. 54 (2006) 6343–6351.
[19] J. Ren, S. Meng, C.E. Lekka, E. Kaxiras, Complexation of flavonoids with iron: structure and optical signatures, J. Phys. Chem. B 112 (2008) 1845–1850.
[20] A. Ahmedova, K. Paradowska, I. Wawer, ^{1}H, ^{13}C MAS NMR and DFT GIAO study of quercetin and its complex with Al(III) in solid state, J. Inorg. Biochem. 110 (2012) 27–35.
[21] J.P. Cornard, J.C. Merlin, Spectroscopic and structural study of complexes of quercetin with Al(III), J. Inorg. Biochem. 92 (2002) 19–27.
[22] L. Dangleterre, J.-P. Cornard, C. Lapouge, Spectroscopic and theoretical investigation of the solvent effects on Al(III)–hydroxyflavone complexes, Polyhedron 27 (2008) 1581–1590.
[23] Y.A. Davila, M.I. Sancho, M.C. Almandoz, S.E. Blanco, Structural and spectroscopic study of Al(III)–3-hydroxyflavone complex: determination of the stability constants in water–methanol mixtures, Spectrochim. Acta Part A Mol. Biomol. Spectrosc. 95 (2012) 1–7.
[24] S. Marzena, K. Mateusz, Flavonoids and their properties to form chelate complexes, 76 (1) (2012) 35–41.
[25] P. Cardiano, F. Crea, C. Foti, O. Giuffrè, S. Sammartano, Potentiometric, UV and ^{1}H NMR study on the interaction of Cu^{2+} with ampicillin and amoxicillin in aqueous solution, Biophys. Chem. 224 (2017) 59–66.
[26] M.J. Frisch, G.W. Trucks, H.B. Schlegel, G.E. Scuseria, M.A. Robb, J.R. Cheeseman, G. Scalmani, V. Barone, B. Mennucci, G.A. Petersson, H. Nakatsuji, M. Caricato, X. Li, H.P. Hratchian, A.F. Izmaylov, J. Bloino, G. Zheng, J.L. Sonnenberg, M. Hada, M. Ehara, K. Toyota, R. Fukuda, J. Hasegawa, M. Ishida, T. Nakajima, Y. Honda, O. Kitao, H. Nakai, T. Vreven, J.A. Montgomery, J.E. Peralta, F. Ogliaro, M. Bearpark, J.J. Heyd, E. Brothers, K.N. Kudin, V.N. Staroverov, R. Kobayashi, J. Normand, K. Raghavachari, A. Rendell, J.C. Burant, S.S. Iyengar, J. Tomasi, M. Cossi, N. Rega, J.M. Millam, M. Klene, J.E. Knox, J.B. Cross, V. Bakken, C. Adamo, J. Jaramillo, R. Gomperts, R.E. Stratmann, O. Yazyev, A.J. Austin, R. Cammi, C. Pomelli, J.W. Ochterski, R.L. Martin, K. Morokuma, V.G. Zakrzewski, G.A. Voth, P. Salvador, J.J. Dannenberg, S. Dapprich, A.D. Daniels, J.B. Farkas Foresman, J.V. Ortiz, J. Cioslowski, D.J. Fox, Gaussian 09, Revision D.01, Gaussian, Inc, Wallingford CT, 2016.
[27] Y. Zhao, N.E. Schultz, D.G. Truhlar, Design of density functionals by combining the method of constraint satisfaction with parametrization for thermochemistry, thermochemical kinetics, and noncovalent interactions, J. Chem. Theory Comput. 2 (2006) 364–382.
[28] A.V. Marenich, C.J. Cramer, D.G. Truhlar, Universal solvation model based on solute electron density and on a continuum model of the solvent defined by the bulk dielectric constant and atomic surface tensions, J. Phys. Chem. B 113 (2009) 6378–6396.
[29] G. Mazzone, On the inhibition of hydroxyl radical formation by hydroxycinnamic acids: the case of Caffeic acid as a promising chelating ligand of a ferrous ion, J. Phys. Chem. A 123 (2019) 9560–9566.
[30] G. Mazzone, M.E. Alberto, B.C. De Simone, T. Marino, N. Russo, Can expanded bacteriochlorins act as photosensitizers in photodynamic therapy? Good news from density functional theory computations, Molecules 21 (2016) 288–299.
[31] R. Ditchfield, Self-consistent perturbation theory of diamagnetism, Mol. Phys. 27 (1974) 789–807.
[32] F. London, Théorie quantique des courants interatomiques dans les combinaisons aromatiques, J. Phys. Le Radium. 8 (1937) 397–409.
[33] D. Cesario, E. Furia, G. Mazzone, A. Beneduci, G. De Luca, E. Sicilia, Complexation of Al^{3+} and Ni^{2+} by L -ascorbic acid: an experimental and theoretical investigation, J. Phys. Chem. A 121 (2017) 9773–9781.
[34] R. Álvarez-Diduk, M.T. Ramírez-Silva, A. Galano, A. Merkoçi, Deprotonation mechanism and acidity constants in aqueous solution of flavonols: a combined experimental and theoretical study, J. Phys. Chem. B 117 (2013) 12347–12359.
[35] M. Musialik, R. Kuzmicz, T.S. Pawłowski, G. Litwinienko, Acidity of hydroxyl groups: an overlooked influence on antiradical properties of flavonoids, J. Organomet. Chem. 74 (2009) 2699–2709.
[36] P.K. Agrawal, H.-J. Schneider, Deprotonation induced ^{13}C NMR shifts in phenols and flavonoids, Tetrahedron Lett. 24 (2) (1983) 177–180.
[37] Š. Ramešová, R. Sokolová, I. Degano, J. Bulíčková, J. Žabka, M. Gál, On the stability of the bioactive flavonoids quercetin and luteolin under oxygen-free conditions, Anal. Bioanal. Chem. 402 (2012) 975–982.
[38] E. Furia, G. Sindona, Complexation of L-Cystine with metal Cations, J. Chem. Eng. Data 55 (2010) 2985–2989.
[39] P. Gans, A. Sabatini, A. Vacca, Investigation of equilibria in solution. Determination of equilibrium constants with the HYPERQUAD suite of programs, Talanta 43 (1996) 1739–1753.
[40] Z. Jurasekova, A. Torreggiani, M. Tamba, S. Sanchez-Cortes, J.V. Garcia-Ramos, Raman and surface-enhanced Raman scattering (SERS) investigation of the quercetin interaction with metals: evidence of structural changing processes in aqueous solution and on metal nanoparticles, J. Mol. Struct. 918 (2009) 129–137.
[41] C. Zhang, G.V. Korshin, A.M. Kuznetsov, M. Yan, Experimental and quantum-chemical study of differential absorbance spectra of environmentally relevant species: a study of quercetin deprotonation and its interactions with copper (II) ions, Sci. Total Environ. 679 (2019) 229–236.
[42] J.M. Dimitrić Marković, Z.S. Marković, D.S. Veselinović, J.B. Krstić, J.D. Predojević Simović, Study on fisetin–aluminium(III) interaction in aqueous buffered solutions by spectroscopy and molecular modeling, J. Inorg. Biochem. 103 (2009) 723–730.
[43] J.M. Dimitrić Marković, Z.S. Marković, T.P. Brdarić, V.M. Pavelkić, M.B. Jadranin, Iron complexes of dietary flavonoids: combined spectroscopic and mechanistic study of their free radical scavenging activity, Food Chem. 129 (2011) 1567–1577.
[44] M.M. Kasprzak, A. Erxleben, J. Ochocki, Properties and applications of flavonoid metal complexes, RSC Adv. 5 (2015) 45853–45877.
[45] M.E. Bodini, G. Copia, R. Tapia, F. Leighton, L. Herrera, Iron complexes of quercetin in aprotic medium. Redox chemistry and interaction with superoxide anion radical, Polyhedron 18 (1999) 2233–2239.
[46] A. Torreggiani, A. Trinchero, M. Tamba, P. Taddei, Raman and pulse radiolysis studies of the antioxidant properties of quercetin: Cu(II) chelation and oxidizing radical scavenging, J. Raman Spectrosc. 36 (2005) 380–388.
[47] E.J. Brown, H. Khodr, C.R. Hider, C.A. Rice-Evans, Structural dependence of flavonoid interactions with Cu^{2+} ions: implications for their antioxidant properties, Biochem. J. 330 (1998) 1173–1178.
[48] L. Mira, M.T. Fernandez, M. Santos, R. Rocha, M.H. Florêncio, K.R. Jennings, Interactions of flavonoids with iron and copper ions: a mechanism for their antioxidant activity, Free Radic. Res. 36 (2002) 1199–1208.
[49] A.C. Boudet, J.P. Cornard, J.C. Merlin, Conformational and spectroscopic investigation of 3-hydroxyflavone-aluminum chelates, Spectrochim. Acta - Part A Mol. Biomol. Spectrosc. 56 (2000) 829–839.
[50] T. Marino, N. Russo, M. Toscano, On the copper(II) ion coordination by prion protein HGGGW pentapeptide model, J. Phys. Chem. B 111 (2007) 635–640.
[51] B. Le Guennic, D. Jacquemin, Taking up the cyanine challenge with quantum tools, Acc. Chem. Res. 48 (2015) 530–537.
[52] A. Primikyri, G. Mazzone, C. Lekka, A.G. Tzakos, N. Russo, I.P. Gerothanassis, Understanding zinc(II) chelation with quercetin and luteolin: a combined NMR and theoretical study, J. Phys. Chem. B 119 (2015) 83–95.
[53] V. Exarchou, A. Troganis, I.P. Gerothanassis, M. Tsimidou, D. Boskou, Do strong intramolecular hydrogen bonds persist in aqueous solution? Variable temperature gradient ^{1}H, ^{1}H-^{13}C GE-HSQC and GE-HMBC NMR studies of flavonols and flavones in organic and aqueous mixtures, Tetrahedron 58 (2002) 7423–7429.
[54] P. D'Adamo, S. Ulivi, A. Beneduci, G. Pontoni, G. Capasso, C. Lanzara, G. Andrighetto, U. Hladnik, V. Nunes, M. Palacin, P. Gasparini, Metabonomics and population studies: age-related amino acids excretion and inferring networks through the study of urine samples in two Italian isolated populations, Amino Acids 38 (2010) 65–73.
[55] A. Beneduci, G. Chidichimo, G. Dardo, G. Pontoni, Highly routinely reproducible alignment of ^{1}H NMR spectral peaks of metabolites in huge sets of urines, Anal. Chim. Acta 685 (2011) 186–195.
[56] R.F.V. De Souza, W.F. De Giovani, Synthesis, spectral and electrochemical properties of Al(III) and Zn(II) complexes with flavonoids, Spectrochim. Acta - Part A Mol. Biomol. Spectrosc. 61 (2005) 1985–1990.
[57] S.B. Bukhari, S. Memon, M. Mahroof-Tahir, M.I. Bhanger, Synthesis, characterization and antioxidant activity copper-quercetin complex, Spectrochim. Acta - Part A Mol. Biomol. Spectrosc. 71 (2009) 1901–1906.

Supplementary Material

Experimental and theoretical study on the coordination properties of quercetin towards aluminum(III), iron(III) and copper(II) in aqueous solution

Giuseppina A. Corrente, Luana Malacaria, Amerigo Beneduci, Emilia Furia*, Tiziana Marino and Gloria Mazzone

Dipartimento di Chimica e Tecnologie Chimiche, Via P. Bucci, Cubo 12/D, Università della Calabria, I-87036 Arcavacata di Rende (CS), Italy

Table of Contents

Figure S1

$Al(H)_{-2}(H_5Que)^+$			
(a) $Al(OH)H_4Que^+$	*site*	□	ΔE
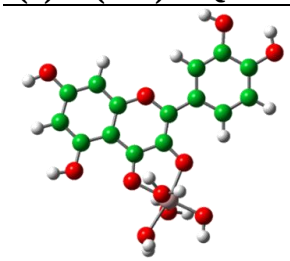	*3-4 s-trans*	-6.7	2.9
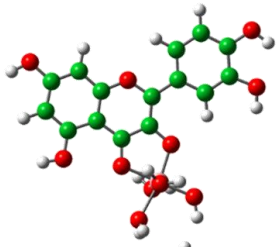	*3-4 s-cis*	-175.7	3.2
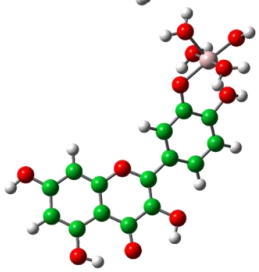	*3'-4'$_H$*	-147.5	9.1
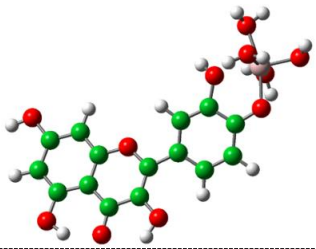	*3'$_H$-4'*	-168.4	10.7
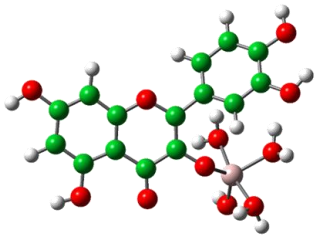	*3*	-34.3	20.4
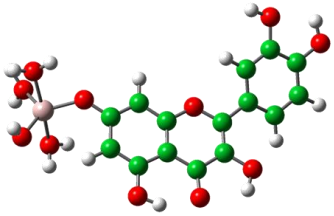	*7*	-150.1	15.1

(b) Al(H_3Que)$^+$	*site*	□	ΔE
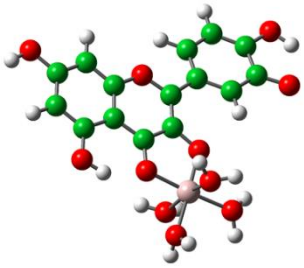	*3-4 s-cis*	13.9	16.6
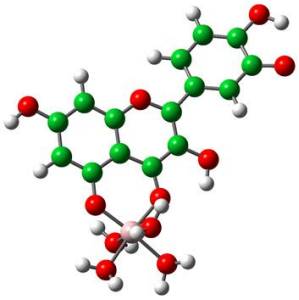	*4-5 s-cis*	28.4	15.1
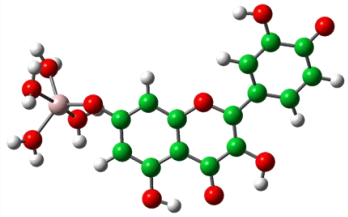	*7*	-164.0	42.4

Table S1

	Al(H)$_{-2}$(H$_5$Que)$^+$		*Fe(H)$_{-4}$(H$_5$Que)$^-$*	*Cu(H)$_{-1}$(H$_5$Que)$^+$*
site	**Al(OH)H$_4$Que$^+$**	**Al(H$_3$Que)$^+$**	**Fe(OH)$_2$H$_3$Que$^-$**	**Cu(H$_4$Que)$^+$**
4,5 *s-trans*	-70.9			-24.3
4,5 *s-cis*	-71.2	-55.8		-24.2
3-4 *s-trans*	-68.3			-22.7
3-4 *s-cis*	-68.6	-57.6		-22.9
3'-4' *s-trans*		-55.9	-98.8	
3'-4' *s-cis*			-99.4	
3'$_H$-4	-57.7			-16.7
3'-4$_H$	-60.1			-14.3
3'			-85.9	-15.7
3	-51.1			
7	-51.8	-7.9		

Gibbs free energy of formation (kcal/mol)

Figure S2

$Fe(H)_{-5}(H_5Que)_2^{2-}$			
$Fe(OH)_2H_3Que^-$	*site*	□	ΔG_f
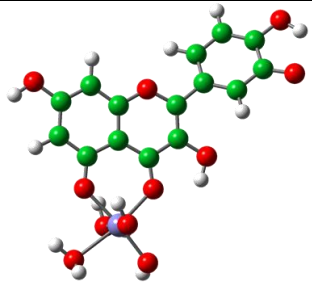	*4-5*	-31.7	5.0
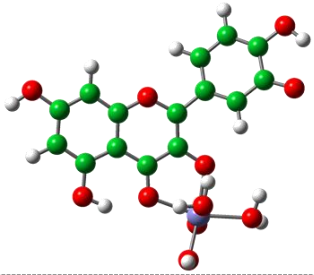	*3-4*	-26.8	4.1
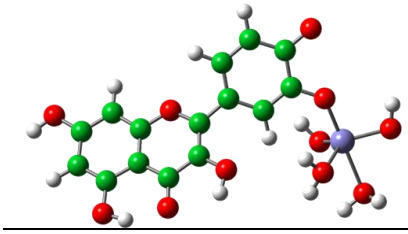	*3′*	35.7	-12.9
$Fe(H)_{-5}(H_5Que)_2^{2-}$			
$Fe(OH)(H_3Que)_2^{2-}$	*site*		ΔG_f
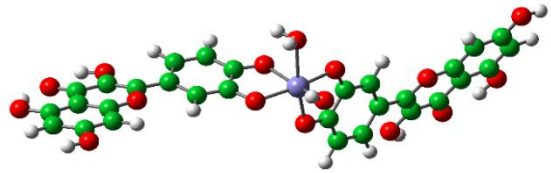	*3′-4′*		-113.7
$Fe(H)_{-6}(H_5Que)_2^{3-}$			
$Fe(OH)_2(H_3Que)_2^{3-}$			
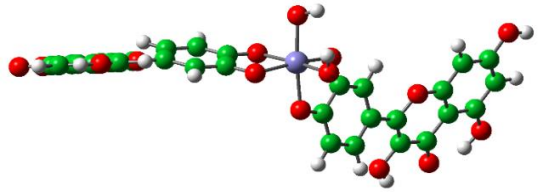	*3′-4′*		-125.8

Figure S3

$Cu(H)_{-1}(H_5Que)^+$			
$Cu(H_4Que)^+$	*site*	Φ	ΔE
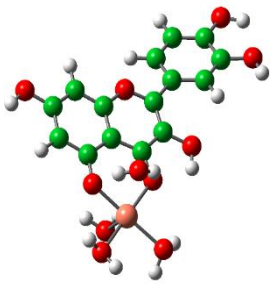	*4-5* *s-cis*	-25.5	0.1
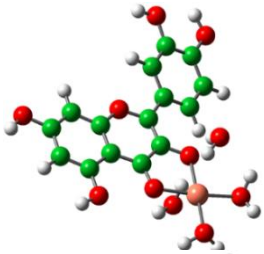	*3-4* *s-trans*	-160.5	2.2
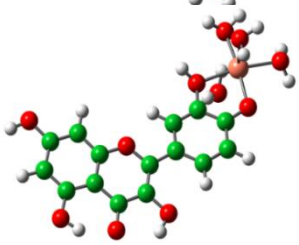	*3'$_H$-4'*	-169.1	5.8
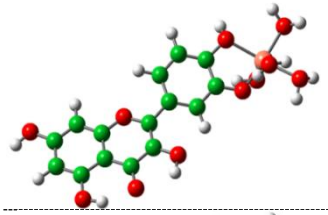	*3'-4'$_H$* *s-cis*	15.4	6.2
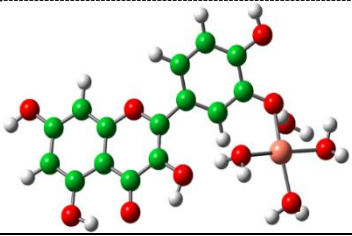	*3'*	33.6	4.7

Figure S4

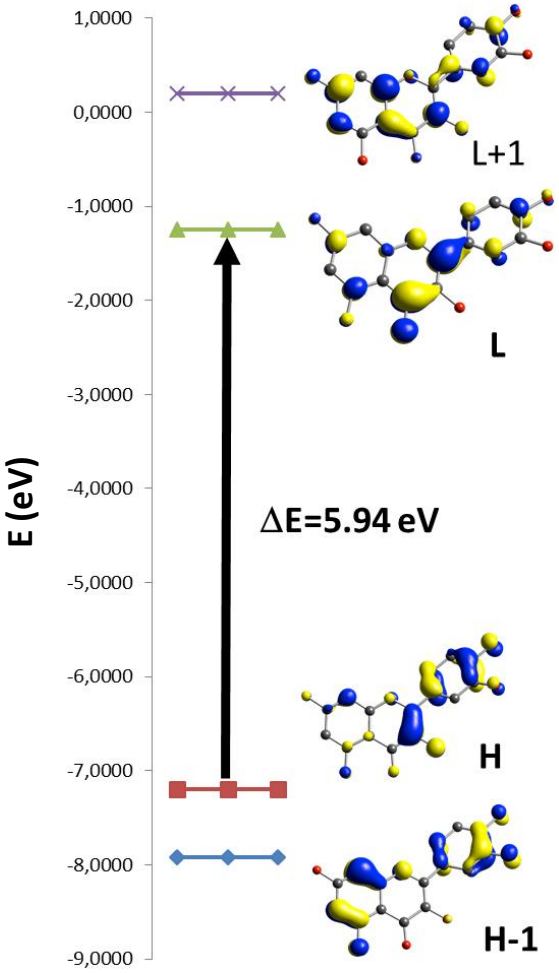
1,0000
0,0000
-1,0000
-2,0000
-3,0000
-4,0000
-5,0000
-6,0000
-7,0000
-8,0000
-9,0000
E (eV)
L+1
L
ΔE=5.94 eV
H
H-1

Table S2

Proton	Free Que	Al(III)-Que complex	Shift	Carbon	Free Que	Al(III)-Que complex	Shift
H 6	6.1867	6.236	0.0493	**C8**	93.3333	93.4003	0.067
	6.1908	6.24	0.0492	**C6**	98.1765	98.2726	0.0961
H 8	6.4014	6.494	0.0926	**C10**	103.0275	102.8863	-0.1412
	6.4055	6.4981	0.0926	**C2'**	115.1221	115.1427	0.0206
H 5'	6.8807	6.9073	0.0266	**C5'**	115.6	115.7525	0.1525
	6.8976	6.9243	0.0267	**C6'**	119.9746	119.9648	-0.0098
H 6'	7.5286	7.5259	-0.0027	**C1'**	121.9857	121.9416	-0.0441
	7.5331	7.5304	-0.0027	**C3**	135.6844	135.6064	-0.078
	7.5456	7.5428	-0.0028	**C3'**	145.0514	145.0833	0.0319
	7.55	7.5473	-0.0027	**C2**	146.8551	146.8181	-0.037
H 2'	7.671	7.6583	-0.0127	**C4'**	147.6954	147.714	0.0186
	7.6754	7.6627	-0.0127	**C9**	156.1646	156.0874	-0.0772
OH 3	9.1694	9.1461	-0.0233	**C5**	160.7272	160.5722	-0.155
OH 3'	9.199	9.2678	0.0688	**C7**	163.8718	164.1508	0.279
OH 4'	9.4511	9.6043	0.1532	**C4**	175.8286	175.7677	-0.0609
OH 7	10.6646	11.0099	0.3453				
OH5	12.4467	12.4065	-0.0402				

Table S3

Atom	Free Que *s-cis*	Free Que *s-trans*	Al(III) – Que 3-4 complex	Shift	Al(III) – Que 4-5 complex	Shift	Al(III) – Que 3'-4' complex	Shift
OH 3	6.83	7.02			6.72	-0.11	7.24	0.22
OH 5	12.06	12.04	10.58	-1.48			12.38	0.34
H 6	6.64	6.65	6.71	0.07	6.55	-0.09	6.69	0.04
OH 7	5.56	5.56	5.60	0.04	5.53	-0.03	6.27	0.72
H 8	6.91	6.94	7.01	0.10	6.85	-0.06	6.97	0.03
H 2'	8.47	8.12	9.33	0.86	8.62	0.14	7.85	-0.27
OH 3'	5.25	5.31	5.23	-0.02	5.27	0.01		
OH 4'	6.03	6.03	6.00	-0.04	6.12	0.09		
H 5'	7.56	7.52	7.54	-0.02	7.58	0.02	7.17	-0.36
H 6'	8.09	8.62	8.17	0.08	8.24	0.15	8.32	-0.30
C2	154.86	154.00	156.56	1.70	156.77	1.91	157.70	3.70
C3	144.60	145.26	151.14	6.54	143.55	-1.05	143.91	-1.35
C4	182.04	181.91	181.81	-0.24	175.66	-6.38	180.97	-0.94
C5	171.85	171.86	169.79	-2.06	174.34	2.49	171.01	-0.85
C6	104.78	104.83	105.33	0.55	108.98	4.21	105.15	0.32
C7	173.48	173.52	173.69	0.21	175.04	1.57	173.10	-0.43
C8	100.24	100.24	100.79	0.55	98.48	-1.76	100.65	0.41
C9	166.14	165.74	165.19	-0.95	166.25	0.12	165.80	0.05
C10	110.64	110.60	109.25	-1.39	112.34	1.70	110.77	0.18
C1'	131.91	132.00	133.29	1.38	131.29	-0.62	127.98	-4.02
C2'	122.67	118.36	122.58	-0.10	123.10	0.43	116.50	-1.85
C3'	150.96	152.75	151.92	0.96	152.07	1.11	164.50	11.75
C4'	157.05	157.26	156.58	-0.47	157.87	0.82	169.88	12.62
C5'	123.60	123.60	123.62	0.02	123.88	0.27	120.63	-2.96
C6'	129.89	132.24	128.28	-1.60	130.43	0.55	130.59	-1.65

Table S4

Proton	Fe(III) – Que complex	Shift	Cu(II) – Que complex	Shift
H 6	6.2415	0.0548	6.1811	-0.0056
	6.2455	0.0547		
H 8	6.5014	0.1	6.3959	-0.0055
	6.5055	0.1		
H 5'	6.9111	0.0304	6.8719	-0.0088
	6.928	0.0304	6.8893	-0.0083
H 6'	7.526	-0.0026	7.5234	-0.0052
	7.5307	-0.0024	7.5261	-0.007
	7.5431	-0.0025	7.5399	-0.0057
	7.5474	-0.0026	7.5414	-0.0086
H2'	7.6583	-0.0127	7.6641	-0.0069
	7.6626	-0.0128	7.6657	-0.0097
OH 3	9.1469	-0.0225	9.1675	-0.0019
OH 3'	9.2779	0.0789	9.1892	-0.0098
OH 4'	9.6218	0.1707	9.4505	-0.0006
OH 7	11.0396	0.375	10.6624	-0.0022
OH5	12.4035	-0.0432	12.4357	-0.011

Figure S5

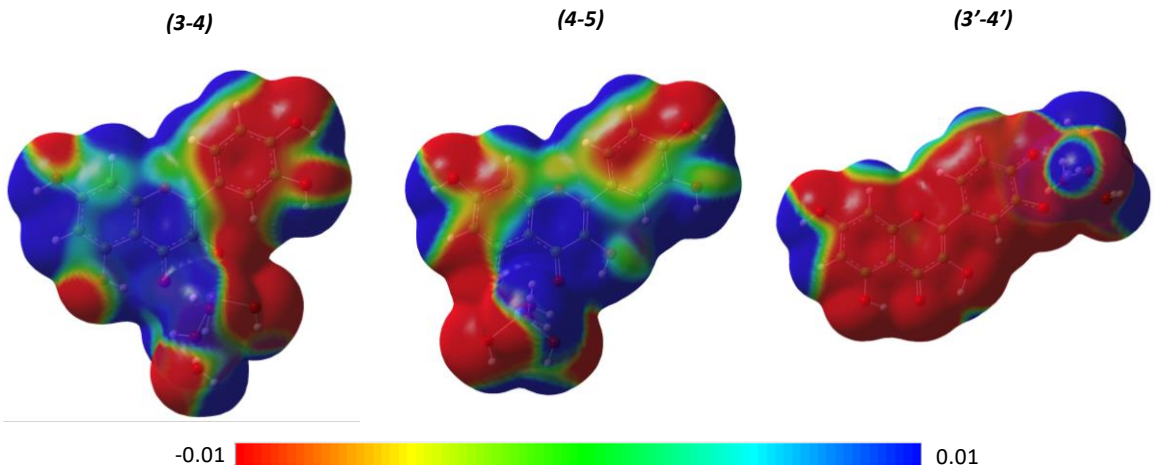

Table S5

Atom	Fe(III) – Que 3-4 complex	Shift	Fe(III) – Que 4-5 complex	Shift	Fe(III) – Que 3'-4' complex	Shift
OH 3			7.2	0.4	6.9	0.1
OH 5	11.0	-1.0			12.2	0.2
H 6	6.7	0.1	6.3	-0.3	6.6	0.0
OH 7	5.6	0.1	5.3	-0.2	5.5	-0.1
H 8	7.0	0.1	6.7	-0.2	6.9	0.0
H 2'	9.3	0.8	8.6	0.1	7.8	-0.7
OH 3'	5.4	0.1	5.2	0.0		
OH 4'	6.1	0.0	6.0	0.0		
H 5'	7.5	0.0	7.5	0.0	6.7	-0.8
H 6'	8.2	0.1	8.2	0.1	8.1	0.0
C2	151.1	-3.7	153.2	-1.6	156.2	1.3
C3	153.9	9.3	144.3	-0.3	144.0	-0.6
C4	184.7	2.6	178.4	-3.6	181.3	-0.8
C5	168.8	-3.0	179.3	7.4	171.7	-0.1
C6	105.6	0.8	105.1	0.3	104.4	-0.4
C7	173.7	0.2	174.1	0.7	173.1	-0.4
C8	100.7	0.4	97.6	-2.7	99.9	-0.3
C9	165.5	-0.6	167.2	1.1	165.9	-0.3
C10	110.0	-0.7	114.6	4.0	110.5	-0.2
C1'	132.5	0.6	131.9	0.0	129.9	-2.0
C2'	124.9	2.2	122.4	-0.3	117.6	-5.1
C3'	152.2	1.3	152.1	1.1	165.9	15.0
C4'	156.9	-0.2	156.9	-0.1	170.8	13.7
C5'	123.7	0.1	123.6	0.0	119.4	-4.2
C6'	129.8	-0.1	129.2	-0.6	128.9	-1.0

Figure S6

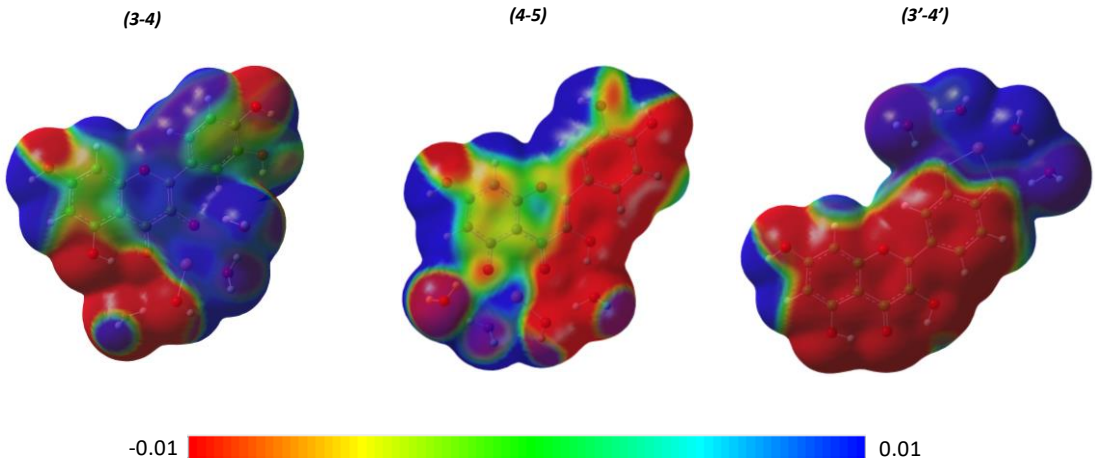

Table S6

Atom	Cu(II) – Que 3-4 complex	Shift	Cu(II) – Que 4-5 complex	Shift	Cu(II) – Que 3'-4' complex	Shift
OH 3			10.8	3.8	6.8	-0.2
OH 5	10.6	-1.4			12.2	0.2
H 6	6.7	0.0	6.3	-0.3	6.6	-0.1
OH 7	5.6	0.0	5.3	-0.3	5.4	-0.1
H 8	6.9	0.0	6.7	-0.2	6.8	-0.1
H 2'	8.2	-0.2	8.1	0.0	7.6	-0.5
OH 3'	5.2	0.0	5.3	0.0		
OH 4'	6.0	-0.1	6.0	0.0		
H 5'	7.5	0.0	7.5	-0.1	6.9	-0.6
H 6'	7.9	-0.2	8.8	0.2	8.2	-0.4
C2	158.8	3.9	153.7	-0.3	156.4	2.4
C3	151.8	7.2	147.6	2.3	143.6	-1.6
C4	186.7	4.6	177.9	-4.0	180.8	-1.1
C5	170.3	-1.5	176.0	4.2	171.6	-0.3
C6	105.5	0.7	107.6	2.8	104.3	-0.5
C7	173.3	-0.2	173.5	-0.1	172.8	-0.7
C8	100.1	-0.2	97.1	-3.2	99.9	-0.3
C9	165.4	-0.8	166.5	0.7	165.6	-0.2
C10	110.6	-0.1	113.2	2.6	110.3	-0.3
C1'	132.8	0.9	132.5	0.5	127.6	-4.4
C2'	122.5	-0.2	118.6	0.3	117.9	-0.5
C3'	151.5	0.6	152.7	-0.1	165.4	12.7
C4'	156.7	-0.4	156.9	-0.4	170.1	12.8
C5'	123.7	0.1	123.3	-0.3	121.7	-1.9
C6'	130.3	0.4	133.7	1.5	129.6	-2.6

molecules

MDPI

Article

Modeling the Solubility of Phenolic Acids in Aqueous Media at 37 °C

Emilia Furia [1], Amerigo Beneduci [1,*], Luana Malacaria [1], Alessia Fazio [2], Chiara La Torre [2] and Pierluigi Plastina [2]

[1] Department of Chemistry and Chemical Technologies, University of Calabria, 87036 Arcavacata di Rende (CS), Italy; emilia.furia@unical.it (E.F.); luana.malacaria@unical.it (L.M.)
[2] Department of Pharmacy, Health and Nutritional Sciences, University of Calabria, 87036 Arcavacata di Rende (CS), Italy; alessia.fazio@unical.it (A.F.); latorre.chiara@libero.it (C.L.T.); pierluigi.plastina@unical.it (P.P.)
* Correspondence: amerigo.beneduci@unical.it

Abstract: In this work, the solubility of vanillic, gallic, syringic, *p*-coumaric, ferulic and caffeic acids was determined at 37 °C under different conditions, namely pure water and two different ionic media, NaCl(aq) and $NaClO_4$(aq), at different ionic strengths (i.e., 0.16, 0.50, 1.0, 2.0 and 3.0 M). The solubility in water of all the acids was found to be higher than that in both of the ionic media. Moreover, the solubility of hydroxycinnamic acids was lower than that of hydroxybenzoic acids. The activity coefficients of neutral species were calculated from these data; this knowledge is necessary when modeling the dependence of equilibrium constants on the ionic strength. Results obtained in this work can be useful for further studies regarding complex formation equilibria between these ligands and bioavailable metal cations.

Keywords: solubility; phenolic acids; activity coefficients; salting out constant; ionic medium

Citation: Furia, E.; Beneduci, A.; Malacaria, L.; Fazio, A.; La Torre, C.; Plastina, P. Modeling the Solubility of Phenolic Acids in Aqueous Media at 37 °C. *Molecules* **2021**, *26*, 6500. https://doi.org/10.3390/molecules26216500

Academic Editors: Piotr Cysewski, Tomasz Jeliński and Maciej Przybyłek

Received: 7 October 2021
Accepted: 27 October 2021
Published: 28 October 2021

1. Introduction

A variety of phenolic compounds are currently among the most studied categories of natural antioxidants [1]. Phenolic acids contain one or more hydroxyl groups (polar part) attached to an aromatic ring (non-polar part) and are often found in plants as esters or glycosides [1–6]. Due to their ubiquitous presence in plant-based foods (fruit, vegetables, grain, tea, coffee, spices), the intake of phenolic acids is estimated as 25×10^{-3}–1 g per day, depending on diet [7]. The interest in phenolic compounds lies mainly in their known health benefits, including their antioxidant activity and ability as free radical scavengers [8–11]. These properties give them great potential as active principles in the pharmaceutical industry as well as antioxidants in the food industry. For this reason, there is increasing interest in isolating these compounds from their natural matrices [12–14]. The efficient design of any extraction process requires the knowledge of the solute's solubility. Aqueous solubility is a parameter of particular importance for assessing the environmental partitioning of different compounds. It has been reported that the low solubility of some solutes in water can be modified by the presence of co-solutes such as salts or by increasing the temperature [15–21]. Two phenomena related to solubility changes caused by the presence of co-solutes can be observed: salting-in and salting-out. In general, the solubility of a non-electrolyte can increase or decrease by the addition of an electrolyte, but the effect is dependent on the solvent salt used. Equation (1) relates the solubility of the neutral species, S°, to its activity coefficients, γ:

$$\log \gamma = \log (S^\circ{}_0 / S^\circ) \quad (1)$$

where S°_0 is the solubility at zero ion concentration. The activity coefficient of the neutral species is related to the molality, m, of the solvent electrolyte by Equation (2), also valid for weak electrolytes:

$$\log \gamma = k \cdot m \quad (2)$$

where k is the salting-out (positive) or salting-in (negative) coefficient, also known as the Setschenow coefficient, which may depend on the ionic strength [22]. For a generic non-electrolyte, the effect depends upon the solvent salt; in general, for a given solvent salt, it depends upon the saturating non-electrolyte. According to Debye [23], the salting-out constant generally increases as the polar properties of the non-electrolyte decrease. This theory does not clarify how certain electrolytes salt-out a specified non-electrolyte while others do the opposite. A possible explanation has been proposed by Kruyt and Robinson [24]: in a solution of a non-electrolyte in water, the water dipoles are arranged around a molecule of the non-electrolyte, with their positive or negative end towards the non-electrolyte depending upon the polar properties of the latter. When an electrolyte is added to the solution, due to the hydration of the ions, less water is available to the saturating non-electrolyte and salting-out of the non-electrolyte is expected. There is an opposite effect: water molecules are organized in a manner differing to the arrangement about the non-electrolyte. The result of the approach of the ion to the non-electrolyte is the packing-in of water molecules about the non-electrolyte, i.e., salting-in. The present work represents the continuation of efforts concerning the evaluation of the effect of salt addition on the solubility of organic compounds [25–29]. We report here on the solubility at 37 °C of six phenolic acids of both subclasses, i.e., hydroxybenzoic and hydroxycinnamic acids, generically indicated as H_nPh—vanillic (VA), gallic (GA), syringic (SA), *p*-coumaric (*p*-CA), ferulic (FA) and caffeic (CafA) acids (Scheme 1)—in pure water as well as in aqueous solutions of different ionic strength in sodium chloride and in sodium perchlorate.

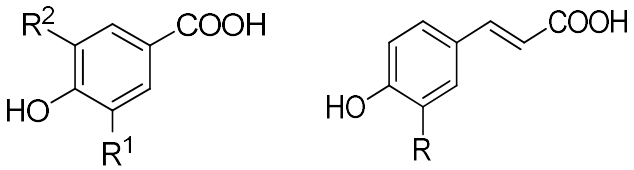

(**a**) (**b**)

Scheme 1. Chemical structure of (**a**) hydroxybenzoic acids (vanillic acid: $R^1 = OCH_3$, $R^2 = H$; syringic acid: $R^1 = R^2 = OCH_3$; gallic acid: $R^1 = R^2 = OH$); (**b**) hydroxycinnamic acids (caffeic acid: R = OH; ferulic acid: $R = OCH_3$; *p*-coumaric acid: R = H).

Previous literature data report on the solubility of these phenolic acids in pure organic solvents, in mixed organic–aqueous solutions [10,30–43], or in aqueous media but under experimental conditions far from biological. The interaction of these acids with aqueous media is important because such compounds display their antioxidant activity in the biological systems involving water as the natural solvent.

2. Results

The determination of phenolic acid solubility was achieved by measuring the absorbance values between 200 and 300 nm, every 1 nm, taking the ionic medium as a blank. Three replicates were run for each point. The typical spectra recorded for hydroxybenzoic (Figure 1a–c) and hydroxycinnamic (Figure 1d–f) acids are reported.

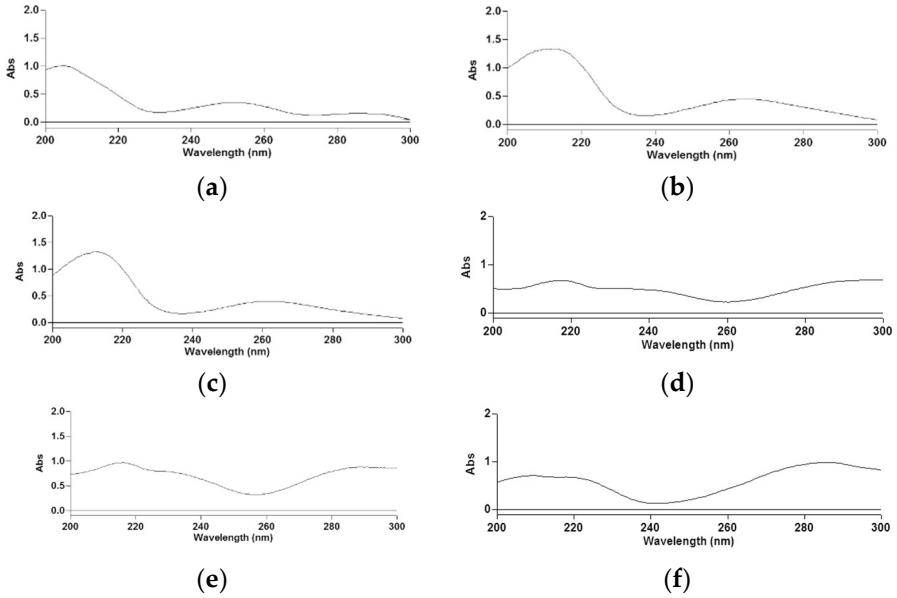

Figure 1. Absorption spectra of vanillic (**a**), syringic (**b**), gallic (**c**), caffeic (**d**), ferulic (**e**) and *p*-coumaric (**f**) acids.

For the solubility determination of vanillic, syringic and gallic acids, peaks at 251, at 262 and at 258 nm, respectively, were considered. Concerning hydroxycinnamic acids, peaks at 287 for the quantitative determination of caffeic and ferulic acids and at 288 nm for *p*-coumaric acid were considered. The absorbance, A_λ, of phenolic acids, generically H_nPh, was expressed according to Equation (3):

$$A_\lambda = l\ \varepsilon_\lambda\ [H_nPh] \quad (3)$$

where l is the optical path and ε_λ is the molar absorptivity. The total solubility in pure water, $S_T{}^\circ$, as well as in aqueous solutions of different ionic strength in sodium chloride and in sodium perchlorate, generically S_T, was deduced by interpolation on a calibration curve, based on standard solutions prepared in the range 2.0×10^{-3} and 25.0×10^{-3} molal for hydroxybenzoic acids and in the range 1.0×10^{-3} and 10.0×10^{-3} molal for hydroxycinnamic acids. In all cases, the correlation coefficient, R^2, was $\geq$0.999 and the limit of detection was 0.50×10^{-3} molal. The total solubility values obtained at 37 °C are reported in Table 1, along with the outcomes of the statistical analysis.

As a general trend, the solubility in water of all the acids was higher than that in both ionic media at each of the electrolyte concentrations. The hydroxybenzoic acids were more soluble than the hydroxycinnamic ones and, among them, gallic acid showed the highest solubility, more than one order of magnitude higher. As expected, among the hydroxybenzoic acids, syringic acid was the least soluble, due to the presence of two methoxy groups, and the solubility of the hydroxycinnamic acids was generally lower than that of the hydroxybenzoic acids in all the media investigated. The salting-out effect is related to the strong tendency of ionic solutes to form hydration shells. In fact, as the concentration of the ionic salt increased, more and more water molecules were bound up in the hydration shells, and therefore the solubility decreased. The solubility trend of hydroxybenzoic and hydroxycinnamic acids as a function of the ionic strength can be better appreciated in Figure 2, in the two electrolyte media.

Table 1. Total solubility at 37 °C of phenolic acids in water and in aqueous solutions of NaCl and $NaClO_4$ at different ionic strengths.

	S_T 10^3, Molal					
	VA	**SA**	**GA**	**CafA**	**FA**	***p*-CA**
H_2O	$^{z}12.47 \pm 0.01^{a}$	$^{y}8.8 \pm 0.3^{a}$	$^{x}114.5 \pm 0.3^{a}$	$^{w}6.4 \pm 0.2^{a}$	$^{v}5.47 \pm 0.01^{a}$	$^{w}6.61 \pm 0.01^{a}$
***I* , molal NaCl**						
0.16	$^{z}11.52 \pm 0.06^{b}$	$^{y}8.62 \pm 0.03^{ab}$	$^{x}104.6 \pm 0.3^{b}$	$^{w}6.26 \pm 0.03^{ab}$	$^{v}5.35 \pm 0.01^{a}$	$^{w}6.24 \pm 0.01^{a}$
0.51	$^{z}9.74 \pm 0.03^{c}$	$^{y}8.36 \pm 0.06^{ab}$	$^{x}104.2 \pm 0.4^{bc}$	$^{w}5.67 \pm 0.04^{bc}$	$^{v}4.59 \pm 0.09^{b}$	$^{w}5.31 \pm 0.01^{b}$
1.02	$^{z}7.7 \pm 0.6^{d}$	$^{z}7.99 \pm 0.05^{bc}$	$^{y}101.1 \pm 0.1^{d}$	$^{x}4.76 \pm 0.01^{d}$	$^{w}3.82 \pm 0.03^{c}$	$^{xw}4.19 \pm 0.01^{cg}$
2.09	$^{z}7.42 \pm 0.05^{d}$	$^{z}7.5 \pm 0.1^{cde}$	$^{y}98.7 \pm 0.2^{e}$	$^{x}3.50 \pm 0.01^{e}$	$^{xw}3.24 \pm 0.01^{cd}$	$^{w}2.64 \pm 0.02^{d}$
3.20	$^{z}7.36 \pm 0.03^{d}$	$^{z}7.36 \pm 0.03^{ce}$	$^{y}94.4 \pm 0.5^{f}$	$^{x}2.11 \pm 0.03^{f}$	$^{w}3.15 \pm 0.01^{d}$	$^{x}1.92 \pm 0.08^{e}$
***I*, molal $NaClO_4$**						
0.16	$^{z}11.92 \pm 0.04^{ab}$	$^{y}8.42 \pm 0.03^{ab}$	$^{x}104.6 \pm 0.3^{b}$	$^{w}5.79 \pm 0.04^{bc}$	$^{w}5.37 \pm 0.01^{a}$	$^{w}6.12 \pm 0.01^{af}$
0.51	$^{z}11.66 \pm 0.04^{b}$	$^{y}8.33 \pm 0.04^{ab}$	$^{x}103.7 \pm 0.3^{c}$	$^{w}5.41 \pm 0.01^{c}$	$^{w}5.32 \pm 0.01^{a}$	$^{w}6.05 \pm 0.05^{af}$
1.05	$^{z}11.33 \pm 0.03^{b}$	$^{y}8.10 \pm 0.09^{bd}$	$^{x}102.6 \pm 0.8^{g}$	$^{w}5.18 \pm 0.06^{cd}$	$^{w}5.16 \pm 0.01^{ab}$	$^{w}5.59 \pm 0.04^{bf}$
2.21	$^{z}10.1 \pm 0.1^{c}$	$^{y}7.12 \pm 0.02^{e}$	$^{x}97.1 \pm 0.1^{h}$	$^{w}4.65 \pm 0.04^{d}$	$^{w}4.54 \pm 0.07^{b}$	$^{w}4.65 \pm 0.04^{c}$
3.50	$^{z}8.9 \pm 0.3^{e}$	$^{y}6.27 \pm 0.01^{f}$	$^{x}95.1 \pm 0.1^{i}$	$^{w}3.98 \pm 0.02^{e}$	$^{w}3.78 \pm 0.03^{cd}$	$^{w}3.75 \pm 0.07^{g}$

The values with different superscripts (a, b, c, d, e, f, g, h and i) in the same column are significantly different ($p < 0.05$). The values with different superscripts (v, w, x, y and z) in the same row are significantly different ($p < 0.05$).

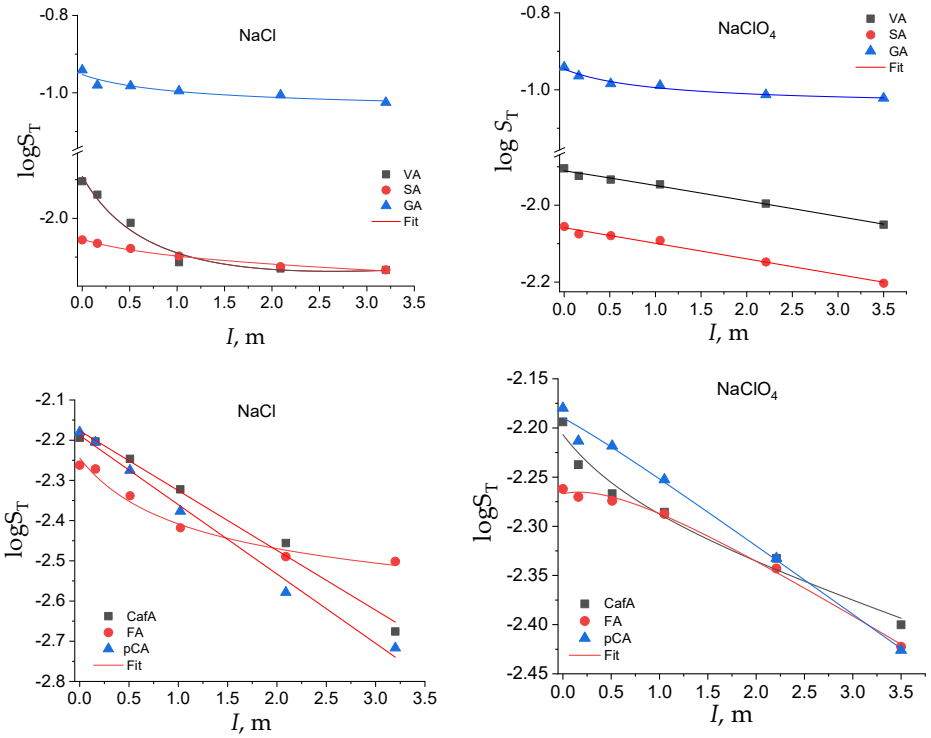

Figure 2. Total solubility in the logarithmic scale of the hydroxybenzoic and hydroxycinnamic acids as a function of the solvent salts and of the ionic strength.

In both sets of acids, the solubility was affected by the -OH and -OCH_3 substituents on the phenyl moiety, with the hydroxy and methoxy groups contributing to an increase and a decrease in the solubility, respectively, especially at lower ionic strengths. The following order of solubility, that holds up to approximately I = 1 m, was found: GA > VA > SA and CafA > *p*-CA > FA. The effect of the substituents on the total solubility was more evident on the benzoic acid series. If we look at the dependence of S_T on the ionic strength for the benzoic acid series, the salting-out effect of the electrolyte was different for the two salts.

In sodium chloride, the solubility dropped to low values in a smoothed way, at low ionic strength, and then it tended towards a plateau value. In perchlorate, instead, the solubility decreased almost linearly with I (except for GA).

In the hydroxycinnamic acid series the solubility decreased quite linearly with the ionic strength, independently of the ionic medium used, except for the least soluble ferulic acid, which showed a nonlinear dependence of its S_T vs. I (Table S1 in Supplementary Material). The solid lines are the best fitting curves obtained by Equation (5) or by a line. The related fitting parameters are reported in Table S1.

The order of solubility traced above seems to be related to a polarity decrease in the acids as the hydroxyl groups are replaced by either a hydrogen or a methoxy group, and to the decrease in the capability of the molecule to make hydrogen bonds with water. This argument may explain why gallic acid has the highest solubility, almost one order of magnitude higher than the other acids of both series, at all ionic strengths, and why its solubility is slightly affected by the increase in the molality of the solvent salt.

However, this consideration is mostly important for the benzoic acids, while, in the hydroxycinnamic ones, the unsaturated alkyl chain plays a major role in determining the overall solubility behavior.

In a recent computational study, it was shown that the free energy of solvation in water is negative for gallic and caffeic acids and positive for ferulic acid, with gallic acid having the most negative solvation free energy [44], indicating that the highest solubility of gallic acid is due to the high polar interaction density formed between the phenolic and carboxylic hydroxyl groups with water. In the same study, the authors showed also that the phenolic hydroxyl and the carboxyl functions tend to form hydrogen bonds with water, giving rise to a twist in the molecule structure close to the carboxyl group in the case of ferulic and caffeic acids. The effects of the phenyl hydroxy and methoxy substituents on the solid–liquid equilibrium of syringic and vanillic acids in water was recently investigated by the Abraham solvation model [45]. It was found that vanillic acid, with two hydroxyl substituents, had the highest value for the H-bond acidity (solute acidity descriptor), which described the tendency of the solute to form hydrogen bonds with its acid hydrogens, followed by syringic acid, which had one hydroxyl and two methoxy substituents. Moreover, the H-bond acidity of the carboxyl group increased by the electron-donating resonance effect of the methoxy substituents in the aromatic ring. In contrast, the H-bond acidity decreased due to the intramolecular hydrogen bond between two adjacent OH-OR substituents [46].

These acids may also form hydrogen bonds by sharing an oxygen lone electron pair of one of their substituents, i.e., they have hydrogen bond basicity. This is the highest for syringic acid due to the higher number of available lone electron pairs, even though intramolecular H-bonds may lead to a decrease in this parameter for vanillic acid [46]. Analogous results were obtained for ferulic and *p*-coumaric acids, the latter showing the highest value for the H-bond acidity parameter, which is partially reduced in ferulic acid due to the intramolecular hydrogen bond between the hydroxyl group and the methoxy group in the *meta* position. In contrast, the H-bond basicity character decreases from ferulic acid to *p*-coumaric acid, according to the increase in the number of hydrogen acceptors in the molecules [47].

Thus, the presence of hydroxyl groups increases the H-bond acidity, i.e., the strength of the hydrogen bonds formed by the donor hydroxyl groups with water, whereas the H-bond basicity descriptor, related to the strength of the hydrogen bonds formed by the acceptor groups in the molecules with water, increases with the number of methoxy substituents on the ring. On the other hand, when the hydroxy and/or the methoxy groups are absent, the above solute descriptors significantly decrease in value, such as in the case of veratric and cinnamic acids [46,47].

The largest salting-out effect calculated at the highest ionic strength is reported in Figure 3 in terms of the percentage decrease in the total solubility with respect to the value in pure water (Equation (4)).

$$Salting - out\ \% = \left(S_T^0 - S_T\right) \times 100/S_T^0 \quad (4)$$

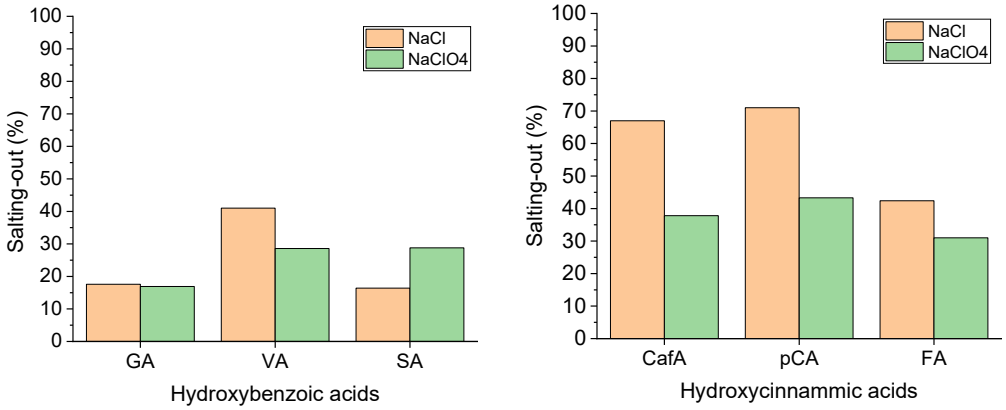

Figure 3. Salting-out effect calculated at the highest ionic strength for the two series of acids and in both electrolytes.

The salting-out effect is remarkable especially for the hydroxycinnamic acids, with values ranging from 40 up to 70% and mostly in NaCl. The strong decrease in the solubility with the ionic strength determines this result and highlights the low tendency of the hydroxycinnamic acids to interact with water, which becomes worse in the presence of highly polar salts such as sodium chloride. On the other hand, the salting-out effect seems to depend less on the type of electrolyte in the hydroxybenzoic acid series. It is interesting to note that in both ionic media and for both the acid series, the maximum salting-out occurs for the acids that have intermediate solubility in each series (i.e., vanillic and *p*-coumaric), which are the ones that respond mainly to ionic strength changes (Figure 2) mostly in NaCl medium.

3. Discussion

The knowledge of the activity coefficients of the neutral species is useful when modeling the dependence of equilibrium constants on the ionic strength [48,49]. For example, to evaluate the sequestering ability of these acids towards biological metal cations in a natural system, such as the ocean or biological fluids, the activity coefficients must be used to extrapolate their equilibrium constants at the infinite dilution reference state from those determined in constant ionic medium [50,51].

The activity coefficients of the neutral species as a function of I and of the solvent electrolyte are plotted in Figures 4 and 5. The solubility of the neutral species at all the ionic strengths investigated is reported in Table S2 in the Supplementary Material.

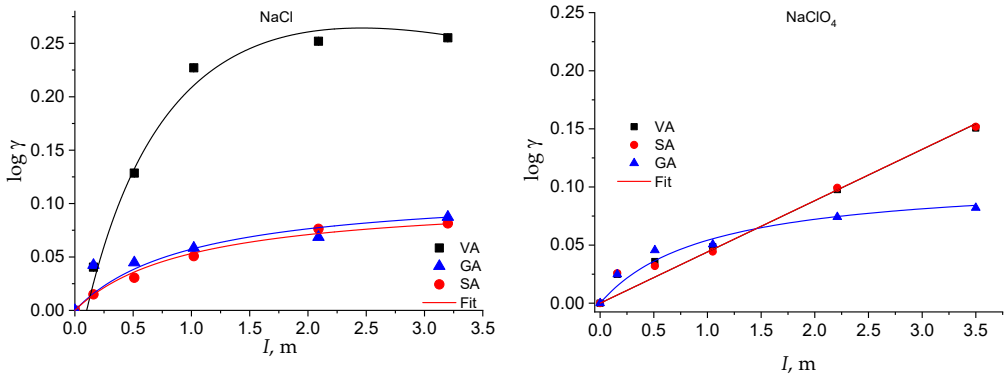

Figure 4. log γ of the hydroxybenzoic acids as a function of the solvent salt and of the ionic strength.

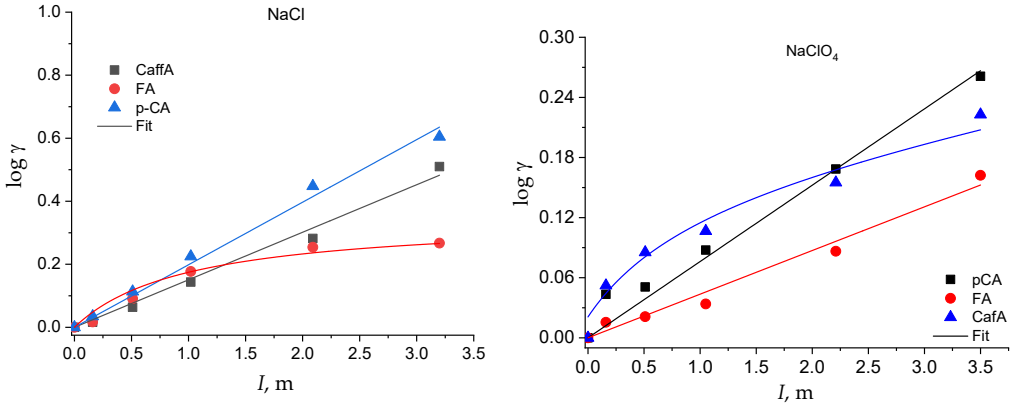

Figure 5. log γ of the hydroxycinnamic acids as a function of the solvent salt and of the ionic strength.

The activity coefficient of the neutral species of all the acids increases with the ionic strength in both the solvent electrolytes (Figures 4 and 5). However, some of them show a linear trend that can be well fitted by Equation (1), with Setschenow coefficients ranging from 0.7 up to 0.53 kg mol^{-1}, while others show a nonlinear trend that is modeled by Equation (7) (Table S3 in Supplementary Material). In the latter cases, the Setschenow coefficient depends on the concentration of the solvent electrolyte and the log γ tends towards a plateau value for ionic strengths larger than around 2 molal. These data show that a salting-out effect in the total solubility corresponds to a salting-in effect on the activity coefficients, as already observed for other acids in aqueous solution [48].

Therefore, while, in NaCl medium, the solubility of the phenolic acids tends towards zero (and the activity coefficient tends towards infinity) at infinite *I*, in $NaClO_4$, the solubility tends towards a minimum value (and the activity coefficient towards a maximum value) at very high *I*. This different behavior in the two electrolyte media is intriguing and deserves further study to be explained by changing the experimental conditions (i.e., the nature of inert salt) and extending the evaluation to other classes of analytes.

Table 2 collects literature data [6,30,32,34,39,41,43,46,52–55] for a comparison with our solubility results. All data are expressed as mass fraction (χ).

Table 2. Solubility of phenolic acids, as mass fraction (χ), in water and in 1 molal NaCl at 37 °C from this work and from the literature.

				χ·10³										
Phenolic Acids	**This Work**	**Ref. [6]**	**Ref. [30]**	**Ref. [32]**	**Ref. [34]**	**Ref. [39]**	**Ref. [41]**	**Ref. [43]**	**Ref. [46]**	**Ref. [52]**	**Ref. [53]**	**Ref. [54]**		**Ref. [55]**
				H_2O										
VA	0.23								0.22 [b]			0.24 [c] 0.26 [d]		0.24
GA	2.10		1.33	2.79	2.16	2.50	2.66					1.31 [c] 1.38 [d]		1.40
SA	0.16	0.36	0.84						0.22 [b]			0.79 [c] 0.92 [d]		0.85
CafA	0.12			0.19										
FA	0.10			0.14					0.11 [b]	0.113 [c]; 0.079 [d]	0.0807 [c]; 0.109 [d]			0.90
***p*-CA**	0.12	0.086							0.12 [b]					
				χ·10³										
Phenolic Acids	**This Work**													
				1 m NaCl								**1 m KNO_3**	**1 m $NaNO_3$**	
VA	0.14											0.19 [c] 0.23 [d]	0.17 [c] 0.20 [d]	
GA	1.85		0.98 [a]									1.27 [c] 1.34 [d]	1.15 [c] 1.21 [d]	
SA	0.14											0.76 [c] 0.88 [d]	0.71 [c] 0.88 [d]	
FA	0.07													

[a] Calculated at 37 °C in 1 m Na_2SO_4; [b] Calculated from the experimental solubility values at 40 °C expressed as g solute/100 solvent by the equation: $\chi = \frac{\left(\frac{m}{M}\right)_{acid}}{\left(\frac{m}{M}\right)_{acid}+\left(\frac{m}{M}\right)_{water}}$; [b] Measured at 35 °C; [c] Measured at 35 °C; [d] Measured at 40 °C.

Our results are in line with previous literature data for vanillic, gallic, caffeic and *p*-coumaric acids. The agreement is also satisfactory for syringic and ferulic acids in pure water. There is less agreement with the data at 1 m NaCl and those reported previously in sulphate [30] and nitrate media [54], where the salting-out effect is higher than in chloride for syringic and vanillic acid and lower for gallic. This behavior has been already observed previously for syringic acid at room temperature [54] and clearly highlights the significant effect of the anion of the electrolyte salt. Moreover, the above discrepancies may be related to a substantial difference in the preparation of the saturated solutions: in our experimental approach, the direct contact of the analytes with the magnetic stirring is avoided and this is mainly reflected in the less soluble analytes.

4. Materials and Methods

4.1. Materials

All solutions were prepared by means of analytical-grade reagents and ultrapure water (Millipore MilliQ system). Vanillic (J&K Scientific, Beijing, China, 99%), syringic and gallic (Sigma Aldrich, St. Louis, MI, USA, ≥98% and ≥99%, respectively), *p*-coumaric (Sigma, St. Louis, MI, USA, ≥98%), ferulic and caffeic (Aldrich, St. Louis, MI, USA, 99%) acids were used without further purification. Sodium perchlorate and sodium chloride stock solutions were prepared and standardized according to previous works [56,57].

4.2. Solubility Apparatus and Procedure

The absorption spectra in the UV region were recorded with a Varian Cary 50 Scan UV–Visible spectrophotometer on a series of hydroxybenzoic and hydroxycinnamic acid test solutions, prepared by 100-fold dilution of 50 microliters of saturated solutions. These were prepared with a leaching apparatus suitable to prevent solid particles from coming into contact with the magnetic stirrer. To prevent grinding by the stirrer, hydroxybenzoic and hydroxycinnamic acids were wrapped in highly retentive filter paper (Whatman 42) bags. These were retained in glass cylinders containing pure water as well as sodium chloride and sodium perchlorate solutions at pre-established ionic strength values while continuously stirring with a magnetic bar. The cylinders were then placed in a thermostatic water bath at (37.0 ± 0.1) °C, and the hydroxybenzoic and hydroxycinnamic acid concentrations were monitored over time, until they reached a constant value, which usually occurred in around 4 days. Matched quartz cells of thickness 1 cm and 100 microliter volume were employed. The absorbance, A_λ, was recorded to ±0.001 units. The formulations of the parameters and the acquisition of data were achieved with the aid of a computer connected to the instrument.

4.3. Thermodynamic Modeling

Total solubility data in the molal concentration scale were fitted by the smoothing empirical Equation (5):

$$\log(S_T) = \log\left(S_T^0\right) + \left[a_\infty + \frac{a_0 - a_\infty}{1 + m}\right] m \tag{5}$$

where S_T^0 is the total solubility in pure water, and a_∞ and a_0 are empirical parameters at infinite and at zero ionic strength, respectively. Equation (5) becomes linear for $a\infty = a_0 \equiv a$.

The solubility of the neutral species, S^0, was calculated by Equation (6), considering the deprotonation equilibrium of the phenolic acids (Equation (7)), behaving as a monoprotic acid with constant K_I (Equation (8)):

$$S^0 = \frac{S_T[H^+]}{[H^+] + K_I} \tag{6}$$

$$HA \rightleftarrows H^+ + A^- \tag{7}$$

$$K_I = \frac{[H^+][A^-]}{[HA]} \frac{\gamma_{H^+}\gamma_{A^-}}{\gamma_{HA}} \quad (8)$$

where, according to the specific ion interaction model (SIT) [58,59], the activity coefficients of the ionic species $\gamma_\pm$ and of the neutral one are given by Equations (9) and (10), respectively.

$$log\gamma_\pm = -z_\pm^2 \frac{0.4565I^{0.5}}{1 + 1.11I^{0.5}} + b_\pm I \quad (9)$$

$$log\gamma_{HA} = kI \quad (10)$$

with $b_+ = b\left(H^+, Cl^-/ClO_4^-\right)$, $b_- = b(A^-, Na^+)$ and k is the Setschenow coefficient.

The dependence of the ionization constant of the acids on the ionic strength was explicitly considered in the calculation. Unfortunately, data on the protonation constant of these acids are only reported at a few ionic strengths and in the low molal range (up to 0.1 mol/kg) [60–66]. Therefore, here, the K_I for each acid was measured at 0.16 mol/kg and 0.51 mol/kg and its values at higher ionic strength, up to 3.5 mol/kg, were estimated by the SIT model at 37 °C (Equations (8)–(11)).

$$pK_I = pK_0 - 2D + (b_+ + b_- - k)I \quad (11)$$

where K_0 is the value of K_I at infinite dilution and $D = \frac{0.4565I^{0.5}}{1+1.11I^{0.5}}$ is the extended Debye term. K_0 was calculated by Equation (11) using the experimental values at I = 0.51 mol/kg.

In the SIT model (Equation (9)), the specific ion interaction coefficients relative to the proton with the anion of the electrolyte salt (i.e., Cl^-, ClO_4^-) and that relative to the conjugate base of the acid (A^-) with Na^+ were kept constant in the iterations used for fitting the experimental data, respectively, at 0.12 (in NaCl)/0.14 (in $NaClO_4$) [58] and 0.06 (in both media) [67]. For the specific ion interaction coefficient of A^- with Na^+, we chose a value identical to that of the hydrogen salicylate ion with Na^+, by considering the similarity of the anion structures. Figure S1 displays the dependence of the first ionization acidic constant vs. the ionic strength for all the investigated acids.

Equations (2) and (12), which consider the dependence of the Setschenow coefficients k on the ionic strength, were used to fit the activity coefficient data:

$$\log \gamma = k_\infty + \left[k_\infty + \frac{k_0 - k_\infty}{1 + m}\right] m \quad (12)$$

where k_∞ and k_0 are the Setschenow coefficients at infinite and at zero ionic strength, respectively.

4.4. Statistical Analysis

All the experiments were performed in triplicate, and the data were expressed as means ± standard deviation. To test statistical differences among solubility values of each compound under different experimental conditions, data were evaluated with one-way ANOVA followed by Tukey's multiple comparison test. A p value of < 0.05 was considered statistically significant.

5. Conclusions

The study of the solubility of benzoic and cinnamic acid derivatives is important for at least two aspects: one is on a fundamental thermodynamic basis, and concerns the knowledge of the solubility behavior at different temperatures and in different aqueous media, such as those containing electrolyte salts that may act as co-solvents. Calculation of the activity coefficients from the solubility values allows us to obtain a more complete picture of different aspects of the thermodynamic properties of hydroxybenzoic and hydroxycinnamic acids. Solubility measurements were analyzed to determine the Setschenow coefficients at infinite and at zero ionic strength and the solubility of the neutral species in pure water. Knowledge of these data simplifies the calculation of the activity coefficients of

the charged and uncharged species. For instance, environmental partitioning of these acids in the aqueous phase is determined by their solubility in different conditions. Therefore, solubility studies of these compounds are of crucial interest for modeling the behavior of natural aquatic systems. The other aspect is of practical interest because the acids studied here are biologically active compounds that find applications in different industrial fields, such as pharmaceutical, cosmetic, food and biological wastewater treatment applications. In these cases, it is important to know the solubility in water and in other media in order to better design, for instance, processes aimed at their extraction from different matrices.

In this work, the solubility of hydroxybenzoic and hydroxycinnamic acids was studied in aqueous solutions of different ionic strengths at 37 °C. Here, we have verified that the higher polarity of the first class of phenolic acids reflects their higher solubility in aqueous solutions, independently of the ionic medium and the ionic strength. According to Kruyt and Robinson [24], this trend is due to the lower availability of the water molecules to the solvation of the phenolic acids because they are mainly involved in the ion's hydration. The solubility of hydroxybenzoic acids decreases linearly when the inert salt is NaCl, while in $NaClO_4$, the dependence on the ionic strength is smoothed. The behavior of hydroxycinnamic acids is different; in fact, the solubility of this class of acids decreases linearly with the ionic strength independently of the ionic medium.

Supplementary Materials: The following are available online, Figure S1. Dependence of the ionization constant on the ionic strength in the two salts media. Experimental values (symbols) and values modeled by the SIT theory (lines) with the equation 11. For all of the fitting, an adjusted $R^2 > 0.998$ and a reduced χ^2 as low as 10^{-5} were obtained. Table S1. Smoothed total solubility data as a function of the ionic strength in NaCl and $NaClO_4$. Table S2. Solubility of the neutral species at 37 °C of phenolic acids in water and in aqueous solutions of NaCl and $NaClO_4$ at different ionic strength. The uncertainties represent standard deviation. Table S3. Setschenow coefficients of hydroxybenzoic and hydroxycinnamic acids in NaCl and $NaClO_4$.

Author Contributions: Conceptualization, validation, writing—review and editing, supervision, A.B., E.F. and P.P.; Methodology, software, visualization, data curation, formal analysis, investigation, A.B., E.F., L.M. and C.L.T.; Writing—original draft preparation, A.B., E.F., A.F. and P.P. All authors have read and agreed to the published version of the manuscript.

Funding: This research received no external funding.

Institutional Review Board Statement: Not applicable.

Informed Consent Statement: Not applicable.

Data Availability Statement: Not applicable.

Acknowledgments: The authors thank the University of Calabria for financial support.

Conflicts of Interest: The authors declare no conflict of interest.

Sample Availability: Samples of the compounds are not available from the authors.

References

1. Malacaria, L.; Corrente, G.A.; Beneduci, A.; Furia, E.; Marino, T.; Mazzone, G. A review on coordination properties of Al(III) and Fe(III) towards natural antioxidant molecules: Experimental and theoretical insights. *Molecules* **2021**, *26*, 2603. [CrossRef]
2. Furia, E.; Beneduci, A.; Russo, N.; Marino, T. Structural characterization of aluminium (III) and iron (III) complexes of coumarinic acid in aqueous solution from combined experimental and theoretical investigations. *New J. Chem.* **2018**, *42*, 11006–11012. [CrossRef]
3. Beneduci, A.; Corrente, G.A.; Marino, T.; Aiello, D.; Bartella, L.; Di Donna, L.; Napoli, A.; Russo, N.; Romeo, I.; Furia, E. Insight on the chelation of aluminum(III) and iron(III) by curcumin in aqueous solution. *J. Mol. Liq.* **2019**, *296*, 111805–111814. [CrossRef]
4. Corrente, G.A.; Malacaria, L.; Beneduci, A.; Furia, E.; Marino, T.; Mazzone, G. Experimental and theoretical study on the coordination properties of quercetin towards aluminum(III), iron(III) and copper(II) in aqueous solution. *J. Mol. Liq.* **2021**, *325*, 115171–115182. [CrossRef]
5. Boskou, D. Sources of natural phenolic antioxidants. *Trends Food Sci. Technol.* **2006**, *17*, 505–512.
6. Queimada, A.J.; Mota, F.L.; Pinho, S.P.; Macedo, E.A. Solubilities of Biologically Active Phenolic Compounds: Measurements and Modeling. *J. Phys. Chem. B* **2009**, *113*, 3469–3476. [CrossRef]

7. Du, L.; Yu, P.; Rossnagel, B.G.; Christensen, D.A.; McKinnon, J.J. Physicochemical Characteristics, Hydroxycinnamic Acids (Ferulic Acid, *p*-Coumaric Acid) and Their Ratio, and *in Situ* Biodegradability: Comparison of Genotypic Differences among Six Barley Varieties. *J. Agric. Food Chem.* **2009**, *57*, 4777–4783. [CrossRef]
8. Robbins, R.J. Phenolic Acids in Foods: An Overview of Analytical Methodology. *J. Agric. Food Chem.* **2003**, *51*, 2866–2887. [CrossRef]
9. Cione, E.; La Torre, C.; Cannataro, R.; Caroleo, M.C.; Plastina, P.; Gallelli, L. Quercetin, epigallocatechin gallate, curcumin and resveratrol: From dietary sources to human microRNA modulation. *Molecules* **2020**, *25*, 63. [CrossRef] [PubMed]
10. Galanakis, C.M.; Goulas, V.; Tsakona, S.; Manganaris, G.A.; Gekas, V. A Knowledge Base for The Recovery of Natural Phenols with Different Solvents. *Int. J. Food Prop.* **2013**, *16*, 382–396. [CrossRef]
11. Petrucci, R.; Astolfi, P.; Greci, L.; Firuzi, O.; Saso, L.; Marrosu, G. A spectroelectrochemical and chemical study on oxidation of hydroxycinnamic acids in aprotic medium. *Electrochim. Acta* **2007**, *52*, 2461–2470. [CrossRef]
12. Fernandes, C.I.S.; Rebelo, M.J.F. Polyphenolic Biosensors. Application in Red Wines. *Port. Electrochim. Acta* **2009**, *27*, 457–462. [CrossRef]
13. Arribas, A.S.; Martìnez-Fernàndez, M.; Chicharro, M. The role of electroanalytical techniques in analysis of polyphenols in wine. *Trends Anal. Chem.* **2012**, *34*, 78–96. [CrossRef]
14. Clifford, M.N. Chlorogenic acids and other cinnamates–nature, occurrence and dietary burden. *J. Sci. Food Agric.* **1999**, *79*, 362–372. [CrossRef]
15. Singh, S.K.; Kundu, A.; Kishore, N. Interactions of some amino acids and glycine peptides with aqueous sodium dodecyl sulfate and cetyltrimethylammonium bromide at T = 298.15 K: A volumetric approach. *J. Chem. Thermodyn.* **2004**, *36*, 7–16. [CrossRef]
16. Soto, A.; Arce, A.; Khoshkbarchi, M.K. Thermodynamics of Diglycine and Triglycine in Aqueous NaCl Solutions: Apparent Molar Volume, Isentropic Compressibility, and Refractive Index. *J. Sol. Chem.* **2004**, *33*, 11–21. [CrossRef]
17. Poulson, S.R.; Harrington, R.R.; Drever, J.I. The solubility of toluene in aqueous salt solutions. *Talanta* **1999**, *48*, 633–641. [CrossRef]
18. Gorgényi, M.; Dewulf, J.; Van Langenhove, H.; Héberger, K. Aqueous salting-out effect of inorganic cations and anions on non-electrolytes. *Chemosphere* **2006**, *65*, 802–810. [CrossRef]
19. Bullister, J.L.; Wisegarver, D.P.; Menzia, F.A. The solubility of sulfur hexafluoride in water and seawater. *Deep Sea Res. Part I Oceanogr. Res. Pap.* **2002**, *49*, 175–187. [CrossRef]
20. Falcone, G.; Giuffrè, O.; Sammartano, S. Acid-base and UV properties of some aminophenol ligands and their complexing ability towards Zn^{2+} in aqueous solution. *J. Mol. Liquids* **2011**, *159*, 146–151. [CrossRef]
21. Bretti, C.; Giuffrè, O.; Lando, G.; Sammartano, S. Solubility, protonation and activity coefficients of some aminobenzoic acids in $NaCl_{aq}$ and $(CH_3)_4NCl_{aq}$, at different salt concentrations, at T = 298.15K. *J. Mol. Liq.* **2015**, *212*, 825–832. [CrossRef]
22. Long, F.A.; McDevit, W.F. Activity coefficients of nonelectrolyte solutes in aqueous salt solutions. *Chem. Rev.* **1952**, *50*, 119–169. [CrossRef]
23. Debye, P. Das elektrische Ionenfeld und das Aussalzen. *Z. Phys. Chem.* **1927**, *130*, 56–65. [CrossRef]
24. Kruyt, H.R.; Robinson, C. The Stability of Suspensoids under Influence of Electrolyte Mixture on Lyotropie. *Proc. Acad. Sci. Amst.* **1926**, *29*, 1244.
25. Porto, R.; Furia, E. On the complexation of copper (II) ion with 2-hydroxybenzamide. *Ann. Chim.* **2007**, *97*, 187–198. [CrossRef] [PubMed]
26. Furia, E.; Falvo, M.; Porto, R. Solubility and Acidic Constants of L-Cystine in $NaClO_4$ Aqueous Solutions at 25 °C. *J. Chem. Eng. Data* **2009**, *54*, 3037–3042. [CrossRef]
27. Furia, E.; Nardi, M.; Sindona, G. Standard Potential and Acidic Constants of Oleuropein. *J. Chem. Eng. Data* **2010**, *55*, 2824–2828. [CrossRef]
28. Furia, E.; Napoli, A.; Tagarelli, A.; Sindona, G. Speciation of 2-Hydroxybenzoic Acid with Calcium(II), Magnesium(II), and Nickel(II) Cations in Self-Medium. *J. Chem. Eng. Data* **2013**, *58*, 1349–1353. [CrossRef]
29. Furia, E.; Sindona, G.; Tagarelli, A. Solubility and acidic constants at 25 °C in $NaClO_4$ aqueous solutions of 1-(2-hydroxyphenyl)ethenone. *Monatsh. Chem.* **2016**, *147*, 1009–1014. [CrossRef]
30. Noubigh, A.; Cherif, M.; Provost, E.; Abderrabba, M. Solubility of Gallic Acid, Vanillin, Syringic Acid, and Protocatechuic Acid in Aqueous Sulfate Solutions from (293.15 to 318.15) K. *J. Chem. Eng. Data* **2008**, *53*, 1675–1678. [CrossRef]
31. Calado, M.S.; Branco, A.S.H.; Najdanovic-Visak, V.; Visak, Z.P. Solubility of high-value compounds in environmentally friendly solvents-liquid poly(ethylene glycol) and ionic liquids: Experimental study and thermodynamic analysis. *J. Chem. Thermodyn.* **2014**, *70*, 154–159. [CrossRef]
32. Mota, F.L.; Queimada, A.J.; Pinho, S.P.; Macedo, E.A. Aqueous Solubility of Some Natural Phenolic Compounds. *Ind. Eng. Chem. Res.* **2008**, *47*, 5182–5189. [CrossRef]
33. Alevizou, E.I.; Voutsas, E.C. Solubilities of *p*-coumaric and caffeic acid in ionic liquids and organic solvents. *J. Chem. Thermodyn.* **2013**, *62*, 69–78. [CrossRef]
34. Lu, L.-L.; Lu, X.-Y. Solubilities of Gallic Acid and Its Esters in Water. *J. Chem. Eng. Data* **2007**, *52*, 37–39. [CrossRef]
35. Murga, R.; Sanz, M.T.; Beltrán, S.; Cabezas, J.L. Solubility of three hydroxycinnamic acids in supercritical carbon dioxide. *J. Supercrit. Fluids* **2003**, *27*, 239–245. [CrossRef]
36. Murga, R.; Sanz, M.T.; Beltrán, S.; Cabezas, J.L. Solubility of Syringic and Vanillic Acids in Supercritical Carbon Dioxide. *J. Chem. Eng. Data* **2004**, *49*, 779–782. [CrossRef]

37. Manic, M.S.; Villanueva, D.; Fornari, T.; Queimada, A.J.; Macedo, E.A.; Najdanovic–Visak, V. Solubility of high-value compounds in ethyl lactate: Measurements and modelling. *J. Chem. Thermodyn.* **2012**, *48*, 93–100. [CrossRef]
38. Crea, F.; Crea, P.; De Stefano, C.; Giuffrè, O.; Pettignano, A.; Sammartano, S. Thermodynamic Parameters for the Protonation of Poly(allylamine) in Concentrated $LiCl_{(aq)}$ and $NaCl_{(aq)}$. *J. Chem. Eng. Data* **2004**, *49*, 658–663. [CrossRef]
39. Daneshfar, A.; Ghaziaskar, H.S.; Homayoun, N. Solubility of Gallic Acid in Methanol, Ethanol, Water, and Ethyl Acetate. *J. Chem. Eng. Data* **2008**, *53*, 776–778. [CrossRef]
40. Noubigh, A.; Jeribi, C.; Mgaidi, A.; Abderrabba, M. Solubility of gallic acid in liquid mixtures of (ethanol+water) from (293.15 to 318.15)K. *J. Chem. Thermodyn.* **2012**, *55*, 75–78. [CrossRef]
41. Noubigh, A.; Aydi, A.; Mgaidi, A.; Abderrabba, M. Measurement and correlation of the solubility of gallic acid in methanol plus water systems from (293.15 to 318.15) K. *J. Mol. Liquids* **2013**, *187*, 226–229. [CrossRef]
42. De Stefano, C.; Foti, C.; Giuffrè, O.; Sammartano, S. Acid–base and UV behavior of 3-(3,4-dihydroxyphenyl)-propenoic acid (caffeic acid) and complexing ability towards different divalent metal cations in aqueous solution. *J. Mol. Liquids* **2014**, *195*, 9–16. [CrossRef]
43. Noubigh, A.; Mgaidi, A.; Abderrabba, M.; Provost, E.; Fürst, W. Effect of salts on the solubility of phenolic compounds: Experimental measurements and modelling. *J. Sci. Food Agric.* **2007**, *87*, 783–788. [CrossRef]
44. Delmondes, P.H.; Stefani, R. Computational study of natural phenolic acid solubility and their interactions with chitosan. *MOL2NET* **2016**, *2*. [CrossRef]
45. Abraham, M.H. Scales of solute hydrogen-bonding: Their construction and application to physicochemical and biochemical processes. *Chem. Soc. Rev.* **1992**, *96*, 73–83. [CrossRef]
46. Vilas-Boas, S.M.; Vieira, V.; Brandão, P.; Alves, R.S.; Coutinho, J.A.P.; Pinho, S.P.; Ferreira, O. Solvent and temperature effects on the solubility of syringic, vanillic or veratric acids: Experimental, modeling and solid phase studies. *J. Mol. Liq.* **2019**, *289*, 111089–111098. [CrossRef]
47. Vilas-Boas, S.M.; Vieira, V.; Brandão, P.; Alves, R.S.; Coutinho, J.A.P.; Pinho, S.P.; Ferreira, O. Solid-liquid phase equilibrium of *trans*-cinnamic acid, *p*-coumaric acid and ferulic acid in water and organic solvents: Experimental and modelling studies. *Fluid Phase Equilibria* **2020**, *521*, 112747–112756. [CrossRef]
48. Bretti, C.; Cigala, R.M.; Crea, F.; Foti, C.; Sammartano, S. Solubility and activity coefficients of acidic and basic non-electrolytes in aqueous salt solutions: 3. Solubility and activity coefficients of adipic and pimelic acids in $NaCl_{(aq)}$, $(CH_3)_4NCl_{(aq)}$ and $(C_2H_5)_4NI_{(aq)}$ at different ionic strengths and at t = 25 °C. *Fluid Phase Equilibria* **2008**, *263*, 43–54.
49. Furia, E.; Sindona, G. Interaction of Iron(III) with 2-Hydroxybenzoic Acid in Aqueous Solutions. *J. Chem. Eng. Data* **2012**, *57*, 195–199. [CrossRef]
50. Beneduci, A.; Furia, E.; Russo, N.; Marino, T. Complexation behaviour of caffeic, ferulic and *p*-coumaric acids towards aluminium cations: A combined experimental and theoretical approach. *New J. Chem.* **2017**, *41*, 5182–5190. [CrossRef]
51. Porwal, S.K.; Furia, E.; Harris, M.E.; Viswanathan, R.; Devireddy, L. Synthetic, potentiometric and spectroscopic studies of chelation between Fe(III) and 2,5-DHBA supports salicylate-mode of siderophore binding interactions. *J. Inorg. Biochem.* **2015**, *145*, 1–10. [CrossRef]
52. Bitencourt, R.G.; Cabral, F.A.; Meirelles, A.J.A. Ferulic acid solubility in supercritical carbon dioxide, ethanol and water mixtures. *J. Chem. Thermodyn.* **2016**, *103*, 285–291. [CrossRef]
53. Shakeel, F.; Salem-Bekhit, M.M.; Haqa, N.; Siddiqui, N.A. Solubility and thermodynamics of ferulic acid in different neat solvents: Measurement, correlation and molecular interactions. *J. Mol. Liq.* **2017**, *236*, 144–150. [CrossRef]
54. Noubigh, A.; Cherif, M.; Provost, E.; Abderrabba, M. Solubility of some phenolic compounds in aqueous alkali metal nitrate solutions from (293.15 to 318.15) K. *J. Chem. Thermodyn.* **2008**, *40*, 1612–1616. [CrossRef]
55. Noubigh, A.; Abderrabba, M.; Provost, E. Temperature and salt addition effects on the solubility behaviour of some phenolic compounds in water. *J. Chem. Thermodyn.* **2007**, *39*, 297–303. [CrossRef]
56. Furia, E.; Porto, R. 2-Hydroxybenzamide as a Ligand. Complex Formation with Dioxouranium(VI), Aluminum(III), Neodymium(III), and Nickel(II) Ions. *J. Chem. Eng. Data* **2008**, *53*, 2739–2745. [CrossRef]
57. Cardiano, P.; Giuffrè, O.; Napoli, A.; Sammartano, S. Potentiometric, ^{1}H NMR and ESI-MS investigation on dimethyltin(IV) cation–mercaptocarboxylate interaction in aqueous solution. *New J. Chem.* **2009**, *33*, 2286–2295. [CrossRef]
58. Ciavatta, L. The specific interaction theory in evaluating ionic equilibria. *Ann. Chim.* **1980**, *70*, 551–567.
59. Ciavatta, L. The specific interaction theory in equilibrium analysis. Some empirical rules for estimating interaction coefficients of metal ion complexes. *Ann. Chim.* **1990**, *80*, 255–263.
60. Öhman, L.-O.; Sjöberg, S. Equilibrium and structural studies of silicon(IV) and aluminium(III) in aqueous solution. 1. The formation of ternary mononuclear and polynuclear complexes in the system Al^{3+}-gallic acid-OH^-. A potentiometric study in 0.6 M Na(Cl). *Acta Chem. Scand.* **1981**, *35*, 201–212. [CrossRef]
61. Sedeh, I.F.; Öhman, L.-O.; Sjöberg, S. Equilibrium and structural studies of silicon(IV) and aluminium(III) in aqueous solution. 30. Aqueous complexation between silicic acid and some *ortho*-Di- and triphenolic compounds. *Acta Chem. Scand.* **1992**, *46*, 933–940. [CrossRef]
62. Sandmann, B.J.; Chien, M.H.; Sandmann, R.A. Stability constants of calcium, magnesium and zinc gallate using a divalent ion-selective electrode. *Anal. Lett.* **1985**, *18*, 149–159. [CrossRef]

63. Kipton, H.; Powell, J.; Taylor, M.C. Interactions of Iron(II) and Iron(III) with Gallic Acid and its Homologues: A Potentiometric and Spectrophotometric Study. *Aust. J. Chem.* **1982**, *35*, 739–756.
64. Ambulkar, R.S.; Marathe, D.G.; Munshi, K.N. Complexes of gallium(III) with pyrocatechol, pyrogallol & protocatechuic, α-resorcylic, gallic & 2,3-dihydroxynaphthalene-6-sulphonic acids in aqueous medium. *Ind. J. Chem.* **1981**, *20*, 1044–1046.
65. Ozkorucuklu, S.P.; Beltrán, J.L.; Fonrodona, G.; Barrón, D.; Alsancak, G.; Barbosa, J. Determination of Dissociation Constants of Some Hydroxylated Benzoic and Cinnamic Acids in Water from Mobility and Spectroscopic Data Obtained by CE-DAD. *J. Chem. Eng. Data* **2009**, *54*, 807–811. [CrossRef]
66. Beltrán, J.L.; Sanli, N.; Fonrodona, G.; Barrón, D.; Özkan, G.; Barbosa, J. Spectrophotometric, potentiometric and chromatographic p*K*a values of polyphenolic acids in water and acetonitrile–water media. *Anal. Chim. Acta* **2003**, *484*, 253–264. [CrossRef]
67. Furia, E.; Porto, R. The effect of ionic strength on the complexation of copper (II) with salicylate ion. *Ann. Chim.* **2002**, *92*, 521–530. [PubMed]

Modelling the solubility of phenolic acids in aqueous media at 37 °C

Emilia Furia[1], Amerigo Beneduci[1,*], Luana Malacaria[1], Alessia Fazio[2], Chiara La Torre[2] and Pierluigi Plastina[2]

[1] Department of Chemistry and Chemical Technologies, University of Calabria, Arcavacata di Rende (CS), Italy; emilia.furia@unical.it (E.F.); luana.malacaria@unical.it (L.M.)
[2] Department of Pharmacy, Health and Nutritional Sciences, University of Calabria, Arcavacata di Rende (CS), Italy; alessia.fazio@unical.it (A.F.); chiara.latorre@unical.it (C.L.T.); pierluigi.plastina@unical.it (P.P.)
* Correspondence: amerigo.beneduci@unical.it (A.B.)

Table S1. Smoothed total solubility data as a function of the ionic strength in NaCl and $NaClO_4$[a].

	$\log(S_T^0)$	a_0	a_∞ a (for linear fit)	Reduced $\chi^2 \times 10^4$	Adj. R^2
NaCl					
VA	-1.89 (0.02)	-0.43 (0.062)	0.03 (0.02)	4	0.96135
SA	-2.054 (0.004)	-0.078 (0.01)	-0.009 (0.004)	0.18	0.98234
GA	-0.95 (0.01)	-0.09 (0.04)	-0.002 (0.001)	3	0.97818
CafA	-2.18 (0.01)		-0.145 (0.008)	0.1	0.9903
FA	-2.315 (0.009)		-0.050 (0.005)	5	0.98635
p-CA	-2.19 (0.01)		-0.172 (0.008)	4	0.99048
	$\log(S_T^0)$	a_0	a_∞ a (for linear fit)	Reduced $\chi^2 \times 10^4$	Adj. R^2
$NaClO_4$					
VA	-1.911 (0.006)	-0.04 (0.02)	-0.041 (0.006)	0.4	0.98455
SA	-2.054 (0.004)	-0.078 (0.01)	-0.009 (0.004)	0.18	0.98234
GA	-0.946 (0.004)	-0.096 (0.008)	0[b]	0.3	0.9598
CafA	-2.21 (0.01)	-0.13 (0.04)	-0.03 (0.01)	0.2	0.96067
FA	-2.267 (0.004)	-0.53 (0.03)	-0.071 (0.008)	1	0.98718
p-CA	-2.187 (0.005)		-0.067 (0.003)	0.9	0.98977

[a]Values in parentheses are the standard deviations of the data as determined by the fit; [b]The parameter a_∞ has been kept fixed to zero during the iteration because it is more than one order of magnitude smaller than a_0.

Table S2. Solubility of the neutral species at 37°C of phenolic acids in water and in aqueous solutions of NaCl and $NaClO_4$ at different ionic strength. The uncertainties represent standard deviation.

	S^0 10^3. mol kg^{-1}					
	VA	**SA**	**GA**	**CafA**	**FA**	***p*-CA**
I **mol kg^{-1} NaCl**						
0	12±3	8±2	113±15	6.1±0.9	5±1	6.2±0.9
0.16	11±2	8±2	102±13	5.8±0.8	5±1	5.8±0.8
0.51	9±1	8±2	102±13	5.3±0.7	4±1	4.8±0.6
1.02	7±1	7±2	98±12	4.4±0.6	3±1	3.7±0.5
2.09	7±1	7±2	96±12	3.2±0.4	3±1	2.2±0.3
3.20	7±1	7±2	92±12	1.9±0.3	3±1	1.5±0.2
I **mol kg^{-1} $NaClO_4$**						
0	12±3	8±2	113±16	6.1±0.9	5±1	6.2±0.9
0.16	11±2	8±1	106±15	5.4±0.8	5.0±0.7	5.6±0.8
0.51	11±2	8±1	101±14	5.0±0.7	4.9±0.7	5.6±0.8
1.05	11±2	8±1	100±14	4.8±0.7	4.8±0.7	5.1±0.7
2.21	10±1	7±1	95±13	4.3±0.6	4.2±0.6	4.2±0.6
3.50	9±1	6±1	93±13	3.7±0.6	3.6±0.5	3.4±0.5

Table S3. Setschenow coefficients of hydroxybenzoic and hydroxycinnamic acids in NaCl and $NaClO_4$[a].

	k_0 k (for linear fit)	k_∞	Reduced $\chi^2 \times 10^4$	Adj. R^2
NaCl				
VA	0.57 (0.01)	-0.05 (0.06)	82	0.97706
SA	0.106 (0.003)	0[b]	0.11	0.98948
GA	0.11 (0.01)	0[b]	2	0.92014
CafA	0.151 (0.005)		5	0.99278
FA	0.35 (0.02)	0[b]	4	0.97025
p-CA	0.199 (0.006)		4	0.99486
	k_0 k (for linear fit)	k_∞	Reduced $\chi^2 \times 10^4$	Adj. R^2
$NaClO_4$				
VA	0.044 (0.002)		1	0.96640
SA	0.044 (0.002)		5	0.98505
GA	0.108 (0.005)	0[b]	0.4	0.95551
CafA	0.17 (0.05)	0.02 (0.01)	3	0.95770
FA	0.044 (0.002)		0.82	0.97809
p-CA	0.076 (0.004)		2	0.97401

[a]Values in parentheses are the standard deviations of the data as determined by the fit; [b]The parameter k_∞ has been kept fixed to zero during the iteration because it is more than one order of magnitude smaller than k_0.

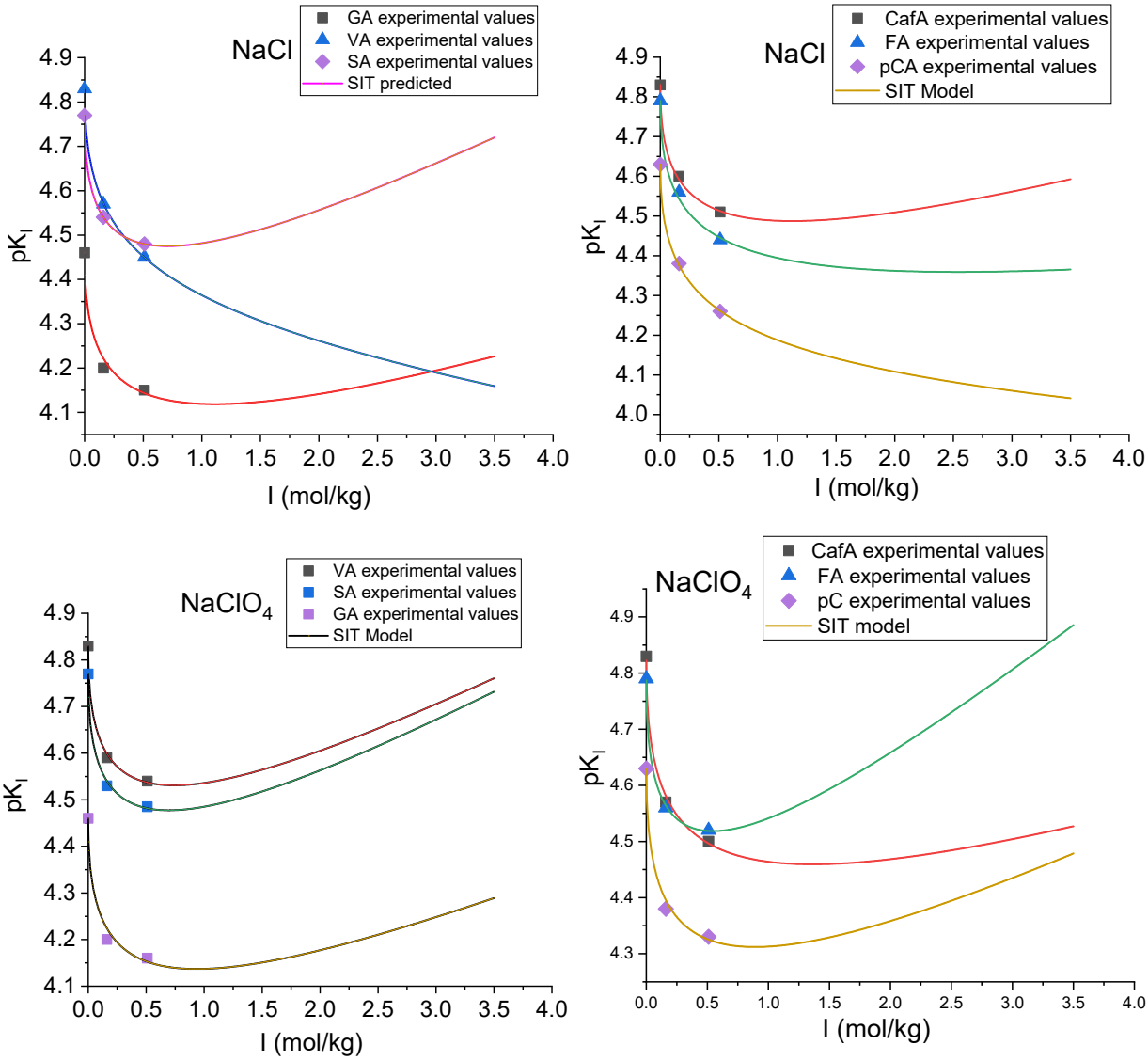

Figure S1. Dependence of the ionization constant on the ionic strength in the two salts media. Experimental values (symbols) and values modeled by the SIT theory (lines) with the equation 11. For all of the fitting, an adjusted $R^2 > 0.998$ and a reduced χ^2 as low as 10^{-5} were obtained.

Journal of Molecular Liquids 345 (2022) 117895

Contents lists available at ScienceDirect

Journal of Molecular Liquids

journal homepage: www.elsevier.com/locate/molliq

Aluminum(III), iron(III) and copper(II) complexes of luteolin: Stability, antioxidant, and anti-inflammatory properties

Luana Malacaria [a], Chiara La Torre [b,1], Emilia Furia [a,*], Alessia Fazio [b,1], Maria Cristina Caroleo [b,1], Erika Cione [b,1], Luca Gallelli [c], Tiziana Marino [a], Pierluigi Plastina [b,1]

[a] Dipartimento di Chimica e Tecnologie Chimiche, Università della Calabria, Via P. Bucci, Cubo 12/D, 87036 Arcavacata di Rende, Cosenza, Italy
[b] Dipartimento di Farmacia e Scienze della Salute e della Nutrizione, Università della Calabria, Via P. Bucci, Edificio Polifunzionale, 87036 Arcavacata di Rende, Cosenza, Italy
[c] Dipartimento di Scienze della Salute, Scuola di Medicina, Università della Magna Graecia, Unità di Farmacologia Clinica, Ospedale Mater Domini, 88100 Catanzaro, Italy

ARTICLE INFO

Article history:
Received 22 August 2021
Revised 15 October 2021
Accepted 18 October 2021
Available online 21 October 2021

Keywords:
Aluminum luteolin complexes
Iron luteolin complexes
Copper luteolin complexes
Stability constants
Antioxidant
Anti-inflammatory

ABSTRACT

In this work complexation of luteolin (H_4Lu) with Al(III), Fe(III) and Cu(II) at 37 °C and in 0.16 M NaCl is discussed. To evaluate the competition of the ligand for the metal cations and H^+, the protonation constant of luteolin was also determined under the same experimental conditions. Speciation profiles obtained by potentiometric titrations show that in aqueous solution a complexation occurs at 1:1 ligand-to-Al(III) ratio, and at 1:1 and 2:1 ligand-to-cation ratios for Fe(III) and Cu(II). The coordination sites of luteolin to the different metal ions were determined by a computational approach, displaying that copper ion shows no selective preference towards any of the complexation sites of luteolin, while the six-membered chelate ring of the 4–5 site (*i.e.*, the 4-carbonyl-5-hydroxyl site of the A and C rings of the ligand) is the preferred one for aluminum and iron ions. Additionally, we have evaluated the antioxidant and anti-inflammatory properties of free luteolin and of the luteolin-metal ion complexes. The complex with iron was found to have a higher activity than the other complexes (*i.e.*, Fe(III)-Lu > Cu(II)-Lu > Al(III)-Lu), and its DPPH radical scavenging ability was even higher than that of free luteolin. Finally, all luteolin metal complexes were found to significantly reduce lipopolysaccharide (LPS)-induced interleukin (IL)-6 levels in monocyte-derived macrophages with the following order: Fe(III)-Lu > Al(III)-Lu > Cu(II)-Lu > free Lu.

1. Introduction

Over the last decades, an increasing interest has been shown towards flavonoids, the largest class of phenolic compounds. More than 8000 flavonoids have been characterized so far, and this number is continuously growing [1–2]. The basic structure of flavonoids contains two aromatic rings (labeled as ring A and ring B) linked by a C3 spacer, which is usually part of another ring (labeled as ring C). Flavonoids are sub-divided into six main subgroups: flavones, isoflavones, flavonols, flavanones, anthocyanins, and flavan-3-ols, depending on the oxidation state of ring C (Fig. 1). The substitution patterns of hydroxy and methoxy groups on rings A and B determine the specific flavonoid. Moreover, these compounds may exist in the free form as well as in the esterified, prenylated, and glycosylated forms [1]. Interest on flavonoids is mainly due to their potent antioxidant activity [2–8], which is essential in preventing and treating oxidation damage [9–10]. Besides being able to act as primary antioxidants, donating an H atom to stabilize a radical species, flavonoids can act as secondary antioxidants due to their ability to chelate pro-oxidant metal ions. This second antioxidant mechanism may result from the interactions between metal ions and flavonoids to produce complexes. The pro-oxidant ion is sequestered, thus preventing its participation in free radical generating reactions [11–13]. Moreover, flavonoids have been reported to possess many beneficial pharmacological properties, such as antibacterial, antitumor, antimutagenic activity and cardiovascular protection [14–15].

Among the various classes of flavonoids, flavones, widely present in herbaceous plants, are characterized by a 2-phenyl-1,4-benzopyrone skeleton and are usually classified by the number and position of their hydroxy and methoxy substituents. Luteolin (3 ▫ ,4 ▫ ,5,7-tetrahydroxyflavone, H_4Lu, Fig. 2) occurs in the leaves, blossoms, and stems of various plants [16–17] and has been recently used in many areas of medicine [18–19], food chemistry [20] and biochemistry [15,21].

Luteolin-rich extract is utilized as a natural yellow dye, which is stable and resistant to fading [22]. Moreover, experimental data indicate that luteolin may prevent diabetes, cardiovascular and

* Corresponding author.
E-mail address: emilia.furia@unical.it (E. Furia).
[1] Dipartimento di Eccellenza 2018-2022.

https://doi.org/10.1016/j.molliq.2021.117895
0167-7322/

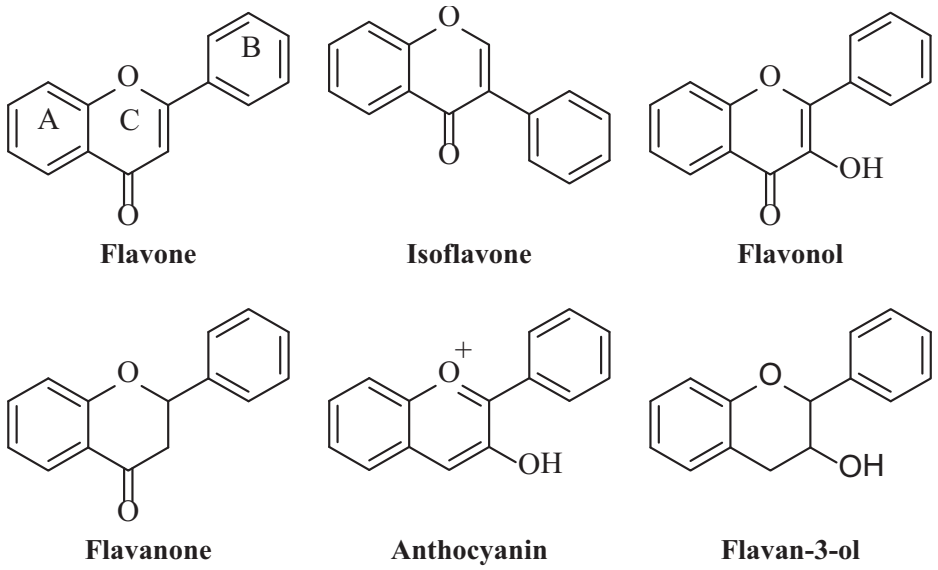

Fig. 1. Structure of the six main subgroups of flavonoids.

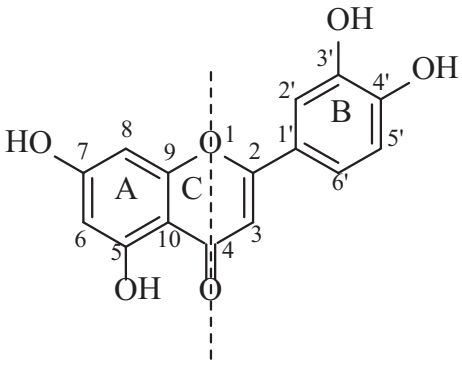

Fig. 2. Chemical structure of luteolin, H_4Lu.

neurodegenerative diseases and shows anti-allergic activity *in vitro* and *in vivo* [23].

Luteolin possesses two possible chelating sites: the 5-hydroxy-4-oxo and 3 ▫ ,4 ▫ -dihydroxyl (catechol) groups (Fig. 2); the 5-hydroxy-4-oxo group is superior to 3 ▫ ,4 ▫ -dihydroxyl group in the complexation process [24]. The chelation of metal ions can be crucial in preventing radical generation, which can cause damage to biomolecules. Moreover, natural metal chelators, such as flavonoids, should be preferred to other synthetic sequestering agents that present associated toxicity problems [25–26]. Due to the importance of metal chelation for the characterization of antioxidant behavior of compounds, we aimed to study luteolin's ability to chelate iron, aluminum, and copper ions.

Following our previous studies on the sequestering ability of quercetin towards the same metal cations [27–29], herein we present an experimental investigation (potentiometric and UV–Vis spectrophotometric measurements) on the complexation ability of luteolin towards aluminum(III), iron(III) and copper(II) at 37 °C and in 0.16 M NaCl, evaluating the stability constants of the complexes and the corresponding structures. Metal-flavonoid complexes display free radical scavenging activity [9–12,30]. Moreover, anti-inflammatory effects of flavonoids are well known [31] and there is the evidence that luteolin *per se* has the capability to reduce interleukin (IL)-6 levels in both peripheral blood and discrete brain areas after peripheral injection of LPS [32]. In this frame, here we have also evaluated the antioxidant and anti-inflammatory effects of luteolin-metal ion complexes on IL-6 levels.

2. Experimental section

2.1. Materials

Sodium chloride, hydrochloric acid and sodium hydroxide titrant solutions were prepared and standardized as previously described [33]. Aluminum(III), iron(III) and copper(II) chloride stock solutions were prepared and standardized as reported previously [28]. Luteolin (Sigma, ≥98%) was kept at 4 °C and used without further purification. All solutions were freshly prepared with bidistilled water. Dimethylsulphoxide (DMSO), absolute ethanol and methanol were purchased from Carlo Erba (Milan, Italy). 2,2-Azinobis(3-ethylbenzothiazoline-6-sulfonic) acid (ABTS), 2,2-diphenyl-1-picrylhydrazyl (DPPH), potassium persulfate ($K_2S_2O_8$), $FeCl_3$, sodium acetate and 2,4,6-tris-pyridyl-*S*-triazine (TPTZ) were purchased from Sigma Aldrich (Milan, Italy).

2.2. Potentiometric and spectrophotometric measurements

The potentiometric apparatus and the set-up of the titrations were described in a previous work [28]. To avoid carbonate interference, a slow stream of nitrogen gas was passed through the gas inlet tube into the test solutions, kept under continuous stirring during titrations. During the EMF measurements, the cell assembly was placed in a thermostatic water bath kept at 37.0 ± 0.1 °C. Spectrophotometric measurements were carried out with a Varian Cary 50 Scan UV Visible Spectrophotometer by measuring the absorbance values, A_λ, (to 0.001 units) between 200 and 500 nm each 1 nm. Matched quartz cells of thickness 1 cm were employed. The temperature of the cell holder was maintained at 37.0 ± 0.3 ° C by a Grant circulating water bath. The acquisition of data and the formulations of the parameters were managed with the aid of a computer connected to the instrument.

2.3. Antioxidant and anti-inflammatory measurements

2.3.1. DPPH assay

The DPPH assay was performed according to a previously reported protocol [34]. An aliquot (0.1 mL) of each sample (from

1 to 0.01 mg mL^{-1} DMSO) was added with 0.1 mL of DPPH (1 mM) solution and MeOH to obtain a total volume of 3 mL. The final concentrations of the different solutions were 33.33, 16.67, 3.3 and 0.33 μg mL^{-1}. The mixtures were let to stir vigorously and allowed to incubate at room temperature (25 ± 3 °C) for 30 min and in the absence of light. The experiments were conducted against a blank (3 mL of MeOH) and a control (3 mL solution obtained by diluting 0.1 mL of DPPH with MeOH), and the scavenging activity of each solution was quantified spectrophotometrically using an UV–Vis spectrophotometer (model V-550, Jasco Europe) at 517 nm. The antioxidant activity is expressed as % of DPPH inhibition and was calculated using the following equation:

$$\%I_{DPPH} = [(A_{control} - A_{sample})/A_{control}]\hat{A} \cdot 100 \quad (1)$$

Trolox (6-hydroxy-2,5,7,8-tetramethylchroman-2-carboxylic acid) was used as a positive control and the results were also expressed as μg of Trolox equivalent (TEAC). All analyses were conducted in triplicate. The percentages obtained were used to calculate EC_{50} values for each sample using GraphPad Prism 8 software (GraphPad Inc., San Diego, CA).

2.3.2. ABTS assay

The radical scavenging effects of samples on $ABTS^{\bullet+}$ radical cation were estimated according to a known protocol [35]. An aliquot (50 mL) of 2 mM ABTS and 0.5 mL of 70 mM $K_2S_2O_8$ were mixed, followed by incubation in the dark for 16 h at room temperature to prepare $ABTS^{\bullet+}$ radical solution. An aliquot (0.030 mL) of each sample (from 1 to 0.01 mg mL^{-1} DMSO) was mixed with 3 mL of the $ABTS^{\bullet+}$ solution and then stirred vigorously at room temperature (25 ± 3 °C) for 5 min, in the dark. The control was prepared by diluting 3 mL of the $ABTS^{\bullet+}$ solution with 0.030 mL of DMSO. The ABTS scavenging activity of each solution was quantified spectrophotometrically at 734 nm using a UV–Vis spectrophotometer (model V-550, Jasco Europe). The ABTS radical scavenging was expressed as % of ABTS inhibition of each compound compared to the initial concentration of ABTS (control) according to the formula:

$$\%I_{ABTS} = \left[(A_{control} - A_{sample})/A_{control}\right] \cdot 100 \quad (2)$$

The percentages obtained were used to calculate EC_{50} values for each sample using GraphPad Prism 8 software (GraphPad Inc., San Diego, CA). The results were also expressed as μg of Trolox equivalent (TAEC), used as positive control.

2.3.3. FRAP assay

The ferric reducing antioxidant power (FRAP) method measures the change in absorbance that occurs when the TPTZ (2,4,6-tripyridyl-*S*-triazine)–Fe(III) complex is reduced to the TPTZ-Fe^{2+} form in the presence of antioxidant compounds [36]. Briefly, the FRAP reagent contained 10 mM tripyridyl-triazine (TPTZ) solution in 40 mM HCl plus 20 mM $FeCl_3$ and 0.25 M sodium acetate buffer (pH 3.6) in a ratio 1:1:10. Extracts were dissolved in DMSO at a concentration of 0.1 mg mL^{-1}. An aliquot (0.1 mL) of solution was mixed with 2 mL of FRAP reagent and 0.9 mL of H_2O and the absorption of the reaction mixture was measured at λ = 593 nm. A solution of $FeSO_4$ (1 mM) were used to obtain the calibration curve.

2.3.4. Monocyte-Derived Macrophages (MDMs) isolation

Peripheral blood mononuclear cells (PBMCs) were obtained from healthy donors. Buffy coat preparations were diluted 1:1 with phosphate-buffered saline (PBS) solution and centrifuged over Ficoll–Hypaque mixture (Pharmacia LKB Biotechnology Inc., Uppsala, Sweden). Monocytes were separated from lymphocytes by adherence, as described in literature [37]. Monocyte isolation techniques significantly impact the phenotype of both isolated monocytes and derived macrophages *in vitro*. Mononuclear cells were counted and plated at a concentration of $2{\cdot}10^6$ /well in 24-well plates (Falcon, MA, USA). PBMCs were cultured at 37 °C under humidified atmosphere enriched with 5% CO_2 in Roswell Park Memorial Institute (RPMI) medium with 10% of fetal calf serum (FCS) heat-inactivated and endotoxin-free (Thermo Fisher Scientific, USA), 50 Units/mL penicillin, 50 μg mL^{-1} streptomycin, 2 mM glutamine (complete medium). Non-adherent cells were then removed by repeated gentle washing with warm medium after 5 days of culture. More than 90% of the adherent cells were monocyte-derived macrophages (MDMs) as revealed through morphology by esterase non-specific technique. Adherent MDMs were then cultured for an additional day in RPMI complete medium supplemented with 5% endotoxin- and mycoplasma-free FCS. Each experiment was run with primary MDMs from a single blood donor.

2.3.5. Cell viability assay

Cell viability was estimated by evaluating the reduction of 3-(4,5-dimethylthiasol-2-yl)-2,4-diphenyltetrazolium bromide (MTT) by mitochondrial succinate dehydrogenase [38]. The absorbance, *A*, was measured with a microtiter plate reader (Synergy H1 by BioTeck, Winooski, VT, USA) at the test wavelength (*tw*, 570 nm) and at the reference wavelength (*rw*, 690 nm). The optical density (*OD*) was calculated as $A_{rw} - A_{tw}$.

2.3.6. IL-6 determination

Cells were pre-treated with luteolin or luteolin-metal complexes for an incubation period of 20 h and stimulated with LPS for further 4 h. IL-6 secretion was measured by enzyme-linked immunosorbent assay (ELISA). The concentration of IL-6 in supernatants from primary M/M cells stimulated with LPS was 40 ± 5 pg mL^{-1}. After twenty-four hours of incubation conditioned media were collected and IL-6 production was analyzed using ELISA Kit (Thermo Fisher Scientific, USA) following the manufacturer's instructions. Briefly, the medium was spun 5 min at 2500 rpm, 4 °C, to pellet down cellular debris and either immediately assayed or frozen in liquid N_2 first and −80 °C successively, for no longer than one week. The sensitivity of the assay was 5 pg mL^{-1}. Results were read with a microtiter plate reader (Synergy H1 by BioTeck, Winooski, VT, USA).

2.3.7. Statistical analysis

Prism GraphPad Prism version 5.0 for Windows (GraphPad Software, San Diego, CA, USA) was used to build graphs. Differences were evaluated by one-way ANOVA, followed by multi-comparison Dunnett's test ($^*p < 0.05$, $^{**}p < 0.02$, $^{***}p < 0.01$, with respect to controls).

2.4. Computational details

All the electronic calculations were performed using the Gaussian 16 computational package [39]. The geometries of all the investigated compounds, including radicals, radical cations and anions, were fully optimized employing the hybrid functional M05-2X [40] combined with the standard 6–31 + G(d) basis set for C, H, O and Al except for Cu and Fe atoms, for which the relativistic compact Stuttgart/Dresden effective core potential with its related split valence basis set was used. All the optimizations were performed in solvent applying the Solvent Model based on Density (SMD) to mimic the environment of the experimental measurements (dielectric constant of 78.0) [41]. The hybrid meta-GGA functional M05-2X proved to better describe short- and medium-range interatomic interactions than traditional DFT methods [42].

Such a functional was also suggested, together with other hybrid functionals, for kinetic data calculations in radical-molecule reactions, including scavenging ones [43].

All the optimized structures in solvent were confirmed to be real minima by harmonic vibrational frequencies calculation. Thermodynamic corrections at 25 °C were included in the calculations of relative energies. The unrestricted open-shell approach was used for radical species. In these cases, no spin contamination was found. The energies were refined by single point calculations on the optimized geometries at the same level of theory employing a larger standard basis set, 6–311++G(d,p), for all atoms unless Fe and Cu described as above reported.

In order to compare the ability of the luteolin to bind Al(III), Fe(III) and Cu(II), metal binding affinity has been also considered by calculating the reaction free energies of the complexation reaction for the substitution of water molecules in the hexaaquo complex and considering the overall process in solution, as already applied for other systems.

There are three major antioxidant mechanisms for exercising the free radical scavenging activity as outlined in the Scheme 1: hydrogen atom transfer (HAT), single electron transfer (SET) and sequential proton loss electron transfer (SPLET). The theoretical evaluation of some key thermochemical parameters can be helpful to gain more insight on their preferred action mechanism, therefore BDE, IP, PDE, PA and ETE were calculated in water at 25 °C by the same procedure already applied on similar systems [44–47], according to the following expressions:

BDE: $H(ArO^{\cdot}) + H(H^{\cdot}) - H(ArOH)$

IP: $H(ArOH^{+\cdot}) + H(e^{-}) - H(ArOH)$

PDE: $H(ArO^{\cdot}) + H(H^{-}) - H(ArOH^{+\cdot})$

PA: $H(ArO^{-}) + H(H^{+}) - H(ArOH)$

ETE: $H(ArO^{\cdot}) + H(e^{-}) - H(ArO^{-})$

The calculated $H(H^{+})$ and $H(e^{-})$ enthalpy values are 1.48 and 0.75 kcal/mol, respectively [42].

The above-mentioned protocol was used to the most stable open shell species for computations of single-point spin densities. This computational procedure was already successfully applied to investigate the antioxidant properties of a large series of polyphenols.

3. Results and discussion

In this study, we evaluated the stability constants of the complexes between luteolin and Al(III), Cu(II) and Fe(III) cations, and the antioxidant and anti-inflammatory behavior of these species.

3.1. Chelating properties of luteolin and stability of formed complexes

The complex formation equilibria between H_4Lu and Al(III), Cu(II) and Fe(III) cations were studied at 37 °C and in 0.16 M NaCl. Luteolin is essentially insoluble in water, for this reason, all the experiments were carried out by adding an accurately weighed quantity of solid luteolin in the titration apparatus. After the addition of the other reagents, the pH of test solutions was stepwise increased from 2 to 7.5 by adding NaOH standard solutions. When the general equilibrium reported in Eq. (3) takes place, luteolin dissolves into the aqueous medium to form complexes.

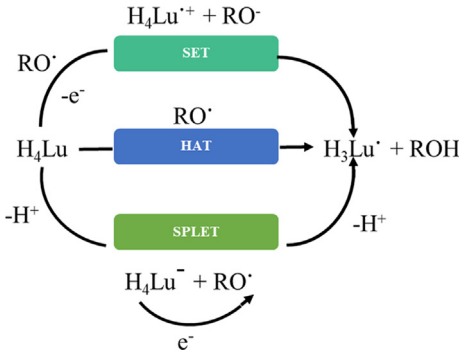

Scheme 1. Major antioxidant mechanisms of the free radical scavenging activity.

$$pM^{n+} + rH_4Lu \rightleftarrows M_p(H)_{-q}(H_4Lu)_r^{(np-q)} + qH^{+} \quad \log \beta_{p,q,r} \tag{3}$$

This equilibrium considers all the possible complexes formed in solution. The most probable p, q, and r values and the corresponding constants $\log \beta_{p,q,r}$ were obtained by a numerical procedure [48], and results obtained are reported in the Table 1. To evaluate complex stability, which is also affected by the acid-base properties of the ligand, preliminarily it was necessary to determine the first acidic constant of luteolin (Eq. (4)) under the same experimental conditions. According to literature this could be related to the deprotonation of the 7-OH group [49].

$$H_4Lu \rightleftarrows H_3Lu^{-} + H^{+} \quad pK_{a1} = 8.93 \pm 0.09 \tag{4}$$

The uncertainty represents 3σ. No additional attempts were made to determine the acidity of the other hydroxy groups as we have experienced that luteolin undergoes degradation in aqueous alkaline medium, which occurs more rapidly than potentiometric measurement time. The constants of main cationic hydrolysis products [28] (*i.e.*, $Al(OH)^{2+}$ and $Al(OH)_2^{+}$, $Cu(OH)^{+}$ and $Cu_2(OH)_2^{2+}$, $Fe(OH)^{2+}$ and $Fe(OH)_2^{+}$) and the acidic constant of the ligand were kept invariant in the numerical treatment to determine stability constants $\beta_{p,q,r}$ [49].

The measurements were performed as potentiometric titrations with cell (G):

Reference Electrode/Test Solution/Glass Electrode (G)

The general composition of Test Solution was C_M M MCl_n, C_L M H_4Lu, C_A M HCl, C_B M NaOH, and $(0.16\text{-}nC_M\text{-}C_A\text{-}C_B)$ M NaCl. Metal and ligand concentrations were ranged from $(0.1\cdot10^{-3})$ to $(1.0\cdot10^{-3})$ M and the ligand to metal ratio was varied between 1 and 5. The pH was ranged from 2 for Fe(III), from 2.5 for Al(III) and from 3 for Cu(II), to the precipitation of a neutral species, which takes place at different pH depending not only on the nature of metal but also on the specific ligand to metal ratio investigated.

Speciation profiles show that in aqueous solution a complexation occurs at 1:1 Al(III) to ligand ratio, and at 1:1 and 1:2 Fe(III)- and Cu(II)- to ligand ratios. It was not possible to make any comparison with previous literature data as this study is the first one entirely carried out in aqueous medium. The distribution diagrams in Fig. 3 a-c show the percentage of metal cations into the luteolin complexes with respect to pH. As can be seen in Fig. 3a, the complexation between luteolin and Al(III) starts at pH higher than 3.5 and the complex $Al(H)_{-3}(H_4Lu)$ reaches a percentage not more than 50%, confirming that the sequestering ability of luteolin towards Al(III) is not so efficient. The speciation diagram of the system Cu(II)-Lu (Fig. 3b) shows that the neutral complex $Cu(H)_{-2}(H_4Lu)_2$ starts to form at pH 4 and reaches a maximum at pH 5, while the other species, $Cu(H)_{-3}(H_4Lu)^{-}$, starts to form at pH 4.5 and is the predominant one at pH 5.5, with percentage higher than 75%. Finally, regarding the system Fe(III)-Lu (Fig. 3c) the complexes $Fe(H)_{-2}(H_4Lu)^{+}$ and $Fe(H)_{-3}(H_4Lu)$ reach significant percentages. The complexation starts from acidic pH for the species $Fe(H)_{-2}(H_4Lu)^{+}$ which is the predominant in the whole investigated pH range. As can be seen, the complex $Fe(H)_{-4}(H_4Lu)_2^{-}$ is a minor species, but its existence is confirmed by a significant decrease of the statistical parameters of the numerical evaluation. Interestingly, the distribution of the hydrolysis complexes, of all the investigated metal cations, shows that their percentages decrease or disappear drastically in the presence of luteolin. This led us to

Table 1
Formation of complexes of luteolin with Al(III), Cu(II), and Fe(III) according to general Eq. (3). Values of log $\beta_{p,q,r}$ in NaCl 0.16 M at 37 °C were obtained by numerical procedure (standard deviations are reported as 3 σ).

	Species	log $\beta_{p,q,r}$ ± 3 σ
Al(III)	$Al(H)_{-3}(H_4Lu)$	−9.5 ± 0.1
Cu(II)	$Cu(H)_{-3}(H_4Lu)^-$	−11.88 ± 0.09
	$Cu(H)_{-2}(H_4Lu)_2$	−3.3 ± 0.2
Fe(III)	$Fe(H)_{-2}(H_4Lu)^+$	−0.42 ± 0.09
	$Fe(H)_{-3}(H_4Lu)$	−6.1 ± 0.2
	$Fe(H)_{-4}(H_4Lu)_2^-$	−6.1 ± 0.1

hypothesize that the complexes between metal ions and ligand could be mixed species also involving hydroxyl ion.

A comparison of the UV–Vis spectra of free ligand (H_4Lu) and the coordinated species (Fig. 4) supports the effective formation of the complexes. The UV–Vis spectrum of free luteolin shows two characteristic absorption bands of flavonoid compounds [50]: the band at 355 nm is due to the conjugation between B and C ring (cinnamoyl system), and the band at 250 nm deriving from the A-C ring (benzoyl system). Moreover, there are two other less intense absorption bands at 295 and at 267 nm. The UV–Vis spectra recorded on the solutions containing metal cations show a significant shift of luteolin's characteristic bands, confirming the occurred complexation. Regarding the Cu(II)- and Fe(III)-luteolin systems the band related to the benzoyl portion (*i.e.*, at 250 nm) undergoes an hypsochromic shift (Δ ∼ 15 nm). On the contrary, the Al(III)-luteolin spectrum shows an evident bathochromic shift (Δ ∼ 60 nm) of the cinnamoyl band (*i.e.*, 355 nm), suggesting that the coordination sites depend on the specific metal cation. All the solids gained at the end of each titration were also analyzed after their solubilization in EtOH. As can be seen in Fig. 4, the difference between these spectra and that of free ligand is not so pronounced, suggesting that the majority of the solid may be unreacted luteolin.

Following the indications arising from the speciation profiles and those acquired under the same conditions for similar systems [27–29,33], we attributed the loss protons to both ligand and water and considered metal coordination to the luteolin occurring mainly *via* the 4-carbonyl-5-hydroxyl site of the A and C rings (4–5 site) or *via* the catechol moiety of the B ring (3′-4′ site) (see Fig. 5). It is well known that the binding site is strictly related to the nature of both ligand and metal ion and to the pH value. In fact, despite the huge number of experimental and theoretical studies on the coordination properties of flavonoids, no confluence on same outcomes is observed regarding the binding site and metal/ligand stoichiometry owing dependent on the variation in experimental conditions in the different studies [50].

In the present work, two complexes (Fig. 5) were obtained for the Al(III)-Lu system considering the loss of protons from both ligand and water molecules coordinated to the metal, as suggested by potentiometric analysis of Table 1. They were enclosed in about 5 kcal/mol (see Table 2) indicating the complex with Al coordinating to the 4–5 site to be the most stable one for the $Al(OH)_2(H_3Lu)$. Similar findings occurred considering the quercetin as ligand [28], evidencing that, also for the luteolin, the six-membered chelate ring of the 4–5 site is preferred to the five-membered chelate ring of the catechol moiety (B ring).

Regarding the Fe(III)-Lu system, since the $Fe(OH)(H_3Lu)^+$ and $Fe(OH)_2(H_3Lu)$ showed significant percentages in the monitored acidic pH range (Fig. 3c), four complexes (Fig. 5) were analyzed considering the catechol moiety and the 4–5 site for both considered species. Irrespective of the species, the complex having the 4–5 site implicated in the coordination of metal ion results to be

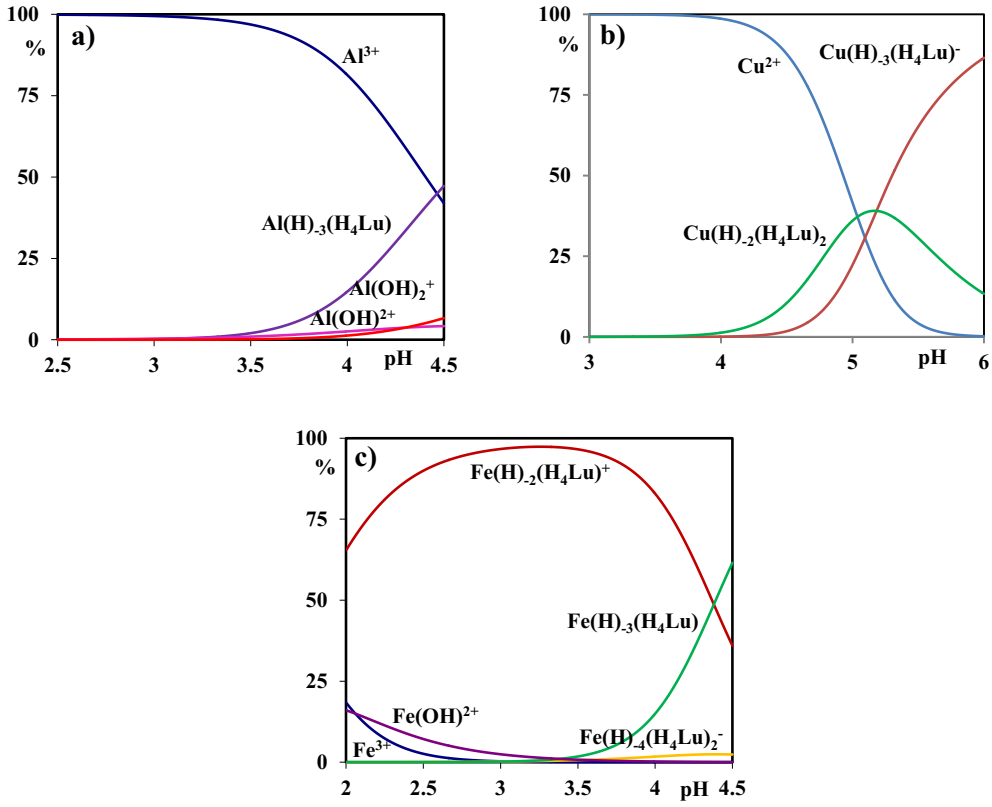

Fig. 3. Distribution diagrams in the presence of H_4Lu of: (a) Al(III) (C_M = 0.12 mM and C_L = 0.3 mM); (b) Cu(II) (C_M = 0.25 mM and C_L = 0.5 mM) and (c) Fe(III) (C_M = 0.1 mM and C_L = 0.5 mM).

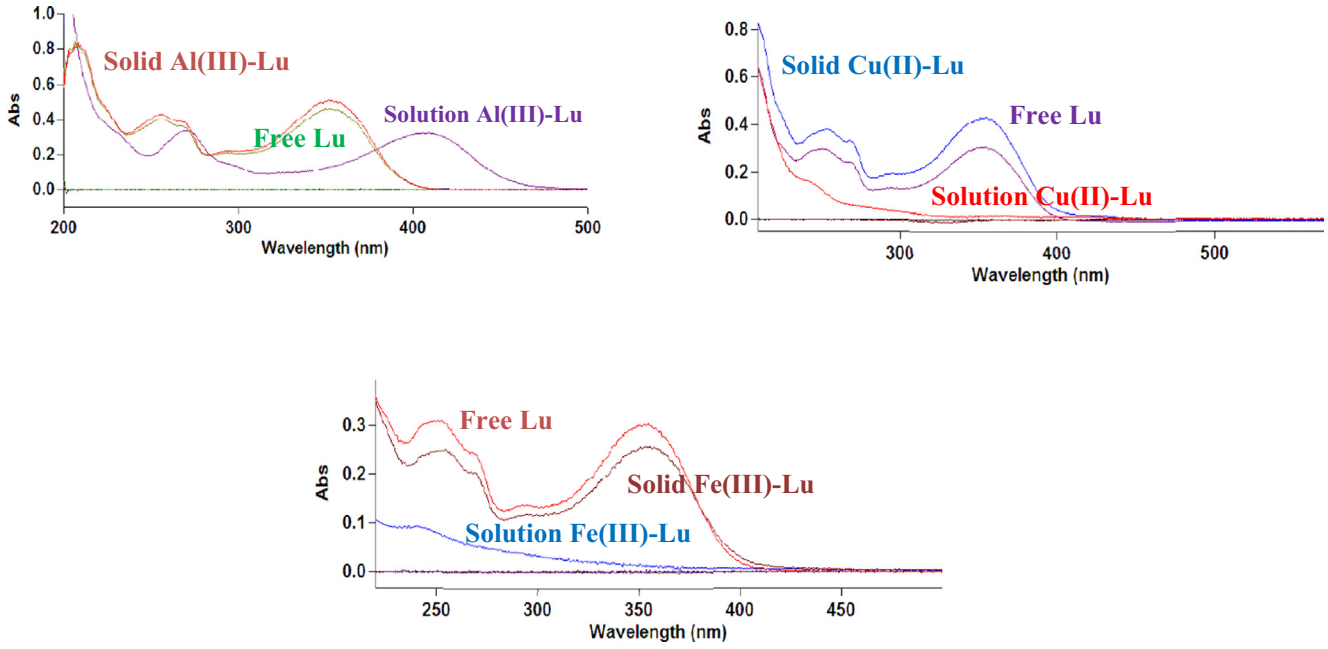

Fig. 4. UV–Vis spectra of the free ligand and of the complexes.

just over stable than the 3 ▫ -4 ▫ site on ring B by 2.8 kcal/mol and 1.4 kcal/mol for $Fe(OH)(H_3Lu)^+$ and $Fe(OH)_2(H_3Lu)$, respectively.

The deviation from the planarity of ring B is less pronounced than that observed in the case of Al(III)-Lu. Similar findings occurred in the analog quercetin complexes under the same conditions.

The Cu(II)-Lu showed a very distinctive behavior compared with that of the Al(III)- and Fe(III)-Lu species. For this system, no substantial energy difference characterizes the two examined complexes (see Table 2) proposing both species as equally populated in the considered environment, in agreement to available data [51]. As observed in a previous work [28], copper assumes a square planar geometry with two water molecules not coordinated to copper but retained in the outer coordination shell by H-bond (see Fig. 5).

In all the considered species the hydroxy groups are oriented in such a way to retain the maximum number of hydrogen bond interactions.

The change of the UV–Vis spectra (Fig. 4) displaying a bathochromic (red) shift can be also rationalized looking the HOMO-LUMO energy gaps related to the first absorption band having π-> π * character. The bathochromic shift can be associated to a strong charge transfer from the flavonoid to the metallic center (Ligand to Metal Charge Transfer, LMCT), or to a decrease in the HOMO-LUMO gap [52]. Fig. 6 reports the energy diagram of the HOMO and LUMO orbitals for Lu and its complexes with Al(III), Fe(III) and Cu(II) on the 4–5 preferred site along with the graphical representation of the frontier orbitals. It is possible to note that the $Al(OH)_2(H_3Lu)$ (**4**–**5**) complex having a lower value of HOMO-LUMO energy gap than that of Lu alone, well reflects the UV–Vis spectra behavior while the effect is less evident in the case of Cu (II) and Fe(III) complexes. This finding indicates that the nature of the metal ion plays an additional role in influencing the electronic spectra, as ligand and coordination site being equal, suggesting a LMCT major contribution for Cu(II) and Fe(III) in the luteolin complexes. However, in agreement with previous works [53], in all the three examined complexes a decrease of the HOMO-LUMO gap was observed. Furthermore, a different behavior in the UV–Vis spectrum by Lu complexes with respect to the analog with quercetin [28] remarks the selective role of the OH free 3 position on the C ring in luteolin.

3.2. Antioxidant properties

Results of the scavenging activity against DPPH radical are reported in Table 3 and graphically in Fig. 7. Data show the antioxidant activities of free luteolin, as well as of Al(III)-Lu, Cu(II)-Lu and Fe(III)-Lu complexes. Cu(II)-Lu complex exhibits the same antioxidant activity as Trolox, a standard used as the positive control, followed by Fe(III)-Lu complex (*i.e.*, 89.5 ± 0.6% and 88.4 ± 0.2%, respectively), at the highest concentration tested (*i.e.*, 33.3 μg mL^{-1}). On the other hand, at the lowest concentrations (from 3.3 to 0.3 μg mL^{-1}) the antioxidant activity of Fe(III)-Lu complex predominates (from 56.7 ± 0.7 to 45.1 ± 5.6%, respectively), even in higher percentages than the free ligand (from 34.2 ± 0.6 to 1.0 ± 0.1%, respectively). Table 4 shows the results of the EC_{50} relative to the percentages of inhibitions against DPPH. Results are also expressed as Trolox equivalents (TEAC, Table 5), and were obtained by using a suitable calibration curve (from 0.1 to 66.7 μg mL^{-1}).

The antioxidant activity of free and metal-complexed luteolin samples was also tested spectrophotometrically by ABTS assay. Results are reported in Table 6 and graphically represented in Fig. 8. Trolox was used as a positive control also for this assay. These data show a positive response to the assay, but with a lower percentage of inhibition of the $ABTS^{\cdot+}$ radical cation compared to the DPPH radical at all tested concentrations (*i.e.*, 10, 5, 1 and 0.1 μg mL^{-1}). At the highest concentration tested (10 μg mL^{-1}), luteolin complexed with Fe(III) exerts the highest antioxidant activity (*i.e.*, 17.9 ± 0.9%) compared to that exhibited by Cu(II)-Lu and Al(III)-Lu complexes (*i.e.*, 9.2 ± 0.9 and 5.5 ± 0.8%, respectively). However, free luteolin exerts, in this assay, a greater antioxidant activity than the complexes, except at the lowest concentration (0.1 μg mL^{-1}) where Cu(II)-Lu and Fe(III)-Lu exert a greater antioxidant activity (*i.e.*, 3.9 ± 0.4 and 4.4 ± 0.1%, respectively) with respect to free luteolin (2.7 ± 0.2%). The percentages of inhibition obtained with the ABTS assay were used to calculate the EC_{50} values (Table 7). In agreement with the trend observed with previously shown inhibitory results, data in Table 7 underline antioxidant activity of the standard and of the complex with Fe (III), albeit in a lower percentage than the values obtained against DPPH. Results obtained are also expressed as Trolox equivalents (TEAC, Table 8), for which it was necessary to construct a suitable

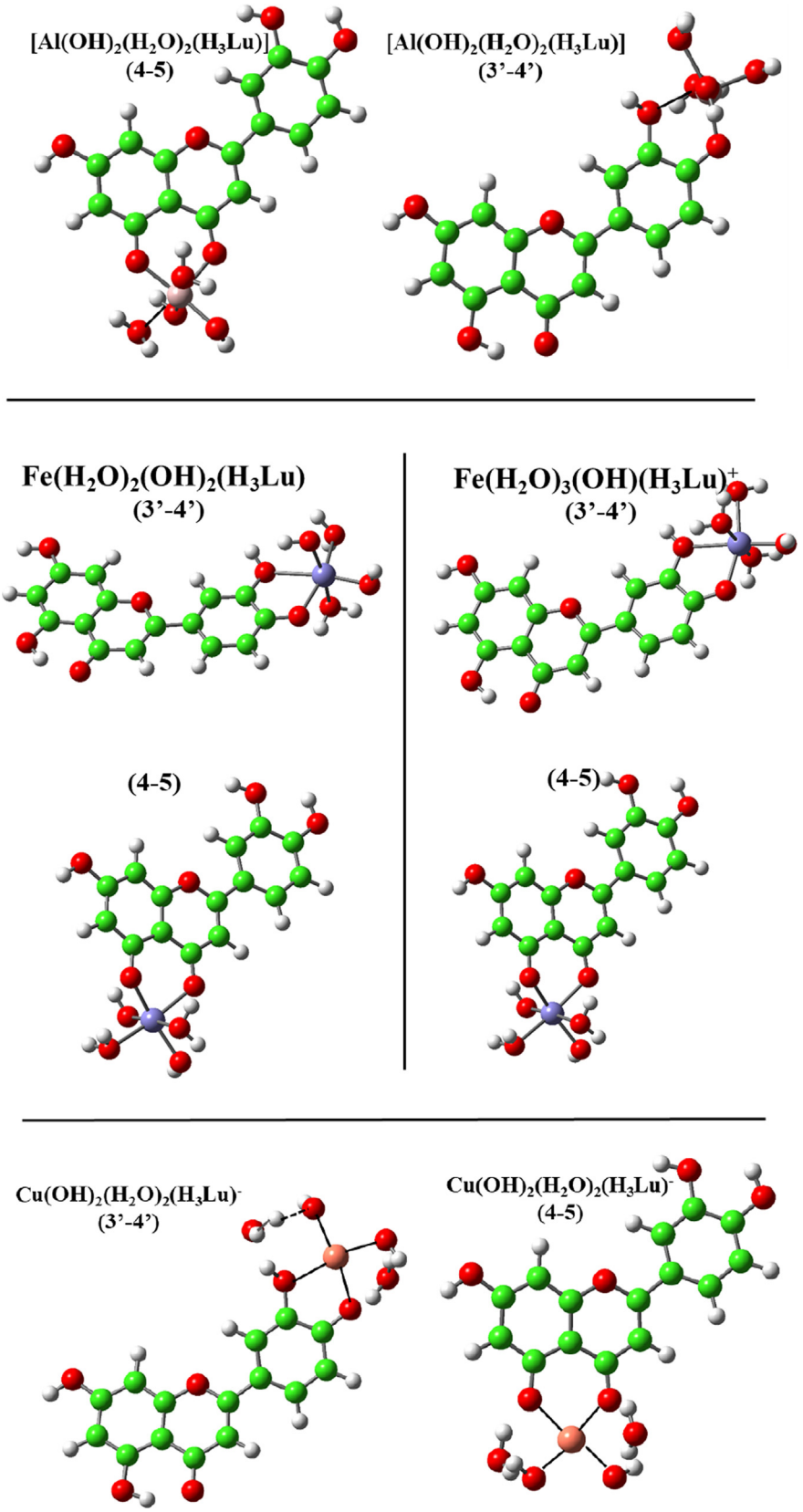

Fig. 5. Optimized Structures for the most plausible complexes of Lu with Al(III), Fe(III) and Cu(II). In parenthesis is reported the coordination site.

calibration curve (from 0.1 to 20 μg mL^{-1}). At the highest concentrations the data obtained are completely comparable, at the lowest concentrations tested the activity of inhibition of the Fe(III)-Lu complex prevails. Results obtained towards the free radical is further confirmed by an EC_{50} value of 1.4 for the Fe(III)-Lu complex (Table 4). Free luteolin was found to be more active against the free

Table 2
Gibbs free energy differences (ΔE) and free energy formation (ΔG_f) in kcal/mol of the considered complexes between the luteolin and Al(III), Fe(III) and Cu(II) calculated according to equations below reported.[a]

Complex	ΔE	ΔG_f
$Al(OH)_2(H_2O)_2(H_3Lu)$ (**3′-4′**)	4.9	−89.9
$Al(OH)_2(H_2O)_2(H_3Lu)$ (**4–5**)	0.0	−94.8
$Fe(OH)_2(H_2O)_2(H_3Lu)$ (**3′-4′**)		
$Fe(OH)_2(H_2O)_2(H_3Lu)$ (**4–5**)	1.4	−82.4
$[Fe(H_2O)_3(OH)(H_3Lu)]$(**3′-4′**)	0.0	−83.9
$[Fe(H_2O)_3(OH)(H_3Lu)]$(**4–5**)	2.8	−61.7
	0.0	−64.4
$Cu(OH)_2(H_2O)_2(H_3Lu)$(**3′-4′**)	0.2	−61.1
$Cu(OH)_2(H_2O)_2(H_3Lu)$(**4–5**)	0.0	−61.2

[a] $\{Lu\}^c + [M(H2O)6]^z \rightarrow [MLu(OH)_n]^{z+c} + (6\text{-}t)H2O$
where c is the total formal charge of luteolin, in this case equal to −1; z is the charge of the hexaaquo complex; n is the OH^- number equal to 1,2; and t = 2 takes into account the possibility that the luteolin is bidentate. Therefore, the formation energies of these complexes were calculated as:
$\Delta Gf = \Delta G([MLu(OH)_n]^{z+c}) + (6\text{-}t)\,\Delta G(H_2O) - \Delta G(Lu)^c - \Delta G(OH^-)_n - \Delta G([M(H_2O)_6]^z)$.

radical in the first three concentrations tested. Only at the lowest concentration Fe(III)-Lu complex appears to show more significant activity than free luteolin. However, luteolin shows to have an excellent response against the cationic radical, as it is also by the EC_{50} values (Table 7).

The FRAP assay treats the antioxidants in the sample as reducing agents in a colorimetric reaction linked to oxidation. As reported in Table 9, Fe(III)-Lu complex demonstrated highest reducing power with a FRAP value of 143.2 μmol g^{-1} (r^2 = 0.983), almost comparable to butylated hydroxytoluene (BHT), a standard used as a positive control (*i.e.*, 145.8 μmol g^{-1}), while free luteolin shows a reducing capacity of 500.5 μmol g^{-1}.

The reactivity to the FRAP test by luteolin and the complexes was found to be comparable to the responses obtained by the DPPH and ABTS assays. The complexed compounds' activity is lower than that of free luteolin, even if the complex with iron showed, also in this test, to have a higher ability than the other complexes (Fe(III)-Lu > Cu(II)-Lu > Al(III)-Lu) and to perform an activity comparable to the positive control.

The antioxidant activity parameters for all the species, including radicals and anions of the Lu and the most stable species for the Al, Cu and Fe complexes are reported in Table 10.

From a first glance to this table emerges that the energy values referred to the considered parameters are of a very different magnitude, this can be a suggestion of the mechanism favored over another.

Among the investigated species, the $Cu(OH)_2(H_2O)_2(H_3Lu)$-(**4–5**) provides a slightly lower BDE value than that characterizing the other species including the ligand alone, thus suggesting a better action as a scavenger following the HAT mechanism, even if they are enclosed in a very close range of energy. In fact, the BDE represents the best reliable thermochemical parameter to describe the HAT mechanism involving the hydrogen transfer from hydroxyl group that in the complexes occurs at the site 7, the most likely ΔH reaction the greatest antioxidant activity. This means that the radicalization of the hydroxyl group in position 7 of the ring A close the metalation site can take place.

Analyzing the IP values of Table 10 it is possible to note that the energy amount required to form the radical cation is lower for copper than for iron and aluminum complexes, proposing the copper containing luteolin as species more susceptible to ionization and with a stronger antioxidant property. This finding can be related to the fact that Cu(II)-Lu species is more reactive for both HAT and electron transfer than luteolin and well fits the observed behavior of the radical scavenger activity studied by $ABTS^{\cdot+}$ assay previously discussed [51].

The stepwise mechanisms, SET-PT and SPLET (see Scheme 1), are both associated to the tendency of chemical species to donate electrons. In the SET-PT an electron is given from the antioxidant to the free radical generating the $ArOH^{+\cdot}$ radical cation that succes-

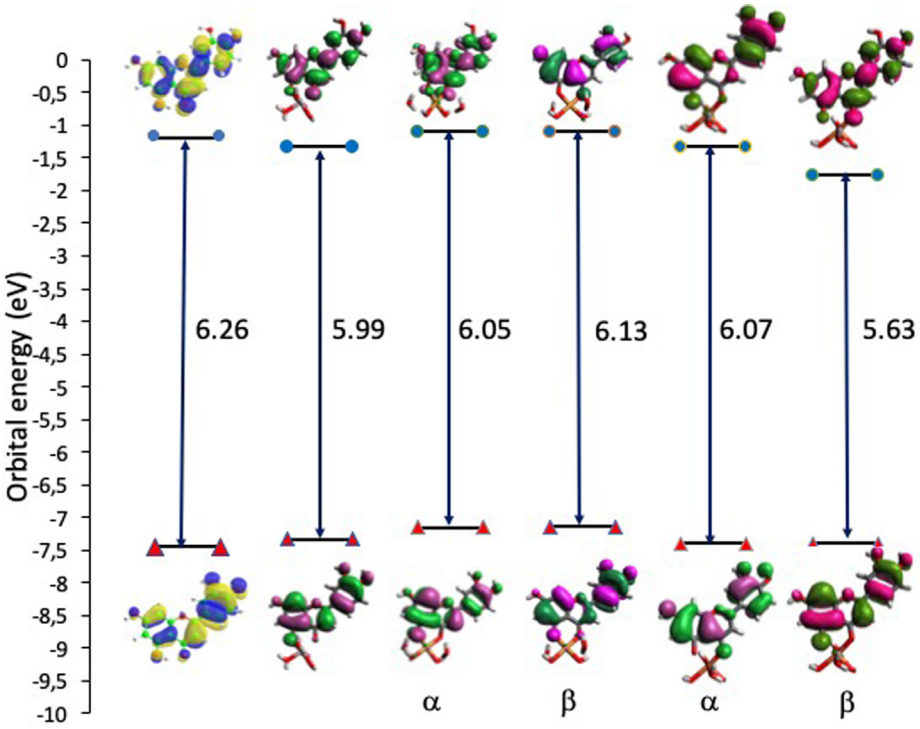

Fig. 6. Energy diagram of the HOMO and LUMO orbitals for the most representative complexes of Al(III)-Lu, Cu(II)-Lu and Fe(III)-Lu with respect to those of Lu alone as reference with different color. Energy gaps (eV) between HOMO and LUMO are reported.

Table 3
$\%I_{DPPH}$ of luteolin and its metal complexes.

μg mL^{-1}	Trolox $\%I_{DPPH}$ ± SD	Lu $\%I_{DPPH}$ ± SD	Al(III)-Lu $\%I_{DPPH}$ ± SD	Cu(II)-Lu $\%I_{DPPH}$ ± SD	Fe(III)-Lu $\%I_{DPPH}$ ± SD
33.3	100.0 ± 0.1	89.5 ± 0.8	88 ± 1	89.5 ± 0.6	88.4 ± 0.2
16.7	99.0 ± 0.1	88 ± 1	76.2 ± 0.1	79.4 ± 0.1	79.7 ± 0.9
3.3	96.0 ± 0.1	34.2 ± 0.6	24.6 ± 0.8	20.2 ± 0.1	56.7 ± 0.7
0.3	89.0 ± 0.1	1.0 ± 0.1	20.7 ± 0.7	13 ± 1	45.1 ± 5.6

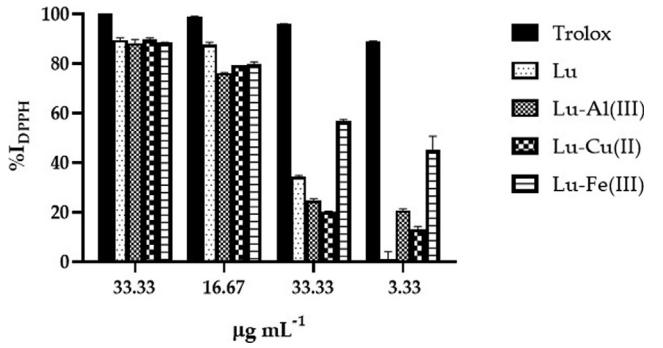

Fig. 7. Histogram of the percentages of inhibition against DPPH. In black the positive control (Trolox), followed by Lu (luteolin), Lu-Al(III) (luteolin-aluminum complex), Lu-Cu(II) (luteolin-copper complex) and finally Lu-Fe(III) (luteolin-iron complex).

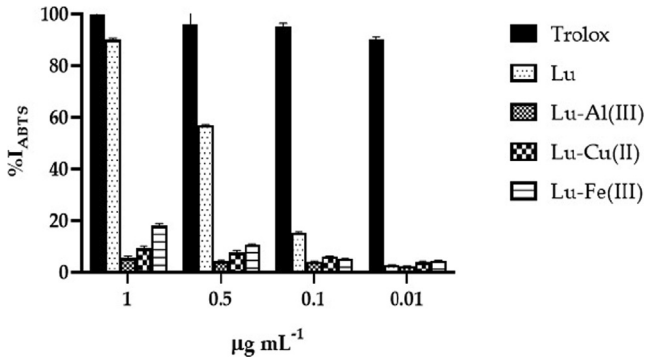

Fig. 8. Histogram of the percentages of inhibition against ABTS. In black the positive control (Trolox), followed by Lu (luteolin), Lu-Al(III) (luteolin-aluminum complex), Lu-Cu(II) (luteolin-copper complex) and finally Lu-Fe(III) (luteolin-iron complex).

Table 4
EC_{50} values of luteolin and its metal complexes.

Samples	μg mL^{-1} ± SD
Trolox	0.04 ± 0.01
Lu	4.8 ± 0.2
Al(III)-Lu	6.4 ± 0.2
Cu(II)-Lu	6.7 ± 0.3
Fe(III)-Lu	1.4 ± 0.1

Table 7
EC_{50} values of luteolin and its metal complexes.

Samples	μg mL^{-1} ± SD
Trolox	0.10 ± 0.01
Lu	3 ± 1
Al(III)-Lu	146 ± 2
Cu(II)-Lu	82 ± 1
Fe(III)-Lu	43 ± 1

sively releases a proton. Hence the most relevant properties useful to measure the feasibility of this mechanism are IP and PDE, while PA and ETE those to establish the viability of SPLET.

Since in all the considered species the higher deprotonation of radical cation $ArOH^{+\cdot}$ limits the reaction rate of SET-PT in water, the required lower energy to produce the radical cation (low IP values) makes the species more susceptible to ionization conversely to what happens in the SPLET mechanism.

Anyhow, to unequivocally determine the reasons favoring one particular mechanism, it is mandatory to deeply explore all the possible mechanisms. This goes beyond the comparative analysis of the potential antioxidant properties of the species examined in the present theoretical investigation, mainly based on the evalua-

Table 5
Trolox equivalents or TEAC of luteolin and its metal complexes.

μg mL^{-1}	Lu TE_{DPPH} ± SD	Al(III)-Lu TE_{DPPH} ± SD	Cu(II)-Lu TE_{DPPH} ± SD	Fe(III)-Lu TE_{DPPH} ± SD
33.3	12.0 ± 0.1	11.9 ± 0.2	12.1 ± 0.1	11.94 ± 0.03
16.7	11.8 ± 0.1	10.27 ± 0.01	10.73 ± 0.01	10.7 ± 0.1
3.3	4.49 ± 0.08	3.2 ± 0.1	2.59 ± 0.02	7.58 ± 0.09
0.3	0	2.64 ± 0.09	1.6 ± 0.2	6.0 ± 0.8

Table 6
$\%I_{ABTS}$ of luteolin and its metal complexes.

μg mL^{-1}	Trolox $\%I_{ABTS}$ ± SD	Lu $\%I_{ABTS}$ ± SD	Al(III)-Lu $\%I_{ABTS}$ ± SD	Cu(II)-Lu $\%I_{ABTS}$ ± SD	Fe(III)-Lu $\%I_{ABTS}$ ± SD
10	100 ± 0.2	90.1 ± 0.6	5.5 ± 0.8	9.2 ± 0.9	17.9 ± 0.9
5	96 ± 1.7	56.9 ± 0.3	4.2 ± 0.5	7.5 ± 0.9	10.8 ± 0.1
1	95 ± 1.5	15.4 ± 0.2	4.1 ± 0.2	6.2 ± 0.1	5.2 ± 0.1
0.1	90 ± 1.2	2.7 ± 0.2	2.3 ± 0.1	3.9 ± 0.4	4.4 ± 0.1

Table 8
Trolox equivalents or TEAC of luteolin and its metal complexes.

$\mu g\ mL^{-1}$	Lu TE_{ABTS} ± SD	Al(III)-Lu TE_{ABTS} ± SD	Cu(II)-Lu TE_{ABTS} ± SD	Fe(III)-Lu TE_{ABTS} ± SD
10	6.77 ± 0.05	0.15 ± 0.06	0.44 ± 0.07	1.12 ± 0.07
5	4.17 ± 0.02	0.05 ± 0.04	0.31 ± 0.07	0.56 ± 0.01
1	0.93 ± 0.02	0.04 ± 0.02	0.21 ± 0.01	0.13 ± 0.01
0.1	0	0	0.02 ± 0.04	0.07 ± 0.01

Table 9
FRAP assay of luteolin and its metal complexes.

Samples	Fe(III) ($\mu mol\ g^{-1}$)
BHT	145.8 ± 0.1
Lu	500.5 ± 0.1
Al(III)-Lu	21.8 ± 0.2
Cu(II)-Lu	38.1 ± 0.1
Fe(III)-Lu	143.2 ± 0.1

tion of their known descriptors for Lu and their Al(III), Fe(III) and Cu(II) complexes.

All the antioxidant measurements performed in the present work are electron transfer based assays in particular the FRAP assay is governed by SET, TEAC or ABTS assays involve both SET and HAT, even if they are frequently classified as SET assays [54–56], so the trend of the above mentioned antioxidant descriptors collected in Table 10 can be helpful to better rationalize the experimentally observed behavior that cannot be unequivocally assigned to a particular mechanism but rather to a combinations of several mechanisms depending also on the environment they are conducted in. Likewise, the ABTS and DPPH methods although based on the PA and IP, not always retain the same trend.

The antioxidant activity of flavonoids can be also related to the change in the energetic state as a consequence of metal ion chelation [56]. For this purpose, the frontier orbital energies E_{HOMO} and E_{LUMO} and in particular their difference ($\Delta E_{H\text{-}L}$), reported in Fig. 6, can be connected also with antioxidant activity. The higher the HOMO energy the better the electron donor, as a consequence the higher HOMO value present in copper system indicates the best donor among the studied compounds, followed by aluminum, iron and luteolin, in agreement with the IP trend. This means that since the H-abstraction reaction involves the electron transfer, the HOMO composition of the flavone allows to qualitatively indicate the sites easily attacked by free radicals and other reactive molecules.

Analyzing the H-L energy gaps, the electron promotion from HOMO to LUMO is easier in Fe(III)-Lu followed by Al(III)-Lu and Cu(II)-Lu than in the ligand.

On the basis of these results, it is noteworthy that the different charge of the ions as in Fe(III) and Cu(II) can play also a role in the different applied assays.

Moreover, the HAT mechanism represents the crucial reaction mechanism in the antioxidant activity of several compounds and metal complexes [42,57]. This does not mean that other reaction mechanisms generating the same products as HAT must be excluded by the scavenging activity but the present calculations in conjunctions with the experimental measurements can concur to discriminate among them.

3.3. Anti-inflammatory activity

Luteolin and the three luteolin-metal complexes were investigated as potential anti-inflammatory agents by verifying their ability to suppress lipopolysaccharide (LPS used at 10 ng mL^{-1}) induced IL-6 secretion in primary adherent MDMs. The production profile of IL-6 monitored with ELISA technique in conditioned medium of human MDMs cultures after LPS treatment was examined. We found that the exposure of human MDMs to LPS led to an increase of IL-6 production compared to control cultures. Treatment of LPS primed MDMs with luteolin or luteolin-metal complexes significantly reduced IL-6 production compared to LPS stimulation with a remarkable effect in the case of Fe(III)-Lu (14 ± 2 pg mL^{-1}) exposed cultures (Fig. 9). IL-6 is a cytokine known to promote the innate inflammatory response. Controlling its levels is crucial for the treatment of several diseases; it is fundamental for CAR T-cell therapy and for the current infection giving COVID-19 [58–60]. *In vivo* studies demonstrated that luteolin *per se* has the capability to reduce IL-6 levels in both peripheral blood and discrete brain areas after peripheral injection of LPS [32]. Here we showed that chelation with metal ions significantly enhances its ability.

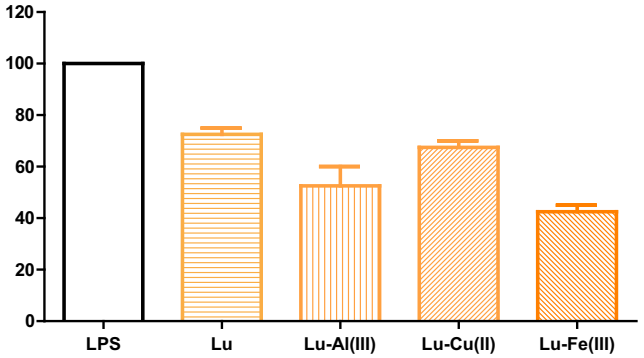

Fig. 9. Effect of luteolin and its metal complexes at 10 μM on IL-6 release by human macrophage. Data are presented as percentage of IL-6 release compared with IL-6 level of LPS alone treatment (100%). Bars represent the mean ± SD from three independent experiments.

Table 10
M05-2X/6–31 + G(d) bond dissociation enthalpies (BDE), proton dissociation enthalpies (PDE), proton affinities (PA), electron transfer enthalpies (ETE) and adiabatic ionization potentials (IP) for the most stable complexes are reported in kcal/mol.

Species	BDE	PDE	IP	PA	ETE*
Luteolin	403	513	158	521	139
$Al(OH)_2(H_2O)_2(H_3Lu)$ (**4**–**5**)	403	517	154	532	139
$[Fe(H_2O)_3(OH)(H_3Lu)]$ (**4**–**5**)	404	517	155	656	140
$Cu(OH)_2(H_2O)_2(H_3Lu)$ (**4**–**5**)	402	526	143	525	119

*Values obtained without considering the H(e-) that is the same in all of the cases.

4. Conclusions

The coordination properties of luteolin towards Al(III), Fe(III) and Cu(II) in aqueous solution at 37 °C and in 0.16 M NaCl were discussed. Speciation profiles from potentiometric titrations show that a complexation occurs at 1:1 ligand-to-Al(III) ratio and at 1:1 and 2:1 ligand-to-Fe(III) and -Cu(II) ratios. The favorite coordination sites of luteolin, determined by a computational approach, depend on the different metal ions. In particular, copper ion shows no selective preference towards any of the complexation sites of luteolin, while the six-membered chelate ring of the 4–5 site (*i.e.*, the 4-carbonyl-5-hydroxyl site of the A and C rings of the ligand) is the preferred one for aluminum and iron ions. On the contrary, redox behavior of ligands in complexes depends on the presence of hydroxy groups in their structure [61]. Metal-flavonoid complexes have been reported to possess higher antioxidant against free radicals than free flavonoid [62]. Among these reactions, the chelation of iron is of particular interest since the binding of iron improves the antioxidant activity of flavonoids [62]. Accordingly, in this work we found that the complex with iron had a higher activity than the other complexes (Fe(III)-Lu > Cu(II)-Lu > Al(III)-Lu), and its DPPH radical scavenging ability was even higher than that of free luteolin. Chelation of luteolin leads to the formation of complexes with enhanced anti-inflammatory properties. In fact, all the complexes tested were found to significantly reduce LPS-induced IL-6 levels in monocyte-derived macrophages with the following order: Fe(III)-Lu > Al(III)-Lu > Cu(II)-Lu > free Lu.

CRediT authorship contribution statement

Luana Malacaria: Investigation. **Chiara La Torre:** Investigation. **Emilia Furia:** Conceptualization, Resources, Writing – original draft, Writing – review & editing. **Alessia Fazio:** Conceptualization, Writing – original draft. **Maria Cristina Caroleo:** Investigation. **Erika Cione:** Conceptualization, Writing – original draft. **Luca Gallelli:** Investigation. **Tiziana Marino:** Conceptualization, Resources, Writing – original draft, Writing – review & editing. **Pierluigi Plastina:** Conceptualization, Writing – original draft.

Declaration of Competing Interest

The authors declare that they have no known competing financial interests or personal relationships that could have appeared to influence the work reported in this paper.

Acknowledgements

The authors thank Università della Calabria and Università della Magna Graecia for the financial support.

References

[1] E. Cione, C. La Torre, R. Cannataro, M.C. Caroleo, P. Plastina, L. Gallelli, Quercetin, epigallocatechin gallate, curcumin, and resveratrol: from dietary sources to human microRNA modulation, Molecules 25 (2020) 63–83.
[2] S.A.B.E. van Acker, M.J. de Groot, D.-J. van den Berg, M.N.J.L. Tromp, G. Donné-Op den Kelder, W.J.F. van der Vijgh, A. Bast, A quantum chemical explanation of the antioxidant activity of flavonoids, Chem. Res. Toxicol. 9 (8) (1996) 1305–1312.
[3] P.J. Cox, Y. Kumarasamy, L. Nahar, S.D. Sarker, M. Shoeb, Luteolin, Acta Crystallogr. E E 59 (7) (2003) o975–o977.
[4] M. Leopoldini, I.P. Pitarch, N. Russo, M. Toscano, Structure, conformation, and electronic properties of apigenin, luteolin, and taxifolin antioxidants. A first principle theoretical study, J. Phys. Chem. A 108 (1) (2004) 92–96.
[5] M.R. Webb, S.E. Ebeler, Comparative analysis of topoisomerase IB inhibition and DNA intercalation by flavonoids and similar compounds: structural determinates of activity, Biochem. J. 384 (2004) 527–541.
[6] N. Russo, M. Toscano, N. Uccella, Semiempirical molecular modeling into quercetin reactive site: structural, conformational, and electronic features, J. Agric. Food Chem. 48 (8) (2000) 3232–3237.
[7] S.A.B.E. Van Acker, D.-J. Van Den Berg, M.N.J.L. Tromp, D.H. Griffioen, W.P. Van Bennekom, W.J.F. Van Der Vijgh, A. Bast, Structural aspects of antioxidant activity of flavonoids, Free Radical Biol. Med. 20 (3) (1996) 331–342.
[8] O.S. Wolfbeis, M. Begum, H. Geiger, The fluorescence properties of luteolinesdie fluoreszenzeigenschaften der luteoline, Monatsh. Chem. 118 (12) (1987) 1403–1411.
[9] S. Rafat Husain, J. Cillard, P. Cillard, Hydroxyl radical scavenging activity of flavonoids, Photochem. 26 (9) (1987) 2489–2491.
[10] S.A.B.E. van Acker, G.P. van Balen, D. van den Berg, A. Bast, W.J.F. van der Vijgh, Influence of iron chelation on the antioxidant activity of flavonoids, Biochem. Pharmacol. 56 (8) (1998) 935–943.
[11] I.B. Afanas'ev, A.I. Dcrozhko, A.V. Brodskii, V.A. Kostyuk, A.I. Potapovitch, Chelating and free radical scavenging mechanisms of inhibitory action of rutin and quercetin in lipid peroxidation, Biochem. Pharmacol. 38 (11) (1989) 1763–1769.
[12] I. Morel, G. Lescoat, P. Cillard, J. Cillard, Role of flavonoids and iron chelation in antioxidant action, Methods Enzymol. 234 (1994) 437–443.
[13] N.J. Miller, C. Castellucio, L. Tijburg, C. Rice-Evans, The antioxidant properties of theaflavins and their gallate esters-radical scavengers or metal chelators?, FEBS Lett 392 (1996) 40–44.
[14] M.L. Brandi, Flavonoids: biochemical effects and therapeutic applications, Bone Mineral 19 (1992) S3–S14.
[15] B.H. Havsteen, The biochemistry and medical significance of the flavonoids, Pharmacol. Therapeut. 96 (2-3) (2002) 67–202.
[16] K.R. Markham, Techniques of Flavonoid Identification, Academic Press London, 1982.
[17] R. Karadað, E. Dölen, Examination of historical textiles with dyestuff analyses by TLC and derivative spectrophotometry, Tr. J. Chem. 21 (1997) 126–133.
[18] R. Garcia-Closas, A. Agudo, C.A. Gonzalez, E. Riboli, Intake of specific carotenoids and flavonoids and the risk of lung cancer in women in Barcelona, Spain, Nutr. Cancer 32 (3) (1998) 154–158.
[19] P. Knekt, R. Jarvinen, A. Reunanen, Flavonoid intake and coronary mortality in Finland: a cohort study, Br. Med. J. 312 (1996) 478–481.
[20] E. Miller, P. Schreier, Studies on flavonol degradation by peroxidase (donor: H_2O_2-oxidoreductase, EC 1.11.1.7): Part 1—Kaempferol, Food Chem. 17 (1985) 143–154.
[21] Q. Wang, L. Zhao, H. Zhao, X. Liu, L. Gao, N. Cheng, W. Cao, Complexation of luteolin with lead (II): Spectroscopy characterization and theoretical researches, J. Inorg. Biochem. 193 (2019) 25–30.
[22] R. Karadag, H. Böhmer, Dye analyses using derivate UV-Visible spectrophotometry and fibre-safe extraction with EDTA, Dyes His. Arch. 16 (2001) 106.
[23] M. López-Lázaro, Distribution and biological activities of the flavonoid luteolin, Mini Rev. Med. Chem. 9 (2009) 31–59.
[24] A. Primikyri, G. Mazzone, C. Lekka, A.G. Tzakos, N. Russo, I.P. Gerothanassis, Understanding zinc (II) chelation with quercetin and luteolin: a combined NMR and theoretical study, J. Phys. Chem. B 119 (2015) 83–95.
[25] V. Uivarosi, S.F. Barbuceanu, V. Aldea, C.-C. Arama, M. Badea, R. Olar, D. Marinescu, Synthesis, spectral and thermal studies of new rutin vanadyl complexes, Molecules 15 (3) (2010) 1578–1589.
[26] O.I. Aruoma, Characterization of drugs as antioxidant prophylactics, Free Radic. Biol. Med. 20 (5) (1996) 675–705.
[27] E. Furia, T. Marino, N. Russo, Insights into the coordination mode of quercetin with the Al(III) ion from a combined experimental and theoretical study, Dalt. Trans. 43 (2014) 7269–7274.
[28] G.A. Corrente, L. Malacaria, A. Beneduci, E. Furia, T. Marino, G. Mazzone, Experimental and theoretical study on the coordination properties of quercetin towards aluminium(III), iron(III) and copper(II) in aqueous solution, J. Mol. Liq. 325 (2021) 115171–115182.
[29] L. Malacaria, G.A. Corrente, A. Beneduci, E. Furia, T. Marino, G. Mazzone, A review on coordination properties of Al(III) and Fe(III) towards natural antioxidant molecules: experimental and theoretical insights, Molecules 26 (9) (2021) 2603.
[30] S. Selvaraj, S. Krishnaswamy, V. Devashya, S. Sethuraman, U.M. Krishnan, Flavonoid-metal ion complexes: a novel class of therapeutic agents, Med. Res. Rev. 34 (4) (2014) 677–702.
[31] S.J. Maleki, J.F. Crespo, B. Cabanillas, Anti-inflammatory effects of flavonoids, Food Chem. 299 (2019) 125124–125134.
[32] S. Jang, K.W. Kelley, R.W. Johnson, Luteolin reduces IL-6 production in microglia by inhibiting JNK phosphorylation and activation of AP-1, Proc. Natl. Acad. Sci. 105 (21) (2008) 7534–7539.
[33] A. Beneduci, G.A. Corrente, T. Marino, D. Aiello, L. Bartella, L. Di Donna, A. Napoli, N. Russo, I. Romeo, E. Furia, Insight on the chelation of aluminium(III) and iron(III) by curcumin in aqueous solution, J. Mol. Liq. 296 (2019) 111805–111814.
[34] P. Plastina, B. Gabriele, A. Fazio, Characterizing traditional rice varieties grown in temperate regions of Italy: free and bound phenolic and lipid compounds and in vitro antioxidant properties, Food Quality and Safety 2 (2) (2018) 89–95.
[35] P. Plastina, A. Fazio, B. Gabriele, Comparison of fatty acid profile and antioxidant potential of extracts of seven Citrus rootstock seeds, Nat. Prod. Res. 26 (23) (2012) 2182–2187.
[36] M. Leporini, M.R. Loizzo, R. Tundis, C. La Torre, A. Fazio, P. Plastina, Non-pungent *n*-3 polyunsaturated fatty acid (PUFA)-derived capsaicin analogues as potential functional ingredients with antioxidant and carbohy-drate-hydrolysing enzyme inhibitory activities, Antioxidants 8 (2019) 162–169.

[37] M.C. Nielsen, M.N. Andersen, H.J. Møller, Monocyte isolation techniques significantly impact the phenotype of both isolated monocytes and derived macrophages *in vitro*, Immunology 159 (1) (2020) 63–74.
[38] C. Benincasa, C. La Torre, P. Plastina, A. Fazio, E. Perri, M.C. Caroleo, L. Gallelli, R. Cannataro, E. Cione, Hydroxy-tyrosyl oleate: improved extraction procedure from olive oil and by-products, and *in vitro* antioxidant and skin re-generative properties, Antioxidants 8 (2019) 233–242.
[39] M.J. Frisch, G.W. Trucks, H.B. Schlegel, G.E. Scuseria, M.A. Robb, J.R. Cheeseman, G. Scalmani, V. Barone, G.A. Petersson, H. Nakatsuji, X. Li, M. Caricato, A.V. Marenich, J. Bloino, B.G. Janesko, R. Gomperts, B. Mennucci, H.P. Hratchian, J.V. Ortiz, A.F. Izmaylov, J.L. Sonnenberg, D. Williams-Young, F. Ding, F. Lipparini, F. Egidi, J. Goings, B. Peng, A. Petrone, T. Henderson, D. Ranasinghe, V.G. Zakrzewski, J. Gao, N. Rega, G. Zheng, W. Liang, M. Hada, M. Ehara, K. Toyota, R. Fukuda, J. Hasegawa, M. Ishida, T. Nakajima, Y. Honda, O. Kitao, H. Nakai, T. Vreven, K. Throssell, J.A. Montgomery Jr., J.E. Peralta, F. Ogliaro, M.J. Bearpark, J.J. Heyd, E.N. Brothers, K.N. Kudin, V.N. Staroverov, T.A. Keith, R. Kobayashi, J. Normand, K. Raghavachari, A.P. Rendell, J.C. Burant, S.S. Iyengar, J. Tomasi, M. Cossi, J.M. Millam, M. Klene, C. Adamo, R. Cammi, J.W. Ochterski, R. L. Martin, K. Morokuma, O. Farkas, J.B. Foresman, D.J. Fox, Gaussian 16, Revision C.01, Gaussian, Inc., Wallingford CT, 2016
[40] Y. Zhao, D.G. Truhlar, The M06 suite of density functionals for main group thermochemistry, thermochemical kinetics, noncovalent interactions, excited states, and transition elements: two new functionals and systematic testing of four M06-class functionals and 12 other functionals, Theor. Chem. Acc. 120 (2008) 215–241.
[41] A.V. Marenich, C.J. Cramer, D.G. Truhlar, Universal solvation model based on solute electron density and on a continuum model of the solvent defined by the bulk dielectric constant and atomic surface tensions, J. Phys. Chem. B 113 (18) (2009) 6378–6396.
[42] Z. Marković, J. Tošović, D. Milenković, S. Marković, Revisiting the solvation enthalpies and free energies of the proton and electron in various solvents, Comput. Theor. Chem. 1077 (2016) 11–17.
[43] A. Galano, J.R. Alvarez-Idaboy, Kinetics of radical-molecule reactions in aqueous solution: a benchmark study of the performance of density functional methods, J. Comput. Chem. 35 (2014) 2019–2026.
[44] G. Mazzone, M. Toscano, N. Russo, Density functional predictions of antioxidant activity and UV spectral features of Nasutin A, Isonasutin, Ellagic Acid, and one of its possible derivatives, J. Agric. Food Chem. 61 (40) (2013) 9650–9657.
[45] G. Mazzone, N. Malaj, A. Galano, N. Russo, M. Toscano, Antioxidant properties of several coumarin–chalcone hybrids from theoretical insights, RSC Adv. 5 (1) (2015) 565–575.
[46] Z. Marković, D. Amić, D. Milenković, J.M. Dimitrić-Marković, S. Marković, Examination of the chemical behavior of the quercetin radical cation towards some bases, Phys. Chem. Chem. Phys. 15 (19) (2013) 7370, https://doi.org/10.1039/c3cp44605k.
[47] E. Klein, V. Lukes, DFT/B3LYP study of the substituent effect on the reaction enthalpies of the individual steps of single electron transfer–proton transfer and sequential proton loss electron transfer mechanisms, J. Phys. Chem. A 110 (2006) 12312–12320.
[48] P. Gans, A. Sabatini, A. Vacca, Investigation of equilibria in solution. Determination of equilibrium constants with the HYPERQUAD suite of programs, Talanta 43 (10) (1996) 1739–1753.
[49] A. Amat, F. De Angelis, A. Sgamellotti, S. Fantacci, Acid-base chemistry of Luteolin and its methyl-ether derivatives: A DFT and ab initio investigation, Chem. Phys. Lett. 462 (2008) 313–317.
[50] M.M. Kasprzak, A. Erxleben, J. Ochocki, Properties and applications of flavonoid metal complexes, RSC Adv. 5 (57) (2015) 45853–45877.
[51] Y.i. Xu, J. Yang, Y. Lu, L.-L. Qian, Z.-Y. Yang, R.-M. Han, J.-P. Zhang, L.H. Skibsted, Copper(II) coordination and translocation in Luteolin and effect on radical scavenging, J. Phys. Chem. B 124 (2) (2020) 380–388.
[52] J. Ren, S. Meng, C.E. Lekka, E. Kaxiras, Complexation of flavonoids with iron: structure and optical signatures, J. Phys. Chem. B 112 (2008) 1845–1850.
[53] J.M. Dimitrić Marković, Z.S. Marković, T.P. Brdarić, N.D. Filipović, Comparative spectroscopic and mechanistic study of chelation properties of fisetin with iron in aqueous buffered solutions. Implications on *in vitro* antioxidant activity, Dalton Trans. 40 (17) (2011) 4560, https://doi.org/10.1039/c0dt01834a.
[54] A. Jiménez, A. Selga, J.L. Torres, L. Julià, Reducing activity of polyphenols with stable radicals of the TTM series. Electron transfer versus H-abstraction reactions in flavan-3-ols, Org. Lett. 6 (24) (2004) 4583–4586.
[55] R.L. Prior, X. Wu, K. Schaich, Standardized methods for the determination of antioxidant capacity and phenolics in foods and dietary supplements, J. Agr. Food Chem. 53 (10) (2005) 4290–4302.
[56] J.M. Alvarez-Suarez, S. Tulipani, S. Romandini, A. Vidal, M. Battino, Methodological aspects about determination of phenolic compounds and in vitro evaluation of antioxidant capacity in the honey: a review, Curr. Anal. Chem. 5 (2009) 293–302.
[57] G. Mazzone, N. Russo, M. Toscano, Antioxidant properties comparative study of natural hydroxycinnamic acids and structurally modified derivatives: Computational insight, Comput Theor. Chem. 1077 (2016) 39–47.
[58] T. Tanaka, M. Narazaki, T. Kishimoto, IL-6 in inflammation, immunity, and disease, Cold Spring Harb. Perspect. Biol. 6(10) (2014) 1-17.
[59] J. Wei, Y. Liu, C. Wang, Y. Zhang, C. Tong, G. Dai, W. Wang, J.E.J. Rasko, J.J. Melenhorst, W. Qian, A. Liang, W. Han, The model of cytokine release syndrome in CAR T-cell treatment for B-cell non-Hodgkin lymphoma, Sig. Transduct. Target. Ther. 5 (2020) 1–9.
[60] F. Luciani, E. Cione, M.C. Caroleo, M. Colosimo, A. Zanolini, A. Barca, S. Cosimo, P. Pasqua, L. Gallelli, SARS-CoV-2 Translocate from Nasopharyngeal to Bronchoalveolar Site: A Case Presentation, Reports 3 (2020) 23-27.
[61] Y.S. Tarahovsky, Y.A. Kim, E.A. Yagolnik, E.N. Muzafarov, Flavonoid membrane interactions: Involvement of flavonoid-metal complexes in raft signaling, Biochim. Biophys. Acta 1838 (5) (2014) 1235–1246.
[62] M. Grzesik, G. Bartosz, A. Dziedzic, D. Narog, J. Namiesnik, I. Sadowska-Bartosz, Antioxidant properties of ferrous flavanol mixtures, Food Chem. 268 (2018) 567–576.

Journal of Molecular Liquids 346 (2022) 118302

Contents lists available at ScienceDirect

Journal of Molecular Liquids

journal homepage: www.elsevier.com/locate/molliq

Experimental insights on the coordination modes of coumarin-3-carboxilic acid towards Cr(III)-, Co(II)-, Ni(II)-, Cu(II)- and Zn(II): A detailed potentiometric and spectroscopic investigation in aqueous media

Luana Malacaria, Rosaria Bruno, Giuseppina Anna Corrente, Donatella Armentano, Emilia Furia *, Amerigo Beneduci

Dipartimento di Chimica e Tecnologie Chimiche, Università della Calabria, Via P. Bucci, Cubo 12/D, Arcavacata di Rende, Cosenza 87036, Italy

ARTICLE INFO

Article history:
Received 14 October 2021
Revised 2 December 2021
Accepted 6 December 2021
Available online 9 December 2021

Keywords:
Coumarin-3-carboxilic acid
Cr(III), Co(II), Ni(II), Cu(II) and Zn(II) complexes
Stability constants
Coordination modes
Structural characterization

ABSTRACT

Here complexation of coumarin-3-carboxilic acid (HCCA) with Cr(III), Co(II), Ni(II), Cu(II) and Zn(II) at 37 °C and in 0.16 M $NaClO_4$ is discussed. Speciation profiles obtained by potentiometric titrations show that in aqueous solution a complexation occurs at a ligand-to-Cr(III), -Ni(II) and -Cu(II) ratio of 1:1, and at a ligand-to-Co(II) and -Zn(II) ratio of 1:1, 2:1 and 3:1. For Co(II)-HCCA system also a polynuclear species is formed (*i.e.*, $Co_2(OH)(CCA)_2^+$). The coordination sites of HCCA to the different metal ions were determined with the aid of UV–Vis, IR and X-ray diffraction. Solid state chemistry of HCCA was enriched of two new X-ray resolved structures for cobalt and nickel metal cations, which are also reported and discussed. From crystal packing analysis results the intricate motif of weak interactions that leads to a supramolecular interesting arrangement, not yet disclosed and argued in the previous literature about coumarin-3-carboxilic acid isostructural coordination compounds.

1. Introduction

Coumarin and its derivatives have attracted the interest of researchers in consideration of their antibiotic, anticoagulant, anti-cancer and anti-inflammatory properties [1–5]. The coordination chemistry and biological activity of coumarin derivatives and some metal cations have been reported in previous studies [6–12]. Among these, several coumarin-3-carboxylic acid-derived complexes were synthesized, and bidentate coordination through the lactone carbonylic oxygen and the deprotonated carboxylic oxygen atoms has been proposed [13,14]. Coumarin-3-carboxilic acid (HCCA, Fig. 1) ligand, when reacting with metals, can exhibit different coordination modes [15–22]. It can acts as monodentate *via* carboxylic moiety involving one or both oxygen atoms [16,17,18], as well as bidentate ligand through the lactone and the carboxylic oxygen to realize a high stabilized 6-membered metallocycle [5,19–22]. Furthermore, simultaneous bidentate and monodentate coordination mode by the free carbonyl oxygen has been shown in presence of lanthanides [23]. Recently, gold mononuclear complex [16] exhibiting biological activity and ruthenium binuclear [18] have been synthesized to obtain secondary building units (SBUs) for metal–organic fraimworks (MOFs) design, exploiting CCA^- as ligand. In 2001, attempts to determine structure of copper(II) complex of HCCA, analyzing spectroscopic data, suggested a binuclear structure [5]. Synthesis was carried out using copper(II) chloride as the salt yielding a very insoluble product. Ten years later, the slow solvent diffusion of aqueous solutions of $Cu(NO_3)_2{\cdot}6H_2O$ salt and HCCA afforded crystals suitable to be analyzed by single crystal X-ray diffraction (SCXRD). Its crystal structure unveiled a mononuclear complex in which copper (II) cation binds two anions of CCA^- in chelating coordination mode. Two water molecules occupy the *trans* positions of the Jahn-Teller elongated octahedral environment [19]. Overall complexes of Ni(II), Co(II), Zn(II) and Mn(II) with HCCA have been studied at experimental and theoretical levels. The complexes were characterized by elemental analyses, FT-IR, ^1H NMR, ^{13}C NMR and UV–Vis spectroscopy and by magnetic susceptibility measurements [24]. For each one an arrangement isostructural to the one previously reported for Cu(II) was suggested. However as far as we know, only for Mn(II) [20] and Zn(II) [22] crystallographic characterizations have been previously reported.

Recently, we have described the complexation of coumarin-3-carboxylic acid with Al(III) and Fe(III), and with Nd(III) and uranyl,

* Corresponding author.
E-mail address: emilia.furia@unical.it (E. Furia).

https://doi.org/10.1016/j.molliq.2021.118302
0167-7322/

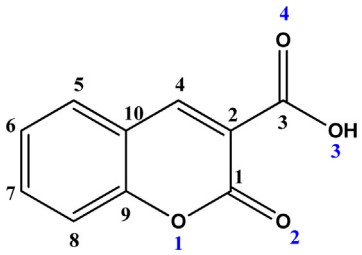

Fig. 1. Chemical structure of HCCA.

in aqueous solutions at 37 °C and in 0.16 M NaCl and $NaClO_4$, respectively, to evaluate the selectivity of this ligand towards bioavailable metal cations [15,25,26]. With the same purpose, herein we present a study on the complexation ability of HCCA towards Cr(III), Co(II), Ni(II), Cu(II) and Zn(II) at 37 °C and in 0.16 M $NaClO_4$, evaluating the stability constants of the complexes by potentiometric measurements and the corresponding structures by UV–Vis and IR characterizations. Furthermore, the crystal structures of two new Co(II) and Ni(II) coumarinic acid adducts were solved by single-crystal X-ray diffraction for the first time.

2. Experimental section

2.1. Materials

The sodium hydroxide titrant solutions, the perchloric acid and sodium perchlorate stock solutions were prepared and standardized as previously described [27]. The chromium(III), cobalt(II), nickel(II), copper(II) and zinc(II) perchlorate stock solutions were prepared and standardized as reported previously [28–32]. HCCA (Sigma, ≥99%), kept in a desiccator over silica gel, was used without further purification. All solutions were freshly prepared with bidistilled water.

2.2. Potentiometric and spectrophotometric measurements

The complex formation equilibria between investigated cations [Cr(III), Co(II), Ni(II), Cu(II) and Zn(II)] and HCCA were studied by performing potentiometric titrations with cell (G) and measuring the competition of the ligand for the metal cations and H^+ with a glass electrode, GE, at 37 °C and in 0.16 M $NaClO_4$.

This background salt was chosen to control the ionic strength due to its high inertia towards complexation and was preferred to NaCl, which it is not suitable for the metals investigated that belong to the borderline category. Moreover, in the case of $NaClO_4$ it is possible to prepare solutions with a high degree of purity.

RE/TestSolution/GE

where RE, reference electrode, = Ag / AgCl / 0.01 M NaCl / (0.16 – 0.01) M $NaClO_4$ / 0.16 M $NaClO_4$ and Test Solution = C_M M $M(ClO_4)_n$, C_A M $HClO_4$, C_B M NaOH, (0.16 – n C_M – C_A – C_B) M $NaClO_4$. The metal (C_M) and ligand (C_L) concentrations were varied from 1.0 to 5.0 mM. The ligand-to-metal ratio was varied between 1 and 5. The hydrogen ion concentration was varied from 10 mM (pH 2.0) to incipient precipitation of a neutral salt, which takes place in the range $[H^+]$ = 0.6–3·10^{-5} mM (pH 3.2–7.5) depending on the specific metal ion and on the ligand-to-metal ratio. As an example, some primary data for the Co(II)-HCCA system are reported in the Supplementary Material (*i.e.*, Table S1 and Fig. S1).

The glass electrode by Metrohm acquired, after the addition of the reagents, a constant potential within 30–40 min which remained unchanged within 0.1 mV.

The EMF of cell (G) can be written, in mV, at the temperature of 37 °C, as (1):

$$\boldsymbol{E} = \boldsymbol{E}_0 + 61.54\boldsymbol{log}[\boldsymbol{H}^+] + \boldsymbol{E}_j \quad (1)$$

where E_0 is constant in each series of measurements and E_j, whose value was taken from literature [25], is the liquid junction potential which is a function of $[H^+]$ only. In the first part, E_0 was determined for each titration in the absence of ligand and metal cations. In particular, the acidity of test solution (*i.e.*, 20 mL 0.16 M $NaClO_4$) was varied by adding 2.5 mL of 10 mM $HClO_4$ titrant solution. In the $[H^+]$ range 10^{-4} – 10^{-2} M constant values in the range from 310 to 350 mV, to within 0.1 mV, were calculated. In the second part the acidity was decreased stepwise by adding NaOH standard solution by using a manual burette. The titrant's concentration was varied from 5.0 to 25.0 mM and the final titrant volume from 10 to 50 mL, depending on the specific metal-to-ligand ratio investigated. To avoid carbonate interference, a slow stream of nitrogen gas was passed into the test solutions, stirred magnetically during titrations. The cell assembly was placed in a thermostat kept at (37.0 ± 0.1) °C.

Spectrophotometric measurements were carried out with a Varian Cary 50 Scan UV Visible Spectrophotometer by measuring the absorbance values, A_λ, (to 0.001 units) between 200 and 550 nm each 1 nm. Matched quartz cells of thickness 1 cm were employed. The temperature of the cell holder was maintained at (37.0 ± 0.3) °C by a Grant circulating water bath. The acquisition of data and the formulations of the parameters were managed with the aid of a computer connected to the instrument.

2.3. Synthesis

2.3.1. $Co(CCA)_2(H_2O)_2$ (1)

The reaction of an aqueous solution of $Co(ClO_4)_2{\cdot}6(H_2O)$ (0.0182 g, 0.05 mmol) added to an ethanolic solution of HCCA (0.0190 g, 0.1 mmol), under magnetic stirring, leads to a final light orange solution. After a week for slow evaporation at room temperature were obtained cubic light orange crystals adapt for SCXRD (Single Crystal X-Ray Diffraction). Yield: 77%; Anal. calc. (%) for $C_{20}H_{14}CoO_{10}$ (473.24): C, 50.76; H, 2.98; O, 33.81; found: C, 50.26; H, 2.38; O, 33.92.

2.3.2. $Ni(CCA)_2(H_2O)_2$ (2)

Similarly, to the previous synthesis, an aqueous solution of $Ni(ClO_4)_2{\cdot}6(H_2O)$ (0.0182 g, 0.05 mmol) reacts with HCCA in ethanol (0.0190 g, 0.1 mmol), under magnetic stirring, to give a pale green solution. Cubic light green crystals suitable for SCXRD characterization were grown in a month after a process of slow evaporation at room temperature. Yield: 78%; Anal. calc. (%) for $C_{20}H_{14}NiO_{10}$ (473.02): C, 50.78; H, 2.98; O, 33.82; found: C, 50.12; H, 3.20; O, 31.82.

2.4. Single-Crystal X-ray diffraction

A Crystal of **1** and **2** was selected and mounted on a MITIGEN holder in Paratone oil. Diffraction data were collected at room temperature on a Bruker-Nonius X8APEXII CCD area detector diffractometer using graphite-monochromated Mo-Kα radiation (λ = 0.71073 Å). The data were processed through the SAINT [33] reduction and SADABS [34] multi-scan absorption software. The structure was solved with the SHELXT [35] structure solution program, using the direct method. The model was refined with version 2018/3 of SHELXL against F^2 on all data by full-matrix least squares [36].

All non-hydrogen atoms were refined anisotropically, the hydrogen atoms of the ligand were set in calculated positions

and refined as riding atoms. Water hydrogen atoms in **1** and **2** were assigned and refined with restrained distances.

A summary of the crystallographic data and structure refinement for crystal structure is given in Table 1. Cambridge Crystallographic Data Centre (CCDC) reference numbers are 2,015,450 and 2,015,451 for **1** and **2**, respectively.

The final geometrical calculations on free voids and the graphical manipulations were carried out with PLATON [36] implemented in WinGX [37] and CRYSTAL MAKER [38] programs, respectively.

3. Results and discussion

3.1. Chelating properties of HCCA and stability of formed complexes

The experimental data were explained according to the following general equilibrium (eq. (2)):

$$pM^{(n+)} + qOH^- + rCCA^- \rightleftarrows M_p(OH)_q(CCA)_r^{(np-q-r)} \qquad \beta_{pqr} \qquad (2)$$

The most probable p, q and r values and the corresponding constants β_{pqr} were obtained by a least square fitting of the potentiometric data [39]. This computer program has been developed to determine formation constants of species in solution equilibria from data obtained by potentiometric titration, in particular, by minimization of an error-square sum based on measured electrode potentials. There exists a model of the equilibrium system, which adequately accounts for the experimental observations. The model is specified by a set of coefficients, one for each species formed, and all least-squares refinements are performed in terms of an assumed model. Examination of a sequence of models should yield that best which is not significantly different from that true. Choice of the best model is known as species selection.

Hydrolysis equilibria of Cr(III) were also studied according to a method already reported [40], as they were unknown under our experimental conditions from literature, and were kept invariant in the numerical evaluation of the stability constants. The equilibrium constants $K_{p,q}$, where p and q are the stoichiometric coefficients for the metal species and protons, respectively, for the formation of $Cr(OH)^{2+}$, $Cr(OH)_2^+$ and $Cr_3(OH)_4^{5+}$ (Eqs. (3)–(5)) were reported with the corresponding standard deviations (3σ).

$$Cr^{3+} + H_2O \rightleftarrows Cr(OH)^{2+} + H^+ \qquad logK_{1-1} = -4.19 \pm 0.06 \qquad (3)$$

$$Cr^{3+} + 2H_2O \rightleftarrows Cr(OH)_2^+ + 2H^+ \qquad \log K_{1-2} = -9.6 \pm 0.2 \qquad (4)$$

$$3Cr^{3+} + 4H_2O \rightleftarrows Cr_3(OH)_4^{5+} + 4H^+ \qquad \log K_{3-4} = -11.0 \pm 0.3 \qquad (5)$$

The constants of the predominant hydrolysis products of the Co (II), Ni(II), Cu(II) and Zn(II) cations under our experimental conditions were taken from the literature [41–44] and were kept also invariant, as well as the acidic constant of the ligand, determined in a previous work [15]. The stability constants of a chosen ternary species (p,q,r) were allowed to vary systematically to seek the best data fitting. Results obtained for the metal ions–HCCA systems are reported in Table 2. As can be seen, the sequestering ability of HCCA towards the Cu(II) cation is comparable with that of Cr(III), and stronger than that towards the other metal cations. This behavior was unexpected by considering the different nature of the metal cations; chromium belongs to the hard metal groups with higher affinity with oxygen donor ligands, while copper is a borderline metal, and it is expected to form more stable complexes with borderline ligands. However, this tendency has been already revealed in a previous work [15] in which was highlighted that HCCA forms more stable complexes with Al(III) ion respect to Fe(III).

In the numerical evaluation for the chromium–, nickel– and copper–HCCA systems, we have tried to explain experimental data with one complex; the best minimum was obtained with the Cr $(OH)_2(CCA)$, $Ni(OH)_2(CCA)^-$ and $Cu(OH)_2(CCA)^-$ species, respectively. The square error sum U decreased by taking into account also $Cr(OH)(CCA)^+$, $Ni(OH)(CCA)$ and $Cu(OH)_3(CCA)^{2-}$ species. No other complexes, introduced to improve the fit, were retained for these systems. The distribution diagrams reported in Fig. 2 a-c show that all the complexes reach significant percentages and start to form in acidic pH range.

Regarding the cobalt– and zinc–HCCA systems we have tried to explain the experimental data with a two complexes model. The best fit was achieved with the species $Co(CCA)_3^-$ and $Co_2(OH)(CCA)_2^+$, and $Zn(CCA)^+$ and $Zn(CCA)_3^-$, respectively. A significant improve to the fit was obtained by considering the presence of the M(OH)(CCA) and M

Table 1
Crystallographic data for compound **1** and **2**.

	1	2
CCDC	2,015,450	2,015,451
Formula	$C_{20}H_{14}CoO_{10}$	$C_{20}H_{14}NiO_{10}$
Fw / g mol-1	473.24	473.02
Crystal system	Triclinic	Triclinic
Space group	*P-1*	*P-1*
a/Å	6.6343(4)	6.6973(7)
b/Å	6.8527(4)	6.9594(7)
c/Å	10.4094(6)	10.4750(11)
a/°	85.253(4)	85.928(6)
β/°	89.491(4)	88.973(6)
γ/°	66.118(3)	65.388(5)
V/Å^3	431.08(4)	442.72(8)
Z	2	2
Dc/g cm $^{-3}$	1.823	1.774
T/K	296(2)	296(2)
μ/mm^{-1}	1.061	1.160
F(000)	241	242
Reflec. Collected26.278°. Reflec. Collected	7010	7638
Indep. Reflections [R(int)]	1747	1796
Data/restraints/ parameters	1747 /3 / 148	1796 / 2 / 150
Goodness-of-fit (Goof)[c]	1.112	1.071
Final R indices [a,b] [I > 2σ(I)]	R_1 = 0.0349	R_1 = 0.03457
	wR_2 = 0.0876	wR_2 = 0.0776
R indices (all data)	R_1 = 0.0430	R_1 = 0.0453
	wR_2 = 0.0920	wR_2 = 0.0824
Largest diff. peak/hole, Å-3	0.614/-0.401	0.367/-0.483

[a] $R_1 = \sum||F_o| - |F_c||/\sum|F_o|$.
[b] $wR_2 = \{\sum w(F_o^2 - F_c^2)^2/\sum[w(F_o^2)^2\}^{1/2}$ and $w = 1/[\sigma^2(F_o)^2 + (mP)^2 + nP]$ with $P = (F_o^2 + 2F_c^2)/3$.

Table 2
Survey of the log β, according to eq.(2), for Cr(III)–, Co(II)–, Ni(II)–, Cu(II)– and Zn(II) –HCCA complexes. The uncertainties represent 3 σ.

M^{n+}	Species	log $\beta_{p,q,r}$ ± 3σ
Cr(III)	$Cr(OH)(CCA)^+$	15.1 ± 0.9
	$Cr(OH)_2(CCA)$	26.5 ± 0.2
Co(II)	Co(OH)(CCA)|	9.8 ± 0.3
	$Co(OH)(CCA)_2^-$	12.44 ± 0.03
	$Co(CCA)_3^-$	8.2 ± 0.2
	$Co_2(OH)(CCA)_2^+$	16.59 ± 0.02
Ni(II)	Ni(OH)(CCA)	8.46 ± 0.02
	$Ni(OH)_2(CCA)^-$	15.13 ± 0.02
Cu(II)	$Cu(OH)_2(CCA)^-$	24.28 ± 0.06
	$Cu(OH)_3(CCA)^{2-}$	34.08 ± 0.09
Zn(II)	$Zn(CCA)^+$	5.2 ± 0.2
	$Zn(HCCA)(CCA)^+$	9.1 ± 0.3
	$Zn(CCA)_3^-$	10.31 ± 0.09
	Zn(OH)(CCA)	11.8 ± 0.2
	$Zn(OH)(CCA)_2^-$	14.4 ± 0.2

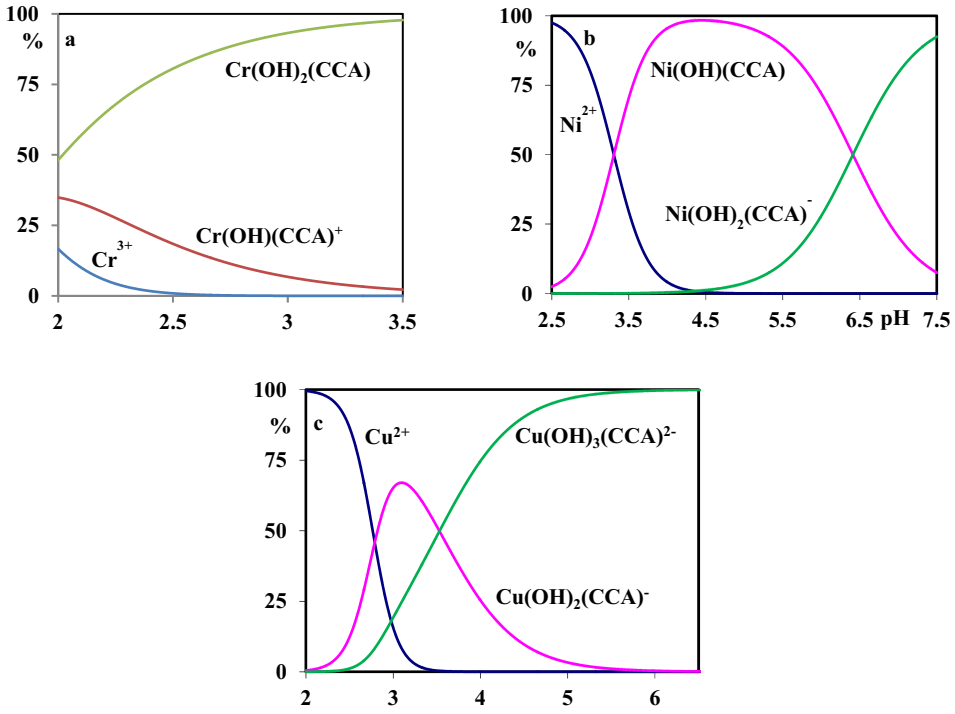

Fig. 2. Distribution diagrams in the presence of HCCA of: a) Cr(III) (C_M = 1.0 mM and C_L = 5.0 mM); b) Ni(II) (C_M = 0.1 mM and C_L = 1.0 mM) and c) Cu(II) (C_M = 0.1 mM and C_L = 1.0 mM).

$(OH)(CCA)_2^-$ species, for both systems. No other complexes introduced to improve the fit were retained for Co(II)-HCCA system, while for Zn(II)-HCCA the best agreement with the experimental data was obtained by considering also the presence of $Zn(HCCA)CCA^+$ species. In the distribution diagrams reported in Fig. 3 a–c the percentage of Co(II) and Zn(II) on the complexes with HCCA *versus* pH are depicted.

Considering the different existence regions of the various zinc complexes, it was necessary to report two different concentration ratios (*i.e.*, Fig. 3b and 3c).

As can be seen in the Figs. 2 and 3, none of the metal hydrolytic species reaches significant percentages. The formation of the complexes between Co(II)-HCCA is relevant from pH 3.0, while for Ni

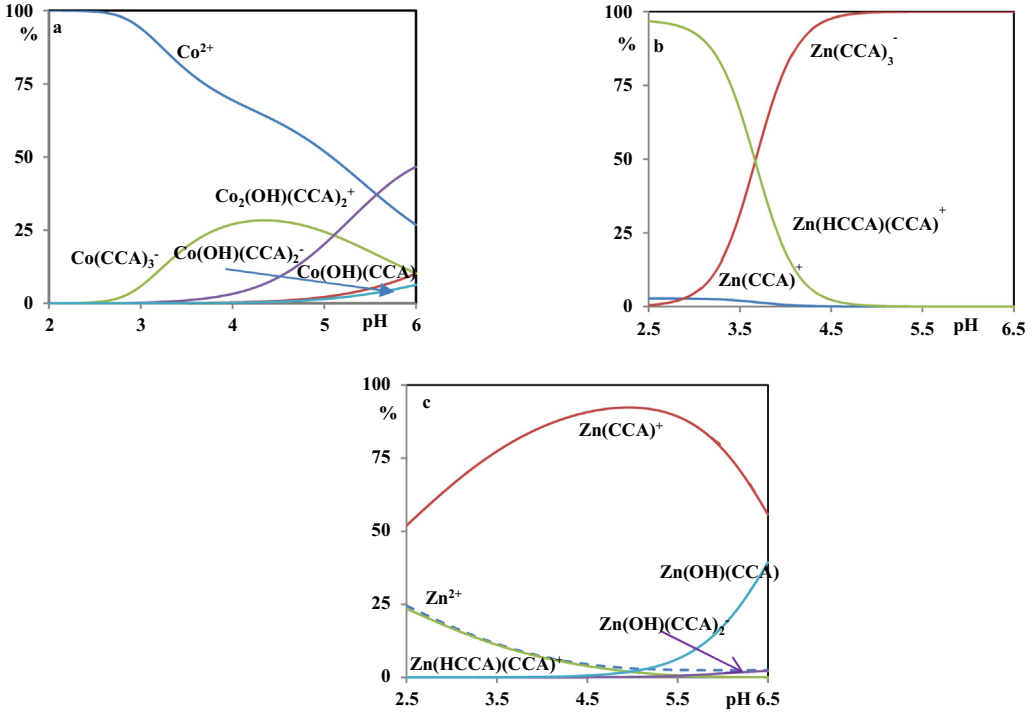

Fig. 3. Distribution diagrams in the presence of HCCA of: a) Co(II) (C_M = 1.0 mM and C_L = 5.0 mM); b) Zn(II) (C_M = 0.5 mM and C_L = 5.0 mM) and c) Zn(II) (C_M = 5.0 mM and C_L = 5.0 mM).

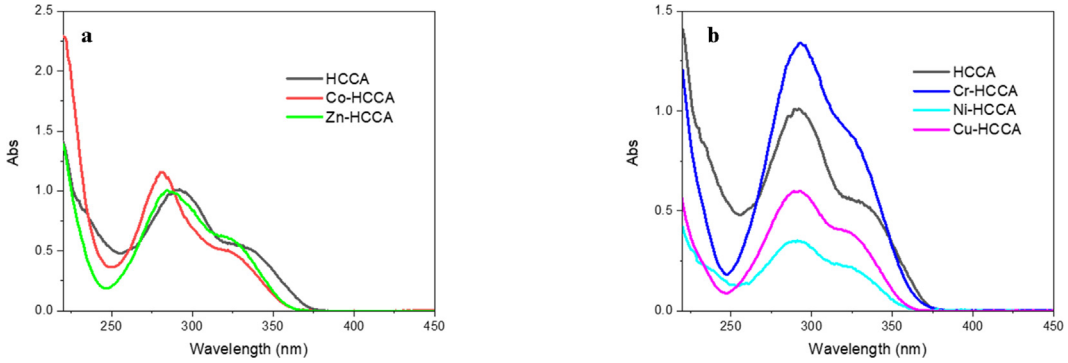

Fig. 4. UV–Vis spectra of the free ligand (HCCA) and of the solutions: (a) Co-HCCA and Zn-HCCA; (b) Cr-HCCA, Ni-HCCA and Cu-HCCA.

(II)- and Zn(II)-HCCA from pH 2.5. For Cr(III)- and Cu(II)-HCCA systems the formation of the complexes is relevant from pH 2.0, highlighting the different nature of these metal ions which form high stability species with the ligand, as evident from results reported in Table 2. $Co(CCA)_3^-$ and Ni(OH)CCA have similar stability constant values and reach high concentrations in a more acidic pH range; similarly, $Cr(OH)_2(CCA)$ and $Cu(OH)_2(CCA)^-$ have comparable stability and reach high percentages at a pH range between 3 and 3.5. $Co_2(OH)(CCA)_2^+$, $Ni(OH)_2CCA^-$, $Cu(OH)_3(CCA)^{2-}$ and $Zn(CCA)_3^-$ complexes are predominant at less acidic pH values (*i.e.*, pH > 6). The other Zn(II)-HCCA species are distributed in a wide pH range, between 2.5 and 6.5, depending on the specific ligand to metal ratio considered.

Information about structural features and binding modes were obtained from UV–Vis, IR and crystallographic characterizations.

3.2. UV–Vis and IR characterization

In order to verify the effective formation of the complexes and to obtain useful insight on the coordination properties, all solutions and solids gained at the end of each titration were analyzed by UV–Vis spectroscopy, and the solids by IR spectroscopy too. The UV–Vis spectrum of HCCA shows two distinctive absorption bands, one peaked at 291 nm (band I) and a broader one at 342 nm (band II). These bands correspond to two π-π* transitions, from a HOMO-1 – LUMO (band I) and from a HOMO – LUMO (band II) [15,24]. The UV–Vis spectra of the complexes (Fig. 4) can be separated into two groups based on the differences with respect to that of the free ligand: Co(II)/Zn(II) and Cr(III)/Ni(II)/Cu(II). It is clear from Fig. 4, and from the deconvolution analysis reported in the Supplementary Material (*i.e.*, Fig. S2), that the overall effect caused by the metal complexation is a relatively modest blue spectral shift (up to 16 nm), more evident for Co(II) and Zn(II) where, both bands I and II, shift at lower wavelengths (Table 3). This effect is less marked for the other three metals, where the blue shift occurs mainly on the band II. Table 3 reports also the area percentage of each absorption band, highlighting that the relative contribution of the band II to the overall spectrum increases slightly in all the complexes with respect to the free ligand. According to previous reports [15], the band at 330 nm (band II) of the complexes may be attributed to either ligand-to-mixed metal/ligand charge transfer transitions or to metal-to-ligand charge transfer transitions, which occur at lower wavelength with respect to the vertical excitation energy of the first excited state $^1A \square (\pi\pi^*)$ of the free ligand. While, the band at 290 nm mainly arises from intraligand charge transfer contribution, almost similar to the vertical excitation energy of the second excited state $^1A \square (\pi\pi^*)$ of the free ligand [24].

For Co(II), Ni(II), Cu(II) and Zn(II) a solid was also obtained during titration (Fig. 5). The deconvolution analysis of the absorption spectra of these compounds (Fig. S3) shows a general slight decrease of the peak wavelength, especially of the band II, compared to the free ligand (Table 3). However, the appearance of a new broad band in the range 375–475 nm can be observed for the complexes with Co and Cr, while a strong absorption band at 238 nm is found for the Ni-HCCA complex (Fig. S3). The latter may be interpreted as a significant red shift of the strong π-π* transition characteristic of HCCA in the UV range, which is only partially displayed in Fig. 5b.

The solid compounds obtained during the titrations were also analyzed by FT-IR spectroscopy. The vibrational analysis of HCCA and metals-HCCA complexes is very useful for the assignment of the ligand structural changes upon complexation. All the IR data and assignments for HCCA and the M(II)-HCCA (M = Co, Cu, Ni, Zn) complexes are reported in Table 4. The IR spectra are reported

Table 3
Relative contribution of each absorption band to the overall absorption spectrum of HCCA and of the complexes, calculated by spectral deconvolution.

Area % (λ nm)							
		UV Band	Band I	Band II	Band III	R^2	X^2 ($/10^{-4}$)
Solution	HCCA		89 (291)	12 (342)		0.9821	20
	Co-HCCA		73 (**281**)	27 (**326**)		0.9906	13
	Cr-HCCA		76 (**293**)	24 (**333**)		0.999	22
	Ni-HCCA		82 (**291**)	17 (**332**)		0.9923	0.9
	Cu-HCCA		78 (**291**)	22 (**331**)		0.998	0.7
	Zn-HCCA		75 (**287**)	25 (**329**)		0.9982	2
Solid	Co-HCCA		62 (**285**)	28 (**335**)	10 (**416**)	0.9976	1
	Ni-HCCA	50 (**238**)	36 (**290**)	14 (**335**)		0.9954	0.02
	Cu-HCCA		84 (**291**)	16 (**341**)		0.9884	2
	Zn-HCCA		72 (**290**)	28 (**334**)		0.9974	0.7

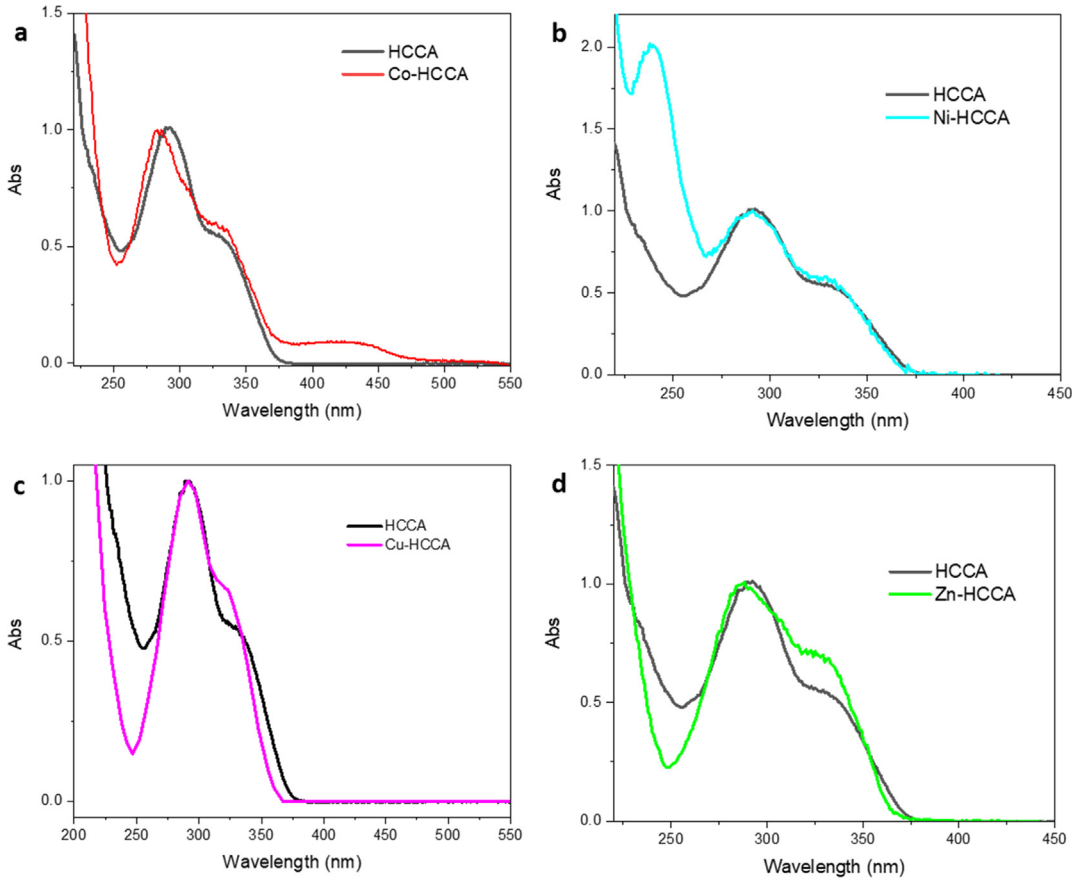

Fig. 5. UV–Vis spectra of the solids: (a) Co-HCCA; (b) Ni-HCCA; (c) Cu-HCCA; (d) Zn-HCCA with respect to that of the free ligand (HCCA).

in Fig. 6, where the two spectral regions, in which significant differences between the complexes and the free ligand were observed, are highlighted by vertical red lines. The strong IR bands observed in all the complexes, in the range 3150–3550 cm^{-1}, were assigned to the ν(OH) stretching vibration of the hydroxyl groups belonging to the coordination sphere of the metal ion. The most important and distinctive changes in the IR spectra were detected on the carbonyl stretching vibration $\nu(C1O2)_{carbonyl}$, on the in-plane $\nu(COH)_{ip}$ bending vibration of the acid group and on the stretching vibration of the C-O bond relative to carboxylic acid group (Table 4). In contrast, no significant changes were observed on the C = O stretching vibration of the carboxyl double bond. All these features strongly

Table 4
IR frequencies (cm^{-1}) and band assignment of HCCA and metals-HCCA complexes.

Vibration	Frequencies (cm^{-1})				
	HCCA	Co-HCCA	Cu-HCCA	Ni-HCCA	Zn-HCCA
ν(OH)	/	3356	3179	3410	3564
		3217			
$\nu(C3O4)_{carbonyl}$	1744	1743	1744	1744	1744
$\nu(C1O2)_{carbonyl}$	1682	1666	1690	1677	1681
ν(C = C)	1612	1612	1612	1612	1612
$\nu(COH)_{ip}$	1419	1419	1419	1419	1419
		1396	1396	1396	
$\delta(CCH)_{ip}$	1374	1373	1373	1373	1373
				1350	
ν(CO1)	1227	these bands changes and there	these bands changes and there	these bands changes and there	these bands changes and there
ν(C3O3)	1203	are many new bands:	are many new bands:	are many new bands:	are many new bands:
$\delta(CCH)_{ip}$	1042	1188	1180	1165	1144
		1141	1149	1141	1114
		1141	1118	1118	1087
		1087	1087	1087	
$ring_{ip}$	833	833	833	833	833
$\delta(COH)_{op}$	802	802	802	802	802
$\delta(CCC)_{ip}$	648	624	640	648	640
			624		624

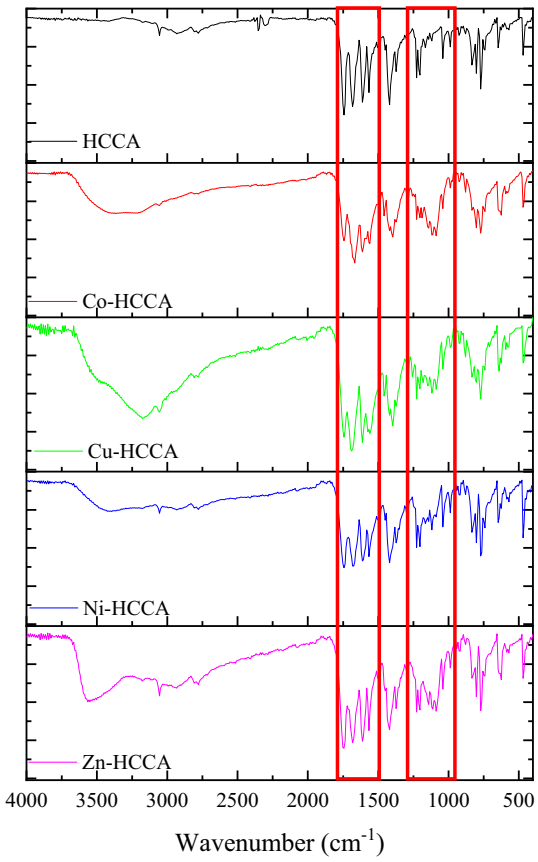

Fig. 6. FT-IR spectra of HCCA and metals-HCCA complexes.

indicate that the complexation between the HCCA ligand and the investigated metal ions occurs by chelation through the involvement of the carbonyl group of the lactone and the hydroxyl of the acidic group. A strong support to this hypothesis comes from the single crystal X-ray diffraction characterization of that complexes which we were able to isolate as single crystals, *i.e.*, Co$(CCA)_2(H_2O)_2$ and Ni$(CCA)_2(H_2O)_2$.

3.3. Single crystal X-ray diffraction characterization

Compound **1** of formula Co$(CCA)_2(H_2O)_2$ and compound **2** of formula Ni$(CCA)_2(H_2O)_2$ crystallize in *P-1* space group of the triclinic system. These compounds are isostructural and consist of a metal ion M(II) residing in a distorted octahedral geometry, bond to two CCA^- ligands and two water molecules in *trans* conformation (Fig. 7).

Molecular moiety is reproduced by inversion symmetry operation on the central atom of the crystallographic asymmetric unit. Coordination environment for compound **1** is denoted by cobalt

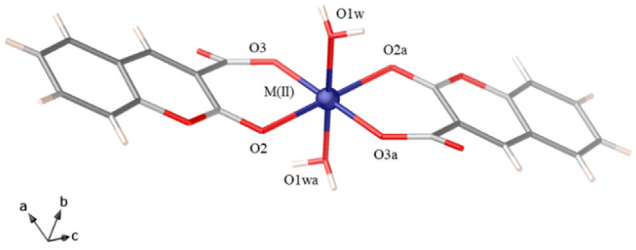

Fig. 7. Crystal structure of $M(CCA)_2(H_2O)_2$ with M = Co(II) (1) and Ni(II) (2).

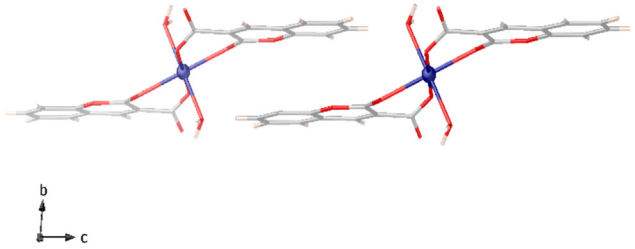

Fig. 8. Perspective view of adjacent mononuclear complexes along *a* crystallographic axis, perfectly interacting via π•••π interactions.

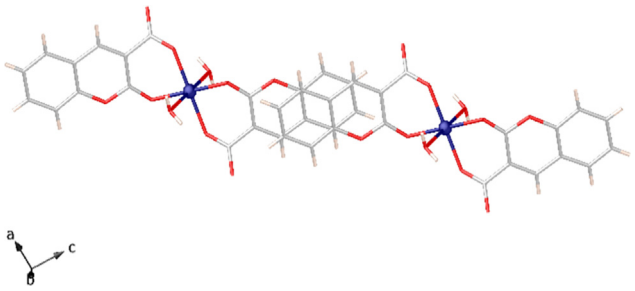

Fig. 9. Representative figure of π stacking interactions between two symmetry related molecules, generated by translation. Perspective view down *b* crystallographic axis.

oxygen distances of 2.143(2) and 2.025(2) Å for Co-O2 and Co-O3, respectively. Water molecules reside at a bond distance for Co-O1w of 2.101(2) Å. For compound **2**, nickel oxygen distances are 2.322(2) Å for Ni-O2 and 1.926(2) Å for Ni-O3 with the coordinated water molecule at a distance of 2.001(2) Å. A very robust packing is built by means π···π stacking (Figs. 8-9) and H-bond interactions (Fig. 10). Each molecular unit takes part in six H-bonds, involving water molecules as H-donor and carbonyl oxygen as H-acceptor. Water molecules build strong intermolecular interactions with oxygen atoms of the carboxylic moiety of two molecules related by symmetry [O···O distances of 2.702(3) Å and 2.752(3)] (Table 5). Furthermore, the carboxylic group interacts with four adjacent units [O4···H(2wa) and O4···H(1wb); symmetry codes *a* = -x + 1, -y + 1, -z + 1 and *b* = x-1, y, z] yielding a pretty hydrogen bonded cluster.

Additional π stacking interactions, contribute to stabilize the supramolecular network establishing chains developing along *b* crystallographic axes. The mean centroid·centroid distance is of 3.66 Å (Figs. 8-9).

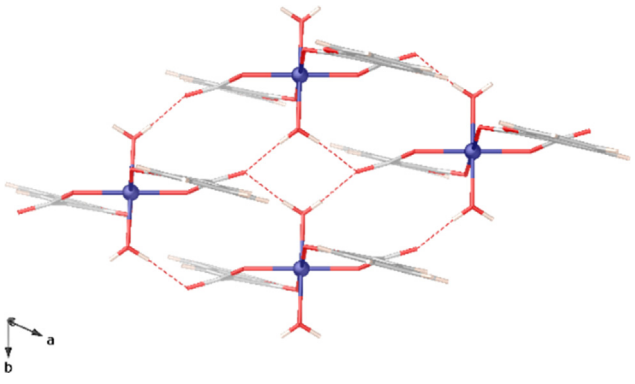

Fig. 10. Perspective view along *c* axis of the 3D supramolecular structure.

Table 5
Hydrogen bonds for **1** and **2** [Å and °].

D-H...A	d(H...A) [Å]	<(DHA)[°]
Compound **1**		
O(1 W)...O(4) [a]	2.701(2)	167(3)
O(1 W)...O(4) [b]	2.751(2)	173(3)
Compound **2**		
O(1 W)...O(4) [a]	2.796(2)	172(2)
O(1 W)...O(4) [b]	2.726(2)	164(2)

a: [-x + 1,-y + 1,-z + 1]; *b:* [x-1,y,z]

4. Conclusion

In this work the formation of the Cr(III), Co(II), Ni(II), Cu(II) and Zn(II) complexes with coumarin-3-carboxilic acid in aqueous medium for the first time was investigated. From our results the following conclusions can be drawn: in the considered pH range, only 1:1 stoichiometric ratio species between ligand and Cr(III), Ni(II) and Cu(II) in aqueous medium are possible, while Co(II) and Zn(II) form complexes with stoichiometry 1:1, 1:2 and 1:3 with HCCA. For Co(II)-HCCA system also a polynuclear species is formed (*i.e.*, $Co_2(OH)(CCA)_2^+$). The stability of Cu(II) species is significantly higher than that of Co(II), Ni(II) and Zn(II) complexes, and it is comparable to that of hard metal cations as Cr(III), Al(III) and Fe(III) [15]. This behavior was unexpected by considering the borderline nature of copper(II) and the hardness of the ligand. The complexation between HCCA and the investigated metal ions occurs by chelation through the carbonyl group of the lactone and the hydroxyl of the acidic group. This hypothesis, based on results obtained from UV–Vis and IR characterization, was supported by the single crystal X-ray diffraction analysis of very stable mononuclear structures for Co(II) and Ni(II) with the CCA^- anionic moiety acting as chelating ligand. Solid state chemistry of coumarin-3-carboxilic acid was enriched of two new X-ray resolved structures of cobalt and nickel metal ions. Crystal packing, for both, unveils an extended supramolecular network of synergistic H-bond and π stacking interactions.

CRediT authorship contribution statement

Luana Malacaria: Investigation. **Rosaria Bruno:** Investigation. **Giuseppina Anna Corrente:** Investigation, Writing – original draft. **Donatella Armentano:** Conceptualization, Resources, Writing – original draft. **Emilia Furia:** Conceptualization, Resources, Writing – original draft. **Amerigo Beneduci:** Conceptualization, Resources, Writing – original draft.

Declaration of Competing Interest

The authors declare that they have no known competing financial interests or personal relationships that could have appeared to influence the work reported in this paper.

Acknowledgements

This work was supported by the Ministero dell'Istruzione, dell'Università e della Ricerca (Italy). R.B. thanks the MIUR (Project PON R&I FSE-FESR 2014–2020) for predoctoral grant.

Appendix A. Supplementary material

Supplementary data to this article can be found online at https://doi.org/10.1016/j.molliq.2021.118302.

References

[1] F.E. Arias Arias, A. Beneduci, F. Chidichimo, E. Furia, S. Straface, Study of the adsorption of mercury (II) on lignocellulosic materials under static and dynamic conditions, Chemosphere 180 (2017) 11–23.
[2] J. Kim, H.J. Lee, K.W. Lee, Naturally occurring phytochemicals for the prevention of Alzheimer's disease, J. Neurochem. 112 (6) (2010) 1415–1430.
[3] G. Crisponi, V.M. Nurchi, V. Bertolasi, M. Remelli, G. Faa, Chelating agents for human diseases related to aluminium overload, Coord. Chem. Rev. 256 (1-2) (2012) 89–104.
[4] C. Exley, Aluminum should now be considered a primary etiological factor in alzheimer's disease, J. Alzheimer Dis. Rep. 1 (1) (2017) 23–25.
[5] A. Karaliota, O. Kretsi, C. Tzougraki, Synthesis and characterization of a binuclear coumarin-3-carboxylate copper (II) complex, J. Inorg. Biochem. 84 (1-2) (2001) 33–37.
[6] B.S. Creaven, M. Devereux, D. Karcz, A. Kellett, M. McCann, A. Noble, M. Walsh, Copper (II) complexes of coumarin-derived schiff bases and their anti-Candida activity, J. Inorg. Biochem. 103 (9) (2009) 1196–1203.
[7] B.S. Creaven, D.A. Egan, D. Karcz, K. Kavanagh, M. McCann, M. Mahon, A. Noble, B. Thati, M. Walsh, Synthesis, characterisation and antimicrobial activity of copper(II) and manganese(II) complexes of coumarin-6,7-dioxyacetic acid ($cdoaH_2$) and 4-methylcoumarin-6,7-dioxyacetic acid ($4\text{-}MecdoaH_2$): X-ray crystal structures of $[Cu(cdoa)(phen)_2] \cdot 8.8H_2O$ and $[Cu(4\text{-}Mecdoa)(phen)_2] \cdot 13H_2O$ (phen = 1,10-phenanthroline), J. Inorg. Biochem. 101 (2007) 1108-1119.
[8] B.S. Creaven, D.A. Egan, K. Kavanagh, M. McCann, M. Mahon, A. Noble, B. Thati, M. Walsh, Synthesis and antimicrobial activity of copper(II) and silver(I) complexes of hydroxynitrocoumarins: X-ray crystal structures of $[Cu(hnc)_2(H_2O)_2] \cdot 2H_2O$ and [Ag(hnc)] (hncH = 4-hydroxy-3-nitro-2H-chromen-2-one), Polyhedron 24 (2005) 949–957.
[9] B.S. Creaven, D.A. Egan, K. Kavanagh, M. McCann, A. Noble, B. Thati, M. Walsh, Synthesis, characterization and antimicrobial activity of a series of substituted coumarin-3-carboxylatosilver (I) complexes, Inorg. Chim. Acta 359 (12) (2006) 3976–3984.
[10] B. Thati, A. Noble, R. Rowan, B.S. Creaven, M. Walsh, M. McCann, D. Egan, K. Kavanagh, Mechanism of action of coumarin and silver (I)–coumarin complexes against the pathogenic yeast *Candida albicans*, Toxicol. *in Vitro* 21 (5) (2007) 801–808.
[11] M. Grazul, E. Budzisz, Biological activity of metal ions complexes of chromones, coumarins and flavones, Coord. Chem. Rev. 253 (21-22) (2009) 2588–2598.
[12] A. Kulkarni, S.A. Patil, P.S. Badami, Synthesis, characterization, DNA cleavage and *in vitro* antimicrobial studies of La (III), Th (IV) and VO (IV) complexes with Schiff bases of coumarin derivatives, Eur. J. Med. Chem. 44 (7) (2009) 2904–2912.
[13] T.z. Mihaylov, N. Trendafilova, I. Kostova, I. Georgieva, G. Bauer, DFT modeling and spectroscopic study of metal–ligand bonding in La (III) complex of coumarin-3-carboxylic acid, Chem. Phys. 327 (2-3) (2006) 209–219.
[14] I. Georgieva, N. Trendafilova, W. Kiefer, V.K. Rastogi, I. Kostova, Vibrational and theoretical study of coumarin-3-carboxylic acid binding mode in Ce(III) and Nd(III) complexes, Vib. Spectrosc. 44 (1) (2007) 78–88.
[15] E. Furia, A. Beneduci, N. Russo, T. Marino, Structural characterization of aluminium(III) and iron(III) complexes of coumarinic acid in aqueous solutions from combined experimental and theoretical investigations, New J. Chem. 42 (2018) 11006–11012.
[16] S. Carboni, A. Zucca, S. Stoccoro, L. Maiore, M. Arca, F. Ortu, C. Artner, B.K. Keppler, S.M. Meier-Menches, A. Casini, M.A. Cinellu, New Variations on the Theme of gold(III) C^N^N cyclometalated complexes as anticancer agents: synthesis and biological characterization, Inorg. Chem. 57 (2018) 14852–14865.
[17] S.W. Ng, Coordination complexes of triphenyltin coumarin-3-carboxylate with O-donor ligands: (coumarin-3-carboxylato)triphenyltin-L (L = ethanol, diphenylcyclopropenone and quinoline N-oxide) and bis[(coumarin-3-carboxylato)triphenyltin]-L (L = triphenylphosphine oxide and triphenylarsine oxide), Acta Crystallogr., Sect. C: Cryst. Struct. Commun. C 55 (1999) 523–531.
[18] N.F. O'Rourke, M. Ronaldson, T. Stanley Cameron, R. Wang, M.A.S. Aquino, Equatorial π-stacking interactions in diruthenium (II, III) tetracarboxylate complexes containing extended π-systems, J. Mol. Struct. 1052 (2013) 17–23.
[19] Y. Cui, Q. Gao, H.-H. Wang, L. Wang, Y.-B. Xie, Diaquabis(2-oxo-2 H -chromene-3-carboxylato)copper(II), Acta Crystallogr., Sect. E: Struct. Rep. Online 67 (6) (2011) m782.
[20] Y. Cui, Q. Gao, H.-H. Wang, L. Wang, Y.-B. Xie, Diaquabis(2-oxo-2*H*-chromene-3-carboxylato-κ^2O^2, $^{O}3$)manganese(II), Acta Crystallogr., Sect. E: Struct. Rep. Online 67 (6) (2011) m727.
[21] Y. Cui, Q. Gao, H.-H. Wang, L. Wang, Y.-B. Xie, Diaquabis(2-oxo-2*H*-chromene-3-carboxylato-κ^2O^2, O3)cadmium, Acta Crystallogr., Sect. E: Struct. Rep. Online 67 (1) (2011) m126.
[22] Y. Cui, Q. Gao, H.-H. Wang, L. Wang, Y.-B. Xie, Diaquabis(2-oxo-2 H -chromene-3-carboxylato)zinc(II), Acta Crystallogr., Sect. E: Struct. Rep. Online 67 (1) (2011) m69.
[23] Y. Shuping, H. Lijun, W. Daqi, P. Yan, Y. Zhiqun, Y. Haiyan, Solvothermal synthesis, crystal structure of a 1D coordination polymer $[Er(CCA)_3(H_2O)_2]_n \bullet 2nH_2O$ (HCCA = coumarin-3-carboxylic acid) and the interaction between the polymer and bovine serum albumin (BSA), Huaxue Xuebao (Chin.) (Acta Chim. Sinica) 69 (2011) 2319–2327.

[24] B.S. Creaven, M. Devereux, I. Georgieva, D. Karcz, M. McCann, N. Trendafilova, M. Walsh, Molecular structure and spectroscopic studies on novel complexes of coumarin-3-carboxylic acid with Ni(II), Co(II), Zn(II) and Mn(II) ions based on density functional theory, Spectrochim. Acta Part A Mol. Biomol. Spectrosc. 84 (1) (2011) 275–285.
[25] L. Malacaria, G.A. Corrente, E. Furia, Thermodynamic study on the dissociation and complexation of coumarinic acid with neodymium (III) and dioxouranium (VI) in aqueous media, Appl. Sci. 11 (2021) 4475.
[26] L. Malacaria, G.A. Corrente, A. Beneduci, E. Furia, T. Marino, G. Mazzone, A review on coordination properties of Al(III) and Fe(III) towards natural antioxidant molecules: experimental and theoretical insights, Molecules 26 (9) (2021) 2603.
[27] E. Furia, G. Sindona, Interaction of iron (III) with 2-hydroxybenzoic acid in aqueous solutions, J. Chem. Eng. Data 57 (1) (2012) 195–199.
[28] E. Furia, G. Sindona, Complexation of L-cystine with metal cations, J. Chem. Eng. Data 55 (2010) 2985–2989.
[29] E. Vasca, S. Materazzi, T. Caruso, O. Milano, C. Fontanella, C. Manfredi, Complex formation between phytic acid and divalent metal ions: a solution equilibria and solid state investigation, Anal. Bioanal. Chem. 374 (2002) 173–178.
[30] E. Furia, A. Napoli, A. Tagarelli, G. Sindona, Speciation of 2-hydroxybenzoic acid with calcium (II), magnesium (II), and nickel (II) cations in self-medium, J. Chem. Eng. Data 58 (5) (2013) 1349–1353.
[31] K. Emerson, W.M. Graven, Equilibria in acidic solutions of chromium (III) perchlorate, J. Inorg. Nucl. Chem. 11 (4) (1959) 309–313.
[32] E. Furia, D. Aiello, L. Di Donna, F. Mazzotti, A. Tagarelli, H. Thangavel, A. Napoli, G. Sindona, Mass spectrometry and potentiometry studies of Pb (II)–, Cd (II)– and Zn (II)–cystine complexes, Dalton Trans. 43 (2014) 1055–1062.
[33] SAINT, version 6.45, Bruker Analytical X-ray Systems, Madison, WI (2003).
[34] a) G.M. Sheldrick, SADABS Program for Absorption Correction, version 2.10, Analytical X-ray Systems, Madison, WI (2003); b) L. Krause;
b) L. Krause, R. Herbst-Irmer, G.M. Sheldrick, D. Stalke, Comparison of silver and molybdenum microfocus X-ray sources for single-crystal structure determination, J. Appl. Cryst. 48 (2015) 3–10.
[35] a) G.M. Sheldrick, SHELXT - integrated space-group and crystal-structure determination, Acta Cryst. C 71 (2015) 3–8;
b) G.M. Sheldrick, Acta crystallographica a-foundation and advances, Acta Cryst. A64 (2008) 112–122;
c) SHELXTL-2013/4, Bruker Analytical X-ray Instruments, Madison, WI (2013).
[36] a) A.L. Spek, Structure validation in chemical crystallography, Acta Crystallogr. Sect. D Biol. Crystallogr. 65 (2009) 148–155;
b) A.L. Spek, PLATON SQUEEZE: a tool for the calculation of the disordered solventcontribution to the calculated structure factors, Acta Crystallogr. Sect. C-Struct. Chem. 71 (2015) 9–18.
[37] L.J. Farrugia, WinGX suite for small-molecule single-crystal crystallography, J. Appl. Cryst. 32 (1999) 837–838.
[38] D. Palmer, CRYSTAL MAKER, Cambridge University Technical Services (1996).
[39] P. Gans, A. Sabatini, A. Vacca, Superquad,, An improved general program for computation of formation constants from potentiometric data, J. Chem. Soc., Dalton Trans. 6 (1985) 1195–1200.
[40] D. Aiello, E. Furia, C. Siciliano, D. Bongiorno, A. Napoli, Study of the coordination of *ortho*-tyrosine and *trans*-4-hydroxyproline with aluminum (III) and iron (III), J. Mol. Liq. 269 (2018) 387–397.
[41] H.P. Srivastava, D. Tiwari, Equilibrium studies of poly nucleating dye with bivalent metal ions, Indian J. Chem. 34A (1995) 550–555.
[42] N.V. Plyasunova, Y. Zhang, M. Muhammed, Critical evaluation of thermodynamics of complex formation of metal ions in aqueous solutions. IV. Hydrolysis and hydroxo-complexes of Ni^{2+} at 298.15 K, Hydrometallurgy 48 (1) (1998) 43–63.
[43] C. Rigano, A. De Robertis, S. Sammartano, Computer analysis of equilibrium data in solution. a method for computing the formation constants of two mass balance systems, from potentiometric measurements, applied to the hydrolysis of copper(II), Trans. Metal Chem. 10 (1) (1985) 1–4.
[44] P. Cardiano, R.M. Cigala, F. Crea, C. De Stefano, O. Giuffrè, S. Sammartano, G. Vianelli, Potentiometric, UV and ^{1}H NMR study on the interaction of penicillin derivatives with Zn (II) in aqueous solution, Biophys. Chem. 223 (2017) 1–10.

Supplementary Material

Experimental insights on the coordination modes of coumarin-3-carboxilic acid towards Cr(III)-, Co(II)-, Ni(II)-, Cu(II)- and Zn(II): a detailed potentiometric and spectroscopic investigation in aqueous media

Luana Malacaria, Rosaria Bruno, Giuseppina Anna Corrente, Donatella Armentano, Emilia Furia*, Amerigo Beneduci

Dipartimento di Chimica e Tecnologie Chimiche, Università della Calabria, Via P. Bucci, Cubo 12/D, 87036 Arcavacata di Rende, Cosenza, Italy

Table of Contents

Table S1. Some primary data for Co(II)-HCCA system.

V_T, mL 5.01 mM OH^-	E, mV	C_L, mM	C_M, mM	$[H^+]$, mM	C_H, mM	pH	$([H^+]- C_H)/ C_L$
0	168.59	0.001197	0.00117	0.001545193	0.00109234	2.811017	0.38
0.6	166.16	0.001167	0.001141	0.0014109	0.000940415	2.850504	0.40
1.1	164	0.001143	0.001118	0.001301359	0.000819472	2.885603	0.42
1.55	162	0.001123	0.001098	0.00120753	0.00071475	2.918102	0.44
2.1	159.52	0.001098	0.001074	0.001100523	0.000591758	2.958401	0.46
2.7	156.64	0.001073	0.00105	0.000988098	0.000463473	3.0052	0.49
3.3	153.58	0.001049	0.001026	0.000881204	0.000340933	3.054924	0.51
3.8	150.99	0.00103	0.001007	0.000799816	0.00024293	3.09701	0.54
4.4	147.71	0.001008	0.000986	0.000707443	0.000129964	3.150309	0.57
4.9	144.8	0.00099	0.000968	0.000634461	3.94718E-05	3.197595	0.60
5.4	141.67	0.000973	0.000952	0.000564344	-4.78893E-05	3.248456	0.63
5.8	138.88	0.00096	0.000939	0.000508402	-0.000115631	3.293793	0.65
6.25	135.65	0.000945	0.000924	0.000450527	-0.000189664	3.346279	0.68
6.6	132.98	0.000934	0.000914	0.000407694	-0.000245714	3.389665	0.70
7	129.5	0.000922	0.000902	0.00035792	-0.000308197	3.446214	0.72
7.35	126.21	0.000912	0.000891	0.000316464	-0.00036154	3.499675	0.74
7.65	123.46	0.000903	0.000883	0.000285521	-0.000406308	3.544361	0.77
8	119.82	0.000893	0.000873	0.000249167	-0.00045746	3.60351	0.79
8.3	116.21	0.000884	0.000865	0.000217685	-0.000500409	3.662171	0.81
8.55	112.75	0.000877	0.000858	0.000191252	-0.000535585	3.718395	0.83
8.8	109.27	0.000871	0.000851	0.000167902	-0.000570217	3.774943	0.85
9	106.08	0.000865	0.000846	0.000149012	-0.000597538	3.826779	0.86
9.2	102.74	0.00086	0.000841	0.000131506	-0.000624526	3.881053	0.88
9.4	98.89	0.000855	0.000836	0.000113864	-0.000651185	3.943614	0.90
9.55	95.68	0.000851	0.000832	0.000100978	-0.000670968	3.995775	0.91
9.7	92.21	0.000847	0.000828	8.86827E-05	-0.000690572	4.052161	0.92
9.85	88.15	0.000843	0.000825	7.61843E-05	-0.00071	4.118135	0.93
10	83.54	0.000839	0.000821	6.41143E-05	-0.000729254	4.193045	0.95
10.15	78.76	0.000836	0.000817	5.36144E-05	-0.000748336	4.270718	0.96
10.25	75.33	0.000833	0.000815	4.71569E-05	-0.000760963	4.326454	0.97
10.35	71.13	0.000831	0.000812	4.02993E-05	-0.000773516	4.394703	0.98
10.4	68.97	0.000829	0.000811	3.71705E-05	-0.000779764	4.429802	0.98

10.5	64.01	0.000827	0.000809	3.08745E-05	-0.000792206	4.5104	1.00
10.55	61.48	0.000826	0.000808	2.80859E-05	-0.000798399	4.551511	1.00
10.6	58.49	0.000825	0.000806	2.51132E-05	-0.000804575	4.600097	1.01
10.65	55.37	0.000823	0.000805	2.23462E-05	-0.000810732	4.650796	1.01
10.7	52.15	0.000822	0.000804	1.98098E-05	-0.000816871	4.70312	1.02
10.75	48.53	0.000821	0.000803	1.73004E-05	-0.000822993	4.761943	1.02
10.8	44.67	0.00082	0.000802	1.49738E-05	-0.000829096	4.824667	1.03
10.85	40.38	0.000819	0.000801	1.27533E-05	-0.000835182	4.894378	1.04
10.9	35.87	0.000817	0.000799	1.0773E-05	-0.00084125	4.967663	1.04
10.95	31.4	0.000816	0.000798	9.11383E-06	-0.0008473	5.040299	1.05
11	26.55	0.000815	0.000797	7.60135E-06	-0.000853333	5.11911	1.06
11.05	22.01	0.000814	0.000796	6.41383E-06	-0.000859349	5.192883	1.06
11.15	8.71	0.000812	0.000794	3.8994E-06	-0.000871328	5.409002	1.08
11.2	2.97	0.00081	0.000793	3.14576E-06	-0.000877291	5.502275	1.09
V_T, mL 20.5 mM OH^-	***E*, mV**	**C_L, mM**	**C_M, mM**	**$[H^+]$, mM**	**C_H, mM**	**pH**	**$([H^+]- C_H)/ C_L$**
2.1	168.54	0.0037625	0.001074219	0.001014699	-0.000678945	2.993662658	0.45
2.5	165.48	0.003704615	0.001057692	0.000904927	-0.000984038	3.043386415	0.51
2.85	161.92	0.003655408	0.001043643	0.000792073	-0.001243397	3.101234969	0.56
3.15	159.31	0.003614259	0.001031895	0.000718379	-0.001460281	3.143646409	0.60
3.5	154.73	0.003567407	0.001018519	0.000605244	-0.001707222	3.218069548	0.65
3.75	151.04	0.003534679	0.001009174	0.000527193	-0.001879725	3.278030549	0.68
4.15	147.72	0.003483544	0.000994575	0.000465608	-0.002149241	3.331979201	0.75
4.35	144.25	0.003458528	0.000987433	0.000408917	-0.002281095	3.388365291	0.78
4.5	141.33	0.00344	0.000982143	0.000366594	-0.00237875	3.435814105	0.80
4.65	138.03	0.00342167	0.000976909	0.000324013	-0.002475364	3.489437764	0.82
4.8	134.4	0.003403534	0.000971731	0.000282863	-0.002570954	3.548423789	0.84
4.95	130.44	0.003385589	0.000966608	0.000243909	-0.002665536	3.612772181	0.86
5.1	125.62	0.003367832	0.000961538	0.00020366	-0.002759126	3.691095223	0.88
5.25	121.26	0.003350261	0.000956522	0.000173004	-0.002851739	3.761943451	0.90
5.45	112.7	0.003327116	0.000949914	0.000125591	-0.002973731	3.901039974	0.93
5.55	107.43	0.003315663	0.000946644	0.000103116	-0.003034096	3.986675333	0.95
5.6	104.46	0.003309966	0.000945017	9.22706E-05	-0.003064124	4.034936627	0.95
5.65	100.81	0.003304288	0.000943396	8.04919E-05	-0.003094048	4.094247644	0.96
5.7	95.76	0.00329863	0.000941781	6.66334E-05	-0.00312387	4.176308092	0.97

5.75	91.32	0.003292991	0.000940171	5.64344E-05	-0.00315359	4.248456289	0.97
5.8	86.16	0.003287372	0.000938567	4.6526E-05	-0.003183208	4.332304192	0.98
5.85	81.81	0.003281772	0.000936968	3.95376E-05	-0.003212726	4.402989925	0.99
5.9	76.22	0.00327619	0.000935374	3.20756E-05	-0.003242143	4.493825154	1.00
5.95	62.03	0.003270628	0.000933786	1.88622E-05	-0.00327146	4.72440689	1.01
6	51.3	0.003265085	0.000932203	1.26251E-05	-0.003300678	4.898765031	1.01
6.05	39.31	0.00325956	0.000930626	8.06125E-06	-0.003329797	5.09359766	1.02
6.1	29.72	0.003254054	0.000929054	5.63078E-06	-0.003358818	5.249431264	1.03
6.15	19.27	0.003248567	0.000927487	3.80856E-06	-0.00338774	5.419239519	1.04
6.2	8.71	0.003243098	0.000925926	2.56546E-06	-0.003416566	5.590835229	1.05
6.25	-3.21	0.003237647	0.00092437	1.64236E-06	-0.003445294	5.784530387	1.06
6.3	-17.72	0.003232215	0.000922819	9.54307E-07	-0.003473926	6.020311992	1.08
6.35	-36.05	0.003226801	0.000921273	4.80654E-07	-0.003502462	6.318167046	1.09

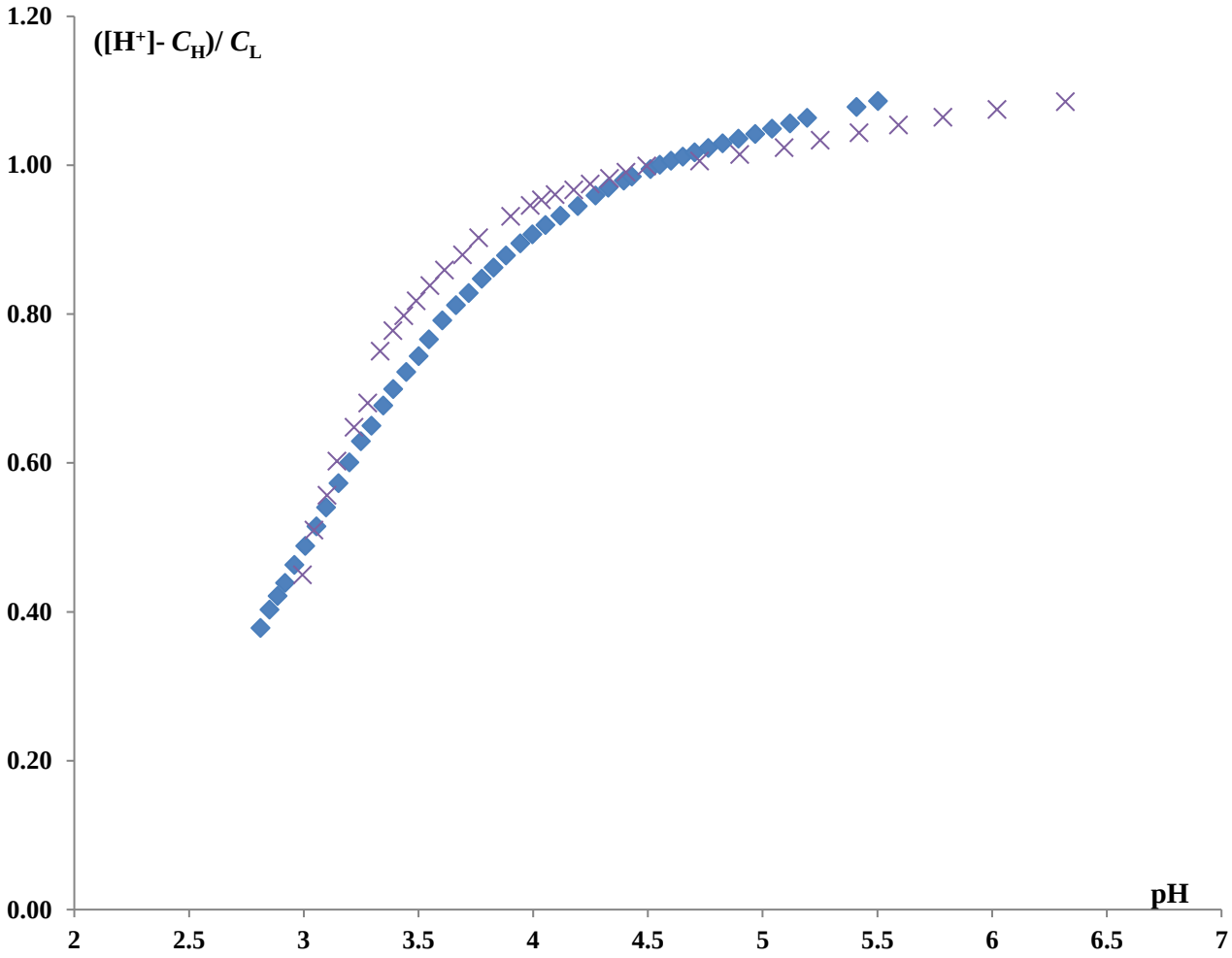

Fig. S1. Average number of protons released by the ligand *vs* pH.

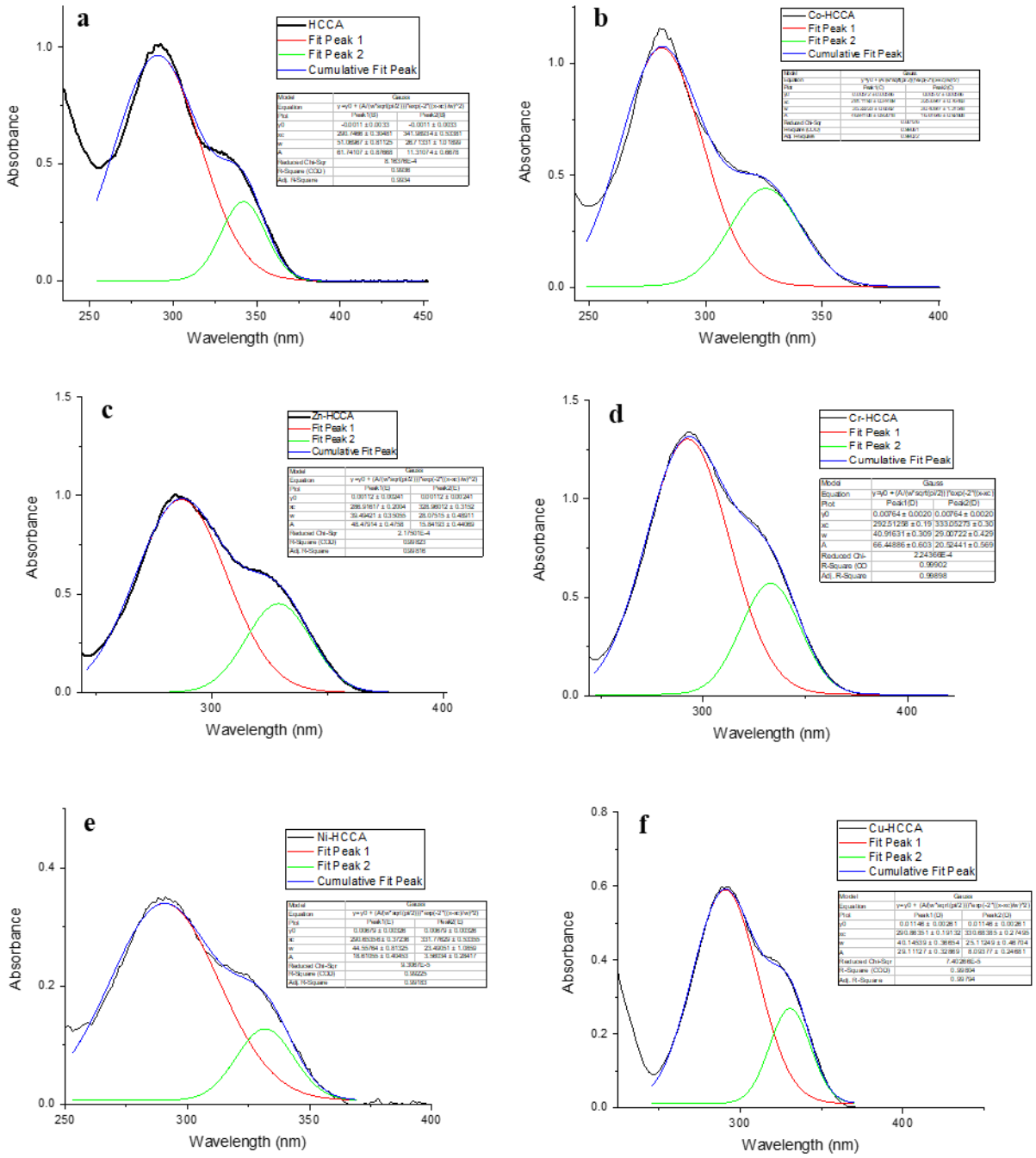

Fig. S2. Deconvolution of UV-Vis spectra of the (a) free ligand (HCCA) and of the complexes (b) Co-HCCA, (c) Zn-HCCA, (d) Cr-HCCA, (e) Ni-HCCA and (f) Cu-HCCA.

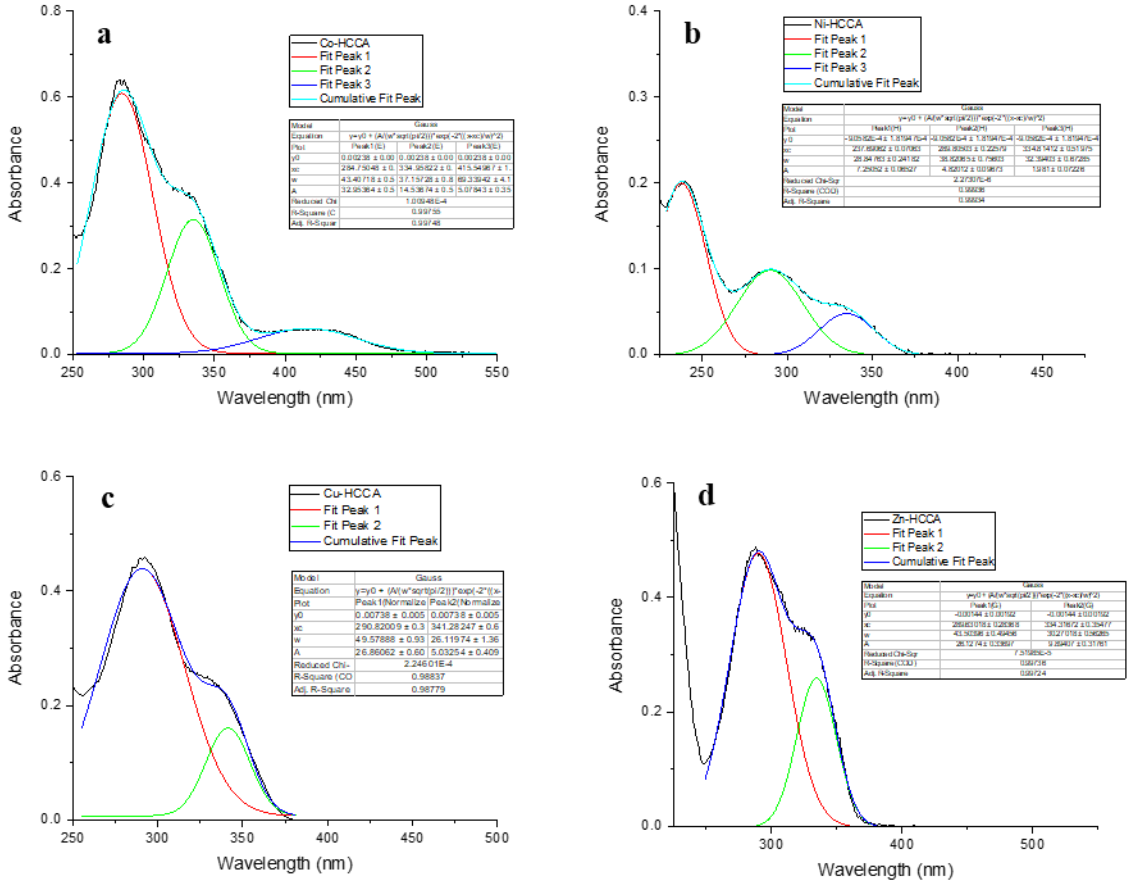

Fig. S3. Deconvolution of UV-Vis spectra of the solid compounds obtained during titration (a) Co-HCCA, (b) Ni-HCCA (c) Cu-HCCA and (d) Zn-HCCA.

Journal of Molecular Liquids 355 (2022) 118973

Contents lists available at ScienceDirect

Journal of Molecular Liquids

journal homepage: www.elsevier.com/locate/molliq

Experimental and theoretical study of the complexation of Fe^{3+} and Cu^{2+} by L-ascorbic acid in aqueous solution

Alessandra G. Ritacca [1], Luana Malacaria [1], Emilia Sicilia, Emilia Furia *, Gloria Mazzone *

Dipartimento di Chimica e Tecnologie Chimiche, Via P. Bucci, Università della Calabria, I-87036 Arcavacata di Rende (CS), Italy

ARTICLE INFO

Article history:
Received 12 January 2022
Revised 16 March 2022
Accepted 18 March 2022
Available online 22 March 2022

Keywords:
Ascorbic acid
Iron ascorbate complexes
Copper ascorbate complexes
Stability constants
DFT
TDDFT

ABSTRACT

In this study, the ability of L-ascorbic acid to form complexes with Fe^{3+} and Cu^{2+} ions was investigated by using a combination of potentiometric measurements and DFT computations with the aim to recognize the coordination modes of the ligand and the most reliable complexes. Speciation profiles obtained by potentiometric titrations in aqueous solution (*i.e.*, 0.16 M NaCl), and supported by UV–Vis data, show that a complexation occurs at 1:1 and 1:2 Fe(III)-to-ligand ratios and at 1:1, 1:2 and 1:3 Cu(II)-to-ligand ratios. The most plausible structures were firstly hypothesized by considering a general equilibrium that considers the effective ligands which enter in the coordination sphere of the metal ions: the anionic forms of ascorbic acid and hydroxide ion. Computational tools were, thus, exploited to ascertain the feasibility of the hypothesized complexes formation.

1. Introduction

Antioxidants are substances that protect the body from destructive oxidation reactions by interacting with free radicals and other reactive oxygen species within the body. Among them, L-ascorbic acid (vitamin C, H_2Asc, Scheme 1) is an extremely interesting molecule that possesses many important biochemical properties.

It is a water-soluble antioxidant that exists in pure form as a white crystalline solid and it is found naturally in a wide variety of plants and animals [1,2]. It has also been associated with the prevention of many degenerative diseases [2]. Vitamin C is the term frequently used to refer to L-ascorbic acid in a nutritional context, and it also encloses the oxidation product, the dehydroascorbic acid, which has similar activity *in vivo* to the parent compound [3]. The L-ascorbic acid has a high reactivity that makes the storage in the liquid and solid phases difficult due to the presence in its structure of an ene-diol group that boosts a high biological activity and powerful reducing properties. In aqueous environments, it exists as an acid that is easily deprotonated to ascorbate anion. L-Ascorbic acid is essential to man and, such as other vitamins, is not produced by the human body; thus, the only source is from diet. A fundamental characteristic of the L-ascorbic acid chemistry is its redox behavior, and much of the loss of vitamin C from foods and drinks seems to be due to the oxidation process by dioxygen. Thus, the degradation of ascorbic acid is related to juice flavor and color changes [4]. When stored, this substance is very unstable against moisture, air oxygen, light, heat, metal ions and can be easily transformed into biologically inactive or harmful products [5]. In particular, the oxidizing mechanisms of ascorbic acid in aqueous solutions are known to involve its partially dissociated forms [6–9].

Particularly interesting in the context of transition metal chemistry is the ability of L-ascorbic acid to form chelate complexes with transition metal ions. The structures of these complexes, deduced from spectroscopic studies, reveal that a five-membered ring with the ene-diol part of the molecule can be formed [1]. Many studies of equilibria occurring between ascorbate and metal ions [10] were reported and most of them have involved spectroscopic, potentiometric and kinetic measurements. The stabilities of metal ion complexes with ascorbic acid and ascorbate anions are in general lower than might were expected. The combination of problems associated with rapid redox reactions, hydrolysis and precipitation of metal ions, very likely, explains why only few studies of complex formation with ascorbate at pH higher than 7 were performed [11–19].

In a previous work we have investigated the formation of Al^{3+} and Ni^{2+}–L-ascorbic acid complexes in aqueous solution by using a combination of experimental and computational tools [20]. The metal-to-ligand ratios obtained by a potentiometric approach were

* Corresponding authors.
E-mail addresses: emilia.furia@unical.it (E. Furia), gloria.mazzone@unical.it (G. Mazzone).
[1] these authors contributed equally to this work.

https://doi.org/10.1016/j.molliq.2022.118973
0167-7322/

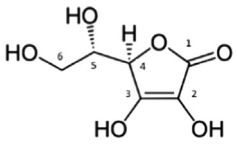

Scheme 1. Chemical structure of L-ascorbic acid, H_2Asc.

theoretically examined to obtain the most plausible structures of the proposed species. DFT computational exploration indicated that the preferred complexation sites of L-ascorbic acid are the deprotonated donor oxy-groups at C2 and C3 (see Scheme 1). In this framework, the present experimental and computational investigation aims at determining the stoichiometry and the corresponding stability of the complexes formed by Fe^{3+} and Cu^{2+} ions with L-ascorbic acid at 37 °C in aqueous media (*i.e.*, 0.16 M NaCl) and their structural properties. This background salt was chosen to control the ionic strength as it is possible to prepare solutions with a high degree of purity and due to its high inertia towards complexation with the investigated metals.

Some works reported computational exploration of Cu^{2+} and Fe^{3+} complexes formations with some advanced glycation end products (AGEs) inhibitors, including ascorbic acid [21–23]. However, such investigations were based exclusively on the acid-base properties of the ligands at physiological pH (mono-anionic $HAsc^-$ as the most abundant species of H_2Asc) and on the most probable structural arrangements around the metal centers (square-planar and octahedral for Cu^{2+} and Fe^{3+}, respectively). No influences of the metal nature on the behavior of the ligand were explicitly taken into consideration. Accordingly, in searching for complexes with 1:2 and 1:3 metal to ligand stoichiometric ratios for Cu^{2+} and Fe^{3+}, respectively, the most stable complexes were found to be square-planar and octahedral with two and three ascorbate ligands coordinated in an η^2 fashion, respectively [22,23]. The monoanion $HAsc^-$ was, thus, considered as a bidentate ligand that coordinates to the metal through the O^- and OH set of donors. A more recent study traces such exploration, but the obtained complexes are all characterized by a mono-coordination of the $HAsc^-$ ligand and the presence of water molecules used to complete the coordination sphere of the metal [21]. Our computational exploration aims to detect the most plausible complexes of Cu^{2+} and Fe^{3+} with H_2Asc in an aqueous solution using potentiometric titrations as a guide. These redox-active metal ions exert their toxic action by forming reactive oxygen species (ROS) [24]. Current treatment options for metal cations overload aim at removing tissue deposits, which cause the toxic effects, by using a selective and specific natural ligand. In this context, stability of metal-chelator complexes is extremely important for the choice of the most adequate chelating agent. The knowledge of metal–ligand speciation profiles at 37 °C in aqueous media (*i.e.*, 0.16 M NaCl) allows to reveal the chelating agent activity *in vitro* or *in vivo*.

2. Experimental section

2.1. Materials

Sodium chloride, hydrochloric acid and sodium hydroxide titrant solutions were prepared and standardized as reported in a previous study [20]. Iron(III) and copper(II) chloride stock solutions were prepared and standardized as reported previously [25]. L-Ascorbic acid (Sigma-Aldrich p.a., 99.2%) was kept in a desiccator over silica gel and was used without further purification. The ligand is susceptible to oxidation thus each experiment was started from a freshly prepared solution and the measurements were performed under nitrogen atmosphere.

2.2. Potentiometric and spectrophotometric measurements

The potentiometric apparatus was the same described in a previous work [25]; during the EMF measurements, the cell assembly was placed in a thermostat kept at (37.0 ± 0.1) °C.

The complex formation equilibria between H_2Asc and Fe(III) and Cu(II) cations were studied by measuring with a glass electrode, GE, the competition of H^+ and metal cations for the ascorbate ion. To minimize activity coefficient changes, test solutions were made to contain 0.16 M NaCl. Measurements were performed as potentiometric titrations with cell (G)

RE / Test Solution / GE (G)

where the reference electrode, RE, has the composition

Ag / AgCl / 0.01 M NaCl / (0.16 −0.01) M NaCl / 0.16 M NaCl

and Test Solution = C_M M $M(Cl)_n$, C_L M H_2Asc, C_A M HCl, C_B M NaOH, (0.16 − n C_M − C_A − C_B) M NaCl. The metal concentration, C_M, ranged from 0.1 to 1.0 mM, the ligand concentration, C_L, was varied between 1 and 10 mM and $1 \leq C_L/C_M \leq 10$.

The hydrogen ion concentration was varied from 10^{-2} M to incipient precipitation of basic salts, which takes place in the range $[H^+] = 3.55 \cdot 10^{-4}$–$1 \cdot 10^{-5}$ M (*i.e.*, pH = 3.45–5) depending on the metal ion involved and on the specific metal to ligand ratio investigated. Since the effects of composition changes on activity coefficients can be considered negligible, the EMF of cell (G) can be written, in mV and at 37 °C, as equation (1):

$$E = E^{\circ} + 61.54 \log[H^+] + E_j \quad (1)$$

where E° is constant in each series of measurements, E_j is the liquid junction potential which is a function of $[H^+]$ only [26]. In a previous study we have determined the value of j (mV/M) under the same experimental conditions [27]. In the first part of each titration E° was determined in the absence of ligand and metal ions, and the alkalinization was attained by adding NaOH standard solutions.

To verify the formation of complexes, spectrophotometric measurements, achieved with a Varian Cary 50 Scan UV Visible Spectrophotometer, were realized by registering the absorbance values, A_λ, (to 0.001 units) between 200 and 500 nm each 1 nm. Matched quartz cells of thickness 1 cm were used. The temperature of the cell holder was kept at (37.0 ± 0.3) °C by a Grant circulating water bath. The data acquisition of and the formulations of the parameters were managed with the aid of a computer directly connected to the spectrophotometer by using the supplied software.

2.3. Computational details

All the electronic calculations involving copper(II) and iron(III) complexes were carried out at the DFT level of theory using the hybrid Becke three parameter exchange functional and the Lee-Yang-Parr correlation functional B3LYP [28,29] by means of the Gaussian16 software package [30]. Since nonbonding interactions play a very important role in such case, Grimme's dispersion correction [31] were included using atom pair-wise additive scheme, DFT-D3 method. The standard 6-311G** basis set was adopted to describe all the atoms. All structures were fully relaxed without imposing any constrain and were confirmed to be minima by harmonic vibrational frequencies calculation. In order to simulate the aqueous environment, the implicit continuum solvation model based on density (SMD) [32], with a dielectric constant of 78.35, was employed in all the optimizations. For the assessment of the final free energy changes, single point calculations at M05 [33]/6–311+G** level in water solvent were carried out. For every complexation reaction, free energy was computed replacing water molecules in the reference *hexa*-aquo complexes. The reference

complex is octahedral for Fe(III) and square planar with four water molecules in the first shell and two water molecules in the second coordination shell for Cu(II) [34,35].

The whole process in solution is described as follows:

$$[M(H_2O)_6]^z + nL^c \rightarrow [ML_n]^{c+z} + (6 - n - t)H_2O \quad (2)$$

where L could be the ascorbic acid ligand, in its neutral, deprotonated and di-deprotonated forms, or the OH^- one, c is the total formal charge of the n ligands and z the charge of the *hexa*-aquo complex, whereas the possibility that the ligands are mono or bidentate is taken into consideration by the parameter t = 0, 1, 2, 3. Therefore, the free energies of formation of these complexes are calculated as:

$$\Delta G = \Delta G([ML_n]^{c+z}) + (6 - n - t)\,\Delta G(H_2O) - \Delta G([M(H_2O)_6]^z - \Delta G(nL)^c \quad (3)$$

Enthalpies and Gibbs free energies were obtained using standard statistical procedures [36] at 298 K and 1 atm from total energies, including zero-point and thermal corrections. As the free energy corrections in the Gaussian default standard state correspond to an ideal gas at a standard pressure of 1 atm, the computed free energies were converted [37] to yield Gibbs energies with a solution phase standard state of 1 mol L^{-1} for all the species except water solvent. For water molecules a standard state of 55.5 M was used. The most stable spin state of the Cu(II) and Fe(III) complexes was established through the optimization of the respective *hexa*-aquo reference compounds and resulted to be doublet and sextet, respectively. In order to test and confirm that the spin multiplicity is conserved after complexation, some of the metal–ligand systems were also checked for their stability as a function of spin multiplicity. To explore the behavior upon metal complexation, UV–vis spectra were calculated in water including 50 electronic excitations using the time-dependent extension of DFT, TDDFT. To carry out TDDFT calculations the B3LYP/6-311G** protocol was adopted.

3. Results and discussion

3.1. Stability of Cu(II) and Fe(III) complexes with L-ascorbic acid

The general equilibrium leading to the formation of the investigated complexes can be written schematically as reported in equation (4), which considers all the possible complexes formed in solution (*i.e.*, simple $q = r$, mixed $q \neq r$, mononuclear p and $r = 1$, and polynuclear p and r greater than 1 species), and all the potential chelation sites of ascorbic acid which correspond to a different number of protons involved in the coordination.

$$pM^{n+} + rH_2Asc \rightleftarrows M_p(H)_{-q}(H_2Asc)_r^{(np-q)} + qH^+ \log \beta_{p,q,r} \quad (4)$$

The ascorbic acid acidic constants, already both computationally and experimentally estimated [20], as well as the constants of principal cationic hydrolysis products taken from literature [38,39] (*i.e.*, $Fe(OH)^{2+}$ and $Fe(OH)_2^+$, $Cu(OH)^+$ and $Cu_2(OH)_2^{2+}$), were kept invariant in the numerical treatment to determine stability constants $\beta_{p,q,r}$.

The most probable p, q, and r values and the corresponding constants log $\beta_{p,q,r}$ were computed by a numerical approach [40]. Speciation profiles show that in aqueous solution a complexation occurs at 1:1 and 1:2 Fe(III)-to-ligand ratios and at 1:1, 1:2 and 1:3 Cu(II)-to-ligand ratios and results obtained are reported in the Table 1.

The effective formation of the complexes was verified by analyzing, by UV–Vis spectrophotometry, all solutions obtained at the end of each titration. A comparison of the UV–Vis spectra of the free ligand, free metal ion solutions and coordinated species is reported in the Supplementary data (Fig. S1 a-b). According to literature, the UV–Vis spectrum of free ascorbic acid shows a single band centered at 260 nm [41]. The UV–Vis spectra recorded in solutions containing metal cations show a significant shift of this characteristic band, confirming the occurred complexation.

Table 1
Formation of complexes of H_2Asc with Fe(III) and Cu(II), according to Eq. (4). Values of log $\beta_{p,q,r}$ in NaCl 0.16 M at 37 °C were obtained by numerical procedure (standard deviations are reported as 3 σ).

	p,q,r	Species	log $\beta_{p,q,r}$ ± 3 σ
Fe(III)	1,-2,1	$Fe(H)_{-2}(H_2Asc)^+$	−2.4 ± 0.1
	1,-3,1	$Fe(H)_{-3}(H_2Asc)$	−4.1 ± 0.1
	1,-4,1	$Fe(H)_{-4}(H_2Asc)^-$	−6.90 ± 0.09
	1,-4,2	$Fe(H)_{-4}(H_2Asc)_2$	−5.0 ± 0.1
Cu(II)	1,-3,1	$Cu(H)_{-3}(H_2Asc)^-$	−5.11 ± 0.06
	1,-4,2	$Cu(H)_{-4}(H_2Asc)_2^{2-}$	−4.0 ± 0.2
	1,-6,3	$Cu(H)_{-6}(H_2Asc)_3^{4-}$	−5.6 ± 0.1

3.2. Identification of the most plausible complexes

In order to identify the most probable complexes between the titled metal cations and L-ascorbic acid, we have first hypothesized plausible structures by considering the general equilibrium reported in equation (5), taking into account the effective ligands which enter in the coordination sphere of the metal ions. For this purpose, both the acid-base properties of the ligand [20] and the nature of metal centers and, thus, their behavior in aqueous environment was taken into consideration.

$$pM^{n+} + qOH^- + rAsc^{2-} \rightleftarrows M_p(OH)_q(Asc)_r^{(np-q-2r)} \log \beta \quad (5)$$

In this equilibrium the di-anionic (Asc^{2-}) form was considered. The existence of such species is plausible, even at low pH, as consequence of metal coordination due to the ability of the metal ions to compete with protons for the binding of ascorbate oxy groups. The stability constants were, thus, calculated according to such equilibrium and outcomes are summarized in Table 2.

The distribution diagrams in (Fig. 1 a-c) show the percentage of metal cations into the hypothesized complexes as a function of the pH. For the Fe(III)-H_2Asc system this percentage is independent on the specific investigated metal to ligand ratio, while for the Cu(II)-H_2Asc system is strongly dependent on the studied ratio. For that reason, it was necessary to report two different C_M/C_L ratios (*i.e.*, Fig. 1 b-c) for Cu(II).

Since this work is the first one entirely in aqueous medium, any comparison with previous literature data is not possible. Hence, in order to confirm the hypothesized structures (Table 2), a computational study was achieved. Due to the possibility that even the mono-anionic species could be involved in the complexation of both metal cations at the working pH, the number of complexes to take into consideration significantly increased. Indeed, given the value of the first pK_a, H_2Asc should easily lose the first proton to form the ascorbate anion $HAsc^-$ which can play a role in the investigated range of pH, whereas the loss of the second proton to form the Asc^{2-} species can be hypothesized only upon metal coordination. Accordingly, even though the hypotheses formulated from potentiometric measurements consider only the Asc^{2-} species as plausible ascorbic acid-based ligand, computational exploration was carried out by taking into account also its mono-anionic form. Combining the data of Fig. 1 and Table 2 with the *p,q,r* triads established by potentiometric data, we searched for all the plausible combinations amongst ascorbic acid (mono- and di-anion), OH^- and water ligands and the two metal cations generating the observed complexes. Several structures corresponding to different combinations of the named ligands were taken into consideration and only those considered more plausible on the basis of the

Table 2
Stability constants of complexes of H_2Asc with Fe(III) and Cu(II), according to Eq. (5).

	p,q,r	Species	log β ± 3 σ
Fe(III)	1,0,1	$Fe(Asc)^+$	9.5 ± 0.2
	1,1,1	$Fe(OH)(Asc)$	21.1 ± 0.1
	1,2,1	$Fe(OH)_2(Asc)^-$	31.63 ± 0.09
	1,0,2	$Fe(Asc)_2^-$	18.8 ± 0.2
Cu(II)	1,1,1	$Cu(OH)(Asc)^-$	20.10 ± 0.06
	1,0,2	$Cu(Asc)_2^{2-}$	19.8 ± 0.3
	1,0,3	$Cu(Asc)_3^{4}$	30.1 ± 0.1

Table 3
Calculated complexation Gibbs free energies (ΔG, kcal mol^{-1}) of Fe(III) and Cu(II) complexes with ascorbic acid in water.

	General formula	Complexes	ΔG
Fe(III)	$Fe(Asc)^+$	$[Fe(H_2O)_4(Asc)]^+$	−62.6
		$[Fe(H_2O)_5(Asc)]^+$	−52.1
		$[Fe(OH)(H_2O)_4(HAsc)]^+$	−46.9
	$Fe(OH)(Asc)$	$[Fe(OH)(H_2O)_3(Asc)]$	−80.4
	$Fe(OH)_2(Asc)^-$	$[Fe(OH)_2(H_2O)_2(Asc)]^-$	−99.6
	$Fe(Asc)_2^-$	$[Fe(H_2O)_2(Asc)_2]^-$	−89.4
		$[Fe(OH)_2(H_2O)_2(HAsc)_2]^-$	−68.1
Cu(II)	$Cu(OH)(Asc)^-$	$[Cu(OH)(H_2O)(Asc)]^- + 2H_2O$	−46.2
	$Cu(Asc)_2^{2-}$	$[Cu(H_2O)(Asc)_2]^{2-} + H_2O$	−46.0
		$[Cu(OH)(H_2O)_2(HAsc)(Asc)]^{2-}$	−46.2
	$Cu(Asc)_3^{4-}$	$[Cu(Asc)_3]^{4-}$	−58.3
		$[Cu(OH)(HAsc)(Asc)_2]^{4-}$	−57.6

behavior of both metals and ligands in aqueous solution were reported here. The outcomes of the computational exploration were collected in Table 3 and Fig. 2.

3.2.1. Fe(III) complexes

The complexation between H_2Asc and Fe(III) starts at pH lower than 2.0 (Fig. 1a) and all the formed complexes reach high percentages, particularly the mixed species $Fe(OH)_2Asc^-$ which is the predominant one at pH higher than 3, confirming the strong affinity between the ligand and this hard metal ion. Interestingly, the percentage of the hydrolytical complex $Fe(OH)^{2+}$ decreases drastically in presence of ascorbic acid and, furthermore, $Fe(OH)_2^+$ is missing in the distribution diagram reported in (Fig. 1a). This behavior confirms the hypothesis that structures including hydroxide ions in addition to ascorbic acid in the coordination sphere of the metal ion can be formed. Therefore, considering the equilibrium sketched in equation (5), in the pH range between 2 and 3, four Fe-H_2Asc complexes can be distinguished. Two complexes involve the presence of the OH^- ligand in the first coordination shell of the metal. Among the other two species, named as $FeAsc^+$ and $Fe(Asc)_2^-$, the former is mostly present at very low pH and it is characterized by the lowest stability constant (Table 2).

Computational exploration of the plausible complexes with formula $FeAsc^+$ returns two octahedral complexes in which the metal is surrounded by four and five water molecules as the Asc^{2-} ligand

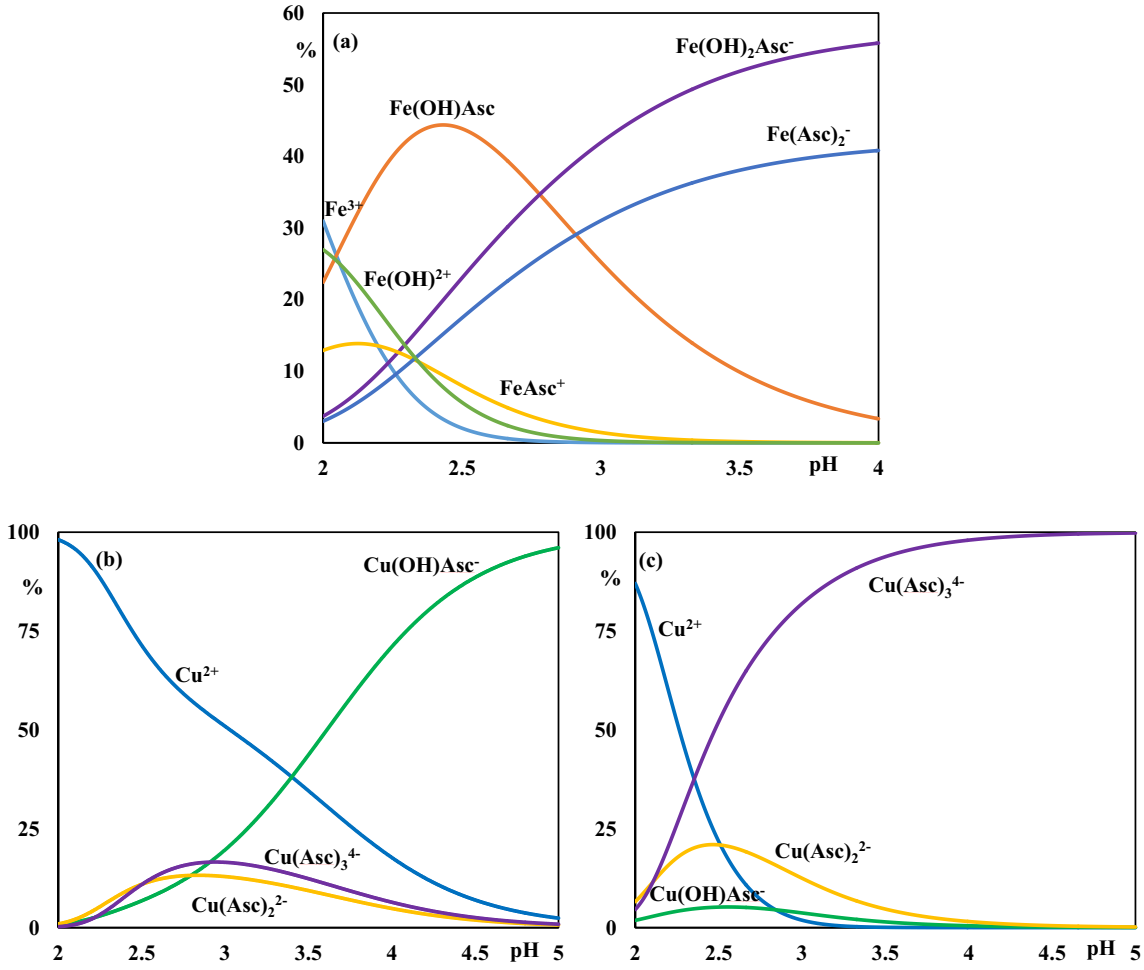

Fig. 1. Distribution diagrams in the presence of H_2Asc of: (a) Fe(III) (C_M = 1.0 mM and C_L = 10.0 mM); (b) Cu(II) (C_M = 1.0 mM and C_L = 1.0 mM) and (c) Cu(II) (C_M = 1.0 mM and C_L = 10.0 mM).

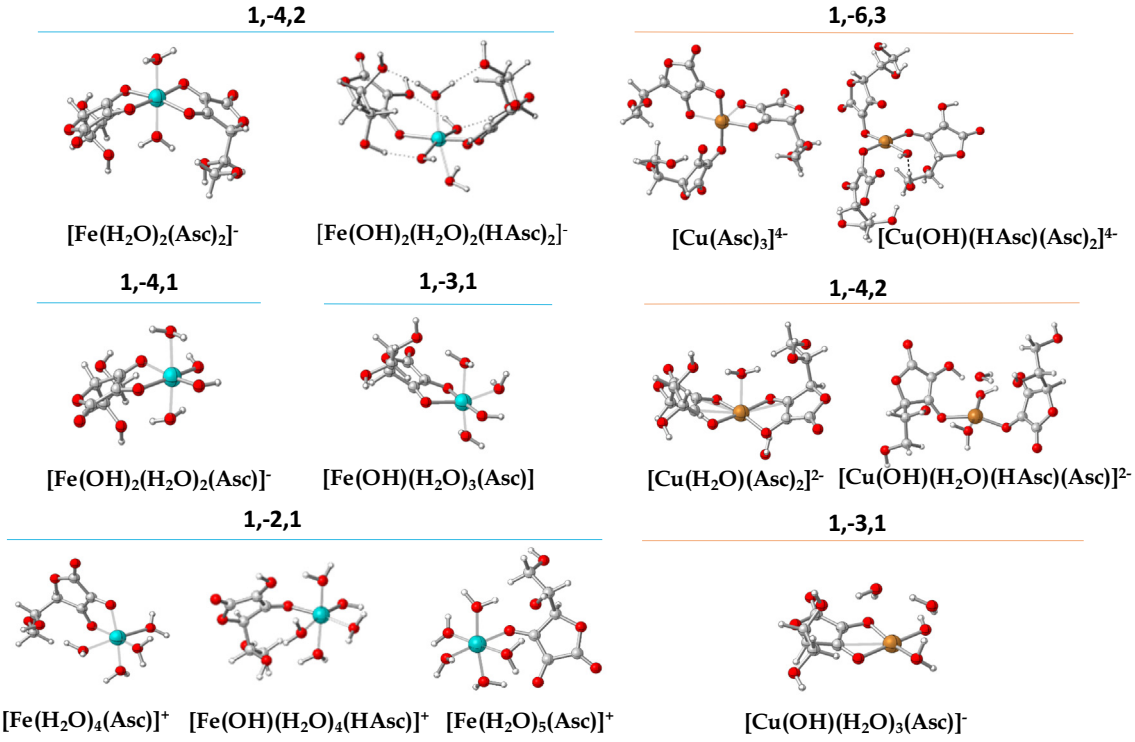

Fig. 2. B3LYP-D3/6-311G** optimized structures of Fe(III) and Cu(II) complexes with L-ascorbic acid.

is η^2- or η^1-coordinated, respectively. The first complex, labeled $[Fe(H_2O)_4(Asc)]^+$, is 10 kcal mol^{-1} more stable than the other because of chelate effect. Another complex involving coordination of $HAsc^-$ in η^1 mode and OH^-, which establishes a H-bond with a coordinated water molecule, was taken into consideration, $[Fe(OH)(H_2O)_4(HAsc)]^+$. However, on the basis of the calculated ΔG value, its formation is less probable than the others, confirming the assumption that the OH^- ligand is not involved in such formation. As regards complexes with general formula $Fe(Asc)_2^-$, two complexes were hypothesized: one in which only water molecules were considered for saturating the coordination sphere of the metal center together with the di-deprotonated ascorbate, Asc^{2-}, bi-coordinated, and another where $HAsc^-$ and OH^- ligands were supposed to surround the metal ion. The latter was found to be less stable by more than 20 kcal mol^{-1} than the first one, corroborating the involvement of Asc^{2-} species in the complexation process.

Among the species present in solution at higher pH, that with two OH^- ligands and the doubly deprotonated ascorbate bi-coordinated to the metal center, $[Fe(OH)_2(H_2O)_2(Asc)]^-$, results to be the most stable for 1:1 complexes, mirroring the highest stability constant measured for such combination in iron complexes formation (Table 2). The other plausible 1:1 complex again involves ascorbate in its di-anionic form coordinated in η^2 fashion to the metal, $[Fe(OH)(H_2O)_3(Asc)]$.

The computed complexation Gibbs free energies (Table 3) return relative stabilities of the hypothesized complexes in agreement with the experimental findings (Table 2) that suggest the complexes with general formula $Fe(OH)_2(Asc)^-$ and $Fe(Asc)^+$ to be the most and the less stable, respectively, whereas the stability of the other two plausible complexes is comparable.

It is expected that all the complexes evidenced in the distribution diagram at the final pH (Fig. 1a) should contribute to the recorded UV–vis spectrum for the Fe(III)-H_2Asc system (Figure S1a). Indeed, keeping together the three computationally characterized complexes, $[Fe(OH)_2(H_2O)_2(Asc)]^-$, $[Fe(H_2O)_2(Asc)_2]^-$ and $[Fe(OH)(H_2O)_3(Asc)]$, belonging to the general classes $Fe(OH)_2(Asc)^-$, $Fe(Asc)_2^-$ and $Fe(OH)(Asc)$, respectively, and weighting them on the basis of their abundance detected by potentiometric studies, the obtained spectrum reproduces the experimental one with a peak centered at 279 nm *vs* 266 nm experimentally found (Figure S2).

3.2.2. Cu(II) complexes

Regarding the system Cu(II)-H_2Asc we have reported two different C_L/C_M ratios (Fig. 1b and c). When the ligand and metal concentrations are comparable (Fig. 1b) the complexation becomes meaningful at pH 3.5 and the predominant species is the mixed complex $Cu(OH)Asc^-$ in the whole investigated pH range, whose percentage is higher than 95%. The other two complexes, *i.e.*, $Cu(Asc)_2^{2-}$ and $Cu(Asc)_3^{4-}$, reach percentages of almost 15%. When the ligand concentration is higher than that of the metal (Fig. 1c) the $Cu(Asc)_3^{4-}$ species is predominant in the whole investigated pH range, and the complexation starts from pH 2. The other two species, $Cu(OH)Asc^-$ and $Cu(Asc)_2^{2-}$, reach percentages lower than 25%.

In driving the computational exploration of Cu(II)-H_2Asc complexes formation, the two experimental conditions were separately taken into consideration. As stated above, when the metal and the ligand have the same concentration (*i.e.*, 1.0 mM), the complexation process starts at pH slightly higher than 3 with the formation of three species with different stoichiometry and general formula $Cu(OH)(Asc)^-$, $Cu(Asc)_2^{2-}$ and $Cu(Asc)_3^{4-}$. However, the presence of $Cu(Asc)_2^{2-}$ and $Cu(Asc)_3^{4-}$ species remains rather low within the investigated pH range. At the highest considered pH, the Cu(II) complexation preferentially leads to formation of complexes having 1:1 metal to ligand stoichiometric ratio (green line), $Cu(OH)Asc^-$. For such combination of M:L:OH ratio, exploring various coordination arrangements, the same square-planar complex was obtained, $[Cu(OH)(Asc)(H_2O)]^-$, where the ascorbate is η^2 coordinated to the metal center, whereas an OH^- ligand and a water molecule complete the coordination sphere of the metal.

For 1:2 and 1:3 metal-to-ligand stoichiometric ratios, essentially, two types of complexes for each combination were considered plausible, which differ for the presence or absence of the

OH^- ligand. For the former ratio, the structure of the complex in which only two water molecules were placed around the metal to draw an octahedral structure, during the optimization evolved to a square-pyramidal geometry, $[Cu(Asc)_2(H_2O)]^{2-}$. On the other side, when OH^- was included in the first coordination sphere of the metal centre, both mono- and di-anionic forms of ascorbic acid participated in the complexation process. Even in this case a water molecule was released and the Asc^{2-} remained anchored to the metal by one site only. The resulted two 1:2 complexes are equally stable, suggesting that, in this case, the hydroxide complex can be formed. Even for 1:3 metal to ligand stoichiometric ratio, the two hypothesized complexes, that is one in which only the ascorbate chelates the metal center, $[Cu(Asc)_3]^{4-}$, and one where the mono-anionic ascorbate ($HAsc^-$) together with OH^- were considered as plausible ligands, $[Cu(OH)(HAsc)(Asc)_2]^{4-}$, are characterized by a similar energy of formation. When the complexation was studied with an excess of ligand (Fig. 1c) the role of the two species Cu(OH)Asc^- and $Cu(Asc)_3^{4-}$ is inverted and the latter becomes the only plausible Cu(II)-H_2Asc complex. Therefore, to discern between the found 1:3 complexes, the absorption spectra were simulated and compared with the experimental one. A substantial difference between them is found. Indeed, while $[Cu(Asc)_3]^{4-}$ complex essentially exhibits the same behavior experimentally observed (Figure S1b), the hydroxide-containing complex shows an additional band around 500 nm suggesting that such complex is absent in the analyzed solution (Figure S3). Hence, the $[Cu(Asc)_3]^{4-}$ complex should be the most probable 1:3 Cu:H_2Asc complex.

Interestingly, Cu(II) complexes retain the octahedral structure only for 1:3 metal to ligand stoichiometric ratio. The neutral ligands, water molecules, were automatically released during the optimization process in all the other cases to afford both square-planar and square pyramidal structures.

In analogy with Fe(III) complexes, the relative stability of the hypothesized complexes is confirmed by the computational outcomes. Indeed, the $[Cu(Asc)_3]^{4-}$ complex is characterized by the highest energy of formation and the other two complexes, labeled with the general formula Cu(OH)Asc^- and $Cu(Asc)_2^{2-}$, exhibit the same stability.

4. Conclusions

The sequestering ability in aqueous solution at 37 °C and in 0.16 M NaCl of L-ascorbic acid towards Fe(III) and Cu(II) cations is debated in the present paper. Speciation profiles from potentiometric titrations show that a complexation occurs at 1:1 and 1:2 Fe(III)-to-ligand ratios and at 1:1, 1:2 and 1:3 Cu(II)-to-ligand ratios. To get insights on the binding modes of the examined metal ions when coordinating the ascorbic acid ligand in its neutral, mono- and di-anionic forms, a careful and detailed DFT analysis was performed. The most plausible structures were firstly hypothesized considering the effective ligands which enter the coordination sphere of the metal ions in the equilibrium reactions for deriving the stability constants. Computational approaches were, thus, used to ascertain the feasibility of the hypothesized complexes formation. The calculations confirmed the relative stability of the various complexes for different metal-to-ligand stoichiometric ratios experimentally found and helped in ascertaining whether or not hydroxido ligand could be involved in the complexation process of Fe(III) and Cu(II) cations by ascorbic acid.

Declaration of Competing Interest

The authors declare that they have no known competing financial interests or personal relationships that could have appeared to influence the work reported in this paper.

Acknowledgements

The authors thank Dipartimento di Chimica e Tecnologie Chimiche, Università della Calabria for the financial support.

Appendix A. Supplementary material

Supplementary data to this article can be found online at https://doi.org/10.1016/j.molliq.2022.118973.

References

[1] Michael B. Davies, Reactions of L-ascorbic acid with transition metal complexes, Polyhedron. 11 (3) (1992) 285–321, https://doi.org/10.1016/S0277-5387(00)83175-7.
[2] Reeshemah N. Allen, M.K. Shukla, Demarcio Reed, Jerzy Leszczynski, Ab initio study of the structural properties of ascorbic acid (vitamin C), Int. J. Quantum Chem. 106 (14) (2006) 2934–2943, https://doi.org/10.1002/qua.21118.
[3] J Mårtensson, A Meister, Glutathione deficiency increases hepatic ascorbic acid synthesis in adult mice, Proc. Natl. Acad. Sci. U. S. A. 89 (23) (1992) 11566–11568, https://doi.org/10.1073/pnas.89.23.11566.
[4] A. Fazio, C. la Torre, M.C. Caroleo, P. Caputo, R. Cannataro, P. Plastina, E. Cione, Effect of addition of pectins from jujubes (Ziziphus jujuba Mill.) on Vitamin C production during heterolactic fermentation, Molecules. 25 (2020) 2706, https://doi.org/10.3390/molecules25112706.
[5] R. Austria, A. Semenzato, A. Bettero, Stability of vitamin C derivatives in solution and topical formulations, J. Pharm. Biomed. Anal. 15 (6) (1997) 795–801, https://doi.org/10.1016/S0731-7085(96)01904-8.
[6] M. M. Taqui. Khan, Arthur E. Martell, Metal Ion and Metal Chelate Catalyzed Oxidation of Ascorbic Acid by Molecular Oxygen. II. Cupric and Ferric Chelate Catalyzed Oxidation, J. Am. Chem. Soc. 89 (26) (1967) 7104–7111, https://doi.org/10.1021/ja01002a046.
[7] Y. Abe, S. Okada, R. Nakao, T. Horii, H. Inoue, S. Taniguchi, S. Yamabe, A molecular orbital study on the reactivity of L-ascorbic acid towards OH radical, J. Chem. Soc. Perkin Trans. 2 (1992) 2221–2232, https://doi.org/10.1039/p29920002221.
[8] L.C. Bichara, H.E. Lanús, C.G. Nieto, S.A. Brandán, Density functional theory calculations of the molecular force field of L -ascorbic acid, vitamin C, J. Phys. Chem. A. 114 (2010) 4997–5004, https://doi.org/10.1021/jp912251g.
[9] Xiang-Guang Meng, Xing-Ming Kou, Jia-Qing Xie, Juan Du, Xian-Cheng Zeng, Microcalorimetric investigation on the kinetics of the oxidation of ascorbic acid with hydrogen peroxide, Chinese J. Chem. 22 (6) (2004) 515–520, https://doi.org/10.1002/cjoc.20040220605.
[10] P.A. Seib, B.M. Tolbert, Ascorbic Acid: Chemistry, Metabolism, and Uses, in: P.A. Seib, B.M. Tolbert (Eds.), AMERICAN CHEMICAL SOCIETY, WASHINGTON, D. C., 1982. https://doi.org/10.1021/BA-1982-0200
[11] D.A. Köse, B. Zümreoglu-Karan, Complexation of boric acid with vitamin C, New J. Chem. 33 (2009) 1874–1881, https://doi.org/10.1039/b902812a.
[12] E. Kleszczewska, The Spectrophotometry Determination of Chelate Complex: L-Ascorbic Acid with Cuprum (II) and Mercury (II) in Alkaline Solution, Polish, J. Environ. Stud. 8 (1999) 313–318.
[13] Joshua A. Obaleye, Chike L. Orjiekwe, Synthesis and characterization of some metal complexes of vitamin c. part 21 - ascorbate complexes of Mn(II), Fe(III) and Co(II), Synth. React. Inorg. Met. Chem. 22 (7) (1992) 1015–1029, https://doi.org/10.1080/15533179208016608.
[14] M.H. Zareie, Y. Zencir, C. Ünaleroğlu, B. Zümreoğlu-Karan, E. Pişkin, PH-Independent decomposition reactions of L-ascorbic acid in aqueous metal solutions. 2. Imaging by scanning tunneling microscopy, Polyhedron. 17 (16) (1998) 2633–2638, https://doi.org/10.1016/S0277-5387(98)00009-6.
[15] J.N. Cape, D.H. Cook, D.R. Williams, Thermodynamic considerations in coordination. Part XIX. In vitro studies of complexing equilibria involved in oral iron(II) therapy, J. Chem. Soc. Dalt. Trans. (1974) 1849–1852, https://doi.org/10.1039/DT9740001849.
[16] Nikolas Benetis, Kim Holmén, Jozef Kowalewski, Lars Nordenskiöld, Olof Wahlberg, Investigation of Nickel(II)–Ascorbic Acid Complex Formation in Aqueous Solution Using Potentiometric Measurements, Optical Spectroscopy and 13C NMR Spectroscopy, Acta Chem. Scand. 35a (1981) 513–520, https://doi.org/10.3891/acta.chem.scand.35a-0513.
[17] A.M.D.S. Chandrathilaka, O.A. Ileperuma, C.V. Hettiarachchi, Spectrophotometric and pH-metric studies on Pb(II), Cd(II), Al(III) and cu(II) complexes of paracetamol and ascorbic acid, J. Natl. Sci. Found. Sri Lanka. 41 (2013) 337–344, https://doi.org/10.4038/jnsfsr.v41i4.6253.
[18] B ZUMREOGLUKARAN, The coordination chemistry of Vitamin C: an overview, Coord. Chem. Rev. 250 (17-18) (2006) 2295–2307, https://doi.org/10.1016/j.ccr.2006.03.002.
[19] Katherine M. Buettner, Joseph M. Collins, Ann M. Valentine, Titanium(IV) and vitamin C: aqueous complexes of a bioactive form of Ti(IV), Inorg. Chem. 51 (20) (2012) 11030–11039, https://doi.org/10.1021/ic301545m.
[20] D. Cesario, E. Furia, G. Mazzone, A. Beneduci, G. De Luca, E. Sicilia, Complexation of Al^{3+} and Ni^{2+} by l -Ascorbic Acid: an Experimental and Theoretical Investigation, J. Phys. Chem. A. 121 (2017) 9773–9781, https://doi.org/10.1021/acs.jpca.7b10847.

[21] G. García-Díez, R. Monreal-Corona, N. Mora-Diez, Complexes of copper and iron with pyridoxamine, ascorbic acid, and a model amadori compound: exploring pyridoxamine's secondary antioxidant activity, Antioxidants. 10 (2021) 1–20, https://doi.org/10.3390/antiox10020208.
[22] J. Ortega-Castro, J. Frau, R. Casasnovas, D. Fernández, J. Donoso, F. Muñoz, High- and low-spin Fe(III) complexes of various AGE inhibitors, J. Phys. Chem. A. 116 (11) (2012) 2961–2971, https://doi.org/10.1021/jp210188w.
[23] J. Ortega-Castro, M. Adrover, J. Frau, J. Donoso, F. Muñoz, Cu2+ complexes of some AGEs inhibitors, Chem. Phys. Lett. 475 (4-6) (2009) 277–284, https://doi.org/10.1016/j.cplett.2009.05.074.
[24] R.A. Goyer, M.G. Cherian, eds., Toxicology of Metals: Biochemical Aspects, Springer-Verlag, Berlin Heidelberg, 1995. https://doi.org/10.1007/978-3-642-79162-8.
[25] Giuseppina A. Corrente, Luana Malacaria, Amerigo Beneduci, Emilia Furia, Tiziana Marino, Gloria Mazzone, Experimental and theoretical study on the coordination properties of quercetin towards aluminum(III), iron(III) and copper(II) in aqueous solution, J. Mol. Liq. 325 (2021) 115171, https://doi.org/10.1016/j.molliq.2020.115171.
[26] G. Biedermann, L.G. Sillén, Studies on the hydrolysis of metal ions. IV. Liquid junction potentials and constancy of activity factors in $NaClO_4$–$HClO_4$ ionic medium, Ark. Kemi. 5 (1952) 425–440.
[27] L. Malacaria, G.A. Corrente, E. Furia, Thermodynamic study on the dissociation and complexation of coumarinic acid with neodymium(III) and dioxouranium (VI) in aqueous media, Appl. Sci. 11 (2021) 4475, https://doi.org/10.3390/app11104475.
[28] Axel D. Becke, Density-functional thermochemistry. III. The role of exact exchange, J. Chem. Phys. 98 (7) (1993) 5648–5652, https://doi.org/10.1063/1.464913.
[29] Chengteh Lee, Weitao Yang, Robert G. Parr, Development of the Colle-Salvetti correlation-energy formula into a functional of the electron density, Phys. Rev. B. 37 (2) (1988) 785–789, https://doi.org/10.1103/PhysRevB.37.785.
[30] M.J. Frisch, G.W. Trucks, H.B. Schlegel, G.E. Scuseria, M.A. Robb, J.R. Cheeseman, G. Scalmani, V. Barone, G.A. Petersson, H. Nakatsuji, X. Li, M. Caricato, a. V. Marenich, J. Bloino, B.G. Janesko, R. Gomperts, B. Mennucci, H.P. Hratchian, J. V. Ortiz, A.F. Izmaylov, J.L. Sonnenberg, D. Williams-Young, F. Ding, F. Lipparini, F. Egidi, J. Goings, B. Peng, A. Petrone, T. Henderson, D. Ranasinghe, V.G. Zakrzewski, J. Gao, N. Rega, G. Zheng, W. Liang, M. Hada, M. Ehara, K. Toyota, R. Fukuda, J. Hasegawa, M. Ishida, T. Nakajima, Y. Honda, O. Kitao, H. Nakai, T. Vreven, K. Throssell, J.A. Montgomery Jr., J.E. Peralta, F. Ogliaro, M.J. Bearpark, J.J. Heyd, E.N. Brothers, K.N. Kudin, V.N. Staroverov, T.A. Keith, R. Kobayashi, J. Normand, K. Raghavachari, A.P. Rendell, J.C. Burant, S.S. Iyengar, J. Tomasi, M. Cossi, J.M. Millam, M. Klene, C. Adamo, R. Cammi, J.W. Ochterski, R. L. Martin, K. Morokuma, O. Farkas, J.B. Foresman, D.J. Fox, G16_C01, (2016) Gaussian 16, Revision C.01, Gaussian, Inc., Wallin.
[31] Stefan Grimme, Jens Antony, Stephan Ehrlich, Helge Krieg, A consistent and accurate ab initio parametrization of density functional dispersion correction (DFT-D) for the 94 elements H-Pu, J. Chem. Phys. 132 (15) (2010) 154104, https://doi.org/10.1063/1.3382344.
[32] Aleksandr V. Marenich, Christopher J. Cramer, Donald G. Truhlar, Universal solvation model based on solute electron density and on a continuum model of the solvent defined by the bulk dielectric constant and atomic surface tensions, J. Phys. Chem. B. 113 (18) (2009) 6378–6396, https://doi.org/10.1021/jp810292n.
[33] Yan Zhao, Donald G. Truhlar, A new local density functional for main-group thermochemistry, transition metal bonding, thermochemical kinetics, and noncovalent interactions, J. Chem. Phys. 125 (19) (2006) 194101, https://doi.org/10.1063/1.2370993.
[34] Raquel Rios-Font, Mariona Sodupe, Luis Rodríguez-Santiago, Peter R. Taylor, The role of exact exchange in the description of Cu^{2+}-(H_2O)n (n = 1–6) complexes by means of DFT methods, J. Phys. Chem. A. 114 (40) (2010) 10857–10863, https://doi.org/10.1021/jp105376s.
[35] Attila Bérces, Tomoo Nukada, Peter Margl, Tom Ziegler, Solvation of Cu^{2+} in water and ammonia. Insight from static and dynamical density functional theory, J. Phys. Chem. A. 103 (48) (1999) 9693–9701, https://doi.org/10.1021/jp992612f.
[36] D.A. McQuarrie, J.D. Simon, Molecular thermodynamics, University Science Books, Sausalito, CA, 1999.
[37] R. Ashcraft, S. Raman, W. Green, Ab initio Aqueous Thermochemistry: Application to the Oxidation of Hydroxylamine in Nitric Acid Solution, J. Phys. Chem. B. 111 (2007).
[38] Amerigo Beneduci, Giuseppina Anna Corrente, Tiziana Marino, Donatella Aiello, Lucia Bartella, Leonardo Di Donna, Anna Napoli, Nino Russo, Isabella Romeo, Emilia Furia, Insight on the chelation of aluminum(III) and iron(III) by curcumin in aqueous solution, J. Mol. Liq. 296 (2019) 111805, https://doi.org/10.1016/j.molliq.2019.111805.
[39] E. Furia, G. Sindona, Complexation of l-Cystine with Metal Cations, J. Chem. Eng. Data. 55 (2010) 2985–2989, https://doi.org/10.1021/je901042y.
[40] P Gans, A Sabatini, A Vacca, Investigation of equilibria in solution, Determination of equilibrium constants with the HYPERQUAD suite of programs, Talanta. 43 (10) (1996) 1739–1753, https://doi.org/10.1016/0039-9140(96)01958-3.
[41] Yeong-Jae Seok, Kap-Seok Yang, Sa-Ouk Kang, A simple spectrophotometric determination of dissociation constants of organic compounds, Anal. Chim. Acta. 306 (2-3) (1995) 351–356, https://doi.org/10.1016/0003-2670(95)00011-N.

Supplementary Material

Experimental and theoretical study of the complexation of Fe^{3+} and Cu^{2+} by L-ascorbic acid in aqueous solution

Alessandra G. Ritacca, [a] Luana Malacaria, [a] Emilia Sicilia, [a] Emilia Furia,* [a] and Gloria Mazzone.* [a]

*corresponding authors: e.furia@unical.it; gloria.mazzone@unical.it

[a]Dipartimento di Chimica e Tecnologie Chimiche, Via P. Bucci, Università della Calabria, I-87036 Arcavacata di Rende (CS), Italy

Figure S1

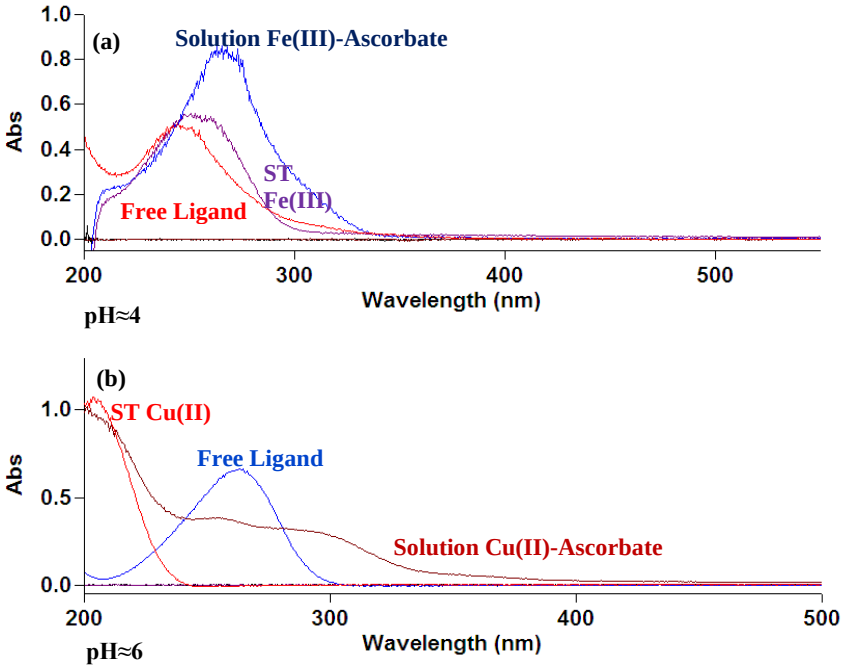
(a)
Solution Fe(III)-Ascorbate
ST Fe(III)
Free Ligand
Abs
1.0
0.8
0.6
0.4
0.2
0.0
200
300
400
500
Wavelength (nm)
pH≈4
(b)
ST Cu(II)
Free Ligand
Solution Cu(II)-Ascorbate
Abs
1.0
0.5
0.0
200
300
400
500
Wavelength (nm)
pH≈6

Figure S2

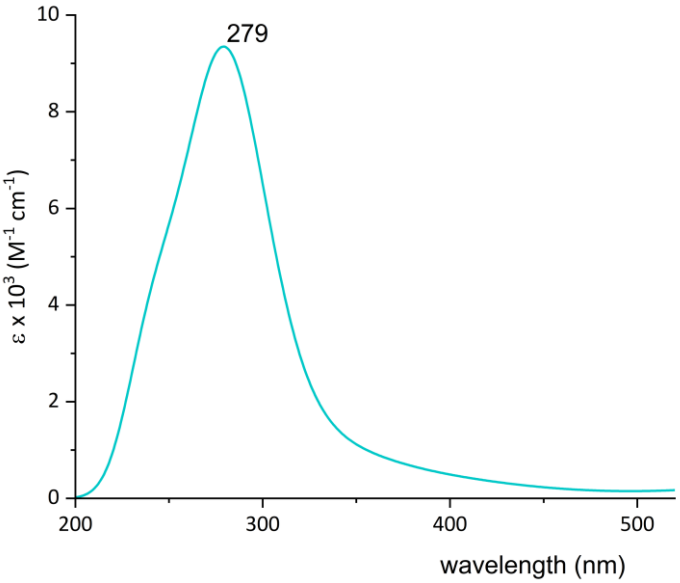

Figure S3

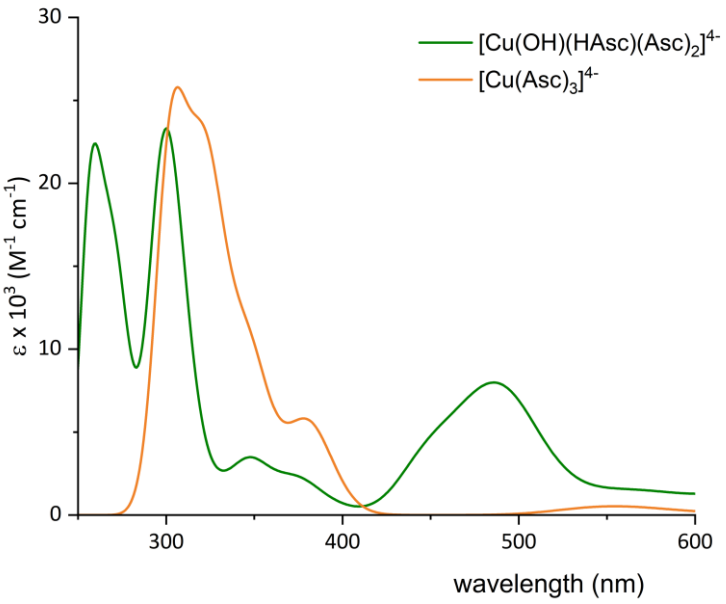
[Cu(OH)(HAsc)(Asc)2]4-
[Cu(Asc)3]4-
ε x 10^3 (M^-1 cm^-1)
30
20
10
0
300
400
500
600
wavelength (nm)

Organic & Biomolecular Chemistry

ROYAL SOCIETY OF CHEMISTRY

COMMUNICATION

View Article Online
View Journal | View Issue

Check for updates

Cite this: *Org. Biomol. Chem.*, 2022, **20**, 9093

Received 14th October 2022,
Accepted 11th November 2022

DOI: 10.1039/d2ob01884e

rsc.li/obc

Transition metal cations catalyze $^{16}O/^{18}O$ exchange of catechol motifs with $H_2{}^{18}O$†

Roelant Hilgers, [a] Judith Bijlsma, [a] Luana Malacaria,[b] Jean-Paul Vincken, [a] Emilia Furia[b] and Wouter J. C. de Bruijn *[a]

Catechol motifs are ubiquitous in nature, as part of plant, animal and microbial metabolites, and are known to form complexes with various metal cations. Here, we report for the first time that complexation with transition metal cations, especially Fe(III), results in rapid $^{16}O/^{18}O$ exchange of the catecholic hydroxyl groups with $H_2{}^{18}O$. We discuss the implications of this finding for mechanistic studies using $H_2{}^{18}O$ and potential relevance for production of ^{18}O-labeled catechol derivatives.

Isotopic labeling studies are widely used in many fields of chemistry, typically in combination with mass spectrometric detection. For example, $^{18}O_2$ and $H_2{}^{18}O$ are often used to investigate chemical, enzymatic and microbial oxidation and degradation reactions.[1–4] In addition, when compounds of interest are available in a stable isotopically labeled form, they can be used for isotope dilution mass spectrometry,[5–7] determination of kinetic isotope effects,[8–10] mass spectrometric monitoring of reaction kinetics,[11,12] and even to follow the metabolic fate of biologically active compounds in human or animal studies.[13,14] In recent (to be published) work, we employed $H_2{}^{18}O$ to investigate degradation reactions of several catechol derivatives in the presence of metal cations, and observed unexpected rapid $^{16}O/^{18}O$ exchange between the $H_2{}^{18}O$ and the aromatic hydroxyl groups under mild conditions (37 °C, neutral or slightly acidic pH). $^{16}O/^{18}O$ exchange of catecholic hydroxyl groups with $H_2{}^{18}O$ has been previously reported, yet only under harsh catalyst-free conditions (3 M HCl, 150 °C, 20 days).[15] To the best of our knowledge, rapid exchange under mild conditions has not been previously described. We investigated this metal-induced $^{16}O/^{18}O$ exchange in further detail, as it may open up a new and simple approach to produce stable ^{18}O-labeled catechol derivatives. Additionally, this communication serves as a warning for researchers who intend to study the reactions of catechol derivatives in the presence of metal cations using $H_2{}^{18}O$.

The starting point of our work was the observation that 3,4-dihydroxybenzoic acid (3,4-DHBA, Fig. 1) showed rapid $^{16}O/^{18}O$ exchange of two oxygen atoms in the presence of various metal cations. These ^{18}O labels were exclusively inserted on the aromatic hydroxyl groups, as evidenced by the neutral loss of 44 Da (*i.e.*, unlabeled CO_2) in both unlabeled and ^{18}O labeled catechols (Fig. 2).

Many metal cations are known to form catecholato complexes in the presence of catechol and its derivatives.[16] Seemingly, this complexation somehow catalyzes the $^{16}O/^{18}O$ exchange with $H_2{}^{18}O$. To investigate this phenomenon in greater detail, we first screened the ability of four metal cations to catalyze this $^{16}O/^{18}O$ exchange. Hereto, catechol and 3,4-DHBA were incubated with the chloride salts of Fe(III), Al(III), Cu(II), and Zn(II) in $H_2{}^{18}O$. We selected these metal cations because they are all able to form catecholato complexes,[17,18] but are fundamentally different in terms of redox activity.

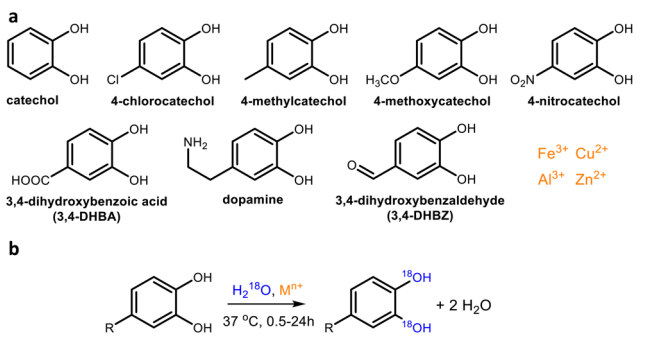

Fig. 1 Catechol derivatives and metal cations used for the ^{18}O labeling study (a) and schematic representation of the observed ^{18}O labeling (b). Unless stated otherwise, cations and catechols were used in equimolar concentrations. The R-group in figure (b) represents any of the substituents shown in figure (a).

[a]*Laboratory of Food Chemistry, Wageningen University & Research, Bornse Weilanden 9, 6708 WG Wageningen, The Netherlands. E-mail: wouter.debruijn@wur.nl*
[b]*Dipartimento di Chimica e Tecnologie Chimiche, Via P. Bucci, Cubo 12/D, Università della Calabria, I-87030 Arcavacata di Rende (CS), Italy*

†Electronic supplementary information (ESI) available. See DOI: https://doi.org/10.1039/d2ob01884e

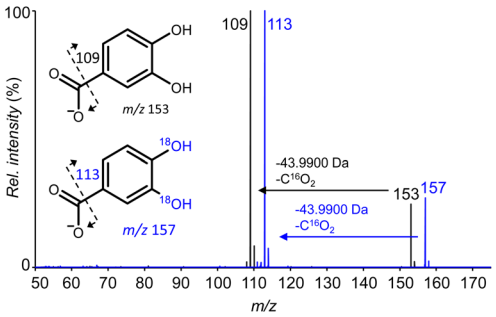

Fig. 2 Overlayed Higher-energy Collisional Dissociation (HCD) fragmentation patterns of unlabeled (black) and doubly ^{18}O-labeled (blue) 3,4-DHBA obtained using high resolution ESI-MS in negative ionization mode. The spectrum of doubly labeled 3,4-DHBA was obtained after incubation with $FeCl_3$ (equimolar, 1 h, 37 °C). Fragmentation patterns of other (un)labeled catechol derivatives can be found in Fig. S1.†

Whereas Fe(III) and Cu(II) have been described to oxidize catechol derivatives,[19] Al(III) and Zn(II) are redox inactive.[20] Samples of the incubation mixture were taken at 2 and 24 h, and analyzed using high resolution RP-UHPLC-PDA-ESI-MS to determine the percentage of single and double ^{18}O labeling. As complexation of catechol motifs to metal cations has been reported to be pH-dependent,[21] these screening experiments were performed at both pH 7 and pH 3.

For both catechol and 3,4-DHBA, incubation with $FeCl_3$ resulted in extensive labeling at pH 3 and 7, already after 2 hours (Fig. 3). $ZnCl_2$ at pH 7 and $CuCl_2$ at both pH 3 and 7 were found to catalyze ^{16}O/^{18}O exchange in the case of catechol, but no effect was observed in the case of 3,4-DBHA. The higher labeling yield at pH 7 as compared to pH 3 is in line with the expected increased complexation of catechol at elevated pH (Fig. S2†).[22] Despite its ability to form catecholato complexes,[23] Al(III) did not catalyze ^{18}O labeling (Fig. 3 and Fig. S2†). The observed ^{16}O/^{18}O exchange in the presence of Fe(III) and Cu(II) could be the result of valence tautomerism within the catecholato complexes. Such tautomerism has, indeed, been described for several complexes of transition metal cations with partly filled 3d orbitals.[24–26] A $H_2{}^{18}O$ molecule coordinated to the metal or present in the bulk could attack the activated keto-tautomer of the catechol and thereby replace the original ^{16}O hydroxyl group (Fig. 4). Such a mechanism seems, furthermore, fully in line with the lack of ^{16}O/^{18}O exchange in the presence of the redox-inactive Al(III). The proposed mechanism, however, cannot explain the observation of ^{16}O/^{18}O exchange in the presence of Zn(II). Since Zn(II) has a completely filled 3d orbital, valence tautomerism, forming Zn(I), is expected to be highly unfavorable. In addition, when catechol incubations were performed with Mn(II), rapid ^{16}O/^{18}O exchange was observed at pH 7 (Fig. S3†). As we expect valence tautomerism between Mn(II) and Mn(I) to be highly unlikely, this finding also challenges valence tautomerism as the only mechanism. To explore other potential mechanisms, we investigated whether molecular oxygen could, somehow, promote ^{16}O/^{18}O exchange, by repeating the incubations of

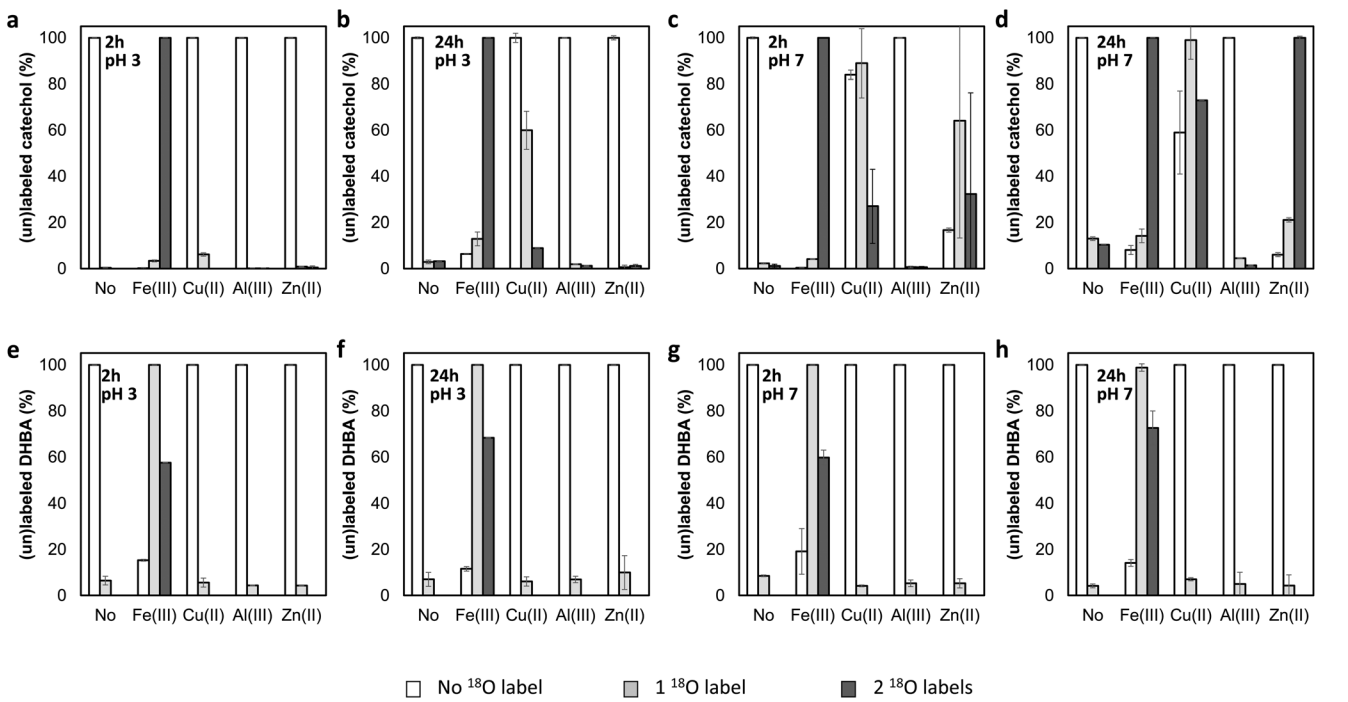

Fig. 3 Percentages of unlabeled, singly labeled, and doubly labeled catechol (a–d) and 3,4-DHBA (e–h) after equimolar incubations (1 mM) with $FeCl_3$, $CuCl_2$, $AlCl_3$, or $ZnCl_2$ at 37 °C for 2 or 24 h, as determined by RP-UHPLC-PDA-ESI-MS. Data are presented as average and standard deviation of two separate incubations.

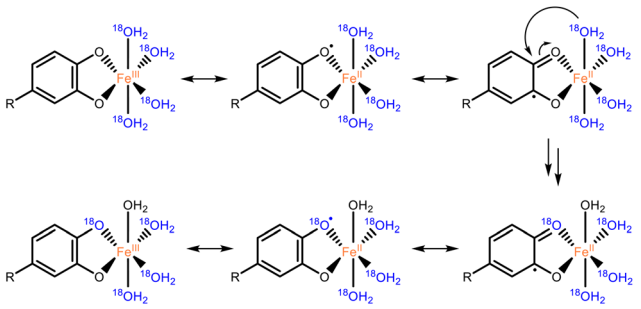

Fig. 4 Proposed mechanism for the Fe(III) or Cu(II) catalyzed $^{16}O/^{18}O$ exchange of catechol motifs, here depicted with Fe(III) as an example. The $H_2{}^{18}O$ attacking the catecholato ligand may also originate from the bulk. Examples of valence tautomerism as a mechanism underlying catalysis in Fe and Cu–catecholato complexes have been reported in earlier research.[25,26]

catechol with $FeCl_3$, $CuCl_2$, and $ZnCl_2$ after N_2 purging of the $H_2{}^{18}O$ solvent and headspace. In none of the incubations, a decrease in ^{18}O labeling was observed after N_2 purging (Fig. S4†), excluding a potential role of O_2 in the $^{16}O/^{18}O$ exchange. We therefore propose that the exchange in the presence of Fe(III) and Cu(II) occurs *via* the mechanism depicted in Fig. 4, whereas the exact mechanism of the Zn(II)-catalyzed exchange remains to be elucidated.

As Fe(III) showed the highest extent of ^{18}O labeling in all cases, we continued our research using only $FeCl_3$. No notable differences were observed between the labeling percentages at pH 3 and pH 7 in $FeCl_3$ incubations. Because of the relatively higher solubility of Fe(III) at acidic conditions,[27] further experiments were performed at pH 3.

Since the initial screening showed limited differences between the timepoints tested, and the $^{16}O/^{18}O$ exchange of catechol seemed already complete within 2 h, we proceeded to follow the exchange kinetics by using time-resolved ESI-MS. Hereto, catechol, 3,4-DHBA, 4-chlorocatechol, 4-methylcatechol, and dopamine solutions in $H_2{}^{18}O$ (pH 3) were mixed with equimolar amounts of $FeCl_3$ in $H_2{}^{18}O$ (pH 3), and infused for ~60 min into an ion trap MS. The kinetics were found to be strongly dependent on the substitution of the aromatic ring. Catechol, 4-chlorocatechol, and 3,4-DHBA were found to undergo near-to-complete ^{18}O labeling within 30 min (Fig. 5a, b and d), whereas 4-methylcatechol and dopamine were labeled considerably slower and reached around 60% labelling within the duration of the experiment (Fig. 5c and e).

No labeling was observed in $H_2{}^{18}O$ in absence of $FeCl_3$, confirming that $^{16}O/^{18}O$ exchange with $H_2{}^{18}O$ only occurs in the presence of a suitable catalyst (Fig. 5f). The latter also indicates that the isotopic labeling will be stable after removal of $FeCl_3$ from the product. When phenol was used instead of the catechols, no labeling was observed after 24 h, which underscores the importance of the catechol motif for the isotope exchange (data not shown).

Although the above described $^{16}O/^{18}O$ exchange may provide an interesting new approach for production of stable ^{18}O-labeled catechols, Fe(III) has been reported to induce oxidative degradation of various catechols.[28] Therefore, we simultaneously determined the labeling yield and recovery of all eight catechol derivatives, shown in Fig. 1, at various time points, using high resolution RP-UHPLC-PDA-ESI-MS. As can be observed from Table 1, complete (*i.e.*, 100% doubly labeled compound) or near-to-complete labeling (*i.e.*, >90% doubly labeled compound) was obtained for catechol, 4-chlorocatechol, 4-methylcatechol, 3,4-DHBA and dopamine with high (*i.e.*, >69%) to very high (*i.e.*, >95%) recoveries. In the case of catechol and 4-chlorocatechol, complete labeling and very high recoveries were obtained for incubations at 0.5 and 1 h. Prolonged incubations (24 h) decreased the recoveries, presumably due to oxidative degradation. For 4-methylcatechol,

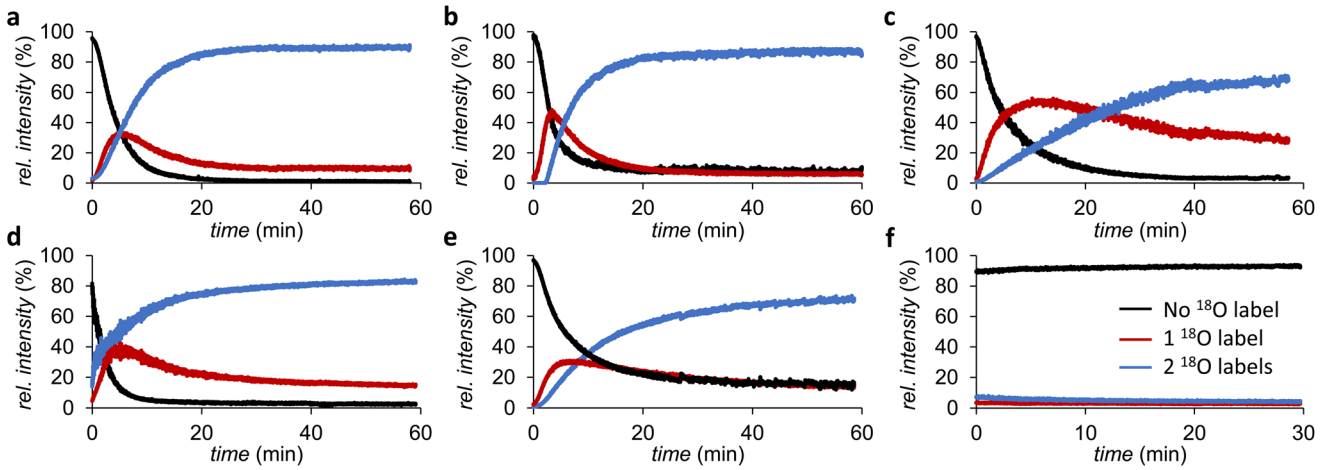

Fig. 5 Kinetics of $FeCl_3$ catalyzed ^{18}O labeling of (a) catechol, (b) 4-chlorocatechol, (c) 4-methylcatechol, (d) 3,4-DHBA, and (e) dopamine. Relative intensities of unlabeled, singly ^{18}O-labeled, and doubly ^{18}O-labeled catechols are shown in black, red, and blue, respectively. In absence of $FeCl_3$, no labeling was observed as indicated in (f) for 4-chlorocatechol. Note: the relative intensities shown are not corrected for the fact that 97% ^{18}O-labeled water was used as solvent.

Table 1 Labeling yields and recoveries of the five catechols after equimolar incubations (0.1 mM) with $FeCl_3$ at 37 °C, as determined by RP-UHPLC-PDA-ESI-MS. Results are shown as the average and standard deviation of two independent incubations. For the 1 h incubation of dopamine and incubations of 4-methoxycatechol no duplicates were included. The labeling percentage has been corrected for the fact that the $H_2{}^{18}O$ contained 97% ^{18}O. Recovery represents relative concentration of the compound (sum of labeled and unlabeled) compared to the initial concentration. Chromatograms and mass spectra are shown in Fig. S5†

Compound	Time (h)	Doubly labeled (%)	Recovery (%)
Catechol	0.5	100 ± 0.1	101 ± 1
Catechol	1	100 ± 0.1	102 ± 5
Catechol	24	100 ± 1	88 ± 5
4-Chlorocatechol	0.5	100 ± 1	95 ± 4
4-Chlorocatechol	1	100 ± 0.5	91 ± 1
4-Chlorocatechol	24	100 ± 0.1	70 ± 3
4-Methylcatechol	1	84 ± 1	69 ± 1
4-Methylcatechol	4	100 ± 0.2	79 ± 2
4-Methylcatechol	24	100 ± 0.1	70 ± 1
3,4-DHBA	1	91 ± 10	86 ± 13
3,4-DHBA	4	94 ± 8	88 ± 15
3,4-DHBA[a]	4	98 ± 2	49 ± 3
3,4-DHBA	24	95 ± 6	80 ± 0.3
Dopamine	1	92	98
Dopamine	4	96 ± 1	92 ± 11
Dopamine[a]	4	97 ± 2	59 ± 3
Dopamine	24	95 ± 2	72 ± 13
4-Nitrocatechol	24	0.2 ± 0.04	65 ± 13
4-Nitrocatechol[a]	24	0.7 ± 0.03	60 ± 4
3,4-DHBZ	24	9 ± 1	87 ± 9
3,4-DHBZ[a]	24	24 ± 9	59 ± 6
4-Methoxycatechol	24	66	2
4-Methoxycatechol[a]	24	N.D.	0

[a] These incubations were performed at a catechol : $FeCl_3$ ratio of 1 : 3.

3,4-DHBA and dopamine, incubations of 4 h were required to achieve >90% doubly ^{18}O labeled products. The double labeling yields of 3,4-DBHA and dopamine stagnated around 95%, and addition of extra iron or incubating at 1 : 3 catechol : Fe ratio did not substantially increase the labeling yield, but mainly resulted in a decreased recovery. Significantly lower labeling yields were obtained for 4-nitrocatechol and 3,4-dihydroxybenzaldehyde (3,4-DHBZ), even though both compounds possess an electron withdrawing substituent. No general trend could be observed on the effect of electron withdrawing and electron donating substituents on the labeling yield. The reason for the poor yields of the $^{16}O/^{18}O$ exchange of 4-nitrocatechol and 3,4-DHBZ remains to be investigated. For 4-methoxycatechol, 66% ^{18}O labeling was observed after 24 h, along with a remarkably low recovery. Various new peaks corresponding to compounds of decreased molecular weight were observed in the RP-UHPLC-PDA-ESI-MS chromatograms, suggesting extensive oxidative degradation of 4-methoxycatechol in the presence of $FeCl_3$ (Fig. S5i†).

Table 2 Labeling yields and recoveries of catechol at various concentrations after equimolar incubations with $FeCl_3$ at 37 °C, as determined by RP-UHPLC-PDA-ESI-MS. Results at 0.1, 1 and 5 mM are shown as the average and standard deviation of two independent incubations. The labeling percentage has been corrected for the fact that the $H_2{}^{18}O$ contained 97% ^{18}O. Recovery presents relative concentration of the compound (sum of labeled and unlabeled) compared to the initial concentration. For incubations at 50 mM no duplicates were included

Concentration (mM)	Time (h)	Doubly labeled (%)	Recovery (%)
0.1	0.5	100 ± 1	101 ± 1
1	0.5	100 ± 0.8	101 ± 8
5	0.5	95 ± 2	90 ± 15
50	4	8	100
50	24	16	85

Results in Table 1 show that $FeCl_3$ is an excellent catalyst for the ^{18}O labeling of various catechols. Although isotopically labeled compounds are mainly used in mass spectrometric studies, requiring low concentrations, the above described experiments (at 0.1 mM) would only allow synthesis of ~10–15 μg of labeled compound per 1 mL of solvent. Therefore, we investigated whether the ^{18}O labeling of catechol could be upscaled to concentrations that are more meaningful for lab-scale synthesis. We note that at increased concentrations the catecholato-complexes partly precipitated, but could be completely resolubilized in ethanol after incubation. RP-UHPLC-PDA-ESI-MS analysis of the resolubilized samples showed that using 10 and 50-fold higher concentrations (1 and 5 mM) still resulted in complete and near-to complete labeling, respectively, within 0.5 h (Table 2). Further upscaling to 50 mM, however, showed a drop in the labeling yield. Presumably this is caused by the poor water solubility of the catechol–iron mixtures at increased concentrations. We are currently investigating approaches to circumvent this. Nonetheless, even partially ^{18}O-labeled compounds can be highly valuable as mechanistic probes and quantification standards.

In summary, we showed that Fe(III), Cu(II), Zn(II) and Mn(II) cations can catalyze $^{16}O/^{18}O$ exchange of catechol motifs with $H_2{}^{18}O$. This may provide a new route for facile production of ^{18}O labeled catechol derivatives. At the same time, our findings indicate that extra caution is required when drawing conclusions from studies on the reactions of catechol derivatives that employ $H_2{}^{18}O$ labeling in the presence of transition metals.

Conflicts of interest

There are no conflicts to declare.

References

1 S. E. Davis, B. N. Zope and R. J. Davis, *Green Chem.*, 2012, **14**, 143–147.
2 K. Norrman, S. A. Gevorgyan and F. C. Krebs, *ACS Appl. Mater. Interfaces*, 2009, **1**, 102–112.

3 G. Vaaje-Kolstad, B. Westereng, S. J. Horn, Z. Liu, H. Zhai, M. Sørlie and V. G. Eijsink, *Science*, 2010, **330**, 219–222.
4 M. D. Hilton and W. J. Cain, *Appl. Environ. Microbiol.*, 1990, **56**, 623–627.
5 C. G. Arsene, R. d. Ohlendorf, W. Burkitt, C. Pritchard, A. Henrion, D. M. Bunk and B. Güttler, *Anal. Chem.*, 2008, **80**, 4154–4160.
6 N. Tretyakova, M. Goggin, D. Sangaraju and G. Janis, *Chem. Res. Toxicol.*, 2012, **25**, 2007–2035.
7 J. Villanueva, M. Carrascal and J. Abian, *J. Proteomics*, 2014, **96**, 184–199.
8 P. Liuni, E. Olkhov-Mitsel, A. Orellana and D. J. Wilson, *Anal. Chem.*, 2013, **85**, 3758–3764.
9 D. A. Singleton and A. A. Thomas, *J. Am. Chem. Soc.*, 1995, **117**, 9357–9358.
10 R. Hilgers, A. Van Dam, H. Zuilhof, J.-P. Vincken and M. A. Kabel, *ACS Catal.*, 2020, **10**, 8650–8659.
11 L. Jasikova, M. Anania, S. Hybelbauerova and J. Roithova, *J. Am. Chem. Soc.*, 2015, **137**, 13647–13657.
12 R. Hilgers, S. Y. Teng, A. Bris, A. Pereverzev, P. White, J. Jansen and J. Roithová, *Angew. Chem., Int. Ed.*, 2022, **61**, e202205720.
13 M. D. Neinast, C. Jang, S. Hui, D. S. Murashige, Q. Chu, R. J. Morscher, X. Li, L. Zhan, E. White and T. G. Anthony, *Cell Metab.*, 2019, **29**, 417–429.
14 B. Kluger, C. Bueschl, N. Neumann, R. Stückler, M. Doppler, A. W. Chassy, A. L. Waterhouse, J. Rechthaler, N. Kampleitner and G. G. Thallinger, *Anal. Chem.*, 2014, **86**, 11533–11537.
15 K. L. Clay and R. C. Murphy, *Biomed. Mass Spectrom.*, 1980, **7**, 345–348.
16 Z. Xu, *Sci. Rep.*, 2013, **3**, 1–7.
17 L. Malacaria, C. La Torre, E. Furia, A. Fazio, M. C. Caroleo, E. Cione, L. Gallelli, T. Marino and P. Plastina, *J. Mol. Liq.*, 2022, **345**, 117895.
18 A. Primikyri, G. Mazzone, C. Lekka, A. G. Tzakos, N. Russo and I. P. Gerothanassis, *J. Phys. Chem. B*, 2015, **119**, 83–95.
19 E. Nkhili, M. Loonis, S. Mihai, H. El Hajji and O. Dangles, *Food Funct.*, 2014, **5**, 1186–1202.
20 M. E. Bodini, G. Copia, R. Robinson and D. T. Sawyer, *Inorg. Chem.*, 1983, **22**, 126–129.
21 J. Bijlsma, W. J. de Bruijn, J. A. Hageman, P. Goos, K. P. Velikov and J.-P. Vincken, *Sci. Rep.*, 2020, **10**, 1–11.
22 M. Elhabiri, C. Carrër, F. Marmolle and H. Traboulsi, *Inorg. Chim. Acta*, 2007, **360**, 353–359.
23 L. Malacaria, G. A. Corrente, A. Beneduci, E. Furia, T. Marino and G. Mazzone, *Molecules*, 2021, **26**, 2603.
24 T. Tezgerevska, K. G. Alley and C. Boskovic, *Coord. Chem. Rev.*, 2014, **268**, 23–40.
25 N. Shaikh, S. Goswami, A. Panja, X.-Y. Wang, S. Gao, R. J. Butcher and P. Banerjee, *Inorg. Chem.*, 2004, **43**, 5908–5918.
26 G. Speier, Z. Tyeklar, P. Toth, E. Speier, S. Tisza, A. Rockenbauer, A. Whalen, N. Alkire and C. Pierpont, *Inorg. Chem.*, 2001, **40**, 5653–5659.
27 P. N. Johnson and A. Amirtharajah, *J. – Am. Water Works Assoc.*, 1983, **75**, 232–239.
28 J. Bijlsma, W. J. de Bruijn, K. P. Velikov and J.-P. Vincken, *Food Chem.*, 2022, **370**, 131292.

Supplementary Information

Transition metal cations catalyze $^{16}O/^{18}O$ exchange of catechol motifs with $H_2{}^{18}O$

Roelant Hilgers,[a] Judith Bijlsma,[a] Luana Malacaria,[b] Jean-Paul Vincken,[a] Emilia Furia[b] and Wouter J.C. de Bruijn,[a]*

[a] Laboratory of Food Chemistry, Wageningen University & Research, Bornse Weilanden 9, 6708 WG Wageningen, The Netherlands

[b] Dipartimento di Chimica e Tecnologie Chimiche, Via P. Bucci, Cubo 12/D, Università della Calabria, I-87030 Arcavacata di Rende (CS), Italy

Table of Contents

Materials and methods

Materials

Catechol (≥99 wt%), 4-chlorocatechol (≥97 wt%), 4-methylcatechol (≥95 wt%), 4-nitrocatechol (≥97 wt%), dopamine hydrochloride (≥98 wt%). Copper(II) chloride (≥97 wt%), aluminum(III) chloride hexahydrate (≥99 wt%), hydrochloric acid (HCl, 37 wt%), sodium hydroxide (NaOH , ≥98 wt%) and ethanol (EtOH) were obtained from Merck (St. Louis, MO, USA). 3,4-Dihydroxybenzoic acid (≥98 wt%) was purchased from TCI Europe NV (Zwijndrecht, Belgium). 4-Methoxycatechol (≥95 wt%) was purchased from Toronto Research Chemicals (North York, Canada). Iron(III) chloride (≥97 wt%), zinc(II) chloride (≥98 wt%), and 3,4-dihydroxybenzaldehyde (≥95 wt%) were purchased from Fisher Scientific (San Jose, CA, USA). $H_2{}^{18}O$ (GMP grade, $^{18}O \geq 97$ %) was purchased from ABX advanced biochemical compounds-Biomedizinische Forschungsreagenzien GmbH (Radeberg, Germany). ULC-MS grade acetonitrile (ACN) and water, both containing 0.1 vol.% formic acid (FA) were purchased from Biosolve (Valkenswaard, the Netherlands). Water for other purposes than UHPLC was prepared using a Milli-Q water purification system (Merck Millipore, Billerica, MA, USA).

General experimental procedure

High resolution RP-UHPLC-PDA-ESI-MS of catechol and derivatives

Stock solutions of catechol and derivatives in acetone were added to an Eppendorf and the acetone was evaporated under nitrogen flow. Water ($H_2{}^{18}O$) and metal chloride solution (10 mM in $H_2{}^{18}O$) were added to obtain a final concentration of 1.0 mM of metal (*i.e.*, $FeCl_3$, $CuCl_2$, $AlCl_3$, and $ZnCl_2$) and ligand for the initial screening with catechol and 3,4-DHBA and 0.1 mM of $FeCl_3$ and catechol and derivatives (*i.e.*, 4-chlorocatechol, 4-methylcatechol, 3,4-DHBA, dopamine, 4-nitrocatechol, 3,4-DHBZ, and 4-methoxycatechol) for the continuation experiments. The pH was adjusted to 3 or 7 for the initial screening and to 3 for the continuation experiments using 0.5 M NaOH or HCl prepared in $H_2{}^{18}O$. Samples were incubated at 37 °C at 1000 rpm using an Eppendorf Thermomixer® F1.5 (Eppendorf, Hamburg, Germany). For UHPLC-MS analysis, 80 µL aliquots of the reaction mixture were taken after 2 and 24 h for the initial screening and 0.5, 1, 4, and 24 h for the continuation experiments, and centrifuged (5 min, 15,000 × *g*) prior to RP-UHPLC-PDA-ESI-MS analysis.

RP-UHPLC-PDA-ESI-MS^n analysis was performed using a Thermo Vanquish UHPLC system (Thermo Scientific, San Jose, CA, USA), equipped with a pump, degasser, and autosampler, coupled to a PDA detector and a Thermo Q Exactive Focus hybrid quadrupole-orbitrap mass spectrometer. Samples (1 µL) were injected onto an Acquity UPLC BEH C18 column (150 × 2.1 mm, particle size 1.7 µm) with a VanGuard guard column (5 × 2.1 mm) of the same material (Waters, Milford, MA, USA). The flow rate was 400 µL min^{-1} and the column temperature was 45 ºC. Water (A) and ACN (B), both acidified with 0.1% FA, were used as eluents. The following solvent gradient was used: 0-1.09 min at 1% B (isocratic), 1.09-6.18 min from 1 to 15% B (linear gradient), 6.18-7.27 min from 15 to 100% B (linear

gradient), 7.27-12.72 min at 100% B (isocratic), 12.72-13.81 min from 100 to 1% B (linear gradient) and 13.81-19.27 min at 1% B (isocratic). The PDA detector was set to measure the wavelength range of 190–680 nm. Mass spectrometric data were collected over the *m/z* range of 100–1,000 in negative and positive ionization mode by using source voltages of 2.5 and 3.5 kV, respectively. Nitrogen was used as a sheath gas (50 arbitrary units) and auxiliary gas (13 arbitrary units). For both modes, the S-lens RF level was set at 50 %, the ion transfer tube temperature was 263 °C and the source heater temperature 425 °C. Data acquisition and processing were performed using Xcalibur (version 4.1, Thermo Scientific). Recoveries of catechol and derivatives were calculated based on integrals of the chromatographic UV_{280} peaks and comparison to an external calibration curve of the corresponding authentic standard (0.0125-0.1 mM, in duplicate, R^2 >0.99). Labeling yields were determined as the average distribution of the accurate masses corresponding to unlabeled, singly labeled and doubly labeled compound under the chromatographic peak. The labeling yield was corrected for labeling percentage of the used $H_2{}^{18}O$ (97%), by dividing the uncorrected percentage of doubly ^{18}O labeled catechols by 0.941 (the theoretical percentage expected after complete ^{18}O labeling of the two catechol hydroxyl groups; 0.97^2).

Time-resolved ESI-MS of catechol and derivatives in $H_2{}^{18}O$ in presence of $FeCl_3$

Solutions (400 µL) of catechol and derivatives at 0.2 mM were prepared in $H_2{}^{18}O$ and placed in a glass vial, the pH of the solution was adjusted to 3 by 0.5 M HCl in $H_2{}^{18}O$. The solution was stirred at 37 °C for 5 minutes after which it was directly infused into the ESI-IT-MS source via a capillary by applying a slight overpressure of N_2 (approximately 0.25 bar). When the MS signal was stable, the measurement was started and after 0.5 min measurement of the ligand, a solution (400 µL) of 0.2 mM $FeCl_3$ in $H_2{}^{18}O$ (pH 3) was added to the glass vial to obtain final concentrations of 0.1 mM catecholate and iron. The ESI-IT-MS measurements were acquired using an LTQ Velos Pro linear ion trap mass spectrometer (Thermo Scientific) equipped with a heated electrospray ionization (ESI) probe. Data were collected for 60 min over the *m/z* range of 100-600 in negative or positive ionization mode by using source voltages of 4.0 and 3.5 kV in positive ionization (PI) and negative ionization (NI) mode, respectively. The S-lens RF level was set at 67.9% in PI and 69.5% in NI, the ion transfer tube and the source heater temperatures were 275 and 45 °C, respectively. Nitrogen was used as a sheath gas (50 arbitrary units) and auxiliary gas (13 arbitrary units). Data were processed using Xcalibur 4.1 (Thermo Scientific).

HCD fragmentation spectra of unlabeled and doubly ^{18}O labeled catechol derivatives

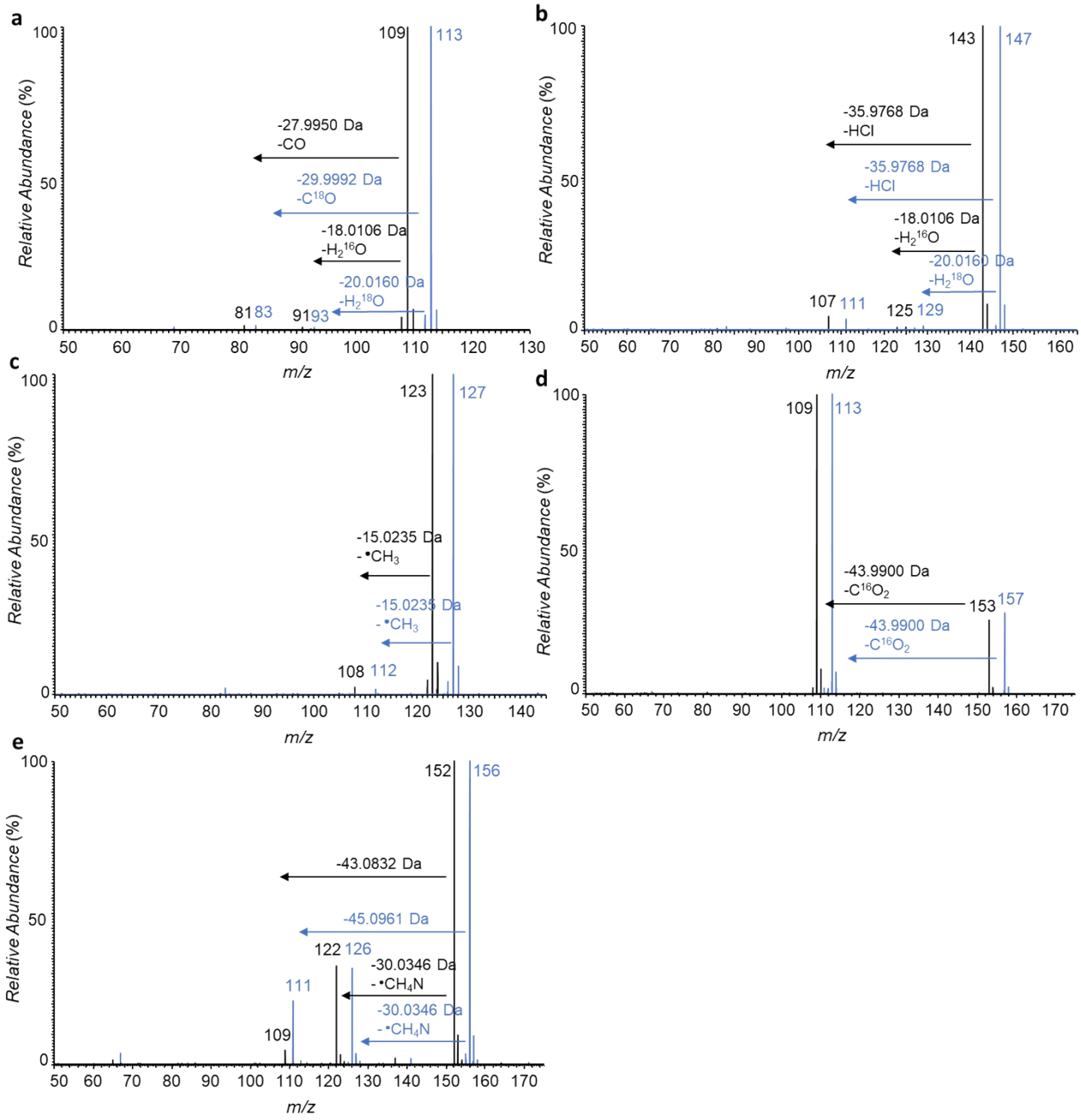

Fig. S1 HCD fragmentation spectra of unlabeled (black) and doubly ^{18}O-labeled catechol (a), 4-chlorocatechol (b), 4-methylcatechol (c), 3,4-dihydroxybenzoic acid (d), and dopamine (e).

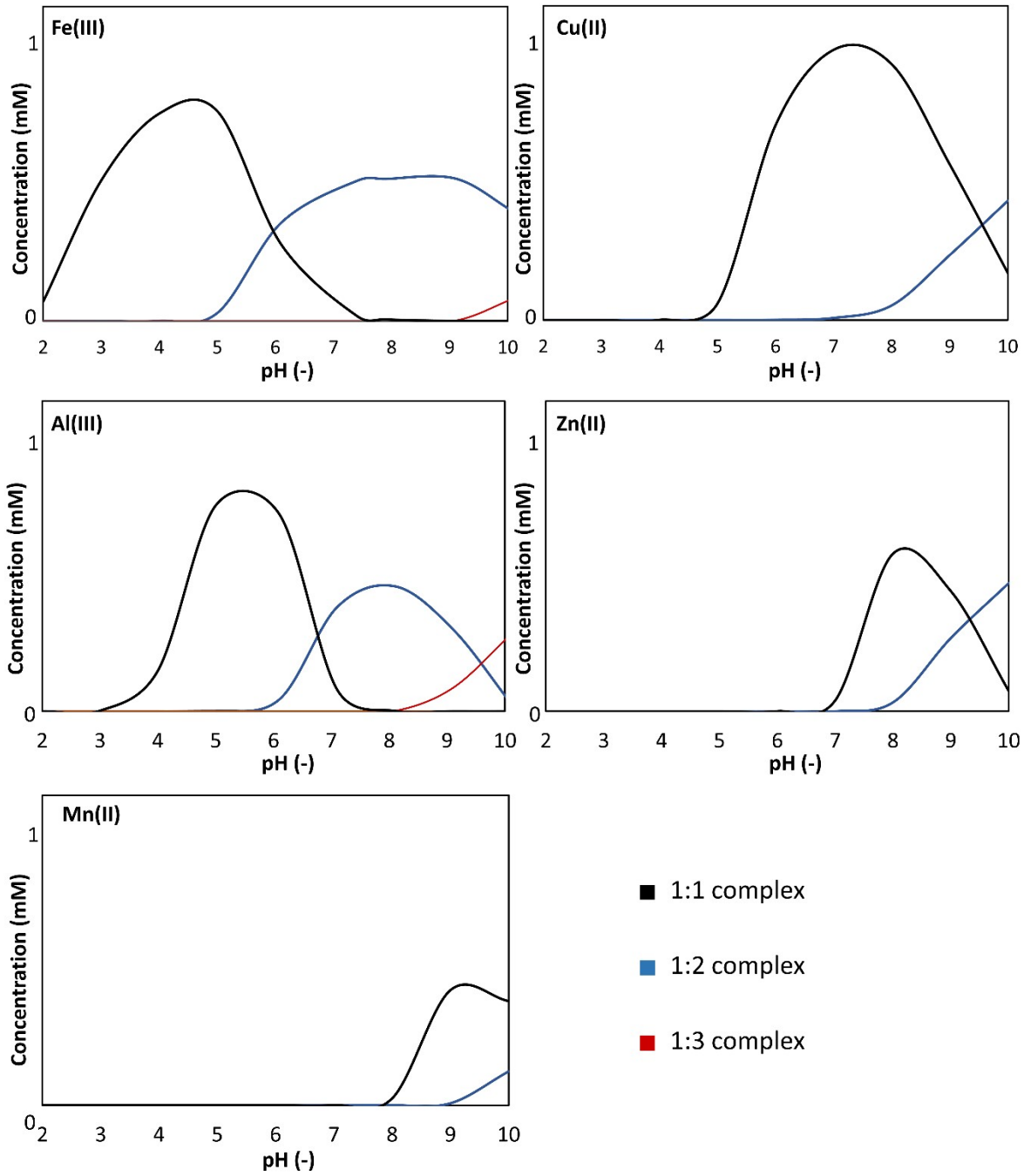

Fig. S2 Predicted concentration of 1:1, 1:2, and 1:3 complexes of catechol with Fe(III), Cu(II), Al(III), Zn(II) and Mn(II) at different pH. Visual MINTEQ (version 3.1) was used for the simulation. The metal-catechol and metal hydrolysis species and stability constants (log K) were obtained from the standard database in Visual MINTEQ 3.1 and not fixed to a constant ionic strength.

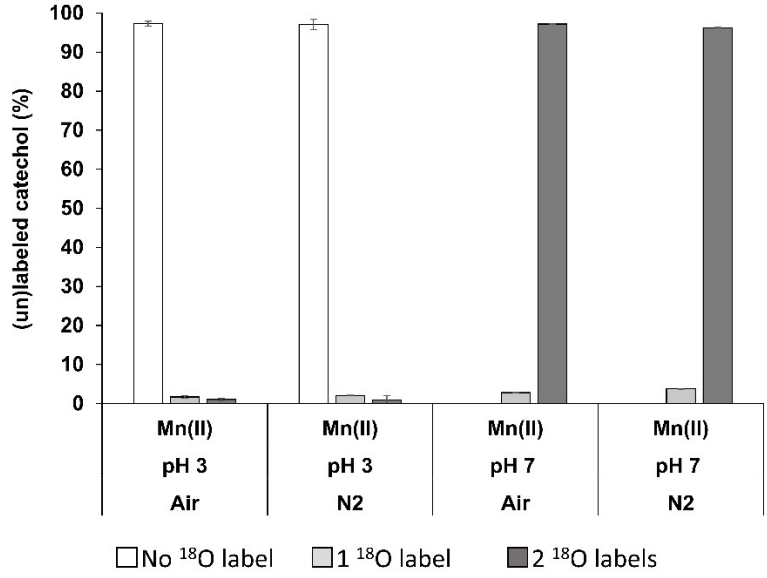

Fig. S3 Percentages of unlabeled, singly labeled, and doubly labeled catechol after equimolar incubations (1 mM) with $MnCl_2$ at 37 °C for 2 h, at pH 3 or 7 in presence of air or after purging with N_2. Purging with N_2 was performed for 2 min through the $H_2{}^{18}O$ solvent and headspace of the Eppendorf tube. Data are presented as average and standard deviation of two separate incubations. The large difference in $^{16}O/^{18}O$ exchange between pH 3 and 7 matches with the low tendency of Mn(II) to form catecholato complexes at low pH.

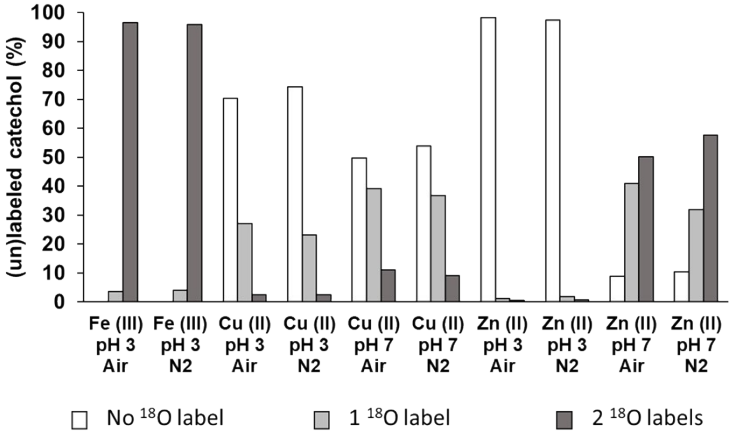

Fig. S4 Relative abundance of unlabeled, singly labeled and doubly labeled catechol in equimolar (1 mM) incubations of catechol with $FeCl_3$, $CuCl_2$, or $ZnCl_2$ at pH 3 or 7 in presence of air or after purging with N_2. Purging with N_2 was performed for 2 min through the $H_2{}^{18}O$ solvent and headspace of the Eppendorf tube. Incubation times were 30 min for the samples containing $FeCl_3$ and 24 h for the samples containing $CuCl_2$ or $ZnCl_2$.

RP-UHPLC-PDA-ESI-MS chromatograms and spectra

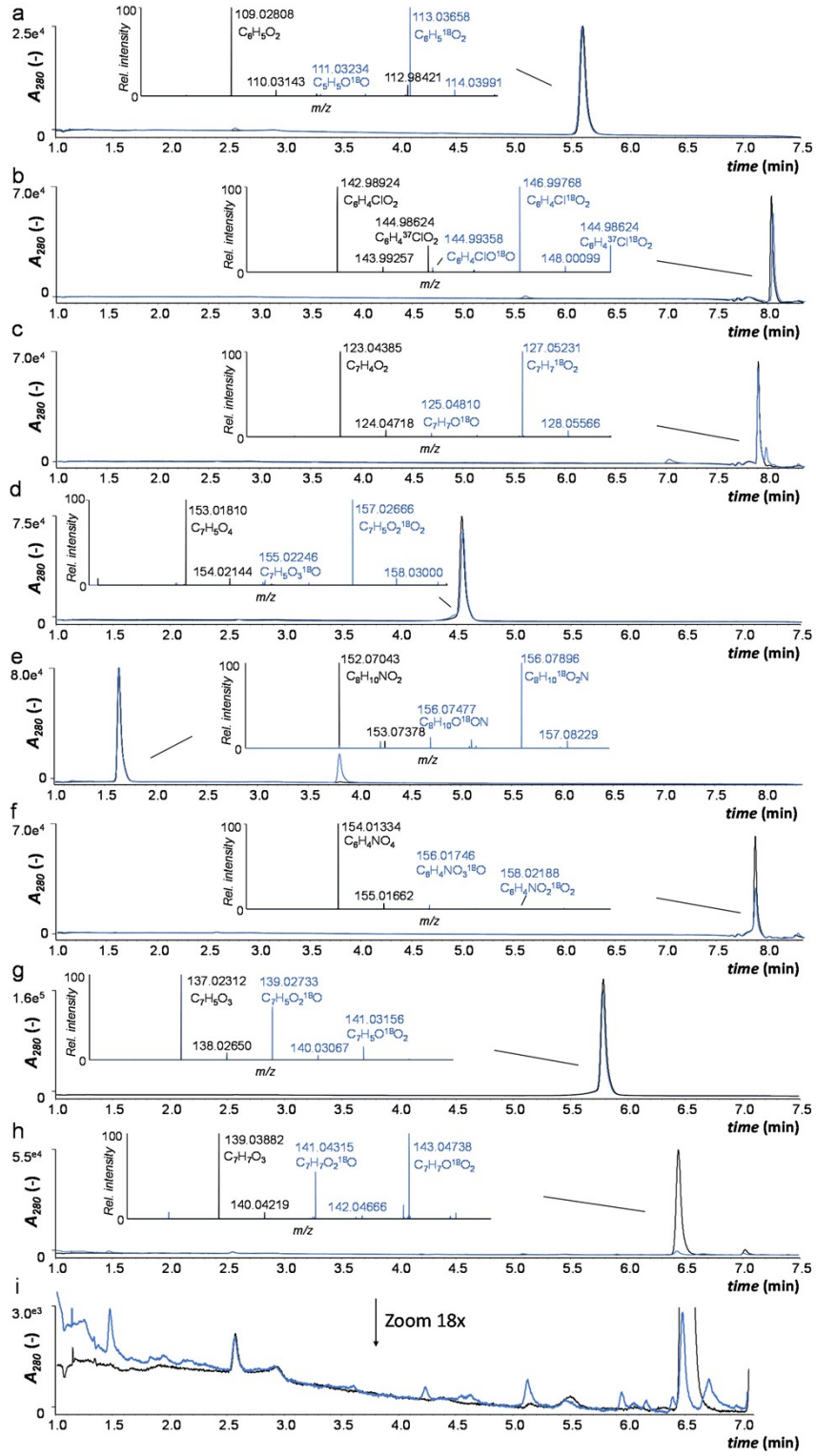

Fig. S5 Overlayed RP-UHPLC-UV_{280} chromatograms and HRMS spectra of catechol (a), 4-chlorocatechol (b), 4-methylcatechol (c), 3,4-dihydroxybenzoic acid (d), dopamine (e), 4-nitrocatechol (f), 3,4-dihydroxybenzaldehyde (g), and 4-methoxycatechol (h) after incubation at 37 °C in absence (black) and presence (blue) of $FeCl_3$. Incubation times were 1 h for a-c and e, 4 h for d and 24 h for f-i. Chromatogram i is an 18-fold zoomed version of h, displaying several (unidentified) degradation products of 4-methoxycatechol. Equimolar concentrations (0.1 mM) were used in all incubations. The inserts depict the overlayed high resolution Full MS spectra under the corresponding peaks. Masses without molecular formula label correspond to the natural ^{13}C isotope peak of the preceding peak.

Journal of Molecular Liquids 369 (2023) 120840

Contents lists available at ScienceDirect

Journal of Molecular Liquids

journal homepage: www.elsevier.com/locate/molliq

Insights into the complexation and oxidation of quercetin and luteolin in aqueous solutions in presence of selected metal cations

Luana Malacaria [a,b,1], Judith Bijlsma [b,1], Roelant Hilgers [b], Wouter J.C. de Bruijn [b], Jean-Paul Vincken [b], Emilia Furia [a,*]

[a] Dipartimento di Chimica e Tecnologie Chimiche, Via P. Bucci, Cubo 12/D, Università della Calabria, I-87030 Arcavacata di Rende, CS, Italy
[b] Laboratory of Food Chemistry, Wageningen University & Research, Bornse Weilanden 9, P.O. Box 17, 6700 AA Wageningen, the Netherlands

ARTICLE INFO

Article history:
Received 21 October 2022
Revised 15 November 2022
Accepted 18 November 2022
Available online 23 November 2022

Keywords:
Flavonoids
UV–Vis Spectroscopy
UHPLC-MS
^{1}H NMR
Metal chelation
Oxidation

ABSTRACT

Flavonoids are natural antioxidants that can be used for the chelation of metal ions to treat metal toxicity. Ideal chelators should form stable metal complexes and be resistant to oxidative degradation reactions in aqueous solutions at physiological conditions (pH 7.4 and 37 °C). In this work, the complexation and oxidation of quercetin and luteolin with selected metal cations (*i.e.* Cr(III), Mn(II), Fe(III), Co(II), Ni(II), Cu(II), Zn(II), and Al(III)) in aqueous solutions at pH 4 and 7.4 is discussed. Using UV–Vis, RP-UHPLC-PDA-MS, ESI-MS and ^{1}H NMR, information about the complexing ability, stoichiometry, and the preferred metal binding sites was obtained. At pH 7.4, all metal ions were complexed by luteolin and quercetin, whereas at pH 4 both flavonoids only formed complexes with the trivalent metal cations (*i.e.* Cr(III), Fe(III), and Al(III)). No clear preference for any of the complexation sites was observed for quercetin and luteolin. UV–Vis and RP-UHPLC-PDA-MS showed that, at pH 7.4, chelation of quercetin was followed by metal-mediated oxidation resulting in degradation of quercetin. On the contrary, luteolin complexes with metal cations were stable and no oxidative degradation of luteolin was observed. The oxidative degradation pathway of quercetin was investigated by incubation in $H_2^{18}O$, which showed that the oxidation occurs via both oxygenation and hydroxylation mechanisms, the latter being the preferred pathway for the trivalent metal ions.

Our results indicate that luteolin is a more suitable chelating agent of Al(III) and first-row transition metal cations due to its higher oxidative stability and its ability to form stable complexes in aqueous solutions at pH 7.4.

1. Introduction

Flavonoids, a group of phenolic compounds produced in plants as secondary metabolites, possess a broad variety of bioactivities, and are widely found in fruits, vegetables, and herbs [1–5]. The main biological activity of flavonoids is their antioxidant activity, which allows them to alleviate oxidative stress by scavenging of free radicals and chelating metal ions [6]. The latter is relevant in clinical settings because accumulation of metal ions in the body at concentrations higher than the optimum level can lead to metal toxicity. This is caused by metal-induced formation of reactive oxygen species (ROS) and reactive nitrogen species (RNS) resulting in (per)oxidation of biological molecules. Metal chelation therapy is used to treat metal toxicity. In order for chelating agents to be effectively used in chelation therapy, they should form a stable chelate [7–10]. Most of the currently used (synthetic) chelating agents show serious side effects, therefore, new chelation strategies should be investigated [11]. Flavonoids can be employed as natural chelating agents that are desired over synthetic chelating agents [12].

Important metal ions to investigate are Al(III) and the first-row transition metal cations (*i.e.* Cr(III), Mn(II), Fe(III), Co(II), Ni(II), Cu(II), Zn(II)), as they are associated with degenerative diseases, such as Alzheimer's disease [13–15]. In this work, quercetin (3,3 ▫ ,4 ▫ ,5,7-pentahydroxyflavone, Q, Fig. 1a), one of the most common flavonols present in nature, and the flavone luteolin (3 ▫ ,4 ▫ ,5,7-tetrahydroxyflavone, L, Fig. 1b) were studied as chelating agents. As can be observed in Fig. 1, quercetin has three possible complexation sites: (i) the 3-hydroxy-4-ketone moiety

* Corresponding author.
E-mail addresses: luana.malacaria@unical.it (L. Malacaria), judith.bijlsma@wur.nl (J. Bijlsma), roelant.hilgers@wur.nl (R. Hilgers), wouter.debruijn@wur.nl (W.J.C. de Bruijn), jean-paul.vincken@wur.nl (J.-P. Vincken), emilia.furia@unical.it (E. Furia).
[1] These authors contributed equally to this work

https://doi.org/10.1016/j.molliq.2022.120840
0167-7322/

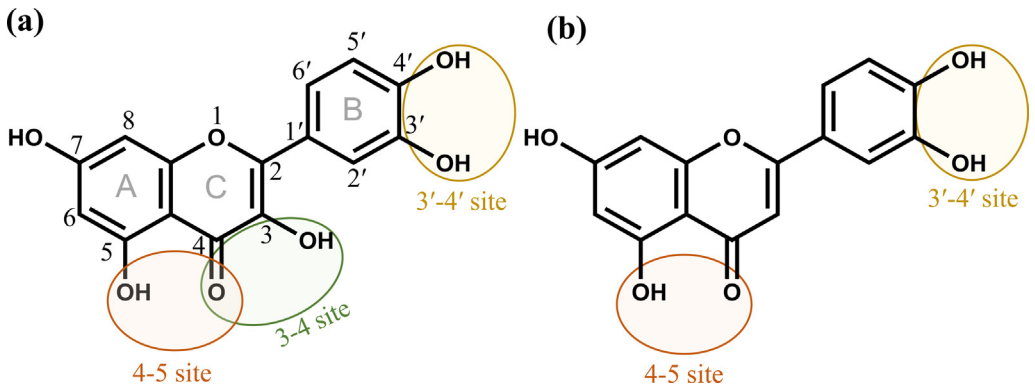

Fig. 1. Flavonoids investigated in this study: (a) quercetin and (b) luteolin. The possible metal binding sites are shown for both ligands.

(3–4 site), the 5-hydroxy-4-ketone moiety (4–5 site), and the 3 ▫ ,4 ▫ -dihydroxy moiety (3 ▫ -4 ▫ site) in the B-ring, whereas luteolin only possesses the 4–5 and the 3 ▫ -4 ▫ sites. Deprotonation of the hydroxyl substituents in these binding sites is a prerequisite for complexation [16,17].

The stability constants of the resulting metal-flavonoid complexes and site specificity (*i.e.*, preferred coordination site) of binding are dependent on the nature of the metal and flavonoid [7–9,18]. A high stability is necessary to guarantee that the metal ions are and remain completely chelated, so that they can be excreted from the body within a few hours or days, thereby preventing harmful effects of the metal [19]. Additionally, the evaluation of the chelators should also include the physiological conditions [11]. Ideal chelators should be soluble in aqueous solutions at physiological pH (*i.e.* 7.4) and be resistant to (bio)chemical transformation (*i.e.* hydrolysis, reduction and oxidation) [11].

Complexation with quercetin and/or luteolin in organic solvent systems has been reported previously for the metal ions selected for this study [18,20–27]. In aqueous solutions the metal-flavonoid complexes may have different structures and stoichiometries from those in organic solvents [28–30]. This can affect the stability of the complex and resistance to subsequent chemical reactions [31]. Complexation of quercetin and luteolin with Fe(III), Al(III), and Cu(II) has also been investigated in aqueous solutions at 37 °C and pH 4 using potentiometric measurements, which showed that they formed stable complexes with cations of Fe(III), Al(III), and Cu(II) at this pH [6–8]. To better resemble physiological conditions, the chelating properties of these flavonoids and their subsequent oxidation should also be investigated in aqueous solution at 37 °C and pH 7.4. However, investigation of the aqueous systems of Fe(III) and Al(III) at pH > 4.5 by potentiometry is hindered by metal hydrolysis [6,7]. Therefore, the complexation of quercetin and luteolin with the selected cations (Cr(III), Mn(II), Fe(III), Co(II), Ni(II), Cu(II), Zn(II), and Al(III)) at pH 7.4 in aqueous solutions should be investigated using a different set-up. Besides complexation, flavonoids, especially flavonols (*e.g.* quercetin), in aqueous solutions are prone to oxidation in presence of Fe(III) [26,32]. Because flavones (*e.g.* luteolin) lack the 3-OH group they are more stable to oxidation reactions [33]. With Fe(III), oxidative degradation of flavonols towards smaller phenolic acids (*i.e.* protocatechuic acid, gallic acid, and phloroglucinol carboxylic acid) was preferred over oxidative coupling [33]. For the other metal cations (*i.e.* Cr(III), Mn(II), Co(II), Ni(II), Cu(II), Zn(II), and Al(III)) it is not known if, and how they affect flavonoid oxidation in aqueous solutions at physiological pH. It is important to better understand the oxidation of these natural chelators by the selected metal ions in aqueous solution, because ideal chelators should be resistant to oxidation [11].

This study aims to investigate the complexation of quercetin and luteolin with Fe(III), Cr(III), Mn(II), Co(II), Ni(II), Cu(II), Zn(II), and Al(III) in aqueous solutions at 37 °C and pH 7.4. For each system, we investigated the ability of flavonoids to coordinate the selected metal cations, metal binding site(s), and stoichiometry of formed complexes. Furthermore, we investigated the flavonoids' oxidative reactivity and possible oxidation pathways in these systems. We hypothesized that (i) due to deprotonated hydroxyl substituents of the flavonoid binding sites at neutral pH, flavonoids chelate the metal cations in aqueous solutions at 7.4, that (ii) the preferred binding site, stoichiometry and reactivity are metal and flavonoid dependent, and that (iii) due to the presence of the 3-OH group, quercetin is more prone to oxidative reactions in presence of the metal cations compared to luteolin.

To this end, a combination of UV–Vis, ESI-ITMS, and ^{1}H NMR can be used to obtain further insight in the complexation, stoichiometries, and complexation sites of flavonoid-metal complexes at pH 4, as a reference for comparison with previously reported results, and pH 7.4. We have used reversed-phase ultra-high performance liquid chromatography (RP-UHPLC) with photodiode array (PDA) detection coupled to ESI-ITMS to identify and quantify the amount of the oxidation products.

2. Experimental section

2.1. Materials

Quercetin hydrate (≥95 wt%), 4-hydroxybenzoic acid (≥99 wt %), 3,4,5-trihydroxybenzoic acid (≥98 wt%), copper(II) chloride (≥97 wt%), aluminum(III) chloride hexahydrate (≥99 wt%), hydrochloric acid (HCl, 37 wt%), and sodium hydroxide (NaOH, ≥98 wt%) were obtained from Merck (St. Louis, MO, USA). 3,4-dihydroxybenzoic acid (≥98 wt%) and 2,4,6-trihydroxybenzoic acid (≥98 wt%) were purchased from TCI Europe NV (Zwijndrecht, Belgium). Luteolin (≥98 wt%) was purchased from Extrasynthese (Genay, France). Chromium(III) chloride hexahydrate (≥98 wt%), manganese(II) chloride (≥97 wt%), iron(III) chloride hexahydrate (≥97 wt%), cobalt(II) chloride hexahydrate (≥98 wt%), nickel(II) chloride hexahydrate (≥97 wt%), and zinc(II) chloride (≥98 wt%) were purchased from Thermo Fisher Scientific (San Jose, CA, USA). Ethanol (EtOH) was obtained from Merck Millipore (Billerica, MA, USA). ULC-MS grade acetonitrile (ACN) and water, both containing 0.1 % (v/v) formic acid (FA) were purchased from Biosolve (Valkenswaard, The Netherlands). Water for other purposes than UHPLC was prepared using a Milli-Q water purification system (Merck Millipore, Billerica, MA, USA).

2.2. Incubation of flavonoids in presence of metal ions

Stock solutions of each metal cation were prepared at 2.0 mM in water. For incubations, a known amount of flavonoid was added (*i.e.*, 3.18 mg of quercetin or 2.86 mg of luteolin) in 10 mL of water, consisting of 5 mL of metal stock solutions and 5 mL of water, to obtain a final concentration of 1.0 mM for flavonoid and metal. Subsequently, each sample was adjusted to pH 4 or 7.4 using 0.05 M HCl and/or 0.05 M NaOH; the pH was maintained constant during the experiments by automatic addition of 0.05 M HCl and/or 0.05 M NaOH using a pH-stat device (Metrohm, Herisau, Switzerland). This experimental approach was chosen as buffer compounds can cause interference with complexation and oxidation reactions [34,35]. After pH adjustment, the samples were incubated at 37 °C and under magnetic stirring (*i.e.*, 300 rpm). Incubations were performed under atmospheric oxygen concentrations; no measures were taken to reduce oxygen levels. The incubations were stopped after 24 h and the samples were centrifuged (10 min, 15,000 × *g*). The supernatants were separated from the solid to obtain the water soluble (WS) fractions. The solid fractions were solubilized with pure EtOH. The resulting suspensions were centrifuged once more (10 min, 15,000 × *g*) and the supernatants were separated to obtain the EtOH soluble (ES) fraction. The WS and ES fractions were analyzed by UV–Vis (section 2.4) and RP-UHPLC-ESI-ITMS (section 2.5 and 2.6).

2.3. Incubation of quercetin with metal ions in $H_2^{18}O$

To obtain more insight into the pathway(s) of metal-induced quercetin degradation, the incubations were also performed in a 50/50 (*v/v*) mixture of $H_2^{18}O/H_2O$. Fifty μL of each metal stock solution in H_2O was thoroughly mixed with 50 μL of quercetin in $H_2^{18}O$ to obtain a final concentration of 1.0 mM metal and quercetin and 50/50 (*v/v*) of $H_2^{18}O/H_2O$. The pH of samples was adjusted to ~ 7.4, by using the same experimental approach described previously. Each sample was then incubated for 24 h at 37 °C and centrifuged (10 min, 15,000 × *g*). Incubations of the quercetin metal solutions in $H_2^{18}O$ were performed under atmospheric oxygen concentrations; no measures were taken to reduce oxygen levels. To check whether spontaneous $^{16}O/^{18}O$ exchange occurred in the main quercetin oxidation products (*i.e.*, 3,4-dihydroxybenzocic acid and 2,4,6-trihydroxybenzoic acid [32]), we carried out control experiments where we incubated 3,4-dihydroxybenzoic acid and 2,4,6-trihydroxybenzoic acid with metal stock solutions to obtain a final concentration of 0.1 mM of 3,4-dihydroxybenzoic acid or 2,4,6-trihydroxybenzoic acid, 1.0 mM metal and 50/50 (*v/v*) of $H_2^{18}O/H_2O$. These samples were analyzed by RP-UHPLC-ESI-FTMS (section 2.5 and 2.7).

2.4. Monitoring complexation and oxidation by UV–Vis spectroscopy

The effect of metal addition on the complexation and on the oxidation reactions was monitored using UV–Vis spectroscopy. Spectra of the WS and ES fraction appropriate dilution were obtained with a Scientific™ Genesys™ 150 UV–Vis spectrophotometer, using a high precision quartz cell with a 10 mm light path (Hellma Analytics). Spectra were recorded at room temperature in the range from 210 to 650 nm. Not all samples were diluted similarly, therefore these data were only used for qualitative comparisons. The UV–Vis spectra were analyzed using a deconvolution program (Origin, Version 2022). The deconvolution of spectra for the systems containing the metal cations is useful to identify the presence of new bands and/or the shift of the characteristic flavonoid bands.

2.5. Separation of flavonoids and oxidation products by reversed phase liquid chromatography (RP-UHPLC)

Flavonoids and their oxidation products in the WS and ES fractions were separated on a Thermo Vanquish UHPLC system (Thermo Scientific, San Jose, CA, USA) equipped with an autosampler, a pump, a degasser, and a photodiode array (PDA) detector. The injection volume, column, temperature, eluents, and gradient elution program was used as reported in Method S1 (supplementary information). The PDA detector was set to measure the wavelength range of 190 – 680 nm. Quantification of each flavonoid in the WS and ES fraction was performed based on PDA peak area (*i.e.*, 280 nm) and an external calibration curve of the corresponding authentic standard (0.03–1.0 mM, in duplicate, $R^2 \geq 0.999$).

2.6. Electrospray ionization ion trap mass spectrometry (ESI-ITMS^n)

Mass spectrometric data of the flavonoids and their oxidation products were acquired using an LTQ Velos Pro linear ion trap mass spectrometer (Thermo Scientific) equipped with a heated electrospray ionization (ESI) probe coupled *in-line* to the Vanquish UHPLC system as described elsewhere [32].

To evaluate the metal-flavonoid complexes the WS and ES solutions at pH 4 and 7.4 were directly infused (30 μL min^{-1}) in the MS. The capillary voltage was set to 4.0 kV and 2.5 kV in positive (PI) and negative ionization mode (NI), respectively. The sample cone was operated at 30 V and 40 V for PI and NI, respectively, with the source temperature set at 150 °C. MS and MS^2 spectra were acquired between *m/z* 100–1500 for 0.5 min. The trap collision energy was varied between 20 and 35 V in MS^2 mode. Data were processed using Xcalibur 4.1 (Thermo Scientific).

2.7. Electrospray ionization hybrid quadrupole Orbitrap mass spectrometry (ESI-FTMS^n)

Accurate mass data were acquired using a Thermo Q Exactive Focus hybrid quadrupole-Orbitrap Fourier transform mass spectrometer (FTMS) (Thermo Scientific) equipped with a heated ESI probe coupled *in-line* to the Vanquish UHPLC system. Prior to analysis, the mass spectrometer was calibrated in the negative and positive ionization mode using Tune 2.11 (Thermo Scientific) by injection of Pierce negative and positive ion calibration solutions (Thermo Scientific). Gas flows and source conditions were the same as for ESI-ITMS. Full MS and higher energy collisional dissociation (HCD) fragmentation data were recorded at 70.000 and 35.000 resolution, respectively. Normalized collision energy was 35 %. MS^n fragmentation was performed on the most intense product ion in the MS^{n-1} spectrum and known quercetin degradation products [32] were inserted in an inclusion list. Data were processed using Xcalibur 4.1 (Thermo Scientific).

2.8. ^1H NMR analysis of metal-flavonoid systems

NMR Spectra of the ES were recorded on a Bruker AVANCE 700 MHz NMR spectrometer (Bruker BioSpin, Rheinstetten, Germany). EtOH was evaporated under nitrogen flow and the solid was dissolved in 0.5 mL DMSO d_6 (99.8 atom%, Isotec) and dried with 3 Å deuterated molecular sieves. ^1H NMR spectra were recorded at a probe temperature of 300 K. The spectral width was 15 ppm with an off-set of 7.5 ppm (δ_H 15 to 0 ppm), 128 scans were recorded. The solvent peak (DMSO d_6) was used as an internal reference (δ_H 2.49 ppm). Data acquisition and processing was performed using Topspin 4.1.3 (Bruker).

3. Results and discussion

3.1. Characterization of metal-flavonoid complexes

First, complexation of quercetin and luteolin with Cr(III), Mn(II), Fe(III), Co(II), Ni(II), Cu(II), Zn(II), and Al(III) was studied. Hereto, the water soluble (WS) and ethanol soluble (ES) fractions were recovered after the incubation experiments and were characterized using UV–Vis and ^{1}H NMR spectroscopy and mass spectrometric techniques.

3.1.1. Evidence for pH-, flavonoid-, and metal-dependent flavonoid-metal complexation

The observed difference in the λ_{max} of the absorbance bands between the UV–Vis spectra of the quercetin blank and that of quercetin in presence of the metal ions, at pH 4 and 7.4, provided evidence that metal-quercetin complexes were formed (Fig. 2a-d) [36]. More specifically, formation of new absorbance bands between 390 and 650 nm could be ascribed to ligand-to-metal charge transfer (LMCT) due to flavonoid-metal complexation [23,37,38].

In the WS fraction at pH 4 and 7.4, the absorption spectrum of the flavonoid blank differed from that of the ES fraction (Fig. 2a-d). Quercetin is mainly recovered in the ES fraction because of its hydrophobicity. Additional changes in the flavonoid absorption spectra are because of the sensitivity of the transition bands to the environment (*i.e.,* solvent type, pH), as previously observed from shifts in the transition bands when comparing absorption spectra of quercetin in ethanol and water [39,40]. To obtain more insights in the behavior of quercetin in aqueous solutions (*i.e.*, WS) at pH 4 and 7.4, the absorption spectra of free flavonoid were deconvoluted in the wavelength range from 295 to 650 nm (Fig. S1-a-b, Tables S1 and S2), by fitting the experimental spectra with multiple Gaussian functions ($R^2 > 0.99$, $\chi^2 < 3{\cdot}10^{-4}$). Deconvolution revealed a band at 291 nm and two broad and less intense bands at 337 and 364 nm in WS at pH 4. The latter indicated a shift in the cinnamoyl band compared to the ES fraction, likely because of the higher polarity of water compared to ethanol causing a hypsochromic shift. At pH 7.4, deconvolution revealed two new broad and weak bands at 435 and 618 nm, and another sharp and more intense band at 310 nm.

For the quercetin-metal systems also most absorbance was observed in the ES fraction. The higher recoveries in this fraction could be a result of the hydrophobicity of the metal-complexes and/or neutrality. In the spectra of the quercetin-metal systems at pH 4 in the ES fraction, only three of the studied metal cations (*i.e.*, Al(III), Fe(III), and Cu(II)) showed an LMCT band, whereas this was observed for all the quercetin-metal systems at pH 7.4 (Fig. 2c-d, Tables S1 and S2). Increased complexation at pH 7.4 was expected because deprotonation of quercetin at this pH results in higher affinity of quercetin towards metal ions [7,16,32]. The spectral changes of WS fractions in presence of most metal cations, at both pH 4 and 7.4, showed a new absorption band in a wavelength range from 282 to 354 nm (Fig. 2a-b, Tables S1 and S2), which is suggested to be a degradation product of quercetin. The appearance of this band at 290 nm is likely a result of a decreased conjugated system in quercetin and the formation degradation products due to oxidation [41]. These degradation products were further investigated by UHPLC-MS in section 3.2.1. In the WS spectra for Fe(III), Al(III), and Cr(III) at pH 4 and 7.4 (Fig. 2a-b) an LMCT absorption band in the visible region was observed which confirms complexation (Tables S1 and S2). These metal cations are classified as hard Lewis acids and therefore are expected to form metal complexes also at acidic pH [7,42]. Fe(III) was previously also reported to form colored complexes with flavonoids at pH 4 [43]. Interestingly, this band was also observed for Cu(II) at pH 4 and for Co(II) at both pH values (Fig. 2a-b, Table S1 and S2), which confirms complexation of these metal ions with flavonoids. The UV–Vis spectra of WS and ES fractions from luteolin-metal cation systems at pH 4 and 7.4 are shown in Fig. 3a-d. The UV–Vis spectra of the ES fractions of the luteolin-metal systems at pH 4 were similar to that of the luteolin blank, except for the Al(III)-luteolin system, which showed an LMCT band in the visible light region. Similarly, at pH 7.4, luteolin systems with Al(III) and Mn(II) also featured an LMCT band (Fig. 3c-d, Tables S3 and S4). These new absorption bands confirm complexation of only Al(III) and Mn(II) to luteolin in the ES fraction. The occurrence of an LMCT band resulting from metal-luteolin complexation in the WS fractions was dependent on metal and pH. At pH 4, complexation was observed for Al(III), Cr(III), and Co(II), whereas at pH 7.4 complexation was observed for Al(III), Fe(III), and Ni(II). Moreover, at pH 7.4 the cinnamoyl band of Mn(II), Co(II), and Zn(II) also showed a bathochromic shift as a result of the increased conjugated system due to metal complexation [32].

Previously, a bathochromic shift of the cinnamoyl band for luteolin with Cu(II) was also reported [44]. However, in aqueous solution this was not observed at pH 4 and 7.4.

3.1.2. Stoichiometry of flavonoid-metal complexes

Presence of the metal-flavonoid complexes in the ES fractions, and the stoichiometry of the complexes were further investigated by direct injection ESI-ITMS analysis. With MS, charged species can be analyzed irrespective of the nuclear spin, providing the possibility to identify paramagnetic, ferromagnetic, and antiferromagnetic complexes [45]. The metal-flavonoid complexes were tentatively identified based on the m/z values, MS^2 fragmentation, and isotope patterns (Table 1 and Table S5).

In the spectra of ES fractions of flavonoid-Al(III) in positive ionization at pH 4 (Fig. S2) signals were detected, that were not present in absence of Al(III), and corresponded to 1:2 and 1:3 metal:ligand complexes. For Fe(III) with quercetin ions were observed that were tentatively identified as a complex with a 1:3 stoichiometry. At pH 7.4, quercetin complexes with Zn(II), Cu(II), Co(II) and Ni(II) were identified in positive ionization mode in the ES fraction (Fig. S3). These metal ions were found to form complexes with a 1:2 stoichiometry (Table 1, and Fig. S3). Additionally, for nickel a complex with 3:2 stoichiometry was tentatively identified. For Mn(II) we did not find metal complexes, but we did identify an intermediate of quercetin degradation with ethanol attached to the *C*2 position (Fig. S4). This molecule was also observed in the UHPLC-MS chromatogram of the ES fraction of quercetin with Mn(II). Because of the redox chemistry of Mn(II), it allows oxidation of quercetin, resulting in the formation of a quercetin quinone that can react with ethanol [46,47].

At pH 4, luteolin formed complexes with aluminum with M:F stoichiometries of 1:2 and 1:3 (Fig. S5). There were no other signals in the mass spectra that suggested formation of complexes between luteolin and any of the other metal ions at both pH values. However, it was previously shown that quercetin-metal complexes were readily ionized but that for the luteolin-metal complexes showed limited intensity [48]. Thus, the lack of detected luteolin-metal complexes in our MS results could not be considered as evidence for absence of complexation.

Our MS results slightly deviate from what was previously reported based on potentiometric titrations [7,8,21,38,49–54], in which it was shown that (i) at pH 4 Al(III) forms a 1:1 metal:flavonoid complex with quercetin and luteolin, (ii) for Fe(III) a 1:1 complex was observed with luteolin, and (iii) the 1:1 and 1:2 ratios were preferred for quercetin [7,8]. However, these potentiometric studies only took the water soluble complex into account, whereas the present study also analyzed the ES fractions. So, the obtained

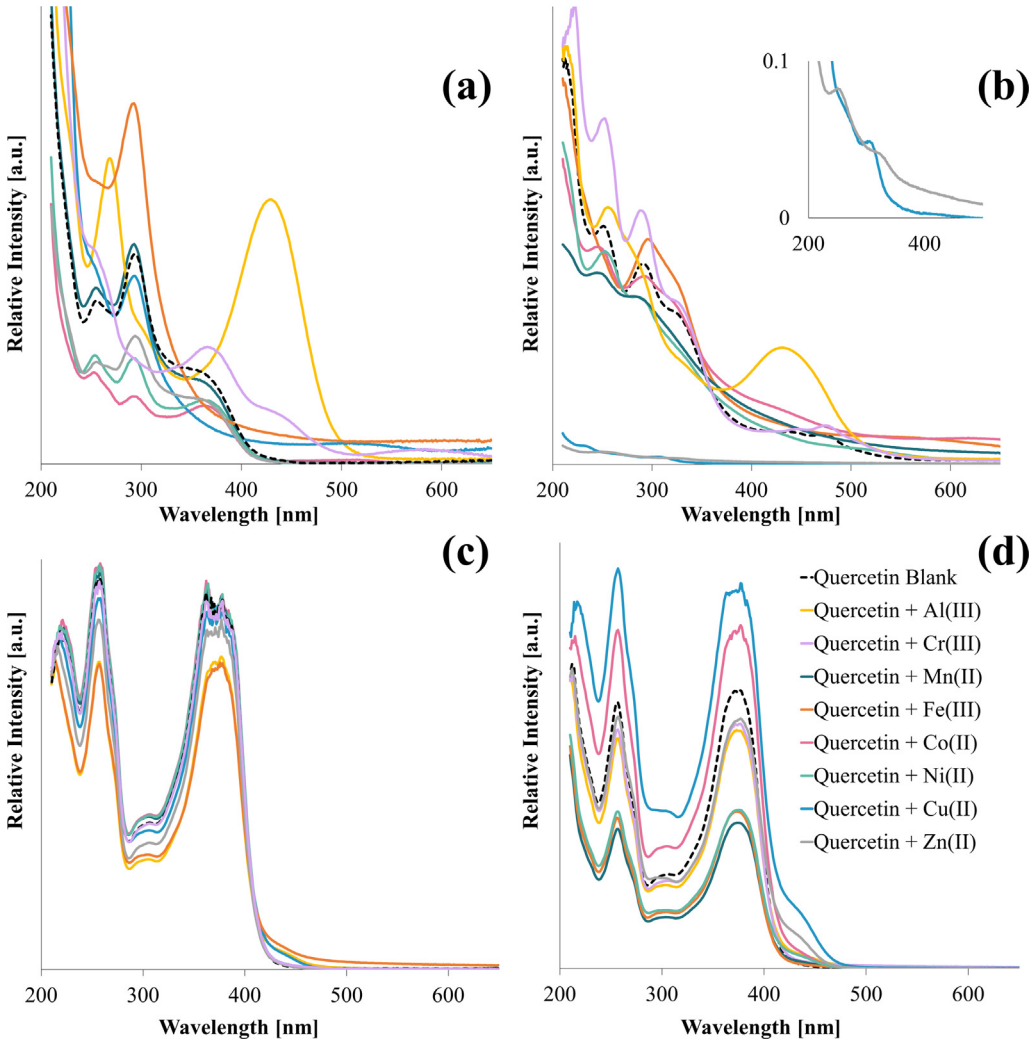

Fig. 2. UV–Vis spectra of WS of quercetin-metal cation systems after 24 h incubation at pH 4 (a) and at pH 7.4 (b), and of ES of quercetin-metal cations systems at pH 4 (c) and at pH 7.4 (d). The inset in (b) is a zoom in on the Zn(II) (grey line) and Cu(II) (light-blue line) spectra from 200 to 500 nm. Spectra can only be used for qualitative comparisons due to differences in dilutions and solubility. (For interpretation of the references to colour in this figure legend, the reader is referred to the web version of this article.)

stoichiometries with a higher metal:flavonoid ratio, and consequently a higher molecular weight and hydrophobicity, are plausible in an ethanolic environment [16,55]. We assumed that our tentatively identified complexes were indeed present as such in the solution and not formed during the electrospray process [56,57], we also confirmed this previously for Fe^{3+}-catechol complexes at 1:1, 1:2, and 1:3 ratios by UV–Vis and electrospray MS [55].

3.1.3. Metal binding sites on quercetin and luteolin

To gain further insight on the quercetin and luteolin binding sites towards the different metal cations, ^{1}H NMR spectra were recorded of the ES fractions after evaporation of EtOH and redissolving the solids in DMSO d_6. In a non-protic solvent, such as DMSO d_6, the complexation of metal to the –OH groups of the flavonoid was expected to lead to a change of the proton signals from the –OH groups [20,22,24,45,58]. The increase of the conjugated system upon complexation is expected to result in an upfield (shielded) shift of the proton signals [20,22]. Because of the paramagnetic nature of Mn(II) and Al(III), the ferromagnetic nature of Fe(III), Co(II), and Ni(II), and the antiferromagnetic nature of Cr (III), broadening of spectral peaks, large splitting, or shielding of the protons were expected upon complexation of flavonoid by these metal ions. Additionally, if specific proton signals show this broadening, splitting, or shielding, it could also be used to identify the binding position [45,58].

In line with the spectroscopic and spectrometric data we did not observe proton shifts in the quercetin spectra for the divalent metal cations at pH 4 (Fig. S6 and Table S6). For Al(III), Fe(III), and Cr(III), peak broadening and shifts in the –OH signals were observed at pH 4 indicating the formation of complexes. For Al (III) and Fe(III) the resonances of 4′-OH and 3′-OH improved, possibly due to metal coordination reducing the proton exchange rate. The upfield shift in the 3′-OH indicates that the quercetin is able to chelate Al(III) and Fe(III) at pH 4 *via* the 3′- or 4′- phenolic groups, in line with previous findings with other metal ions [20,59,60]. However, the shift in 3-OH signal indicated that coordination to the 3–4 site should not be excluded for Al(III) and Fe(III). This shift in signal upon complexation was previously ascribed to the increase of conjugation caused by the effect of coordination [7]. For Cr(III) all signals showed some peak broadening, but no preferred binding site could be ascribed with the current data.

For luteolin at pH 4, small differences in the peak shape in the aromatic region were observed for all metal ions, except Zn(II) (Fig. S7 and Table S7). Because no shifts were observed in the positions of 5-OH, H3 and H6, but differences were observed in the

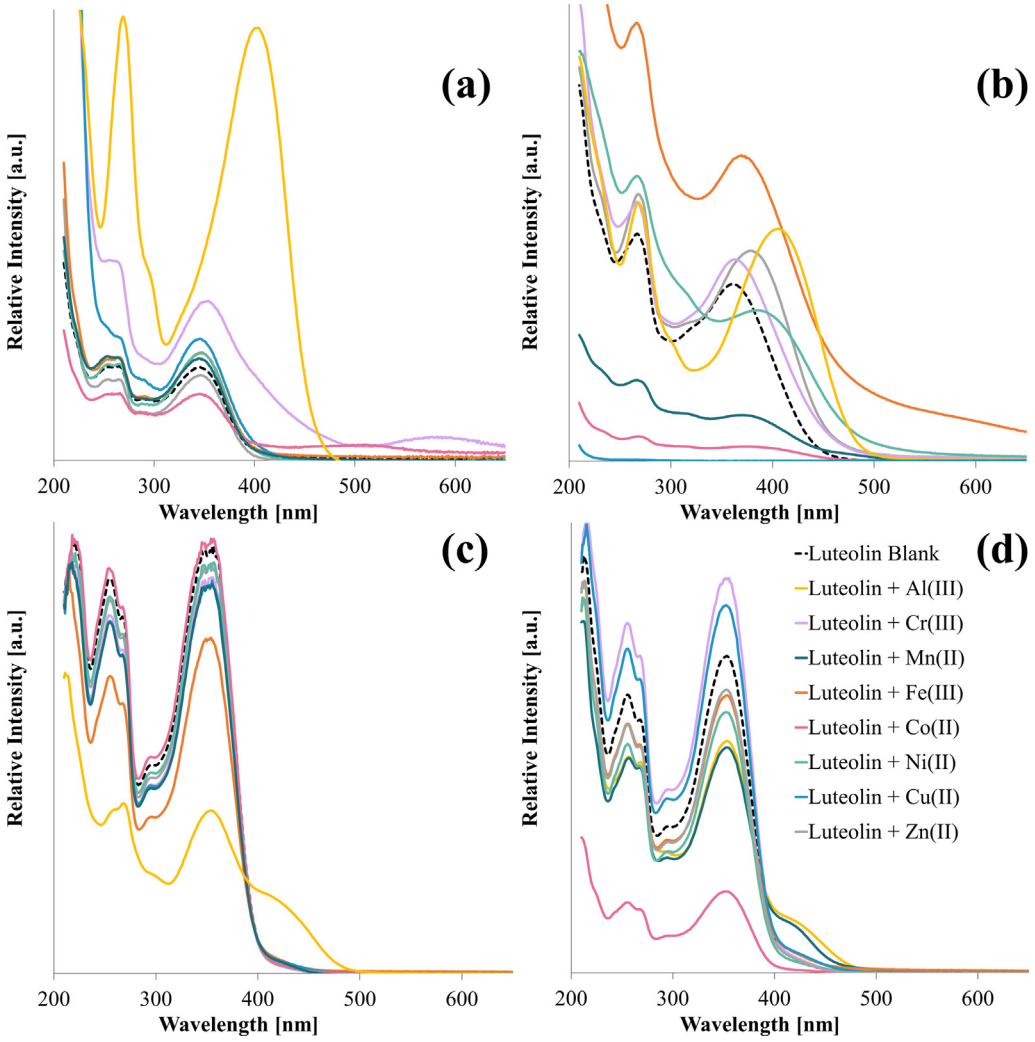

Fig. 3. UV–Vis spectra of WS of luteolin-metal cations systems after 24 h incubation at pH 4 (a) and at pH 7.4 (b), and of ES of luteolin-metal cations systems at pH 4 (c) and at pH 7.4 (d). Spectra can only be used for qualitative comparisons due to differences in dilutions and solubility.

Table 1
Tentative identification of metal-flavonoid complexes (M:F) based on ESI-ITMS.

Metal (M)	pH	*m/z* Exp.	Tentatively identified complex	Stoichiometry M:F
Al(III)	4	629	$[Al(III) + 2(Q^{a} - H)]^{+}$	1:2
		969	$[Al(III) + 3(Q - H) + K]^{+}$	1:3
	4	597	$[Al(III) + 2(L^{b} - H)]^{+}$	1: 2
		653	$[Al(III) + 2(L - H) + OH + K]^{+}$	1:2
		921	$[Al(III) + 3(L - H) + K]^{+}$	1:3
	7.4	n.d.[c]	n.d.	n.d.
Mn(II)	4	n.d.	n.d.	n.d.
	7.4	n.d.	n.d.	n.d.
Fe(III)	4	998	$[Fe(II) + 2Q+(Q - H) + 2H_2O]^{+}$	1:3
	7.4	n.d.	n.d.	n.d.
Co(II)	4	n.d.	n.d.	n.d.
	7.4	662	$[Co(II) + Q+(Q - H)]^{+}$	1:2
Ni(II)	4	n.d.	n.d.	n.d.
	7.4	661	$[Ni(II) + Q+(Q - H)]^{+}$	1:2
		699	$[Ni(II) + 2(Q - H) + K]^{+}$	
		773	$[3Ni(II) +(Q-2H)+(Q - 3H)]^{+}$	3:2
Cu(II)	4	n.d.	n.d.	n.d.
	7.4	704	$[Cu(II) + 2(Q - H) + K]^{+}$	1:2
		688	$[Cu(II) + 2(Q - H) + Na]$	
Zn(II)	4	n.d.	n.d.	n.d.
	7.4	705	$[Zn(II) + 2(Q - H) + K]^{+}$	1:2

[a] Quercetin, [b] Luteolin, [c] n.d., not detected with the ESI-ITMS setup.

peaks of 4′-OH and 3′-OH we interpret that the 3′-4′ binding site is the preferred one for these metal ions at pH 4.

Complexation of the deprotonated flavonoids with the transition metal cations at pH 7.4 resulted in a broadening of some OH signals in the region from 13 to 9 ppm, and in a broadening and/or disappearance of several proton signals in the aromatic region (*i.e.*, from 8 to 6 ppm) (Figs. S8-S9 and Tables S8-S9). All the systems with quercetin at pH 7.4 showed a shift in the 3-OH position, suggesting binding to the 3–4 site. Furthermore, the shifts in signal for 4′-OH and the protons on the B-ring suggest binding on the 3′-4′ sites for all metal ions as well. Finally, the 5–4 site could be excluded in the systems of Al(III) and Ni(II), whereas for the other metal cations also this coordination site is possible (Fig. S8 and Table S8).

For luteolin, at pH 7.4, the ^{1}H NMR data also suggested coordination to the 3′-4′ site for all metal ions. With the exception of Al(III), all the other metal cations coordinated to the 4–5 site as well, as is indicated by the shift and/or broadening of the 5-OH signal (Fig. S9 and Table S9). These results showed that at pH 7.4 most of the metal ions show no preference towards the available binding sites. This absence of a preferred binding site may also explain why contradictory results were reported in literature regarding the preferred binding sites [21,23,38,50,61] and are in line with our previous findings using a computational approach [7].

Fig. 4 summarizes the findings of this work regarding the metal complexation in aqueous solutions by quercetin and luteolin at pH 4 and 7.4. The spectral changes by UV–Vis showed that in slightly acidic conditions (*i.e.*, pH 4) quercetin and luteolin are suitable chelators for trivalent metal cations. The coordination sites as determined by ^{1}H NMR showed no preference towards the 3–4 or 3′-4′ binding sites for quercetin at both pH values. Coordination to the 4–5 binding site at pH 7.4 was also included for all metal ions except for Al(III) and Ni(II). The stoichiometric data that could be obtained for quercetin showed that the divalent metal cations are most likely to coordinate in a 1:2 stoichiometry whereas the trivalent metal ions also showed coordination in a 1:3 fashion. These results demonstrate that the metal complexation and the binding sites are highly dependent on the pH as well as on the nature of the metal ion.

3.2. Reactivity of metal-flavonoid complexes

Ideal chelators should be resistant to metal-induced degradation reactions (*e.g. via* hydrolysis, reduction or oxidation). Complexation of flavonoids by metal ions can, however, be followed up by electron transfer reactions that oxidize flavonoids, which then undergo further degradation [26]. To provide detailed insights into the oxidation and degradation of luteolin and quercetin, the formation of degradation products was monitored by RP-UHPLC-PDA-ESI-MS^{n} at both pH 4 and 7.4.

3.2.1. Stability of the flavonoids in presence of metal ions in aqueous solution

The recovery of quercetin and luteolin in presence of metal cations was quantified using RP-UHPLC-PDA-ESI-MS^{n} at various timepoints of the incubation. Flavonoid recoveries for all metal-

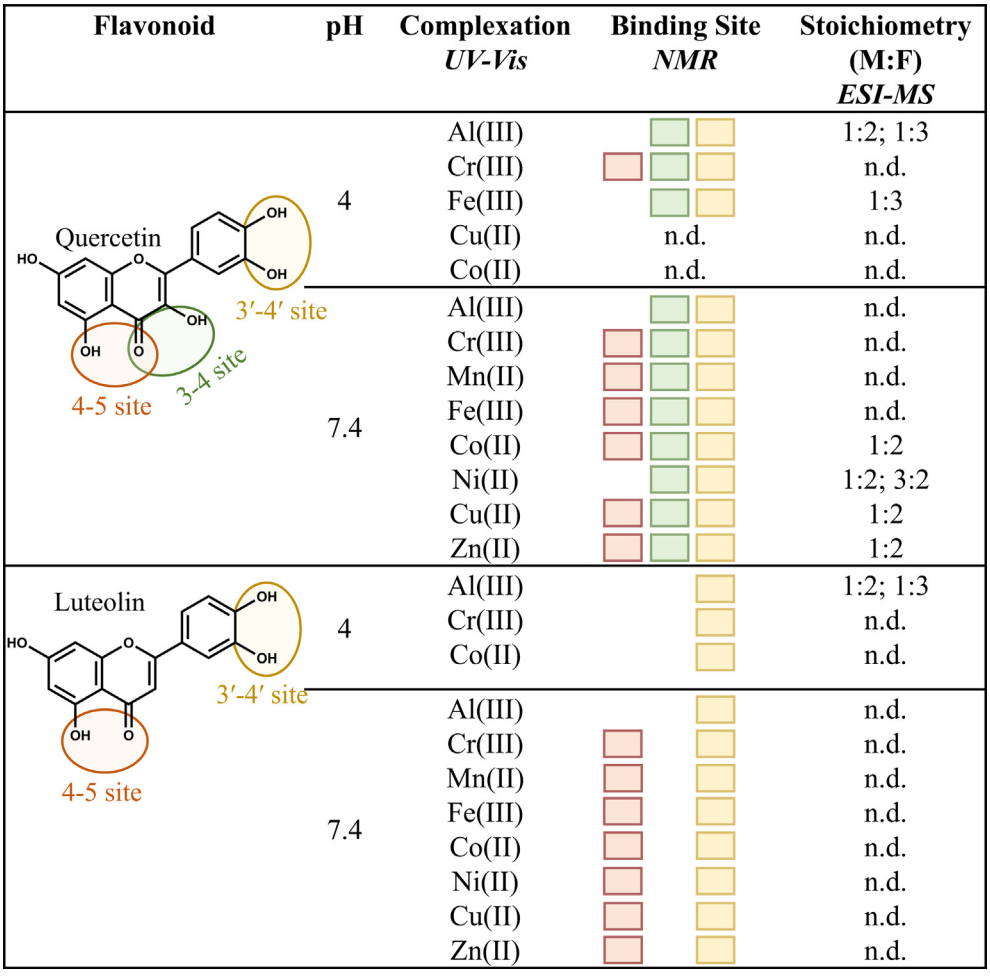

Fig. 4. Overview of characteristics of the metal chelates for quercetin and luteolin at pH 4 and 7.4. M:F, metal:flavonoid.

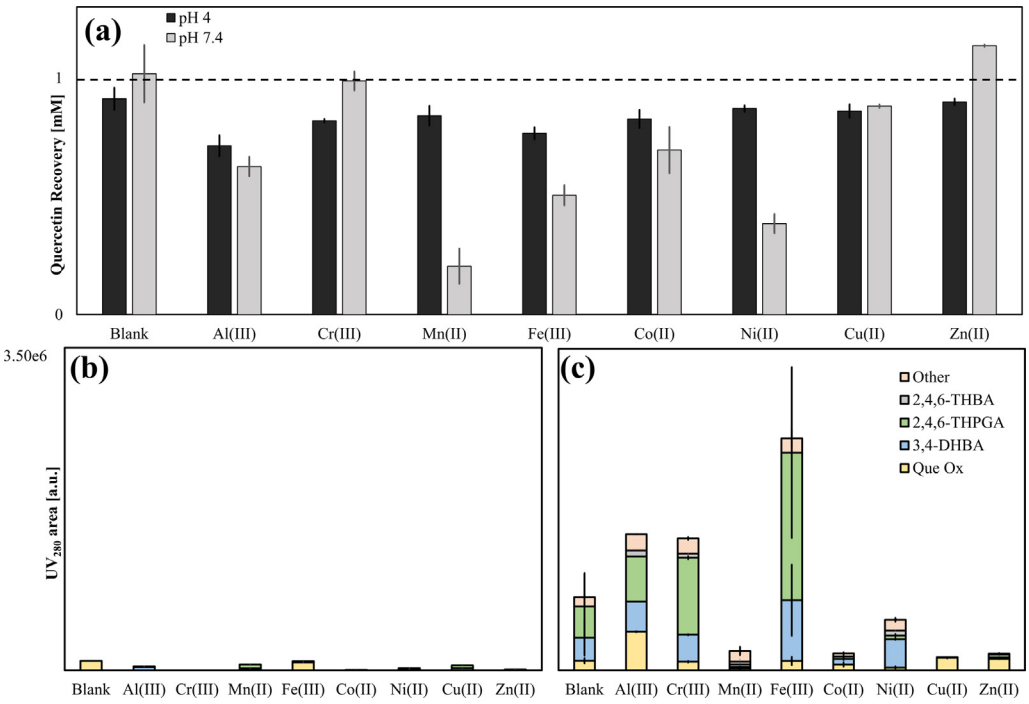

Fig. 5. Recovery based on the sum of the concentrations measured in the WS and ES fraction of the quercetin blank and quercetin metal systems after incubation in aqueous solutions at pH 4 and 7.4 (a); the dotted line indicates the starting concentration of quercetin (*i.e.*, 1.0 mM). Sum of the $UV_{280\ nm}$ peak areas measured in the WS and ES UV for the degradation products after 24 h of incubation of quercetin and quercetin-metal cations systems at pH 4 (b) and pH 7.4 (c).

flavonoid systems were higher at pH 4 than at pH 7.4, except for Cr (III) and Zn(II) (Fig. 5a and Fig. S10). The decreased recovery in the WS and ES fraction after incubation with metal ions can either be a result from oxidation, or from the formation of insoluble metal-phenolic networks [32].

The chromatograms of luteolin in the absence and presence of metal cations, at pH 4 and 7.4, after 24 h of incubation (Figs. S11 and S12) did not show any degradation or coupling products. The decrease in luteolin recovery at pH 7.4 (Fig. S10) is therefore suggested to be due to the formation of insoluble complexes or networks rather than (oxidative) degradation or coupling reactions. Formation of these networks was previously described for luteolin in presence of Fe(III) [32]. For quercetin the recovery at pH 7.4 decreased in the order of Zn(II) > Cr(III) > Cu(II) > Co(II) > Al(III) > Fe(III) > Ni(II) > Mn(II). No direct relation between the recovery and characteristics of the metal (Table S10), such as Lewis hardness, redox potential, ionic radius, or the number of empty shells in the d-orbital, was found.

The chromatograms of the quercetin-containing systems showed that aqueous incubation resulted in the formation of new peaks (Figs. S13 and S14). The peaks were tentatively identified based on spectroscopic and spectrometric data (Table S11) [32]. These identified compounds were previously also reported as oxidative products of quercetin [62]. In the ES fractions we observed one peak with a difference in m/z of 16 amu: this peak was identified as oxidized quercetin (Que Ox), a hydroxylated intermediate of quercetin degradation [32]. In the WS fractions at pH 4 and 7.4, we detected 3,4-dihydroxybenzoic acid (3,4-DHBA; protocatechuic acid), 2,4,6-trihydroxyphenylglyoxylic acid (2,4,6-THPGA; phloroglucinol carboxylic acid), and 2,4,6-trihydroxybenzoic acid (2,4,6-THBA). An overview of the peak areas of the main characteristic degradation products for quercetin in presence of the different metal ions at pH 4 and 7.4 is shown in Fig. 5 (b-c).

Depending on pH and the type of metal, different degradation products and ratios of the oxidation products were observed: at pH 4 the main product in absence of metal ions was Que Ox, while we observed formation of degradation products only in presence of Al(III), Mn(II), Fe(III), and Cu(II). As these were the metal ions that were able form complexes with quercetin at pH 4 (Section 3.1), these results confirm that metal complexation could induce flavonoid degradation.

At pH 7.4 more oxidation products were identified in presence of the trivalent metal cations Cr(III), Fe(III), and Al(III) compared to the blanks and also to divalent ones. For Mn(II), Ni(II), and Co (II) we observed a decrease in recovery of quercetin of 80, 64, and 32 % compared to the quercetin blank, respectively. However, we did not observe increased quantities of degradation products in these samples. Several new peaks were detected in the UV_{280} chromatograms of these samples, but we could not identify the products in the MS chromatograms due to a lack of signal in the MS chromatograms. Given their relatively low polarity, we assume that these UV peaks at 280 nm also correspond to oxidative degradation products, and they are named 'other' in Fig. 5 (b-c). Moreover, the decrease in recovery of these samples can also be due to the formation of insoluble metal-flavonoid complexes or networks. Even after addition of EtOH a black precipitate remained, which was previously also observed for iron-flavonoid networks [32].

Interestingly, for Zn(II) no lower recovery was observed after 24 h incubation and less oxidation product was observed compared to the blank quercetin. These results indicate that Zn(II) is no oxidizing agent for quercetin, in line with literature [24,63]. This can be explained by the fact that the 3d orbital of zinc contains 10 electrons and is filled, which makes electron transfer from quercetin to zinc unfavorable. Also for Cu(II), no degradation products were observed and the recovery at pH 7.4 did also not show a steep decrease. Considering the lower recovery of intact quercetin at pH 7.4 for Fe(III), Mn(II), and Ni(II) compared to the other metal cations (Fig. 5a), the oxidation reaction was further investigated by incubation of these systems with Fe(III), Mn(II), and Ni(II) for 8 and 48 h (Fig. S15). All the identified oxidation products reached

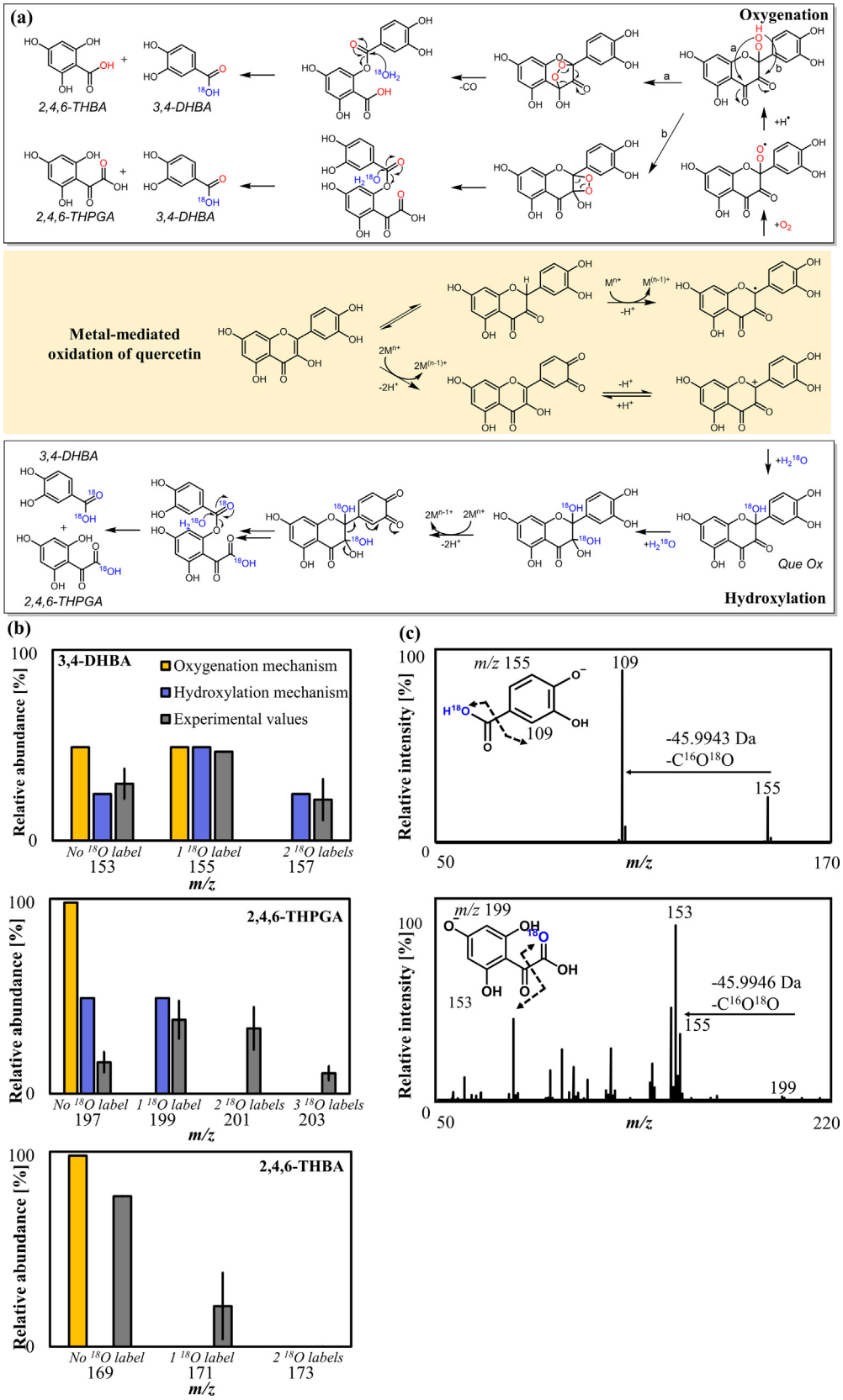

Fig. 6. Putative pathways of quercetin oxidation in $H_2^{18}O$ labeled water after metal coordination; quercetin oxygenation reaction pathway involving the incorporation of an oxygen atom and quercetin hydroxylation reaction pathway involving the incorporation of hydroxyl (a); theoretical abundances of labeled oxidation products according to the oxygenation and hydroxylation mechanism and the experimental values observed as an average of all quercetin-metal incubations with the error bar indicating the differences between the different metal samples (b); fragmentation of single labeled 3,4-DHBA and 2,4,6-THPGA, indicating that the ^{18}O oxygen is present on the carboxylic acid moiety (c).

a maximum value after 24 h of incubation whereupon they decreased or disappeared. These results imply that the formed 3,4-DHBA, 2,4,6-THPGA and 2,4,6-THBA are intermediate reaction products that can be further oxidized towards products that were not observed by RP-UHPLC-PDA-MS^n. Overall, these findings show that luteolin is resistant towards oxidative degradation reactions upon metal-complexation with the metal ions tested in this study. Quercetin-metal complexes show degradation within 24 h in aqueous solution at pH 7.4 in presence of Al(III), Cr(III), Mn(II), Fe(III), Co (II), and Ni(II).

3.2.2. Insights into the metal-mediated oxidation of quercetin

Results of present study show that the established chelator quercetin is prone to oxidative reactions at physiological pH in aqueous solution. Upon (metal-mediated) oxidation of flavonoids an oxygen atom is introduced, for which different origins (*e.g.*,O_2 or H_2O) have been proposed [32,64–67]. To better understand whether quercetin oxidation and degradation in aqueous solutions are dependent on O_2 or H_2O we aimed to identify the origin of the oxygen atom by performing the reaction in $H_2^{18}O$ in presence of atmospheric oxygen (*i.e.* ^{16}O). This is valuable information to better understand if the metal-mediated oxidative degradation can also occur in the anaerobic conditions in the colon at physiological pH [68,69]. The proposed oxidation pathways and degradation products, involving oxygenation and/or hydroxylation, after incubation in $H_2^{18}O$ are shown in Fig. 6a. While the two putative oxidative pathways via oxygenation or hydroxylation can yield similar reaction products, the products will show a distinct ^{18}O-labeling pattern (Fig. 6a). If upon hydroxylation one oxygen atom from $H_2^{18}O$ is incorporated, the product will be observed with an m/z value of 2 Da higher as compared to an incorporation from O_2, if two ^{18}O oxygen atoms are incorporated the m/z will be 4 Da higher compared to incorporation from O_2.

We calculated the theoretical abundance of the ^{18}O isotopes in 3,4-DHBA, 2,4,6-THBA, and 2,4,6-THPGA according to the oxygenation and hydroxylation mechanism and compared these to the experimentally obtained abundances (Fig. 6b). For the calculation of the theoretical values, we corrected for the fact that the incubations were performed in 50 vol% $H_2^{18}O$ (Table S12).

The experimental labeling of 3,4-DHBA after incubation of quercetin with the different metal ions showed a similar profile as the theoretical one of the hydroxylation mechanism. However, the presence of 2,4,6-THBA was linked to the oxygenation mechanism. For 2,4,6-THPGA we observed more labeling then was theoretically assumed based on the putative pathways of quercetin, we found experimental m/z values corresponding to the m/z of the phenolic + 2, + 4 and + 6 Da (Fig. 6b), indicating the presence of one, two or three ^{18}O atoms on the phenolic acids, respectively.

Besides labeling of the carboxylic acid groups as a result of hydrolysis during the oxidation reaction, the labeling may also be a result of $^{16}O/^{18}O$ exchange. Previously we observed $^{16}O/^{18}O$ exchange of catechol motifs in $H_2^{18}O$ in presence of transition metal cations [70]. However, the MS^2 fragmentation of 3,4-DHBA as degradative products from quercetin confirmed that the ^{18}O label on the products that are formed from quercetin are present on the carboxylic acid group rather than the catecholate moiety (Fig. 6c; Fig. S16). The MS^2 fragmentation patterns of 3,4-DHBA therefore indicates that the labeling observed in the quercetin oxidation products is resulting from a hydrolysis reaction rather than $^{16}O/^{18}O$ exchange of the catechol motif. For 2,4,6- THPGA we also confirmed that the labels were present on the glyoxylic acid group. However, it should be noted that the high experimental labeling values obtained for 2,4,6-THPGA can be a result of from spontaneous $^{16}O/^{18}O$ exchange on the glyoxylic acid moiety. The extra carbonyl group makes the glyoxylic acid moiety more electrophilic than the carboxylic acid moiety of 3,4-DHBA, and therefore more prone to $^{16}O/^{18}O$ exchange via reversible addition of water.

Based on the obtained experimental abundances of the labeled oxidation products in comparison with the theoretical values of the oxygenation or hydroxylation mechanism, we cannot yet make a conclusion about the origin of oxygen and the preferred quercetin oxidation pathway in presence of metal ions. Thus, it seems plausible that these two degradation mechanisms may occur concurrently and possibly not exclusively. In presence of trivalent metal cations (Cr(III), Al(III), and Fe(III)), relatively more 2,4,6-THPGA was observed compared to the other metal cations (Fig. 5c). Formation of more 2,4,6-THPGA for the trivalent metal ions hints that the hydroxylation pathway (Fig. 6b) is the preferred pathway for quercetin oxidation in presence of Al(III), Cr(III), and Fe(III). Future work should further investigate the fate of these flavonoid-metal chelates *in vivo* in the gastrointestinal tract.

Table 2
Proposed guideline of the preferred flavonoid-metal chelation systems in aqueous solutions at pH 4 and 7.4. For each of the metal ions it is indicated if quercetin (Q) or luteolin (L) is complexing, if oxidation occurs for Q or L or is not detected (n.d.) and what the proposed chelator is.

pH	Metal	Complexation	Oxidation	Proposed chelator
4	Al(III)	Q + L	no	Q + L
	Cr(III)	Q + L	n.d.	Q + L
	Mn(II)	n.d.	n.d.	none
	Fe(III)	Q + L	n.d.	none
	Co(II)	Q	n.d.	Q
	Ni(II)	n.d.	n.d.	none
	Cu(II)	Q	n.d.	Q
	Zn(II)	n.d.	n.d.	none
7.4	Al(III)	Q + L	Q	L
	Cr(III)	Q + L	Q	L
	Mn(II)	Q + L	Q	L
	Fe(III)	Q + L	Q	L
	Co(II)	Q + L	Q	L
	Ni(II)	Q + L	Q	L
	Cu(II)	Q + L	n.d.	Q + L
	Zn(II)	Q + L	n.d.	Q + L

3.3. Characteristics of metal chelates and effects on flavonoid oxidation

In choosing the ideal chelator for metal ions at acidic and neutral pH, the ability of the flavonoids to chelate them and the stability of the formed complex against subsequent oxidation reactions in aqueous solutions should be considered. Table 2 shows an overview of the preferred flavonoid-metal chelation systems at pH 4 and pH 7.4. At pH 4, both quercetin and luteolin are suitable chelators for the trivalent metal cations Al(III), Cr(III), and Fe(III). Additionally, quercetin can also chelate Co(II) and Cu(II). The other metal ions are not chelated at pH 4 by the flavonoids investigated in this work. We propose that luteolin is the best ligand for the chelation of Al(III), Cr(III), Mn(II), Fe(III), Co(II), and Ni(II) at physiological pH (*i.e.*, 7.4), because it is less prone to oxidative degradation reactions compared to quercetin. For the chelation of Cu(II) and Zn(II) at physiological pH, both quercetin and luteolin are suitable chelators. These metal ions appear to be no oxidizing agent for quercetin.

4. Conclusions

This is the first study to investigate the complexation and oxidation of quercetin and luteolin in presence of Cr(III), Mn(II), Fe (III), Co(II), Ni(II), Cu(II), Zn(II), and Al(III) in aqueous solution, at pH 4 and 7.4. Deprotonation of the hydroxyl groups at neutral pH resulted in more complexation at pH 7.4 than pH 4. At pH 7.4, representing the physiological pH, all metal ions showed com-

plexation with quercetin and luteolin although the binding site, stoichiometry, and oxidative stability were metal and flavonoid dependent. Most of the investigated metal ions, except for Al(III) and Ni(II), did not show any binding site preference. Chelation of metal ions by quercetin, but not luteolin, was followed by metal-mediated oxidation reactions. At pH 7.4, the presence of the selected metal cations (except for Zn(II), and Cu(II)) catalyzes this oxidation reaction. Investigation of the oxidation pathway by performing the incubations in $H_2^{18}O$ hints that from the suggested putative pathways of oxidation, the H_2O-dependent hydroxylation mechanism is preferred in presence of the trivalent metal cations. The findings suggest that quercetin oxidation in presence of the divalent ones can occur by either hydroxylation and/or oxygenation. This study shows that luteolin is a suitable flavonoid for chelation of first-row transition metal cations and Al(III), allowing the formation of stable complexes in aqueous solutions at physiological pH without degradation of the flavonoid.

CRediT authorship contribution statement

Luana Malacaria: Conceptualization, Methodology, Investigation, Data curation, Visualization, Writing - original draft. **Judith Bijlsma:** Conceptualization, Methodology, Investigation, Data curation, Visualization, Writing – original draft. **Roelant Hilgers:** Conceptualization, Methodology, Data curation, Supervision, Writing – review & editing. **Wouter J.C. de Bruijn:** Conceptualization, Methodology, Data curation, Supervision, Writing – review & editing. **Jean-Paul Vincken:** Conceptualization, Supervision, Writing – review & editing. **Emilia Furia:** Conceptualization, Methodology, Data curation, Visualization Supervision, Writing – original draft.

Data availability

Data will be made available on request.

Declaration of Competing Interest

The authors declare that they have no known competing financial interests or personal relationships that could have appeared to influence the work reported in this paper.

Acknowledgements

L.M. and E.F. thank the Dipartimento di Chimica e Tecnologie Chimiche, Università della Calabria for the financial support. The authors are grateful to Annemiek van Zadelhoff (Laboratory of Food Chemistry, Wageningen University & Research) for her help with the NMR measurements. Part of the presented results were obtained using a Thermo Scientific Velos Pro MS system and a Thermo Scientific Q Exactive Focus Orbitrap MS system which are owned by WUR-Shared Research Facilities. Investment by WUR-Shared Research Facility was made possible by the 'Regio Deal Foodvalley' of the province of Gelderland, the Netherlands.

Appendix A. Supplementary data

Supplementary data to this article can be found online at https://doi.org/10.1016/j.molliq.2022.120840.

References

[1] H. Guven, A. Arici, O. Simsek, Flavonoids in our foods: A short review, J. Bas. Clin. Health Sci. 3 (2019) 96–106, https://doi.org/10.30621/jbachs.2019.555.
[2] E. Barrajón-Catalán, M. Herranz-López, J. Joven, A. Segura-Carretero, C. Alonso-Villaverde, J.A. Menéndez, V. Micol, Molecular promiscuity of plant polyphenols in the management of age-related diseases: Far beyond their antioxidant properties, In J. Camps (Ed.), Oxidative stress and inflammation in non-communicable diseases-molecular mechanisms and perspectives in therapeutics. Springer International Publishing Switzerland (2014) 141-159. https://doi.org/10.1007/978-3-319-07320-0
[3] D. Ribeiro, C. Proenca, S. Rocha, J.L. Lima, F. Carvalho, E. Fernandes, M. Freitas, Immunomodulatory effects of flavonoids in the prophylaxis and treatment of inflammatory bowel diseases: A comprehensive review, Curr. Med. Chem. 25 (2018) 3374–3412, https://doi.org/10.2174/0929867325666180214121734.
[4] P.I. Oteiza, C.G. Fraga, D.A. Mills, D.H. Taft, Flavonoids and the gastrointestinal tract: Local and systemic effects, Mol. Asp. Med. 61 (2018) 41–49, https://doi.org/10.1016/j.mam.2018.01.001.
[5] D. Taverna, L. Di Donna, F. Mazzotti, A. Tagarelli, A. Napoli, E. Furia, G. Sindona, Rapid discrimination of bergamot essential oil by paper spray mass spectrometry and chemometric analysis, J. Mass Spect. (2016) 761–767, https://doi.org/10.1002/jms.3820 [[5].
[6] G. Williamson, C.D. Kay, A. Crozier, The bioavailability, transport, and bioactivity of dietary flavonoids: A review from a historical perspective, Comp. Rev. Food Sci. Food Saf. 17 (2018) 1054–1112, https://doi.org/10.1111/1541-4337.12351.
[7] G.A. Corrente, L. Malacaria, A. Beneduci, E. Furia, T. Marino, G. Mazzone, Experimental and theoretical study on the coordination properties of quercetin towards aluminum(III), iron(III) and copper(ii) in aqueous solution, J. Mol. Liq. 325 (2021), https://doi.org/10.1016/j.molliq.2020.115171.
[8] L. Malacaria, C. La Torre, E. Furia, A. Fazio, M.C. Caroleo, E. Cione, L. Gallelli, T. Marino, P. Plastina, Aluminum(III), iron(III) and copper(ii) complexes of luteolin: Stability, antioxidant, and anti-inflammatory properties, J. Mol. Liq. 345 (2022), https://doi.org/10.1016/j.molliq.2021.117895.
[9] L. Malacaria, G.A. Corrente, A. Beneduci, E. Furia, T. Marino, G. Mazzone, A review on coordination properties of Al(III) and Fe(III) toward natural antioxidant molecules: Experimental and theoretical insights, Molecules 26 (2021) 2603, https://doi.org/10.3390/molecules26092603.
[10] E. Furia, R. Porto, 2-Hydroxybenzamide as a Ligand. Complex Formation with Dioxouranium(VI), Aluminum(III), Neodymium(III), and Nickel(II) Ions, J. Chem. Eng. Data 53 (12) (2008) 2739–2745.
[11] S.J.S. Flora, V. Pachauri, Chelation in metal intoxication, Int. J. Env. Res. Pub. Health 7 (2010) 2745–2788, https://doi.org/10.3390/ijerph7072745.
[12] S.J.S. Flora, A. Mehta, R. Gupta, Prevention of arsenic-induced hepatic apoptosis by concomitant administration of garlic extracts in mice, Chem.-Bio. Int. 177 (2009) 227–233, https://doi.org/10.1016/j.cbi.2008.08.017.
[13] I. Angel, A. Bar, T. Horovitz, G. Taler, M. Krakovsky, D. Resnitsky, G. Rosenberg, S. Striem, J.E. Friedman, A. Kozak, Metal ion chelation in neurodegenerative disorders, Drug Dev. Res. 56 (2002) 300–309, https://doi.org/10.1002/ddr.10083.
[14] M.L. Hegde, P. Bharathi, A. Suram, C. Venugopal, R. Jagannathan, P. Poddar, P. Srinivas, K. Sambamurti, K.J. Rao, J. Scancar, L. Messori, L. Zecca, P. Zatta, Challenges associated with metal chelation therapy in Alzheimer's disease, J. Alz. dis. 17 (2009) 457–468, https://doi.org/10.3233/JAD-2009-1068.
[15] R. Squitti, Metals in alzheimer's disease: A systemic perspective, Front. Bio.-Land. 17 (2012) 451, https://doi.org/10.2741/3938.
[16] N.R. Perron, J.L. Brumaghim, A review of the antioxidant mechanisms of polyphenol compounds related to iron binding, Cell Biochem. Biophys. 53 (2009) 75–100, https://doi.org/10.1007/s12013-009-9043-x.
[17] R.C. Hider, Z.D. Liu, H.H. Khodr, Metal chelation of polyphenols, In Methods in enzymology. Elsevier (2001) 190-203. https://doi.org/10.1016/s0076-6879(01)35243-6.
[18] V. Uivarosi, A.C. Munteanu, A. Sharma, H. Singh Tuli, Metal complexation and patent studies of flavonoid, In H. Singh Tuli (Ed.), Current aspects of flavonoids: Their role in cancer treatment. Springer Singapore (2019) 39-89. https://doi.org/10.1007/978-981-13-5874-6_4
[19] G. Flora, M. Mittal, S.J. Flora, Medical countermeasures—chelation therapy, in: Handbook of arsenic toxicology, Elsevier, 2015, pp. 589–626, https://doi.org/10.1016/B978-0-12-418688-0.00026-5.
[20] S.B. Bukhari, S. Memon, M. Mahroof-Tahir, M.I. Bhanger, Synthesis, characterization and antioxidant activity copper–quercetin complex, Spectrochim, Acta Part A: Mol. Biomol. Spect. 71 (2009) 1901–1906, https://doi.org/10.1016/j.saa.2008.07.030.
[21] J.P. Cornard, J.C. Merlin, Spectroscopic and structural study of complexes of quercetin with Al(III), J. Inorg. Biochem. 92 (2002) 19–27, https://doi.org/10.1016/S0162-0134(02)00469-5.
[22] R.F.V. de Souza, E.M. Sussuchi, W.F. De Giovani, Synthesis, electrochemical, spectral, and antioxidant properties of complexes of flavonoids with metal ions, Synt. React. Inorg. Metal-Org. Chem. 33 (2003) 1125–1144, https://doi.org/10.1081/sim-120023482.
[23] M.M. Kasprzak, A. Erxleben, J. Ochocki, Properties and applications of flavonoid metal complexes, RSC Adv. 5 (2015) 45853–45877, https://doi.org/10.1039/C5RA05069C.
[24] A. Primikyri, G. Mazzone, C. Lekka, A.G. Tzakos, N. Russo, I.P. Gerothanassis, Understanding zinc(ii) chelation with quercetin and luteolin: A combined nmr and theoretical study, J. Phys. Chem. B 119 (2015) 83–95, https://doi.org/10.1021/jp509752s.
[25] R. Ravichandran, M. Rajendran, D. Devapiriam, Antioxidant study of quercetin and their metal complex and determination of stability constant by spectrophotometry method, Food Chem. 146 (2014) 472–478, https://doi.org/10.1016/j.foodchem.2013.09.080.
[26] P. Ryan, M.J. Hynes, The kinetics and mechanisms of the reactions of iron(III) with quercetin and morin, J. Inorg. Biochem. 102 (2008) 127–136, https://doi.org/10.1016/j.jinorgbio.2007.07.041.

[27] S. Selvaraj, S. Krishnaswamy, V. Devashya, S. Sethuraman, U.M. Krishnan, Flavonoid–metal ion complexes: A novel class of therapeutic agents, Med. Res. Rev. 34 (2014) 677–702, https://doi.org/10.1002/med.21301.
[28] A. Hernandez-Valdes, R. Zarate, A.I. Martinez, M.I. Pech-Canul, M. Garcia-Lobato, R. Villaroel, The role of solvents on the physical properties of sprayed iron oxide films, Vacuum 105 (2014) 26–32, https://doi.org/10.1016/j.vacuum.2014.02.001.
[29] D. Ushakou, T. Wróblewski, Scutellarein in organic solvents: Changes in spectroscopic properties caused by solute-solvent interactions, Spectrochim. Acta Part A: Mol. Biomol. Spectr. 273 (2022), https://doi.org/10.1016/j.saa.2022.121027.
[30] M. Michalík, M. Biela, D. Cagardová, V. Lukeš, Chelates of 3- and 5-hydroxyflavone: Quantum chemical study, Chem. Phys. Lett. 762 (2021), https://doi.org/10.1016/j.cplett.2020.138142.
[31] X. Li, K. Binnemans, Oxidative dissolution of metals in organic solvents, Chem. Rev. 121 (2021) 4506–4530, https://doi.org/10.1021/acs.chemrev.0c00917.
[32] J. Bijlsma, W.J.C. de Bruijn, K.P. Velikov, J.-P. Vincken, Unravelling discolouration caused by iron-flavonoid interactions: Complexation, oxidation, and formation of networks, Food Chem. 370 (2022), https://doi.org/10.1016/j.foodchem.2021.131292.
[33] M. Pinelo, L. Manzocco, M.J. Nuñez, M.C. Nicoli, Solvent effect on quercetin antioxidant capacity, Food Chem. 88 (2004) 201–207, https://doi.org/10.1016/j.foodchem.2004.01.034.
[34] M. Andjelković, J. Van Camp, B. De Meulenaer, G. Depaemelaere, C. Socaciu, M. Verloo, R. Verhe, Iron-chelation properties of phenolic acids bearing catechol and galloyl groups, Food Chem. 98 (2006) 23–31, https://doi.org/10.1016/j.foodchem.2005.05.044.
[35] C.M. Ferreira, I.S. Pinto, E.V. Soares, H.M. Soares, (Un)suitability of the use of ph buffers in biological, biochemical and environmental studies and their interaction with metal ions – a review, RSC Adv. 5 (2015) 30989–31003, https://doi.org/10.1039/C4RA15453C.
[36] R.F.V. de Souza, W.F. De Giovani, Antioxidant properties of complexes of flavonoids with metal ions, Red. Rep. 9 (2004) 97–104, https://doi.org/10.1179/135100004225003897.
[37] M. Guo, C. Perez, Y. Wei, E. Rapoza, G. Su, F. Bou-Abdallah, N. Chasteen, Iron-binding properties of plant phenolics and cranberry's bio-effects, Dalton Trans. (2007) 4951–4961, https://doi.org/10.1039/b705136k.
[38] J. Ren, S. Meng, C.E. Lekka, E. Kaxiras, Complexation of flavonoids with iron: Structure and optical signatures, J. Phys. Chem. B 112 (2008) 1845–1850, https://doi.org/10.1021/jp076881e.
[39] C. Reichardt, T. Welton, Solvents and solvent effects in organic chemistry, John Wiley & Sons, New York, 2011.
[40] S. Selvaraj, S. Shanmugasundaram, M. Maruthamuthu, B. Venkidasamy, S. Shanmugasundaram, Facile synthesis and characterization of quercetin-loaded alginate nanoparticles for enhanced in vitro anticancer effect against human leukemic cancer u937 cells, J. Clust. Sci. 32 (2021) 1507–1518, https://doi.org/10.1007/s10876-020-01913-5.
[41] A. Zhou, S. Kikandi, O.A. Sadik, Electrochemical degradation of quercetin: Isolation and structural elucidation of the degradation products, Electrochem. Comm. 9 (2007) 2246–2255, https://doi.org/10.1016/j.elecom.2007.06.026.
[42] R.G. Pearson, Hard and soft acids and bases, J. Am. Chem. Soc. 85 (1963) 3533–3539, https://doi.org/10.1021/ja00905a001.
[43] J.M. Dimitrić Marković, Z.S. Marković, I.A. Pašti, T.P. Brdarić, A. Popović-Bijelić, M. Mojović, A joint application of spectroscopic, electrochemical and theoretical approaches in evaluation of the radical scavenging activity of 3-oh flavones and their iron complexes towards different radical species, Dalton Trans. 41 (2012) 7295–7303, https://doi.org/10.1039/C2DT30220A.
[44] M. Šimunková, M. Biela, M. Štekláč, A. Hlinčík, E. Klein, M. Malček, Cu(II) complexes of flavonoids in solution: Impact of the Cu(II) ion on the antioxidant and DNA-intercalating properties, J. Mol. Liq. 359 (2022), https://doi.org/10.1016/j.molliq.2022.119230.
[45] F.D. Doty, G. Entzminger, Y.A. Yang, Magnetism in high-resolution nmr probe design. I: General methods, Conc, Mag. Res.: Ed. J. 10 (1998) 133–156, https://doi.org/10.1002/(SICI)1099-0534.
[46] K.J. Kadassery, S.N. MacMillan, D.C. Lacy, Resurgence of organomanganese(i) chemistry. Bidentate manganese(i) phosphine–phenol(ate) complexes, Inorg. Chem. 58 (2019) 10527–10535, https://doi.org/10.1021/acs.inorgchem.9b00941.
[47] V.B. Di Marco, G.G. Bombi, Electrospray mass spectrometry (ESI-MS) in the study of metal–ligand solution equilibria, Mass Spect. Rev. 25 (2006) 347–379, https://doi.org/10.1002/mas.20070.
[48] M. Satterfield, J.S. Brodbelt, Enhanced detection of flavonoids by metal complexation and electrospray ionization mass spectrometry, Anal. Chem. 72 (2000) 5898–5906, https://doi.org/10.1021/ac0007985.
[49] A. Torreggiani, M. Tamba, A. Trinchero, S. Bonora, Copper(II)–quercetin complexes in aqueous solutions: Spectroscopic and kinetic properties, J. Mol. Struct. 744 (2005) 759–766, https://doi.org/10.1016/j.molstruc.2004.11.081.
[50] M. Leopoldini, N. Russo, S. Chiodo, M. Toscano, Iron chelation by the powerful antioxidant flavonoid quercetin, J. Agr. Food Chem. 54 (2006) 6343–6351, https://doi.org/10.1021/jf060986h.
[51] A. Ahmedova, K. Paradowska, I. Wawer, 1H, 13C MAS NMR AND DFT GIAO study of quercetin and its complex with al(III) in solid state, J. Inorg. Biochem. 110 (2012) 27–35, https://doi.org/10.1016/j.jinorgbio.2012.02.007.
[52] L. Dangleterre, J.-P. Cornard, C. Lapouge, Spectroscopic and theoretical investigation of the solvent effects on al(III)–hydroxyflavone complexes, Polyhedron 27 (2008) 1581–1590, https://doi.org/10.1016/j.poly.2008.01.038.
[53] Y.A. Davila, M.I. Sancho, M.C. Almandoz, S.E. Blanco, Structural and spectroscopic study of al(III)–3-hydroxyflavone complex: Determination of the stability constants in water–methanol mixtures, Spectrochim. Acta A: Mol. Biomol. Spect. 95 (2012) 1–7, https://doi.org/10.1016/j.saa.2012.04.034.
[54] M. Symonowicz, M. Kolanek, Flavonoids and their properties to form chelate complexes, Biotec. Food Sci. 76 (2012) 35–41.
[55] J. Bijlsma, W.J.C. de Bruijn, J.A. Hageman, P. Goos, K.P. Velikov, J.-P. Vincken, Revealing the main factors and two-way interactions contributing to food discolouration caused by iron-catechol complexation, Sci. Rep. 10 (2020) 1–11, https://doi.org/10.1038/s41598-020-65171-1.
[56] R.B. Cole, Electrospray ionization mass spectrometry: Fundamentals, instrumentation, and applications, In Electrospray ionization mass spectrometry: Fundamentals, instrumentation, and applications (1997) 577-577.
[57] L. Gianelli, V. Amendola, L. Fabbrizzi, P. Pallavicini, G.G. Mellerio, Investigation of reduction of cu (ii) complexes in positive-ion mode electrospray mass spectrometry, Rapid Comm. Mass Spec. 15 (2001) 2347–2353, https://doi.org/10.1002/rcm.510.
[58] J. Novotný, J. Vícha, P.L. Bora, M. Repisky, M. Straka, S. Komorovsky, R. Marek, Linking the character of the metal–ligand bond to the ligand nmr shielding in transition-metal complexes: Nmr contributions from spin–orbit coupling, J. Chem. Theo. Comp. 13 (2017) 3586–3601, https://doi.org/10.1021/acs.jctc.7b00444.
[59] S.B. Bukhari, S. Memon, M.M. Tahir, M. Bhanger, Synthesis, characterization and investigation of antioxidant activity of cobalt–quercetin complex, J. Mol. Struc. 892 (2008) 39–46, https://doi.org/10.1016/j.saa.2008.07.030.
[60] R.F.V.d. Souza, W.F. De Giovani, Synthesis, spectral and electrochemical properties of al(III) and zn(ii) complexes with flavonoids, Spec. Acta A: Mol. Biomol. Spec. 61 (9) (2005) 1985–1990.
[61] J.M. Dimitrić Marković, Z.S. Marković, T.P. Brdarić, V.M. Pavelkić, M.B. Jadranin, Iron complexes of dietary flavonoids: Combined spectroscopic and mechanistic study of their free radical scavenging activity, Food Chem. 129 (2011) 1567–1577, https://doi.org/10.1016/j.foodchem.2011.06.008.
[62] A. Zhou, O.A. Sadik, Comparative analysis of quercetin oxidation by electrochemical, enzymatic, autoxidation, and free radical generation techniques: A mechanistic study, J. Agr. Food Chem. 56 (2008) 12081–12091, https://doi.org/10.1021/jf802413v.
[63] Y. Song, S.W. Leonard, M.G. Traber, E. Ho, Zinc deficiency affects DNA damage, oxidative stress, antioxidant defenses, and DNA repair in rats, J. Nutr. 139 (2009) 1626–1631, https://doi.org/10.3945/jn.109.106369.
[64] A. Photiades, S. Grigorakis, D.P. Makris, Kinetics and modeling of l-cysteine effect on the cu(ii)-induced oxidation of quercetin, Chem. Eng. Comm. 207 (2020) 139–152, https://doi.org/10.1080/00986445.2019.1574767.
[65] A. Osman, D.P. Makris, P. Kefalas, Investigation on biocatalytic properties of a peroxidase-active homogenate from onion solid wastes: An insight into quercetin oxidation mechanism, Proc. Biochem. 43 (2008) 861–867, https://doi.org/10.1016/j.procbio.2008.04.003.
[66] A. Osman, D.P. Makris, Comparison of fisetin and quercetin oxidation with a cell-free extract of onion trimmings and peel, plant waste, containing peroxidase enzyme: A further insight into flavonol degradation mechanism, Int. J. Food Sci. Tech. 45 (2010) 2265–2271, https://doi.org/10.1111/j.1365-2621.2010.02408.x.
[67] I.G. Zenkevich, A.Y. Eshchenko, S.V. Makarova, A.G. Vitenberg, Y.G. Dobryakov, V.A. Utsal, Identification of the products of oxidation of quercetin by air oxygen at ambient temperature, Molecules (Basel, Switzerland) 12 (2007) 654–672, https://doi.org/10.3390/12030654.
[68] M.G. Espey, Role of oxygen gradients in shaping redox relationships between the human intestine and its microbiota, Free Rad. Bio. Med. 55 (2013) 130–140, https://doi.org/10.1016/j.freeradbiomed.2012.10.554.
[69] S. Mettu, Z. Hathi, S. Athukoralalage, A. Priya, T.N. Lam, K.L. Ong, N.R. Choudhury, N.K. Dutta, R. Curvello, G. Garnier, C.S.K. Lin, Perspective on constructing cellulose-hydrogel-based gut-like bioreactors for growth and delivery of multiple-strain probiotic bacteria, J. Agr. Food Chem. 69 (2021) 4946–4959, https://doi.org/10.1021/acs.jafc.1c00468.
[70] R. Hilgers, J. Bijlsma, L. Malacaria, J.-P. Vincken, E. Furia, W.J.C. de Bruijn, Transition metal cations catalyze $^{16}O/^{18}O$ exchange of catechol motifs with $H_2^{18}O$, Org. Biomol. Chem. (2022), https://doi.org/10.1039/D2OB01884E.

Supplementary Material

Insights in the complexation and oxidation of quercetin and luteolin in aqueous solution in presence of selected metal cations

Luana Malacaria[‡ a], Judith Bijlsma[‡ b], Roelant Hilgers[b], Wouter J.C. de Bruijn[b], Jean-Paul Vincken[b], Emilia Furia[a]*

[a]Dipartimento di Chimica e Tecnologie Chimiche, Via P. Bucci, Cubo 12/D, Università della Calabria, I-87030 Arcavacata di Rende (CS), Italy

[b]Laboratory of Food Chemistry, Wageningen University & Research, Bornse Weilanden 9, P.O. Box 17, 6700 AA, Wageningen, The Netherlands

*Corresponding author: Email address: emilia.furia@unical.it

[‡]These authors contributed equally to this work.

Email addresses authors:

Luana Malacaria: luana.malacaria@unical.it

Judith Bijlsma: judith.bijlsma@wur.nl

Roelant Hilgers: roelant.hilgers@wur.nl

Wouter J.C. de Bruijn: wouter.debruijn@wur.nl

Jean-Paul Vincken: jean-paul.vincken@wur.nl

Emilia Furia: emilia.furia@unical.it

Table of Contents

Method S1.

RP-UHPLC Settings

Sample (1 µL) was injected on an Acquity UPLC BEH C18 column (150 mm × 2.1 mm i.d., 1.7 µm) with a VanGuard (5 mm × 2.1 mm i.d., 1.7 µm) guard column of the same material (Waters, Milford, MA). Water (A) and acetonitrile (B), both acidified with 0.1 % (v/v) formic acid, were used as eluents. The flow rate was 400 µL min^{-1}, and the temperature of the column oven was 45 °C with the post-column cooler set to 40 °C.

The following elution profile was used: 0.00–1.09 min, isocratic at 1 % (v/v) B; 1.09–20.72 min, linear gradient from 1 to 55 % (v/v) B; 20.72–21.81 min linear gradient from 55 to 100 % (v/v) B; 21.81–27.26 min isocratic at 100 % (v/v) B; 27.26–28.35 min linear gradient from 100 to 1 % (v/v) B; 28.35–33.81 min isocratic at 1 % (v/v) B.

Table S1. Maximum absorbance wavelengths (λ_{max}) of quercetin after 24 hours incubation in the absence and presence of metal ions at pH 4.

Metal	WS				ES		
	Benzoyl	Degradation Product	Cinnamoyl	LMCT	Benzoyl	Cinnamoyl	LMCT
Blank	256	291	337, 364	-	257	378 (307)[a]	-
Al(III)	269	-	344	431	257	374 (307)	443
Cr(III)	248	-	354, 441	466, 581	257	378 (306)	-
Mn(II)	255	289	337, 365	-	258	378 (305)	-
Fe(III)	-	294	-	532	257	375 (312)	464
Co(II)	253	292	315, 371	494	256	375 (307)	-
Ni(II)	254	288	352, 379	-	257	378 (306)	-
Cu(II)	-	297	-	533	258	369 (307)	390
Zn(II)	256	292	336, 364	-	256	377 (307)	-

[a] the value in between brackets is the less intense absorption band.

Table S2. Maximum absorbance wavelengths (λ_{max}) of quercetin after 24 hours incubation in the absence and presence of metal ions at pH 7.4.

Metal	WS				ES		
	Benzoyl	Degradation Product	Cinnamoyl	LMCT	Benzoyl	Cinnamoyl	LMCT
Blank	251	291	310, 435, 618	-	256	377 (307)[a]	-
Al(III)	234	354	432	566	257	375 (312)	445
Cr(III)	252	300	409	464	256	375 (306)	505
Mn(II)	244	282	-	-	257	374 (292)	445
Fe(III)	257	298	396	507	256	374 (309)	461
Co(II)	244	284	-	637	257	375 (310)	441
Ni(II)	253	283	432	-	257	374 (292)	440
Cu(II)	269	305	415	-	257	374 (288)	438
Zn(II)	250	-	319	-	257	375 (291)	435

[a] the value in between brackets is the less intense absorption band.

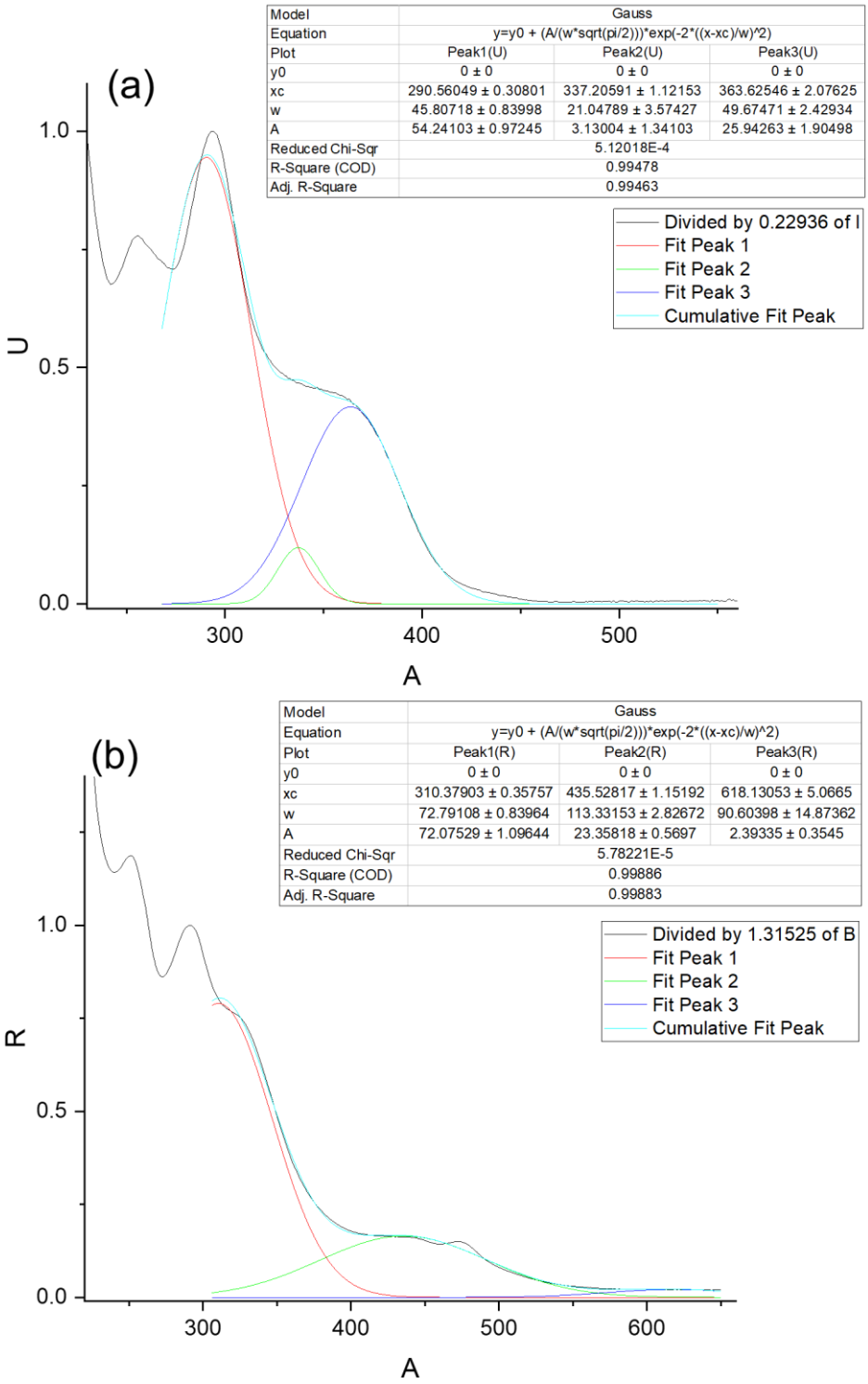

Fig. S1. Deconvolution analysis of WS fractions of the spectrum of quercetin at pH 4 (a) and 7.4 (b).

Table S3. Maximum absorbance wavelengths (λ_{max}) of luteolin after 24 hours incubation in the absence and presence of metal ions at pH 4.

	WS			ES		
Metal	**Benzoyl**	**Cinnamoyl**	**LMCT**	**Benzoyl**	**Cinnamoyl**	**LMCT**
Blank	253 (264)	346 (289)	-	256 (267)[a]	355 (295)	-
Al(III)	(269)	355	407	259 (269)	351 (288)	417
Cr(III)	255	349	444, 583	254 (267)	354 (296)	-
Mn(II)	254 (264)	345 (289)	-	255 (267)	355 (295)	-
Fe(III)	254 (264)	347 (287)	-	255 (267)	354 (295)	-
Co(II)	255 (264)	349 (246)	505, 647	254 (267)	354 (295)	-
Ni(II)	253 (265)	347 (288)	-	255 (267)	357 (296)	-
Cu(II)	254 (265)	345 (290)	-	255 (267)	355 (295)	-
Zn(II)	254 (265)	346 (289)	-	254 (267)	353 (296)	-

[a] the value in between brackets is the less intense absorption band.

Table S4. Maximum absorbance wavelengths (λ_{max}) of luteolin after 24 hours incubation in the absence and presence of metal ions at pH 7.4.

	WS			ES		
Metal	**Benzoyl**	**Cinnamoyl**	**LMCT**	**Benzoyl**	**Cinnamoyl**	**LMCT**
Blank	267	362	-	256 (268)[a]	353 (296)	-
Al(III)	268	288	407	256 (268)	355 (250)	423
Cr(III)	267	362	-	255 (268)	353 (295)	-
Mn(II)	266	372 (314)	-	257 (267)	355 (285)	418
Fe(III)	267	357	563	256 (267)	353 (295)	-
Co(II)	269	377 (309)	-	255 (267)	352 (295)	-
Ni(II)	267	369	588	256 (267)	352 (296)	-
Cu(II)	264	-	-	255 (267)	352 (295)	-
Zn(II)	268	378 (319)	-	256 (268)	353 (295)	-

[a] the value in between brackets is the less intense absorption band.

Table S5. Tentatively identified flavonoid metal complexes with corresponding experimental and theoretical mass-to-charge ratios (*m/z*) and isotope abundances, as well as the fragments and neutral losses used to tentatively identify the complex.

m/z		**Isotopes**	***m/z***		**Isotope abundance**		**MS^2 data[a]**	
Experimental	**Tentatively identified complex**		**Exp.**	**Theoretical**	**Exp.**	**Theoretical**	**Fragments *m/z***	**Neutral losses (amu)**
629	**$[Al(III)+2(Q-H)]^+$**	$^{12}C_{30}H_{18}O_{14}{}^{27}Al$ $^{12}C_{29}{}^{13}CH_{18}O_{14}{}^{27}Al$ $^{12}C_{28}{}^{13}C_2H_{18}O_{14}{}^{27}Al$	629 630 631	629 630 631	100% 32% 8%	100% 33% 8%	601, 573, 327	28 (CO) 56 (C_4H_8) 302 (Quer)
969	**$[Al(III)+3(Q-H)+K]^+$**	$^{12}C_{45}H_{27}O_{21}K^{27}Al$ $^{12}C_{44}{}^{13}CH_{27}O_{21}K^{27}Al$ $^{12}C_{43}{}^{13}C_2H_{27}O_{21}K^{27}Al$	969 970 971	969 970 971	100% 49% 24%	100% 50% 24%	667	302 (Quer)
998	**$[Fe(II)+2Q+(Q-H)+2(H_2O)]^+$**	$^{12}C_{45}H_{33}O_{23}{}^{56}Fe$ $^{12}C_{44}{}^{13}CH_{33}O_{23}{}^{56}Fe$ $^{12}C_{43}{}^{13}C_2H_{33}O_{23}{}^{56}Fe$ $^{12}C_{45}H_{33}O_{23}{}^{45}Fe$	998 999 1000 996	998 999 1000 996	100% 53% 25% 7%	100% 50% 18% 6%	696	302 (Quer)
705	**$(Zn(II)+2(Q-H)+K]^+$**	$^{12}C_{30}H_{18}O_{14}K^{64}Zn$ $^{12}C_{30}H_{18}O_{14}K^{66}Zn$ $^{12}C_{30}H_{18}O_{14}K^{68}Zn$ $^{12}C_{29}{}^{13}CH_{18}O_{14}K^{64}Zn$ $^{12}C_{29}{}^{13}CH_{18}O_{14}K^{66}Zn$	705 707 709 706 708	705 707 709 706 708	100% 73% 42% 33% 31%	100% 72% 50% 33% 30%	687, 677, 669, 659, 631, 555	18 (H_2O) 28 (CO) 36 ($2H_2O$) 46 ($COOH_2$) 74 ($C_3H_6O_2$) 150
688	**$[Cu(II)+2(Q-H)+Na]^+$**	$^{12}C_{30}H_{18}O_{14}Na^{63}Cu$ $^{12}C_{30}H_{18}O_{14}Na^{65}Cu$ $^{12}C_{29}{}^{13}CH_{18}O_{14}Na^{63}Cu$ $^{12}C_{29}{}^{13}CH_{18}O_{14}Na^{65}Cu$	688 690 689 691	688 690 689 691	100% 54% 33% 17%	100% 53% 33% 16%		
704	**$[Cu(II)+2(Q-H)+K]^+$**	$^{12}C_{30}H_{18}O_{14}K^{63}Cu$ $^{12}C_{30}H_{18}O_{14}K^{65}Cu$ $^{12}C_{29}{}^{13}CH_{18}O_{14}K^{63}Cu$ $^{12}C_{29}{}^{13}CH_{18}O_{14}K^{65}Cu$	704 706 705 707	704 706 705 707	100% 58% 32% 17%	100% 60% 33% 19%	686, 676, 402, 340	18 (H_2O) 28 (CO) 302 (Quer) 364 (Cu-Quer)
661	**$[Ni(II)+Q+(Q-H)]^+$**	$^{12}C_{30}H_{19}O_{14}{}^{58}Ni$ $^{12}C_{30}H_{19}O_{14}{}^{60}Ni$ $^{12}C_{29}{}^{13}CH_{19}O_{14}{}^{58}Ni$ $^{12}C_{29}{}^{13}CH_{19}O_{14}{}^{60}Ni$ $^{12}C_{30}H_{19}O_{14}{}^{62}Ni$ or $^{12}C_{28}{}^{13}C_2H_{19}O_{14}{}^{60}Ni$	661 663 662 664 665	661 663 662 664 665	100% 47% 36% 16% 9%	100% 48% 33% 16% 9%	633, 359	28 (CO) 302 (Quer)

699	**[Ni(II)+2(Q−H)+K]$^+$**	$^{12}C_{30}H_{18}O_{14}K^{58}Ni$ $^{12}C_{30}H_{18}O_{14}K^{60}Ni$ $^{12}C_{29}{}^{13}CH_{18}O_{14}K^{58}Ni$ $^{12}C_{29}{}^{13}CH_{18}O_{14}K^{60}Ni$	699 701 700 702	699 701 700 702	100% 53% 34% 18%	100% 54% 33% 18%	681, 671, 663, 643, 625, 549	18 (H_2O) 28 (CO) 36 ($2H_2O$) 56 (C_4H_8) 74 ($C_3H_6O_2$) 150
773	**[3Ni(II)+(Q−2H)+(Q−3H)]$^+$**	$^{12}C_{30}H_{15}O_{14}{}^{58}Ni_3$ $^{12}C_{30}H_{15}O_{14}{}^{58}Ni_2{}^{60}Ni$ $^{12}C_{30}H_{15}O_{14}{}^{58}Ni^{60}Ni_2$ $^{12}C_{29}{}^{13}CH_{15}O_{14}{}^{58}Ni_3$ $^{12}C_{29}{}^{13}CH_{15}O_{14}{}^{58}Ni_2{}^{60}Ni$	773 775 777 774 776	773 775 777 774 776	100% 98% 41% 37% 34%	87% 100% 39% 29% 38%	737, 699	36($2H_2O$) 74($C_3H_6O_2$)
662	**[Co(II)+Q+(Q−H)]$^+$**	$^{12}C_{30}H_{19}O_{14}{}^{59}Co$ $^{12}C_{29}{}^{13}CH_{19}O_{14}{}^{59}Co$ $^{12}C_{28}{}^{13}C_2H_{19}O_{14}{}^{59}Co$	662 663 664	662 663 664	100% 33% 8%	100% 33% 8%	634, 588, 512, 360	28 (CO) 74 ($C_3H_6O_2$) 150 302 (Quer)
807	**Unidentified Co(II) complex**		807 808 809		100% 42% 13%			
597	**[Al(III)+2(L−H)]$^+$**	$^{12}C_{30}H_{18}O_{12}{}^{27}Al$ $^{12}C_{29}{}^{13}CH_{18}O_{12}{}^{27}Al$ $^{12}C_{28}{}^{13}C_2H_{18}O_{12}{}^{27}Al$	597 598 599	597 598 599	100% 32% 8%	100% 33% 8%	569, 541	28 (CO) 56 (C_4H_8)
653	**[Al(III)+2(L−H)+OH+K]$^+$**	$^{12}C_{30}H_{19}O_{13}K^{27}Al$ $^{12}C_{29}{}^{13}CH_{19}O_{13}K^{27}Al$ $^{12}C_{28}{}^{13}C_2H_{19}O_{13}K^{27}Al$	653 654 655	653 654 655	100% 33% 16%	100% 33% 15%		
921	**[Al(III)+3(L−H)+K]$^+$**	$^{12}C_{45}H_{27}O_{18}K^{27}Al$ $^{12}C_{44}{}^{13}CH_{27}O_{18}K^{27}Al$ $^{12}C_{43}{}^{13}C_2H_{27}O_{18}K^{27}Al$	921 922 923	921 922 923	100% 48% 23%	100% 50% 23%	635	286 (Lut)

[a] Fragments are derived from fragmentation of the most abundant isotopic species detected.

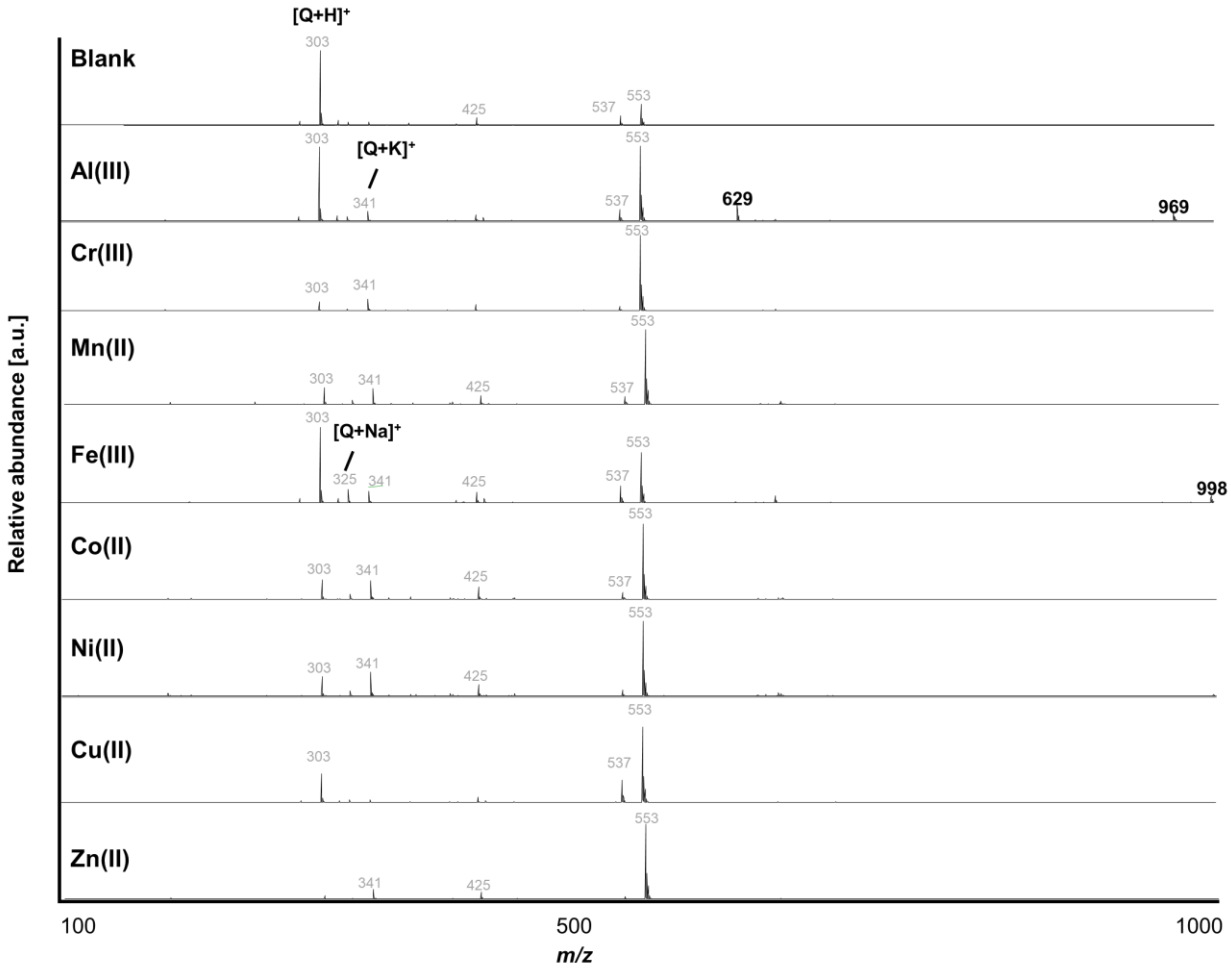

Fig. S2 Electrospray ionization mass spectra in positive mode of the ES fraction from quercetin in absence or presence of metal cations at pH 4. The grey *m/z* values were also found in the quercetin blank in absence of the metal ions, the bold black *m/z* values were formed in presence of the metal and tentatively identified.

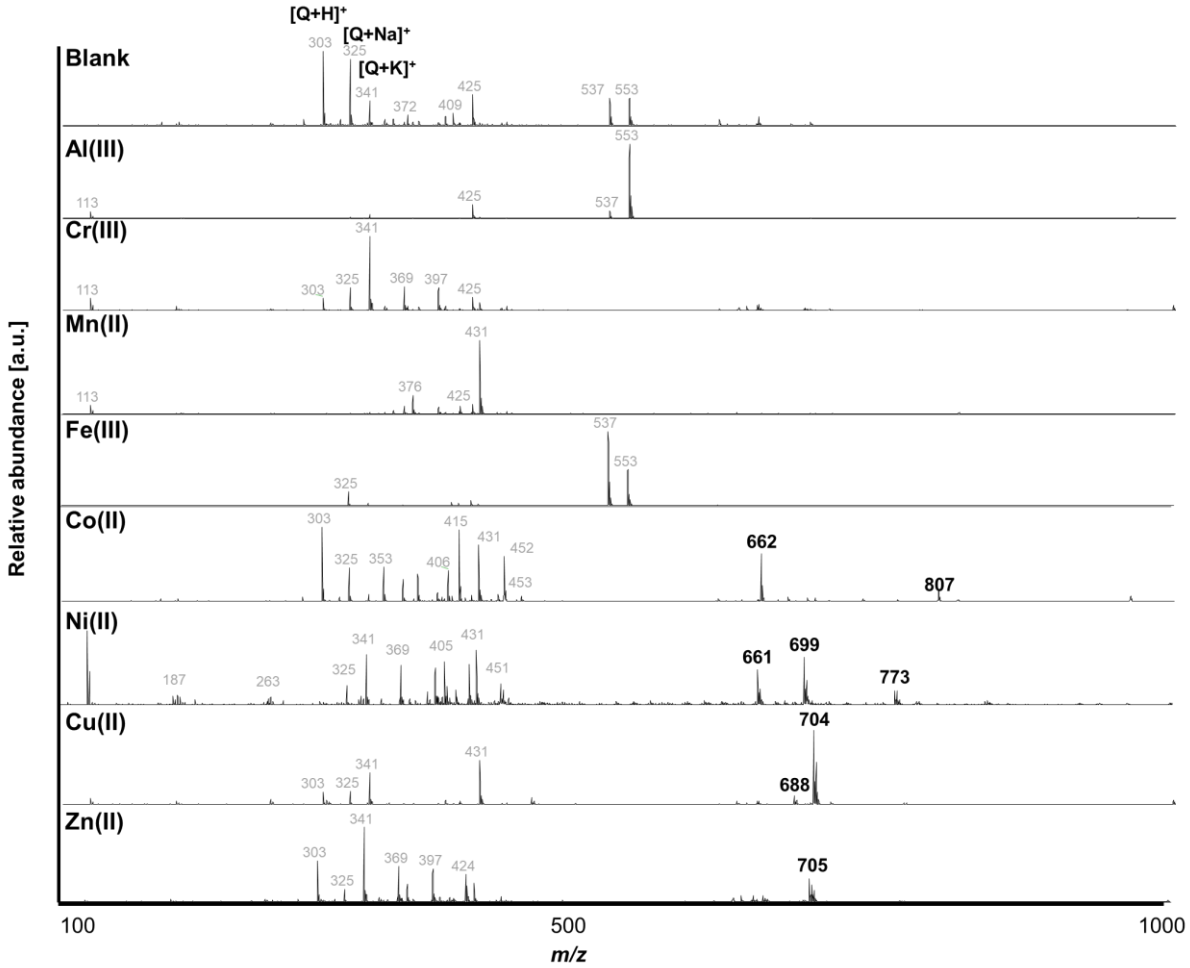

Fig. S3 Electrospray ionisation mass spectra in positive mode of the ES fraction from quercetin in absence or presence of metal cations at pH 7.4. The grey *m/z* values were also found in the quercetin blank in absence of the metal ions, the bold black *m/z* values were formed in presence of the metal and tentatively identified.

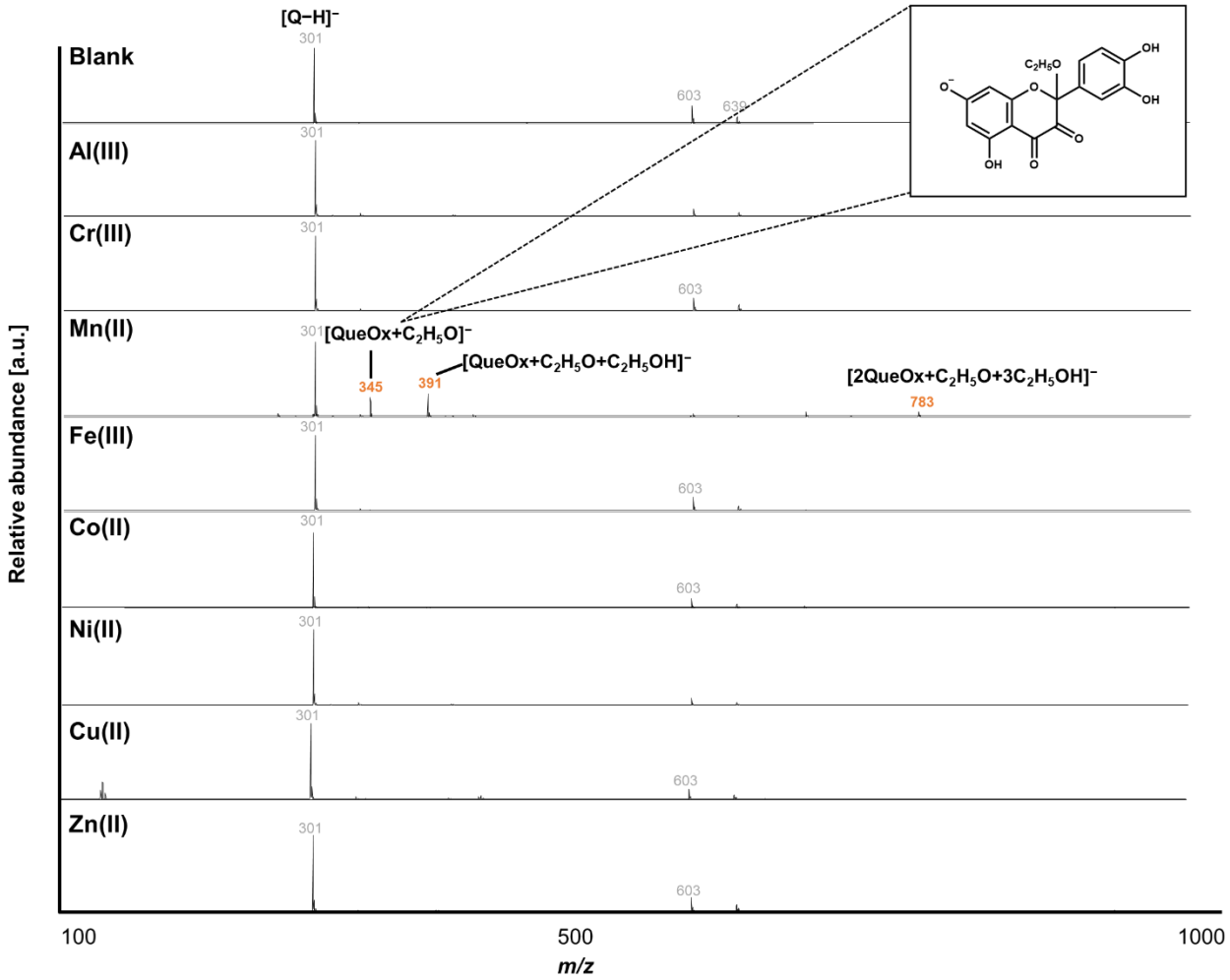

Fig. S4 Electrospray ionisation mass spectra in negative mode of the ES fraction from quercetin in absence or presence of metal cations at pH 7.4. The grey *m/z* values were also found in the quercetin blank in absence of the metal ions, the bold orange *m/z* values in the Mn(II) containing sample were tentatively identified as an ethanol intermediate of quercetin degradation (see inset).

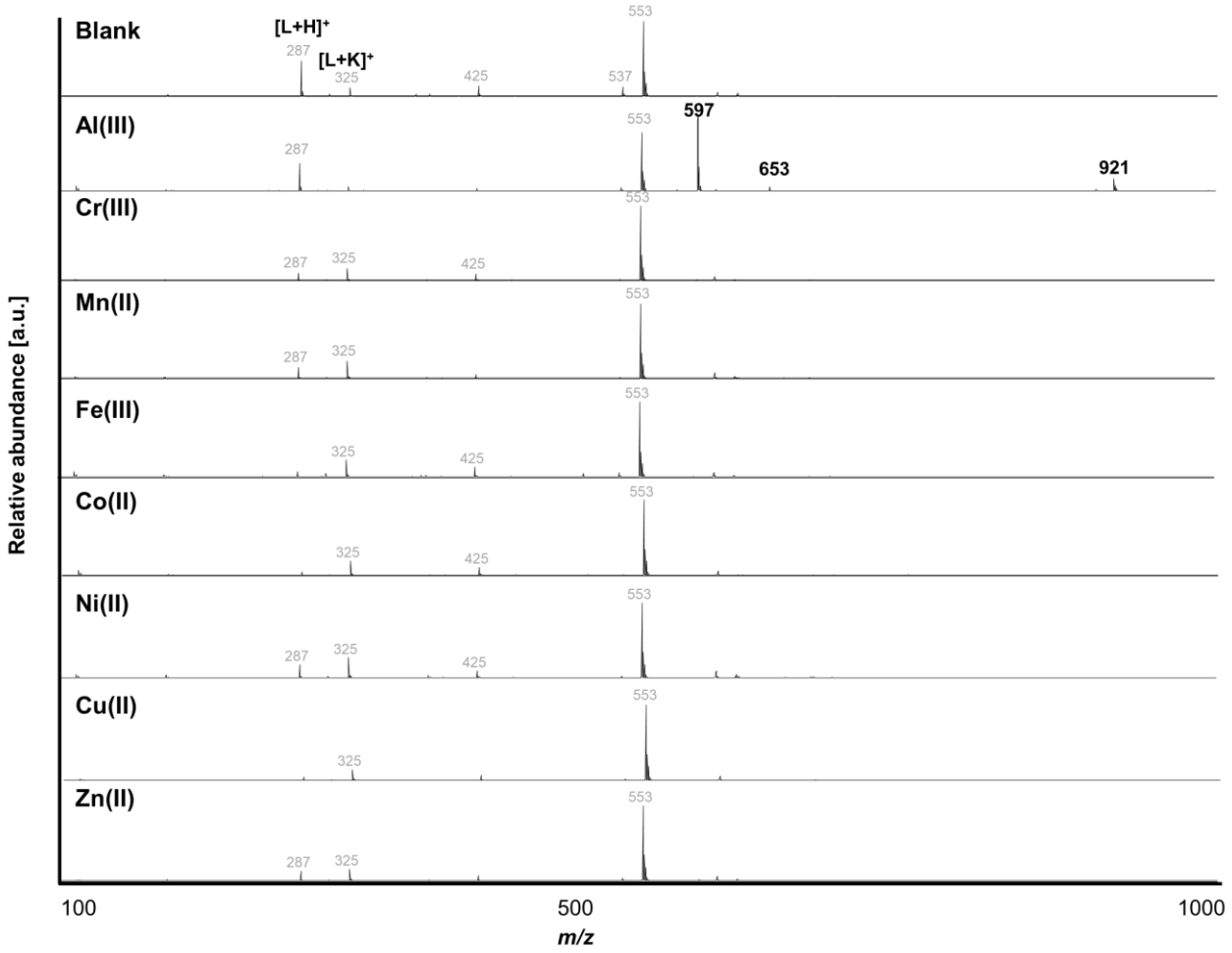

Fig. S5 Electrospray ionization mass spectra in positive mode of the ES fraction from luteolin in absence or presence of metal cations at pH 4. The grey *m/z* values were also found in the luteolin blank in absence of the metal ions, the bold black *m/z* values were formed in presence of the metal and tentatively identified.

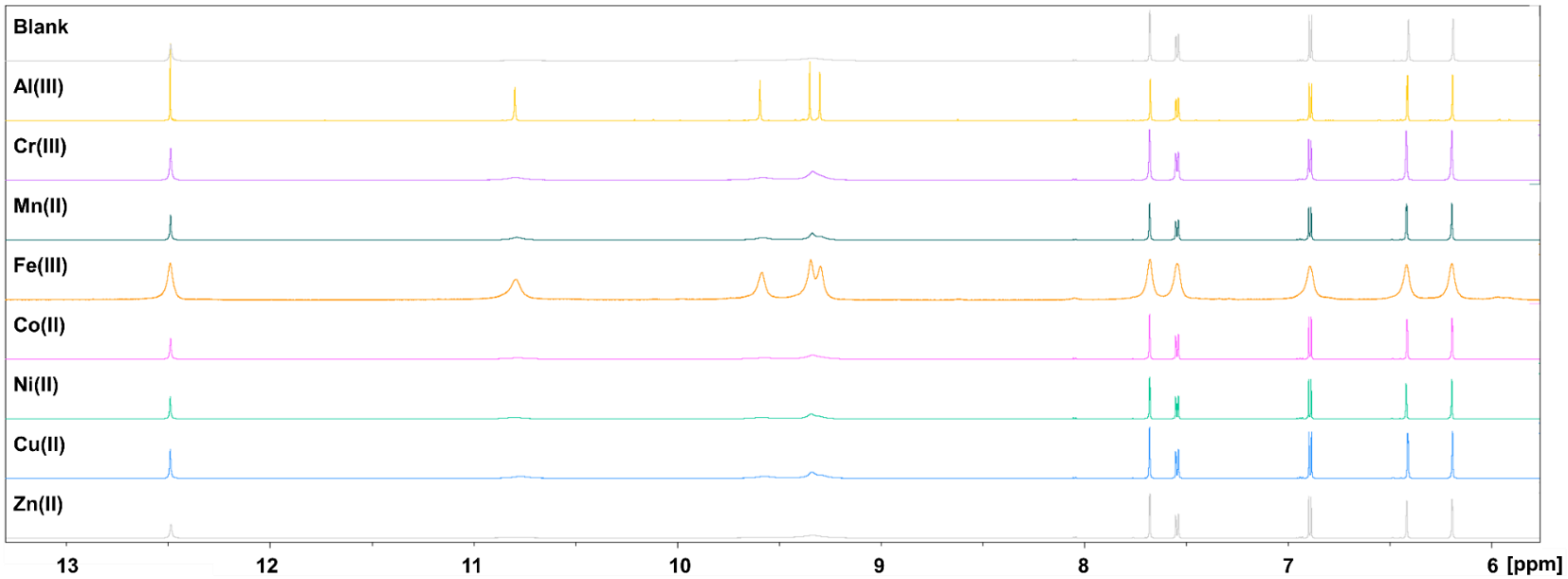

Figure S6. ^{1}H NMR spectra of the quercetin blank and in presence of metal ions at pH 4 in DMSO-d_6.

Table S6. ^{1}H NMR peak data (δh (ppm), mult. (J in Hz)) of the quercetin blank and in presence of the metal ions at pH 4 in DMSO-d_6. bs, broad singlet; d, doublet; dd, doublet of doublets; s, singlets.

	5-OH	7-OH	3-OH	4′-OH	3′-OH	H2′	H6′	H5′	H8	H6
Blank	12.49, s	10.78, bs	9.56, bs	9.34, bs		7.68, d (2)	7.54, dd 2, (8)	6.89, d (8)	6.41, d (2)	6.19, d (2)
Al(III)	12.49, s	10.79, bs	9.59, bs	9.35, bs	9.30, bs	7.67, d (2)	7.54, dd 2, (8)	6.89, d (8)	6.42, d (2)	6.19, d (2)
Cr(III)	12.49, s	10.79, bs	9.58, bs	9.34, bs		7.68, d (2)	7.54, dd 2, (8)	6.89, d (8)	6.42, bs	6.19, bs
Mn(II)	12.49, s	10.79, bs	9.58, bs	9.34, bs		7.68, d (2)	7.54, dd 2, (8)	6.89, d (8)	6.42, d (2)	6.19, d (2)
Fe(III)	12.49, s	10.79, bs	9.59, bs	9.34, bs	9.29, bs	7.68, bs	7.54, bs	6.89, bs	6.42, bs	6.19, bs
Co(II)	12.49, s	10.79, bs	9.57, bs	9.34, bs		7.68, d (2)	7.54, dd 2, (8)	6.89, d (8)	6.42, d (2)	6.19, d (2)
Ni(II)	12.49, s	10.79, bs	9.58, bs	9.34, bs		7.68, d (2)	7.54, dd 2, (8)	6.89, d (8)	6.42, d (2)	6.19, d (2)
Cu(II)	12.49, s	10.77, bs	9.57, bs	9.34, bs		7.68, d (2)	7.54, dd 2, (8)	6.89, d (8)	6.41, d (2)	6.19, d (2)
Zn(II)	12.49, s	10.79, bs	9.55, bs	9.34, bs		7.68, d (2)	7.54, dd 2, (8)	6.89, d (8)	6.42, d (2)	6.19, d (2)

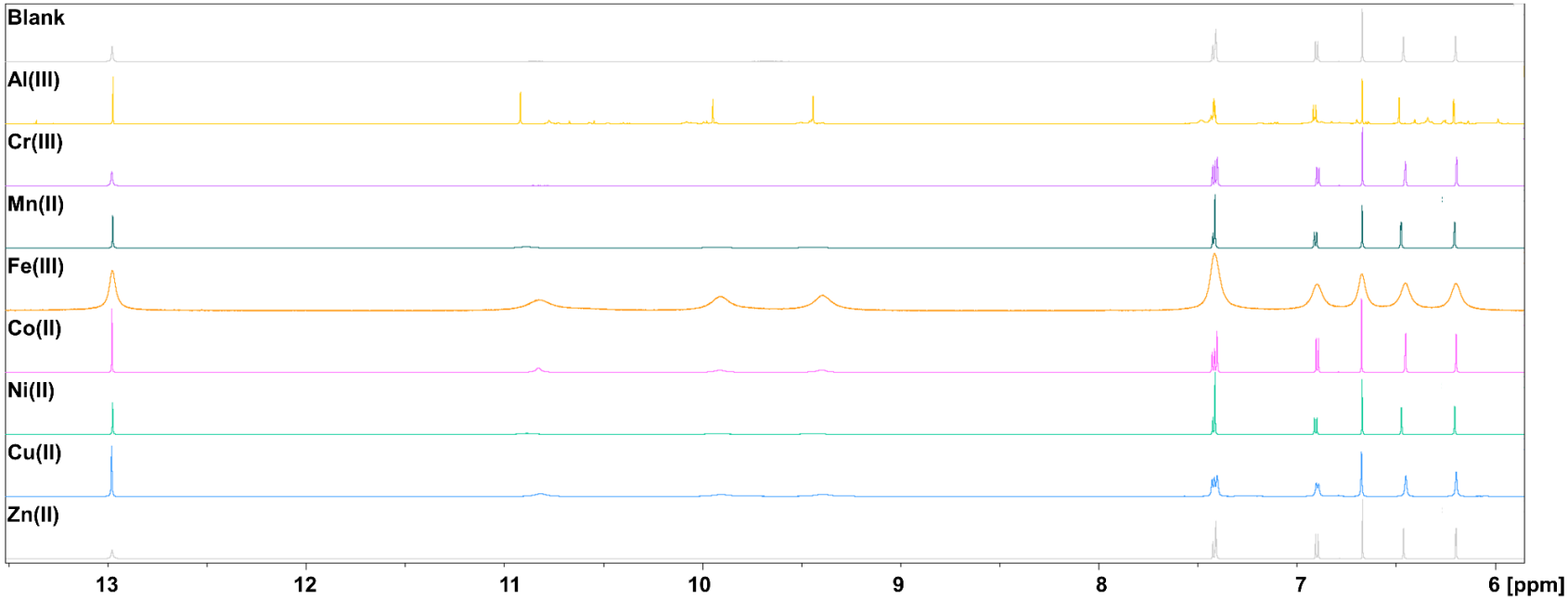

Figure S7. ^{1}H NMR spectra of the luteolin blank and in presence of the metal ions at pH 4 in DMSO-d$_6$.

Table S7. ^{1}H NMR peak data (δh (ppm), mult. (J in Hz)) of the luteolin blank and in presence of the metal ions at pH 4 in DMSO-d$_6$. bs, broad singlet; d, doublet; dd, doublet of doublets; s, singlets.

	5-OH	7-OH	4′-OH	3′-OH	H2′	H6′	H5′	H3	H8	H6
Blank	12.97, s	10.83, bs	9.67, bs		7.42, d (2)	7.41, dd	6.90, d (8)	6.67, s	6.46, d (2)	6.20, d (2)
Al(III)	12.97, s	10.91, bs	9.95, bs	9.44, bs	7.42 d (2)	7.41, dd	6.91, d (8)	6.67, s	6.48, d (2)	6.21, d (2)
Cr(III)	12.97, s	10.82, bs	9.67, bs		7.42, d (2)	7.41, dd	6.90, d (8)	6.67, s	6.45, d (2)	6.20, d (2)
Mn(II)	12.97, s	10.89, bs	9.93, bs	9.44, bs	7.42, d (2)	7.41, bs	6.90, d (8)	6.67, s	6.47, d (2)	6.20, d (2)
Fe(III)	12.97, s	10.83, bs	9.91, bs	9.40, bs	7.41, bs		6.90, bs	6.67, bs	6.45, bs	6.20, bs
Co(II)	12.97, s	10.83, bs	9.91, bs	9.40, bs	7.42, d (2)	7.41, dd	6.90, d (8)	6.67, s	6.45, d (2)	6.20, d (2)
Ni(II)	12.97, s	10.88, s	9.91, bs	9.44, bs	7.42, d (2)	7.41, bs	6.90, d (8)	6.67, s	6.46, d (2)	6.20, d (2)
Cu(II)	12.97, s	10.83, bs	9.91, bs	9.39, bs	7.43, bs	7.42, bs	6.90, d (8)	6.67, s	6.45, bs	6.20, bs
Zn(II)	12.97, s	10.79, bs	9.67, bs		7.42, d (2)	7.41, dd	6.90, d (8)	6.67, s	6.46, d (2)	6.20, d (2)

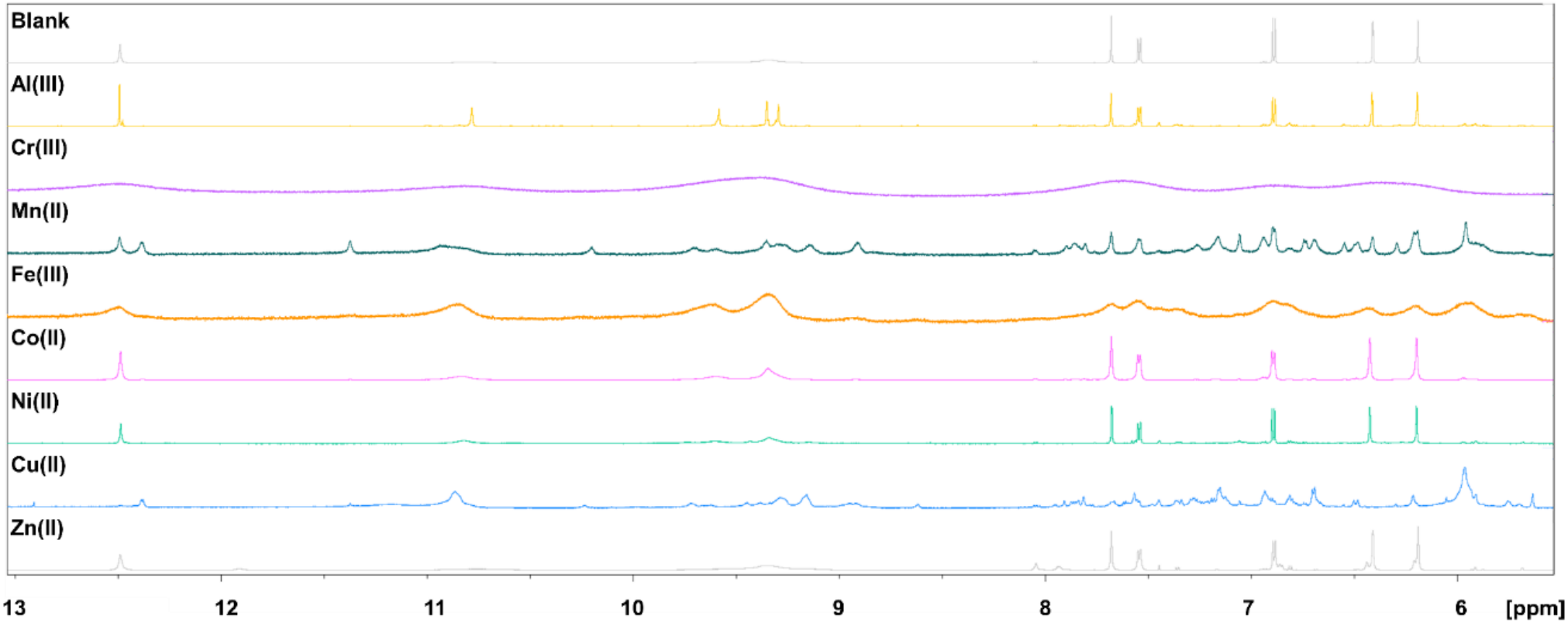

Figure S8: ^{1}H NMR spectra of the quercetin blank and in presence of the metal ions at pH 7.4 in DMSO-d_6.

Table S8. ^{1}H NMR peak data (δh (ppm), mult. (J in Hz)) of the quercetin blank and in presence of the metal ions at pH 7.4 in DMSO-d_6. bs, broad singlet; d, doublet; dd, doublet of doublets; s, singlets.

	5-OH	7-OH	3-OH	4′-OH	3′-OH	H2′	H6′	H5′	H8	H6
Blank	12.49, s	10.79, s	9.56, s	9.34, s		7.68, d (2)	7.54, dd 2, (8)	6.88, d (8)	6.41, d (2)	6.18, d (2)
Al(III)	12.49, s	10.78, s	9.58, s	9.35, s	9.29, s	7.68, d (2)	7.54, dd 2, (8)	6.88, d (8)	6.41, d (2)	6.18, d (2)
Cr(III)	12.49, s	10.79, bs		9.41, bs		7.6, bs		6.90, bs	6.40, bs	
Mn(II)	12.49, s 12.38, s	10.86, bs	9.71, bs 9.59, bs	9.35, bs 9.13, bs	9.29, bs 8.91, bs	7.68, s 7.26, bs	7.54, bd (8) 7.15, bs	6.88, bd (8) 6.69, bs	6.41, bs 6.29 bs	6.20, bd 5.95, bs
Fe(III)	12.49, s	10.86, bs	9.60, bs	9.35, bs		7.68, bs	7.54, bs	6.88, bs	6.41, bs	6.18, bs
Co(II)	12.49, s 12.38, s	10.83, s	9.60, s	9.34, s		7.68, s	7.54, bd (8)	6.88, bd (8)	6.42, bs	6.20, bs
Ni(II)	12.49, s	10.80, bs	9.74, bs 9.59, bs	9.34, bs	9.15, bs	7.68, d (2)	7.54, dd 2, (8)	6.88, d (8)	6.42, d (2)	6.20, d (2)
Cu(II)	12.91, s 12.39, s	10.85, s	9.72, bs 9.63, bs	9.44, bs 9.36, bs	9.29, bs 9.15, bs	7.66, bs 7.36, bs	7.57, bs 7.15, bs	6.92, bs 6.69, bs	6.42, d	6.21, bs 5.96, bs
Zn(II)	12.49, s 11.90, s	10.77, s	9.55, s	9.34, bs		7.68, s 8.04, s	7.54, bd (8) 7.93, bd (8)	6.88, d (8) 6.85, d (8)	6.41, d (2)	6.19, d (2)

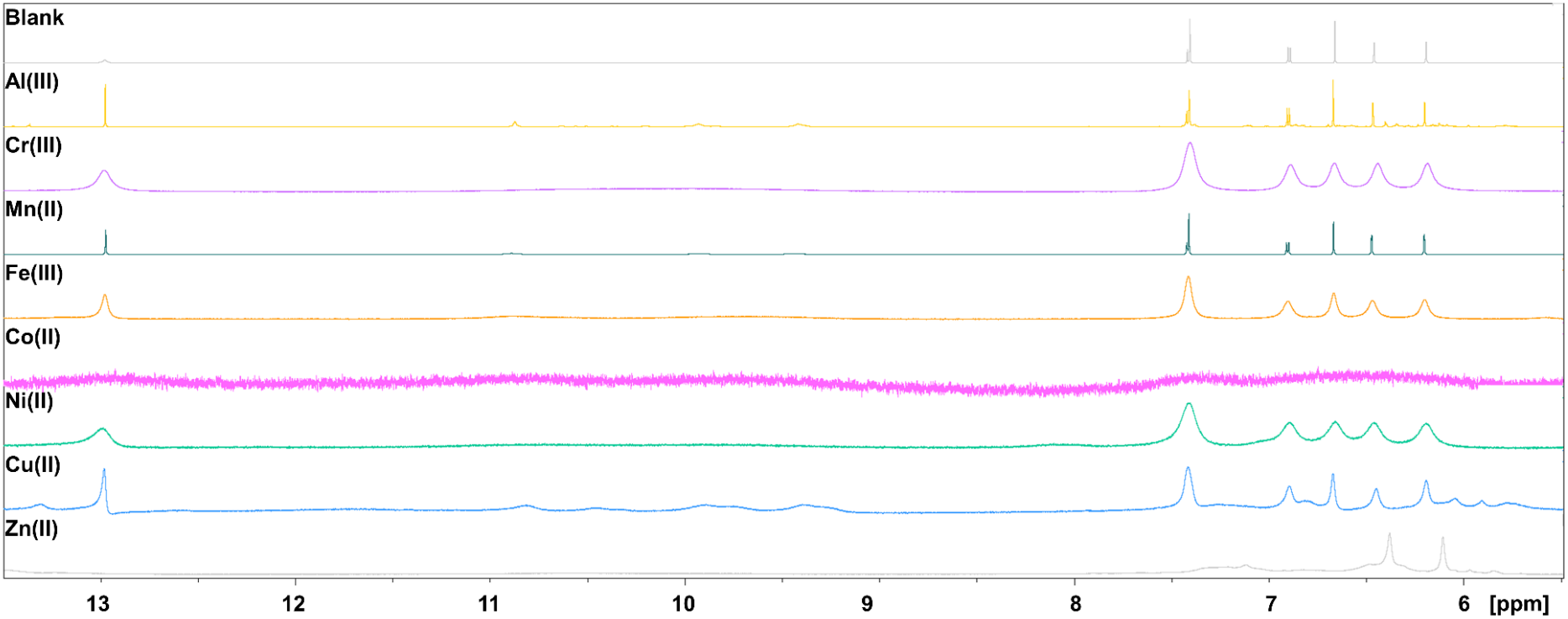

Figure S9. ^{1}H NMR spectra of the luteolin blank and in presence of the metal ions at pH 7.4 in DMSO-d_6.

Table S9. ^{1}H NMR peak data (δh (ppm), mult. (J in Hz)) of the luteolin blank and in presence of the metal ions at pH 7.4 in DMSO-d_6. bs, broad singlet; d, doublet; dd, doublet of doublets; s, singlets.

	5-OH	7-OH	4′-OH	3′-OH	H2′	H6′	H5′	H3	H8	H6
Blank	12.97, s		10.17, bs		7.42, d (2)	7.41, dd	6.90, d (8)	6.66, s	6.46, d (2)	6.20, d (2)
Al(III)	12.97, s	10.88, bs	9.94, bs	9.42, bs	7.42, d (2)	7.41, dd	6.90, d (8)	6.67, s	6.48, d (2)	6.20, d (2)
Cr(III)	12.98, s		10.15, bs		7.41, bs		6.89, bs	6.67, bs	6.44, bs	6.19, bs
Mn(II)	13.02, bs	10.89, bs	9.93, bs	9.49, bs	7.42, d (2)	7.41, bs	6.90, d (8)	6.67, s	6.47, d (2)	6.20, d (2)
Fe(III)	12.98, s	10.87, bs	9.72, bs		7.41, bs		6.89, bs	6.67, bs	6.47, bs	6.20, bs
Co(II)	12.96, bs	10.81, bs	9.76, bs		p.b.				6.45, d (2)	
Ni(II)	12.98, s	10.81, bs	9.91, bs		7.41, bs		6.89, bs	6.67, bs	6.47, bs	6.19, bs
Cu(II)	13.31, s 12.98, s	10.83, bs 10.45, bs	9.91, bs 9.75, bs	9.38, bs	7.41, bs		6.89, bs	6.67, bs	6.45, bs	6.19, bs
Zn(II)	13.48, s		10.50, bs						6.38, bs	6.11, bs

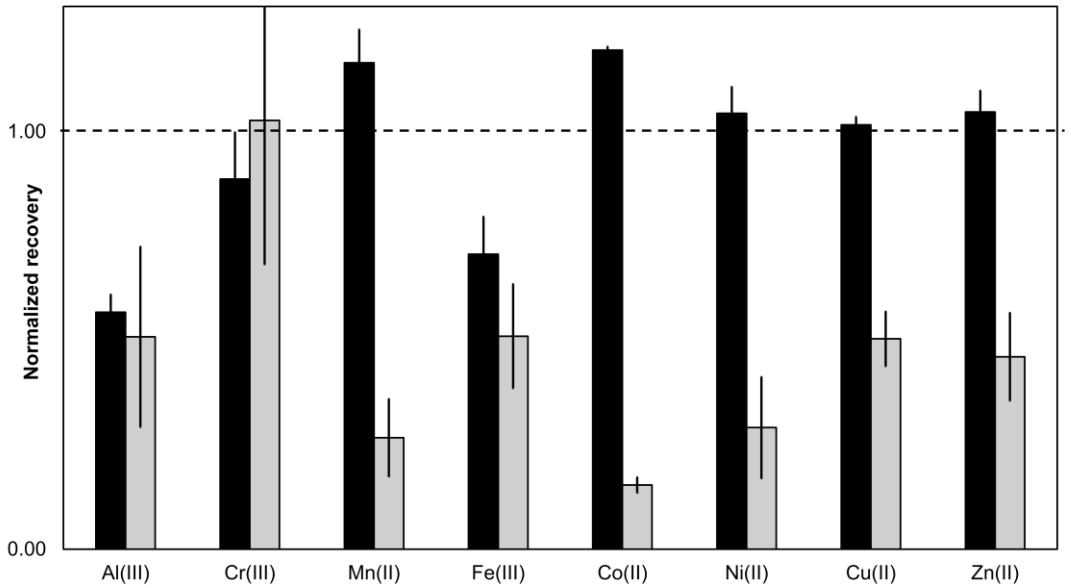

Fig. S10. Normalized recovery of luteolin-metal cation systems at pH 4 (black) and pH 7.4 (grey). The recovery was normalized versus the luteolin blank, where a similar recovery as the luteolin blank was indicated as 1.00 as is indicated by the dashed line. Values above 1.00 indicated that more luteolin was recovered compared to the blank.

Table S10. Lewis hardness, redox potential and empty shells in the d-orbital of the selected metal cations.

Metal	Lewis hardness η (eV) [1]	Redox potential E^o (V vs. SHE) [2]	Ionic radius (Å) [3]	Empty shells d-orbital
Al(III)	45.77	-1.67	0.53	n.a.[a]
Cr(III)	9.1	-0.42	0.76	7
Mn(II)	9.02	-1.19	0.81	5
Fe(III)	12.08	0.77	0.69	5
Co(II)	8.22	-0.28	0.0.54	3
Ni(II)	8.5	-0.26	0.70	2
Cu(II)	8.27	0.34	0.71	1
Zn(II)	10.88	-0.76	0.74	0

[a] n.a. not applicable because Al(III) is no first-row transition metal and has no d-orbital

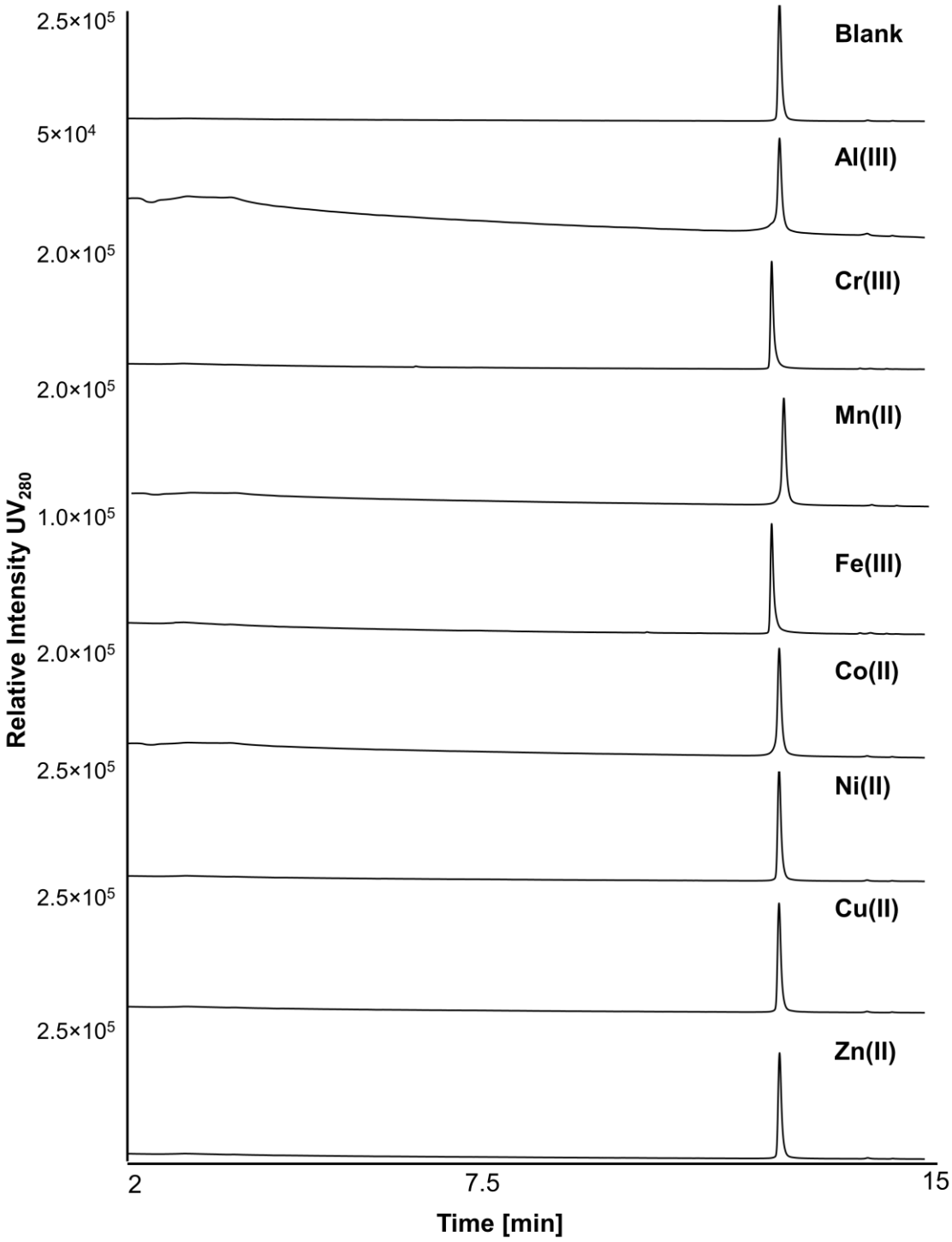

Fig. S11. Sum of relative UV intensities at 280 nm from the RP-UHPLC-PDA chromatograms of the WS and ES fraction of luteolin at pH 4 in absence and presence of the different metal cations. Here the sum of the intensities from both fractions was used to quickly indicate if oxidative luteolin products were formed.

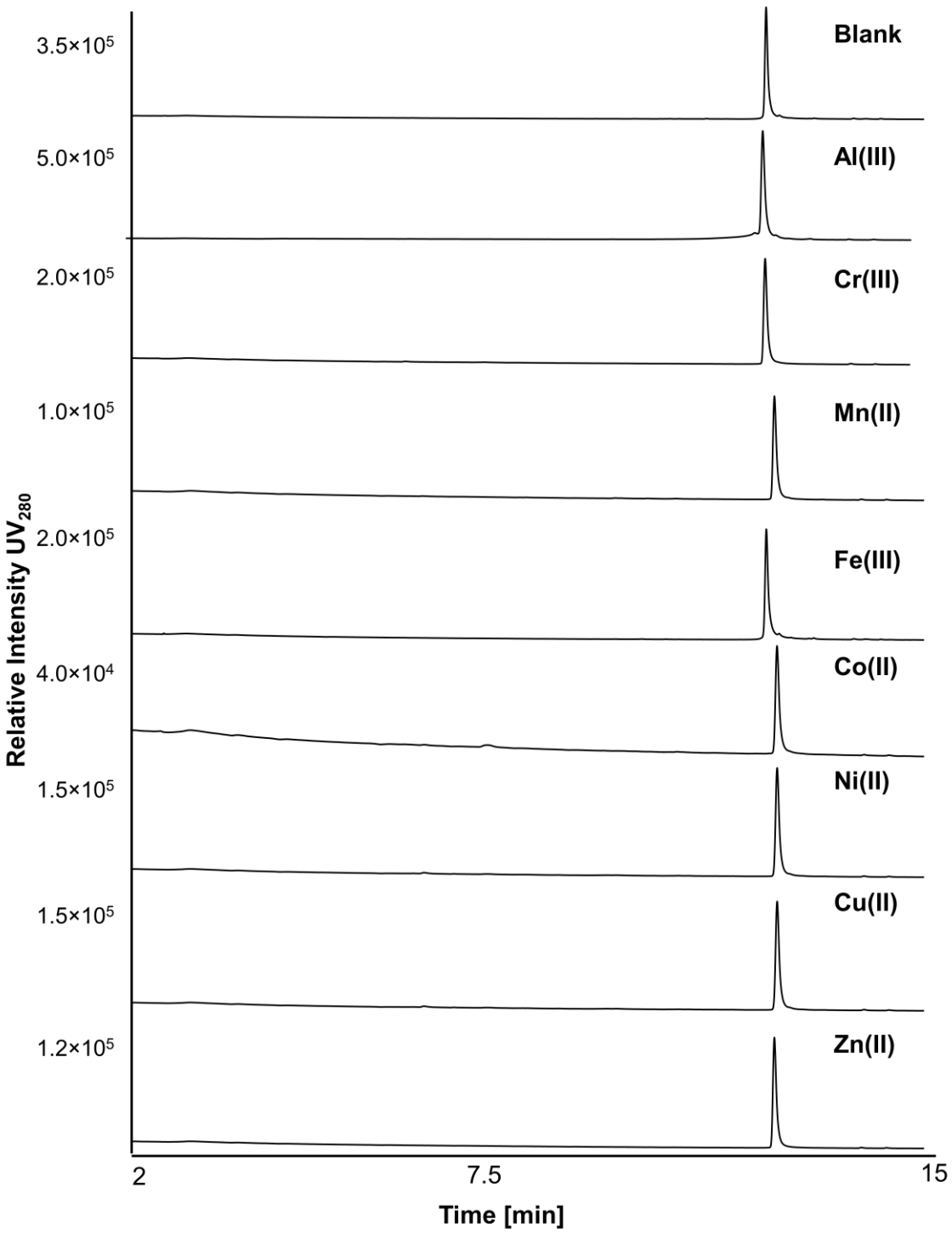

Fig. S12. Sum of relative UV intensities at 280 nm from the RP-UHPLC-PDA chromatograms of the WS and ES fraction of luteolin at pH 7.4 in absence and presence of the different metal cations. Here the sum of the intensities from both fractions was used to quickly indicate if oxidative luteolin products were formed.

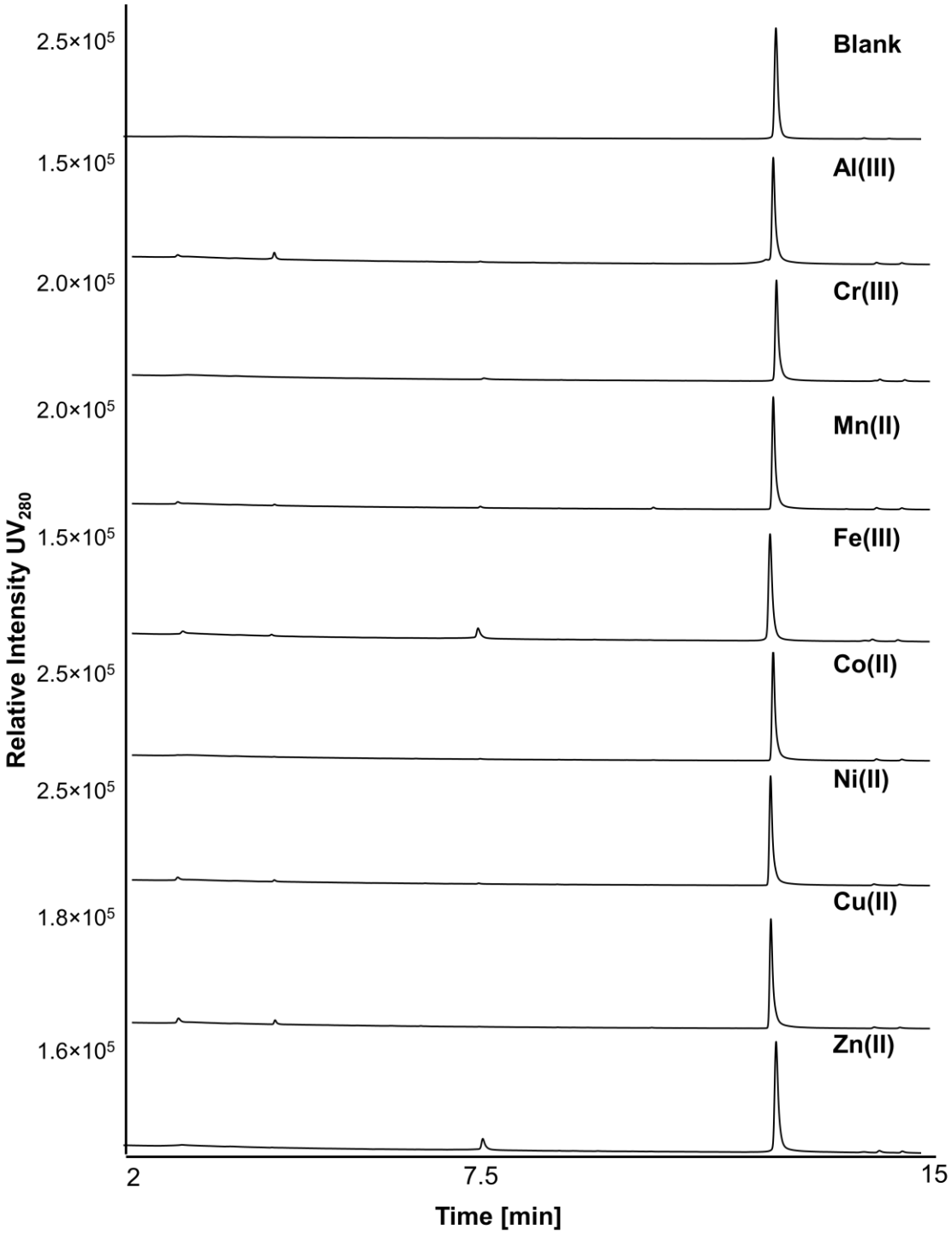

Fig. S13. Sum of relative UV intensities at 280 nm from the RP-UHPLC-PDA chromatograms of the WS and ES fraction of quercetin at pH 4 in absence and presence of the different metal cations. Here the sum of the intensities from both fractions was used to quickly indicate if oxidative quercetin products were formed.

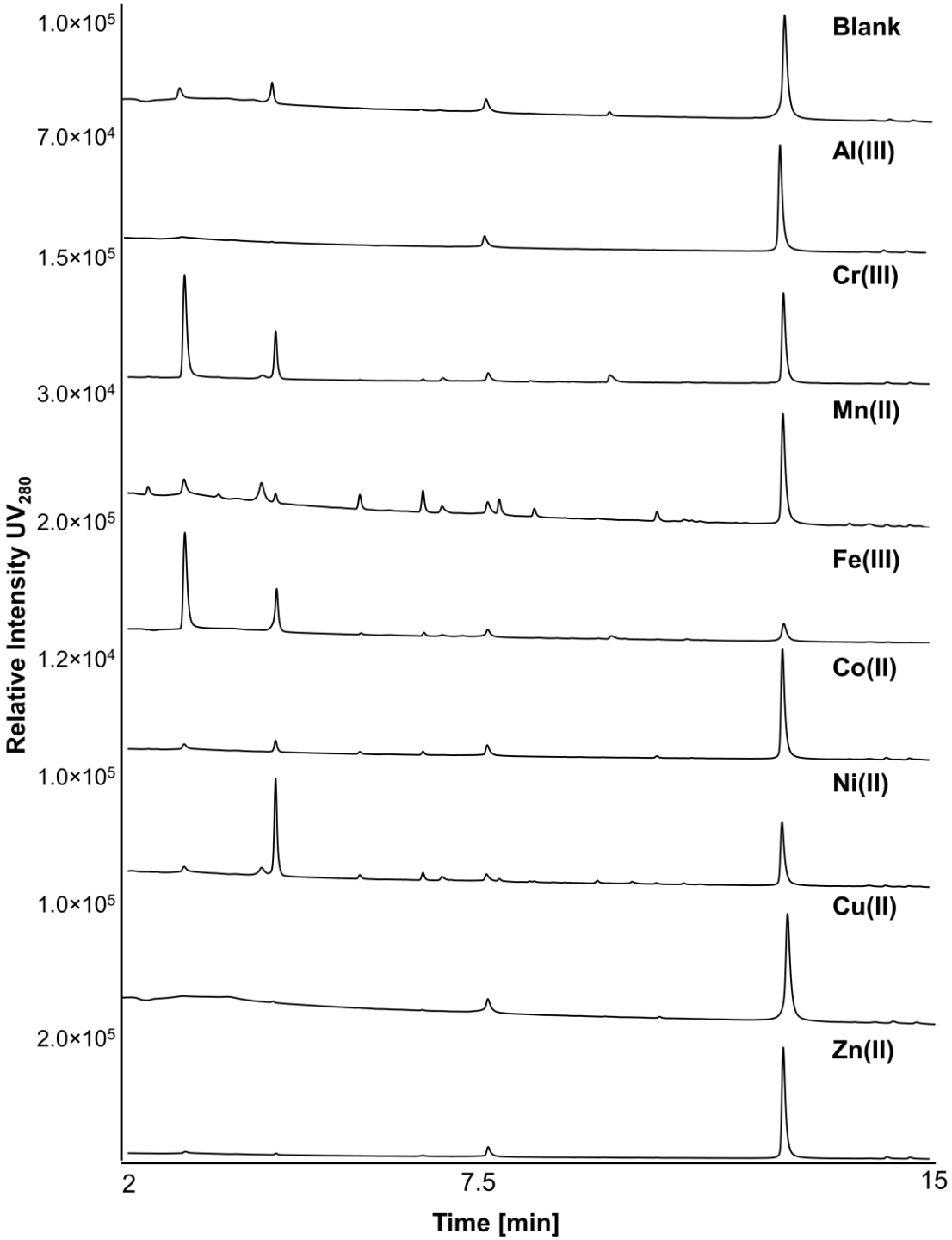

Fig. S14. Sum of relative UV intensities at 280 nm from the RP-UHPLC-PDA chromatograms of the WS and ES fraction of quercetin at pH 7.4 in absence and presence of the different metal cations. Here the sum of the intensities from both fractions was used to quickly indicate if oxidative quercetin products were formed.

Table S11. Flavonoid oxidation products tentatively identified by RP-UHPLC-PDA-MS^2.

Rt (min)	λ_{max} (nm)	$[M-H]^-$ *m/z*	MS^2 product ion *m/z* (relative intensity) [a]	$[M+H]^+$ *m/z*	MS^2 product ion *m/z* (relative intensity) [a]	Tentatively identified	Ref.
Intermediate oxidation products							
	294	317	191, 299 (57), 207 (45), 163 (24), 273 (17)	319	n.d.	Quercetin-ox	[4-6] [7]
Cleavage products							
2.33	286	n.d.	n.d.				
2.92	294	197	153	n.d.	n.d.	2,4,6-trihydroxyphenylglyoxylic acid	[7]
4.19	254, 294	169	151	n.d.	n.d.	2,4,6-trihydroxybenzoic acid [b]	[7]
4.40	260, 294	153	109	n.d.	n.d.	3,4-dihydroxybenzoic acid [b]	[7]
5.76	260	137	n.d.	n.d.	n.d.	4-hydroxybenzoic acid [b]	
6.79	260, 294	n.d.	n.d.	n.d.	n.d.	n.d.	
7.11	n.d.	n.d.	n.d.	n.d.	n.d.	n.d.	
8.03	270	n.d.	n.d.	n.d.	n.d.	n.d.	
8.59	n.d.	n.d.	n.d.	n.d.	n.d.	n.d.	
9.82	298	497	299, 301 (60), 452 (55), 179 (17)	409	n.d.		
Coupling products [c]							
16.84	366	601	299, 271 (10)	603	n.d.	Dehydrodiquercetin	[7]

n.d. not detected; [a] relative intensity threshold for fragments was ≥10. The most intense fragment is underlined; [b] identification confirmed with authentic standard; [c] only oxidative coupling products with a $UV_{250-400\ nm}$ area >1000 after 24 h incubation in presence of metal ions were shown.

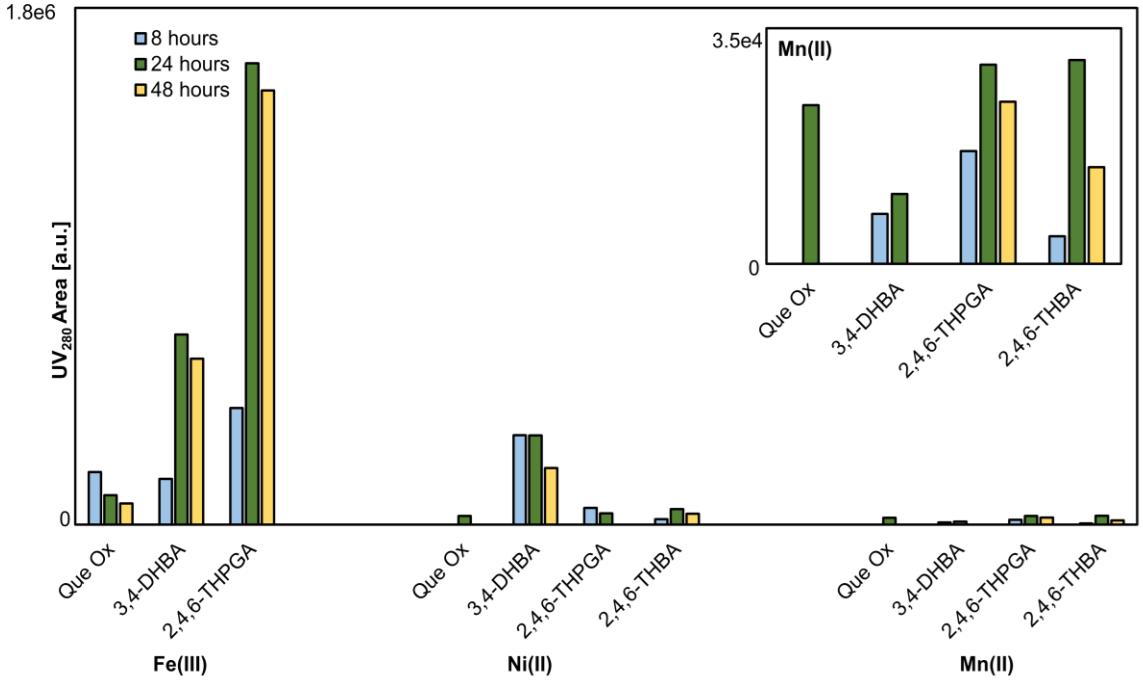

Fig. S15. Oxidation products for Fe(III)-, Mn(II)- and Ni(II)-quercetin systems at 8, 24, and 48 hours at pH 7.4.

Table S12. The theoretical *m/z* values of the reaction products from the oxygenation and hydroxylation pathways in 100 vol.% $H_2{}^{18}O$ and when incubations are performed in 50 vol.% $H_2{}^{18}O$.

Products	***m/z* of unlabeled product**	***m/z* of labeled product in 100 vol.% $H_2{}^{18}O$**	***m/z* of labeled product corrected for 50 vol.% $H_2{}^{18}O$**
Oxygenation reaction			
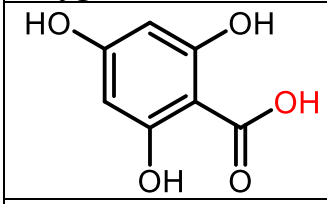	169	169	169 (100%)
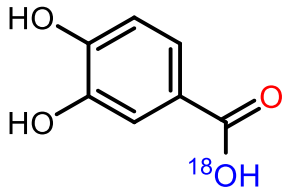	153	155	153 (50%), 155 (50%)
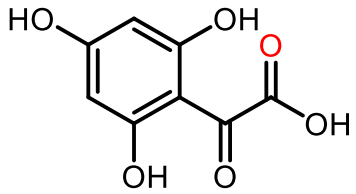	197	197	197 (100%)
Hydroxylation reaction			
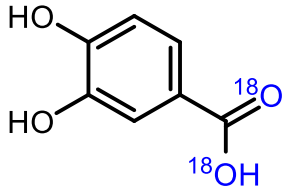	153	157	153 (25%), 155 (50 %), 157 (25%)
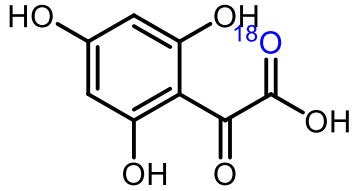	197	199	197 (50%), 199 (50%)

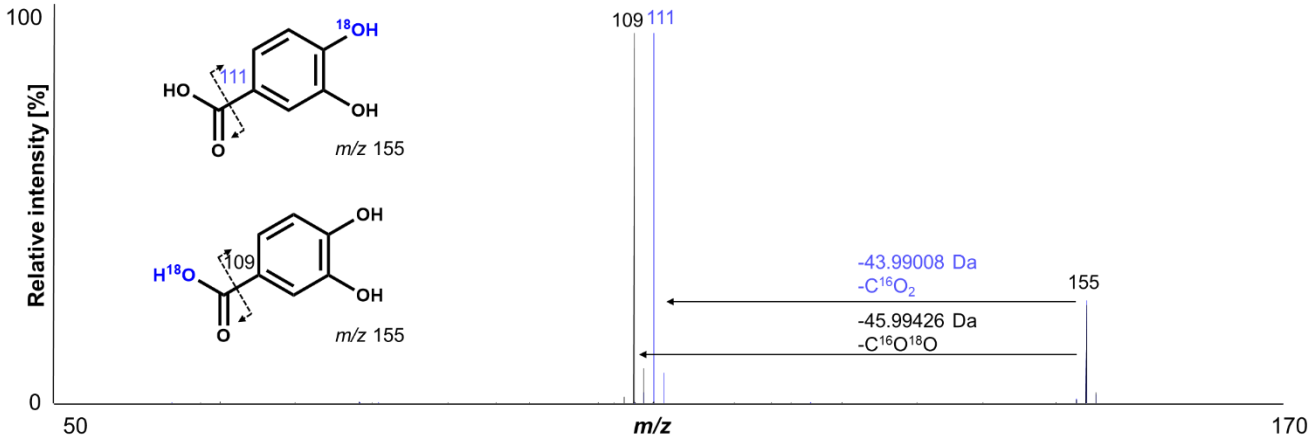

Fig. S16 Higher-energy collisional dissociation (HCD) fragmentation patterns of labelled 3,4-DHBA with the ^{18}O label on the carboxylic acid (black) and catecholate (blue) obtained using high resolution ESI-MS in negative ionization mode. The spectrum from the 3,4-DHBA with the ^{18}O label on the carboxylic acid (black) was obtained after incubation of quercetin with $FeCl_3$ (equimolar, 37 °C, 24 h), the 3,4-DHBA with the ^{18}O label on the catecholate moiety (blue) was obtained after incubation of 3,4-DHBA with $FeCl_3$ (1:10 ratio, 37 °C, 24 h).

References

[1] R.G. Pearson, Absolute electronegativity and hardness: Application to inorganic chemistry, Inorg. Chem. 27 (1988) 734-740.

[2] S.G. Bratsch, Standard electrode potentials and temperature coefficients in water at 298.15 K, J. Phys. Chem. Ref. Data 18 (1989) 1-21.

[3] R.D. Shannon, Revised effective ionic radii and systematic studies of interatomic distances in halides and chalcogenides, Acta cryst. A: cryst. phys. diff. theo. gen. cryst. 32 (1976) 751-767.

[4] G. Jungbluth, W. Ternes, HPLC separation of flavonols, flavones and oxidized flavonols with UV-, DAD-, electrochemical and ESI-ion trap MS detection, Fres. J. Anal. Chem. 367 (2000) 661-666.

[5] J. Fuentes, E. Atala, E. Pastene, C. Carrasco-Pozo, H. Speisky, Quercetin oxidation paradoxically enhances its antioxidant and cytoprotective properties, J. Agr. Food Chem. 65 (2017) 11002-11010.

[6] R. Sokolová, Š. Ramešová, J. Kocábová, V. Kolivoška, I. Degano, E. Pitzalis, On the difference in decomposition of taxifolin and luteolin vs. Fisetin and quercetin in aqueous media, Monatsh. Chemie - Chemical Monthly 147 (2016) 1375-1383.

[7] A. Zhou, O.A. Sadik, Comparative analysis of quercetin oxidation by electrochemical, enzymatic, autoxidation, and free radical generation techniques: A mechanistic study, J. Agr. Food Chem. 56 (2008) 12081-12091.

applied sciences

MDPI

Article

Wide pH Range Potentiometric and Spectrophotometric Investigation into the Acidic Constants of Quercetin, Luteolin and L-ascorbic Acid in Aqueous Media

Luana Malacaria and Emilia Furia *

Department of Chemistry and Chemical Technologies, University of Calabria, 87036 Rende, Italy
* Correspondence: emilia.furia@unical.it; Tel.: +0039-0984-492831

Abstract: It is now well established that the dissociation constants of an organic compound are characteristic of the types of groups, or the combinations of groups, contained in it. Furthermore, the acid–base dissociation constants are important parameters to fully understand the properties of a molecule in biological systems. In this framework, the aim of the present study was to determine the acidic constants of three natural molecules with well-known antioxidant properties, namely quercetin, luteolin and L-ascorbic acid. The evaluation was carried out in aqueous media (i.e., 0.16 M NaCl) at 37 °C in a wide pH range by using a combined approach based on potentiometric and spectrophotometric measurements. The results underline the necessity to employ both experimental techniques to obtain accurate values for acidic constants, preventing uncertainties related to undesirable oxidation reactions.

Keywords: quercetin; luteolin; ascorbic acid; acidic constants; potentiometry; UV-vis spectrophotometry

Citation: Malacaria, L.; Furia, E. Wide pH Range Potentiometric and Spectrophotometric Investigation into the Acidic Constants of Quercetin, Luteolin and L-ascorbic Acid in Aqueous Media. *Appl. Sci.* **2023**, *13*, 776. https://doi.org/10.3390/app13020776

Academic Editors: Antonio Boccaccio, Antony C. Calokerinos, Dario Di Stasio, Maria Contaldo, Andrea Ballini and Michele Covelli

Received: 25 November 2022
Revised: 26 December 2022
Accepted: 1 January 2023
Published: 5 January 2023

1. Introduction

The thermodynamic properties of bioactive molecules in aqueous solutions are of significant scientific and practical interest. In this context, the acidic constants are important physicochemical parameters of a molecule, as they reflect its reactivity, solubility, affinity for a macromolecule and/or ability to establish intermolecular interactions. In addition, the acid and basic functional groups of a molecule strongly influence its pharmacokinetics and toxicity. The experimental evaluation of the pK_a values of the molecules of biological interest, which could be hygroscopic and very unstable in an extreme pH range, is still unsolved, as it is related to the conditions in which the experiments are performed. The most useful and widely employed conventional methods are potentiometric and spectrophotometric titrations and conductometry [1–3]. However, only a few of them have referred to measurements conducted in aqueous media, where they show low water solubility.

In this framework, the present study intends to evaluate the acidic constant values of quercetin, luteolin and L-ascorbic acid (Figure 1a–c), three natural antioxidants (generically H_nL) whose beneficial properties are well known, in aqueous solution. The experimental approach provides measurements via potentiometric and UV-vis spectrophotometric titrations in a wide pH range, at 37 °C and ionic strengths of 0.16 M, using NaCl as a background electrolyte. The constant ionic medium method has proved to be indispensable in equilibrium studies of complex ionic reactions as it is necessary to minimize activity coefficient variation, even though the modification is in the concentration of the reagent. The method, which consists of using concentrated aqueous solutions of inert salts as the solvent, allows for the use of concentrations instead of activities in the evaluation of equilibrium constants. Additionally, it was useful to minimize the liquid junction potential, owing to the hydrogen ion concentration, which was varied in a wide pH range to assess the acidic constants of H_nL.

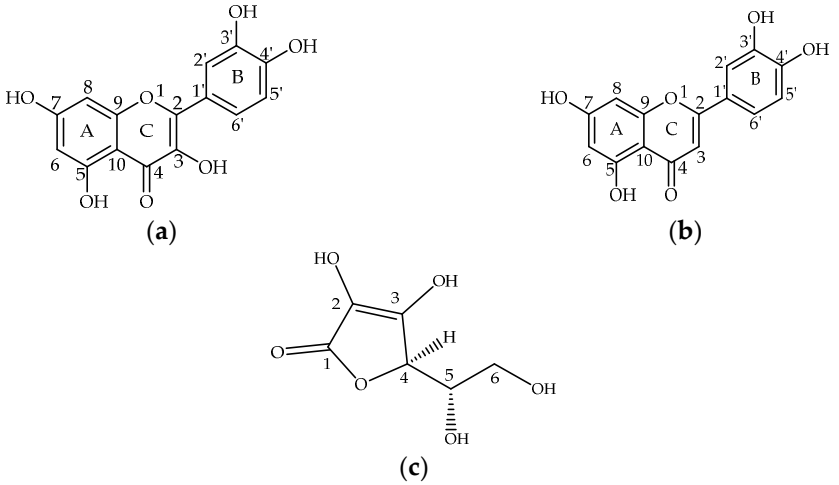

Figure 1. Chemical structure of the investigated natural antioxidants: quercetin (**a**), luteolin (**b**) and L-ascorbic acid (**c**).

Quercetin and luteolin belong to flavonoids that are secondary plant metabolites of the phenolic family. The most common flavonoids contain three rings, indicated as A, B and C (Figure 1a,b), and the oxidation state of C ring provides their classification into several subgroups, as quercetin and luteolin belong to flavonol and flavone subclasses, respectively. L-ascorbic acid is a water-soluble vitamin required for the prevention of scurvy and is known to be active as a cellular hydrogen transfer carrier for the redox enzyme in live cells [4]. Structurally, ascorbic acid is a γ-lactone and an ene-diol (Figure 1c).

All these plant-derived natural compounds are found in significantly high quantities in fruits and vegetables and are considered valuable health-promoting compounds [4–9]. Choosing these natural antioxidants is also related to their well-known capability to chelate several metal ions of relevant importance for biological systems, and they have attracted our research interest in the past 10 years [10–17]. Their ability to bind cations depends on their structure, characterized by functional groups such as phenol, enol and enediol moieties that can undergo deprotonation via metal interaction, whatever their pK_a value. In this context, the accurate knowledge of the acidity of -OH is fundamental to understanding how these molecules can counteract the metal-related damage [18–25]. Furthermore, their antioxidant ability could be correlated to the relative acidity of -OH groups.

2. Materials and Methods

2.1. Chemicals

All chemicals were of analytical grade. The titrant carbonate-free solutions of sodium hydroxide, the hydrochloric acid and the sodium chloride stock solutions were prepared and standardized as previously described [12].

Quercetin (Sigma, ≥95%), luteolin (Sigma, ≥98%) and L-ascorbic acid (Sigma, 99.2%), were stored in a desiccator over silica gel and used as such.

To avoid variations during dilution, all the solutions were prepared by adding the appropriate amount of NaCl, as the background electrolyte, to set the ionic strength at 0.16 M. Double-distilled water, freed from any organic impurities by means of a Milli-Q system (Millipore), was used to prepare fresh solutions.

2.2. Potentiometry and Spectrophotometry

The potentiometric arrangement and the titrations were conducted with the same apparatus described previously [12]. The glass electrodes were from Metrohm. Following the addition of the reagents, they acquired a constant potential (within ±0.01 mV) by 30 min. To prevent any interference due to carbonate formation, nitrogen gas was gently introduced into the test solutions, which were magnetically stirred throughout titrations.

Nitrogen commercial cylinders were used, and the gas was further purified by passing it through 1 M NaOH, 1 M H_2SO_4, double-distilled water and 0.16 M NaCl. The cell apparatus was kept in a thermostatic bath at (37.0 ± 0.1) °C.

The acid–base equilibria were investigated by performing potentiometric titrations, at 37 °C and in 0.16 M NaCl, and by measuring, with a glass electrode (GE), the electromotive force (EMF) of cell:

RE|Test Solution|GE

where RE corresponds to the reference electrode (Ag|AgCl|0.01 M NaCl|0.16 M NaCl), while the test solution was made of C_L M of H_nL, C_A M HCl, C_B M NaOH and 0.16 M NaCl. The primary C_L, C_A, C_B and $[H^+]$ represent the basic data in the treatment to obtain the acidic constants.

The EMF of the cell can be expressed, in mV, at the temperature of 37 °C, as Equation (1):

$$E = E° + 61.54 \log[H^+] + E_j \quad (1)$$

where $E°$ was constant for each series of measurements and E_j is the liquid junction potential, which depends on $[H^+]$ only [26]. The E_j value at 37 °C and 0.16 M NaCl was determined by acid–base titration using cell (G) without H_nL. The obtained results for $[H^+] \leq 0.100$ M could be accurately fitted by the linear slope E_j ($[H^+]$)$I = -j\ I$ $[H^+]$. The value of j (mV/M) was 631 ± 1.

All titrations were separated into two parts. In the first one, $E°$ constant value (within ±0.05 mV), was determined in accordance with the Gran's method [27,28] in the $[H^+]$ range 10^{-4}–10^{-2} M and without H_nL. $[H^+]$ was stepwise reduced by coulometrically generating OH^- ions with the circuit C:

- Pt/Test Solution/AE +

where AE is the auxiliary electrode of generical composition: 0.16 M NaCl/0.1 M NaCl, (0.16–0.1) M NaCl/Hg_2Cl_2/Hg.

Under the chosen experimental condition, the only electroreducible species was water. Hence, suppose that at the cathode the only reaction that occurs is the water reduction (Equation (2)):

$$H_2O + e^- \rightleftarrows \tfrac{1}{2} H_2 + OH^- \quad (2)$$

In the test solution of a known volume, V, C_B can be expressed as ($\mu F \cdot 10^{-6}$/V) M, where μF stands for the microfaradays passed through the cell.

In the second part, after the addition of H_nL, the acidity was gradually decreased by adding known volumes of the standard NaOH solution.

All titrations were conducted with a programmable computer-controlled data acquisition switch unit 34,970 A from Hewlett and Packard. The constant–current source of the coulometric circuit was a system DC power supply 6614 C by Hewlett and Packard. The EMF values were measured at a precision of $\pm 10^{-5}$ V using an OPA 111 low-noise precision DIFET operational amplifier.

Given the low solubility of quercetin and luteolin in water [12,14] and by using the same experimental approach tested in a previous study [29], all the titrations were carried out by adding an exactly known and weighed amount of solid in the cell apparatus. When equilibria (*i.e.*, Equations (2) and (3)) take place, quercetin and luteolin dissolved into the aqueous medium. C_L varied between 0.5 and 5×10^{-3} M, while the hydrogen ion concentration varied from 5.0×10^{-3} M (pH 2.3) to 1.6×10^{-9} M (pH 8.8). The higher pH limit was imposed on the accuracy in the EMF measurements by glass electrode. For this reason, all systems were studied by UV-vis spectrophotometric titrations to investigate the more alkaline pH range (*i.e.*, up to pH 12). C_L was varied between 0.01 and 0.04×10^{-3} M. The spectrophotometric measurements were carried out with a Varian Cary 50 Scan UV Visible Spectrophotometer, by controlling the temperature of the cell holder at (37.0 ± 0.3) °C by using a Grant circulating water bath. Matched quartz cells of thickness 1 cm were employed.

The absorbance values, A_λ, recorded to 0.001 units between 200 and 600 nm for quercetin and luteolin, and between 200 and 340 nm for L-ascorbic acid, were measured each 2 nm to collect data for numerical elaboration by using a Hyperquad [30]. The spectra were recorded 2 minutes after mixing with a strong base. This period was thought short enough to avoid any photochemical degradation. The acquisition of data was controlled with the aid of a computer linked to the instrument.

3. Results

Potentiometry and spectrophotometry were used to determine the acidic constants of quercetin, luteolin and L-ascorbic acid—generically H_nL. To acquire accurate results, the physical integrity of the molecules and the stability at different pH values in which the study was carried out must be taken into consideration during the whole experiment. So the systems were kept under an inert atmosphere and prevented from being exposed to light radiation.

The general equilibria reported in Equations (3) and (4) fully explain the potentiometric data, treated by numerical and graphical methods:

$$H_nL + H_3O^+ \rightleftarrows H_{n+1}L^+ + H_2O \qquad \log K^*(\pm 3\sigma) \qquad (3)$$

$$H_nL + H_2O \rightleftarrows H_{n-m}L^{m-} + m\ H^+ \qquad \log K_{am}\ (\pm 3\sigma) \qquad (4)$$

These correspond to the protonation of the carbonyl moiety, according to [31], and to the protolysis of the -OH groups, respectively. The data used to determine the acidic constants, according to Equations (3) and (4), were obtained by conducting two titrations for each compound.

The interpretation of the potentiometric experimental points, in terms of species and equilibrium constants, was carried out with the least-squares computer program Superquad [32] to get the minimum of the function reported by Equation (5):

$$U = \sum (E_i^{obs} - E_i^{cal})^2 \qquad (5)$$

The results are reported in Table 1.

The graphical evaluation was carried out by analyzing the trend of experimental points, depicted as Z_H and obtained at different C_L values, with respect to the pH. Z_H represents the mean number of protons released for ligand [33], and it is equal to $([H^+] - C_A + C_B + K_w/[H^+])/C_L$. The values for the ion product of water, in our experimental condition (*i.e.*, 37 °C and 0.16 M NaCl), was taken from [34].

The results are reported in Figure A1a–c, for quercetin, luteolin and L-ascorbic acid, respectively. For different C_L values, the experimental points overlap, within the limit of experimental error.

As can be seen in Figure A1, the data are fully explained by Equations (3) and (4). In particular, at pH values lower than 3, Z_H tends to be −1 for all the investigated systems, confirming that a protonation occurs, according to Equations (3) and (4).

Furthermore, as expected, the protolysis equilibria of quercetin and luteolin occur in the alkaline range (−log [H+] > 8) at the expenses of the hydroxylic groups (see Figure 1a,b). In contrast, for L-ascorbic acid, the dissociation starts at a pH higher than 3 (Figure A1c) with the protolysis of -OH in position 3 (see Figure 1c).

Accurate values for the constants of protolysis equilibria (Equation (4)) were determined for quercetin and luteolin only. By performing a back titration, whose points are depicted in Figure A1c as orange crosses, we have verified that L-ascorbic acid undergoes a degradation in an alkaline medium (i.e., pH higher than 7.5), which occurs faster than the potentiometric measurement time.

Therefore, we have performed UV-vis spectrophotometric titrations at different C_L values (i.e., between 0.01 and 0.04 mM). UV-vis absorption spectrophotometry is a simple and accurate method for determining acidic constants, whose determination is based on

a change in the shape and intensity of the absorption spectra with a change in the pH of the test solutions.

The region of pH close to the pK_a values of corresponding acids was supposed to be optimal to obtain accurate values, in the choice of the pH range for all the compounds. Additionally, the spectral range for all compounds was designated according to the variations in the spectra at both acidic and basic solutions.

Consequently, the hydrogen ion concentration was varied by adding small and exactly known volumes of a standard NaOH solution (C_B), from 1.0×10^{-5} M to 1.0×10^{-12} M for quercetin and luteolin and from 1.0×10^{-2} M to 1.0×10^{-11} M for L-ascorbic acid, and the absorbance values were recorded at 93 wavelengths between 230 and 457 nm for quercetin and luteolin and at 50 wavelengths between 211 and 330 nm for L-ascorbic acid.

The typical recorded spectra are depicted in Figure A2a–c, for quercetin, luteolin and L-ascorbic acid, respectively.

The UV-vis spectra of quercetin and luteolin (Figure A2a,b, respectively) show two main absorption bands, which are comparable to signals observed for most flavonoids [12,14]: band I in the 350–400 nm range, as a result of the conjugation between the B and C ring (cinnamoyl system), and band II in the 240–270 nm range, deriving from the A-C ring (benzoyl system). Moreover, two other less-intense absorption bands at 303 and 280 nm for quercetin and at 295 and at 267 nm for luteolin were observed. The UV-vis spectrum of L-ascorbic acid exhibits a single band centered at 260 nm, in accordance with the literature [11,15].

Figure A2a shows that the maximum of band I was blue shifted (*i.e.*, from 367 to 320 nm) by moving from pH 5.5 to pH 6.5. The absorption profile changed negligibly upon raising the pH from 6.5 to 12.0, indicating, according to [35], that the acid–base sites of quercetin were not appreciably rearranged during the dissociation in this pH range.

In contrast, for luteolin and L-ascorbic acid (Figure A2b,c) the maxima of the principal absorption bands were red shifted (*i.e.*, from 352 to 402 nm and from 243 to 267 nm, for luteolin and L-ascorbic acid, respectively) by moving from acidic to basic pH, attesting to the formation of a new spectrally active species in the solution.

The numerical elaboration of spectrophotometric data was carried out by simulating each titration from the knowledge of the total concentrations, C_B and C_L. The minimum of the function, described by Equation (6), was sought by employing the Hyperquad program [30]:

$$U = \sum_i \sum_k w_k \, (A_{ik} - A_{ik}^c)^2 \quad (6)$$

The ion product of water was taken from [34] and was kept invariant.
The results are given in Table 1.

Table 1. Survey of the log K^* and log K_m values, according to general equilibria 3 and 4, by numerical methods. The uncertainties represent 3 σ.

	log K^*	log K_{a1}	log K_{a2}	log K_{a3}	log K_{a4}	log K_{a5}
			Superquad			
Quercetin	2.00 ± 0.06	−8.29 ± 0.03	−8.61 ± 0.01	−9.5 ± 0.1	−9.7 ± 0.3	−10.4 ± 0.3
			Hyperquad			
	/	−8.5 ± 0.6	−9.0 ± 0.3	−9.5 ± 0.6	−10.0 ± 0.3	−10.5 ± 0.9
			Superquad			
Luteolin	2.3 ± 0.1	−8.29 ± 0.03	−8.6 ± 0.1	−8.8 ± 0.3	−9.3 ± 0.3	
			Hyperquad			
	/	−8.1 ± 0.3	−8.80 ± 0.05	−9.6 ± 0.6	−9.8 ± 0.6	
	log K^*		**log K_{a1}**		**log K_{a2}**	
			Superquad			
L-Ascorbic Acid	1.2 ± 0.1	-	−3.86 ± 0.03		/	
			Hyperquad			
	1.16 ± 0.05		−3.75 ± 0.06		−10.6 ± 0.1	

4. Discussion

It has been suggested in previous studies that the antioxidant ability of a series of compounds is strongly affected by pH, which influences the relative abundance of the corresponding acid–base forms [36]. Acid–base equilibria have been reported to strongly affect the UV-vis spectra of several phenolics, including flavonoids. This is observed as significant changes in both the shapes and the intensities of the bands owing to variation in the pH values [37]. The absorption and fluorescence spectra of luteolin have been reported to strongly depend on pH [38]. Therefore, the corresponding acidity constant values are an essential parameter in predicting the functional mechanism of proteins in chemistry and biochemistry.

We calculated here the acidic constants of all the possible sites of quercetin, luteolin and L-ascorbic acid. According to our results, the increase in the pH of the medium at values higher than 3 prompted the proton removal from the protonated carbonyl group (*i.e.*, from $H_{n+1}L^+$ in Equation (3)), leading to the formation of an electroneutral compound (generically H_nL). In contrast, in the narrow pH range of 8–10, in an aqueous solution of quercetin and luteolin, six or five species can simultaneously exist, respectively. These ion molecular forms are in dynamic equilibrium in the aqueous solution, depending on the acidity of the medium. The experimental assignment for the constants of quercetin and luteolin could not be assessed. Although some efforts have been carried out in this way, a systematic and detailed study factoring in all the possible acid forms has not been carried out, and the computational evaluation is still debated [31,35–39]. On the basis only of their structures and, in particular, on the number of phenolic -OH groups, the existence of five and four pK_a values for quercetin and luteolin, respectively, can be hypothesized. However, for quercetin, in previous works dealing with its acidity constants, sets of only two [40,41], three [41–44] and four [43] pK_a values have been reported. Interestingly, in the work of Álvarez-Diduk and colleagues [36], through a combined experimental and computational approach, a complete set of constants has been reported for quercetin. In particular, the deprotonation order was supposed to be 4′, 7, 3, 3′ and 5. Luteolin is structurally analogous to quercetin—except that it has four phenolic -OH groups, as there is no -OH group on ring C. Indeed, the K_{a1} and K_{a2} of quercetin and those of luteolin are the same. Hence, we can suppose that the first two protolysis equilibria involve -OH groups that are less influenced by the deprotonation on the C ring. Only the first acidity constant has been experimentally measured in an aqueous medium [14], and the -OH group in position 4′ has been theoretically calculated as the most acidic site [38]. In the case of L-ascorbic acid, the monoanionic form, derived from the deprotonation of the hydroxy group linked to carbon 3 [O(3)-H] (see Figure 1c), is particularly stable thanks to the delocalization of the negative charge on the oxygen atoms at positions 1 and 3. The second deprotonation occurs at higher pH values, and the corresponding constant is difficult to measure in aqueous media [45–47].

An analysis of the acidity constants in the literature shows major variation among the published values. Furthermore, most of the reported pK_a values were acquired using alcohol and water combinations; thus, there is limited knowledge on pK_a values found in aqueous solutions. Therefore, the acidic constant values determined in this work are not directly comparable with the others in literature, owing to differences in the experimental conditions (Table A1)—except in [11] and [14], which have reported values that are in excellent agreement with our data.

Only a qualitative comparison can be carried out with the values obtained in other works, which reveals acceptable agreement. The difference between those values and those determined here could be related mainly to the different temperatures rather than to the medium used.

Our results showed excellent agreement between the two experimental approaches, providing a valuable method to determine acidic constants values, in a wide range of acidity, with accuracy and in aqueous media (*i.e.*, from pH 2 to pH 12). The acidic constants determined in this work can be considered significant values in the chemistry of

these ligands, and they could be indispensable to understanding ligand behavior in biological systems. Of particular biomedical importance is the ability of these compounds to form stable complexes with biologically active metal ions. The studies in this area have focused on the enhanced curing ability in the case of vitamin C and metal ion deficiencies; on the development of therapeutic agents with potential antitumor, antibacterial, antioxidant and anti-inflammatory properties with enhanced potency with respect to the non-complexed ligands; and on their use as synthetic models for metal containing complex biological systems [13,18,48].

Author Contributions: Conceptualization: E.F. Investigation: L.M. Resources: E.F. Writing—original draft: L.M. and E.F. Writing—review and editing: E.F. All authors have read and agreed to the published version of the manuscript.

Funding: This research received no external funding. We thank the University of Calabria.

Institutional Review Board Statement: Not applicable.

Informed Consent Statement: Not applicable.

Data Availability Statement: Data sharing not applicable.

Conflicts of Interest: The authors declare no conflict of interest.

Appendix A

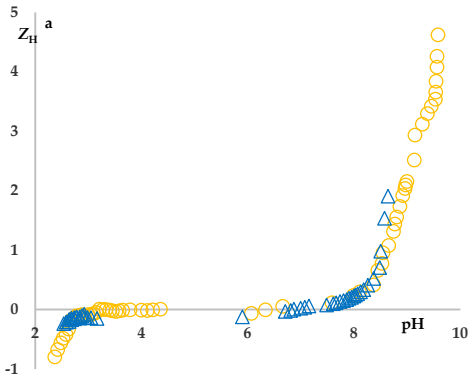

(**a**)

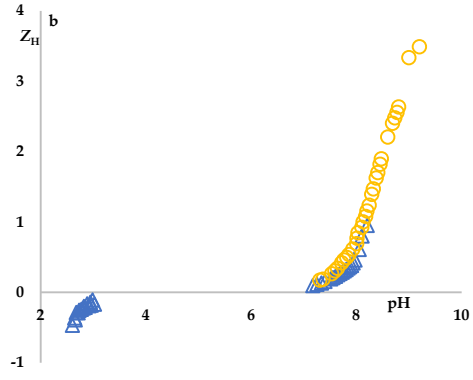

(**b**)

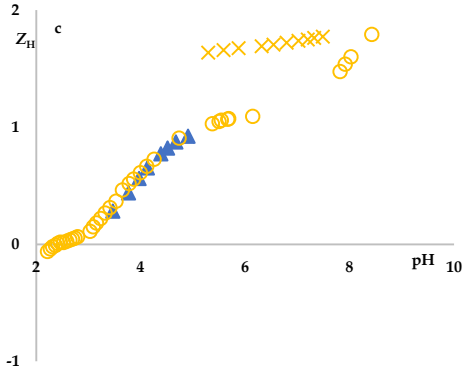

(**c**)

Figure A1. Z_H as a function of -log [H^+] for quercetin (**a**), luteolin (**b**) and L-ascorbic acid (**c**), at 37 °C and in 0.16 M NaCl. Orange circles and orange crosses refer to C_L 0.5 × 10^{-3} M, while blue triangles refer to C_L 5 × 10^{-3} M.

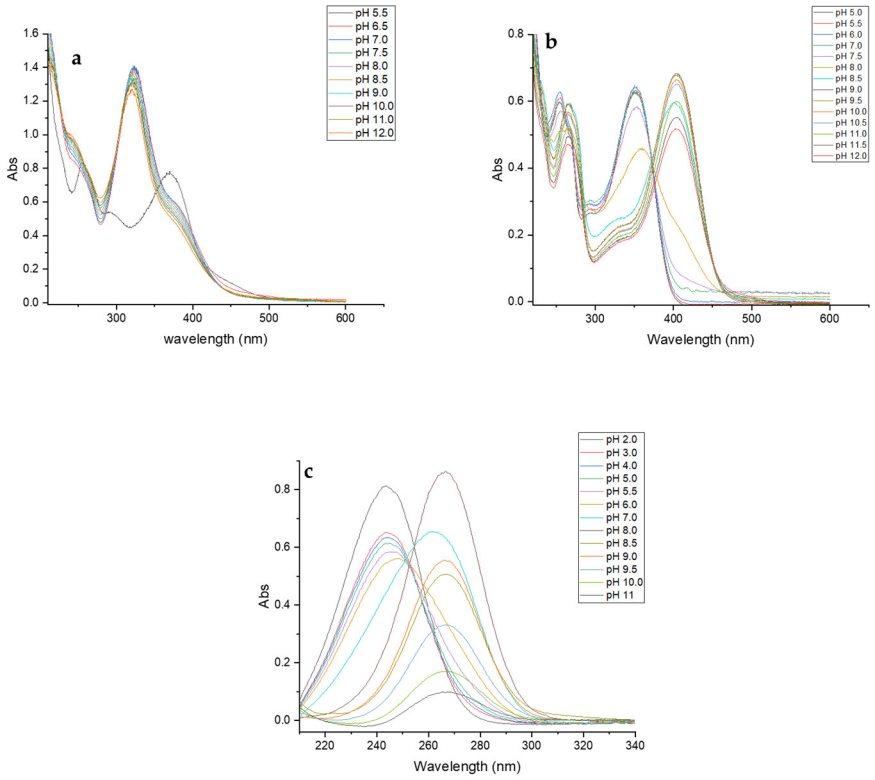

Figure A2. UV-vis spectra recorded for quercetin 0.025 mM (**a**), luteolin 0.010 mM (**b**) and L-ascorbic acid 0.040 mM (**c**), at 37 °C and in 0.16 M NaCl.

Table A1. Acidic constants of quercetin (Que), luteolin (Lut) and L-ascorbic acid (A.A.) from the literature. The uncertainties on the log values represent σ.

	Method	Medium	°C	log *K**	pK_{a1}	pK_{a2}	pK_{a3}	pK_{a4}	pK_{a5}	Ref.
Que	Electroph.	H_2O	25	1.8 ± 0.1	7.1 ± 0.1	9.1 ± 0.1	11.1 ± 0.4			[42]
	Colorim.	H_2O	25		6.4 ± 0.1	8.1 ± 0.1	9.0 ± 0.1	9.6 ± 0.1	11.3 ± 0.1	[31]
	Spectr.				6.6 ± 0.1	8.1 ± 0.1			11.4 ± 0.1	
Lut	Pot.	0.16 M NaCl	37		8.9 ± 0.1					[14]
A.A.	Cond.	H_2O	25		4.147					[45]
	Pot.	0.16 M NaCl	37		3.86 ± 0.01					[11]
	Spectr.	H_2O	25		4.16 ± 0.01	11.73 ± 0.02				[46]
	Titr.	H_2O	16–18		4.14	11.43				[47]

References

1. Beltran, J.L.; Sanli, N.; Fonrodona, G.; Barron, D.; Ozkan, G.; Barbosa. J. Spectrophotometric, potentiometric and chromatographic p*K*a values of polyphenolic acids in water and acetonitrile–water media. *Anal. Chim. Acta* **2003**, *484*, 253–264.
2. Erdemgil, F.Z.; Sanli, S.; Sanli, N.; Ozkan, G.; Barbosa, J.; Guiteras, J.; Beltran, J.L. Determination of p*K*(a) values of some hydroxylated benzoic acids in methanol-water binary mixtures by LC methodology and potentiometry. *Talanta* **2007**, *72*, 489–496.
3. Ragnar, M.; Lindgren, C.T.; Nilvebrant, N.-O. p*K*a-Values of guaiacyl and syringyl phenols related to lignin. *J. Wood Chem. Technol.* **2000**, *20*, 277–305.
4. Lee, S.K.; Mbwambo, Z.H.; Chung, H.S.; Luyengi, L.; Gamez, E.J.C.; Mehta, R.G.; Kinghorn, A.D.; Pezzuto, J.M. Evaluation of the antioxidant potential of natural products. *Comb. Chem. High Throughput Screen.* **1998**, *1*, 35–46.
5. Di Donna, L.; Bartella, L.; De Vero, L.; Gullo, M.; Giufrè, A.M.; Zappia, C.; Capocasale, M.; Poiana, M.; D'Urso, S.; Caridi, A. Vinegar production from *Citrus bergamia* by-products and preservation of bioactive compounds. *Eur. Food Res. Technol.* **2020**, *246*, 1981–1990.
6. Bartella, L.; Mazzotti, F.; Talarico, I.R.; De Luca, G.; Santoro, I.; Prejanò, M.; Riccioni, C.; Marino, T.; Di Donna, L. Structural Characterization of Peripolin and Study of Antioxidant Activity of HMG Flavonoids from Bergamot Fruit. *Antioxidants* **2022**, *11*, 1847.
7. Nijveldt, R.J.; van Nood, E.; van Hoorn, D.E.C.; Boelens, P.G.; van Norren, K.; van Leeuwen, P.A.M. Flavonoids: A review of probable mechanisms of action and potential applications. *Am. J. Clin. Nutr.* **2001**, *74*, 418–425.
8. Taverna, D.; Di Donna, L.; Mazzotti, F.; Tagarelli, A.; Napoli, A.; Furia, E.; Sindona, G. Rapid discrimination of bergamot essential oil by paper spray mass spectrometry and chemometric analysis. *J. Mass Spectrom.* **2016**, *51*, 761–767.
9. Corradini, E.; Foglia, P.; Giansanti, P.; Gubbiotti, R.; Samperi, R.; Laganà, A. Flavonoids: Chemical properties and analytical methodologies of identification and quantitation in foods and plants. *Nat. Prod. Res.* **2011**, *25*, 469–495.
10. Furia, E.; Marino, T.; Russo, N. Insights into the coordination mode of quercetin with Al(III) ion from a combined experimental and theoretical study. *Dalton Trans.* **2014**, *43*, 7269–7274.
11. Cesario, D.; Furia, E.; Mazzone, G.; Beneduci, A.; De Luca, G.; Sicilia, E. The Complexation of Al^{3+} and Ni^{2+} by L-Ascorbic Acid: An Experimental and Theoretical Investigation. *J. Phys. Chem. A* **2017**, *121*, 9773–9781.
12. Corrente, G.A.; Malacaria, L.; Beneduci, A.; Furia, E.; Marino, T.; Mazzone, G. Experimental and theoretical study on the coordination properties of quercetin towards aluminum(III), iron(III) and copper(II) in aqueous solution. *J. Mol. Liq.* **2021**, *325*, 115171.
13. Malacaria, L.; Corrente, G.A.; Beneduci, A.; Furia, E.; Marino, T.; Mazzone, G. A review on coordination properties of Al(III) and Fe(III) towards natural antioxidant molecules: Experimental and theoretical insights. *Molecules* **2021**, *26*, 2603.
14. Malacaria, L.; La Torre, C.; Furia, E.; Fazio, A.; Caroleo, M.C.; Cione, E.; Gallelli, L.; Marino, T.; Plastina, P. Aluminum(III), iron(III) and copper(II) complexes of luteolin: Stability, antioxidant, and anti-inflammatory properties. *J. Mol. Liq.* **2022**, *345*, 117895.
15. Ritacca, A.G.; Malacaria, L.; Sicilia, E.; Furia, E.; Mazzone, G. Experimental and theoretical study of the complexation of Fe^{3+} and Cu^{2+} by L-ascorbic acid in aqueous solution. *J. Mol. Liq.* **2022**, *355*, 118973.
16. Hilgers, R.; Bijlsma, J.; Malacaria, L.; Vincken, J.-P.; Furia, E.; De Bruijn, W.J.C. Transition metal cations catalyze $^{16}O/^{18}O$ exchange of catechol motifs with $H_2{}^{18}O$. *Org. Biomol. Chem.* **2022**, *20*, 9093–9097. https://doi.org/10.1039/d2ob01884e.
17. Malacaria, L.; Bijlsma, J.; Hilgers, R.; De Bruijn, W.J.C.; Vincken, J.-P.; Furia, E. Insights into the complexation and oxidation of quercetin and luteolin in aqueous solutions in presence of selected metal cations. *J. Mol. Liq.* **2023**, *369*, 120840.
18. Crisponi, G.; Nurchi, V.M.; Bertolasi, V.; Remelli, M.; Faa, G. Chelating agents for human diseases related to aluminium overload. *Coord. Chem. Rev.* **2012**, *256*, 89–104.
19. Nurchi, V.M.; Crespo-Alonso, M.; Toso, L.; Lachowicz, J.I.; Crisponi, G. Chelation Therapy for Metal Intoxication: Comments from a Thermodynamic Viewpoint. *Mini-Rev. Med. Chem.* **2013**, *13*, 1541–1549.
20. Hofer, T.; Jørgensen, T.O.; Olsen, R.L. Comparison of food antioxidants and iron chelators in two cellular free radical assays: Strong protection by Luteolin. *J. Agric. Food Chem.* **2014**, *62*, 8402–8410.
21. Crisponi, G.; Dean, A.; Di Marco, V.; Lachowicz, J.I.; Nurchi, V.M.; Remelli, M.; Tapparo, A. Different approaches to the study of chelating agents for iron and aluminium overload pathologies. *Anal. Bioanal. Chem.* **2013**, *405*, 585–601.
22. Drüeke, T.B. Intestinal absorption of aluminium in renal failure. *Nephrol. Dial. Transplant.* **2002**, *17*, 13–16.
23. Cherrak, S.A.; Mokhtari-Soulimane, N.; Berroukeche, F.; Bensenane, B.; Cherbonnel, A.; Merzouk, H.; Elhabiri, M. In Vitro Antioxidant versus Metal Ion Chelating Properties of Flavonoids: A Structure-Activity Investigation. *PLoS ONE* **2016**, *11*, e0165575.
24. Selvaraj, S.; Krishnaswamy, S.; Devashya, V.; Sethuraman, S.; Krishnan, U.M. Flavonoid-Metal Ion Complexes: A Novel Class of Therapeutic Agents. *Med. Res. Rev.* **2014**, *34*, 677–702.
25. Kostyuk, V.A.; Potapovich, A.I.; Kostyuk, T.V.; Cherian, M.G. Metal complexes of dietary flavonoids: Evaluation of radical scavenger properties and protective activity against oxidative stress in vivo. *Cell. Mol. Biol.* **2007**, *53*, 62–69.
26. Biedermann, G.; Sillén, L.G. Studies on the hydrolysis of metal ions. IV. Liquid junction potentials and constancy of activity factors in $NaClO_4$–$HClO_4$ ionic medium. *Arkiv Kemi.* **1953**, *5*, 425–440.

27. Gran, G. Determination of the equivalent point in potentiometric titrations. *Acta Chem. Scand.* **1950**, *4*, 559–577.
28. Gran, G. Determination of the equivalence point in potentiometric titrations. Part II. *Analyst* **1952**, *77*, 661–670.
29. Beneduci, A.; Corrente, G.A.; Marino, T.; Aiello, D.; Bartella, L.; Di Donna, L.; Napoli, A.; Russo, N.; Romeo, I.; Furia, E. Insight on the chelation of aluminum(III) and iron(III) by curcumin in aqueous solution. *J. Mol. Liq.* **2019**, *296*, 111805.
30. Gans, P.; Sabatini, A.; Vacca, A. Investigation of equilibria in solution. Determination of equilibrium constants with the HYPERQUAD suite of programs. *Talanta* **1996**, *43*, 1739–1753.
31. Chebotarev, A.N.; Snigur, D.V. Study of the Acid Base Properties of Quercetin in Aqueous Solutions by Color Measurements. *J. Anal. Chem*. **2015**, *70*, 55–59.
32. Gans, P.; Sabatini, A.; Vacca, A. SUPERQUAD: An improved general program for computation of formation constants from potentiometric data. *J. Chem. Soc. Dalton Trans.* **1985**, 1195–1200. https://doi.org/10.1039/DT9850001195.
33. Sillén, L.G. Some Graphical Methods for Determining Equilibrium Constants. II. On "Curve-fitting" Methods for Two-variable Data. *Acta Chem. Scand.* **1956**, *10*, 186–202.
34. De Stefano, C.; Foti, C.; Giuffrè, O.; Sammartano, S. Dependence on Ionic Strength of Protonation Enthalpies of Polycarboxylate Anions in NaCl Aqueous Solution. *J. Chem. Eng. Data* **2001**, *46*, 1417–1424.
35. Zhang, C.; Korshin, G.V.; Kuznetsov, A.M.; Yan, M. Experimental and quantum-chemical study of differential absorbance spectra of environmentally relevant species: A study of quercetin deprotonation and its interactions with copper (II) ions. *Sci. Total Environ.* **2019**, *679*, 229–236.
36. Álvarez-Diduk, R.; Ramírez-Silva, M.T.; Galano, A.; Merkoçi, A. Deprotonation mechanism and acidity constants in aqueous solution of flavonols: A combined experimental and theoretical study. *J. Phys. Chem. B* **2013**, *117*, 12347–12359.
37. Musialik, M.; Kuzmicz, R.; Pawłowski, T.S.; Litwinienko, G. Acidity of Hydroxyl Groups: An Overlooked Influence on Antiradical Properties of Flavonoids. *J. Org. Chem.* **2009**, *74*, 2699–2709.
38. Amat, A.; De Angelis, F.; Sgamellotti, A.; Fantacci, S. Acid-base chemistry of Luteolin and its methyl-ether derivatives: A DFT and ab initio investigation. *Chem. Phys. Lett.* **2008**, *462*, 313–317.
39. Agrawal, P.K.; Schneider, H.-J. Deprotonation induced ^{13}C NMR shifts in phenols and flavonoids. *Tetrahedron Lett.* **1983**, *24*, 177–180.
40. Tyukavkina, N.A.; Pogodaeva, N.N. Ultraviolet Absorption of Flavonoids VIII. Ionization Constants of Kaempferol and Quercetin. *Chem. Nat. Compd*. **1975**, *11*, 741–743.
41. Zenkevich, I.G.; Guschina, S.V. Determination of Dissociation Constants of Species Oxidizable in Aqueous Solution by Air Oxygen on an Example of Quercetin. *J. Anal. Chem.* **2010**, *65*, 371–375.
42. Herrero-Martínez, J.M.; Sanmartin, M.; Rosés, M.; Bosch, E.; Ràfols, C. Determination of dissociation constants of flavonoids by capillary electrophoresis. *Electrophoresis* **2005**, *26*, 1886–1895.
43. Jovanovic, S.V.; Steenken, S.; Tosic, M.; Marjanovic, B.; Simic, M.G. Flavonoids as Antioxidants. *J. Am. Chem. Soc.* **1994**, *116*, 4846–4851.
44. Herrero-Martínez, J.M.; Repollés, C.; Bosch, E.; Rosés, M.; Ràfols, C. Potentiometric Determination of Aqueous Dissociation Constants of Flavonols Sparingly Soluble in Water. *Talanta* **2008**, *74*, 1008–1013.
45. Rimpapa, Z.; Pleho-Kapić, A.; Galijašević, S.; Šapčanin, A.; Korać, F. Change in Acidity of L-Ascorbic Acid in the Mixed Solvent DMSO—Water Followed by Conductometric Determination of Dissociation Constants. *Bull. Chem. Technol. Bosnia. Herzeg.* **2013**, *40*, 35–38.
46. Seok, Y.-J.; Kap-Seok, Y.; Sa-Ouk, K. A simple spectrophotometric determination of dissociation constants of organic compounds. *Anal. Chim. Acta* **1995**, *306*, 351–356.
47. Birch, T.W.; Harris, L.J. The titration curve and dissociation constants of vitamin C. *Biochem. J.* **1933**, *27*, 595.
48. Zumreoglu-Karan, B. The coordination chemistry of Vitamin C: An overview. *Coord. Chem. Rev.* **2006**, *250*, 2295–2307.